Statistical geological discrete fracture network model

Forsmark modelling stage 2.2

Aaron Fox, Paul La Pointe,

Golder Associates, Inc.

Jan Hermanson, Johan Öhman,

Golder Associates AB

November 2007

SKB

Statistical geological discrete fracture network model

Forsmark modelling stage 2.2

Aaron Fox, Paul La Pointe,
Golder Associates, Inc.

Jan Hermanson, Johan Öhman,
Golder Associates AB

November 2007

Abstract

The Swedish Nuclear Fuel and Waste Management Company (SKB) is performing site characterization at two different locations, Forsmark and Laxemar, in order to locate a site for a final geologic repository for spent nuclear fuel. The program is built upon the development of Site Descriptive Models (SDMs) at specific timed data freezes. Each SDM is formed from discipline-specific reports from across the scientific spectrum.

This report describes the methods, analyses, and conclusions of the geological modeling team with respect to a geological and statistical model of fractures and minor deformation zones (henceforth referred to as the geological DFN), version 2.2, at the Forsmark site. The geological DFN builds upon the work of other geological modelers, including the deformation zone (DZ), rock domain (RD), and fracture domain (FD) models. The geological DFN is a statistical model for stochastically simulating rock fractures and minor deformation zones as a scale of less than 1,000 m (the lower cut-off of the DZ models). The geological DFN is valid within four specific fracture domains inside the local model region, and encompassing the candidate volume at Forsmark: FFM01, FFM02, FFM03, and FFM06.

The models are build using data from detailed surface outcrop maps and the cored borehole record at Forsmark. The conceptual model for the Forsmark 2.2 geological revolves around the concept of orientation sets; for each fracture domain, other model parameters such as size and intensity are tied to the orientation sets. Two classes of orientation sets were described; Global sets, which are encountered everywhere in the model region, and Local sets, which represent highly localized stress environments. Orientation sets were described in terms of their general cardinal direction (NE, NW, etc).

Two alternatives are presented for fracture size modeling:

- the tectonic continuum approach (TCM, TCMF) described by coupled size-intensity scaling following power law distributions. These models describe fracture intensity and size as a single range from borehole to outcrop scale; and

- the combined outcrop scale and tectonic fault models (OSM+TFM), where separate distributions for size and intensity describe the fractures observed at outcrop scale (largely joints) and the features observed at regional scales (lineaments that are largely faults or deformation zones). Fracture intensity and fracture size are not rigidly coupled.

The stochastic intensity model is build using power laws, and combines fracture intensity data from outcrops (P_{21}) and boreholes (P_{10}) to simultaneously match both data sets. Intensity statistics are presented for each fracture set in each domain, and the spatial variation of intensity described as a function of lithology or as a gamma distribution where possible. This report also describes the sources of uncertainty in the methodologies, data, and analyses used to build the version 2.2 geological DFN, and offers insight as to the potential magnitudes of their effects on downstream models. The outputs of the geological DFN modeling process are recommended paramters or statistical distributions describing fracture set orientations, radius sizes, volumetric intensities, spatial correlations and models, and other parameters necessary to build stochastic models (lithology and scaling corrections, termination matrices).

Contents

1   Introduction

1.1   Previous modeling work

The most recent complete version of the Forsmark discrete fracture network model (DFN),
as incorporated into the Forsmark 1.2 Site Descriptive Model (SDM), is described in
/La Pointe et al. 2005/. Since that time, additional studies and data have been gathered to further
develop and refine the SDM for the proposed Forsmark repository site. These include a study
of the dominant rock types in the rock domains and the fracture geology in deformation zones
/Stephens and Forssberg 2006/, the completion of several new boreholes that were logged
for fracturing (KFM01C, KFM01D, KFM06A, KFM06B, KFM06C, KFM07A, KFM07B,
KFM07C, KFM08A, KFM08B, KFM08C, KFM09A, KFM09B and KFM10A) and outcrop
maps of fracturing (AFM001243, AFM001244, AFM001264 and AFM001265), and the
continuing revision of the Forsmark deformation zone (DZ) model based on new borehole and
high-resolution ground magnetic survey data.

The conceptual model underlying version 1.2 of the Forsmark DFN consisted of four sub-vertical
fracture sets and one sub-horizontal fracture set. The four sub-vertical sets appeared to be related
to the orientations of major lineament trends, and were referred to as the NW, NS, NE and EW
global sets. All of these global sets, as well as the sub-horizontal set, were believed to be old,
based upon their mineral fillings, lack of strong intensity variation with depth, and structural
relations. Likewise, the sub-horizontal set was believed to be as old as the sub-vertical sets, with
perhaps minor development of additional fractures within a few tens of meters of the surface due
to deglaciation processes and associated stress-relief after the most recent glacial period.

No consistent evidence was found in Forsmark 1.2 that indicated that fracture intensities
systematically decreased with depth. Plots of intensity vs. depth indicated that there were zones
of higher and lower intensity, and that sometimes there was a zone of high intensity within a few
tens of meters of the present surface, but that no systematic pattern was discernable. A statistical
investigation of the fracture intensity as a function of geological factors suggested no associa-
tions that were sufficiently strong as to be of use for estimating fracture intensity. Some of the
observations made during Forsmark 1.2 were that:

1. Orientations of fractures were not constant with depth within the same borehole;

2. Intervals of higher intensity within the same borehole often corresponded to sections with
   distinct fracture orientation differences, usually including the presence of an additional
   sub-vertical set.

It was found that the fracture intensity varied significantly between rock domains. Within each
rock domain, the spatial pattern of intensity was best characterized by a Poissonian model,
rather than a spatially correlated geostatistical model or a scaling fractal model, for model scales
greater than a few tens of meters.

Key uncertainties identified in version 1.2 of the Forsmark DFN were:

1. the causes for intensity variation within rock domains, the uncertainty about certain rock
   domains that had few or no data sets to characterize them;

2. the "tectonic continuum" assumption used to calculate the size models for the global sets;

3. the size model for the sub-horizontal fractures, especially how large these fractures might
   actually be; and

4. whether the zones of high fracture intensity were part of the background fracture sets or
   constituted a distinct population, perhaps related to deformation zones.

The new outcrop studies, boreholes, structural re-interpretations and other analyses carried out
subsequent to SDM 1.2 were designed to obtain data to reduce these uncertainties.

1.2 Objectives

The goal of the Forsmark geological DFN, version 2.2, was to produce a model of fracturing within and adjacent to the proposed Forsmark repository to facilitate hydrologic and geomechanical modeling in support of safety assessments, and to provide engineering data related to fracturing for repository design and construction, with reduced uncertainty, greater transparency, increased confidence and greater ease-of-use for the intended users of the model.

A key change in the modeling methodology in version 2.2 of the geological DFN is the parameterization of fractures within specific spatial limits (fracture domains). The definition and derivation of these domains are defined in the Fracture Domain report /Olofsson et al. 2007/ a document jointly produced by SKB and the Swedish Geological Survey (SGU). Because of the closer link of these domains to geological and tectonics as they might relate to fracture development, using fracture domains as the highest level partitioning of the fracture model should produce an improved data stratification that reduces overall model uncertainty, and makes it easier to identify and exploit for predictive modeling relations between geological factors and fracture intensity and orientation, since the "noise" is reduced by stratifying data into fracture domains.

The issues regarding the "tectonic continuum" hypothesis and the related issue of how large the regional fractures sets might be, were addressed through the consideration of excavation mapping and data analysis carried out during the construction of the Forsmark nuclear power plant /Carlsson 1979/, the construction of the version 2.2 deformation zone (DZ) model, a desktop study of possible additional minor deformation zones (MDZs) in cored borehole data, /Fox and Hermanson 2006/, and the preliminary analysis of new ground magnetic lineament data /Isaksson et al. 2006ab/ at a scale intermediate between the regional deformation zones and the joints mapped on outcrops.

The identification of MDZs in the borehole data was designed to separate what might be small-scale portions of faults and fault zones from "background" fractures; the hypothesis is that most background fractures that are primarily joints. This separation and the analyses based on the remaining "background' population should, if indeed these MDZs are not part of the background fracturing, make it possible to develop better predictive models for variations in fracture intensity, to develop statistical models for the background fracturing with reduced uncertainty due to the elimination of population mixing effects, and clarify the spatial and scaling patterns of fracture intensity, also through the reduction of population mixing impacts.

To build increased confidence in the model, a validation case was developed to predict the fracture intensity of a recent borehole whose data formed no part of the model development.

All models have uncertainty. In version 2.2 of the geological DFN, the uncertainties that are identified are evaluated as to their possible impacts on hydrology and rock mechanics.

1.3 Model use and applicability

The intended use of the Forsmark version 2.2 geological DFN is as input for hydrological and mechanical modeling for safety assessment and licensing, and to provide fracture-related data for repository design and engineering planning. The model is presented as a mathematical description of the fracturing, not as a static model. As such, the model parameters can be implemented in different forms, such as a discrete fracture network (DFN) model for direct stochastic simulation or as upscaled block properties (fracture permeability, porosity, storage volume) for a continuum model. The implementation of the mathematical description is a function of the downstream modeling or engineering needs, and is not part of the SDM model, although every effort has been made to present the mathematical description in a form that is convenient to the downstream modeling teams and engineers.

The goal of this model is to provide downstream users with a means to estimate the fracture orientations, intensity, size, spatial patterns and fracture geology at a location within the current proposed Forsmark repository area (Figure 1-2), along with the variability of these estimates over a scale range of 0.5 m to 564 m (in terms of fracture radius). The model is only applicable within the local model boundaries shown in Figure 1-1, from the surface to a depth of 1,000 m. It is valid for a size range scale of 0.5 m up to 564 m, expressed as the radius of the area of an equivalent disc-shaped fracture. In addition, the model is only valid within the target fracture domains FFM01, FFM02, FFM03, and FFM06, as borehole and outcrop data were only available for these fracture domains. Applicability outside these limits has not been established, and users who wish to use the model outside the range of applicability should carefully evaluate the parameters and limitations of the 2.2 Geological DFN prior to using the model outside of the context for which it was constructed.

The SDM Forsmark version 2.2 geological DFN is based upon the data described in Section 2.1, the software versions described in Section 2.2, and the assumptions listed in Section 4. Any future data additions or revisions, new conceptual understandings, or changes in assumptions or definitions could require this model to be revised.
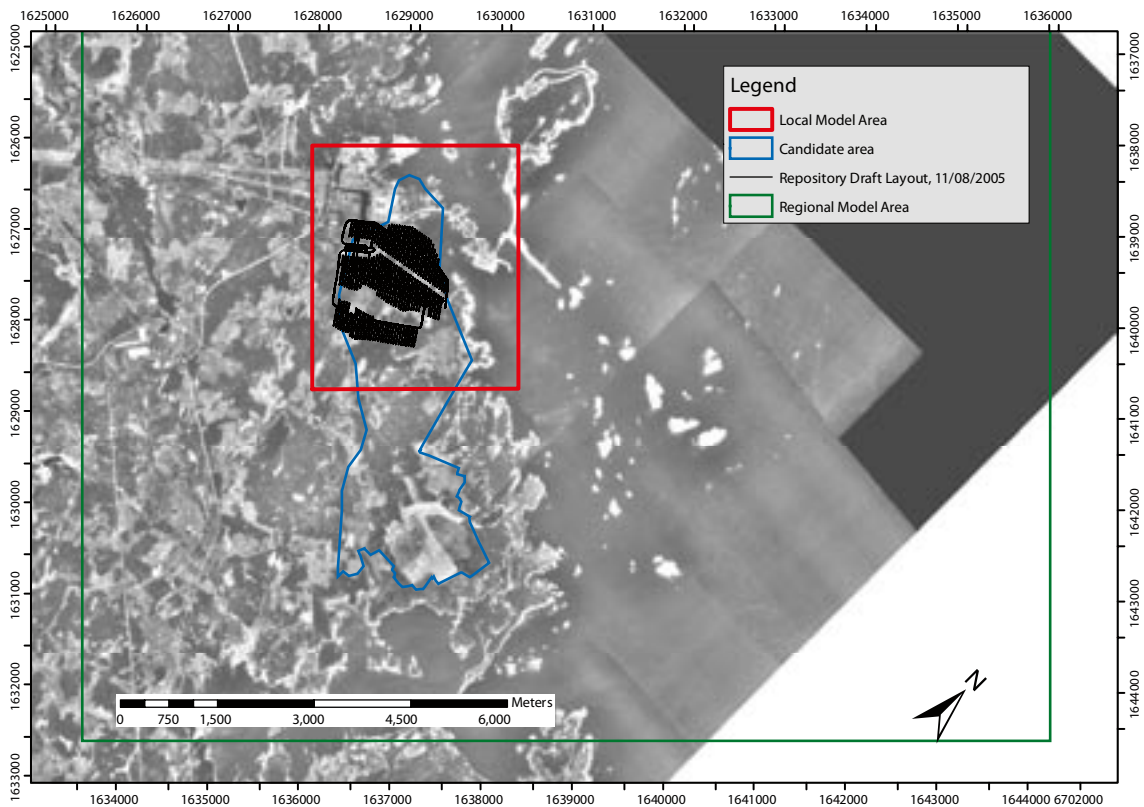
Figure 1-1. *Spatial limits of applicability of the Forsmark geological DFN, version 2.2. The GeoDFN model is defined only within the Local Model area.*

9
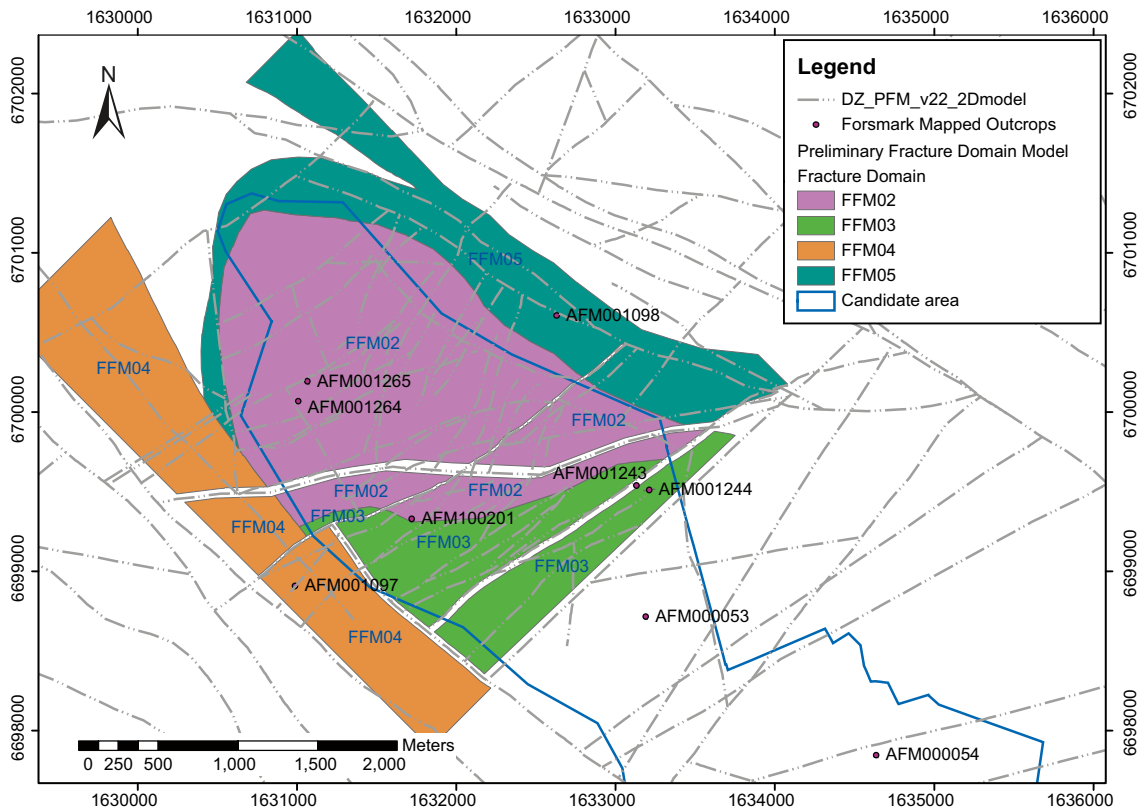
Figure 1-2. *Fracture domains for SDM Forsmark 2.2 modeling at the approximate ground surface (z = 0). Note that the geological DFN is only valid for domains FFM01, FFM02, FFM03, and FFM06.*
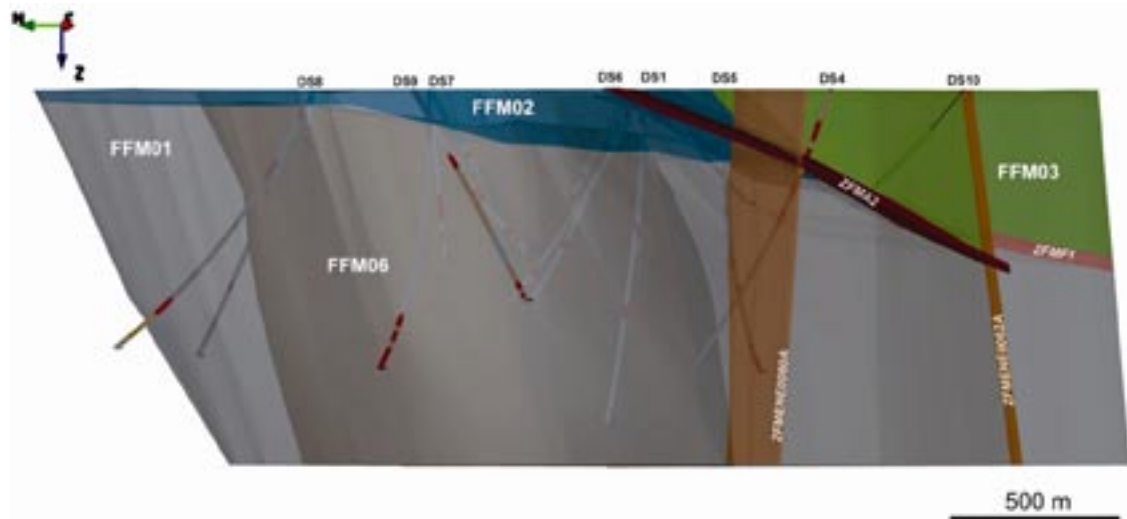
Figure 1-3. *Three-dimensional image of the fraction domain model, viewed towards the east-north-east. Fracture domains FFM01, FFM02, FFM03 and FFM06 are colored grey, dark grey, blue and green, respectively. The gently dipping and sub-horizontal zones ZFMA2 and ZFMF1 as well as the steeply dipping deformation zones ZFMENE0060A and ZFMENE0062A are also shown. Figure borrowed from the Forsmark Fracture Domain Report /Olofsson et al. 2007/.*

1.4 Acronyms & terminology

CDF – Cumulative Density Function: A function that quantifies the cumulative probability of a distribution. The term is used in this report in the description of tracelength and radius distributions. It is the probability that the value of a randomly selected value is *less* than a specified value.

CCDF – Complementary Cumulative Density Function: A function that quantifies the cumulative probability of a distribution. The term is used in this report in the description of tracelength and radius distributions. It is the probability that the value of a randomly selected value is *greater* than a specified value. The CCDF is equal to 1 – CDF.

CCN – Complementary Cumulative Number: A type of plot in which the number of data values greater than or equal to a specific value is plotted as a function of the value. CCN plots are used in this report for estimating the size model for the Tectonic Continuum alternative model.

CFI – Cumulative Fracture Intensity: A type of plot used to identify fractured zones and quantify their characteristic fracture intensity.

DFN – Discrete Fracture Network model: A three-dimensional numerical model in which fractures are represented as finite surfaces with specified mechanical and hydraulic properties.

DZ – Deformation Zone.

Euclidean Scaling, Euclidean Dimension: A scaling behavior characterized by a first-order relation between the number or density of some object, and the extent of the space in which it is embedded. In this report it is used to describe fracture intensity; a Euclidean scaling model for fracture intensity would be characterized by a linear, first order relation between the number of fractures in a volume of rock and the volume itself. Doubling the volume would lead to a doubling of the number of fractures in a Euclidean scaling model. The Euclidean dimension is a fractal mass dimension that characterizes Euclidean scaling. It is 1.0 for line samples, such as borehole fracture data, 2.0 for areal samples, such as outcrop fracture trace data, and 3.0 for volumetric samples, such as rock volumes.

Exfoliation – also *Sheeting*: The development of fractures subparallel to a free surface due to a reduction in stress normal to the free surface. In SDM 2.2, exfoliation or sheeting is thought to have occurred after the last deglaciation, producing new fractures sub-parallel to the present-day rock surface, and possibly causing existing subhorizontal fractures to propagate or enlarge.

Fracture Domain – A fracture domain refers to a rock volume outside deformation zones in which rock units show similar fracture frequency characteristics. Fracture domains are defined on the basis of the single-hole interpretation work and the results of the initial statistical treatment of fractures. The minor modifications of the single-hole interpretation performed during the modeling stage and the higher-resolution, extended single-hole interpretation work are also accounted for in the recognition of fracture domains. The term is used in connection with the discrete fracture network modeling work (geological DFN) and different fracture domains at Forsmark are referred to as FFMxxx /Olofsson et al. 2007/.

GML – Ground magnetic lineaments. A data set created at Forsmark using very high resolution ground-magnetic surveys in localized areas inside the candidate region.

Mass Dimension – A measure of the scaling behavior of a group of objects. In this report, the mass dimension is used to quantify the scaling behavior of fracture intensity in boreholes and outcrops

MDZ – Minor Deformation Zone. A small deformation zone that it is simulated stochastically rather than deterministically. In the Forsmark 2.2 geological model, MDZ are structures with a surface trace length less than 1,000 m.

OSM – Outcrop Scale Model, an alternative size model based on the linked outcrop trace data population in domains FFM02 and FFM03. The OSM was parameterized both through the use of FracSize and through visual fitting of the trace length scaling exponent in Microsoft Excel.

P_{10} – A measure of lineal fracture intensity, expressed in this report as the number of fractures per meter (1/m).

P_{20} – A measure of fracture intensity, expressed in this report as the number of fractures/mapped area in units of the number fractures per square meter ($1/m^2$).

P_{21} – A measure of areal fracture intensity, expressed in this report as the fracture trace length per unit of mapped area (m/m^2).

P_{30} – A measure of volumetric fracture intensity, expressed in this report as the numbers of fractures per unit of rock volume ($1/m^3$).

P_{32} – A measure of volumetric fracture intensity, expressed in this report as fracture surface area per unit of rock volume (m^2/m^3).

SDM – Site Domain Model.

SDE – Standard Errror.

SSQ – Sum of Squares.

Statistical Significance – This relates to the outcome of a statistical test of a hypothesis. It is the probability of the results of the statistical tests given that the hypothesis is true with reference to a specified value of probability for which the hypothesis is rejected or not rejected. The test of statistical significance does not prove that the hypothesis is true, but rather that the data do or do not reach the probability level of falsifying the hypothesis. Statistical significance is quantified as the parameter α, which represents the probability that the null hypothesis for the statistical test being performed will be rejected when it is fact true (a Type I error). In general, α of 0.05 has been used as a level of significance in the Forsmark 2.2 geological DFN modeling.

Tectonic Continuum Hypothesis – The hypothesis that a fracture population extends in size over a very large scale range; for example, from meters to kilometers. In the tectonic continuum model, the fractures in outcrop with traces on the scales of meters are part of the same fracture population as lineaments or deformation zones with traces on the scale of kilometers. This model allows for the combination of data sets at multiple scales.

TCM – Tectonic Continuum Model, an alternative model based on the tectonic continuum hypothesis. Note that this is fundamentally a coupled size-intensity model; it is not possible to separate the two components.

TFM – Tectonic Fault Model, an alternative size model based on the deformation zones and the ground magnetic lineaments. The Tectonic Fault Model is not by itself a stand-alone model; it is necessary to combine it with the Outcrop Scale Model (OSM) for a complete size-intensity parameterization.

2 Data and software

2.1 Data

This section of the report describes the specific data sources utilized during the geological DFN modeling process. Where applicable, references to specific tables, queries, or object within approved SKB databases have been used.

Note that not all of the data sources have a specific SDE table number; early deliveries from SKB (GIS request numbers 06_44, 06_73, and 06_76) arrived with custom names, rather than SDE feature class names.

2.1.1 Data freeze version

Site characterization data for the geological DFN parameterized as a component of the Forsmark site descriptive model (SDM) version 2.2 is based on data stored in SKB databases (SICADA, SDE, RVS) at the time of the Forsmark 2.2 data freeze (date). However, additional data, such as the geometry and extents of faults contained within the finalized Forsmark 2.2 deformation zone (DZ) model, arrived after the data freeze date and were included in the geological DFN modeling process.

2.1.2 Surface data

Surface data, including the fractures mapped in detail on various outcrops across the Forsmark region, was primarily used to develop the orientation and size models of the fracture sets in the geological DFN. In addition, lineaments derived from both regional (airborne gravity, magnetic, electrical, and coordinated lineaments) and local (high resolution ground magnetic lineaments) were investigated for use as components of the 'tectonic continuum' model case.

Detailed Fracture Outcrop Mapping

Specific data sources for the detailed fracture outcrop mapping analysis include the following exported shapefiles (.shp) from SDE:

Outcrop mapping limits:

- Begränsning_av_hällkartering_på_AFM000053 (SDE Delivery 06_44)
- Begränsning_av_hällkartering_på_AFM000054 (SDE Delivery 06_44)
- Begränsning_av_hällkartering_på_AFM001097 (SDE Delivery 06_44)
- Begränsning_av_hällkartering_på_AFM001098 (SDE Delivery 06_44)
- Begränsning_av_hällkartering_på_AFM100201 (SDE Delivery 06_44)
- SDEADM_GOL_FM_GEO_2669 – Outcrop AFM001243
- SDEADM_GOL_FM_GEO_2671 – Outcrop AFM001244
- SDEADM_GOL_FM_GEO_4096 – Outcrop AFM001264

Mapped bedrock geology:

- Bergarter__borrplats_2 – Outcrop AFM000053 (SDE Delivery 06_44)
- Bergarter__borrplats_3 – Outcrop AFM000054 (SDE Delivery 06_44)
- Bergarter__borrplats_5 – Outcrop AFM100201 (SDE Delivery 06_44)
- Berggrundsenheter__borrplats_4 – Outcrop AFM001097 (SDE Delivery 06_44)

- Berggrundsenheter__Klubbudden – Outcrop AFM001098 (SDE Delivery 06_44)
- SDEADM_GOL_FM_GEO_2662 – Outcrop AFM001243
- SDEADM_GOL_FM_GEO_2664 – Outcrop AFM001244
- SDEADM_GOL_FM_GEO_4094 – Outcrop AFM001264
- SDEADM_GOL_FM_GEO_4421 – Outcrop AFM001265

Outcrop Fractures (unlinked):
- Sprickkartering_på_AFM000053 (SDE Delivery 06_44)
- Sprickkartering_på_AFM000054 (SDE Delivery 06_44)
- Sprickkartering_på_AFM001097 (SDE Delivery 06_44)
- Sprickkartering_på_AFM001098 (SDE Delivery 06_44)
- Sprickkartering_på_AFM100201 (SDE Delivery 06_44)
- SDEADM_GOL_FM_GEO_2670_VIEW – Outcrop AFM001243
- SDEADM_GOL_FM_GEO_4089_VIEW – Outcrop AFM001244
- SDEADM_GOL_FM_GEO_4090_VIEW – Outcrop AFM001264
- SDEADM_GOL_FM_GEO_4097_VIEW – Outcrop AFM001265

The linked outcrop fracture data set was delivered to SKB in February 2007 as a component of the Forsmark interim DFN project. However, the data files were NOT re-requested from SDE. As such, a formal reference for these files was not obtained.

Outcrop Fractures (linked):
- AFM000053_NEW_FINAL_Complete
- AFM000054_FINAL_Complete
- AFM001097_FINAL_Complete
- AFM001098_FINAL_Complete
- AFM100201_FINAL_Complete
- AFM001243_FINAL_Complete
- AFM001244_FINAL_Complete
- AFM001264_FINAL_Complete
- AFM001265_FINAL_Complete

In additional to the data contained in the attribute tables of the outcrop mapping GIS files, full mapping parameter data for each fracture was extracted from the following SICADA data tables:
- fracture_area_map
- fracture_line_map

Lineaments

Lineament data derived from high-resolution ground magnetic surveys /Isaksson et al. 2006ab/ was utilized in the parameterization of the fracture size and intensity models, as well as an independent check on the fracture orientation models. A preliminary version of the ground magnetic lineament data, delivered by SKB via email in December 2006, was used in this analysis. The following shapefiles (.shp) were contained in the December 2006 data delivery:
- AFM100206_1292_1293_1314_LL_061115_line

- AFM100206_V1V2_Linked_Lineament_line
- MFM_Edit_polyline

Final versions of the ground magnetic lineament traces were delivered by SKB via email on 20070630. There were no significant differences in the geometries of the ground magnetic lineaments between the December delivery and the June delivery; however, there were slight differences in the parameter (attribute) tables. The following feature classes were contained in the June 2007 delivery:

- SDEADM_GV_FM_GEO_5204

The lineaments mapped in the ground magnetic data generally consist of two types; 'minima connections' and 'minima/edges'. Minima connections are currently interpreted to represent large-scale bedrock structures, such as tectonic foliations, bedrock contacts, and folding. Minima/edge features are interpreted to represent brittle deformation structures such as faults and deformation zones (Stephens M, in response to Fox A, 4/2/2007 and 4/5/2007, email correspondence entitled "Magnetic foliation at Forsmark?" and "Question on Ground Magnetic Survey Data").

It is possible that the ductile structures interpreted from the minima connections may have re-activated in a brittle fashion at some time. However, for the purposes of geological DFN modeling, we have not included the minima connections in the parameterization of the DFN size and intensity models.

2.1.3   Borehole data

Only fracture data from cored boreholes was used in geological DFN parameterization and modeling process. Data from the following boreholes was used:

- KFM01A, B, C, and D
- KFM03A, KFM03B
- KFM04A
- KFM05A
- KFM06A, B, and C
- KFM07A, B, and C
- KFM08A, B, and C
- KFM09A and B
- KFM10A

Fracture and geology data in Forsmark cored boreholes were extracted from the following SICADA tables:

- p_fract_core_eshi
- p_rock
- p_rock_occur
- p_one_hole_interpret
- p_freq_1 m
- object_location

Revised borehole geology charts, which simultaneously present the single-hole interpretation results, the DZ modeling results, and the fracture domain modeling results, were also used. These figures are documented in Appendix 4 of the fracture domain report /Olofsson et al. 2007/.

2.1.4 Deformation zone model

Both preliminary and final versions of the Forsmark deformation zone (DZ) model were used during the geological DFN modeling process; as most of the changes to the final DZ model involved changes to the DZ property tables and not to the zone geometries, there is little difference between the two versions. Two-dimensional traces of the DZ mid-planes, projected to the ground surface in ArcGIS, were used for size model parameterization (the 'tectonic continuum model alternative) and in uncertainty calculations. Parametric data (orientation, trace lengths) were obtained from the DZ model property tables, which were delivered as Microsoft Word tables.

The deformation zone model data sources used include:

Interim Property Tables, delivered via email by Mike Stephens (SGU) on 20070205:

- DZ_properties_ENE_NNE_NE_v.2.2_Forsmark_070205.doc
- DZ_properties_gentle_v.2.2_Forsmark_070205.doc
- DZ_properties_NNW_EW_v.2.2_Forsmark_070205.doc
- DZ_properties_WNW-NW_v.2.2_Forsmark_070205.doc

Surface trace projections, delivered via email by Mike Stephens (SGU) on 20070129.

- DZ_PFM_v22_2Dmodel.shp

Final versions of the surface trace projections were delivered via email by SKB on 20070630. The DFN models were re-analyzed using the final DZ trace model; however, almost no difference between the January and June deliveries was noted.

- SDEADM_POS_FM_GEO_5032

2.1.5 Fracture domain model

A draft two-dimensional projection of the Forsmark fracture domains at the ground surface ($z = 0$ m AMSL) was used for visualization purposes and for classifying detailed outcrop maps into fracture domains. The file used (Export_Output.shp) was a draft version, and was shipped via email by Raymond Munier on 20070401.

During geological DFN parameterization, the fracture domain model was primarily used as a discriminator in queries against the SICADA table p_fract_core_eshi; no additional geometric modeling was performed on the domains themselves. The geological DFN is only quantified within domains FFM01, FFM02, and FFM03, which are the domains that exist within the proposed repository footprint.

2.2 Software

Table 2-1 lists all of the software used to carry out the calculations in this report, including their name, version numbers, modules, address of vendor and what model parameters they were used for. Modules are listed in the case where there might be ambiguity as to which options were selected.

The Manifold GIS package (listed below) was used in addition to ESRI, Inc.'s ArcGIS software package due to the presence of some additional features not available in the standard ArcMap desktop install. Specifically, Manifold allowed for the manipulation of shapefile intrinsic fields to obtain the calculated strike and dip of the entire polyline (fracture or fault trace), rather than the strike and dip of its component segments. This made extracting feature data from the deformation zone model files much easier. No data transformations or analyses were performed using Manifold GIS. This feature is available in an ArcEditor desktop install, which was not available during the modeling time frame.

Table 2-1. List of software used in the production of this report.

Software name	Version	Company	Calculation performed
Excel 2003	11.8120.8122 SP2	Microsoft Corporation One Microsoft Way Redmond, WA 98052 www.microsoft.com	Trace length scaling calculations; general data preparation for other programs, moving-average intensity tables
Analyze-It	1.71 and 1.73	Analyze-It Software, Ltd. PO Box 77, Leeds LS12 5XA, England, UK. www.analyse-it.com Tel: +44 (0)113 229 5599	Summary tables for fracture intensity as a function of alteration zones and rock types; variation of fracture intensity with depth
DIPS	5.106	Rocscience, Inc. 31 Balsam Avenue Toronto, Ontario M4E 3B5 +1 416 698-8217 www.rocscience.com	Orientation and display of fracture orientations; calculation of modal poles to fracture sets, Terzaghi weighting of contoured pole plots Trace length scaling calculations; general data preparation for other programs, moving-average intensity tables
GeoFractal	1.2, Build 321	Golder Associates Inc. 18300 NE Union Hill Rd. Redmond, WA 98052 +1 (425) 883-0777 frac-man.golder.com	Calculation of fractal mass dimension and box dimension
FracMan DOS	2.606	Golder Associates Inc. 18300 NE Union Hill Rd. Redmond, WA 98052 +1 (425) 883-0777 fracman.golder.com	Analysis of fracture orientation statistics and size statistics for fracture sets
FracMan	7.00 (beta)	Golder Associates Inc. 18300 NE Union Hill Rd. Redmond, WA 98052 +1 (425) 883-0777 fracman.golder.com	Visualization of simulated fracture orientations, conditional sampling of test DFN models
SamEdit	4.11 2006	Golder Associates Inc. 18300 NE Union Hill Rd. Redmond, WA 98052 +1 (425) 883-0777 fracman.golder.com	Creation and editing of sampling structure control files for FRED/ FracWorks7/FracMan DOS
ArcGIS	9.2 SP1 and SP2	ESRI Inc 380 New York St. Redlands, CA 92373 +1 909 793 2853 www.esri.com	Display of fracture and deformation zone traces, creation of new GIS files and metadata to aid data analysis. Visual analysis of outcrop fracturing for set parameterization
BestFit	4.5.5 Sep. 2005	Palisade Corporation 798 Cascadilla Street Ithaca, NY 14850 (607)-277-8000 www.palisade.com	Curve-fitting and analysis of statistical significance, P_{32} as a gamma distribution
Manifold GIS	7.x	Manifold .Net, Ltd. 1805 North Carson St. Suite 700 Carson City, NV 89701 +1 800 556 5919 www.manifold.net	Extraction of feature data from lineament and deformation zone shapefiles,
SPSS	13.0	SPSS, Inc. 11th Floor 233 S. Wacker Dr. Chicago, Illinois 60606 +1 312 651 3000 www.spss.com	Contingency table analyses for relation between alteration, lithology & intensity, hypothesis testing, statistical modeling of spatial patterning and intensity variation of fracture sets

GoLink	N/A	Golder Associates AB P.O. Box 20127 104 60 Stockholm Sweden www.golder.se	Algorithmic linking of 3D fracture traces based on geometrical and morphological properties
CoumputeC13	N/A	Golder Associates, Inc. 18300 NE Union Hill Road, Suite 200 Redmond, WA 98052 www.fracturedreservoirs.com/	A C++ batch-mode implementation of the Wang C13 conversion factor for $P10 > P_{32}$
PolyTrans 3D	4.3.8	Okino Computer Graphics 3397 American Dr. Unit #1 Mississauga, Ontario L4V 1T8 Canada www.okino.com	Translation of polyface DXF meshes into 3DFace format for use in FracMan

3 Modeling methodology

3.1 Strategy for geological DFN improvement

The methodology for version 2.2 of the Forsmark geological DFN has implemented many of the comments elucidated during past review sessions (INSITE, SR-CAN, SKB and other external reviewers); such is the nature of an evolutionary model. Specifically, the modeling approach in version 2.2 focuses on:

1. Providing a robust fracture network parameterization with estimates of individual parameter uncertainty, with a goal of making the construction of probabilistic scenario models by downstream users easier;

2. A better incorporation of spatial variability and correlation of fracture patterns to geological indicators, such as lithology, alteration, or location. The spatial distribution of fracture areal intensity per volume (P_{32}) has been given special attention based on previous review comments and geology team discussions /Munier 2006/; and

3. Parameterization within the fracture domains defined during preliminary site modeling efforts. The fracture domain concept, defined in /Munier 2004/ and applied in /Olofsson et al. 2007/, is an attempt to reduce DFN model uncertainty by subdividing the SDM volume into regions of geologically unique and homogenous (relative to adjacent domains) rock fracturing.

3.2 Modeling workflow

3.2.1 Fundamental model assumptions and limitations

The model is intended only to be valid for the rock volume described by the boundaries of the target fracture domains (FFM01, FFM02, FFM03, and FFM06), and only for the data on which it was based, as described in Section 2.1. Use of this model outside of these boundaries is not within the scope of this report, and all conclusions and parameters provided in this study should be evaluated for any use outside the described target volume.

The key assumptions required to generate the Forsmark geological DFN, version 2.2, are:

- All data retrieved from SICADA are correct. No systematic checking of data validity from this database was carried out, although if suspicions arose that bad data existed during analyses, those suspicions were checked out;

- The length of a deformation zone trace or a linked fracture in outcrop is an accurate and appropriate measure of a single fracture's trace length for the purpose of deriving the radius distribution of geologic structures.

- The software used is valid for its intended purpose. In some cases, some commercial software (such as Microsoft Excel) has not been formally validated for its intended purpose in this study.

- There is no error in the geological properties assigned to the fractures seen in the BIPS logs. The statistical analyses for development of the spatial model as a function of geological properties assumes that the geological category, for example, rough, is correct, and that the location of the fractures in borehole or outcrop is correct. This assumption does not apply to fracture orientations in boreholes, whose uncertainty has been quantified /Munier and Stigsson 2007/ and is recognized for the purposes of development of the Forsmark geological DFN, version 2.2.

- Only fractures marked VISIBLE IN BIPS are used in the DFN parameterization, due to the uncertainty in the orientations of fractures that are visible in the core but not in the BIPS imagery. In addition, orientation data from boreholes KFM02A and KFM09B has been excluded from the fracture set orientation modeling; these holes possess a total average uncertainty (Ω) greater than 10°. This exclusion is per the recommendations of the orientation uncertainty memorandum and report /Munier and Stigsson 2007/.

- Deformation zones and minor deformation zones constitute a distinct population of fractures from the "background" fractures. As such, the mathematical model for the background fractures is a distinct model from that describing the deformation and minor deformation zones.

- Deformation zones and minor deformation zones identified in boreholes are complete and correct. All fractures assigned to DZ or MDZ are correctly assigned, and all intervals outside of these zones represent background fractures exclusively.

- Fractures can be approximated as planar, circular discs with thickness described as a parameter (aperture), and having radii independent of position. No statements are made regarding the aperture (width) or hydraulic properties of the DFN fractures. While the fractures in the rock are probably neither circular nor planar, there is not sufficient data to mathematically characterize deviations from these two idealizations. In outcrop, the deviations from planarity do not appear to be large. The major impact would be in the trace length computations, as the linked trace length will be equal to or longer than a straight line (or planar surface) connecting the fracture endpoint. The longer trace lengths will tend to promote greater fracture network connectivity and are thus conservative. There are also mechanical reasons to suppose that the actual fracture shapes may tend towards being equant, as the mechanical layering present in sedimentary rocks which promotes non-equant fracture shape is far less well-developed in the crystalline rocks of the Fennoscandian Shield.

- Since existing outcrop data is insufficient for making detailed studies of fracture size throughout the regions of interest, it has been assumed that sizes may vary by sub-area and rock domain, but that within each domain and sub-area, sizes are homogeneous. It is not obvious whether this is a conservative assumption. Resolution will require a much greater amount of outcrop and borehole data.

- Fracture sets can be usefully parameterized based only upon orientation. In developing set definitions from outcrops and boreholes, sets were defined based only on orientation, although the delineation of the sets also relied upon parameters such as length, rock structure, and set termination relationships.

- Both outcrop and borehole data was locally fitted to multiple spherical probability distributions such as the bivariate Fisher or Bingham. However, in many cases, these distributions did not provide significantly better statistical fits to the observed data than the univariate Fisher distribution. A decision was then made, based on the needs of downstream modelers and the ease of model implementation, to parameterize orientation using only univariate Fisher probability distributions.

- DFN model statistical properties will only be valid within their target fracture domains. The spatial analysis results (Section 4.3) suggest that the current fracture domains, as defined in /Olofsson et al. 2007/ are appropriate boundaries for subdivision of the background fracture model. However, some model properties (specifically, fracture intensity and fracture location) may vary spatially or lithologically within a fracture domain and will require either additional subdivision or conditional simulation.

Additional assumptions relevant to specific model components, such as the size or spatial models, are discussed in the relevant sections.

3.2.2 DFN orientation model

The fracture set orientation model was developed primarily from the orientations, geologic properties, and geometric relationships recorded during the mapping of nine outcrop exposures within the Forsmark project domain. Six of the outcrops (AFM000053, AFM000054, AFM001097, AFM001098, AFM100201, and AFM001264) are roughly rectangular in extent; these surface and represent either natural bedrock exposures or areas cleared of overburden during the construction of core drilling pads. The remaining three outcrops (AFM001243, AFM001244, and AFM001265) consist of trench or strip outcrops, constructed across or near mapped, modeled, or potential (based on airborne or ground geophysical surveys) faults and deformation zones. As these outcrops are much longer (10–30 m) than they are wide (2–5 m), there is a risk for orientation and size bias in the fracture data recorded on these outcrops.

Two sets of outcrop fracture data were used; the recorded outcrop fractures as mapped (hereafter referred to as the 'unlinked' data set), and a set of modified traces joined together using a geometric algorithm combined with expert review (hereafter referred to as the 'linked' data set) /Öhman et al. in press/.

The process of linking outcrop fractures together (if possible) is crucial to correctly assessing the fracture radius distribution estimates made from outcrop trace length data. The longer the stochastic DFN fractures are, the more likely they are to intersect in manners that may prove significant to downstream modeling teams (kinematic block failure analysis, fracture network flow and transport calculations, and the acceptance or rejection of specific canister deposition holes). In addition, the linking process addresses a conceptual inconsistency commented on in previous SDMs as to how DZs (linked) and outcrop fractures (unlinked) were treated.

The linking process was performed in a manner similar to the studies completed in Oskarshamn and Forsmark for the DZ model /Triumf 2003, 2004, Johansson and Isaksson 2006, Isaksson 2003/. However, it should be noted that additional data (geophysics) was not used in the outcrop trace linking efforts.

Set definitions were derived from both the linked and unlinked traces; however, the final geological DFN includes orientation (and size) parameterization is based upon the linked trace data set. In addition, fractures identified as being inside of deformation zones (both DZ and MDZ) were excluded from the orientation analyses.

The workflow for the development of the orientation model is as follows:

1. A map for each individual outcrop was created in GIS that contained the fracture trace data, the mapped geology and the 3D topography of the outcrop surface. In addition, orientation and fracture property files for each outcrop were prepared and imported into DIPS for stereographic and qualitative analysis.

2. Tentative fracture sets are identified based on pole clustering in DIPS. Tentative geological association set associations, such as fracture morphology, mineralogy, or host lithology are evaluated through the use of symbolic pole plots in DIPS. Formal statistical analyses of geologic characteristics of fracture sets were performed during the development of the DFN spatial model.

3. The pole cluster boundaries identified in DIPS are utilized to produce a 'first cut' of fracture sets, based on a manual hard-sectoring in ArcGIS.

4. The tentative fracture sets identified in DIPS are further refined through manual analysis in GIS. The objective of the analysis was to develop a model with the fewest sets necessary, but that still did not lump together fractures that appeared to belong to more than one population. In some instances (the NE and ENE sets), the outcrops clearly showed distinct sets that were not obvious in the pole data due to the closeness in mean poles and the overlap of orientations in the data for the two sets. Set membership was determined by similarities in trace orientation, trace length, abutting relationships with other traces or characteristic relation to any underlying rock type or structural element. Set definitions for each outcrop were developed independently for each outcrop.

5. Once set assignment was completed in DIPS, the outcrop fractures were exported to ASCII text orientation files (.ORS) and their orientation probability distributions parameterized using the code FracSys/ISIS for DOS /Dershowitz et al. 1998/. The orientations of fractures in a fracture set are characterized by a mean pole vector (φ, θ) and a set of concentration parameters (κ; κ_1 and κ_2 for bivariate distributions) that describe how the fracture pole vectors cluster around the mean pole. Univariate Fisher, bivariate Fisher, bivariate normal and bivariate Bingham spherical probability distributions were fitted to the sets identified on each outcrop, both for linked AND unlinked traces.

6. Identified outcrop sets were assigned names based on their general strike orientations. The sets were then listed in a matrix and classified into one of two categories:
    a. Global: A fracture orientation set visible in all or nearly all of the mapped outcrops. In the case of the EW and WNW sets, the two sets were combined into a single global set based on their mutual exclusion (any outcrop with the WNW set did not possess the EW set, and vice versa).
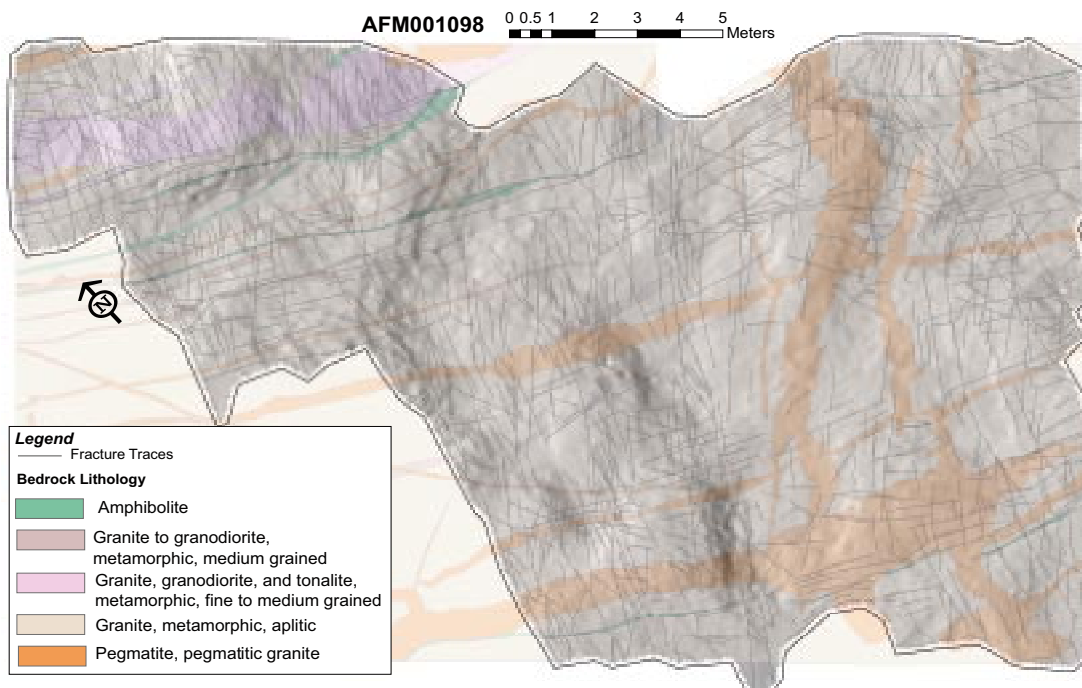
Figure 3-1. *Example fracture outcrop map, illustrating outcrop topography and lithology.*
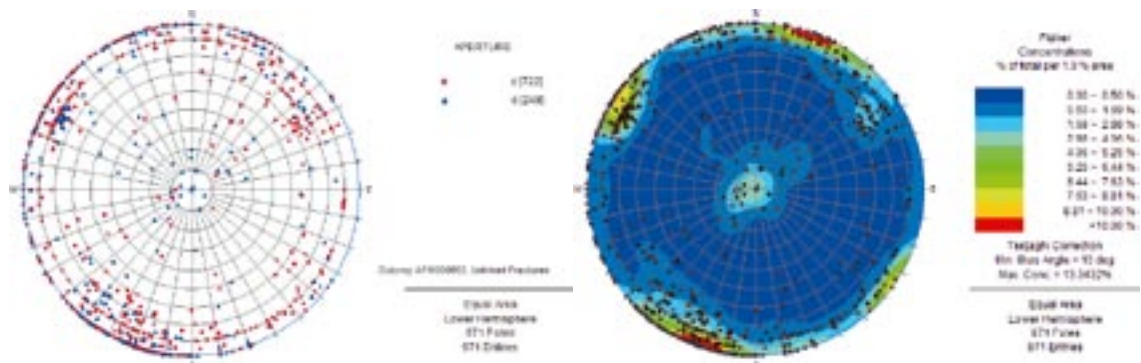
Figure 3-2. *Example symbolic pole and contoured stereo plots. These plots were used to qualitatively gauge whether specific geologic associations were easily visible in the outcrop fracture data.*
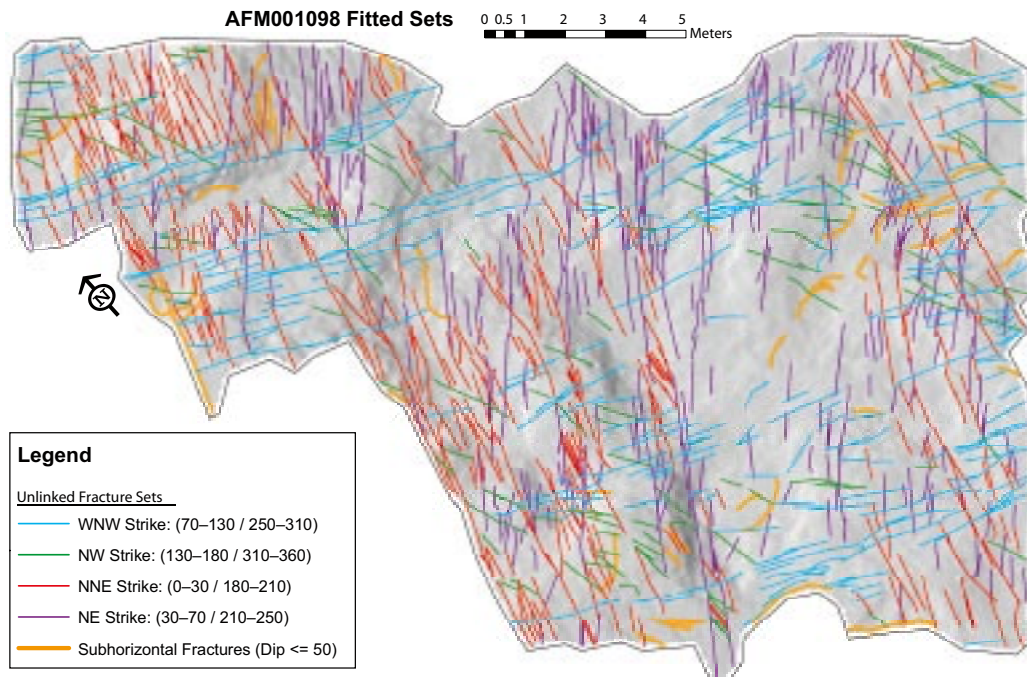
Figure 3-3. *Example of final fitted fracture sets on a detail-mapped outcrop.*

    b. Local: A fracture orientation set visible only in a small subset of the mapped outcrops or boreholes. Local sets may represent variations in local stress conditions or tectonic history that are not applicable across the entire modeling region. A key point is that, in terms of model parameterization, local sets do not exist across the entire modeling volume or domain.

7. The global and local set definitions were then grouped by fracture domain. Note that several outcrops (AFM000054, AFM001097, and AFM001098) are outside of the target fracture domains and candidate model regions. Orientation distributions were fit to these outcrops; however they were not included in the orientation model parameterized inside the mapped fracture domains. The domain groupings were:

    a. Domain FFM01 – No outcrops

    b. Domain FFM02 – Outcrops AFM100201, AFM001264, and AFM001265

    c. Domain FFM03 – Outcrops AFM000053, AFM001243, and AFM001244

    d. Domain FFM06 – No outcrops

8. The outcrop set definitions were then used as guides to assign borehole fractures into discrete sets. Note that, unlike in past geological DFN models, hard-sectored orientations were NOT used to divide the fractures into sets. Rather, the generic outcrop sets (NE, ENE, NW, etc) were used as initial starting points for the orientation modeling. Within every fracture domain, fracture sets were locally defined for each borehole, for multiple types of spherical probability distributions, using ISIS /Dershowitz et al. 1998/. All set assignments utilized Terzaghi-corrected data with a maximum correction value of 5; however, the fractures added to the data set by the Terzaghi correction were deleted after the set assignment was completed.

9. Once fractures were divided into outcrop sets, further subdivisions were then applied. Fractures were additionally classed by fracture domain, presence inside deformation zones, and by presence inside of rock volumes mapped as "Affected by DZ". The orientation analysis was performed separately on fractures labeled 'Affected by DZ' and on fractures labeled "Not Affected by DZ".

A word about borehole intervals labeled 'Affected by DZ'. The "Affected by DZ" label denotes sections of the borehole where the geological modelers have determined that the fracture intensity pattern represents not just background fracturing, but also a tectonic

overprint from a nearby fault or deformation zone. Including fractures from these zones in calculating fracture orientations, sizes, or intensity, creates a risk of introducing bias into the DFN parameterization. As such, where necessary, fractures in zones labeled "Affected by DZ" are treated separately.

10. Fitted orientation distributions for each fracture set in each fracture domain for borehole and outcrop data were compiled into a single data set. Only the univariate Fisher distribution fits were included in this data set.

11. The final orientation model for each fracture set consists of:

    a. A mean pole (φ, θ) of all the mean poles of the data points fitted for a single domain. For example, the mean pole orientation for the NE fracture set in domain FFM02 was calculated by placing the fitted mean poles for the NE sets for both borehole AND outcrop data into FracSys/ISIS, and then calculating the mean pole of the aggregated mean poles.;

    b. A univariate Fisher concentration parameter representing the potential variation in the mean pole location (κ_{mp}). This value is calculated when the orientation of the mean pole of all the fitted sets is assigned. The κ_{mp} value should only be used if, for a given set (NE, NW, etc), the modeler wishes to simulate a variable set mean pole (i.e. a set where the average orientation varies spatially according to a univariate Fisher distribution) instead of a single fixed mean pole value, and;

    c. An average value for the Fisher concentration parameter (κ). The average concentration parameter is calculated by computing the mean value of the individual κ-values for all set fits. For example, for the NE set in Domain FFM02, each borehole and each outcrop has its own univariate Fisher distribution fit. The κ-values from each of these individual fits are aggregated and the mean value is calculated.

12. An approximate 95% confidence interval of the mean pole of the mean poles was calculated for all sets in all fracture domains, using the following approximation /Fisher et al. 1987/ for the univariate Fisher distribution:

$$\delta_{95} \approx 140 \big/ \sqrt{\kappa n} \qquad\qquad \text{Equation 3-1}$$

where κ represents the arithmetic mean concentration parameter, and n the number of observations. The confidence interval approximation assumes a Fisher $\kappa > 7$, a circular confidence interval (rather than the elliptical formulation more commonly used), and $\alpha = 0.05$.

In addition, the radius of the 95% percentile cone (the radius at which the pole vector of a fracture belonging to that set has a 95% probability of falling inside) for the fitted Fisher distribution was also computed using Equation 3-2.

$$\alpha_{95} = \left(\frac{180°}{\pi}\right) \arccos\left(1 - \left(\left(\frac{N-R}{R}\right)\left(\left(\frac{1}{p}\right)^{\frac{1}{N-1}} - 1\right)\right)\right) \qquad \text{Equation 3-2}$$

where $p = 0.05$ and R is the length of the mean dip vector (resultant) found from the direction cosines for each axial direction.

13. For a given set in a given fracture domain, variation in the Fisher concentration parameter (κ) was documented using standard 'box-and-whisker' plots /NIST 2007a/. Figure 3-4 presents an example box-and-whisker plot. Obvious data outliers were then removed from the data set, and the remaining set of κ-values was tested for normality using the parametric Shapiro-Wilk W test /NIST 2007b/, assuming $\alpha = 0.05$. The Shapiro-Wilk W test does not prove that the test samples are from a normal distribution; rather, it tests for departures from normality. Where the distribution of κ is found to differ from normal, we recommend using the set median κ value, rather than the mean value of κ. All statistics were computed using the Microsoft Excel add-in Analyze-It (see Section 2.2). Only sets with more than three fitted mean poles were evaluated for normality, as per the design of the Shapiro-Wilk W test.
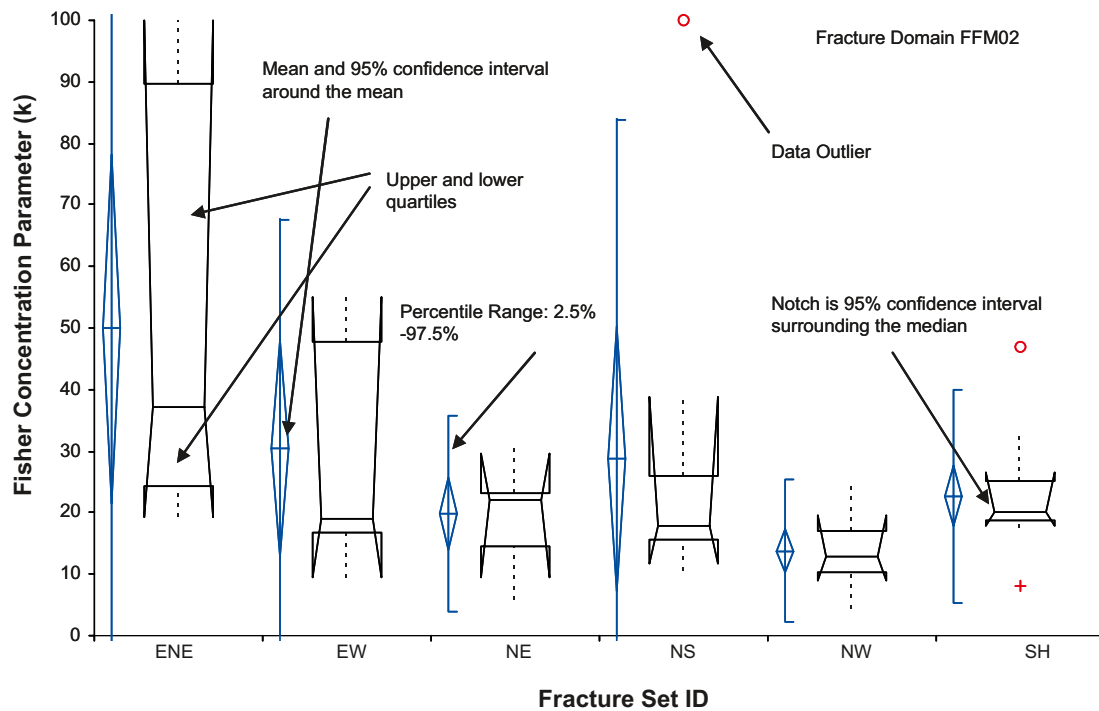
Figure 3-4. *Example 'box and whisker' plot with annotations.*

Discussion: Global versus local fracture sets

The Forsmark version 2.2 Geological DFN describes two different types of orientation sets; Global sets and Local sets. The distinction between the two types of sets was described above (6a,b). However, additional statistical testing was performed using SPSS to determine if there were differences other than orientation between the two types of sets. Specifically, the goal was to determine if the local sets were limited to a specific lithology or combination of geologic factors that could be used as predictor variables. If a key factor was found, it would be possible to constrain the locations of the local sets in the spatial model.

In addition, it was necessary to test whether fracture orientations were different in zones labeled 'Affected by DZ'. As the geological DFN parameterization is fundamentally based on orientation sets, inconsistency between 'Affected by DZ' and 'Not Affected by DZ' could add additional uncertainty into the model.

The methodology for testing the effect of 'Affected by DZ' versus 'Not Affected by DZ' on fracture orientations is as follows:

1. For all mean poles, for a given set and fracture domain, that are not listed as 'Affected by DZ' compute the orientation of the mean pole of the population of mean poles, and the Fisher concentration parameter, κ_{mp}.

2. Compute the 95% confidence interval surrounding the set mean pole using Equation 3-1, for all sections NOT affected by DZ in a given fracture domain, for a given fracture set.

3. Compute the 95% confidence cone of the Fisher distribution using Equation 3-2, for all sections NOT affected by DZ in a given fracture domain, for a given fracture set.

4. If, for a given fracture set in a given fracture domain, the fitted mean pole for a set of fractures labeled 'Affected by DZ' falls within the 95% confidence interval of the mean for the population of fractures labeled 'Not Affected by DZ', we conclude that there is no statistically difference between the two populations, and that the data can be combined

25

5. If, for a given fracture set in a given fracture domain, the fitted mean pole for a set of fractures labeled 'Affected by DZ' falls outside the 95% confidence interval of the mean for the population of fractures labeled 'Not Affected by DZ', then we check to see if the 'Affected by DZ' mean pole falls within the 95% confidence cone for the Fisher distribution. If the mean pole is inside the radius of the 95% confidence cone, we conclude that, though not identical to the fractures not affected by deformation zones, the variation in the orientation of the set mean pole of 'Affected by DZ' fractures can be simulated using a univariate Fisher distribution.

6. The final Forsmark 2.2 geologic DFN parameterization makes the additional assumption that if either 4) or 5) are true, then it is appropriate to lump all fractures (both 'Affected by DZ' and 'Not Affected by DZ") into a single population for orientation set parameterization. The increased uncertainty is offset by a smaller Fisher concentration parameter (κ_{mp}) for use in stochastic simulation of variable mean pole vectors for a single orientation set.

7. If the fitted mean pole for a population of fractures labeled 'Affected by DZ' falls outside both the 95% confidence interval of the mean, and the 95% confidence cone of the univariate Fisher distribution, then we conclude that it represents a separate orientation set, and must be treated as a new orientation set for that fracture domain

The results of the global set versus local set analysis are presented in Chapter 4.1.3.

3.2.3 DFN size model

The size model refers to a mathematical description of the area of the fractures. Previous analyses /La Pointe et al. 2005/ performed during SDM Forsmark version 1.2 indicated that different fracture sets are likely to require different (and potentially unique) size models. Also, since fracture domains have been identified that are distinguished from one another by geology and degree of tectonic deformation, it is reasonable to presume that the size model for the fractures differs by fracture domain. Therefore, as a point of departure for the analysis of the size model, models were developed for individual sets within single fracture domains. Whether or not the size models could be combined for certain sets or fracture domains was later evaluated based on the models for each set and domain.

The approach to fitting a size model for domains FFM02 and FFM03 differs from that used for FFM01 and FFM06, because there is no outcrop trace data for domains FFM01 and FFM06.

Linking of outcrop traces

The trace data provide indispensable information for the parameterization of fracture size distribution in DFN modeling. The past DFN models for Forsmark assumed a Poissonian spatial distribution of fractures /La Pointe et al. 2005/. However, some specific trace data reveal spatial patterns which deviate from the Poissonian assumption. One such particular spatial pattern may be described as "sequentially located traces (i.e., closely located trace endpoints) with similar orientations" (Figure 3-5a). It is possible that such fractures may form a well-connected structure below the ground surface (Figure 3-5b), even though the traces are not actually connected in the outcrop surface.

Failure to represent this type of possibly connected structures in fracture network modeling may have severe implications on downstream modeling of different processes; e.g., underestimate the risk of planes of failure or connectivity along flow paths (Figure 3-5c). The goal of the linking efforts were to provide a more reasonable definition of fractures at the outcrop scale, where the length of the surface traces directly affects the final size model parameterization in the geological DFN. This is also consistent with the procedure used in lineament interpretation.
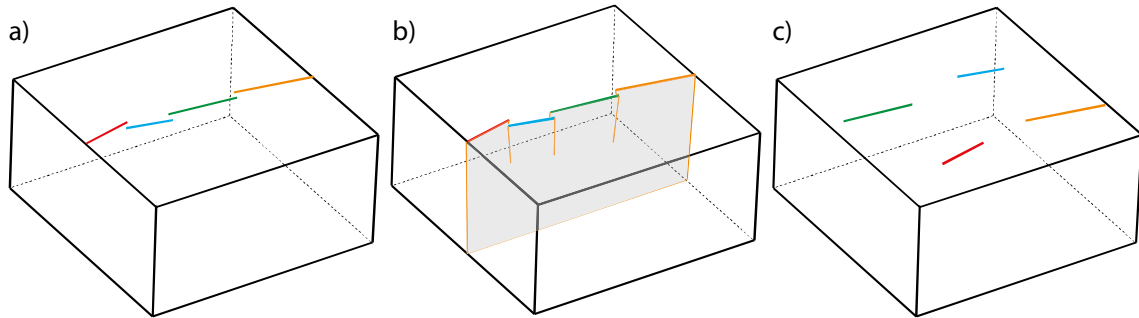
Figure 3-5. *Conceptual figure: a) a hypothetical set of sequentially located traces with similar orientations observed in the field, b) possible underground connectivity of fracture planes, with implications for downstream modeling, e.g., hydrological or rock-mechanical properties of the fracture system, and c) illustration of the error resulting from failure to represent this spatial aspect in DFN modeling.*

The general approach taken to link traces in the Forsmark outcrops was to divide the problem into two steps. In the first step a computer code (GoLink) is used to link traces strictly based on geometrical criteria. In the second step, the results of the previous step are reviewed in a geologic context by expert judgment, and the results are refined based on this evaluation.

The benefits of the numerical algorithm are:

- Efficiency: the trace data set is large and time consuming to interpret; it also facilitates consideration of three-dimensional fracture orientations, which is difficult to asses in a trace map.

- Consistency: as the data set is large, it is difficult to perform a manual linking consistently for all outcrops, for example, to ensure that no links have been overlooked.

The draw-back of the numerical algorithm is the lack of geologic context; it is impossible to include all structural geologic aspects which are essential to avoid unrealistic links.

The GoLink numerical algorithm used the following geometric criteria to determine if two traces from the detailed outcrop mapping results should be linked:

1. The minimum separation distance between the endpoints of two candidate traces must not exceed a specified threshold value, r_{max} (in meters).

2. The difference in orientations of two candidate traces must not exceed a specified maximum polar angle, θ_{max}.

3. The linking must propagate in one general direction.

4. No links are made between traces that are separated by a trace showing shear offset.

Once the results of the GoLink process were integrated into GIS, an expert review of the linked traces was performed. The goal of the expert review was to assess the difference between what a trained field geologist would link to what a fully algorithmic approach would link.

As previously discussed, the advantage of using an algorithm to link traces is repeatability. The process is transparent, repeatable, and largely free of observer-induced bias. It is entirely possible that three different geologists, mapping the same outcrop, would come up with three different sets of linked traces, based on their judgment of the conditions and relationships observed. A computer program has the potential to eliminate this observer bias.

However, an algorithm-based approach, unless expertly programmed and very comprehensive (such as a well-trained probabilistic neural net), cannot match the human brain when it comes to combining optical pattern analysis with experiences from past work at other field sites.

Table 3-1. Demonstration of criteria used in the linking of trace data.

Criterion 1: maximum gap between trace endpoints $< r_{max}$
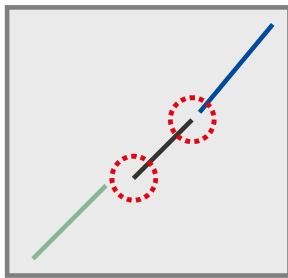
The green trace is not linked to the black trace, as the gap exceeds r_{max} (i.e. neither of its termination points are located within the distance rmax of either termination points of the black trace; r_{max} is shown by red circles).

The blue trace is linked to the black trace, as the gap between their endpoints is less than r_{max}.

Criterion 2: fractures must be "semi-parallel"
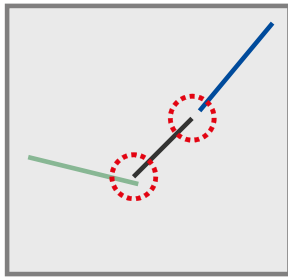
The green trace is not linked to the black trace, as the orientation of their poles deviates more than θ_{max}.

The blue trace is linked to the black trace, as their fracture-plane poles are of similar orientation (e.g. the deviation angle $< \theta_{max}$).

Criterion 3: trace linking must propagate in one general direction
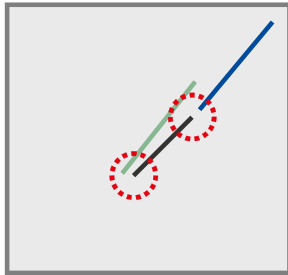
The green trace is not linked to the black trace, although it fulfills the conditions on maximum gap and "semi-parallelity" (see above). Links in the "reverse direction" are avoided by requiring that the distance between endpoints of the linked trace must always increase in every linking step.

Criterion 4: traces separated by shear fractures are not linked
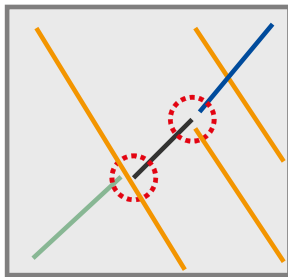
The green trace is not linked to the black trace, as the gap is intersected by a fracture that has signs of shear movement (sheared traces shown as orange lines).

The blue trace is linked to the black trace, as:
1) the gap (= distance between endpoints) is not strictly intersected by any shear fracture, and
2) although the blue trace is intersected by a sheared fracture, the trace has been mapped as "intact" in the field.

In particular, a trained professional is much better at looking at the 'big pictures; the relationship of the trace not only to other traces, but to the outcrop as a whole.

A wide variety of parameters were investigated during the expert review to determine whether two traces should be linked together. Of particular importance were the following characteristics:

1. Do the traces cross or end at or near a lithologic boundary? What is the relationship between the trace and the outcrop geology?

2. Do the traces bend near a shear structures, or do they show clean shear offset?

3. Do the traces terminate against other traces? What are the termination relationships

4. Do groups of traces appear to represent a larger-scale single feature? For example, closely-spaced parallel traces with identical orientations and morphologies may represent the results of a single fracture propagating towards a free surface.

It should be noted that the GoLink process, like many computer algorithms, is not perfect. The expert analysis noted that GoLink had problems linking the correct traces in the following specific cases:

- When there are several small traces, all of which strike in the same direction at roughly the same dip. The algorithm picks the trace closest to the endpoint of the currently-selected analysis trace. This may not necessarily be the correct trace; the results may be stereologically correct but appear visually inadequate to the trained eye.

- When there are complex geologic structures. GoLink is designed to include a search neighborhood around each fracture, specifically to search for parallel structures that might represent larger-scale features (minor deformation zones). However, this functionality was not used during the linking efforts. The result was that GoLink performed poorly at linking structures with any width (i.e. 2–3 parallel, closely spaced joints that represent the possible interaction of a single fracture near a free surface).

- Linking across sheared structures. GoLink has been programmed not to link structures across a shear boundary. In cases like this, geometry alone is not sufficient to match up traces, and human input is required.

- Linking very long (> 10 m) traces.

The end result of the linking process was a set of GIS files containing the linked fracture traces for each detail-mapped outcrop at Forsmark, along with a modified attribute table listing the orientations, sizes, and SICADA identification numbers of the smaller traces used to create the new linked fractures.

The orientation of a linked trace was estimated from the orientations of its individual trace components. The resultant-vector method was used for this calculation, and the relative contribution from each trace component was weighed by its trace length. The reason for weighing orientations by trace length was that larger trace exposures to the surface are assumed to be more representative of the structure that is formed in the linking procedure.

The orientation of each component fracture, i, can be characterized by its fracture pole $\mathbf{n}_i$ (a unit-length vector normal to the fracture plane). This fracture pole is defined by its three vector co-ordinates so that $[\mathbf{n}_i] = [n_{ix}, n_{iy}, n_{iz}]$. The maximum resultant vector V, for a given set of N trace components, is calculated to estimate the mean pole orientation of the linked structure using the following relationship:

$$\mathbf{V} = \sum_{i=1}^{N} w_i \mathbf{n}_i$$

where w_i is the weigh of each fracture component i, and is set equal to its trace length in meters. It should be noted it is possible to calculate two fracture poles with opposite directions from a fracture plane. Which one of these fracture-pole directions are used to define fracture orientation is generally irrelevant. However, in the calculation of the resultant vector, each fracture-pole direction must be chosen so as to maximize the resultant vector length (i.e., the fracture poles must have the same general direction). Otherwise, the resultant vector will not reflect the overall orientation of the fracture components.

For more information on the trace linking project at Forsmark and Laxemar, please see the method-specific project memorandum by /Öhman and Hermanson 2007/.

Domains FFM02 and FFM03

The methodology for quantifying a fracture size distribution for a fracture set in either of these two domains involves fitting a scalar probability distribution based on r (the radius, in meters, of a disc-shaped equivalent-area fracture) to fracture trace length data observed in outcrop data, derived from lineament interpretations of regional and local geophysical anomalies, and the lengths of the intercepts of the mid-planes of the Forsmark version 2.2 DZ structures.

For both size model alternatives (Tectonic Continuum or Outcrop Scale + Tectonic Fault), the fracture intensity is coupled to the size model. Whether the model is a power law or follows a lognormal or other probability distribution type, the match to the trace lengths is a non-unique combination of minimum fracture size and intensity. Different combinations of minimum size and intensity will match the trace length data, assuming that other parameters (such as the radius exponent for the Pareto distribution) are held constant. As a consequence, the first step in defining the size model parameterization was to assume a minimum size, expressed as fracture radius, of 0.5 m, and to determine the value of P_{32} that matched the measured outcrop and/or lineament trace length data.

The second step in the parameterization was to adjust this model so that it matches the mean borehole fracture intensity. The mean intensity is quantified by calculating the P_{32} that corresponds to the P_{10} in all boreholes within the fracture domain, outside of deformation zones, and not classified as 'affected by DZ'. This mean P_{32} may be higher or lower than the P_{32} that was determined for the arbitrary 0.5 m minimum size. If the borehole P_{32} is greater than the 0.5 m minimum size P_{32} calculated from outcrop trace data, the minimum size (r_0 for power-law distributions) is reduced and P_{32} increased so that it still fits the trace data. Alternatively, if the borehole P_{32} is less than the 0.5 m minimum size P_{32}, then the minimum size is increased and P_{32} decreased so that it still fits the trace data. For a Pareto (power law) distribution, this can be done analytically using Equation 3-10 and verified through simulation. For other types of distributions, this can be approximated using First Order, Second Moment (FOSM) techniques and then verified through simulation. The final result matches the measured distribution of trace lengths in outcrop and/or lineaments, and also the mean fracture intensity measured in boreholes outside of deformation zones.

The geological DFN size model does not assume a fracture shape. Modeling teams are free to choose alternative shape and elongation models, provided that the resulting fractures obey areal equivalence with respect to the chosen size and intensity models. The tectonic continuum size analyses, the global scaling model, the spatial location model, the orientation model, and the intensity models make no assumptions regarding fracture shape. However, the primary outcrop trace size analysis (FracSize) of fitting a size distribution to two-dimension traces does assume circular disk fractures; traces are assumed to be random chords /Dershowitz et al. 1998/. All DFN simulations for model parameterization and validation assumed four-sized square fractures.

Domains FFM01 and FFM06

Fracture domains FFM01 and FFM06 do not have any outcrop trace data to support the parameterization of the fracture size models in these domains. As a result, the procedures used to fit the models in FFM02 and FFM03 do not strictly apply. In order to parameterize sets in these domains, the following additional assumptions were made:

1. FFM02 is more likely to be an analogue for FFM01 and FFM06 than FFM03. This is because FFM03 represents a much more highly deformed tectonic domain in the hanging wall of the large site-scale gently dipping deformation zones (ZFMA3, ZFMA4, ZFMA7, etc).

2. The form of the distribution (power law, lognormal, etc) found to characterize a particular set in FFM02 is the appropriate model for that set in FFM01 and FFM06. Thus, if a power law model was used to characterize sizes of the NE set in FFM02, a power law model is used to parameterize the NE set in FFM01 and FFM06.

3. If the P_{32} match point previously determined for the FFM02 domain for a particular set is less than the P_{32} determined from the borehole data outside of deformation zones, then the minimum size is reduced until a match is made. Likewise, if the P_{32} for the FFM02 model is greater than the P_{32} measured from the borehole data, the minimum size is increased. If the borehole P_{32} cannot be matched even with a very small minimum size, or if the minimum size is so large that only very few large traces in a typical outcrop, this is an indication

that the distribution type or its other parameters in FFM02 are not adequate to describe the particular fracture set in the domain. In this case, the other parameters (the slope, in the case of a Power Law distribution; the mean in the case of other distributions) can be altered to achieve a match.

4. Size-intensity coupling (i.e. a direct correlation between fracture radius and intensity) is not mandatory in domains FFM01 and FFM06; sufficient data does not exist to uniquely parameterize the relationship or to confirm its boundaries. As such, the two alternative conceptual models treat the size-intensity couple differently in FFM01 and FFM06. Treating the two model alternatives using different methodologies allows us to bracket the potential ranges of parameters. The assumptions are as follows:

   a. The Tectonic Continuum models assume that FFM01 and FFM06 obey the same size-intensity coupling relationships. This means that the radius exponent and the minimum size fit to trace data (the P_{32} based on surface outcrops) used are the values from FFM02. The minimum radius is then changed to match the borehole intensity data in FFM01/06 to the outcrop fracture data in FFM02. Geologically, this assumption states that we believe the mechanics and rheology of FFM01 and FFM06 are similar to FFM02, and that the intensity difference between the domains is largely due to an abundance or absence of fractures of a certain size.

   b. The Outcrop Scale Model does not require a size-intensity couple. The model assumes that the fractures in FFM01 and FFM06 follow the same radius exponent (k_r) as FFM02, but that the absolute minimum radius is equal to that of the borehole. Given that the SICADA borehole data set only records fractures that completely cut across the entire core, the smallest fracture recorded in the database should be a circular disc, with a radius equal to that of the borehole (0.0385 m, assuming a borehole diameter of 77 mm), oriented perpendicular to the core axis. The OSM model assumes a minimum radius of 0.0385 m and that the intensity (P_{32}) recorded in the borehole data represents 'truth'. The minimum size of 0.0385 m (the radius of a 77 mm diameter cored borehole) is used, rather than the radius of the core (56 mm diameter core), because we are basing the statistics on fractures 'Visible in BIPS' (i.e. those that cut across the entire diameter of the finished drill hole.

The end result is that, for domains FFM01 and FFM06, the two alternative size models describe different potential size ranges. The TCM model implies that there are fewer overall fractures in FFM01 and FFM06, relative to FFM02, but that they are larger. The OSM model implies that there are more small fractures in FFM01 and FFM06 than FFM02, as well as fewer fractures overall. Together, the models cover a wide range of parameter space.

Clearly, the size model parameterization of the fracture sets in FFM01 and FFM06 are more uncertain than in FFM02 and FFM03, largely due to the lack of trace length or other size data from these domains.

Conceptual uncertainties in the DFN size models

The development of the size model needs to consider several conceptual uncertainties. These conceptual uncertainties that influence the workflow are:

- The 'Tectonic Continuum' hypothesis;

- Fracture trace linkage;

- Whether fractal or Euclidean scaling behavior better characterizes how fracture intensity scales from the scale of meters to the scale of kilometers; and

- Whether the ground magnetic lineaments realistically represent fracture trace length and intensity.

Other uncertainties that do not influence the workflow but can affect the model results are discussed in Chapter 5.

A key assumption for the version 2.2 geological DFN is that DZ and MDZs in boreholes and outcrops are a distinct population of geologic structures, and are not part of the "background" population of fractures in boreholes and outcrop. As such, they are excluded in the parameterization of the stochastic DFN model. However, the tectonic continuum hypothesis presumes that the lineaments related to large-scale deformation zones and magnetic lineaments are the larger size fraction of each regional fracture set. Thus, the deformation zones encountered in boreholes or outcrops belong to respective fracture populations as much as any of the joints encountered in the boreholes or outcrops. The geological modeling for Forsmark 2.2, defined in /Olofsson et al. 2007/, required the exclusion and separate treatment of DZ, mapped MDZ, and Affected by DZ zones in the cored borehole arrays from the parameterization of the Tectonic Continuum Model (TCM). As a result, the tectonic continuum model has increased uncertainty due to the decision to exclude this data from its parametrization.

Another model was developed that does not have this inconsistency. It presumes that the tectonic continuum does not exist, and that the fractures represented by large-scale tectonic lineaments and ground magnetic lineaments manifest themselves in boreholes as DZs and MDs, while joints and smaller-scale re-activated joints constitute the background fracture population. This alternative model consists of the Outcrop Scale Model (OSM) as one component, and the Tectonic Fault Model (TFM) as another component. The combined OSM+TFM alternative size model assumes that the outcrop traces constitute one group of fractures (primarily joints, or joints re-activated as faults but still represented as single surfaces), while the ground magnetic lineaments and the large deformation zones constitute another population (predominantly faults that have zones of secondary fracturing that is sufficiently wide such that a single surface is an inadequate representation).

Fracture trace linkage /Öhman et al. *in press*/ alters the size and number of fractures tabulated from outcrop trace data, and as such, impacts the size model for all hypotheses. Therefore, statistics for both linked and unlinked traces need to be produced and applied to all models. However, the linked models for size, orientation, and outcrop intensities are the ones that are carried through the DFN parameterization.

The scaling behavior uncertainty only impacts size models calculated when the tectonic continuum hypothesis is accepted, because it impacts the area renormalization that is part of the cumulative number vs. trace scaling plots. Scaling considerations do not play a role in the Outcrop Scale size model. Thus the workflow should examine the tectonic continuum hypothesis under all scaling models that are applicable.

Outcrop scale size model (OSM)

The Outcrop Scale Size Model (OSM) is a size-model alternative based solely on matching the sizes and intensities of fractures recorded as outcrop traces to the intensities in borehole data. Fundamentally, it treats fracture traces exposed in outcrop as joints. The OSM is *not* a complete parameterization by itself; it is necessary to also include the Tectonic Fault Model (TFM) to have a complete parameterization across the desired size range for the Forsmark 2.2 Geological DFN (0.5–564 m).

The size model for each fracture set in the Outcrop Scale was produced through an analysis of linked and unlinked trace lengths, as mapped on eight of the nine Forsmark surface outcrops. Outcrop AFM001265, due to its very small size, large censoring, and high potential for bias, was omitted from the size analysis. The size analysis, performed using FracSys/FracSize for DOS /Dershowitz et al. 1998/, centers around stochastically producing a fracture radius probability distribution that, when sampled using a trace plane equivalent to that of the mapped outcrop, will produce similar trace length probability distributions.

Trace planes were created using ArcGIS by calculating the surface normal to a hypothetical 'best-fit' planar surface visually aligned to major outcrop features. A rectangular polygon was then constructed with an orientation parallel to that of the outcrop, with a size just large enough

to enclose the mapped outcrop perimeter. The corner coordinates were exported as a text file, and converted to a FracMan sampling structure (*.SAB) control file using SamEdit.

Next, a probability distribution type was selected for the fracture radius probability density function. A synthetic fracture set composed of discs with an initial "guess" of mean and standard deviation (or other appropriate parameters) was generated and intersected with a plane representing the outcrop surface. The synthetic fracture set assumes the 'best fit' univariate Fisher distribution for a particular fracture set at a particular outcrop; for example, the local size model for the global NE Set on outcrop AFM000053 uses the univariate Fisher mean poles and concentration parameter (κ) for the NE set on that outcrop.

The trace plane intersection produced a set of trace lengths that can be compared with the measured trace lengths. All synthetic fracture sets were generated using the full outcrop trace plane area (which is slightly larger than the dimensions of the outcrop to prevent edge effects). As the outcrop mapping protocol /Danielsson et al. 2006/ avoided mapping fractures with a trace length smaller than 0.5 m, traces less than 0.5 m were eliminated from the simulation. These calculations were carried out on both linked and unlinked outcrop trace data.

Through a Simulated Annealing optimization routine /Press et al. 1992/, values of the mean and standard deviation were iterated until a statistically significant match was achieved. This process was repeated for several probability distribution functions, including lognormal, power law (Pareto), normal, and exponential. The optimization process was performed so as to minimize the Kolmogorov-Smirnov (K-S) statistic, which is based on the single worst match in the cumulative probability distribution. Optimization through K-S minimization produces size distribution matches that minimize the maximum difference between the actual and theoretical cumulative probability distribution /Dershowitz et al. 1998/.

The χ^2 and K-S tests have probability values associated with them that indicate the statistical significance of the test results. Probabilities less than 0.05 or 5% indicate that the observed test results, which are the values of the calculated χ^2 and K-S test values, are unlikely if indeed the tested model and its assumed parameters are true. Thus, if the probability is greater than 0.05 or 5%, the test does not lead to the rejection of the hypothesis that the mode tested is a statistically significant representation of the trace length data. The higher the probability, the more representative the observed trace data is of the selected probability model.

In the case where a statistically-significant match between outcrop and simulated data was not reached at $\alpha = 0.05$, the 'closest match', based on the general shape of the cumulative density function (CDF) and both the K-S and Chi-squared test statistics, was chosen. The local size fits were computed for both linked and unlinked fracture traces.

Once individual fracture set size distributions were calculated for every outcrop, the results were classified into fracture domains for parameterization. The division is as follows:

- Domain FFM01/FFM06: Assumed to have same size population as FFM02
- Domain FFM02: AFM001264, AFM100201
- Domain FFM03: AFM000053, AFM001243, AFM001244

Outcrop AFM001097, which was located atop a deformation zone inside fracture domain FFM04, and Outcrop AFM001098, which is located inside fracture domain FFM05, were not used in the model parameterization. Outcrop AFM000053 was judged to be 'close enough' to domain FFM03 to be used. This decision was based on the geometry of domain FFM03, which is modeled as a domain of rock bounded vertically by a series of southeast-dipping sub-horizontal structures. FFM03 exists in the hanging wall of these structures, which thickens to the south. Figure 1-3 illustrates this relationship. Given the geometry of the domains and the similarity of the lithologies exposed in AFM000053 to the lithologies exposed in boreholes drilled into FFM03, we feel it is a reasonable assumption to include AFM000053 in FFM03.

However, we were unable to determine if outcrop AFM000054 was also representative of FFM03. The outcrop was located a significant distance away from the edge of the Forsmark 2.2 local model region, within which the fracture domains were assigned. There was only limited borehole coverage in the area as well, which made it difficult to determine if AFM000054 was representative of domain FFM03 rock. As such, it too was omitted from the size model parameterization. Finally, outcrop AFM001265 was found to be too highly censored and biased in terms of sets (it is oriented such that it likely over-sampled the NE global set), and was omitted from the size analysis. Only the linked fracture data set was carried forward from the exploratory data analysis phase to the size model parameterization phase.

In addition to stochastic size simulation through FracSize, the fracture size distribution parameters were also determined using the same trace-length scaling methodology as the tectonic continuum models. This process assumed a power-law size distribution; however, the FracSize results generally suggested that all sets could be adequately fitted using power-law distributions. The scaling exponent (k_t) was fit only to outcrop data; no area renormalization or combination with ground magnetic lineaments or deformation zones was performed. The reader is encouraged to read the next subchapter, which describes the trace-length scaling analysis process in great detail.

The final Outcrop Scale Model utilized the radius exponents estimated from trace-length scaling plots. For most samples, the FracSize solutions resulted in adequate fits to shorter (< 2 m) traces, which make up the majority of the outcrop data recorded. However, the FracSize solutions generally over-estimated the intensity of larger (> 5 m) fractures relative to outcrop data; this is a highly censored data set, to be sure, but the over-estimate made it very difficult to simultaneously fit outcrop and borehole data within a fracture domain.

As such, the FracSize fits were used primarily to determine if differences between sets and domains existed, and to determine if a given set in a fracture domain could be simulated assuming a Pareto (power law) distribution. The final OSM size model parameterizations, however, are based on the radius exponent (k_r) calculated through trace length scaling analysis, not FracSize.

For each fracture set on each outcrop within each domain, exploratory statistics such as the sample mean, sample median, sample quartiles, and 'box and whisker' plot (Figure 3-4) were computed. A key question arising during the size model parameterization was whether or not, for a given fracture set in a single domain, trace lengths observed on different outcrops represented different random samples from a single parent population. The non-parametric Kruskal-Wallis 1-way analysis of variance (ANOVA) test, as implemented in the Excel add-on Analyze-It, was used to evaluate this hypothesis. The Kruskal-Wallis procedure evaluates the null hypothesis that a number of samples from potentially different populations actually origi-nate from similar populations, based on the similarities of the sample medians, are concerned /NIST 2007c/.

If the Kruskal-Wallis test at $\alpha = 0.05$ indicated that it was impossible to reject the null hypothesis that, for a given set in a given domain, the samples came from the same population, the traces were combined into a single file, the FracSize analysis re-run, and the size model parameterization based on the combined data set. If it was possible to reject the null hypothesis, a decision was made based on other factors (potential censoring, outcrop area) as to which size alternative to use.

This fitting procedure does not assume a minimum fracture size. The next step is to assume a minimum size of 0.5 m and through analytical equation or OFSM procedure, estimate the P_{32} that would correspond to that minimum size and verify the result through simulation. If the simulation verifies that the 0.5 m minimum size and prescribed distribution still match the trace lengths, then the next step is to compare the P_{32} to the mean borehole P_{32}.

The mean borehole P_{32} is calculated by selecting only those intervals of boreholes that are outside of the deformation zones. The P_{10} was calculated over intervals of 6 m, 15 m and 30 m. The P_{32} for each P_{10} interval is calculated through Wang's formula (described below in the Intensity section). Any interval containing a section designated as being part of a deformation zone (DZ or MDZ) or "Affected by DZ" was excluded.

In other words, for an example section of four consecutive 6 m intervals containing:

• a first not part of any DZ, MDZ or "Affected by DZ" section, with a P_{32} of 5.0,

• a second interval with the ending 2 m of the section labeled "Affected By DZ",

• a third 6 m interval outside of all deformations zones, with a P_{32} of 6.0,

• and a fourth 6 m interval entirely inside a zone labeled 'Affected by DZ';

the second and fourth intervals would be entirely excluded. The mean for the four 6 m sections of boreholes would be reported as 5.5, and would be relevant to a length of 12 m.

The Forsmark geological DFN Outcrop Scale size model presents one probability distribution per fracture set per fracture domain. However, distribution fits for individual outcrops within a fracture domain from FracSize have also been provided so that downstream modelers have a published basis for evaluating other local size alternatives if they so wish, as part of their specific model uncertainty and sensitivity analyses. The Pareto (power-law) distributions fitted by area-normalized trace length scaling plots are the preferred model, however.

A key feature of the Outcrop Scale size model is that it was built entirely upon the trace length distribution exposed on mapped outcrops; deformation zone traces or regional lineaments were not used in the Outcrop Scale data analysis or parameterization.

Tectonic fault size model (TFM)

The Tectonic Fault Model (TFM) is an alternative size model designed to be used in conjunction with the Outcrop Scale size model. The TFM model is fit to the lengths and intensities (P_{21}) of the deformation zone traces inside the Regional and Local model volumes, and to the new high-resolution ground magnetic lineaments inside the candidate region. The fundamental hypothesis is that these structures represent faults, rather than joints. Unlike the Outcrop Scale models, the P_{32} values estimated for TFM sets are based solely on fits to P_{21} from outcrop map data; as it is impossible to assign orientation distributions to the MDZ and ground magnetic lineaments, no P_{10} data from boreholes is available for use in parameterization. The P_{10} of MDZ, however, is used in a validation exercise (see Chapter 6) of the Tectonic Fault Model.

The TFM model includes only Global orientation sets (Chapter 3.2.2); none of the local sets parameterized in the orientation model were found in the ground magnetic lineaments or the deformation zone traces. We also assume that the TFM only covers a portion of the scale of the geological DFN model; the TFM uses an r_{min} value of 28 m, which is the radius of a fracture that will most likely produce a trace length of 50 m (assuming a random chord through a circular disk fracture). Like the OSM, the TFM is valid up to a maximum size (r_{max}) of 564 m (the radius of a fracture that will most likely produce a trace length of 1,000 m, the cut-off for the DZ model). Fundamentally this means that the TFM model assumes all structures mapped as faults or deformation zones are larger than 28 m.

The steps to parameterize the TFM model are identical to the steps taken to parameterize the Tectonic Continuum models described below, with the exception that the intensity/minimum radius pairings are not matched to borehole data.

**OSM Scale: 0.5m - ~ 564 m radius (~1m –
1000 m trace length) – Predominantly Joints**

**TFM Scale: 28m - 564m radius (50m – 1000m
trace length) – Predominantly Faults**
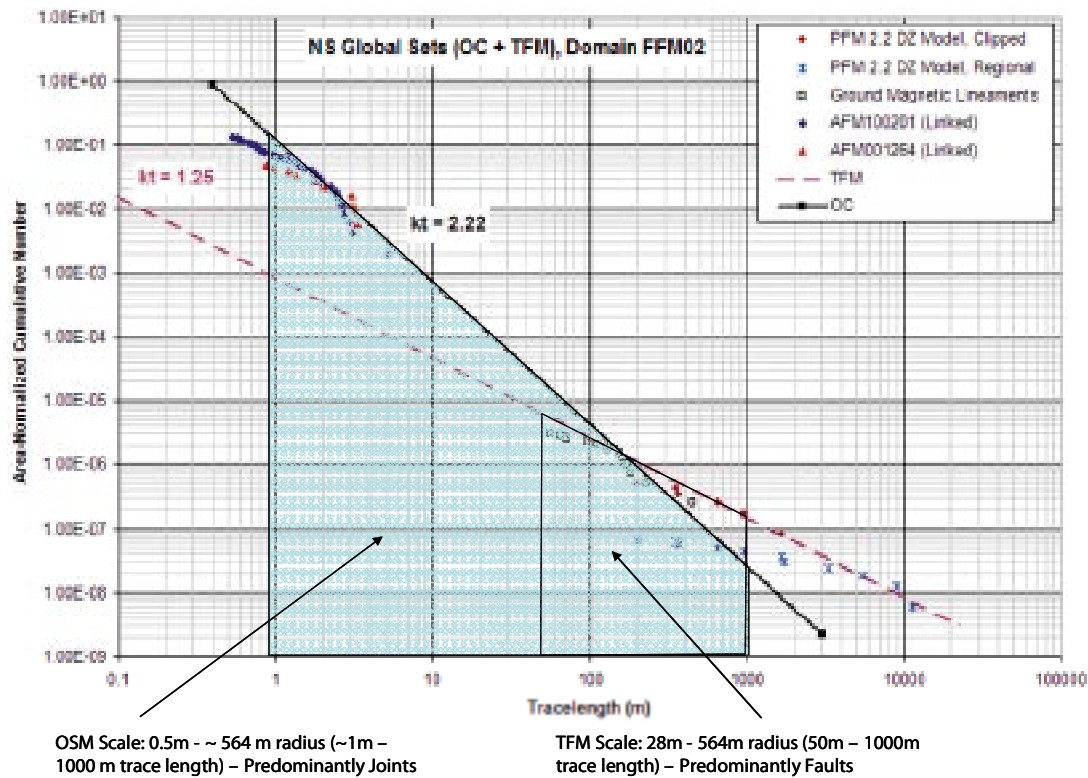
Figure 3-6. *Relationship between the Outcrop Scale and Tectonic Fault models.*

Tectonic continuum models (TCM and TCMF)

The tectonic continuum approach, which has been used in previous SDMs to describe fracture size scaling in geological DFN models, follows a different method towards calculating the DFN size model. In the tectonic continuum approach, fracture traces from outcrops were combined with traces from other sources, including lineament traces derived from high-resolution ground magnetic mapping and the kilometer-scale traces derived from the SDM Forsmark version 2.2 deformation zone (DZ) model, into a trace length frequency plot. The trace length frequency plots were then used to determine the size scaling parameters for the fracture radius distribution, assuming that the size population could be described by a power law (Pareto distribution). The limits of the tectonic continuum models are illustrated graphically in Figure 3-7.

There are two alternatives within the tectonic continuum approach; one assuming Euclidean size-intensity scaling, and one assuming fractal size-intensity scaling based on the fractal mass dimension. The differences between these two alternative approaches are described later in this chapter. It should be noted that the tectonic continuum models exist ONLY for fracture sets that are Global in at least one domain. This limitation exists because, by in large, it was not possible to identify any of the local sets in the DZ trace data or in the ground magnetic lineament data set. We recommend the use of the OSM for simulation of the size and intensity of the local sets.

To construct the plot, the trace lengths actually measured in the domain were ordered from shortest to longest. Each trace was numbered according to its cumulative frequency. If there were 50 traces, then the shortest trace would be assigned the number 50, indicating that there are 50 traces greater than or equal to the length of this shortest trace. The second shortest trace would be assigned the number 49, and so on through the longest trace in the data set, which would have a complimentary cumulative frequency of 1. More generally, if n_i fracture traces were measured in domain i, then the shortest trace has the cumulative frequency value of n_i, and the next longest has the value of $n_i – 1$, and so on such that the longest trace measured has the value of 1. Next, these cumulative frequency numbers were each divided by the appropriate mapped area. The values were plotted with the area-normalized cumulative frequency value on the ordinate (Y-axis), and the trace length value on the abscissa (X-axis) as shown in Figure 3-8.

36

Range of TCM / TCMF models (0.5 m to 564 m radius, ~ 0.89 m–1,000 m trace length)
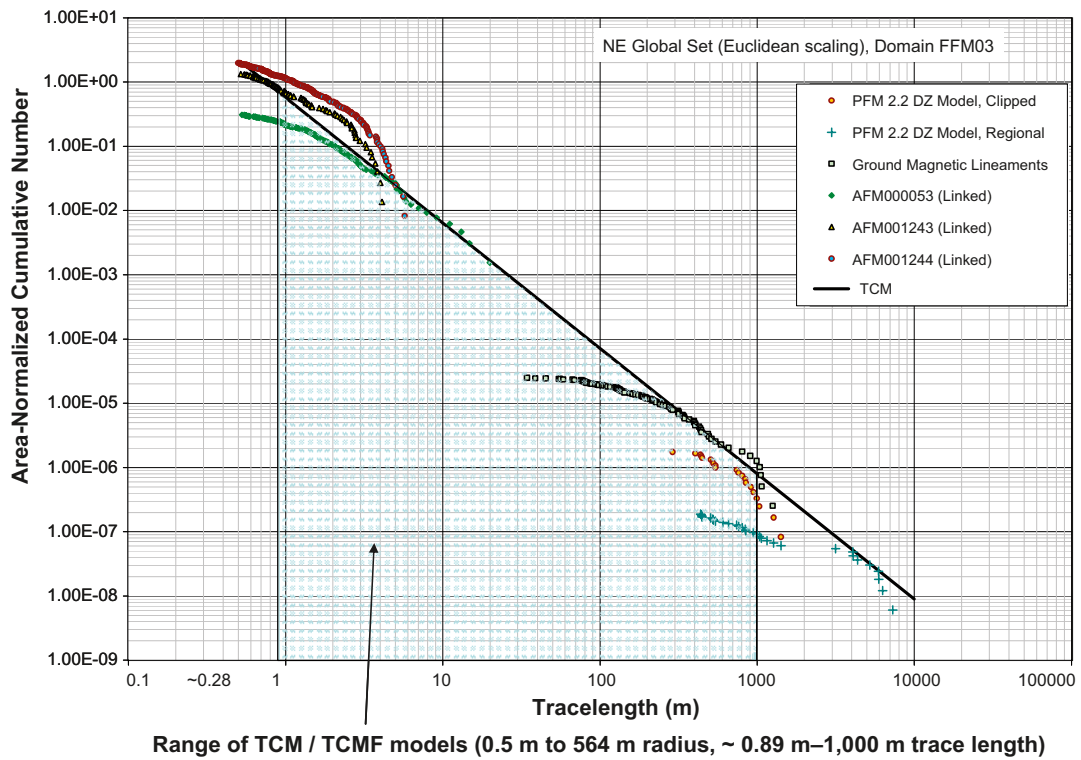
Figure 3-7. *Limits of the tectonic continuum model alternatives, expressed as minimum and maximum trace length values relative to Forsmark outcrop data.*
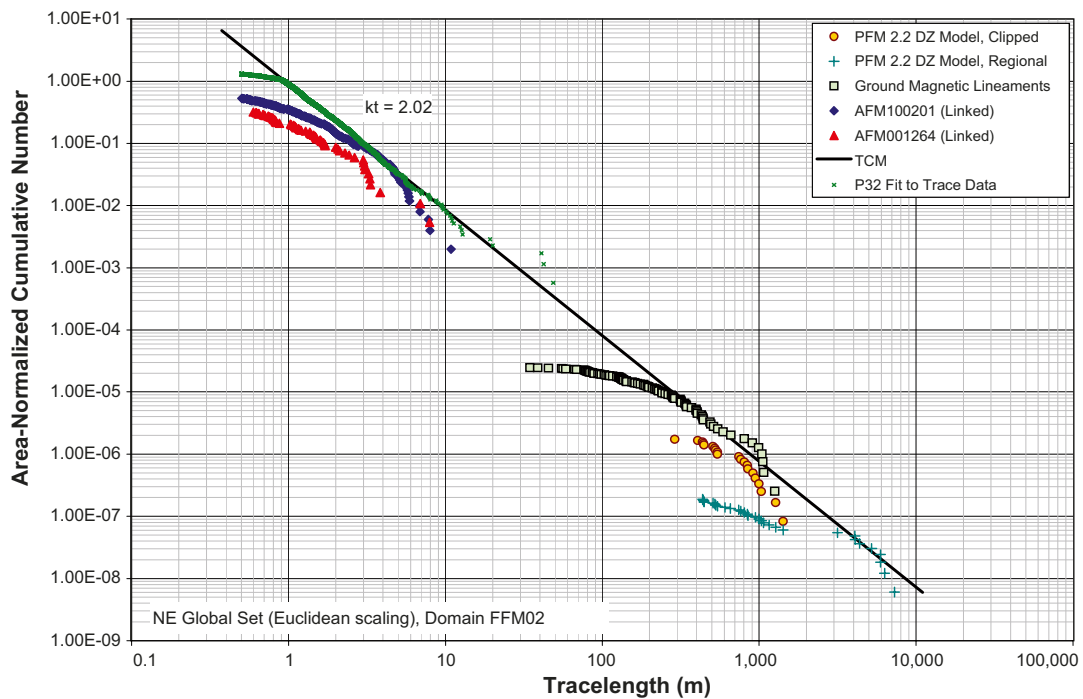
Figure 3-8. *Example area-normalized trace length cumulative frequency plot.*

In order to distinguish between the parameters for the various power law distributions that arise from the parameterization of fracture sizes based on normalized cumulative number plots, the following nomenclature is adopted:

Table 3-2. Power-law distribution nomenclature.

Distribution name	Parameter 1	Parameter 2
Mass dimension	ρ (prefactor)	D_m (mass dimension)
Cumulative number of trace lengths	t_{0n} (coefficient)	k_t (trace length exponent)
Trace length CCDF	x_{0t} (coefficient)	k_t (trace length exponent)
Radius CCDF	r_0 (coefficient)	k_r (radius exponent)
Radius size truncation limits	r_{min}	r_{max}

Note that Parameter 2 for both the cumulative number of trace lengths and the trace length CCDF are identical. The equation of the black line shown in Figure 3-8 conforms to a power law. The complementary cumulative number (CCN) plot shown in Figure 3-8 represents the number of traces, per unit area, greater than or equal to a specific trace length:

$$\text{Number/area} \; (x \geq t_{0n}) = \left(\frac{t_{0n}}{x} \right)^{k_t}$$

Equation 3-3

The value of t_{0n} corresponds to a trace length of which it is expected that there is only one of them per unit area of this length or longer. Note that the relation depicted in Figure 3-8 does not describe a probability distribution, but rather a cumulative number distribution. The parameter k_t is the slope of the black line on Figure 3-8, and the parameter t_{0n} is the abscissa value that corresponds to the ordinate value of 1.0.

It is possible to calculate a probability distribution from the cumulative number distribution, but this requires fixing the value of x_{0t} or r_0. This probability density (PDF) function for trace lengths, which is quantified by this line, has the functional form:

$$P(X \geq x) = \left(\frac{x_{0t}}{x} \right)^{k_t}$$

Equation 3-4

where x_{0t} is the minimum trace length;

       x is any trace length greater than or equal to x0t;

       k_t is the Trace Length Dimension, and

       $P(X \geq x)$ is the probability that a trace length is greater than or equal to x.

The value of x_{0t} is not the same as t_{0n}. x_{0t} corresponds to a minimum trace length of a probability density function, and is not calculated from t_{0n}. r_0 and x_{0t} are related, however, as are k_r and k_t /La Pointe et al. 1999/, according to Equation 3-5:

$$k_r = k_t + 1$$

Equation 3-5

$$r_0 = x_{0t} * \frac{2}{\pi}$$

This equation implies that the exponent describing the radius CCDF can be calculated from the slope of the cumulative number plot by simply adding 1.0 to the slope. The values of r_0 or x_{0t} are not calculated from the cumulative number plot, but are based either on the minimum fracture trace or radius required in the simulation. The methods for calculating P_{32} for a specific combination of minimum fracture size and power-law exponent, as well as a method for re-adjusting P_{32} values for different minimum sizes, are described at the end of this Section and in the context of the Tectonic Continuum spatial model in Section 3.2.5

Note also that the exponent of the parent radius distribution is sometimes specified by a parameter, *b*, often termed the Pareto exponent. This exponent is related to the trace dimension in Equation 3-6 as:

$$k_r = b - 1$$ Equation 3-6

Those using results from these analyses should be aware of which convention is being used in the specification of the radius distribution model parameters in their particular application. All versions of FracMan software assume that the radius exponent is specified as *b*, not k_r. It is important to also note that the parameter k_t is not the same as the mass fractal dimension, D_m! They are, in fact, independent parameters.

As the number of fractures encountered was related to the size of the mapped area, the cumulative number needed to be normalized for this effect. A simple way to compensate for different map areas among the data sets is to divide each data set by the map area (area normalization). This procedure assumes that doubling the area of the outcrop or map would lead to a doubling of the number of traces. This type of intensity scaling, in which the number of fractures is directly proportional to area, is Euclidean in nature and not fractal. The manner in which the fracture intensity scales with area can be quantified by the mass dimension (D_m) of the fracture traces. When the mass dimension of the traces has a value of 2.0, the fracture intensity (number of fractures per unit area) scales proportionately to area, and the spatial pattern of traces can be characterized by a Poissonian density function which inherently has no spatial correlation between the fractures

It is possible that the intensity scaling of fractures is better described by a fractal model /La Pointe et al. 1999/. For the fractal model, the area normalization is a function of the mass dimension of the number of traces per as a function of scale. In this type of model, intensity varies according to:

$$N(r) = \rho * r^{D_m}$$ Equation 3-7

where ρ is a constant, termed the prefactor;

        r is the radius of a circle,

        D_m is the Mass Fractal dimension, and

        N(r) is the number of fracture traces (partial or entire) contained within the circle of radius *r*.

When the Mass Dimension of the traces has a value of 2.0, the intensity (number of fractures per unit area) scales proportionately to area, and the spatial pattern of traces can be characterized by a Poissonian density function which inherently has no spatial correlation among the fractures.

The computation of the mass dimension can take several distinct forms, such as the scaling properties of fracture center points or random points selected along the fracture trace, of the number of traces (P_{20}) themselves, or of the P_{21} (fracture trace length per unit area) measure of fracture intensity. All are useful for certain purposes. For size-scaling analysis, the desired parameter is how the number of fractures (P_{20}) changes with scale.

The procedure for calculating the mass dimension is illustrated in Figure 3-9. The value for D_m in Equation 3-7 is equal to the slope of the line when the data are plotted on doubly logarithmic axes. The value of the prefactor is equal to the ordinate value corresponding to a circle with radius = 1.0, and can be read directly from the graph It is important to make this calculation on individual sets rather than all of the traces at once, as each set may have different scaling properties.
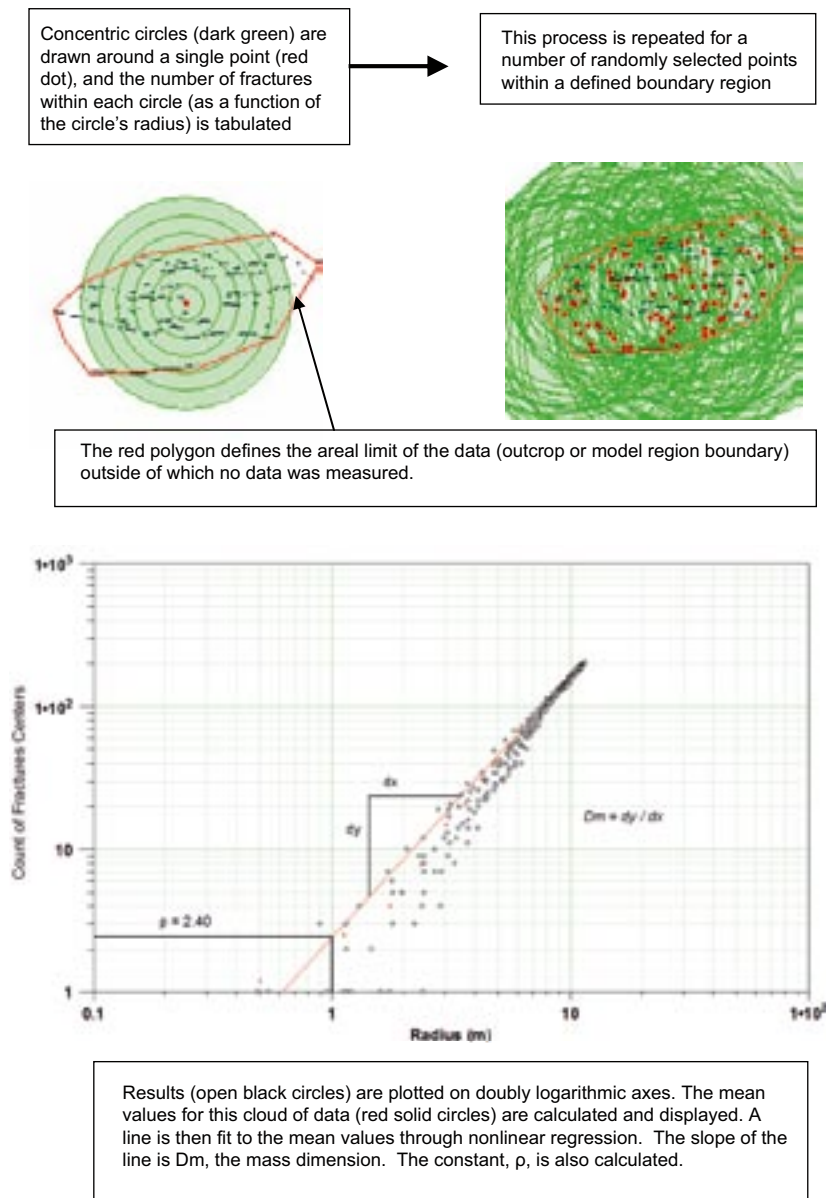
Figure 3-9. *Workflow for calculating the mass dimension from maps of fracture traces.*

The procedure is to calculate and plot the cloud of mass dimension data points, as in Figure 3-9, and then compute a non-linear least-square fit of the Pareto equation to the locus of the mean. The calculations are always performed on the data set with the least censoring on the small trace end of the distribution, as censoring produces an underestimation of the number of fractures per unit area. For this reason, the mass dimensions were always calculated on the outcrop trace data rather than the deformation zone data.

The next step is to combine the data from different data sets. Since the various data sets may have come from maps or outcrops of different areas, the area differences must be accounted for. The process for normalizing for different mapped areas, using the example of an outcrop data set and traces of the deformation zones, is as follows:

Let the "o" subscript denote outcrop fractures, the "z" subscript denote deformation zones, and "1" denote an area equal to 1 m^2. Furthermore, let the variable "A" denote the area of the outcrop or deformation zone map, and "R" denote the radius of an imaginary circle that would have the same area as "A". Also, let "x" represent the trace length of a fracture.

40

Then, from Equation 3-8, it is possible to calculate the number of fracture traces that would be expected in the deformation zone map area based on what was measured in the outcrop area. The radius (R_l) that corresponds to a circle of area 1 m² is

$$A_1 = \pi R_1^2 = 1.0$$

$$R_1 = \sqrt{\frac{1}{\pi}}$$

$$N(R_1) = \rho \left(\sqrt{\frac{1}{\pi}} \right)^{D_m}$$

Equation 3-8

Alternatively, if the scaling were Poissonian and not fractal, the exponent, D_m, would be equal to 2.0. In this case, the number of fractures in an area of 1 m² would be:

$$N(R_1) = \rho \left(\sqrt{\frac{1}{\pi}} \right)^2$$

Equation 3-9

A convenient way to adjust the CCN plots for the fractal scaling is to calculate a pseudo-area. For example, the pseudo-area, A^* for an outcrop of A_o is:

$$A^* = A_o * \frac{\rho \left(\sqrt{\frac{1}{\pi}} \right)^2}{\rho \left(\sqrt{\frac{1}{\pi}} \right)^{D_m}} = A_o * \left(\sqrt{\frac{1}{\pi}} \right)^{2-D_m}$$

Equation 3-10

Instead of dividing the cumulative number of traces by A_o, the number is divided by the pseudo area. The same calculation is repeated for lineaments or any other data sets.

The parameters for the Complementary Cumulative Number (CCN) plots do not directly yield the trace length probability distribution, because they describe the cumulative number of fractures, not the probability of the fractures. The probability distribution will have the same exponent as the radius distribution derived from the CCN plot, but the minimum size value differs from the value calculated from the CCN plot. The minimum size value for the probability distribution can be derived through simulation, however. The simulation steps are as follows, and are based on Equation 3-11:

$$P_{32}(r_{min}, r_{max}) = \frac{[r_{min}^{2-k_r} - r_{max}^{2-k_r}]}{r_0^{2-k_r}} * P_{32}(r_0, \infty)$$

Equation 3-11

1. For a particular set, specify a size model as a power law distribution using the exponent k_r derived from the cumulative trace number plot, and an assumed minimum size value (r_0). Also assume a value for fracture intensity (P_{32}) chosen to produce enough trace intersections for robust computation of simulation trace length statistics. For the simulations used in SDM 2.2, a minimum radius of 10 m and a P_{32} of 0.1 m²/m³ were assumed.

2. Assign the orientation model for the set.

3. Generate the fractures in a volume. If the simulation model volume or area differs from the volume for the data set, then note the ratio of volumes for later plotting adjustment. The volume used in the simulations for SDM 2.2 was 1,000 m by 1,000 m by 1,000 m.

4. Place a horizontal trace plane into the model and compute the fracture intersections with the plane.

5. Export the traces and plot on a CCN plot. If the simulation volume or area differs from the volume or area of the measured data, adjust the Y-value of the simulated data by the ratio so that the volumes or areas are the same.

6. Compare the simulated traces to the measured traces. The ratio of Y-values (cumulative number) for the straight-line portions of the data corresponds to the ratio by which the P_{32T} should be adjusted to achieve a match.

7. Make the P_{32T} adjustment and re-run for verification that the results match the measured data. Everything in Equation 3-11 is known at this point except r_0 and $P_{32}(r_0, \infty)$.

8. Using Equation 3-11, specify a desired value of r_0. Since all other values except $P_{32}(r_0, \infty)$ are known, calculate this value which corresponds to the desired lower limit (r_0) of model applicability.

With consideration of the linked vs. unlinked trace data, and two scaling models, the Tectonic Continuum alternative model has two sub-models: Euclidean size-intensity scaling, and fractal size-intensity scaling. The fits are made visually, because of the many artifacts that are present in the data set due to censoring and truncation effects on the trace length data, and it is difficult to develop an algorithm that would accurately recognize these artifacts and exclude them from the fitting.

An example of the process is shown in Figure 3-10 and Figure 3-11. The initial guess of $P_{32} = 0.1$ m²/m³ for a minimum size of 10 m did not match the fitted line (Figure 3-10). The simulated points lie above the line, which indicates that the intensity is too high. A reduction of P_{32} to 0.052632 m²/m³ resulted in an excellent match (Figure 3-11). Using Equation 3-9, and taking the value of $x_{1r} = 10.0$ m, $x_{2r} = \infty$, $x_{0r} = 0.5$ m, $k_r = 2.8$ and $P_{32}(x_{1r}, x_{2r}) = 0.052632$ m²/m³, yields $P_{32}(x_{0r}, \infty) = 0.5782$ m²/m³.

At this point, any portion of the population from 0.5 m to infinity can be simulated (Figure 3-12). In this example, separate models were generated for the size ranges 1–20 m, 20–200 m, and 200 m to 1,000 m. The simulation did not include fractures greater than 1,000 m as these represent deformation zones that have already been mapped and are not generated stochastically.
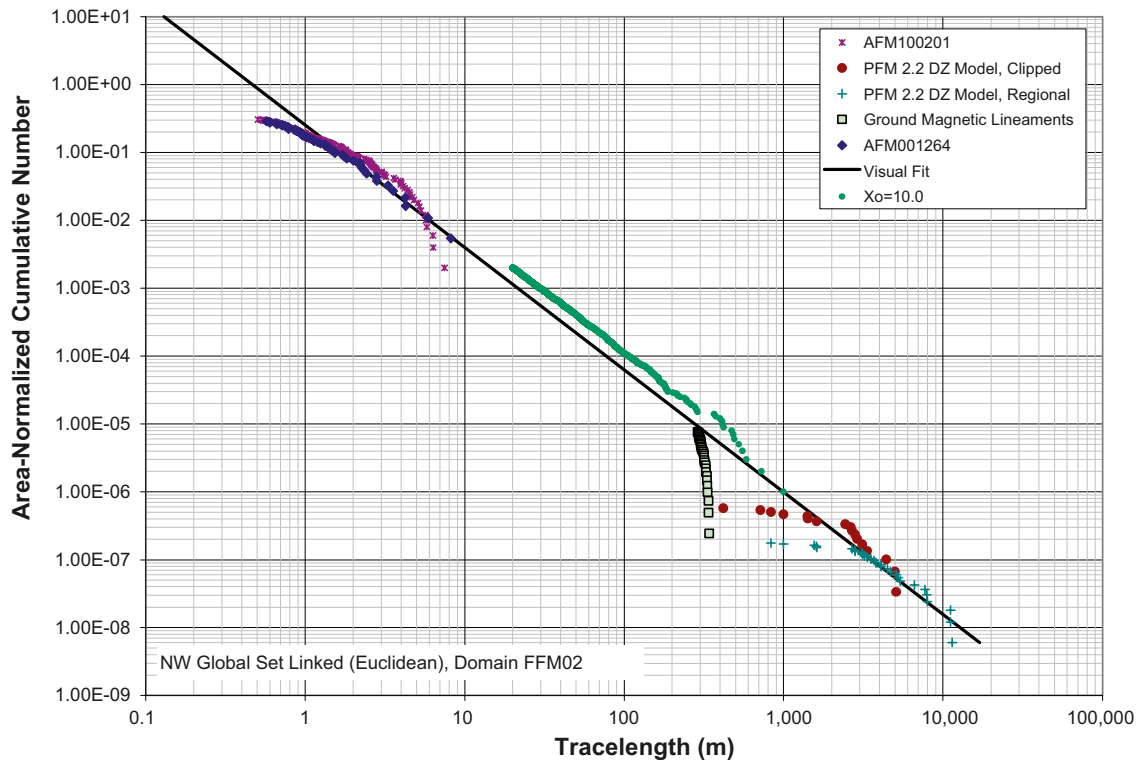
Figure 3-10. *Calculating the minimum size value. The simulations with the minimum size set to 10 m and P_{32} set to 0.1 m²/m³ produced the green points that indicate that the assigned P_{32} is too high.*
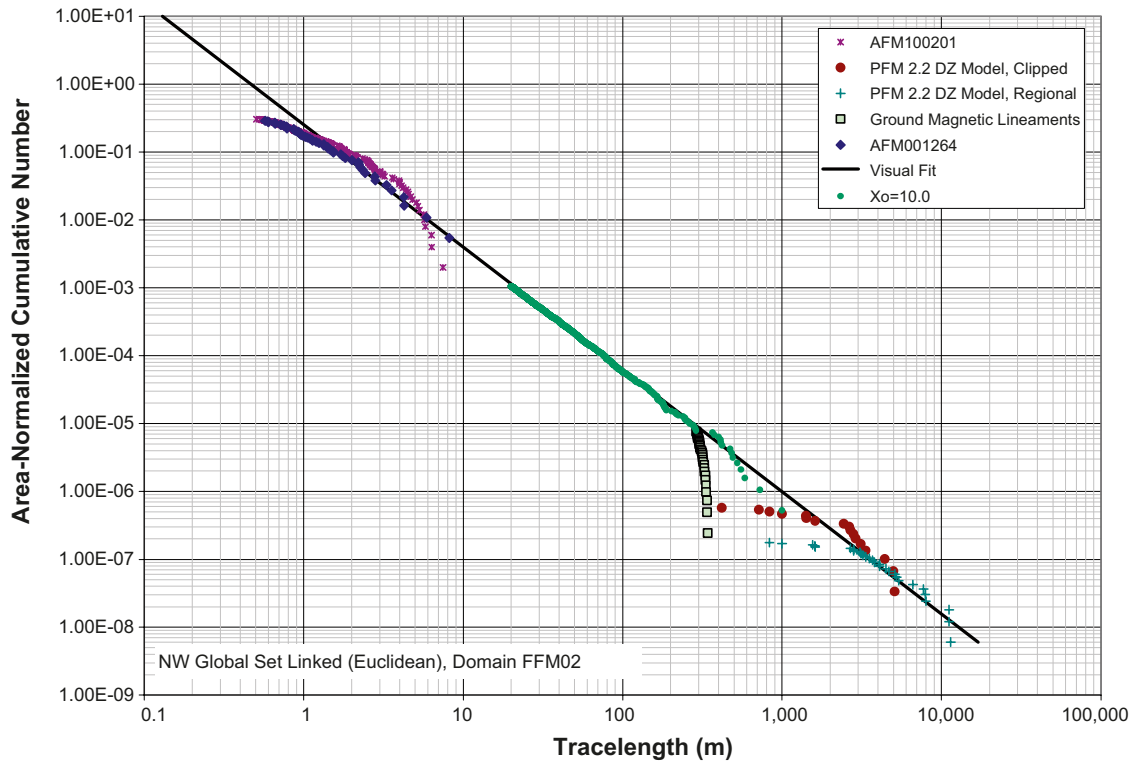
Figure 3-11. *A reduction of P_{32} to 0.0526 m^2/m^3 matches the fitted line very well.*

It should be noted that the size-scaling simulations used to constrain P_{32} have an artifact. This artifact occurs at trace lengths exactly twice the value of the fracture radius. This artifact causes the number of intersected traces to be less than the theoretical number that would be expected if the trace plane or outcrop were infinite in extent. The artifact is negligible at trace lengths greater than twice the minimum radius, and so when a minimum radius of 10 m was used, only traces greater than or equal to 20 m were plotted. Plotting all traces, including those between 10 m and 20 m does not change the location of any of the points shown in the plots, but merely adds some addition points that fall below the straight line fit. Note that the measured traces in the outcrops also deviate from a straight line as they approach 0.5 m below 1.0 m.

By definition, the parameterization for the TCM requires a power law size model. The remainder of the parameterization for the TCM follows the same steps as in the Outcrop Scale Model, in which the minimum size is adjusted to match the mean fracture intensity.

At the end of this procedure, the minimum radius (r_{min}) calculated for a given fracture set inside a given fracture domain represents a coupled size-intensity fit to fracture trace data recorded in outcrop. The final step in producing the coupled size-intensity model parameterization for the geologic DFN is to constrain the size-intensity match to the fracture intensities recorded in the cored boreholes, where possible.

For the tectonic continuum-based models, the assumption is made that the increased P_{32} observed in boreholes represents smaller fractures that were not recorded during the detailed outcrop mapping exercises. The outcrop maps do not record any traces shorter than 0.5 m in length; for outcrop intensity matching, the minimum fracture radius (r_{min}) was set at 0.5 m. Therefore, we can calculate the true distribution minimum radius (r_0) by comparing the ratios of the outcrop and borehole P_{32} values through the following steps:

1. The borehole P_{32} (P_{32BH}) of a given fracture set in a given fracture domain is calculated using the Wang C13 conversion factor (see Chapter 3.2.4) and binned P_{10} values from p_fract_core_eshi. The conversion is done for P_{10} values at 6 m, 15 m and 30 m section lengths.
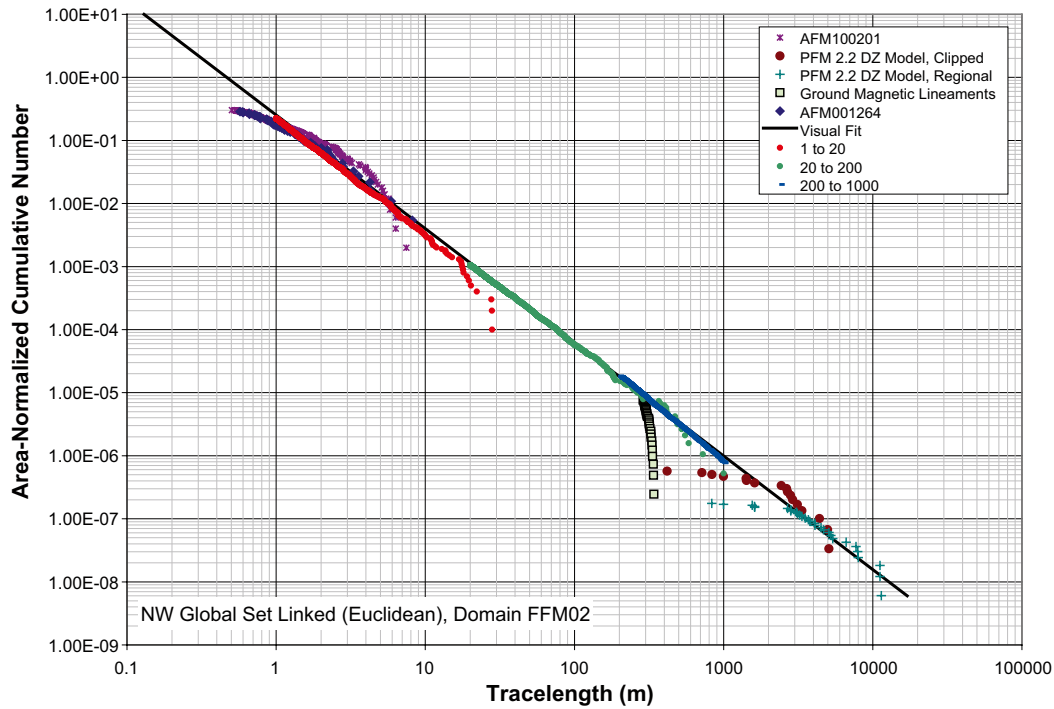
Figure 3-12. *Three separate simulations spanning different size ranges from 0.5 m to 1,000 m.*

2. Given the minimum radius (r_{minOC}) and P$_{32outcrop}$ matched to outcrop data with no imposed maximum fracture sizes, and P$_{32BH}$, r_{minBH} is adjusted according to Equation 3-12 (which is effect a re-statement of Equation 3-11):

$$r_{\min BH} = r_{\min OC} * \left(\frac{P_{32BH}}{P_{32OC}} \right)^{1/(2-k_r)}$$

Equation 3-12

The value of r_{minBH} corresponds to a population of fractures with no imposed maximum size limit

3. In cases where r_{minBH} is larger than the radius of the cored borehole (0.038 m) and <u>smaller</u> than the minimum radius fit calculated for outcrop data ($r_{minBH < r_{minOC}}$), r_{minBH} is used as r_0, the minimum radius for the radius size probability distribution. In these cases, it is possible to simultaneously match borehole and outcrop intensities with a single coupled size-intensity relationship.

4. In cases where is smaller than the diameter of the cored borehole (0.038 m), it is not possible to simultaneously respect both the outcrop size-intensity data and the borehole size-intensity data. In these cases, the radius exponent (k_r) from the outcrop data is used, and the minimum radius is set to the borehole diameter (i.e. $r_0 = 0.038$ m).

5. In cases where the minimum radius fit calculated for the coupled size-intensity model to borehole data is <u>larger</u> than the minimum radius fit calculated for outcrop data ($r_{minBH > r_{minOC}}$), it is <u>not</u> possible to simultaneously fit both data sets (outcrop and borehole) using the fitted values for k_r, r_0, P$_{32OC}$, and P$_{32BH}$. In these cases, we recommend that the P$_{32}$ and r_0 values ($r_0 = r_{minBH}$) calculated from the borehole data be used for all DFN simulations.

The geologic arguments for choosing the borehole intensity data over the outcrop trace data are as follows:

   a. The surface outcrops are most likely to have been disturbed recently by glacial loading or anthropogenic activities.
   b. There is far more intensity data coverage from boreholes than outcrops within any given fracture domain. It is most likely that the borehole data is the best estimate of average domain properties, rather than the outcrops.
   c. There are no outcrops in FFM01 and FFM06.

3.2.4 DFN intensity model

The Forsmark 2.2 geologic DFN presents fracture intensity measurements in several forms:

- As a single matching intensity value in the coupled size-intensity models. These models are based on the arithmetic mean P_{32} intensity in borehole data for a given fracture set within a given fracture domain.

- As a set of descriptive statistics for each fracture set, by fracture domain. Statistics include the arithmetic mean, standard deviation, median, quartiles and percentiles. No assumption is made about the form of the distribution.

- As a gamma distribution, where applicable. The reasoning and methodology behind the use of the Gamma distribution is described in Chapter 4.4.3

Fracture set intensities are based largely upon the data (P10) collected in the cored borehole logs. P_{32} values are calculated for individual borehole sections at multiple intervals (6 m, 15 m and 30 m); the resulting values are then aggregated by set and domain. Outcrop fracture intensity (P21) is used to bound the coupled size-intensity models, and as a validation tool for the final model parameterization.

It should be noted that there are several critical limitations with respect to the usage of the Forsmark cored borehole data suite in DFN modeling. These limitations are discussed in SKB Report R-07-19 /Munier and Stigsson 2007/:

- Only data from cored boreholes with an overall orientation/position uncertainty (Ω) less than 10 was used.

- Only fractures marked 'VISIBLE_IN_BIPS = 1' in the SICADA database were used in all DFN analyses. However, the final intensity parameterization is corrected for fractures not visible in BIPS. The percent of fractures visible in BIPS is computed for each borehole, in each fracture domain. For each bin interval (6 m, 15 m, and 30 m), the calculated P10 value is divided by the percent of fractures visible in BIPS before being multiplied by the C13 conversion factor. As such, P_{32} values in cored boreholes represent all fractures logged.

Fracture intensities are computed in terms of both sealed and open fractures; no distinction between the two classes is made in the geological DFN. However, Global and Local sets are treated differently in terms of model intensity parameterization. Global sets are hypothesized to exist everywhere within the model domain; as such, intervals with no fractures are considered part of the spatial distribution of the Global sets, and are included in the intensity statistics and gamma distribution calculations. Local sets, on the other hand, are hypothesized to represent truly local phenomena; an interval with no Local set fractures is NOT considered part of the spatial distribution of the Local fractures. As such, zero intervals in the Local fracture set data are removed before the intensity statistics and gamma distributions are calculated.

Calculating P_{32} from borehole fracture Logs

Previous geological DFN models have used stochastic simulation to develop a conversion factor between borehole P_{10} and model volume P_{32}. The approach generally relies on calculating a conversion factor, C_{13}, by which the observed borehole P_{10} is then multiplied to obtain a distribution of P_{32}. The stochastic simulation method is quite versatile, as it allows for the use of different orientation, spatial, and intensity models. However, it is very sensitive to several simulation parameters, including the fracture size distribution relative to the diameter of the borehole, the size of the simulation region relative to the fracture size, and to the intensity values used in simulation. It is necessary to use very high P_{32} values (in the range of 30–40 m^2/m^3) to obtain stable solutions; it is difficult to model large regions with small fractures in this approach.

The Forsmark 2.2 geological DFN instead uses another method for the estimation of fracture set intensity distributions; the numerical approximation based on Wang's /Wang 2005/ doctoral

research on stereological relationships between fracture orientation and fracture intensity. Wang's C_{13} is an analytical solution, and is subject to several critical assumptions:

- The method is only applicable to line-sampling; i.e. a zero-radius borehole. This implies that every fracture recorded in the SICADA database for a given cored borehole crosses the entire diameter of the core.

- Wang's C13 assumes constant-sized fractures, but is independent of fracture shape.

- Wang's C13 assumes that the fracture population follows a univariate Fisher spherical probability distribution.

Given a relationship where $C_{13} * P_{10} = P_{32}$, the conversion factor C_{13} is defined by /Wang 2005/ as:

$$C_{13} = \left[\int_0^\pi |\cos\alpha| f_A(\alpha) d\alpha \right]^{-1} \qquad \text{Equation 3-13}$$

where α is the solid angle between the sampling line and the fracture normal. Assuming line sampling (P10) of fractures distributed according to a univariate Fisher spherical probability distribution, the theoretical probability distribution function given by /Wang 2005/ for α is given by:

$$f_A(\alpha) = \frac{1}{\pi} \int_{R_\delta} \frac{\sin\alpha}{\sqrt{\sin^2\delta \sin^2\rho - (\cos\alpha - \cos\delta\cos\rho)^2}} \frac{\kappa e^{\kappa\cos\delta} \sin\delta}{e^\kappa - e^{-\kappa}} d\delta \qquad \text{Equation 3-14}$$

For α in the range $|\delta-\rho| < \alpha < \delta + \rho$, where the range of integration of Rδ is given by :

$$R_\delta = [\rho - \alpha, \rho + \alpha] \text{ if } \alpha < \rho \text{ , or}$$

$$R_\delta = [0, \alpha + \rho] \text{ if } \alpha > \rho$$

In the Forsmark 2.2 geological DFN parameterization, Wang's C_{13} is calculated in the following manner:

1) Borehole coordinate survey data from SICADA table p_object_location are divided into 'bin' intervals of 6 m, 15 m, and 30 m. The bin intervals are based on the borehole length ('ADJUSTED_SECUP', otherwise known as Measured Depth) rather than the true depth or segment elevation (relative to a sea-level datum).

2) object_location contains cored borehole centerline coordinates in the RT90-RHB70 coordinate system at 3 m intervals. The start point and endpoint of each section were used to calculate a trend and plunge of each borehole section.

3) For each fracture set in each domain, the mean pole vector orientation (trend, plunge) and Fisher concentration parameter (κ) was obtained. Note that the Wang C13 analytical solution works only for Univariate Fisher distributed data.

4) For each borehole section, in each bin size range, for each fracture set in each fracture domain, the solid angle (θ) between the fracture set mean pole vector and the unit vector representing the orientation of the borehole section was computed.

5) The solid angle and the Fisher concentration parameter are then used as input parameters to a compiled C++ application (ComputeC13.exe) written. The code uses a numerical integration procedure to approximate the Wang C13. Copies of the executable and/or source code are available upon request; the algorithm will ultimately be included in a future release of FracMan.

The resulting C_{13} values were then input into Microsoft Excel, where the actual P_{10} to P_{32} conversions were performed.

P_{32} as a gamma distribution

It has been suggested /Dershowitz 1984/ that, in the absence of other controlling factors such as lithology or deformation zones, P_{32} for a system exhibiting Euclidean scaling behavior and follow a Poisson point process for fracture centers should follow a Gamma (γ) distribution. Borehole lineal fracture intensity (P10) can be taken as the rate parameter (λ) of a Poisson distribution, with γ as the distribution of the variability of λ within the scale of measurement /Schlaifer and Raiffa 1972/. The gamma distribution is a two-parameter continuous probability distribution, described by a scale parameter (β) and a shape parameter (α); if the α is a positive integer, then the resulting distribution represents the sum of exponentially-distributed random variables, each with a mean of β /NIST 2007e/.

Assuming that the system to be modeled can be reasonably approximated through Euclidean scaling and a Poissonian location model, it is possible to calculate the gamma distribution of P_{32} from borehole data. The method assumes that borehole fracture frequency (P_{10}) has been converted to volumetric fracture intensity (P_{32}), either through simulation or application of the Wang C_{13} factor. Expressing P_{32} as a gamma distribution allows for the implementation of random spatial variability of fracture intensity; this form is most applicable to finite-difference or geocellular-grid style models.

The steps necessary to compute the gamma distribution parameters for a given fracture set within a given fracture domain are as follows:

1) Tabulate fracture frequency (P_{10}) for each fracture set in a given fracture domain for all boreholes. The fracture frequency measurements should be taken from borehole intervals outside of mapped DZ and MDZ, and should not contain sections of rock labeled 'affected by DZ'.

2) If the fracture set being parameterized is a Local fracture set, intervals with no intersections ('zero-intervals') were removed. Zero-intervals were not removed from the data for Global fracture sets. The rationale for this treatment is described below in the section on the DFN Spatial model (Chapter 3.2.5). In essence, Global sets are presumed to be present everywhere in the domain, regardless of geological factors, and if they are absent, then their intensity, 0.0, at these locales is relevant for calculating intensity statistics and distributions. On the other hand, Local sets are presumed to present if certain local geological factors were present. When they are not found in a particular borehole interval or location, it is presumed that the geological factors necessary for their formation were not present. Local Set model distributions and statistics are only based on values where the necessary geological factors were present. In a mathematical sense, the Global sets are a simple probability function of the measured values. The Local sets are a compound probability composed of a conditional probability that the set exists, and a second probability having to do with the values given that the set exists. It was not possible to identify what these local factors may have been; the conditional probability for their existence was calculated for each domain without regard to local geological conditions.

3) The gamma distribution parameters (α, β) for a given fracture set in a given domain was estimated using a squared-difference minimization algorithm based upon curve-fitting of the empirical CDF. Microsoft Excel's solver was used to estimate the distribution parameters; a moments-based approach could also have been used if desired.

4) A goodness-of-fit test of the resulting fitted gamma distribution of P_{32} was performed using BestFit version 4.5.5. Goodness-of-fit was determined through the use of the Kolmogorov-Smirnov test /NIST 2007d/, assuming a significance level of $\alpha = 0.05$.

5) It was not possible to fit a gamma distribution to a few fracture set/fracture domain combinations; in those cases, we recommend using the fracture median and quartiles to represent spatial variability.

3.2.5 DFN spatial model

The spatial model describes how many fractures occur in a specific volume of rock at a specific location in the modeling domain. As such, the model may depend upon the depth, the rock type, the influence of tectonic processes, the volume of interest and other geological factors. It may differ by fracture set as well.

The assessment of the spatial variation and the mathematical description of this variation is based on analysis of the scaling properties of the fractures and multivariate statistical analyses to identify any statistically significant relations between mappable geological parameters and fracture intensity variations.

The mass dimension, which models how fracture intensity may change as a function of scale, was computed for the traces in outcrop and the fracture locations in boreholes. This analysis produces a set of data for each analysis consisting of the scale and the average fracture intensity at that scale, with intensity measured as P_{21} for outcrop traces and P_{10} for borehole data. The results are displayed on a graph with doubly logarithmic axes, which makes it visually apparent as to whether the scaling behavior is a power law, and thus consistent with the tectonic continuum hypothesis, Euclidean or some other mathematical form which might have other implications for the spatial model. The key parameter in these mass dimension plots is whether the data conform to a straight line in the doubly logarithmic display, which would support the tectonic continuum hypothesis, whether it is better modeled by two or more straight line segments, implying different characteristic intensities at different scales, or whether it fails to conform to a straight line over any portion of the data record.

For portions of the data that do conform to straight line segments, the slope of the line that approximates the data describes the scaling model.

A special case of the situation where a straight line well-approximates the data or a portion of the data is Euclidean scaling. Euclidean scaling describes a model in which the number of fractures is linearly proportional to the area, in the case of outcrops, or length, in the case of boreholes, and by extension, to the volume in three dimensions. Euclidean scaling implies that doubling the volume or area or length doubles the number of fractures. In this special case, the fracture intensity is scale independent. For outcrop trace data, a slope of 2.0 indicates Euclidean scaling, while for borehole data, a slope of 1.0 indicates Euclidean scaling. The multivariate statistical analyses of the data were based on a series of statistical analyses to better understand the mathematical structure of the data, and then to use multivariate linear regression to evaluate models to predict fracture intensity. Only borehole data was used for these analyses. Borehole data was used because there was much more data available (more than 20,000 observations) and a greater number of geological parameters were recorded, improving the understanding of the possible controls on fracture intensity and potentially leading to more robust regression models than from outcrop data. Outcrop data was generally too sparse and of narrower geological coverage, making it much less useful for statistical analyses of the type described.

The development of the borehole data set for the multivariate statistical analyses required several steps prior to analyses:

1. Contiguous portions of the fracture record with nearly constant fracture intensity were identified through CFI analyses; these zones of nearly constant intensity are termed mechanical layers (not necessarily implying sheet-like volumes);

2. The P_{10} fracture intensity of each mechanical layer was calculated;

3. The geological variables over each mechanical layer were tabulated. These variables were parameters like MIN1, MIN2, ROUGHNESS and other geological observations made for each recorded fracture;

4. The percentage of each constituent within each layer was calculated. For example, if in a layer 3 out of the 10 fractures were designated as "Open", 4 were designated as "Partially Open", and the remainder as "Sealed", then the numbers 0.30, 0.40 and 0.30 were

assigned to Open, Partially Open and Sealed for this layer. One of the reasons that the data observations were represented by percentages is that most of the geological variables are Class variables rather than continuous variables, and as such, are not appropriate for many types of useful statistical analyses that require continuous variables. The other reason is that individual layers often consist of fractures with multiple characteristics, for example, they are rarely all Partially Open. The representation as percentages affords the mathematical convenience of transforming the class variables into continuous variables, and also accounts for the mixture of geological characteristics for the fracture population in the layer.

5. Any intervals lying partly or completely within any designated deformation or minor deformation zone was removed from the data set;

6. The final data set for analysis was prepared that consisted of the P_{10} for the interval based on the CFI plot, and the geological factors represented as percentages over each layer.

Once this data set was complete, it was available for statistical analyses. The statistical analysis consisted of a preliminary series of calculations to investigate the mathematical relations among the variables, and a second series of calculations to create multivariate regression models and analyses to determine whether geological factors like lithology could be used to usefully reduce the variance or uncertainty in the intensity models. The preliminary investigations are important because they provide information to guide the development of the regression models and to interpret why they may be successful in predicting fracture intensity.

Spatial model for local sets

Local sets are groups of fractures with well-defined orientations, but with a limited spatial extent. These sets are seen in relatively few boreholes or outcrops, and may be tied to highly local stress phenomena. As such, it is inappropriate to simulate the local sets across the entire Forsmark 2.2 model domain; the end result would be an over-estimate of fracture intensity in locations where local sets are not present, but are predicted by the geologic DFN.

The Forsmark 2.2 geological DFN treats Local fracture sets as highly localized phenomena. The P_{32} of local fracture sets, as recorded in boreholes, is based solely on borehole sections (6 m, 15 m or 30 m) that contain Local set intersections; if the borehole section does not contain fractures from a given local set, it is not counted when the distribution of intensity is computed. The distribution of P_{32} given as model parameters in the geological DFN for the Local sets represent the intensity recorded when they were recorded. It does not represent the probability of encountering the Local orientation set, nor does it represent the total intensity of the Local set in a given domain. This is in contrast to the Global sets, where zero intervals are included in the set intensity parameterization. One of the assumptions of the version 2.2 geological DFN model is that Global sets are ubiquitous; a zero-section (one with no intersections) represents the natural variability of the fracture system.

The methodology for handling the spatial distribution of the local sets is as follows:

1. A statistical analysis of fracture morphology, host lithology, and other parameters. The goal of this analysis is to determine if there are any recorded specific factors that control the location of the local sets. If a controlling parameter is found, a correlated spatial model can be built.

2. In the event a geologic correlation for local set location is not found, a probability of intersection model will be built for each set, based on binned borehole fracture intensity data. For any given fracture set within a specific fracture domain, for a given unit in a geocellular model (6 m and 30 m bin sizes were used), the probability of encountering a local set will be defined as the total number of recorded cells with local set intersections, divided by the total number of cells.

For example, the SH2 Local fracture set is only seen in one borehole (KFM07C) in fracture domain FFM01. The OSM model specifies a P_{32} intensity of 0.92 m^2/m^3 for this set (Table 7-2). It was encountered in 79 of the 888 6 m bins (sections of cored boreholes of a set length) in domain FFM01. This suggests that any 6 m section of borehole (and, by extension, any 6 m cubic volume of rock) has a 9% probability of containing fractures belonging to the NNW set. If the set is encountered, it is generated at the full intensity (0.92 m^2/m^3); the intensity is only valid for that 6 m 'bin', and not for the domain as a whole.

4 Derivation of SDM Forsmark version 2.2 geological DFN statistical model

This chapter describes the specific implementation of the geological DFN framework described within Chapter 3. All models are parameterized in terms of the significant identified fracture domains (FFM01, FFM02, FFM03, and FFM06) at Forsmark /Olofsson et al. 2007/.

4.1 Orientation model

The orientation model for the SDM Forsmark version 2.2 geological DFN was defined primarily using data recorded from outcrop fracture mapping. The borehole data record was included in the analysis, and does contribute towards the final parameterization. However, the identification of orientation sets is largely based on outcrop traces. The recorded strikes and dips were used to define spherical probability distributions for individual fracture sets. Set membership was determined primarily by a combination of pole orientation and geometric relationships to other fractures on the outcrops (terminations, apparent history).

4.1.1 Fracture sets identified in outcrop

The first step in building the orientation model for the geological DFN was the identification of orientation sets on each of the detail mapped fracture outcrops. The methodology for this analysis is described in Chapter 3.2.2.

Preliminary fracture set identification through stereonets

The DIPS software package was used to construct stereonet plots of poles to fracture planes, as measured in outcrop. Equal area, Terzaghi bias-corrected, lower hemisphere pole plots, nominal symbolic pole plots, and Fisher contoured stereonets were produced. The stereonets provide a first guess at identifying fracture poles; however, it is difficult to locate overlapping or conjugate sets using only a stereonet with no other information than orientation.

Stereonet plots were created for both linked and unlinked outcrop traces. There was very little difference between the two data sets; only a slight change in the Fisher contours is visible.
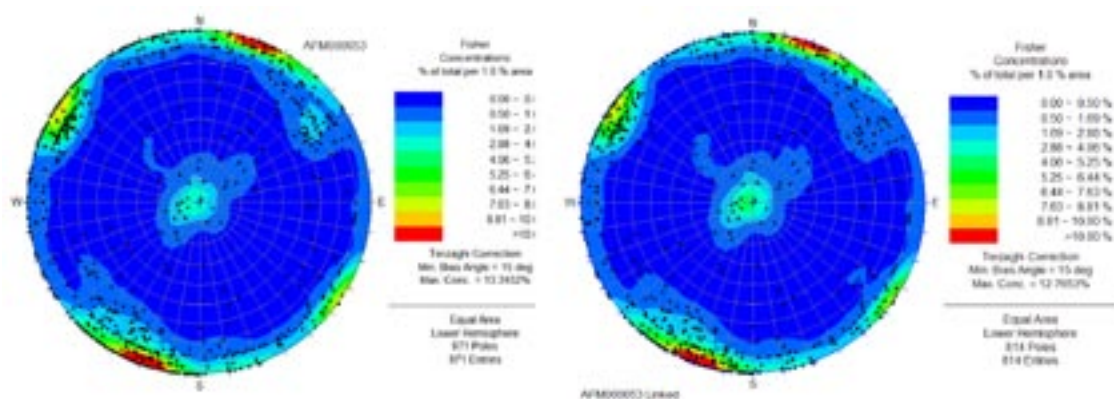
Figure 4-1. *Contoured stereonet plots of unlinked (left) and linked (right) fracture traces, Outcrop AFM000053.*
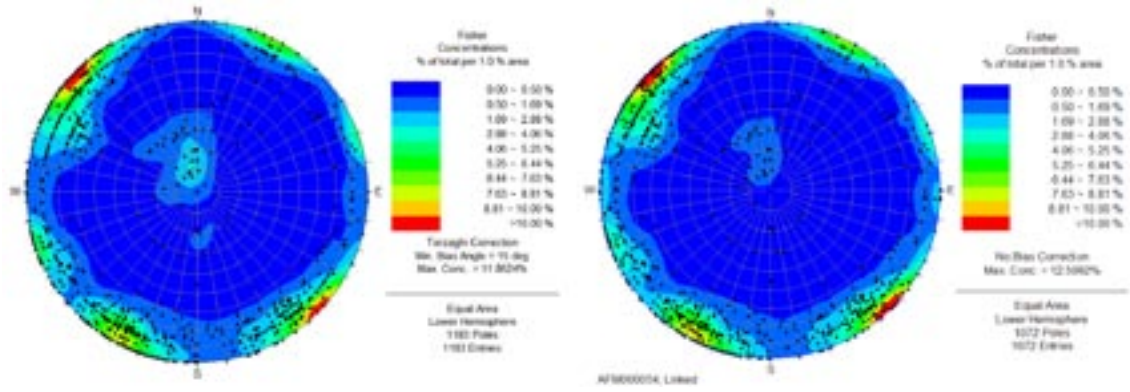
Figure 4-2. *Contoured stereonet plots of unlinked (left) and linked (right) fracture traces, Outcrop AFM000054.*
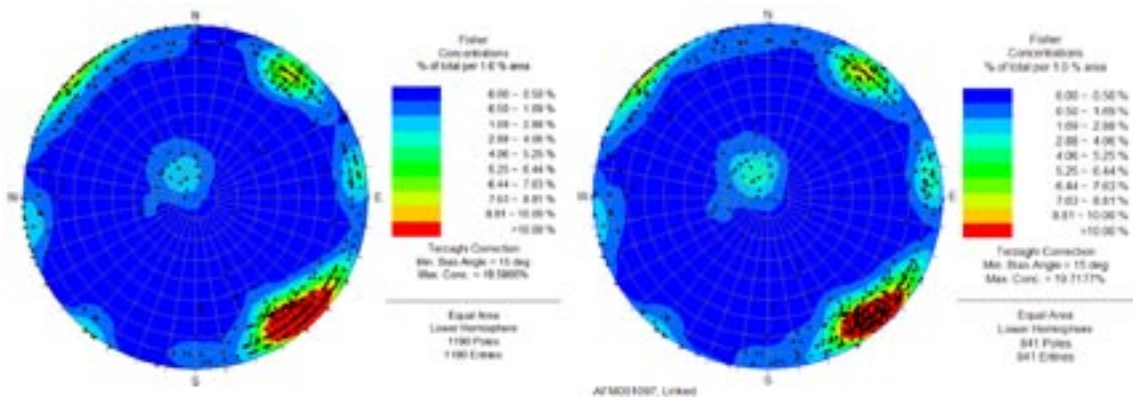
Figure 4-3. *Contoured stereonet plots of unlinked (left) and linked (right) fracture traces, Outcrop AFM001097.*
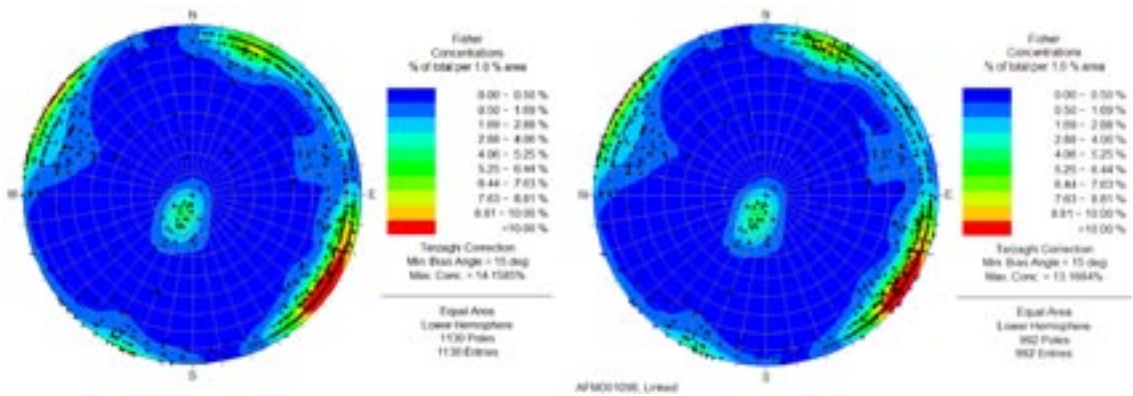
Figure 4-4. *Contoured stereonet plots of unlinked (left) and linked (right) fracture traces, Outcrop AFM001098.*
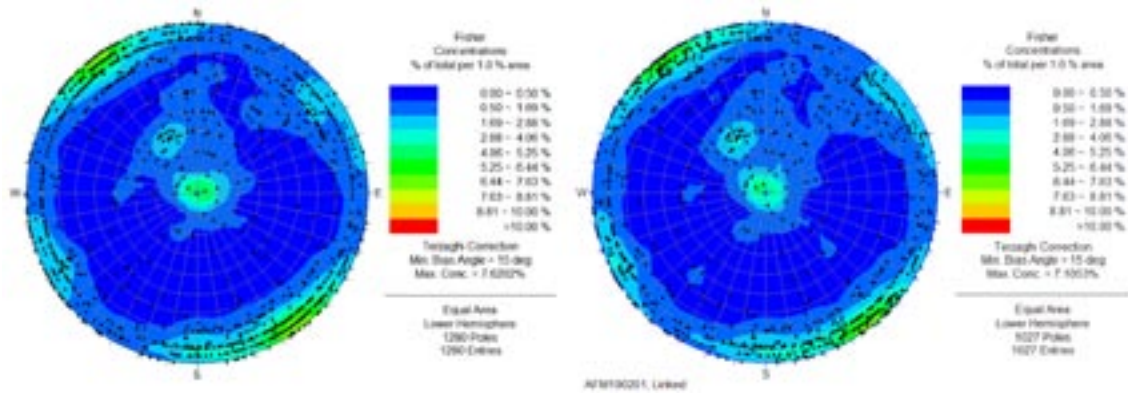
Figure 4-5. *Contoured stereonet plots of unlinked (left) and linked (right) fracture traces, Outcrop AFM100201.*
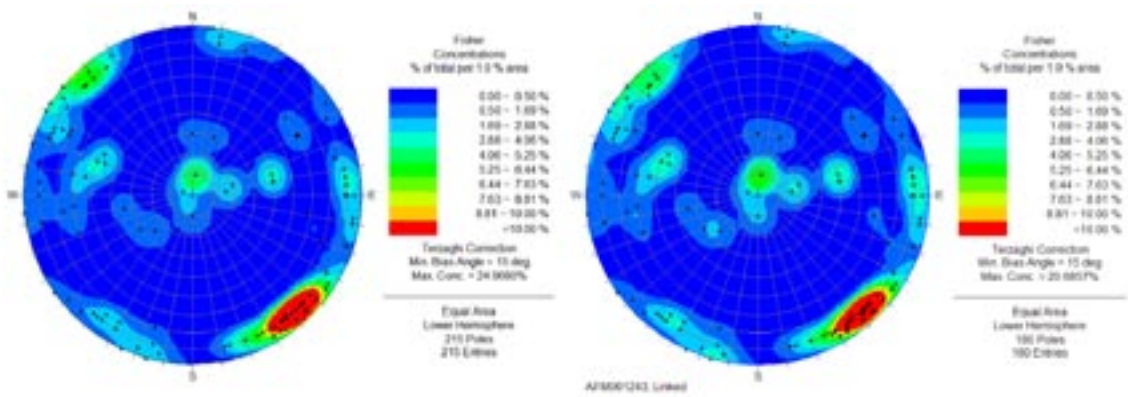
Figure 4-6. *Contoured stereonet plots of unlinked (left) and linked (right) fracture traces, Outcrop AFM001243.*
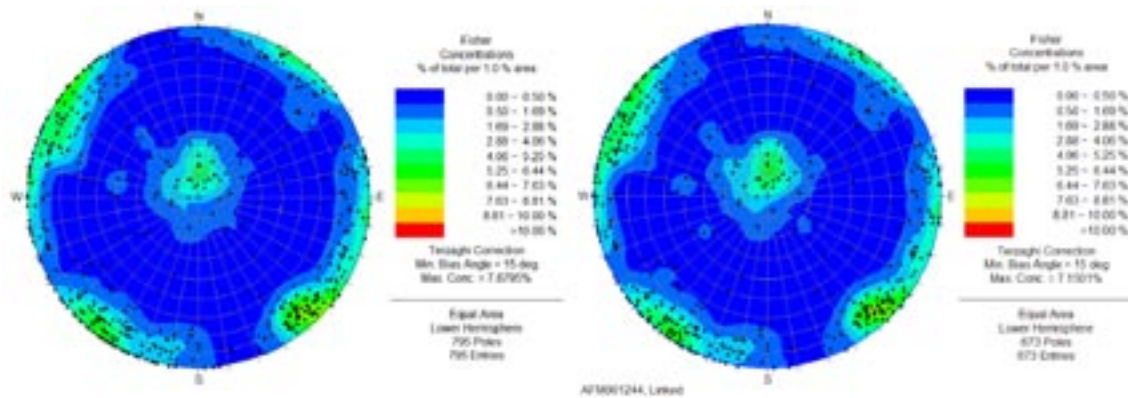
Figure 4-7. *Contoured stereonet plots of unlinked (left) and linked (right) fracture traces, Outcrop AFM001244.*
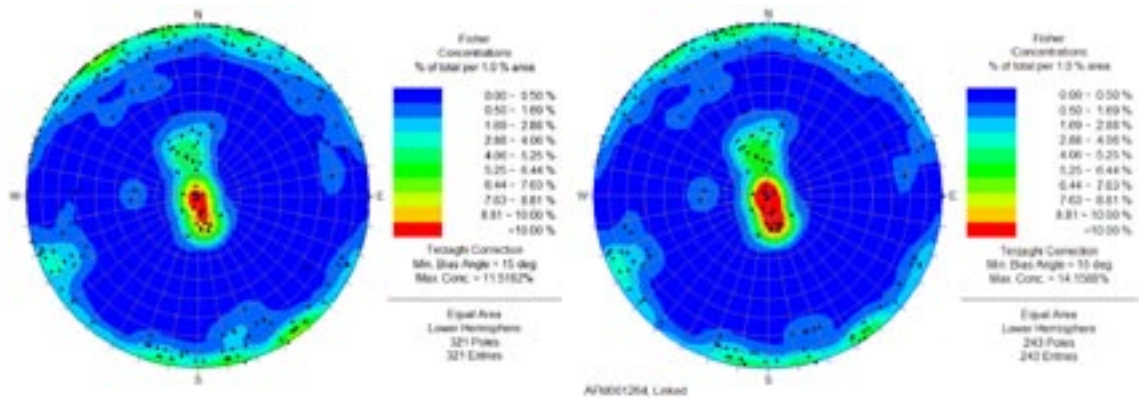
Figure 4-8. *Contoured stereonet plots of unlinked (left) and linked (right) fracture traces, Outcrop AFM001264.*
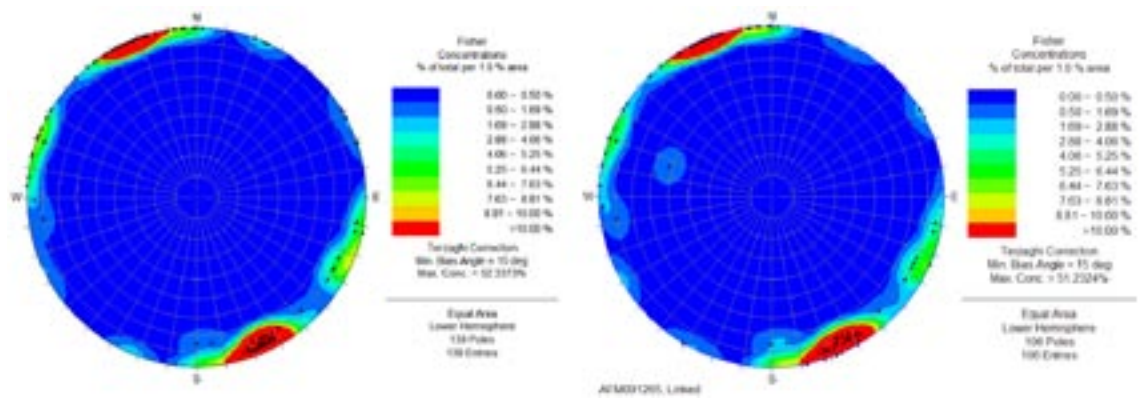
Figure 4-9. *Contoured stereonet plots of unlinked (left) and linked (right) fracture traces, Outcrop AFM001265.*

In general, the contoured stereonet plots showed at least four distinct concentrations of fracture poles per outcrop, suggesting a minimum of four fracture sets. Mapped trace parameters (mineral fillings, aperture, length, alteration, and fracture morphology) were also plotted using symbolic stereonets; an example is presented below (Figure 4-10).
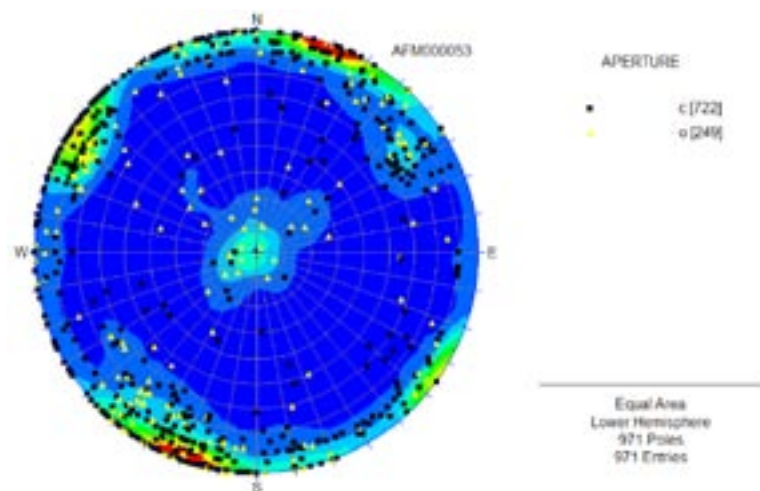
Figure 4-10. *Example of a symbolic pole plot. Figure shows unlinked traces from outcrop AFM00053, classified in terms of fracture aperture ('o' = open, or 'c' = sealed).*

A qualitative analysis of trace parameters showed no easily visible geologic relationships between the trace sets. Note that a more extensive statistical analysis was conducted during the spatial model development; the qualitative analysis only served to help guide the division of traces into orientation sets. Alteration, fracture morphology (stepped versus planar), and fracture roughness showed no visible relationships inside or between sets. Fracture aperture (open versus sealed) did show a few interesting patterns:

- AFM000053: Subhorizontally-oriented traces were predominantly mapped as open. The apertures of the remainder of the traces were a mix of open and sealed.

- AFM000054: Subhorizontally-oriented traces were predominantly mapped as open. The NNW-striking traces appeared to have more open fractures than the other vertical traces.

- AFM001097: Subhorizontally- and east-west-oriented traces were predominantly mapped as sealed, with open fractures largely confined to NE and NW striking traces.

- AFM001098: Open fractures were confined to the NNE striking traces.

- AFM001243: No visible relationships.

- AFM001244: The NS-striking traces were predominantly mapped as sealed, with no other visible relationships in the other trace sets.

- AFM001265: The ENE-striking traces were predominantly mapped as open, with no other visible relationships in the other trace sets.

- AFM100201: This outcrop appears to be anomalous; most traces on the outcrop, regardless of orientation, have been mapped as open. This is a different behavior from all other outcrops.

However, the aperture results were not consistent between 'sets' or between outcrops; there was not a single pattern that could be used as a predictor for set membership. The symbolic pole plots suggested that orientation, combined with trace lengths and trace termination relationships, would be the most useful factors for delineating fracture sets on the outcrops.

Assignment of outcrop fractures to fracture sets

With the aid of the fracture pole plots, initial hard-sector set assignments are made based on fracture strike orientation. Note that true strike, rather than apparent strike, was used to divide the sets. While the set assignment was fundamentally a hard-sector operation (there were no fuzzy orientation boundaries), the trace maps were reviewed and some fractures were manually re-assigned from one set to another based on termination relationships or discrepancies in apparent strike. In general, fewer than five fractures per outcrop required manual re-assignment. The fracture set assignment was done inside ArcGIS 9.1.

Sets were labeled based on the dominant orientation of each trace set; i.e. NE set, WNW set, and so on. This allowed for a consistent set terminology across outcrops, even when the set mean poles did not quite match due to apparent pole rotations, local geologic controls, or local stress field variations.

Though sets were identified for both linked and unlinked trace data, only the linked trace data set was carried through the full orientation model parameterization. As such, only the set fits for the linked trace data are presented in this report. Figure 4-11 through Figure 4-19 illustrates the relationships between the trace sets at the detail mapped outcrops.

Once the 'hard-sectored' assignment of outcrop traces to orientation sets was completed, the resulting classified trace data was fed into FracSys/ISIS /Dershowitz et al. 1998/ to fit spherical probability distributions for the trace data. The ISIS results are presented in Table 4-1 through Table 4-9. For Kolmogorov-Smirnov goodness-of-fit testing, the null hypothesis is that the observed poles are samples from the hypothesized spherical probability distribution (Fisher, Bivariate Bingham, etc). A rejection of the null hypothesis suggests that the distribution of poles is not well-simulated by the current probability distribution. An $\alpha = 0.05$ was used as the level of significance for the goodness-of-fit testing.

Note that at this point, sets are defined solely on an outcrop-by-outcrop basis; the NE set on one outcrop may not have the same mean pole and concentration parameters as on another outcrop. However, the sets in the two outcrops will have the same general strike orientation (i.e. both sets of traces generally strike northeasterly).

Figure 4-11. *Fracture sets (linked) identified through trace data analysis, Outcrop AFM000053.*
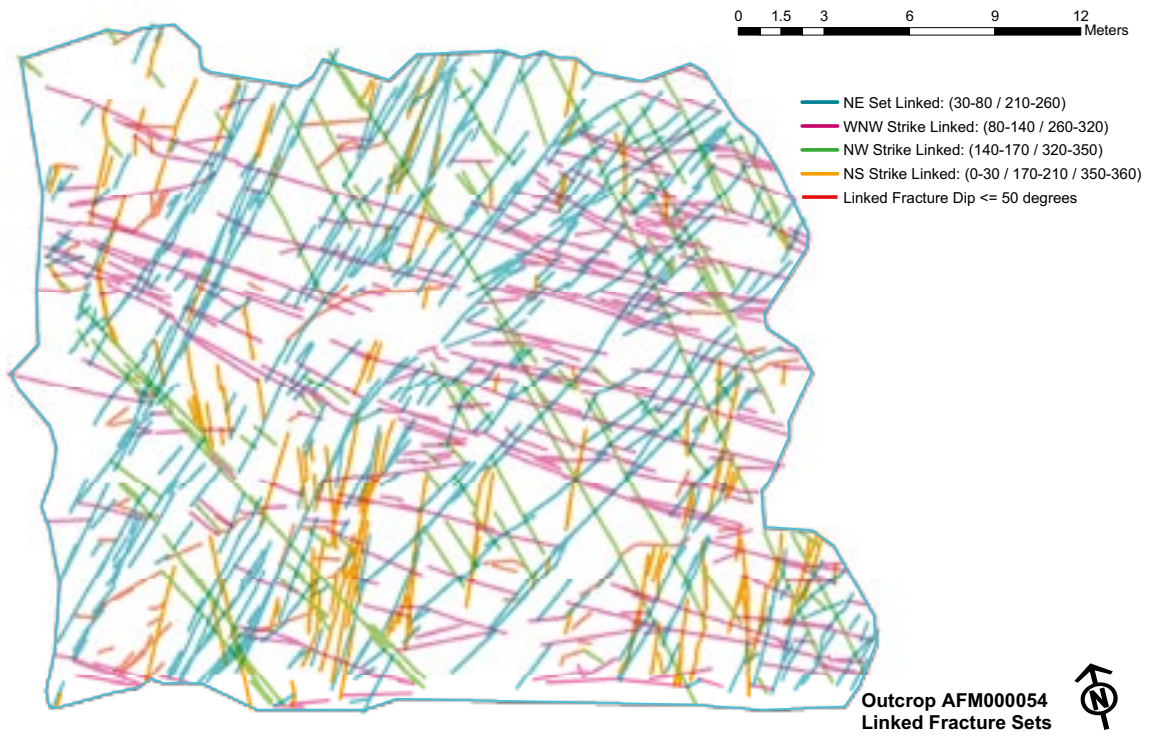
Figure 4-12. *Fracture sets (linked) identified through trace data analysis, Outcrop AFM000054.*
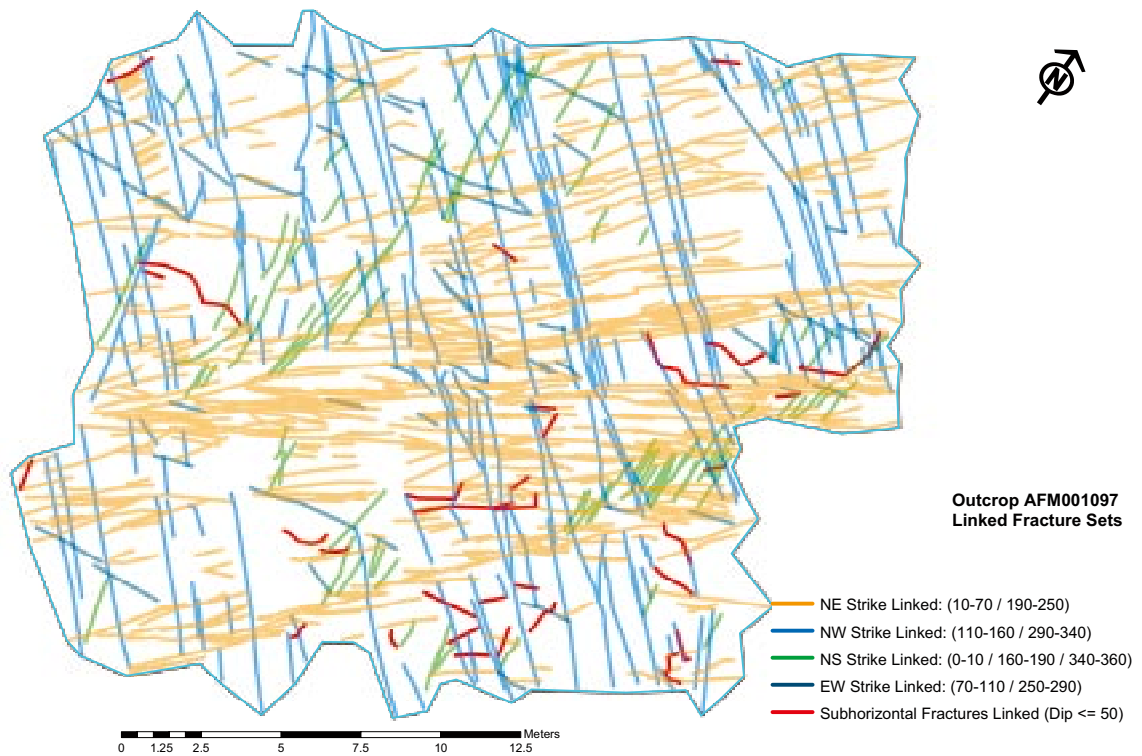
Figure 4-13. *Fracture sets (linked) identified through trace data analysis, Outcrop AFM001097.*

**Outcrop AFM001098
Linked Fracture Sets**

——	WNW Strike: (70-130 / 250-310)
——	NW Strike: (130-180 / 310-360)
——	NNE Strike: (0-30 / 180-210)
——	NE Strike: (30-70 / 210-250)
——	Subhorizontal Fractures (Dip <= 50)
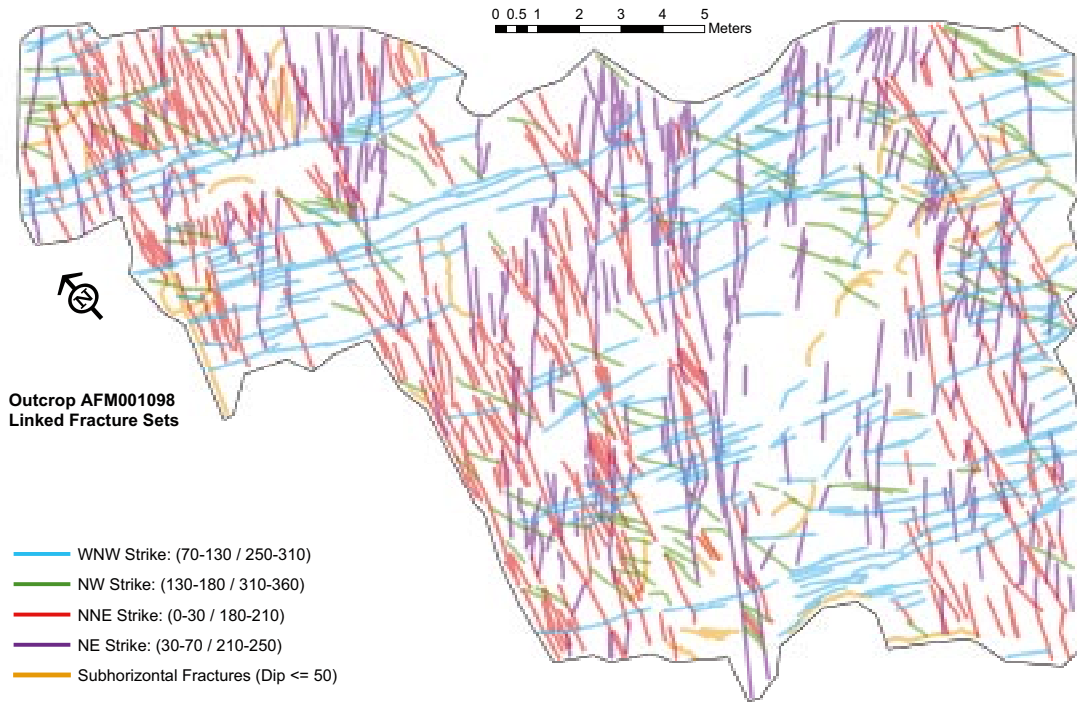
Figure 4-14. *Fracture sets (linked) identified through trace data analysis, Outcrop AFM001098.*

**Outcrop AFM100201
Linked Fracture Sets**

——	NS Strike Linked: (0-30/170-210/350-360)
——	NE Strike Linked: (30-70 / 210-250)
——	EW Strike Linked: (70-120 / 250-290)
——	NW Strike Linked: (120-170 / 300-350)
——	Subhorizontal Fractures Linked (Dip <= 50)

Figure 4-15. *Fracture sets (linked) identified through trace data analysis, Outcrop AFM100201.*

58
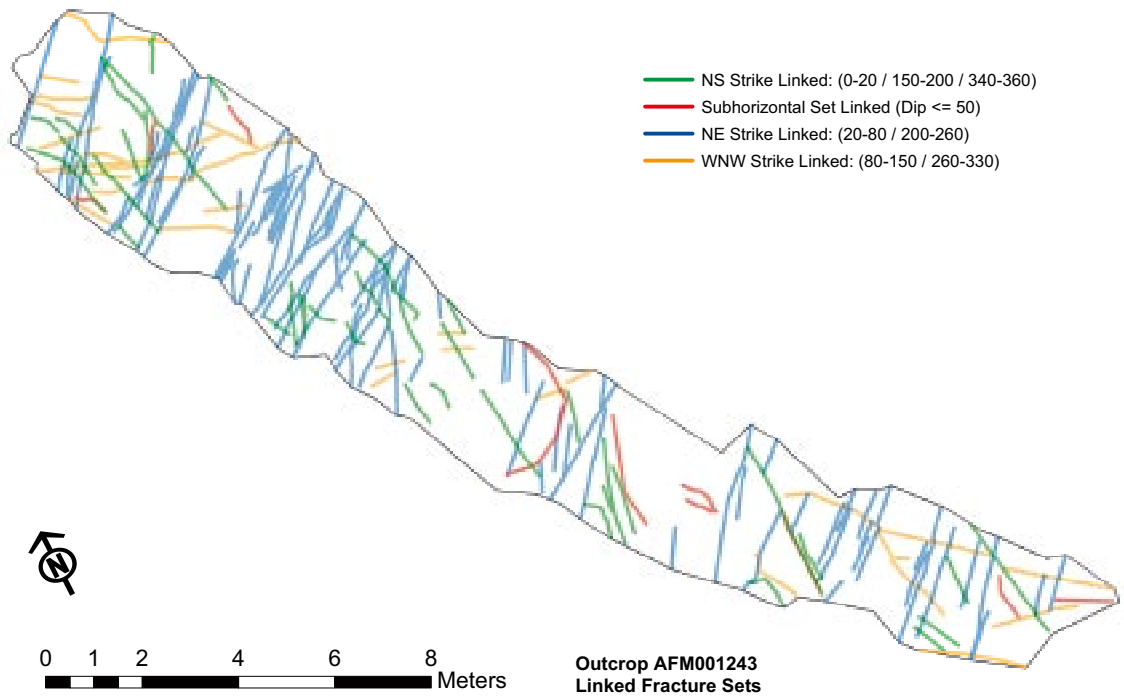
Figure 4-16. Fracture sets (linked) identified through trace data analysis, Outcrop AFM001243.
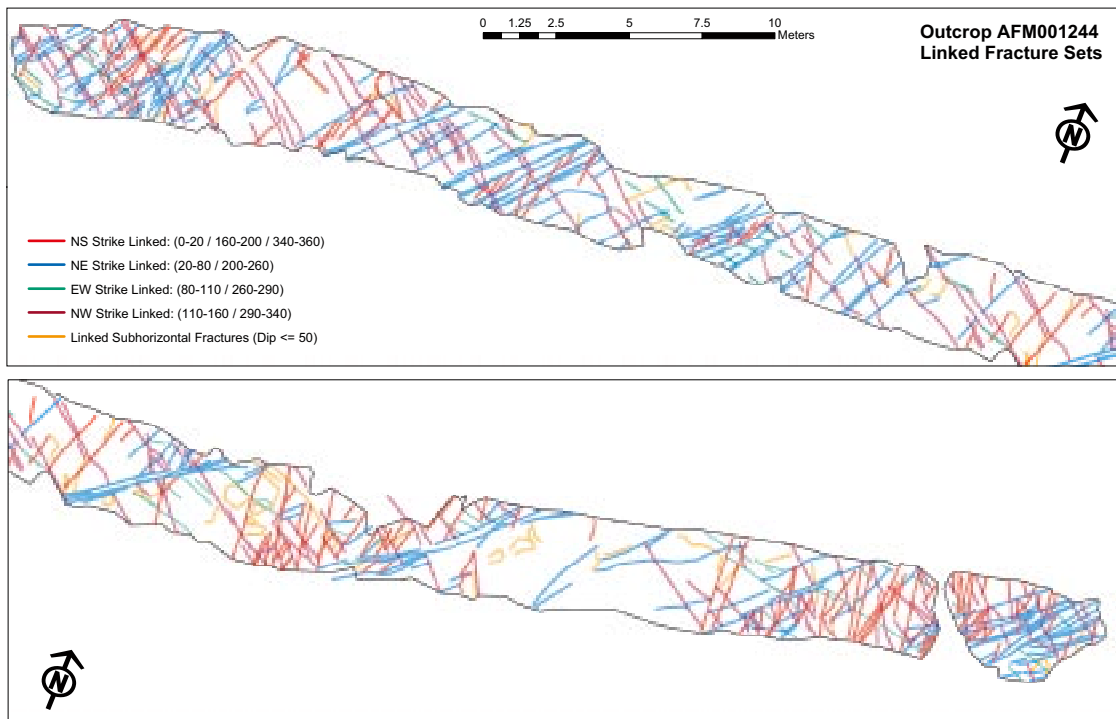
Figure 4-17. Fracture sets (linked) identified through trace data analysis, Outcrop AFM001244.
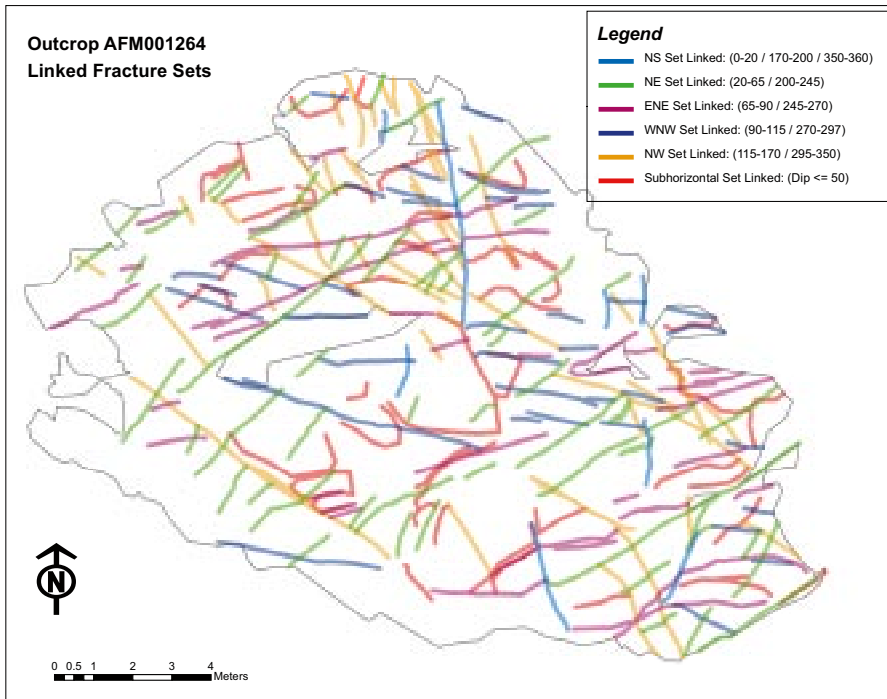
Figure 4-18. *Fracture sets (linked) identified through trace data analysis, Outcrop AFM001264.*

Figure 4-19. *Fracture sets (linked) identified through trace data analysis, Outcrop AFM001265.*

60

Table 4-1. Results of ISIS analysis of linked traces on outcrop AFM000053.

Set ID	# of Fracs.w	Probability distribution	Mean pole		Major axis*		Dispersion			Goodness of fit		K-S crit	Reject null
			Trend	Plunge	Trend	Plunge	$\kappa/\kappa 1$	$\kappa 2$	$\kappa 12$	K-S Stat	% Conf.	$\alpha = 0.05$	Hypothesis?
WNW	244	Fisher	197.1	1.9	NA	NA	51.20	NA	NA	0.143	0.01%	0.087	YES
WNW	244	Bivariate Normal	197.1	1.9	17.1	88.1	7.55	8.57	0.19	0.141	0.01%	0.087	YES
WNW	244	Bivariate Fisher	197.1	1.9	106.1	27.2	24.28	25.00	NA	0.295	0.00%	0.087	YES
WNW	244	Bivariate Bingham	197.1	1.9	106.1	27.2	−34.30	−22.21	NA	0.104	2.80%	0.087	YES
ENE	94	Fisher	164.8	1.2	344.8	88.8	44.00	NA	NA	0.074	67.60%	0.140	NO
ENE	94	Bivariate Normal	164.8	1.2	344.8	88.8	9.00	8.37	0.10	0.087	48.00%	0.140	NO
ENE	94	Bivariate Fisher	164.9	1.1	72.6	64.4	24.64	25.00	NA	0.310	0.00%	0.140	YES
ENE	94	Bivariate Bingham	164.9	1.1	72.6	64.4	−26.54	−20.59	NA	0.100	36.00%	0.140	NO
NE	199	Fisher	303.8	2.1	123.8	87.9	39.87	NA	NA	0.117	0.90%	0.096	YES
NE	199	Bivariate Normal	303.8	2.0	123.8	88.0	8.97	9.32	0.22	0.101	3.40%	0.096	YES
NE	199	Bivariate Fisher	303.7	2.2	35.6	40.0	24.31	25.00	NA	0.234	0.00%	0.096	YES
NE	199	Bivariate Bingham	303.7	2.2	35.6	40.0	−27.19	−17.40	NA	0.099	7.60%	0.096	YES
NS	27	Fisher	91.0	1.4	271.0	88.6	41.05	NA	NA	0.186	31.00%	0.254	NO
NS	27	Bivariate Normal	91.0	1.6	271.0	88.4	4.74	11.85	0.23	0.157	52.10%	0.254	NO
NS	27	Bivariate Fisher	91.0	1.0	0.9	6.1	22.73	25.00	NA	0.106	92.70%	0.254	NO
NS	27	Bivariate Bingham	91.0	1.0	0.9	6.1	−79.89	−26.59	NA	0.244	8.80%	0.254	NO
NW	188	Fisher	46.4	1.2	226.4	88.8	16.83	NA	NA	0.042	88.80%	0.099	NO
NW	188	Bivariate Normal	46.7	1.2	226.7	88.8	13.37	14.95	0.19	0.048	77.10%	0.099	NO
NW	188	Bivariate Fisher	46.0	1.1	315.4	26.6	16.81	18.00	NA	0.135	0.60%	0.099	YES
NW	188	Bivariate Bingham	46.0	1.1	315.4	26.6	−12.22	−7.99	NA	0.054	75.00%	0.099	NO
SH	60	Fisher	322.4	83.9	142.4	6.1	8.22	NA	NA	0.123	32.30%	0.176	NO
SH	60	Bivariate Normal	66.7	65.2	246.7	24.8	117.16	15.81	−0.13	0.172	5.80%	0.176	NO
SH	60	Bivariate Fisher	322.7	83.5	124.0	6.2	7.98	8.64	NA	0.115	44.60%	0.176	NO
SH	60	Bivariate Bingham	322.7	83.5	124.0	6.2	−6.10	4.96	NA	0.135	25.60%	0.176	NO

Table 4-2. Results of ISIS analysis of linked traces on outcrop AFM000054.

Set ID	# of Fracs.	Probability distribution	Mean pole Trend	Plunge	Major axis* Trend	Plunge	Dispersion κ/κ_1	κ_2	κ_{12}	Goodness of fit K-S stat	% Conf.	K-S crit $\alpha = 0.05$	Reject null Hypothesis?
WNW	324	Fisher	205.6	5.2	25.6	84.8	29.94	NA	NA	0.108	0.10%	0.076	YES
WNW	324	Bivariate Normal	205.5	5	25.5	85	11.66	9.43	−0.07	0.116	0.03%	0.076	YES
WNW	324	Bivariate Fisher	205.7	5.1	324.0	79.3	24.22	25.00	NA	0.119	0.20%	0.076	YES
WNW	324	Bivariate Bingham	205.7	5.1	324.0	79.3	−19.86	−13.60	NA	0.085	5.80%	0.076	YES
NE	413	Fisher	139.6	0.9	319.6	89.1	27.52	NA	NA	0.082	0.80%	0.067	YES
NE	413	Bivariate Normal	139.7	0.9	319.7	89.1	11.72	10.31	0.33	0.092	0.20%	0.067	YES
NE	413	Bivariate Fisher	139.4	0.9	48.2	54.3	23.00	24.50	NA	0.067	15.00%	0.067	YES
NE	413	Bivariate Bingham	139.4	0.9	48.2	54.3	−22.24	−11.30	NA	0.057	29.70%	0.067	NO
NS	156	Fisher	288.0	7.3	108.0	82.7	23.71	NA	NA	0.072	39.00%	0.109	NO
NS	156	Bivariate Normal	288.0	7.1	108.0	82.9	11.10	12.65	−0.30	0.117	2.80%	0.109	YES
NS	156	Bivariate Fisher	288.1	7.3	193.6	31.5	21.22	22.75	NA	0.146	0.60%	0.109	YES
NS	156	Bivariate Bingham	288.1	7.3	193.6	31.5	−18.63	−9.98	NA	0.087	26.40%	0.109	NO
NW	118	Fisher	246.9	3.9	66.9	86.1	44.34	NA	NA	0.061	77.80%	0.125	NO
NW	118	Bivariate Normal	246.9	3.8	66.9	86.2	7.66	9.57	0.12	0.063	73.20%	0.125	NO
NW	118	Bivariate Fisher	246.9	3.9	337.9	14.0	24.30	25.00	NA	0.262	0.00%	0.125	YES
NW	118	Bivariate Bingham	246.9	3.9	337.9	14.0	−31.12	−18.67	NA	0.076	58.40%	0.125	NO
SH	61	Fisher	342.1	74.4	162.1	15.6	10.19	NA	NA	0.100	58.00%	0.174	NO
SH	61	Bivariate Normal	24.3	62.7	204.3	27.3	87.50	12.18	−0.04	0.095	63.50%	0.174	NO
SH	61	Bivariate Fisher	342.9	73.2	95.7	6.7	9.34	11.56	NA	0.195	2.50%	0.174	YES
SH	61	Bivariate Bingham	342.9	73.2	95.7	6.7	−9.80	−4.90	NA	0.115	43.00%	0.174	NO

Table 4-3. Results of ISIS analysis of linked traces on outcrop AFM001097.

Set ID	# of Fracs.	Probability distribution	Mean pole Trend	Plunge	Major axis* Trend	Plunge	Dispersion κ / $\kappa1$	$\kappa2$*	$\kappa12$*	Goodness of fit K-S stat	% Conf.	K-S Crit $\alpha = 0.05$	Reject null Hypothesis?
EW	57	Fisher	173.6	1.8	353.6	88.2	25.87	NA	NA	0.116	42.40%	0.180136	NO
EW	57	Bivariate Normal	173.3	1.8	353.7	88.2	9.95	12.61	−0.04	0.124	34.30%	0.180136	NO
EW	57	Bivariate Fisher	173.5	1.7	263.7	5.0	22.70	23.75	NA	0.159	13.10%	0.180136	NO
EW	57	Bivariate Bingham	173.5	1.7	263.7	5.0	−18.21	−11.46	NA	0.133	29.60%	0.180136	NO
NE	498	Fisher	137.3	8.5	317.3	81.5	36.38	NA	NA	0.055	9.50%	0.060943	NO
NE	498	Bivariate Normal	137.3	8.3	317.3	81.7	10.63	8.52	0.34	0.071	1.20%	0.060943	YES
NE	498	Bivariate Fisher	137.3	8.5	32.0	60.4	23.76	25.00	NA	0.159	0.00%	0.060943	YES
NE	498	Bivariate Bingham	137.3	8.5	32.0	60.4	−30.55	−14.29	NA	0.067	10.20%	0.060943	YES
NS	90	Fisher	82.8	3.9	262.8	86.1	36.10	NA	NA	0.211	0.07%	0.143357	YES
NS	90	Bivariate Normal	82.8	3.9	262.8	86.1	6.85	11.81	−0.11	0.137	6.90%	0.143357	NO
NS	90	Bivariate Fisher	82.7	3.7	173.1	5.7	23.30	25.00	NA	0.152	4.30%	0.143357	YES
NS	90	Bivariate Bingham	82.7	3.7	173.1	5.7	−38.55	−13.34	NA	0.092	49.30%	0.143357	NO
NW	164	Fisher	38.7	10.0	218.7	80.0	49.93	NA	NA	0.188	0.00%	0.106198	YES
NW	164	Bivariate Normal	38.8	10.0	218.8	80.0	8.10	8.43	0.01	0.190	0.00%	0.106198	YES
NW	164	Bivariate Fisher	38.6	9.9	132.0	18.4	24.82	25.00	NA	0.395	0.00%	0.106198	YES
NW	164	Bivariate Bingham	38.6	9.9	132.0	18.4	−28.71	−24.84	NA	0.160	0.10%	0.106198	YES
SH	32	Fisher	318.6	77.4	138.6	12.6	23.01	NA	NA	0.187	21.60%	0.240416	NO
SH	32	Bivariate Normal	17.5	70.8	197.5	19.2	100.36	8.69	−0.22	0.119	75.80%	0.240416	NO
SH	32	Bivariate Fisher	319.3	76.9	72.1	5.1	21.17	22.78	NA	0.116	79.60%	0.240416	NO
SH	32	Bivariate Bingham	319.3	76.9	72.1	5.1	−19.04	−9.90	NA	0.097	93.00%	0.240416	NO

Table 4-4. Results of ISIS analysis of linked traces on outcrop AFM001098.

Set ID	# of . Fracs	Probability distribution	Mean pole Trend	Plunge	Major axis* Trend	Plunge	Dispersion κ / $\kappa1$	$\kappa2$	$\kappa12$	Goodness of fit K-S stat	% Conf.	K-S crit $\alpha = 0.05$	Reject null Hypothesis?
NNE	306	Fisher	108.3	1.1	288.3	88.9	35.07	NA	NA	0.106	0.20%	0.078	YES
NNE	306	Bivariate Normal	108.3	1.1	288.3	89.0	7.97	11.25	−0.15	0.049	46.70%	0.078	NO
NNE	306	Bivariate Fisher	108.3	1.3	198.6	11.1	23.79	25.00	NA	0.128	0.10%	0.078	YES
NNE	306	Bivariate Bingham	108.3	1.3	198.6	11.1	−28.57	−14.04	NA	0.050	61.40%	0.078	NO
WNW	229	Fisher	20.8	5.1	200.8	84.9	32.58	NA	NA	0.173	0.00%	0.090	YES
WNW	229	Bivariate Normal	20.7	5.0	200.7	85.0	11.43	8.71	0.06	0.193	0.00%	0.090	YES
WNW	229	Bivariate Fisher	21.0	5.2	148.2	81.4	24.04	25.00	NA	0.189	0.00%	0.090	YES
WNW	229	Bivariate Bingham	21.0	5.2	148.2	81.0	−23.64	−14.13	NA	0.136	0.20%	0.090	YES
NE	285	Fisher	133.2	3.9	313.2	86.1	50.63	NA	NA	0.110	0.20%	0.081	YES
NE	285	Bivariate Normal	133.2	3.9	313.2	86.1	8.98	7.15	−0.10	0.120	0.05%	0.081	YES
NE	285	Bivariate Fisher	133.1	4.0	243.0	78.4	24.44	25.00	NA	0.354	0.00%	0.081	YES
NE	285	Bivariate Bingham	133.1	4.0	243.0	78.4	−34.54	−21.66	NA	0.121	0.30%	0.081	YES
NW	121	Fisher	63.1	9.9	243.1	80.1	22.22	NA	NA	0.087	32.50%	0.124	NO
NW	121	Bivariate Normal	63.1	9.7	243.1	80.3	13.69	10.98	0.23	0.083	38.20%	0.124	NO
NW	121	Bivariate Fisher	63.2	9.9	312.9	63.3	20.62	22.04	NA	0.061	81.30%	0.124	NO
NW	121	Bivariate Bingham	63.2	9.9	312.9	63.3	−17.05	−9.69	NA	0.064	77.60%	0.124	NO
SH	51	Fisher	214.8	86.4	34.8	3.6	8.79	NA	NA	0.171	10.20%	0.168	YES
SH	51	Bivariate Normal	199.3	66.0	19.3	24.0	82.10	14.65	0.04	0.148	21.70%	0.168	NO
SH	51	Bivariate Fisher	212.4	84.9	334.8	2.8	8.70	9.30	NA	0.171	11.70%	0.168	YES
SH	51	Bivariate Bingham	212.4	84.9	334.8	2.8	−6.46	−5.34	NA	0.190	6.10%	0.168	YES

Table 4-5. Results of ISIS analysis of linked traces on outcrop AFM100201.

Set ID	# of Fracs	Probability distribution	Mean pole Trend	Plunge	Major axis* Trend	Plunge	Dispersion κ / κ1	κ2	κ12	Goodness of Fit K-S stat	% Conf.	K-S crit α = 0.05	Reject null Hypothesis?
EW	154	Fisher	178.8	3.2	358.8	86.8	18.84	NA	NA	0.048	86.60%	0.110	NO
EW	154	Bivariate Normal	178.9	3.0	358.9	87.0	13.22	13.62	−0.06	0.054	75.50%	0.110	NO
EW	154	Bivariate Fisher	178.5	3.4	269.4	15.7	19.35	19.68	NA	0.046	93.70%	0.110	NO
EW	154	Bivariate Bingham	178.5	3.4	269.4	15.7	−11.35	−10.01	NA	0.049	90.40%	0.110	NO
NE	266	Fisher	141.2	0.3	321.2	89.7	29.65	NA	NA	0.043	71.10%	0.083	NO
NE	266	Bivariate Normal	141.2	0.3	321.2	89.7	10.06	11.16	0.03	0.046	61.50%	0.083	NO
NE	266	Bivariate Fisher	141.3	0.4	51.2	6.3	24.53	25.00	NA	0.053	59.30%	0.083	NO
NE	266	Bivariate Bingham	141.3	0.4	51.2	6.3	−17.96	−14.37	NA	0.040	89.10%	0.083	NO
NS	67	Fisher	280.9	0.3	100.9	89.7	25.86	NA	NA	0.163	5.70%	0.147	YES
NS	67	Bivariate Normal	280.9	0.3	100.9	89.7	11.61	11.08	−0.05	0.181	2.50%	0.147	YES
NS	67	Bivariate Fisher	281.0	0.3	190.3	62.2	23.36	23.67	NA	0.217	0.60%	0.147	YES
NS	67	Bivariate Bingham	281.0	0.3	190.3	62.2	−14.91	−13.07	NA	0.169	5.60%	0.147	YES
NW	152	Fisher	57.0	3.8	237.0	86.2	17.09	NA	NA	0.128	1.30%	0.110	YES
NW	152	Bivariate Normal	56.8	3.7	236.8	86.3	12.96	15.08	−0.17	0.117	3.00%	0.110	YES
NW	152	Bivariate Fisher	57.2	3.8	148.8	22.2	16.89	18.20	NA	0.151	0.50%	0.110	YES
NW	152	Bivariate Bingham	57.2	3.8	148.8	22.2	−12.57	−7.93	NA	0.138	1.30%	0.110	YES
SH	99	Fisher	346.6	76.4	166.6	13.6	7.97	NA	NA	0.074	65.60%	0.121	NO
SH	99	Bivariate Normal	22.8	61.1	202.8	28.9	89.15	13.84	−0.25	0.078	57.60%	0.121	NO
SH	99	Bivariate Fisher	345.5	74.6	246.6	2.4	7.36	8.74	NA	0.048	98.40%	0.121	NO
SH	99	Bivariate Bingham	345.5	74.6	246.6	2.4	−6.86	−4.36	NA	0.085	52.60%	0.121	NO

Table 4-6. Results of ISIS analysis of linked traces on outcrop AFM001243.

Set ID	# of Fracs.	Probability distribution	Mean pole Trend	Plunge	Major axis* Trend	Plunge	Dispersion κ / κ1	κ2	κ12	Goodness of fit K-S stat	% Conf.	K-S crit α = 0.05	Reject null Hypothesis?
NE	98	Fisher	137.8	4.7	317.8	85.3	34.43	NA	NA	0.154	1.90%	0.137381	YES
NE	98	Bivariate Normal	137.8	4.5	317.8	85.5	11.23	8.30	0.34	0.185	0.30%	0.137381	YES
NE	98	Bivariate Fisher	137.8	4.8	37.9	64.2	23.46	25.00	NA	0.087	50.60%	0.137381	NO
NE	98	Bivariate Bingham	137.8	4.8	37.9	64.2	−31.62	−13.11	NA	0.185	0.40%	0.137381	YES
NS	42	Fisher	269.8	2.8	89.8	87.2	6.10	NA	NA	0.194	8.30%	0.209853	NO
NS	42	Bivariate Normal	93.1	0.7	273.1	89.3	24.04	31.84	0.03	0.291	0.20%	0.209853	YES
NS	42	Bivariate Fisher	270.3	3.8	179.9	7.0	2.00	7.13	NA	0.260	0.90%	0.209853	YES
NS	42	Bivariate Bingham	270.3	3.8	179.9	7.0	−19.09	−6.36	NA	0.289	0.20%	0.209853	YES
SH	10	Fisher	335.6	80.3	155.6	9.7	14.20	NA	NA	0.271	45.50%	0.409	NO
SH	10	Bivariate Normal	41.6	70.1	221.6	19.9	94.05	13.13	0.05	0.280	41.30%	0.409	NO
SH	10	Bivariate Fisher	341.9	80.8	160.0	9.2	14.15	14.88	NA	0.280	41.90%	0.409	NO
SH	10	Bivariate Bingham	341.9	80.8	160.0	9.2	−9.81	−7.42	NA	0.264	49.50%	0.409	NO
WNW	30	Fisher	209.6	1.1	29.6	88.9	16.14	NA	NA	0.110	85.90%	0.242	NO
WNW	30	Bivariate Normal	210.0	0.9	30.0	89.1	16.25	12.64	−0.41	0.147	53.90%	0.242	NO
WNW	30	Bivariate Fisher	208.9	1.8	302.2	60.7	15.64	17.93	NA	0.352	0.10%	0.242	YES
WNW	30	Bivariate Bingham	208.9	1.8	302.2	60.7	−15.26	−6.90	NA	0.174	34.10%	0.242	NO

Table 4-7. Results of ISIS analysis of linked traces on outcrop AFM001244.

Set ID	# of Fracs.	Probability distribution	Mean pole		Major axis*		Dispersion			Goodness of fit		K-S crit	Reject null
			Trend	Plunge	Trend	Plunge	κ / κ1	κ2*	κ12*	K-S stat	% Conf.	α = 0.05	Hypothesis?
EW	57	Fisher	188.7	5.1	8.7	84.9	29.25	NA	NA	0.124	34.30%	0.180	NO
EW	57	Bivariate Normal	188.7	5.1	8.7	84.9	8.03	12.86	0.13	0.114	44.40%	0.180	NO
EW	57	Bivariate Fisher	188.8	5.0	98.2	5.8	23.05	25.00	NA	0.107	56.60%	0.180	NO
EW	57	Bivariate Bingham	188.8	5.0	98.2	5.8	−28.40	−11.20	NA	0.085	83.20%	0.180	NO
NE	238	Fisher	132.1	2.1	312.1	87.9	24.69	NA	NA	0.068	22.60%	0.088	NO
NE	238	Bivariate Normal	132.2	2.0	312.2	88.0	11.14	12.16	0.22	0.074	14.30%	0.088	NO
NE	238	Bivariate Fisher	132.0	2.2	40.6	32.7	22.17	23.26	NA	0.091	8.20%	0.088	YES
NE	238	Bivariate Bingham	132.0	2.2	40.6	32.7	−17.63	−11.00	NA	0.056	58.20%	0.088	NO
NS	146	Fisher	274.6	1.7	94.6	88.3	22.31	NA	NA	0.090	18.90%	0.113	NO
NS	146	Bivariate Normal	274.6	1.7	94.6	88.3	12.32	12.29	−0.34	0.108	6.70%	0.113	NO
NS	146	Bivariate Fisher	274.7	1.7	183.0	45.6	20.67	22.23	NA	0.171	0.10%	0.113	YES
NS	146	Bivariate Bingham	274.7	1.7	183.0	45.6	−17.83	−9.62	NA	0.065	64.90%	0.113	NO
NW	176	Fisher	219.8	0.7	39.8	89.3	17.89	NA	NA	0.165	0.01%	0.103	YES
NW	176	Bivariate Normal	218.8	1.2	38.8	88.8	18.45	16.58	−0.35	0.302	0.00%	0.103	YES
NW	176	Bivariate Fisher	219.6	1.8	309.7	2.3	18.65	20.65	NA	0.237	0.00%	0.103	YES
NW	176	Bivariate Bingham	219.6	1.8	309.7	2.3	−16.97	−8.24	NA	0.060	64.80%	0.103	NO
SH	56	Fisher	334.2	80.5	154.2	9.5	11.75	NA	NA	0.152	14.90%	0.182	NO
SH	56	Bivariate Normal	30.4	67.4	210.4	22.6	93.71	12.26	−0.04	0.104	58.50%	0.182	NO
SH	56	Bivariate Fisher	333.1	79.9	184.9	8.6	12.23	13.69	NA	0.166	10.60%	0.182	NO
SH	56	Bivariate Bingham	333.1	79.9	184.9	8.6	−9.45	−6.02	NA	0.149	18.80%	0.182	NO

Table 4-8. Results of ISIS analysis of linked traces on outcrop AFM001264.

Set ID	# of Fracs	Probability distribution	Mean pole Trend	Plunge	Major axis* Trend	Plunge	Dispersion $\kappa/\kappa 1$	$\kappa 2^*$	$\kappa 12^*$	Goodness of fit K-S stat	% Conf.	K-S crit $\alpha = 0.05$	Reject null Hypothesis?
ENE	38	Fisher	347.6	0.1	NA	NA	47.57	NA	NA	0.208	7.40%	0.221	NO
ENE	38	Bivariate Normal	347.6	0.1	167.6	89.9	5.73	10.34	−0.10	0.131	53.40%	0.221	NO
ENE	38	Bivariate Fisher	347.7	0.1	257.7	4.2	23.62	25.00	NA	0.284	0.50%	0.221	YES
ENE	38	Bivariate Bingham	347.7	0.1	257.7	4.2	−52.73	−17.57	NA	0.108	78.50%	0.221	NO
NE	59	Fisher	316.5	3.1	NA	NA	23.68	NA	NA	0.066	95.70%	0.177	NO
NE	59	Bivariate Normal	316.5	3.1	136.5	86.9	13.03	10.64	−0.19	0.077	87.70%	0.177	NO
NE	59	Bivariate Fisher	316.7	2.8	219.1	69.3	21.51	22.71	NA	0.168	8.50%	0.177	NO
NE	59	Bivariate Bingham	316.7	2.8	219.1	69.3	−17.23	−10.43	NA	0.073	93.10%	0.177	NO
NS	9	Fisher	91.3	6.3	NA	NA	17.59	NA	NA	0.208	83.10%	0.453	NO
NS		Bivariate Normal											
NS		Bivariate Fisher	No other distributions tested due to very small sample size										
NS		Bivariate Bingham											
NW	53	Fisher	232.9	1.9	NA	NA	19.69	NA	NA	0.105	59.90%	0.187	NO
NW	53	Bivariate Normal	233.0	1.8	53.0	88.2	14.73	11.13	−0.50	0.288	0.03%	0.187	YES
NW	53	Bivariate Fisher	233.1	1.9	139.9	58.9	17.44	20.39	NA	0.202	3.20%	0.187	YES
NW	53	Bivariate Bingham	233.1	1.9	139.9	58.9	−23.17	−7.72	NA	0.097	73.30%	0.187	NO
WNW	38	Fisher	12.2	0.9	NA	NA	54.98	NA	NA	0.086	93.90%	0.221	NO
WNW	38	Bivariate Normal	12.2	0.9	192.2	89.1	6.29	9.02	0.00	0.093	89.50%	0.221	NO
WNW	38	Bivariate Fisher	12.2	0.7	282.2	2.0	24.24	25.00	NA	0.363	0.01%	0.221	YES
WNW	38	Bivariate Bingham	12.2	0.7	282.2	2.0	−43.62	−21.56	NA	0.070	99.40%	0.221	NO
SH	46	Fisher	336.3	83.7	NA	NA	19.53	NA	NA	0.137	35.10%	0.201	NO
SH	46	Bivariate Normal	61.4	73.8	241.4	16.2	101.10	10.87	0.21	0.203	4.50%	0.201	YES
SH	46	Bivariate Fisher	336.2	84.0	80.0	1.4	16.57	20.19	NA	0.128	46.90%	0.201	NO
SH	46	Bivariate Bingham	336.2	84.0	80.0	1.4	−29.66	−9.89	NA	0.093	83.90%	0.201	NO

Table 4-9. Results of ISIS analysis of linked traces on outcrop AFM001265.

Set ID	# of . Fracs	Probability distribution	Mean pole Trend	Plunge	Major axis* Trend	Plunge	Dispersion κ/ κ1	κ2	κ12	Goodness of fit K-S stat	% Conf.	K-S crit α = 0.05	Reject null Hypothesis?
EW	13	Fisher	180.9	2.3	0.9	87.7	47.45	NA	NA	0.250	39.20%	0.361	NO
EW	13	Bivariate Normal	181.0	2.3	1.0	87.7	10.52	5.41	−0.14	0.337	10.40%	0.361	NO
EW	13	Bivariate Fisher	180.6	2.3	294.9	84.4	23.47	25.00	NA	0.251	39.60%	0.361	NO
EW	13	Bivariate Bingham	180.6	2.3	294.4	84.4	−58.51	−19.50	NA	0.236	47.10%	0.361	NO
NE	73	Fisher	156.2	2.8	336.2	87.2	100.00	NA	NA	0.291	0.00%	0.159176	YES
NE	73	Bivariate Normal	156.2	2.7	336.2	87.3	5.53	3.59	−0.13	0.190	1.00%	0.159176	YES
NE	73	Bivariate Fisher	156.2	2.7	264.3	81.2	24.66	25.00	NA	0.598	0.00%	0.159176	YES
NE	73	Bivariate Bingham	156.2	2.7	264.3	81.2	−24.66	−20.08	NA	0.544	0.00%	0.159176	YES
NW	2	Fisher	Two data points. Not fitted										
NW	2	Bivariate Normal											
NW	2	Bivariate Fisher											
NW	2	Bivariate Bingham											
NNE	18	Fisher	107.2	1.8	287.2	88.2	45.29	NA	NA	0.128	92.90%	0.309	NO
NNE	18	Bivariate Normal	107.2	1.8	287.2	88.2	10.84	5.41	0.59	0.167	69.90%	0.309	NO
NNE	18	Bivariate Fisher	107.3	1.9	12.0	70.8	22.82	25.00	NA	0.295	9.20%	0.309	NO
NNE	18	Bivariate Bingham	107.3	1.9	12.0	70.8	−94.56	−31.52	NA	0.258	19.00%	0.309	NO

4.1.2 Fracture sets identified in boreholes

In contrast to classification efforts in past SDMs, the ISIS outcrop set definitions were not directly imposed on the observed borehole fracture orientation population (i.e. through hard-sectoring). Instead, the set orientations were used as 'guides', and a complete orientation analysis was run on the borehole fracture data. However, the borehole set identification had to be based primarily on orientations; the extra data of termination relationships and fracture/trace size were not available for set delineation.

Borehole fracture data from SICADA (specifically, table p_fract_core_eshi) was imported to FracMan .ORS orientation sampling files. Data was organized first by fracture domain, then by borehole. The borehole fracture data was filtered based on the following criteria:

- VISIBLE_IN_BIPS = 1

- FRACTURE_DOMAIN = FFM01, FFM02, FFM03, or FFM06

- ACTIVITY_TEXT = GE041 (the combined BOREMAP/BIPS mapping results)

- DEFORMATION_ZONE = <blank>. Fractures inside mapped deformation zones included in the enhanced single-hole interpretation were not included in the analysis.

- 'AFFECTED_BY_DZ'. The Forsmark 2.2 geological DFN parameterization is based upon data outside of core intervals labeled 'affected by deformation zones'. Analyses were run to determine if, in terms of orientation, geology, or morphology, the fractures in these sections are different than the background fracturing in the rock mass. As of October 2007, fractures inside intervals affected by deformation zones are labeled in the SICADA table p_fract_core_eshi, in the data column FRACTURE_DOMAIN. This updated table was not available when the geological DFN modeling work was started. As such, the assignment of the 'Affected By DZ' label was done manually, using a draft version of p_fract_core_eshi (dated 20070319) and the limits of the Affected By DZ zones shipped as a component of the geological model (RFM_ZFM_FFM_tabell_20070425.xls). Copies of the relative tables were submitted to SKB as a component of the geological DFN model.

The resulting borehole data files were imported into FracSys/ISIS /Dershowitz et al. 1998/, where different spherical probability distributions were fitted to each borehole in each fracture domain. A mix of hard sectoring, soft sectoring, and sector pre-conditioning was used to subdivide the fractures into sets; this results in the preservation of some overlap between the sets. Fractures labeled 'affected by DZ' were modeled separately; however, the distinction was later found to have little to no effect on the orientation distributions.

The results of the ISIS analysis are presented in Table 4-10 through Table 4-13, while stereonets of the fracture sets are presented by set, borehole, and domain, in Appendix D. Note that only the univariate Fisher set definitions are presented in the stereonets; this was the only model carried through the full parameterization.

Table 4-10. Fitted univariate Fisher spherical orientation distributions for boreholes within domain FFM01.

Borehole IDCODE	Set ID	# of Fractures	Aff. by DZ?	Prob. Dist.	Mean pole Trend	Plunge	Fisher κ	Goodness of fit K-S stat	% Conf.
KFM06C	ENE	109	No	Fisher	163	6.1	40	0.145	2.00%
KFM07A	ENE	116	No	Fisher	343	4.8	28.13	0.205	0.01%
KFM07B	ENE	102	No	Fisher	153	7.9	23.21	0.12	10.50%
KFM09A	ENE	232	No	Fisher	156.8	10.4	11.54	0.056	45.80%
KFM09B	ENE	66	No	Fisher	330.9	0.9	60.55	0.06	97.20%
KFM09B	ENE	276	Yes	Fisher	338.1	0.2	41.23	0.12	0.07%
KFM01C	EW	203	Yes	Fisher	176.5	0.6	20.19	0.052	64.30%
KFM06A	EW	221	No	Fisher	358.3	19.3	8.12	0.116	0.50%
KFM06C	EW	68	No	Fisher	358.9	31.6	15.94	0.059	97.30%
KFM07A	EW	22	Yes	Fisher	172.4	10.7	13.47	0.102	97.60%
KFM08A	EW	148	No	Fisher	2.9	21	9.48	0.117	3.50%
KFM08A	EW	125	Yes	Fisher	359.9	25	9.54	0.109	10.10%
KFM08B	EW	45	No	Fisher	0.9	9.4	7.34	0.199	5.70%
KFM09B	EW	13	No	Fisher	193.1	0.2	19.06	0.116	99.50%
KFM01A	NE	260	No	Fisher	314.2	7.5	21.9	0.275	0.00%
KFM01B	NE	242	No	Fisher	321.7	0.1	25.77	0.22	0.00%
KFM01C	NE	798	Yes	Fisher	147.6	9	24.55	0.14	0.00%
KFM01D	NE	256	No	Fisher	131.5	0.7	10.98	0.12	0.10%
KFM04A	NE	518	No	Fisher	148.8	16.3	15.46	0.136	0.00%
KFM05A	NE	206	No	Fisher	142.3	0.8	15.65	0.055	55.30%
KFM05A	NE	294	Yes	Fisher	143.3	4.6	12.53	0.04	73.90%
KFM06A	NE	654	No	Fisher	122.6	0.6	26.37	0.185	0.00%
KFM07A	NE	168	No	Fisher	318.1	5.6	22.99	0.047	85.50%
KFM07A	NE	97	Yes	Fisher	310.9	24.1	16.85	0.092	38.60%
KFM07B	NE	74	No	Fisher	307.8	8.2	26.85	0.151	6.90%
KFM07C	NE	472	No	Fisher	148.3	7.1	44.43	0.079	0.60%
KFM08A	NE	485	No	Fisher	311.3	6.1	10.84	0.059	7.00%
KFM08A	NE	252	Yes	Fisher	308.4	7.7	28.91	0.073	13.50%
KFM08B	NE	196	No	Fisher	312.8	0.4	16.09	0.103	3.00%
KFM08C	NE	322	No	Fisher	321.8	0	9.28	0.036	77.40%
KFM09A	NE	229	No	Fisher	302.2	3	17.02	0.191	0.00%
KFM09B	NE	29	No	Fisher	304.5	1.9	39.43	0.143	59.20%
KFM09B	NE	69	Yes	Fisher	124.6	0.5	24.2	0.198	0.90%
KFM06C	NNE	154	No	Fisher	291.7	2.3	12.08	0.071	42.80%
KFM07C	NNE	162	No	Fisher	302.3	14.3	18.58	0.092	13.10%
KFM08C	NNE	595	No	Fisher	107.4	16.6	21.18	0.065	1.30%
KFM01A	NS	249	No	Fisher	279.2	6.4	22.4	0.089	3.89%
KFM01B	NS	106	No	Fisher	269.6	10.3	21.98	0.096	28.80%
KFM01C	NS	125	Yes	Fisher	93.4	0	9.44	0.072	54.20%
KFM04A	NS	437	No	Fisher	279.5	3.4	21	0.086	0.30%
KFM05A	NS	54	No	Fisher	276.5	0.6	18.41	0.142	22.40%
KFM05A	NS	101	Yes	Fisher	269.1	0.4	20.35	0.11	17.10%
KFM06A	NS	197	No	Fisher	265.1	8.7	17.64	0.063	42.00%
KFM07A	NS	128	No	Fisher	266.8	7	17.15	0.064	66.30%
KFM07A	NS	86	Yes	Fisher	272.4	20.6	12.4	0.169	1.50%
KFM07B	NS	59	No	Fisher	273.2	3.9	65.68	0.169	7.00%

Borehole IDCODE	Set ID	# of Fractures	Aff. by DZ?	Prob. Dist.	Mean pole Trend	Plunge	Fisher κ	Goodness of fit K-S stat	% Conf.
KFM08A	NS	373	No	Fisher	266.4	19.4	21.63	0.029	91.30%
KFM08A	NS	125	Yes	Fisher	277.9	16.4	23.54	0.074	49.80%
KFM08B	NS	85	No	Fisher	257.6	11.4	8.54	0.165	1.90%
KFM08C	NS	691	No	Fisher	255.2	3.9	28.04	0.048	8.00%
KFM09B	NS	10	No	Fisher	92.3	19.1	26.5	0.24	61.40%
KFM09B	NS	31	Yes	Fisher	87.6	9.3	20.3	0.08	98.90%
KFM01A	NW	181	No	Fisher	222.3	7.5	8.83	0.06	54.20%
KFM01B	NW	87	No	Fisher	233.9	4.1	24.3	0.18	0.70%
KFM01C	NW	191	Yes	Fisher	221.8	10.3	12.59	0.042	88.10%
KFM01D	NW	475	No	Fisher	246.8	4.4	12.08	0.033	69.50%
KFM04A	NW	425	No	Fisher	61.2	0.4	14.38	0.024	96.30%
KFM05A	NW	137	No	Fisher	56.7	8.2	12.62	0.043	96.40%
KFM05A	NW	111	Yes	Fisher	53.6	0.5	16.18	0.045	97.60%
KFM06A	NW	101	No	Fisher	201.1	19.1	9.36	0.095	32.50%
KFM06C	NW	66	No	Fisher	254	4.8	10.54	0.155	8.40%
KFM07A	NW	102	No	Fisher	223.9	11.8	10.36	0.088	40.60%
KFM07B	NW	48	No	Fisher	55.8	13.2	38.26	0.335	0.00%
KFM07C	NW	107	No	Fisher	239.1	9.7	9.45	0.155	1.20%
KFM08A	NW	115	No	Fisher	224.8	8.6	13.02	0.061	78.30%
KFM08A	NW	43	Yes	Fisher	219	8.1	10.7	0.232	1.90%
KFM08C	NW	307	No	Fisher	210.8	0.1	10.96	0.062	18.60%
KFM09A	NW	217	No	Fisher	241.6	6.4	13.91	0.15	0.01%
KFM09B	NW	19	No	Fisher	225.9	4.2	29.04	0.136	87.30%
KFM09B	NW	8	Yes	Fisher	227.6	3.3	9.84	0.349	28.30%
KFM01A	SH	238	No	Fisher	345.1	79	25.02	0.192	0.00%
KFM01B	SH	78	No	Fisher	16.7	73.6	11.6	0.141	9.10%
KFM01C	SH	430	Yes	Fisher	343.6	82.5	14.36	0.097	0.06%
KFM01D	SH	274	No	Fisher	354.7	75.1	12.7	0.189	0.00%
KFM04A	SH	253	No	Fisher	341.9	74	10.72	0.131	0.03%
KFM05A	SH	95	No	Fisher	26.1	76.7	11.42	0.137	5.60%
KFM05A	SH	110	Yes	Fisher	2.3	79.2	14.08	0.195	0.05%
KFM06A	SH	175	No	Fisher	293.9	78.7	12.64	0.11	2.90%
KFM06C	SH	207	No	Fisher	229.4	84.8	14.44	0.125	0.30%
KFM07A	SH	194	No	Fisher	155.4	83.3	16.29	0.151	0.03%
KFM07A	SH	50	Yes	Fisher	169.5	71.8	18.11	0.253	0.30%
KFM07B	SH	17	No	Fisher	171.9	78.4	19.75	0.246	25.70%
KFM07C	SH	262	No	Fisher	107.9	80.7	26.97	0.267	0.00%
KFM08A	SH	232	No	Fisher	76.9	87.8	21.41	0.225	0.00%
KFM08A	SH	113	Yes	Fisher	90.1	81.2	26.68	0.278	0.00%
KFM08B	SH	150	No	Fisher	307.6	83.4	26.8	0.139	0.60%
KFM08C	SH	304	No	Fisher	183.1	68.3	7.37	0.174	0.00%
KFM09A	SH	158	No	Fisher	317.5	79.8	14.02	0.172	0.02%
KFM09B	SH	23	No	Fisher	82.1	86.5	10.19	0.149	68.60%
KFM09B	SH	207	Yes	Fisher	349.3	77.3	32.81	0.203	0.00%
KFM07C	SH2	123	No	Fisher	169.6	39.5	26.01	0.038	99.50%
KFM08C	SH3	157	No	Fisher	337.9	52.9	10.16	0.049	84.90%
KFM09B	SH3	45	Yes	Fisher	153.7	65.2	23.99	0.179	11.10%

Table 4-11. Fitted univariate Fisher spherical orientation distributions for boreholes within domain FFM02.

Borehole IDCODE	Set ID	# of Fractures	Aff. by DZ?	Prob. Dist.	Mean pole Trend	Plunge	Fisher κ	Goodness of fit K-S stat	% Conf.
AFM001264	ENE	38	No	Fisher	347.6	0.1	47.57	0.208	7.40%
AFM001265	ENE	73	No	Fisher	156.2	2.8	100	0.291	0.00%
KFM05A	ENE	212	No	Fisher	151.8	2.2	20.89	0.162	0.00%
KFM07A	ENE	11	No	Fisher	155.4	16	100	0.287	32.50%
KFM07B	ENE	203	No	Fisher	339.3	1.8	25.37	0.123	0.40%
KFM09A	ENE	276	Yes	Fisher	154.2	2.1	19.39	0.107	0.40%
KFM09B	ENE	63	Yes	Fisher	161	6.5	59.05	0.061	97.10%
AFM001264	EW	38	No	Fisher	12.2	0.9	54.98	0.086	93.90%
AFM001265	EW	13	No	Fisher	180.9	2.3	47.45	0.25	39.20%
AFM100201	EW	154	No	Fisher	178.8	3.2	18.84	0.048	86.60%
KFM01C	EW	5	Yes	Fisher	177.8	6.7	61	0.274	84.70%
KFM05A	EW	49	No	Fisher	4.5	4.3	48.28	0.226	1.40%
KFM06A	EW	14	No	Fisher	193.5	21	18.9	0.507	0.20%
KFM06B	EW	13	No	Fisher	357.4	0.4	9.63	0.249	39.80%
KFM07B	EW	86	No	Fisher	206.3	6.3	14.78	0.113	22.00%
AFM001264	NE	59	No	Fisher	316.5	3.1	23.68	0.066	95.70%
AFM100201	NE	266	No	Fisher	141.2	0.3	29.65	0.043	71.10%
KFM01A	NE	279	No	Fisher	123.2	16.6	23.17	0.127	0.03%
KFM01B	NE	42	No	Fisher	128.7	1.1	9.55	0.157	25.00%
KFM01C	NE	408	No	Fisher	149	7.8	26.96	0.137	0.00%
KFM01C	NE	28	Yes	Fisher	144.6	6.6	99.39	0.09	97.80%
KFM01D	NE	49	No	Fisher	312.8	25.2	5.95	0.13	37.80%
KFM06B	NE	39	No	Fisher	294.2	14.6	30.58	0.2	8.80%
KFM07B	NE	171	No	Fisher	309.5	7.9	22.55	0.143	0.20%
KFM07C	NE	29	No	Fisher	142.1	0.6	17.51	0.156	48.30%
KFM08B	NE	41	No	Fisher	322.8	4.5	13.55	0.143	37.60%
KFM09B	NE	70	Yes	Fisher	137.2	0.9	21.74	0.153	7.60%
AFM001265	NNE	18	No	Fisher	107.2	1.8	45.29	0.128	92.90%
KFM07B	NNW	113	No	Fisher	73	5.6	11.62	0.103	18.30%
AFM001264	NS	9	No	Fisher	91.3	6.3	17.59	0.208	83.10%
AFM100201	NS	67	No	Fisher	280.9	0.3	25.86	0.163	5.70%
KFM01B	NS	37	No	Fisher	262	2.3	38.95	0.241	2.80%
KFM01C	NS	116	No	Fisher	88.6	7.5	11.7	0.189	0.05%
KFM01C	NS	4	Yes	Fisher	112.7	23.4	48.05	0.232	98.30%
KFM05A	NS	103	No	Fisher	267.9	33	15.63	0.129	6.60%
KFM06A	NS	41	No	Fisher	276.7	2.9	10.7	0.255	1.00%
KFM07A	NS	3	No	Fisher	104.5	5	100	0.292	96.00%
KFM09A	NS	77	Yes	Fisher	83.4	1.6	20.4	0.226	0.08%
KFM09B	NS	41	Yes	Fisher	80.3	5.1	17.97	0.192	9.80%
AFM001264	NW	53	No	Fisher	232.9	1.9	19.69	0.105	59.90%
AFM001265	NW	2	No	Fisher	240.5	0	100	0.941	5.80%
AFM100201	NW	152	No	Fisher	57	3.8	17.09	0.128	1.30%
KFM01A	NW	133	No	Fisher	32.4	4	7.04	0.108	8.90%
KFM01B	NW	142	No	Fisher	59.7	12.1	20.75	0.152	0.30%
KFM01C	NW	98	No	Fisher	218.5	5.5	10.67	0.056	92.20%

Borehole IDCODE	Set ID	# of Fractures	Aff. by DZ?	Prob. Dist.	Mean pole Trend	Plunge	Fisher κ	Goodness of fit K-S stat	% Conf.
KFM01C	NW	10	Yes	Fisher	218.4	6.4	15.47	0.219	72.50%
KFM01D	NW	68	No	Fisher	230	0.9	9	0.093	60.40%
KFM05A	NW	72	No	Fisher	53.9	19.3	12.74	0.064	92.60%
KFM06B	NW	17	No	Fisher	37.2	39.9	16.64	0.174	68.20%
KFM07A	NW	14	No	Fisher	244.7	3.6	25.32	0.152	90.20%
KFM07C	NW	18	No	Fisher	37.1	25.3	13.89	0.233	28.30%
KFM08B	NW	19	No	Fisher	236.6	17.2	4.53	0.179	57.50%
KFM09A	NW	71	Yes	Fisher	235.1	3.7	10.38	0.105	40.80%
KFM09B	NW	29	Yes	Fisher	15.5	1	11.87	0.148	54.90%
AFM001264	SH	46	No	Fisher	336.3	83.7	19.53	0.137	35.10%
AFM100201	SH	99	No	Fisher	346.6	76.4	7.97	0.074	65.60%
KFM01A	SH	239	No	Fisher	343.3	84.2	21.14	0.286	0.00%
KFM01B	SH	206	No	Fisher	61.9	79.3	20.8	0.246	0.00%
KFM01C	SH	391	No	Fisher	1	79.2	23.39	0.155	0.00%
KFM01C	SH	61	Yes	Fisher	349.5	85.3	31.7	0.323	0.00%
KFM01D	SH	230	No	Fisher	213.5	85.4	17.74	0.118	0.30%
KFM05A	SH	139	No	Fisher	29.2	80	20.01	0.146	0.60%
KFM06A	SH	41	No	Fisher	307.4	78.4	17.76	0.331	0.02%
KFM06B	SH	137	No	Fisher	266	89.2	17.51	0.084	29.40%
KFM07A	SH	20	No	Fisher	287.2	71.3	33.57	0.279	9.00%
KFM07B	SH	282	No	Fisher	145.5	82.6	19.41	0.151	0.00%
KFM07C	SH	39	No	Fisher	150.8	79.4	19.73	0.193	11.00%
KFM08B	SH	73	No	Fisher	43.6	87.5	28.17	0.31	0.00%
KFM09A	SH	332	Yes	Fisher	6.6	78.2	26.66	0.137	0.00%
KFM09B	SH	100	Yes	Fisher	334.5	80.9	46.85	0.174	0.50%

Table 4-12. Fitted univariate Fisher spherical orientation distributions for boreholes within domain FFM03.

Borehole IDCODE	Set ID	# of Fractures	Aff. by DZ?	Prob. Dist.	Mean pole Trend	Plunge	Fisher κ	Goodness of fit K-S stat	% Conf.
AFM000053	ENE	94	No	Fisher	164.8	1.2	44	0.074	67.60%
AFM000053	EW	244	No	Fisher	197.1	1.9	51.2	0.143	0.01%
AFM001243	EW	30	No	Fisher	209.6	1.1	16.14	0.11	85.90%
AFM001244	EW	57	No	Fisher	188.7	5.1	29.25	0.124	34.30%
KFM10A	EW	45	No	Fisher	190.4	20.8	12.1	0.1	76.30%
AFM000053	NE	199	No	Fisher	303.8	2.1	39.87	0.117	0.90%
AFM001243	NE	98	No	Fisher	137.8	4.7	34.43	0.154	1.90%
AFM001244	NE	238	No	Fisher	132.1	2.1	24.69	0.068	22.60%
KFM03A	NE	796	No	Fisher	313	6.4	11.52	0.073	0.05%
KFM03B	NE	60	No	Fisher	298.8	2.9	20.55	0.327	0.00%
KFM10A	NE	194	No	Fisher	137.2	1.2	19.14	0.126	0.40%
KFM10A	NE	19	Yes	Fisher	315.1	15.1	30.95	0.137	33.30%
AFM000053	NS	27	No	Fisher	91	1.4	41.05	0.186	31.00%
AFM001243	NS	42	No	Fisher	269.8	2.8	6.1	0.194	8.30%
AFM001244	NS	146	No	Fisher	274.6	1.7	22.31	0.09	18.90%
KFM03A	NS	548	No	Fisher	263.8	0.2	17.69	0.064	2.30%
KFM03B	NS	25	No	Fisher	267	16	18.18	0.183	37.40%
KFM10A	NS	87	No	Fisher	271.1	20	12.6	0.092	44.80%
KFM10A	NS	4	Yes	Fisher	274.2	9.2	20.18	0.357	68.90%

Borehole IDCODE	Set ID	# of Fractures	Aff. by DZ?	Prob. Dist.	Mean pole Trend	Mean pole Plunge	Fisher κ	K-S stat	% Conf.
AFM000053	NW	188	No	Fisher	46.4	1.2	16.83	0.042	88.80%
AFM001244	NW	176	No	Fisher	219.8	0.7	17.89	0.165	0.01%
KFM03A	NW	404	No	Fisher	216.7	2.4	9.79	0.091	0.20%
KFM03B	NW	50	No	Fisher	231.6	1.4	31.66	0.241	0.60%
KFM10A	NW	161	No	Fisher	48	13.3	19.17	0.06	60.50%
KFM10A	NW	12	Yes	Fisher	31.9	6.8	14.96	0.187	79.60%
AFM000053	SH	60	No	Fisher	322.4	83.9	8.22	0.123	32.30%
AFM001243	SH	10	No	Fisher	335.6	80.3	14.2	0.271	45.50%
AFM001244	SH	56	No	Fisher	334.2	80.5	11.75	0.152	14.90%
KFM03A	SH	528	No	Fisher	328.9	72.2	9.01	0.033	60.20%
KFM03B	SH	60	No	Fisher	320.2	71.6	11.13	0.052	99.70%
KFM10A	SH	186	No	Fisher	80.9	78.9	12.14	0.1	4.80%
KFM10A	SH	22	Yes	Fisher	51.4	77.6	25.22	0.266	9.00%

Table 4-13. Fitted univariate Fisher spherical orientation distributions for boreholes within domain FFM06. Note that there are no fractures mapped as 'Affected by DZ' in this domain.

Borehole IDCODE	Set ID	# of Fractures	Probability Distribution	Mean pole Trend	Mean pole Plunge	Fisher κ	K-S stat	% Conf.
KFM06A	ENE	53	Fisher	155.4	8.3	20.83	0.089	79.60%
KFM06A	NE	128	Fisher	300	0.5	53.28	0.051	89.00%
KFM06A	NS	44	Fisher	84.1	1.2	14.74	0.156	23.70%
KFM06A	NW	73	Fisher	27.1	0.4	15.88	0.09	59.00%
KFM06A	SH	47	Fisher	248.8	82.4	10.77	0.114	57.50%
KFM06C	NE	306	Fisher	133.2	8.2	20.63	0.113	0.08%
KFM06C	NS	329	Fisher	100.6	2.2	15.24	0.035	82.80%
KFM06C	NW	172	Fisher	37.6	4.4	10.13	0.053	71.70%
KFM06C	SH	163	Fisher	274.7	85.1	15.89	0.139	0.40%
KFM06C	SH2	161	Fisher	0	47.5	12.71	0.04	96.30%
KFM08C	NE	129	Fisher	123.9	22.6	61.24	0.188	0.02%
KFM08C	NS	78	Fisher	88.2	8.9	28.48	0.05	98.90%
KFM08C	NW	69	Fisher	217.6	2.5	22.38	0.078	79.60%
KFM08C	SH	16	Fisher	307.9	71.8	5.67	0.158	82.20%

4.1.3 Fracture orientation model

The final fracture orientation model for the SDM Forsmark 2.2 geological DFN is parameter-ized only in terms of univariate Fisher spherical probability distributions. The reasoning behind this is discussed in the Methodology section. The final orientation model is built from the linked trace data set (as well as the borehole orientation data). Note that the model is divided into global and local sets; global sets are those sets found in nearly every outcrop and borehole. Local sets are hypothesized to have a much smaller spatial extent and are not seen everywhere in the data record. See the set matrix presented as Table 4-14 for more detail.

An important note is that the EW/WNW global set, which is ubiquitous in the detail-mapped outcrop data, is not nearly as widespread in the borehole record; that set is seen in less than one-half of the boreholes encountered. It is included as a global set based primarily on the outcrop record, as well as the possibility that, in the borehole record, the set is obscured by the overlap of the NE and NW global sets. Also note that, in the model parameterization, the EW/WNW set is formed of the composite of two sets identified on outcrop (the EW and WNW sets). The decision was made to combine the sets based on the similarity in strike and the two sets mutual

exclusion on the outcrops (see the set matrix below). The same decision was made with regard to the local sub-horizontal sets (SH2 and SH3) present in several boreholes in several fracture domains. These sets, though identified, were lumped into the Global SH set; the end result is a higher average Fisher κ for these sets.

Table 4-14. Set matrix describing prevalence of global and local fracture sets in Forsmark borehole and outcrop data.

Outcrops	Fracture Domain	Local sets				Global sets					
		NNE	ENE	SH2	NNW	EW	WNW	NS	NE	NW	SH*
AFM000053	FFM03		X				X	X	X	X	X
AFM000054	UNK						X	X	X	X	X
AFM001097	FFM04					X		X	X	X	X
AFM001098	FFM05	X					X		X	X	X
AFM100201	FFM02					X		X	X	X	X
AFM001243	FFM03						X		X		X
AFM001244	FFM03					X		X	X	X	X
AFM001264	FFM02		X					X	X	X	X
AFM001265	FFM02	X	X			X			X	X	
Boreholes											
KFM01A	FFM01							X	X	X	X
KFM01B	FFM01							X	X	X	X
KFM01C	FFM01					X		X	X	X	X
KFM01D	FFM01								X	X	X
KFM04A	FFM01							X	X	X	X
KFM05A	FFM01							X	X	X	X
KFM06A	FFM01					X		X	X	X	X
KFM06C	FFM01	X				X			X	X	X
KFM07A	FFM01		X					X	X	X	X
KFM07B	FFM01	X						X	X	X	X
KFM07C	FFM01	X		X					X	X	X
KFM08A	FFM01					X		X	X		X
KFM08B	FFM01					X		X	X		X
KFM08C	FFM01	X		X				X	X	X	X
KFM09A	FFM01		X						X	X	X
KFM09B	FFM01		X					X	X	X	X
KFM10A	FFM01								X	X	X
KFM01A	FFM02								X	X	X
KFM01B	FFM02							X	X	X	X
KFM01C	FFM02		X					X		X	X
KFM01D	FFM02								X	X	X
KFM05A	FFM02		X			X		X		X	X
KFM06A	FFM02					X		X			X
KFM06B	FFM02					X			X	X	X
KFM07A	FFM02		X					X		X	X
KFM07B	FFM02		X		X	X			X		X
KFM07C	FFM02								X	X	X
KFM08B	FFM02								X	X	X
KFM09A	FFM02		X					X		X	X
KFM09B	FFM02		X					X	X	X	X
KFM03A	FFM03							X	X	X	X

Outcrops	Fracture Domain	Local sets				Global sets					
		NNE	ENE	SH2	NNW	EW	WNW	NS	NE	NW	SH*
KFM03B	FFM03							X	X	X	X
KFM10A	FFM03							X	X	X	X
KFM06A	FFM06		X					X	X	X`	X
KFM06C	FFM06							X	X	X	X
KFM08C	FFM06							X	X	X	X

* Includes SH, SH2, and SH3.

The fracture orientation model is presented as a single mean pole orientation, and a suggestion of Fisher concentration parameters (κ). The model mean pole represents the mean pole of the distribution of fitted mean poles for all data sets. The concentration parameter is given as the arithmetic mean of the population of Fisher κ's for the individually-fitted data sets. It is NOT the average of all of the fracture data lumped together. A second Fisher concentration parameter, Kmp, is also given. This value represents the concentration parameter of the distribution of mean poles, assuming a univariate Fisher distribution. It is used for stochastic simulation of the variation in location of a given set's mean pole vector (i.e. a wandering mean pole for the NE set).

Note also that in Domain FFM02, the ENE local set has been included as a 'Global' set. This is due to the large number of DZ and ground magnetic lineaments with an ENE orientation in domain FFM02, combined with a relatively large number of ENE intersections in the borehole data. FFM02 is anomalous in this way; in all other domains, the ENE is either a minor local set, or appears to be part of a larger NE-trending population.

The mean pole populations, organized by fracture set and fracture domain, are presented below as Figure 4-20 through Figure 4-27. The full fracture set parameterizations are presented as Table 4-15 through Table 4-22. Note: The parameter estimation algorithm used by FracMan/ISIS for set assignment is limited to a maximum Fisher κ value of 100.

Table 4-15. Global sets in fracture domain FFM01, all fractures.

Set ID	Mean pole (°) Trend	Plunge	Fisher κ_{mp}	Distribution of fisher κ Mean	Std. dev.	Median	95% confidence interval (°) Mean pole	Fisher CDF
NE	314.9	1.3	47.4	20.9	9.4	17.8	4.7	20.5
NS	270.1	5.3	47.0	21.3	13.2	20.3	5.1	20.6
NW	230.1	4.6	32.3	15.7	8.1	12.6	5.8	24.9
SH	0.8	87.3	48.9	17.4	7.1	14.4	4.5	20.2

Table 4-16. Local sets in fracture domain FFM01, all fractures.

Set ID	Mean pole (°) Trend	Plunge	Fisher κ_{mp}	Distribution of fisher κ Mean	Std. dev.	Median	95% confidence intervals (°) Mean pole	Fisher CDF
ENE	157.5	3.1	100.0	34.1	17.0	34.1	5.7	14.1
EW	0.4	11.9	30.0	13.9	5.6	13.5	9.0	25.8
NNE	293.8	0.0	33.1	21.8	0.9	NA	14.1	24.6
SH2	164.0	52.6	NA	35.4	NA	NA	23.5	23.7
SH3	337.9	52.9	10.2	17.1	0.1	NA	31.1	45.2

NA: Values not available due to small sample size.

Table 4-17. Global sets in fracture domain FFM02, all fractures.

Set ID	Mean pole (°)		Fisher κ_{mp}	Distribution of fisher κ			95% Confidence interval (°)	
	Trend	Plunge		Mean	Std. dev.	Median	Mean pole	Fisher CDF
NE	315.3	1.8	33.8	27.0	24.0	22.9	7.0	24.3
NS	92.7	1.2	24.1	30.7	27.1	19.2	9.0	28.9
NW	47.6	4.4	18.6	19.7	22.9	13.9	8.4	33.0
SH	347.4	85.6	87.8	23.2	8.8	20.4	3.7	15.0
EW	186.3	4.3	46.5	34.2	20.6	33.2	7.3	20.7
ENE	157.9	4.0	100.0	53.2	35.1	47.6	5.3	14.1

Table 4-18. Local sets in fracture domain FFM02, all fractures.

Set ID	Mean pole (°)		Fisher κ_{mp}	Distribution of fisher κ			95% Confidence intervals (°)	
	Trend	Plunge		Mean	Std. dev.	Median	Mean pole	Fisher CDF
NNE	107.2	1.8	NA	45.3	NA	NA	20.8	21.0
NNW	73.0	5.6	NA	11.6	NA	NA	41.1	42.1

NA: Values not available due to small sample size.

Table 4-19. Global sets in fracture domain FFM03, all fractures.

| Set ID	Mean pole (°)		Fisher κ_{mp}	Distribution of fisher κ			95% Confidence interval (°)	
	Trend	Plunge		Mean	Std. dev.	Median	Mean pole	Fisher CDF
NE	311.1	2.7	81.3	25.9	9.8	24.7	5.9	15.6
NS	270.2	6.9	91.4	19.7	10.8	18.2	5.5	14.7
NW	42.4	2.8	84.8	18.4	7.3	17.4	6.2	15.3
SH	348.8	81.0	77.3	13.1	5.7	11.8	6.0	16.0
EW	196.5	7.3	50.7	27.2	17.6	22.7	9.8	19.8

Table 4-20. Local sets in fracture domain FFM03.

Set ID	Mean pole (°)		Fisher κ_{mp}	Distribution of fisher κ			95% Confidence intervals (°)	
	Trend	Plunge		Mean	Std. dev.	Median	Mean pole	Fisher CDF
ENE	164.8	1.2	NA	44	NA	NA	21.1	21.3

NA: Values not available due to small sample size.

Table 4-21. Global sets in fracture domain FFM06.

Set ID	Mean pole (°)		Fisher κ_{mp}	Distribution of fisher κ			95% Confidence interval (°)	
	Trend	Plunge		Mean	Std. dev.	Median	Mean pole	Fisher CDF
NE	125.7	10.1	54.6	45.1	21.5	53.3	10.9	19.1
NS	91.0	4.1	100.0	19.5	7.8	15.2	8.1	14.1
NW	34.1	0.8	100.0	16.1	6.1	15.9	8.1	14.1
SH	84.3	71.3	100.0	10.8	5.1	10.8	8.1	14.1

Table 4-22. Local sets in fracture domain FFM06.

| Set ID	Mean pole (°)		Fisher κ_{mp}	Distribution of fisher κ			95% Confidence intervals (°)	
	Trend	Plunge		Mean	Std. dev.	Median	Mean pole	Fisher CDF
ENE	155.4	8.3	NA	20.8	NA	NA	4.2	31.1
SH2	0.0	47.5	NA	12.7	NA	NA	3.1	40.2

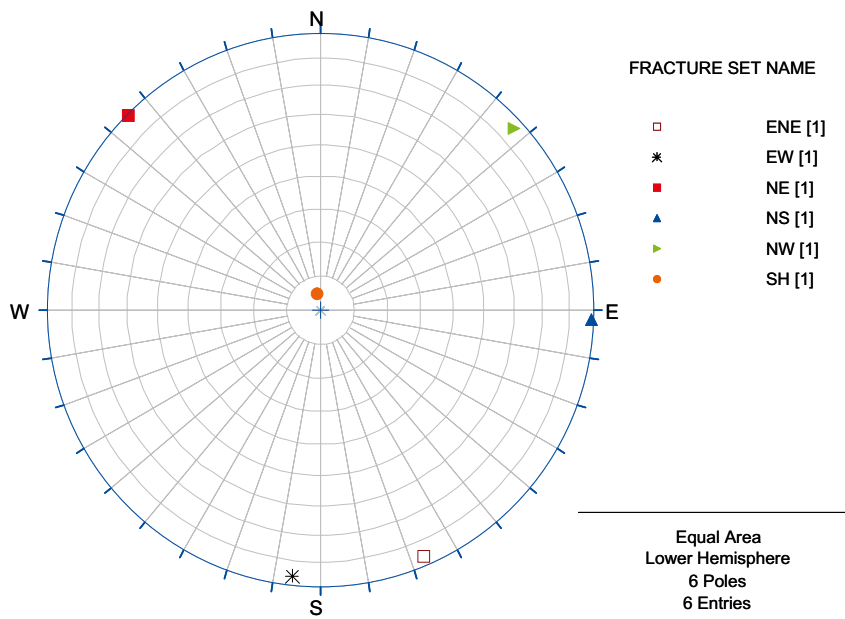NA: Values not available due to small sample size.
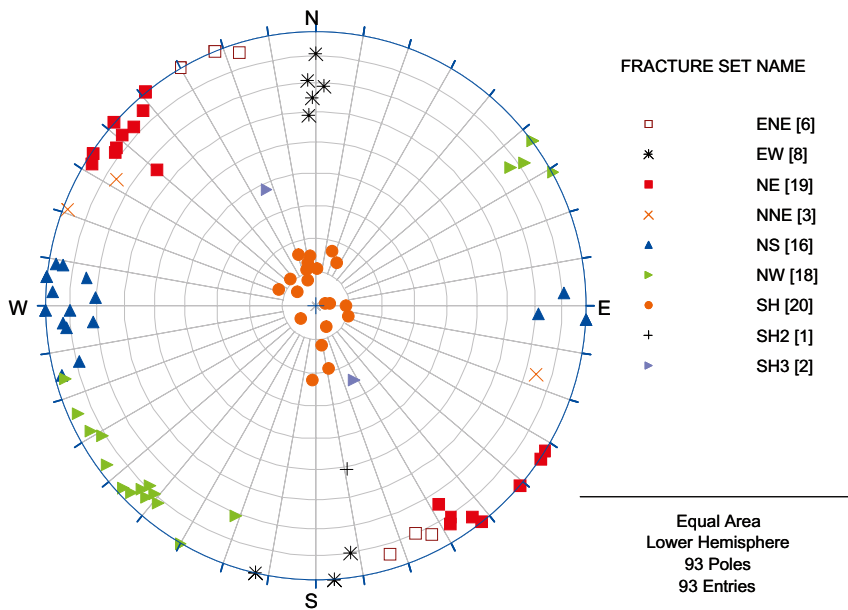
Figure 4-20. *Fitted set mean poles, Domain FFM01. The number of poles indicates the number of data points (boreholes or outcrops) the orientation model is built from.*
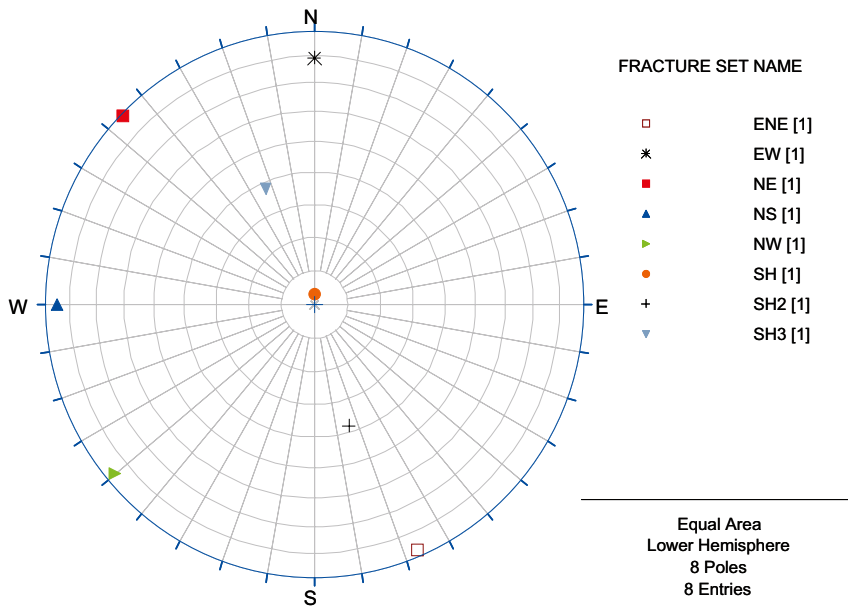
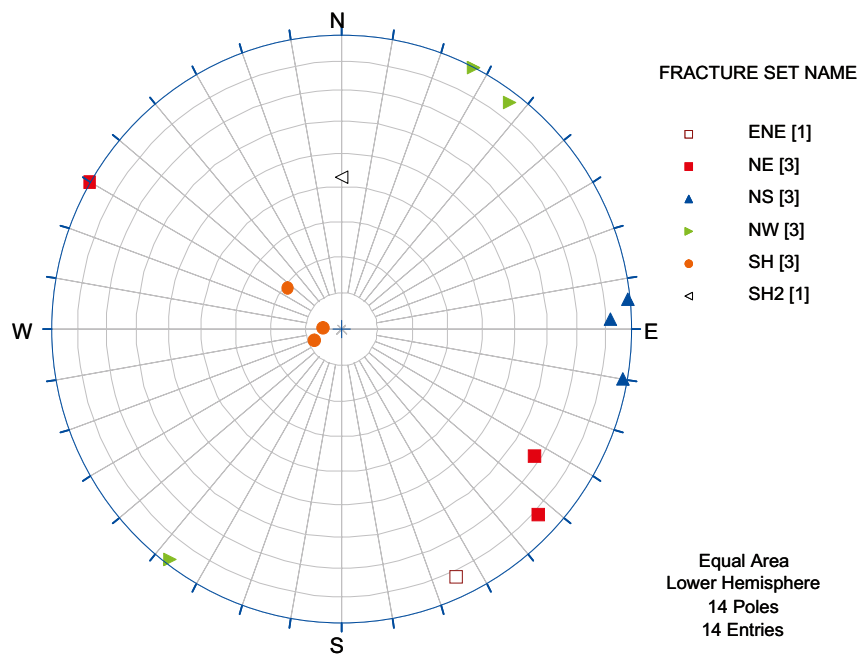***Figure 4-21.*** *Domain FFM01 orientation model.*
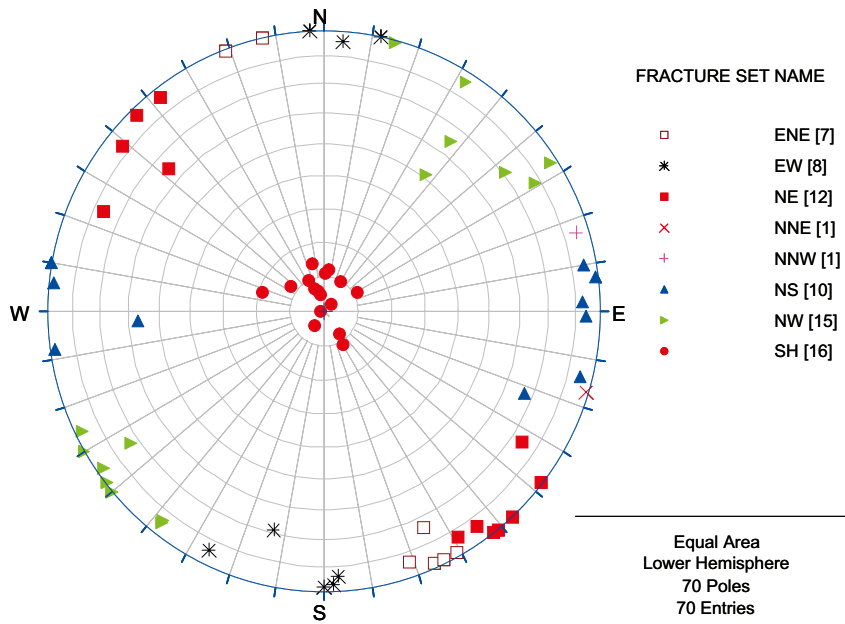
Figure 4-22. *Fitted set mean poles, Domain FFM02. The number of poles indicates the number of data points (boreholes or outcrops) the orientation model is built from.*

Figure 4-23. *Domain FFM02 orientation model.*

Figure 4-24. *Fitted set mean poles, Domain FFM03. The number of poles indicates the number of data points (boreholes or outcrops) the orientation model is built from.*
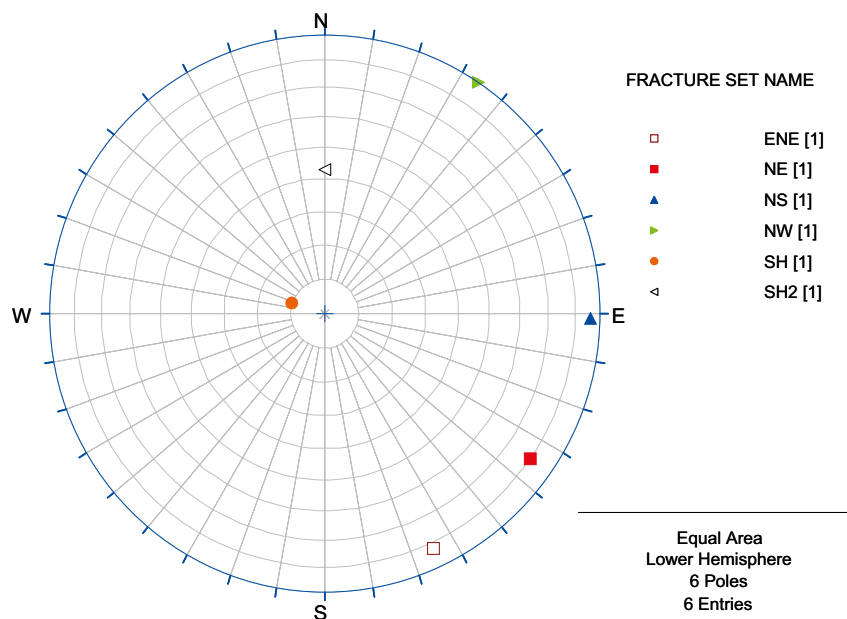

Figure 4-25. *Domain FFM03 orientation model.*

Figure 4-26. *Fitted set mean poles, Domain FFM06. The number of poles indicates the number of data points (boreholes or outcrops) the orientation model is built from.*

Figure 4-27. *Domain FFM06 orientation model.*

Fracture orientation model in rock labeled 'affected by DZ'

A key question addressed during the parameterization of the Forsmark 2.2 geological DFN model was whether or not sections of rock within the candidate volume labeled 'Affected by DZ' were statistically different than the rock mass as a whole. In terms of fracture set orientations, this question was addressed by comparing the mean poles fit to fractures inside sections labeled 'affected by DZ' to the mean poles fit to fractures outside sections labeled 'affected by DZ'. The comparison was completed by fracture domain, fracture set and in each borehole. The test assumes that, for a fracture set whose mean pole wanders spatially, the variability in mean pole orientation can be quantified as a Fisher distribution. The test is described in detail in Chapter 3.2.2.

Results of the analysis are presented below in Table 4-23 through Table 4-25. For Domain FFM01, all sets, save for the EW and SH sets, were able to be combined (i.e. the mean pole of the affected by DZ fractures was inside the 95% confidence interval on the mean). The results in Domains FFM02 and FFM03 were less clear; it was not possible for most of the sets to meet the 95% confidence interval on the mean. However, all sets in Domain FFM02 and Domain FFM03 were able to meet the 95% confidence cone of the Fisher distribution; it is possible to vary the set mean pole stochastically according to a univariate Fisher distribution and not be able to tell the difference between 'Affected by DZ' fractures and 'Not Affected by DZ' fractures. There were no zones labeled 'Affected by DZ' in boreholes intersecting Domain FFM06.

Table 4-23. Results of 'Affected by DZ' orientation analysis, Domain FFM01.

Set ID	Set mean pole		Affected by DZ mean pole		Solid Angle (°)	95% C.I. (°)		Is solid angle < 95% C.I.?	
	Trend	Plunge	Trend	Plunge		Mean Pole	CDF	Mean Pole	CDF
NE	314.8	0.5	315	3.5	3.0	4.8	18.2	Yes	Yes
NS	269.2	5.2	272	5.6	2.8	6.1	20.5	Yes	Yes
NW	231.5	4.3	225.5	5.3	6.1	7.1	27.0	Yes	Yes
SH	349.7	87.3	115.4	86.4	5.6	5.1	20.0	No	Yes
EW	3	16.3	356.2	4.5	13.6	9.3	20.8	No	Yes
ENE	157.3	3.8	338.1	0.2	4.1	6.3	14.1	Yes	Yes

Table 4-24. Results of 'Affected by DZ' orientation analysis, Domain FFM02.

Set ID	Set mean pole		Aff. by DZ mean pole		Solid Angle (°)	95% C.I. (°)		Is solid angle < 95% C.I.?	
	Trend	Plunge	Trend	Plunge		Mean Pole	CDF	Mean Pole	CDF
NE	314.1	2.9	140.9	3.8	9.5	8.1	24.5	No	Yes
NS	273.3	2.7	91.5	10.3	13.1	9.6	25.7	No	Yes
EW	187.6	3.9	177.8	6.7	10.2	8.0	21.2	No	Yes
NW	50.4	6.2	216.4	3.2	16.8	8.9	31.4	No	Yes
SH	344.9	86.5	352.1	81.7	4.8	4.4	16.0	No	Yes
ENE	158.1	3.8	157.6	4.3	0.7	5.9	14.5	Yes	Yes

Table 4-25. Results of 'Affected by DZ' orientation analysis, Domain FFM03.

Set ID	Set mean pole		Aff. by DZ mean pole		Solid Angle (°)	95% C.I. (°)		Is solid angle < 95% C.I.?	
	Trend	Plunge	Trend	Plunge		Mean Pole	CDF	Mean Pole	CDF
NE	310.5	0.6	315.1	15.1	15.2	6.9	17.0	No	Yes
NS	269.6	6.5	274.2	9.2	5.3	6.6	14.8	Yes	Yes
NW	44.5	2	31.9	6.8	13.5	6.6	14.7	No	Yes
SH	337.8	80.3	51.4	77.6	13.4	6.4	15.6	No	Yes

Parameter variability

Parameter variability in the SDM Forsmark geological DFN orientation model is quantified through the following three methods:

- A 95% confidence interval surrounding the mean pole of each model set, in each fracture domain, is given. This allows downstream model users to vary the location of the mean pole stochastically if so desired. The potential effects of choosing a different mean pole from within the 95% confidence interval are documented later in the chapter on uncertainty.

- A 95% confidence cone of the univariate Fisher distribution for each population of set mean poles used to parameterize an orientation set distribution. The radius of this cone on the sphere represents the maximum solid angle from the mean pole vector that a fitted orientation set mean pole (such as from a set of observations in a single outcrop or borehole) can be and still be considered compliant with the orientation set parameterization 95% of the time.

- Variability in the Fisher concentration parameter (κ) is quantified by testing the aggregated κ-values of all sets used to fit an model fracture set (global or local) for normality. The Shapiro-Wilk normality test /NIST 2007b/, as implemented in Analyze-It, was used at an α of 0.05 (i.e. a value of $p > 0.05$). An example of the output is presented below as Figure 4-28. If the variability in the Fisher κ follows a normal distribution, the mean and standard deviation of the distribution are presented for further stochastic simulation. If the Shapiro-Wilk test suggests that the Fisher κ is not normally distributed, we recommend using the sample median and quartiles for further stochastic simulation. The results of the Shapiro-Wilk tests are presented below as Table 4-26. Plots of the overall variability in Fisher κ as a function of fracture set and fracture domain are presented as Figure 4-29 through Figure 4-32.
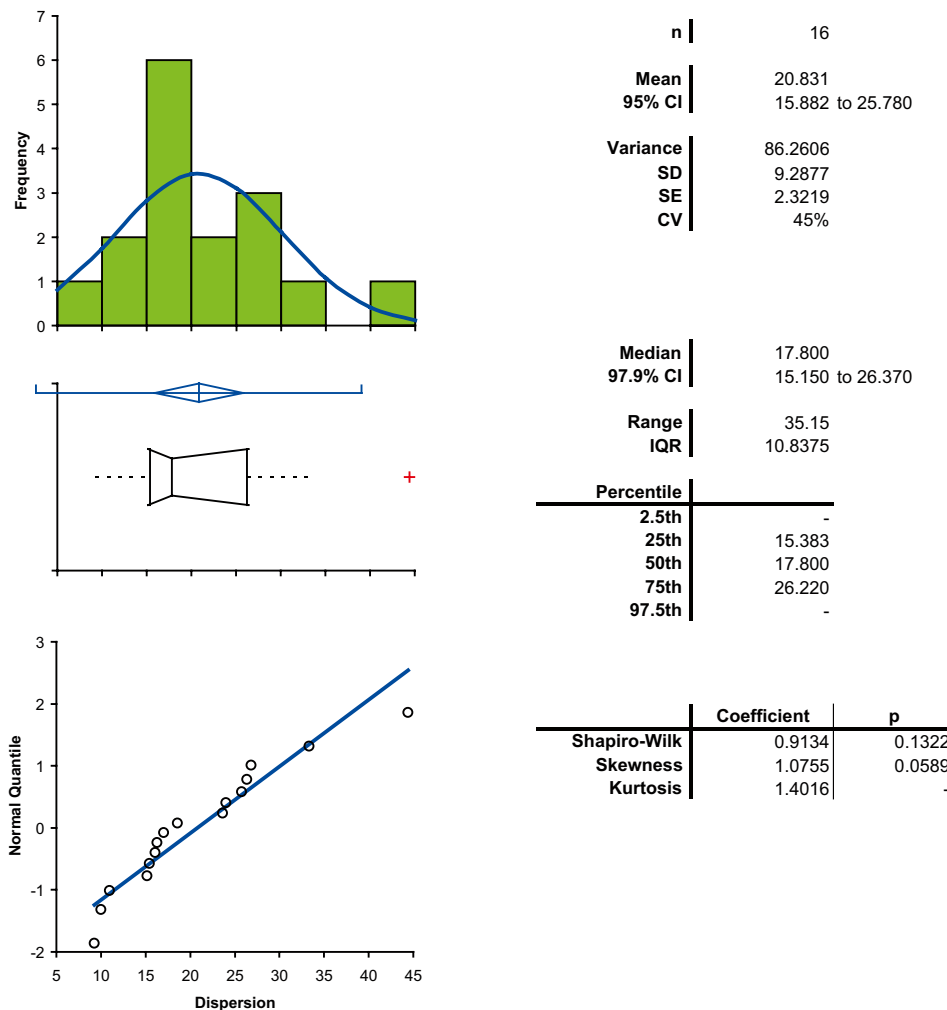
n	16
Mean	20.831
95% CI	15.882 to 25.780
Variance	86.2606
SD	9.2877
SE	2.3219
CV	45%
Median	17.800
97.9% CI	15.150 to 26.370
Range	35.15
IQR	10.8375

Percentile	
2.5th	-
25th	15.383
50th	17.800
75th	26.220
97.5th	-

	Coefficient	p
Shapiro-Wilk	0.9134	0.1322
Skewness	1.0755	0.0589
Kurtosis	1.4016	-

Figure 4 28. *Example results of a Shapiro-Wilk normality test on Fisher κ values.*

**Table 4-26. Summary of variability in the Fisher κ parameter for fracture domains FFM01, FFM02, and FFM03.**

Fracture domain	Fracture set	Shapiro-Wilk W-score	Probability	Set is normally distributed?
FFM01	ENE	0.972	0.574	Yes
FFM01	EW	0.875	0.288	Yes
FFM01	NE	0.913	0.132	Yes
FFM01	NS	0.683	0.001	No
FFM01	NS*	0.951	0.654	Yes
FFM01	NW	0.616	0.000	No
FFM01	NW*	0.949	0.58	Yes
FFM01	SH	0.875	0.022	No
FFM02	ENE	0.816	0.043	No
FFM02	ENE*	0.833	0.115	Yes
FFM02	EW	0.836	0.091	Yes
FFM02	NE	0.944	0.597	Yes
FFM02	NW	0.981	0.982	Yes
FFM02	NS	0.645	0.0003	No
FFM02	NS*	0.871	0.153	Yes
FFM02	SH	0.849	0.017	No
FFM03	NE	0.928	0.567	Yes
FFM03	NS	0.924	0.556	Yes
FFM03	NW	0.901	0.415	Yes
FFM03	SH	0.966	0.862	Yes
FFM06	NE	0.890	0.355	Yes
FFM06	NS	0.777	0.061	Yes
FFM06	NW	0.999	0.933	Yes
FFM06	SH	1.000	1.00	Yes

* Obvious outliers removed.
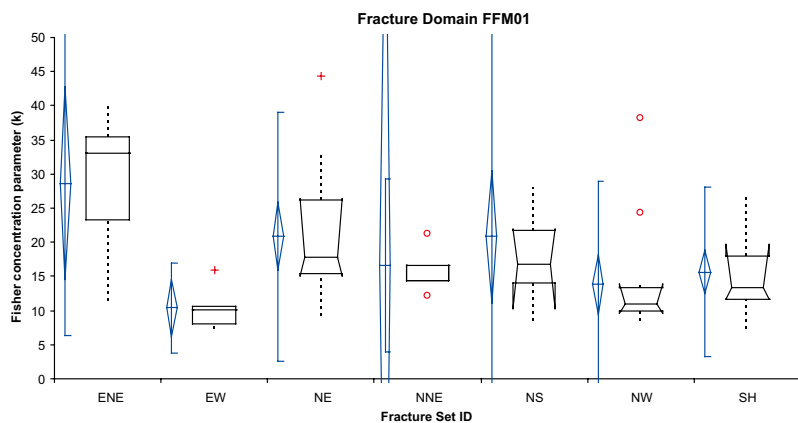
Dispersion by Set ID	n	Mean	SD	SE	95% CI of Mean	Median	IQR	95% CI of Median
ENE	5	28.636	11.3601	5.0804	14.531 to 42.741	32.970	12.250	- to -
EW	5	10.404	3.3684	1.5064	6.222 to 14.586	10.070	2.430	- to -
NE	16	20.831	9.2877	2.3219	15.882 to 25.780	17.800	10.838	15.150 to 26.370
NNE	2	16.630	6.4347	4.5500	-41.183 to 74.443	16.630	0.000	- to -
NS	12	20.866	15.2337	4.3976	11.187 to 30.545	16.705	7.860	10.290 to 21.980
NW	15	13.787	7.7527	2.0017	9.493 to 18.080	11.010	3.435	9.620 to 13.910
SH	18	15.668	6.3772	1.5031	12.496 to 18.839	13.360	6.278	11.600 to 19.750

*Figure 4-29. Variability of Fisher κ, fracture sets in Domain FFM01.*

Figure 4-30. *Variability of Fisher κ, fracture sets in Domain FFM02.*
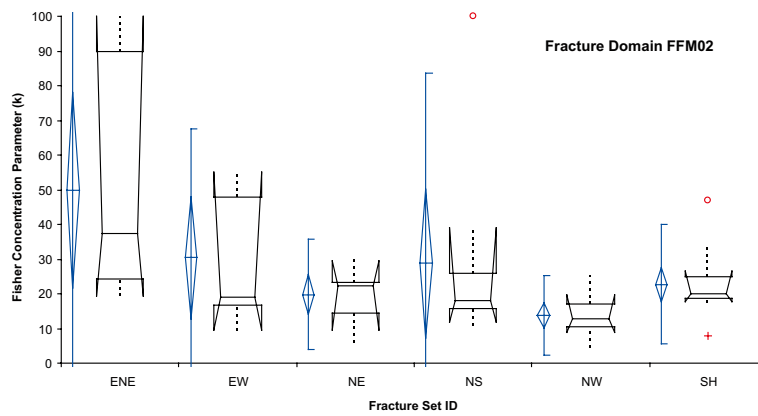
Dispersion by Set ID	n	Mean	SD	SE	95% CI of Mean	Median	IQR	95% CI of Median
ENE	8	49.904	33.8264	11.9594	21.624 to 78.183	37.265	65.513	19.390 to 100.000
EW	7	30.409	18.9554	7.1645	12.878 to 47.939	18.900	31.055	9.630 to 54.980
NE	10	19.793	8.1114	2.5651	13.990 to 25.596	22.145	8.758	9.550 to 29.650
NS	9	28.756	28.0358	9.3453	7.205 to 50.306	17.970	10.230	11.700 to 38.950
NW	13	13.816	5.8851	1.6322	10.260 to 17.372	12.740	6.710	9.000 to 19.690
SH	15	22.683	8.7967	2.2713	17.811 to 27.554	20.010	6.440	17.760 to 26.660

Figure 4-31. *Variability of Fisher κ, fracture sets in Domain FFM03.*

Dispersion by Set ID	n	Mean	SD	SE	95% CI of Mean	Median	IQR	95% CI of Median
EW	3	32.197	17.7148	10.2276	-11.809 to 76.203	29.250	17.530	- to -
NE	6	24.030	11.1411	4.5483	12.338 to 35.722	21.130	10.658	11.520 to 39.870
NS	5	20.734	12.8102	5.7289	4.828 to 36.640	17.690	5.790	- to -
NW	5	15.468	5.8018	2.5946	8.264 to 22.672	16.830	8.100	- to -
SH	6	10.737	2.1465	0.8763	8.484 to 12.989	10.620	2.070	8.220 to 14.200

**Figure 4-31.** *Variability of Fisher κ, fracture sets in Domain FFM03.*

Figure 4-32. *Variability of Fisher κ, fracture sets in domain FFM06.*
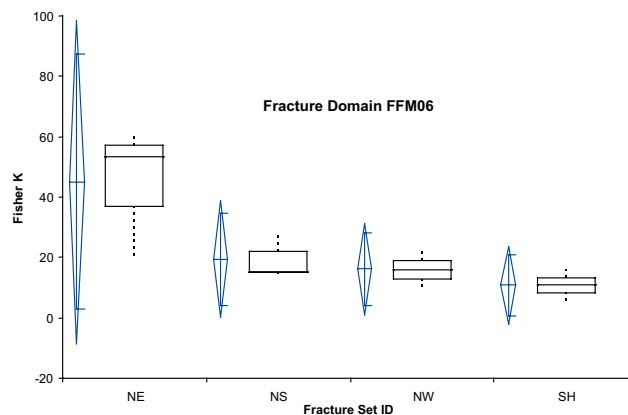
Dispersion by Set ID	n	Mean	SD	SE	95% CI of Mean	Median	IQR	95% CI of Median
NE	3	45.050	21.5196	12.4243	-8.408 to 98.508	53.280	20.305	- to -
NS	3	19.487	7.7925	4.4990	0.129 to 38.844	15.240	6.870	- to -
NW	3	16.130	6.1288	3.5385	0.905 to 31.355	15.880	6.125	- to -
SH	3	10.777	5.1100	2.9503	-1.917 to 23.471	10.770	5.110	- to -

Figure 4-32. *Variability of Fisher κ, fracture sets in domain FFM06.*

86

In summary, for most fracture sets, it is possible to stochastically simulate the variability in the Fisher concentration parameter (κ) for a given orientation set, in a given fracture domain, using a random draw from a normal distribution and the means/standard deviations given in Table 4-15 through Table 4-22. For several sets, it was necessary to remove several obvious outliers (the sets marked with a *). The sole exceptions are the subhorizontal sets in domains FFM01 and FFM02; their κ–values do not appear to be normally distributed. In these cases, we recommend using the median κ-value for all simulations.

4.1.4   Orientation model applied to DZ and ground magnetic lineaments

In order to utilize the SDM Forsmark version 2.2 deformation zone (DZ) model traces and the new high-resolution ground-magnetic lineament data, it was necessary to classify the data into the same basic orientation sets (NE, NNE, SH, etc) as both the outcrop and borehole data. The methodology of computing trace sets on outcrop data was applied directly to the ground magnetic lineament and deformation zone models; all set assignments were done inside ArcGIS. However, neither the ground magnetic lineaments nor the deformation zone data set was used directly in the parameterization of the orientation model.
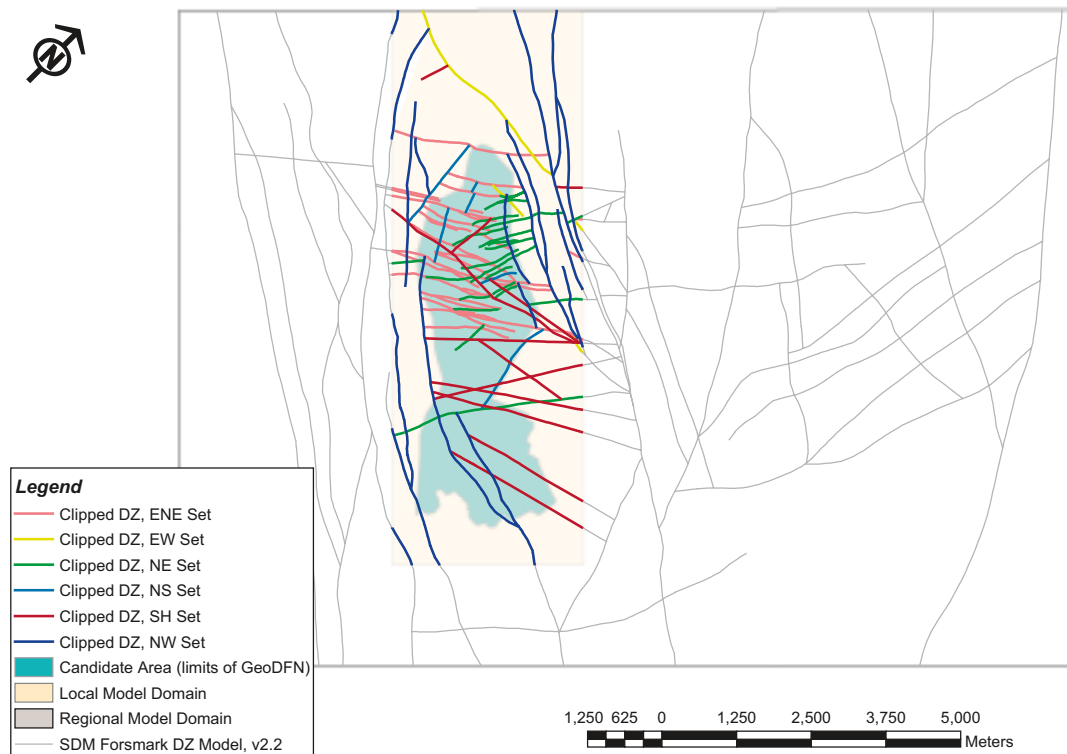
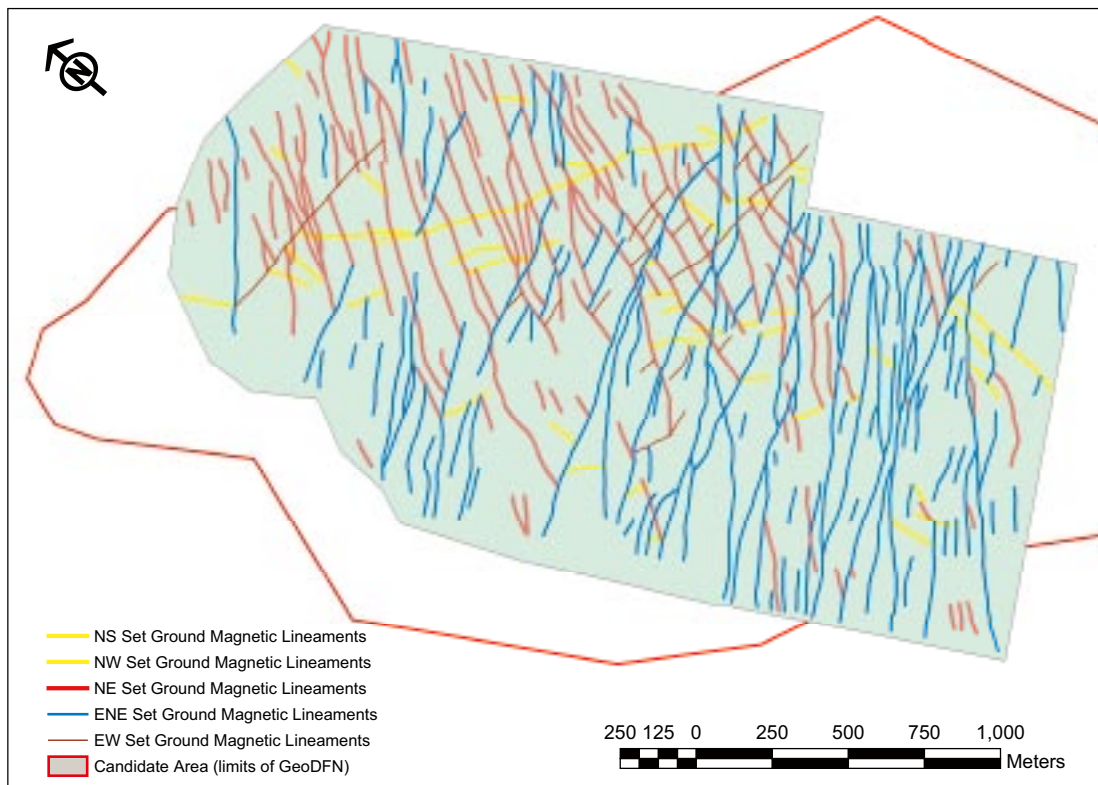*Figure 4-33.* Orientation model applied to SDM Forsmark 2.2 deformation zone (DZ) model.

Figure 4-34. *Orientation model applied to high-resolution ground magnetic lineaments /Isaksson et al. 2006ab/.*
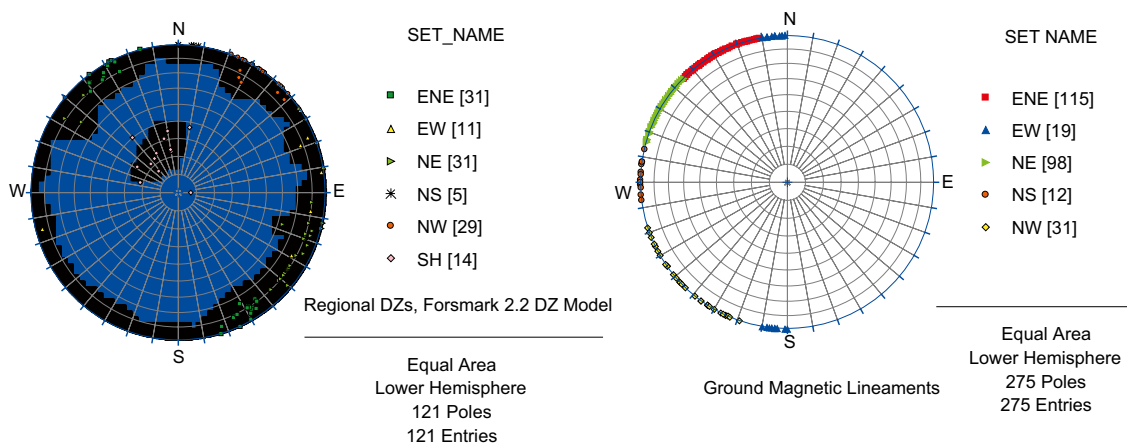

Figure 4-35. *Stereoplots of orientation model sets applied to the SDM Forsmark 2.2 deformation zone model (left) and the high-resolution ground magnetic lineament data set (right).*

4.1.5 Evaluation of uncertainties

The uncertainties associated with the orientation model come from the following sources:

- Linked versus unlinked traces in outcrop;

- The accuracy of the spatial delineation of DZ and MDZ in outcrop and in borehole data;

- Measurement uncertainty of fracture strike and dip on the detail-mapped outcrops. The SKB method description for this activity suggests a general accuracy of 10° in strike and 10° in dip /Danielsson et al. 2006/; and

- The uncertainty in the orientation of both the borehole, and of the orientation of the fractures exposed in core or BIPS. This uncertainty has been dealt with by following the recommendations in the borehole orientation memorandum /Munier and Stigsson 2007/.

4.2 Size model

4.2.1 Outcrop scale model

The Outcrop Scale fracture size model (OSM) is built atop the analysis of fracture traces recorded during detailed mapping of outcrops at Forsmark. The methodology behind the trace analysis for the Outcrop Scale size model is described in Section 3.2.3. Area-normalized cumulative number trace-length scaling plots for the OSM are presented in Appendix A.

Size analysis of linked outcrop traces

Table 4-27. Statistics of linked outcrop traces classified into sets, domains FFM02 and FFM003.

Outcrop ID	Set ID	# of Traces	Mean (m)	Std. dev.	Skewness	Kurtosis
AFM000053	ENE	94	1.96	1.53	1.82	3.42
AFM000053	NE	199	2.16	2.35	4.05	21.70
AFM000053	NS	27	2.60	3.56	2.6	6.57
AFM000053	NW	188	2.58	2.60	3.51	16.50
AFM000053	SH	60	1.47	1.02	2.22	5.57
AFM000053	WNW	244	1.67	1.19	2.43	9.63
AFM001243	NE	98	1.44	0.93	1.24	0.48
AFM001243	NS	42	1.21	0.71	1.5	1.93
AFM001243	SH	10	1.40	0.98	1.19	0.07
AFM001243	WNW	30	1.42	0.88	1.3	1.34
AFM001244	EW	57	1.02	0.68	2.11	4.06
AFM001244	NE	238	1.55	1.10	1.48	1.67
AFM001244	NS	146	1.19	0.71	1.61	2.09
AFM001244	NW	176	1.24	0.74	1.73	2.98
AFM001244	SH	56	1.06	0.51	1.29	1.04
AFM100201	EW	154	1.21	0.84	2.39	6.53
AFM100201	NE	266	1.83	1.53	2.20	6.22
AFM100201	NS	67	1.32	0.85	1.78	4.49
AFM100201	NW	152	1.84	1.46	1.61	2.06
AFM100201	SH	99	1.28	1.50	6.50	51.40
AFM001264	ENE	38	2.02	1.87	1.88	2.88
AFM001264	EW	38	1.58	1.09	2.65	8.25
AFM001264	NE	59	1.69	1.38	2.58	7.91
AFM001264	NS	9	1.97	0.98	0.28	−1.82
AFM001264	NW	53	1.68	1.42	2.53	7.44
AFM001264	SH	46	1.94	1.31	2.73	9.78

Table 4-28. Modeled probability distributions for linked outcrop traces from FracSize, fracture domain FFM03. The green bar represents the 'best fit' model for a particular set and outcrop.

Outcrop ID	Set ID	Prob. dist.	Mean / Min. Radius	Std dev.* / Exponent	Simulation # of traces	Mean	Std. dev.	Skew.	Kurt.	Goodness of fit		χ2 Stat	% Conf.
										K-S stat	% Conf.		
AFM000053	ENE	Normal	0.53	0.70	200	1.67	0.85	0.72	−0.35	0.12	32.00%	14.00	29.80%
AFM000053	ENE	Log Normal	0.47	0.78	200	1.90	1.32	1.22	0.88	0.08	80.80%	22.60	30.70%
AFM000053	ENE	Exponential	0.53		200	1.61	0.95	0.93	0.04	0.12	31.90%	12.30	50.20%
AFM000053	ENE	Power Law	0.44	2.93	200	2.02	1.76	2.30	5.39	0.10	49.30%	10.90	81.80%
AFM000053	NE	Normal	0.49	0.72	200	1.68	0.85	0.66	−0.41	0.12	13.90%	26.60	8.63%
AFM000053	NE	Log Normal	0.56	0.72	200	1.82	1.31	0.20	0.27	0.06	91.80%	29.10	25.90%
AFM000053	NE	Exponential	0.59		200	1.90	1.05	0.88	0.21	0.11	20.00%	25.10	12.30%
AFM000053	NE	Power Law	0.44	2.81	200	1.90	1.39	2.23	6.63	0.06	86.00%	20.70	35.20%
AFM000053	NS	Normal	0.51	0.69	200	1.68	0.75	0.58	−0.22	0.22	21.90%	9.43	49.20%
AFM000053	NS	Log Normal	0.57	0.59	200	1.66	1.09	1.54	2.25	0.13	82.20%	14.80	78.90%
AFM000053	NS	Exponential	0.57		200	1.81	1.09	1.04	0.38	0.17	49.30%	6.20	90.60%
AFM000053	NS	Power Law	0.40	2.87	200	1.73	1.32	2.26	6.65	0.12	91.00%	4.24	99.40%
AFM000053	NW	Normal	0.37	1.11	200	2.19	1.11	0.55	−0.40	0.10	26.50%	25.10	19.80%
AFM000053	NW	Log Normal	0.37	1.23	200	2.22	1.49	1.18	1.09	0.07	67.90%	20.70	70.70%
AFM000053	NW	Exponential	0.75		200	2.29	1.40	0.96	0.15	0.06	82.00%	22.80	30.10%
AFM000053	NW	Power Law	0.58	2.91	200	2.63	2.31	1.90	3.36	0.06	88.20%	19.40	73.20%
AFM000053	SH	Normal	0.31	0.55	200	1.31	0.59	0.92	0.44	0.10	78.20%	6.10	52.80%
AFM000053	SH	Log Normal	0.67	0.35	200	1.31	0.59	0.80	−0.26	0.09	84.90%	11.90	80.70%
AFM000053	SH	Exponential	0.40		200	1.31	0.66	0.83	0.04	0.11	63.20%	9.37	31.20%
AFM000053	SH	Power Law	0.43	3.57	200	1.34	0.80	1.91	3.77	0.10	78.20%	4.53	87.30%
AFM000053	WNW	Normal	0.39	0.69	300	1.61	0.75	0.67	−0.24	0.12	3.15%	25.00	1.50%
AFM000053	WNW	Log Normal	0.17	1.05	300	1.57	0.97	1.07	0.33	0.08	30.30%	21.50	30.80%
AFM000053	WNW	Exponential	0.47		300	1.46	0.79	1.05	0.74	0.08	38.20%	14.50	26.90%
AFM000053	WNW	Power Law	0.42	2.99	300	1.74	1.28	2.08	4.81	0.07	43.70%	6.81	96.30%
AFM001243	NE	Normal	0.35	0.63	200	1.33	0.65	0.88	0.22	0.13	25.00%	18.90	0.85%
AFM001243	NE	Log Normal	0.43	0.53	200	1.37	0.78	1.14	0.46	0.09	71.50%	9.39	85.60%
AFM001243	NE	Exponential	0.45		200	1.39	0.75	1.11	0.79	0.13	25.60%	12.70	8.06%
AFM001243	NE	Power Law	0.35	2.96	200	1.41	0.96	1.74	3.00	0.07	91.70%	4.65	86.40%
AFM001243	NS	Normal	0.63	0.24	200	1.13	0.43	0.50	−0.54	0.15	44.40%	6.28	28.00%

AFM001243	NS	Log Normal	0.44	0.37	200	1.24	0.65	1.25	1.18	0.10	85.60%	12.70	54.90%
AFM001243	NS	Exponential	0.34		200	1.18	0.54	1.09	0.94	0.13	65.50%	6.43	37.70%
AFM001243	NS	Power Law	0.25	2.88	200	1.20	0.78	2.08	5.56	0.10	91.30%	5.23	73.20%
AFM001243	SH*	Normal	0.30	0.55	200	1.26	0.57	0.77	−0.13	0.20	84.10%	1.90	86.30%
AFM001243	SH*	Log Normal	0.11	0.94	200	1.19	0.61	1.04	0.31	0.20	86.20%	6.64	94.80%
AFM001243	SH*	Exponential	0.13		200	0.71	0.15	0.78	−0.25	0.57	0.46%	5.30	25.80%
AFM001243	SH*	Power Law	0.35	3.00	200	1.41	1.02	1.81	2.88	0.14	99.50%	1.99	99.20%
AFM001243	WNW	Normal	0.55	0.50	200	1.38	0.62	0.65	−0.36	0.14	67.20%	2.99	81.00%
AFM001243	WNW	Log Normal	0.34	0.54	200	1.38	0.77	1.33	1.67	0.12	87.00%	13.70	62.10%
AFM001243	WNW	Exponential	0.41		200	1.37	0.74	0.98	0.03	0.11	91.90%	4.07	77.20%
AFM001243	WNW	Power Law	0.39	3.15	200	1.36	0.90	2.50	7.85	0.15	62.90%	3.45	94.40%
AFM001244	EW	Normal	0.29	0.27	200	0.92	0.29	0.84	0.04	0.19	9.27%	13.00	4.24%
AFM001244	EW	Log Normal	0.26	0.23	200	0.93	0.37	1.15	0.80	0.10	75.60%	11.40	65.20%
AFM001244	EW	Exponential	0.21		200	0.91	0.33	0.89	−0.01	0.13	43.10%	12.50	5.21%
AFM001244	EW	Power Law	0.29	3.59	200	0.94	0.46	1.77	2.94	0.08	93.70%	5.39	49.50%
AFM001244	NE	Normal	0.26	0.63	300	1.35	0.64	0.75	−0.18	0.13	4.95%	26.50	0.31%
AFM001244	NE	Log Normal	0.26	0.63	300	1.51	0.92	1.26	1.06	0.08	52.70%	15.60	61.90%
AFM001244	NE	Exponential	0.47		300	1.37	0.66	0.93	0.29	0.12	8.18%	22.50	1.27%
AFM001244	NE	Power Law	0.42	3.41	300	1.38	0.80	1.57	2.12	0.11	11.60%	7.86	64.30%
AFM001244	NS	Normal	0.40	0.36	200	1.07	0.43	0.82	0.09	0.11	29.70%	15.40	1.72%
AFM001244	NS	Log Normal	0.40	0.36	200	1.20	0.64	1.20	0.99	0.08	59.50%	15.20	43.70%
AFM001244	NS	Exponential	0.30		200	1.10	0.48	0.96	0.35	0.09	55.40%	10.70	9.94%
AFM001244	NS	Power Law	0.20	2.01	200	1.09	0.47	0.80	−0.33	0.10	33.50%	14.60	2.40%
AFM001244	NW	Normal	0.38	0.38	200	1.13	0.42	0.68	−0.30	0.10	27.40%	18.20	1.09%
AFM001244	NW	Log Normal	0.46	0.33	200	1.11	0.52	1.24	1.41	0.08	61.30%	15.60	48.30%
AFM001244	NW	Exponential	0.34		200	1.20	0.59	0.89	−0.18	0.07	74.10%	9.90	19.40%
AFM001244	NW	Power Law	0.33	3.16	200	1.29	0.79	1.63	2.55	0.06	82.70%	5.79	67.10%
AFM001244	SH	Normal	0.24	0.39	200	0.99	0.39	0.92	0.37	0.09	87.00%	1.47	83.20%
AFM001244	SH	Log Normal	0.11	0.35	200	1.03	0.45	0.88	−0.17	0.09	83.80%	9.33	67.50%
AFM001244	SH	Exponential	0.30		200	1.12	0.51	0.80	−0.32	0.11	63.30%	1.88	75.80%
AFM001244	SH	Power Law	0.19	2.89	200	1.13	0.67	1.89	4.05	0.09	91.00%	1.99	96.00%

Table 4-29. Modeled probability distributions for linked outcrop traces from FracSize, fracture domain FFM02. The green bar represents the 'best fit' model for a particular set and outcrop.

Outcrop IDCODE	Set ID	Probability Distribution	Mean / Min. radius	Std dev.* Exponent	Simulation # of traces	Mean	Std. dev.	Skewness	Kurtosis	Goodness of fit K-S stat	% Conf.	χ2 Stat	% Conf.
AFM100201	EW	Normal	0.493	0.239	200	1.040	0.347	0.617	−0.416	0.131	9.93%	23.10	0.33%
AFM100202	EW	Log Normal	0.360	0.315	200	1.100	0.529	1.220	0.836	0.074	72.10%	19.30	25.50%
AFM100203	EW	Exponential	0.272		200	1.050	0.472	0.906	−0.185	0.089	50.00%	16.50	3.61%
AFM100204	EW	Power Law	0.330	3.540	200	1.180	0.713	1.560	1.620	0.078	65.90%	6.80	55.80%
AFM100201	NE	Normal	0.367	0.719	300	1.590	0.763	0.798	0.082	0.125	2.45%	45.00	0.00%
AFM100202	NE	Log Normal	0.322	0.692	300	1.640	1.110	1.400	1.630	0.059	71.10%	18.30	63.00%
AFM100203	NE	Exponential	0.539		300	1.650	0.887	0.886	0.220	0.096	14.70%	35.10	0.08%
AFM100204	NE	Power Law	0.369	2.800	300	1.840	1.560	2.010	4.250	0.054	81.10%	9.86	87.40%
AFM100201	NS	Normal	0.376	0.447	200	1.220	0.516	0.408	−0.924	0.139	28.50%	9.76	13.50%
AFM100202	NS	Log Normal	0.315	0.423	200	1.270	0.774	1.480	1.750	0.089	82.50%	16.70	40.60%
AFM100203	NS	Exponential	0.324		200	1.150	0.542	1.010	0.300	0.129	37.90%	5.08	53.40%
AFM100204	NS	Power Law	0.353	3.120	200	1.290	0.888	2.180	5.990	0.093	77.70%	5.71	76.90%
AFM100201	NW	Normal	0.287	0.705	200	1.550	0.777	0.610	−0.523	0.133	9.35%	28.40	48.60%
AFM100202	NW	Log Normal	0.414	0.742	200	1.790	1.250	1.360	1.270	0.078	67.10%	14.70	79.40%
AFM100203	NW	Exponential	0.485		200	1.580	0.841	0.970	0.427	0.114	21.20%	21.00	5.00%
AFM100204	NW	Power Law	0.376	2.860	200	1.800	1.450	2.180	5.290	0.063	87.80%	8.63	80.10%
AFM100201	SH	Normal	0.575	0.152	200	1.020	0.276	0.171	−0.617	0.215	0.44%	30.20	0.01%
AFM100202	SH	Log Normal	0.293	0.295	200	1.060	0.498	1.270	1.180	0.076	83.80%	10.90	81.30%
AFM100203	SH	Exponential	0.263		200	1.050	0.440	0.775	−0.387	0.101	50.80%	10.80	14.70%
AFM100204	SH	Power Law	0.283	3.100	200	1.180	0.755	1.830	3.370	0.056	98.50%	7.77	55.80%
AFM001264	ENE	Normal	0.288	0.816	200	1.620	0.801	0.785	−0.044	0.172	30.20%	12.90	30.10%
AFM001264	ENE	Log Normal	0.307	0.704	200	1.770	1.120	1.030	0.486	0.133	62.60%	20.10	45.20%
AFM001264	ENE	Exponential	0.364		200	1.250	0.609	0.959	0.275	0.232	6.46%	12.10	28.10%

AFM001264	ENE	Power Law	0.384	2.740	200	2.110	1.790	1.860	3.250	0.108	85.10%	10.40	88.80%
AFM001264	WNW	Normal	0.427	0.527	200	1.450	0.653	0.491	−0.525	0.167	33.80%	6.32	50.30%
AFM001264	WNW	Log Normal	0.766	0.338	200	1.410	0.588	0.896	0.902	0.17	31.50%	11.90	75.30%
AFM001264	WNW	Exponential	0.609		200	1.720	1.020	1.070	0.539	0.194	18.00%	8.64	47.10%
AFM001264	WNW	Power Law	0.522	3.930	200	1.460	0.799	1.900	3.810	0.111	83.00%	5.53	78.60%
AFM001264	NE	Normal	0.526	0.540	200	1.520	0.681	0.464	−0.530	0.151	25.00%	10.10	25.70%
AFM001264	NE	Log Normal	0.344	0.601	200	1.530	0.980	1.490	1.950	0.0831	91.20%	11.50	90.50%
AFM001264	NE	Exponential	0.406		200	1.400	0.694	0.765	−0.276	0.144	29.70%	7.61	47.30%
AFM001264	NE	Power Law	0.362	2.900	200	1.630	1.300	2.280	5.650	0.0896	85.80%	7.43	87.90%
AFM001264	NS*	Normal	0.756	0.983	200	2.170	1.150	0.775	0.104	0.174	95.60%	4.12	94.20%
AFM001264	NS*	Log Normal	0.797	0.735	200	2.230	1.330	1.210	1.320	0.2	88.10%	7.26	96.80%
AFM001264	NS*	Exponential	0.735		200	2.140	1.300	0.846	−0.061	0.19	91.50%	3.46	96.80%
AFM001264	NS*	Power Law	0.801	3.620	200	2.140	1.330	1.730	3.970	0.184	93.10%	4.47	98.50%
AFM001264	NW	Normal	0.531	0.508	200	1.420	0.647	0.599	−0.650	0.121	57.20%	8.91	44.50%
AFM001264	NW	Log Normal	0.582	0.483	200	1.450	0.845	1.300	1.360	0.0732	97.80%	10.10	93.00%
AFM001264	NW	Exponential	0.512		200	1.540	0.925	1.120	0.550	0.0792	95.50%	4.54	91.90%
AFM001264	NW	Power Law	0.396	3.040	200	1.600	1.120	2.040	4.690	0.0853	92.10%	5.09	95.50%
AFM001264	SH	Normal	0.554	0.743	200	1.790	0.864	0.537	−0.376	0.119	66.60%	7.35	60.10%
AFM001264	SH	Log Normal	0.963	0.537	200	1.900	0.985	0.997	0.551	0.0839	95.50%	9.88	90.80%
AFM001264	SH	Exponential	0.777		200	2.200	1.420	0.928	0.105	0.211	7.14%	9.92	62.30%
AFM001264	SH	Power Law	0.694	3.510	200	1.910	1.230	2.070	4.870	0.0811	96.70%	5.42	96.50%

Combining and splitting outcrop sets

A key component of the analysis of the outcrop trace length distribution was the assessment of whether individual sets on a single outcrop represented a sample from a larger population of fractures with a given radius distribution. The Kruskal-Wallis test /NIST 2007a/ was used to evaluate this hypothesis; results are presented below as Figure 4-36 through Figure 4-45 and Table 4-30 through Table 4-39.

Table 4-30. Comparative statistics and Kruskal-Wallis test results, linked fracture traces, NE Set, Domain FFM02.

Outcrop	# of fracs.	Mean	Std. Dev.	Std. Err.	95% CI* of Mean		Median	IQR	95% CI of Median	
AFM100201	266	1.83	1.53	0.09	1.65	2.01	1.29	1.25	1.16	1.47
AFM001264	59	1.69	1.38	0.18	1.33	2.04	1.20	1.22	1.03	1.51

Outcrop	# of fracs.	Rank sum	Mean rank
AFM001264	59	9,357	158.6
AFM100201	266	43,618	164

Kruskal-Wallis statistic		0.159
Probability	0.69049	(χ² approximation)
Reject H0 at α = 0.05?	No	
Lump Outcrops?	Yes	

* Confidence Interval.
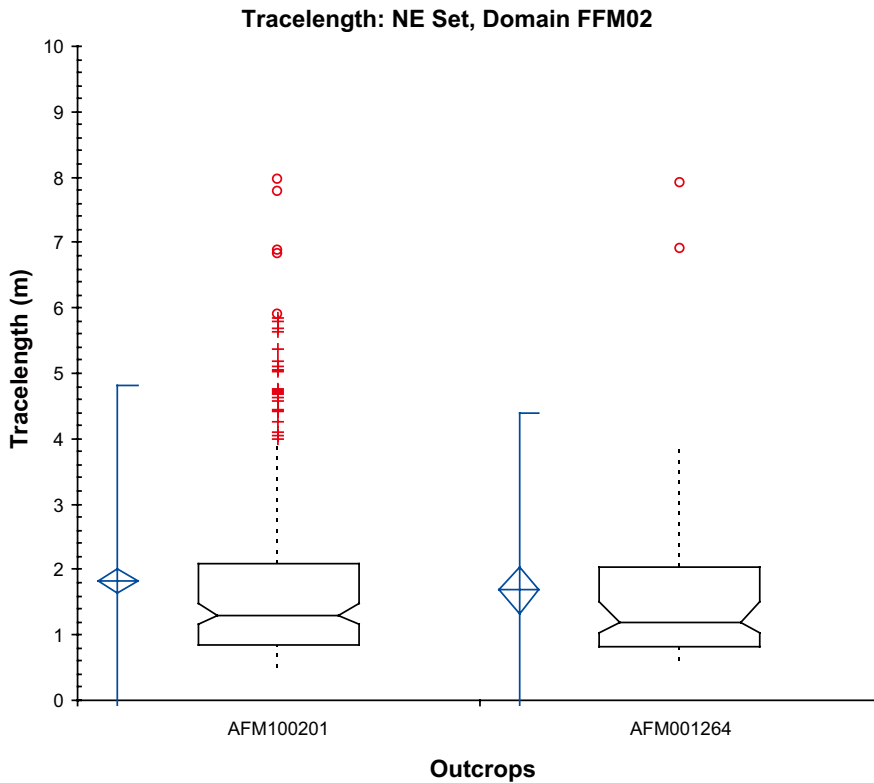
Figure 4-36. *Box and whisker plot, linked fractures, NE Set, Domain FFM02.*
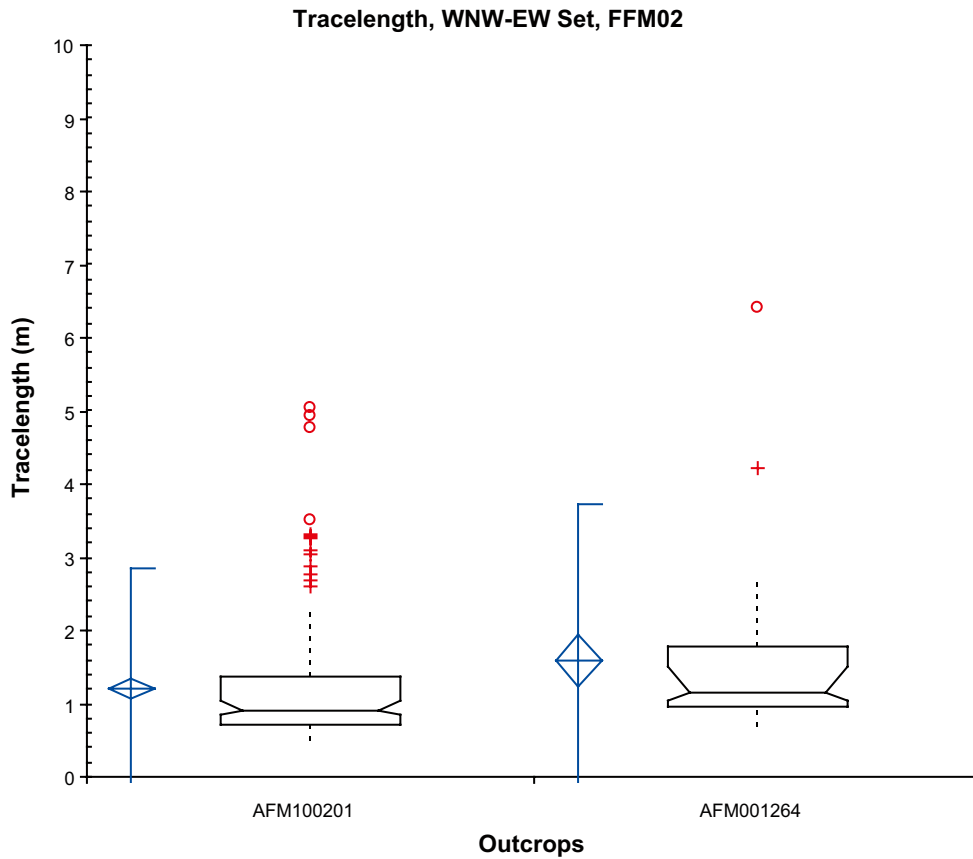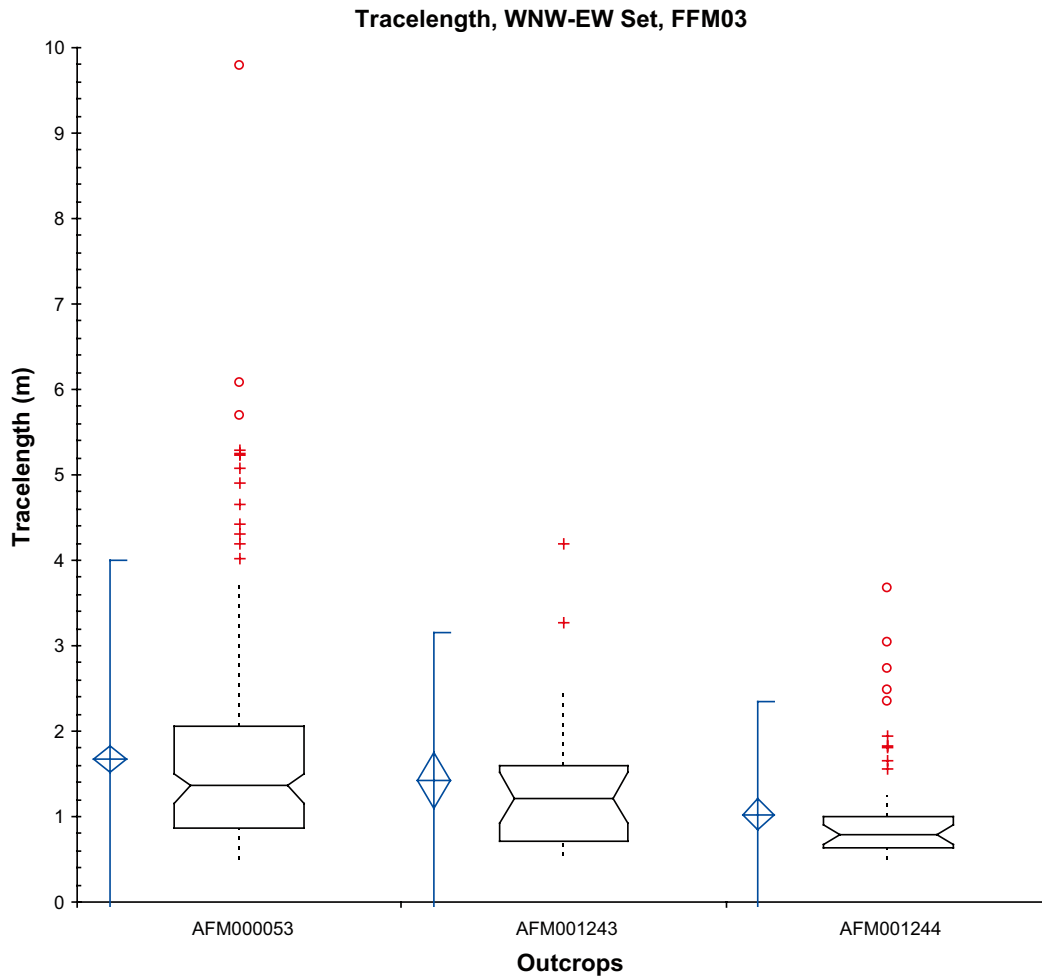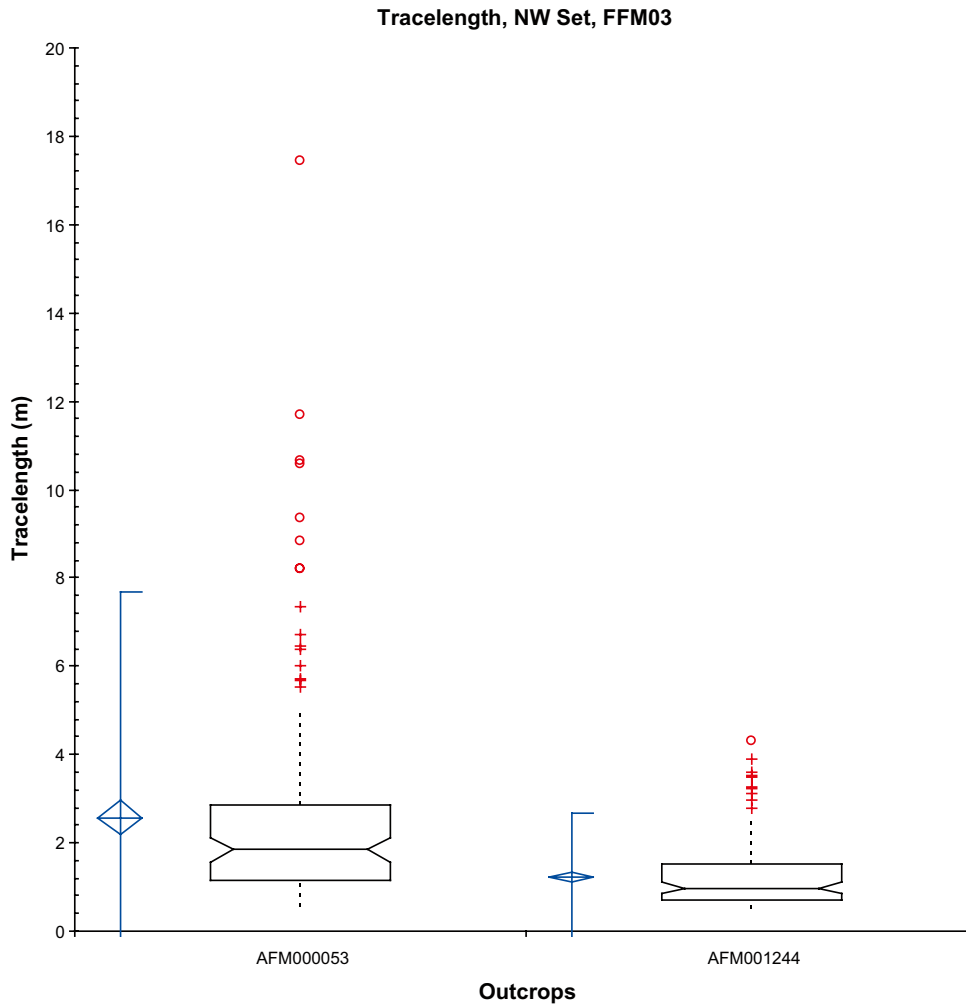
Figure 4-37. *Box and whisker plot, linked fractures, WNW-EW Set, Domain FFM02.*

Table 4-31. Comparative statistics and Kruskal-Wallis test results, linked fractures, WNW-EW Set, Domain FFM02.

Outcrop	# of fracs.	Mean	Std. Dev.	Std. Err.	95% CI of Mean		Median	IQR	95% CI of Median	
AFM100201	154	1.21	0.84	0.07	1.08	1.34	0.90	0.66	0.85	1.03
AFM001264	38	1.58	1.09	0.18	1.23	1.94	1.16	0.82	1.03	1.52

Outcrop	# of fracs.	Rank sum	Mean rank
AFM001264	38	4,696	123.579
AFM100201	154	13,832	89.818

|			
Kruskal-Wallis statistic			11.250
Probability	0.001	(χ^2 approximation)	
Reject H0 at α = 0.05?		Yes	
Lump Outcrops?		No	
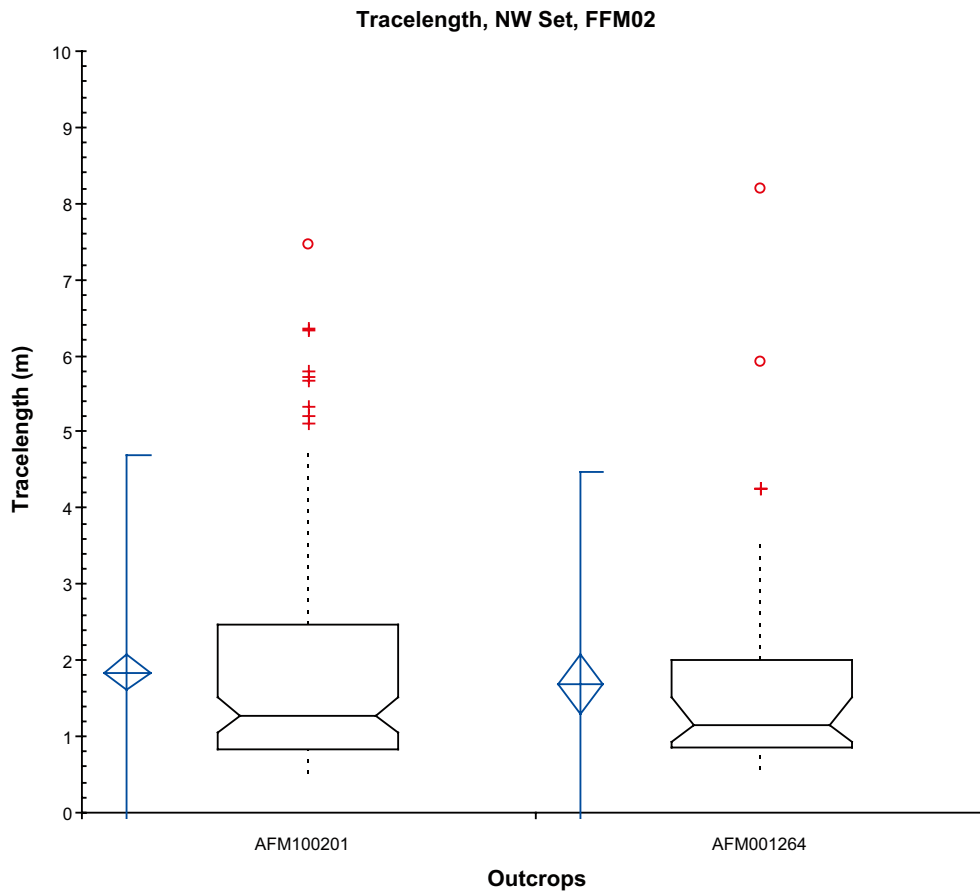
Figure 4-38. *Box and whisker plot, linked fractures, NW Set, Domain FFM02.*

Table 4-32. Comparative statistics and Kruskal-Wallis test results, linked fractures, NW Set, Domain FFM02.

Outcrop	# of fracs.	Mean	Std. Dev.	Std. Err.	95% CI of Mean		Median	IQR	95% CI of Median	
AFM100201	152	1.84	1.46	0.12	1.60	2.07	1.27	1.65	1.06	1.52
AFM001264	53	1.68	1.42	0.19	1.29	2.07	1.14	1.14	0.94	1.53

Outcrop	# of fracs.	Rank sum	Mean rank
AFM001264	53	5,321	100.41
AFM100201	152	15,793	103.91

Kruskal-Wallis statistic			0.137
Probability	0.712	(χ^2 approximation)	
Reject H0 at α = 0.05?		No	
Lump Outcrops?		Yes	
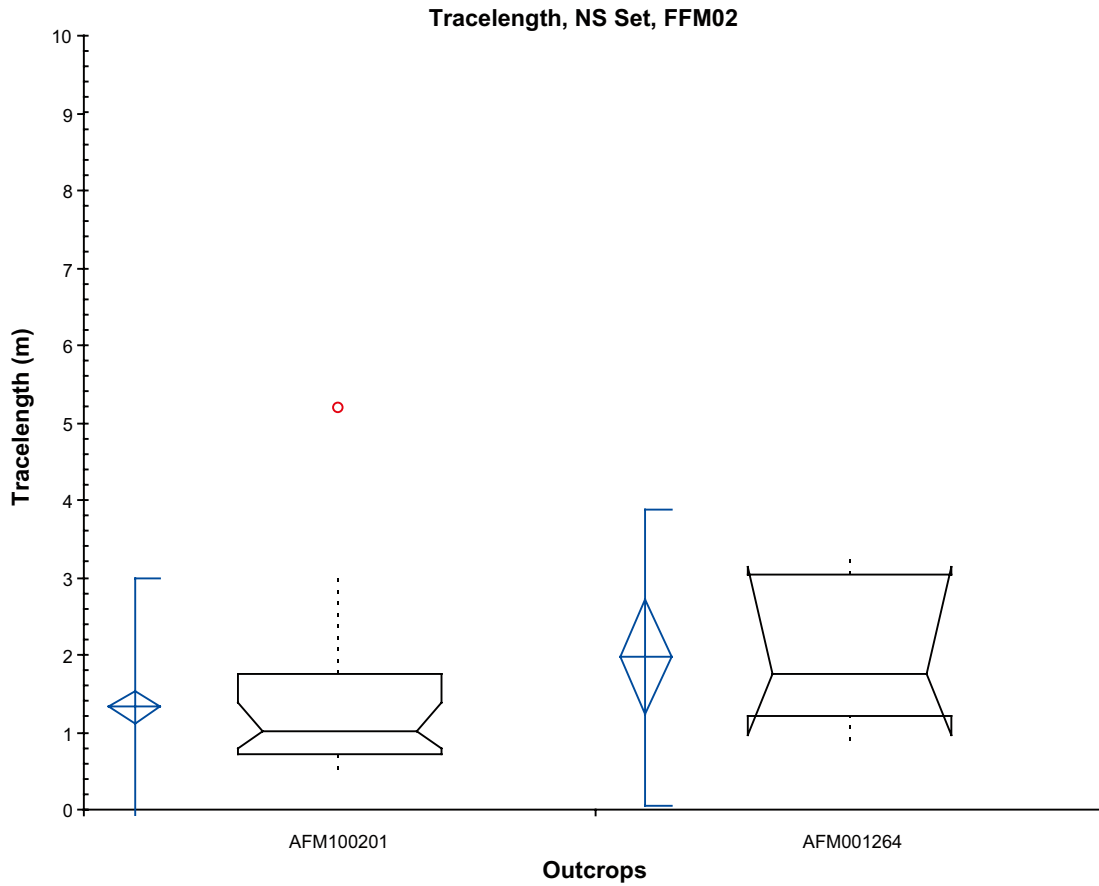
Figure 4-39. *Box and whisker plot, linked fractures, NS Set, Domain FFM02.*

Table 4-33. Comparative statistics and Kruskal-Wallis test results, linked fractures, NS Set, Domain FFM02.
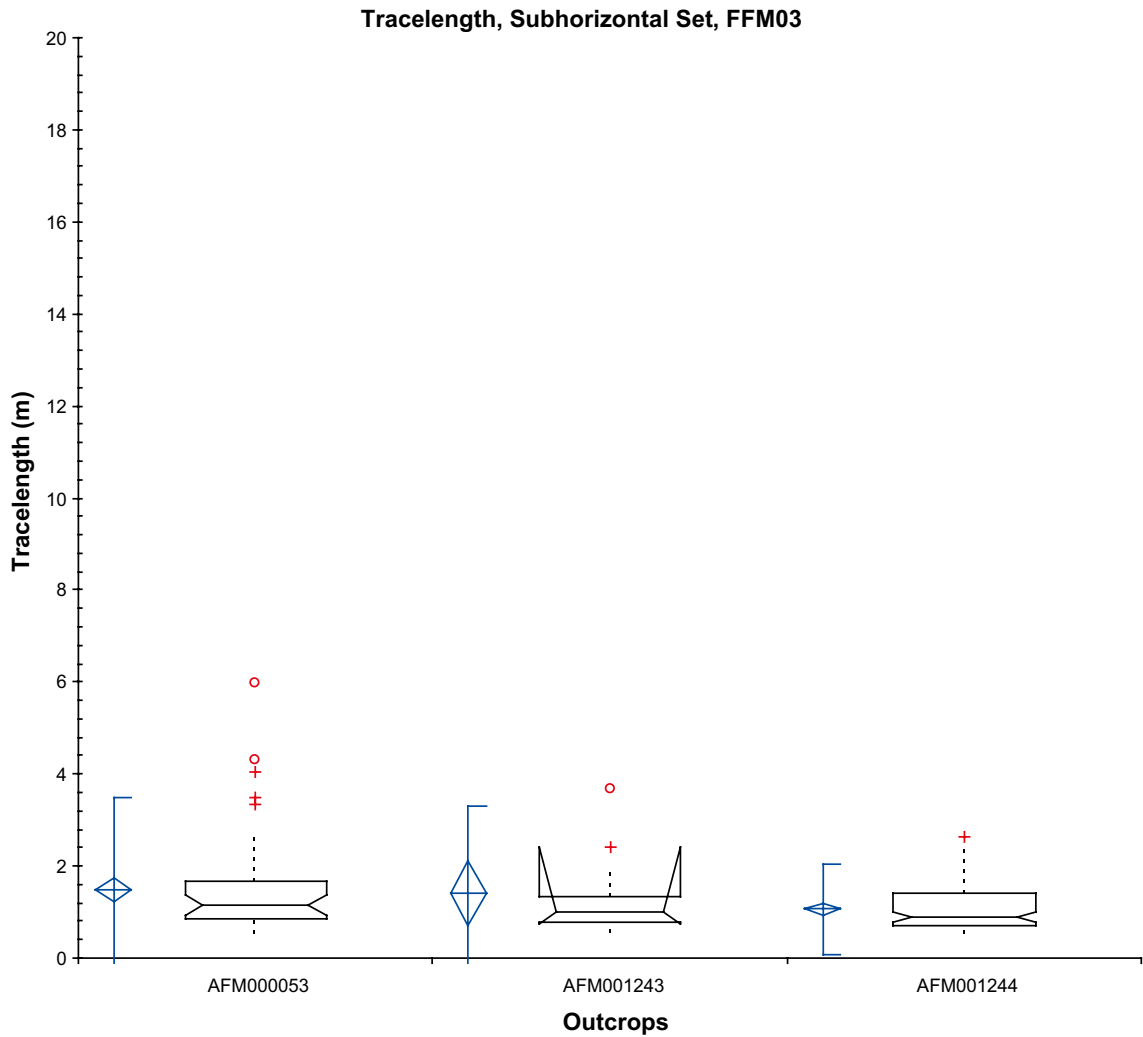
Outcrop	# of fracs.	Mean	Std. Dev.	Std. Err.	95% CI of Mean		Median	IQR	95% CI of Median	
AFM100201	67	1.32	0.85	0.10	1.12	1.53	1.00	1.05	0.78	1.39
AFM001264	9	1.97	0.98	0.33	1.22	2.72	1.76	1.83	0.96	3.14

Outcrop	# of fracs.	Rank sum	Mean rank
AFM001264	9	489	54.333
AFM100201	67	2,437	36.373

Kruskal-Wallis statistic			5.248
Probability	0.022	(χ^2 approximation)	
Reject H0 at α = 0.05?		Yes	
Lump Outcrops?		No	
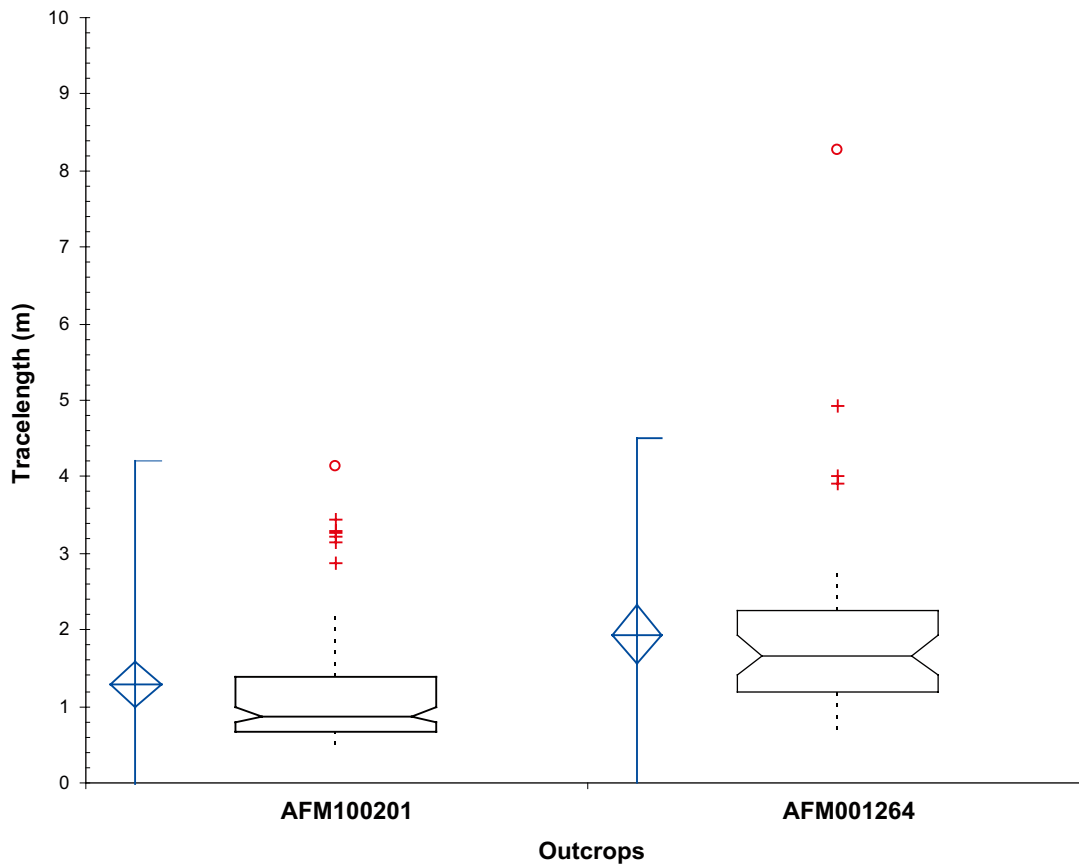
Figure 4-40. *Box and whisker plot, linked fractures, SH Set, Domain FFM02.*

Table 4-34. Comparative statistics and Kruskal-Wallis test results, linked fractures, SH Set, Domain FFM02.

Outcrop	# of fracs.	Mean	Std. Dev.	Std. Err.	95% CI of Mean		Median	IQR	95% CI of Median	
AFM100201	99	1.28	1.50	0.15	0.98	1.58	0.86	0.70	0.80	0.99
AFM001264	46	1.94	1.31	0.19	1.55	2.33	1.66	1.07	1.41	1.93

Outcrop	# of fracs.	Rank sum	Mean rank
AFM001264	46	4,559	99.109
AFM100201	99	6,026	60.869

Kruskal-Wallis statistic			26.003
Probability	0.000	(χ^2 approximation)	
Reject H0 at α = 0.05?			Yes
Lump Outcrops?			No
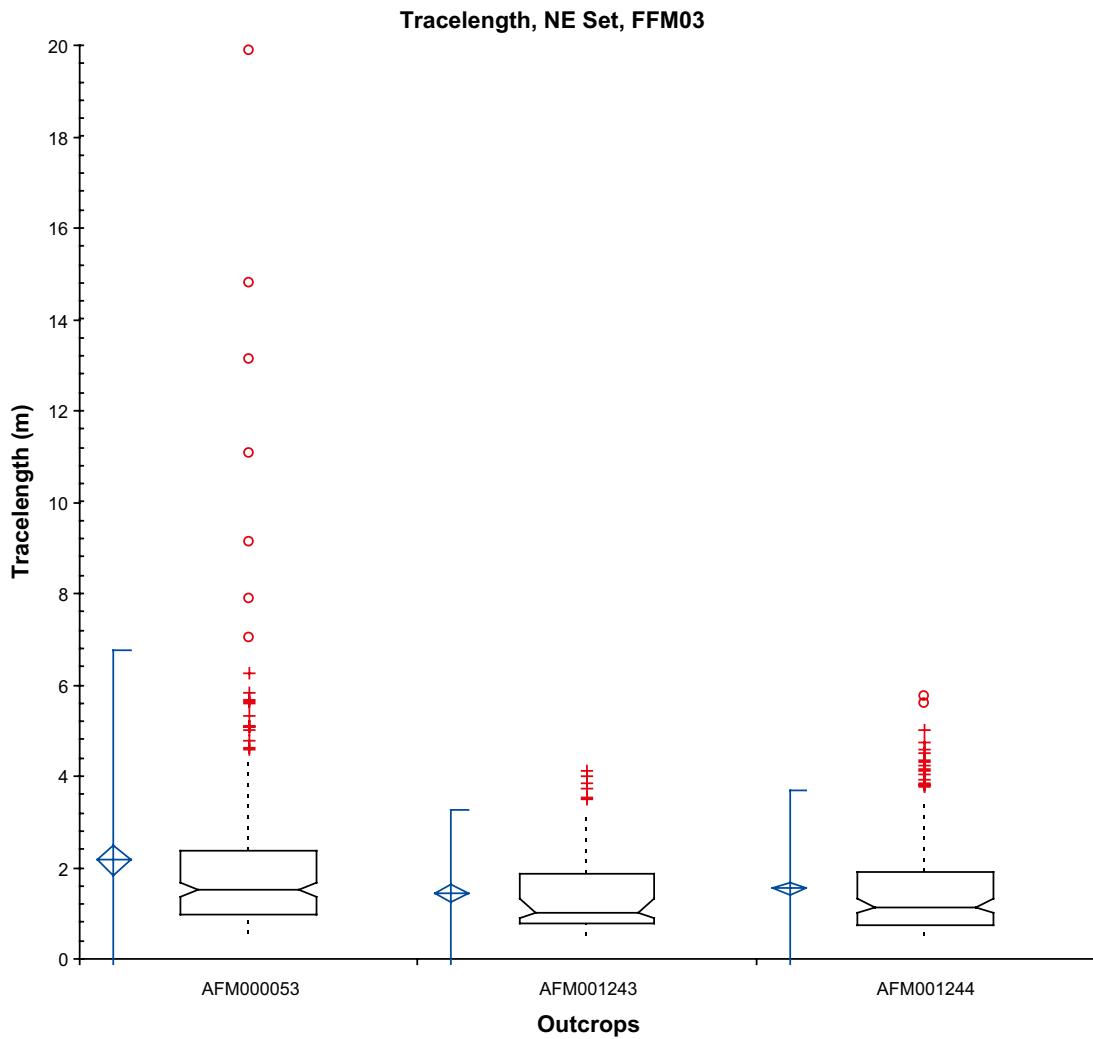
Figure 4-41. *Box and whisker plot, linked fractures, NE Set, Domain FFM03.*

Table 4-35. Comparative statistics and Kruskal-Wallis test results, linked fractures, NE Set, Domain FFM03.

Outcrop	# of fracs.	Mean	Std. Dev.	Std. Err.	95% CI of Mean		Median	IQR	95% CI of Median	
AFM000053	199	2.16	2.35	0.17	1.84	2.49	1.51	1.41	1.35	1.65
AFM001243	98	1.44	0.93	0.09	1.25	1.62	1.00	1.08	0.90	1.31
AFM001244	238	1.55	1.10	0.07	1.41	1.69	1.13	1.18	1.01	1.30

Outcrop	# of fracs.	Rank sum	Mean rank
AFM000053	199	60,325	303.14
AFM001243	98	23,653	241.352
AFM001244	238	59,403	249.592

Kruskal-Wallis statistic			16.569
Probability	0.000	(χ^2 approximation)	
Reject H0 at α = 0.05?		Yes	
Lump Outcrops?		No	

Figure 4-42. *Box and whisker plot, linked fractures, WNW-EW Set, Domain FFM03.*

Table 4-36. Comparative statistics and Kruskal-Wallis test results, linked fractures, WNW-EW Set, Domain FFM03.

Outcrop	# of fracs.	Mean	Std. Dev.	Std. Err.	95% CI of mean		Median	IQR	95% CI of Median	
AFM000053	244	1.67	1.19	0.08	1.52	1.82	1.36	1.20	1.15	1.49
AFM001243	30	1.42	0.88	0.16	1.09	1.75	1.20	0.88	0.91	1.52
AFM001244	57	1.02	0.68	0.09	0.85	1.20	0.79	0.36	0.68	0.91

Outcrop	# of fracs.	Rank sum	Mean rank
AFM000053	244	44,112	180.787
AFM001243	30	4,791	159.700
AFM001244	57	6,043	106.018

Kruskal-Wallis statistic			28.350
Probability	0.000	(χ^2 approximation)	
Reject H0 at α = 0.05?		Yes	
Lump Outcrops?		No	

Figure 4-43. *Box and whisker plot, linked fractures, NW Set, Domain FFM03.*

Table 4-37. Comparative statistics and Kruskal-Wallis test results, linked fractures, NW Set, Domain FFM03.

Outcrop	# of fracs.	Mean	Std. Dev.	Std. Err.	95% CI of mean		Median	IQR	95% CI of Median	
AFM000053	188	2.58	2.60	0.19	2.20	2.95	1.84	1.71	1.57	2.11
AFM001243	176	1.24	0.74	0.06	1.13	1.35	0.96	0.81	0.87	1.11
AFM001244	188	2.58	2.60	0.19	2.20	2.95	1.84	1.71	1.57	2.11

Outcrop	# of fracs.	Rank sum	Mean rank
AFM000053	188	42,297	224.981
AFM001243	176	24,134	137.122
AFM001244	188	42,297	224.981

Kruskal-Wallis statistic			63.377
Probability	0.000	(χ^2 approximation)	
Reject H0 at α = 0.05?		Yes	
Lump Outcrops?		No	
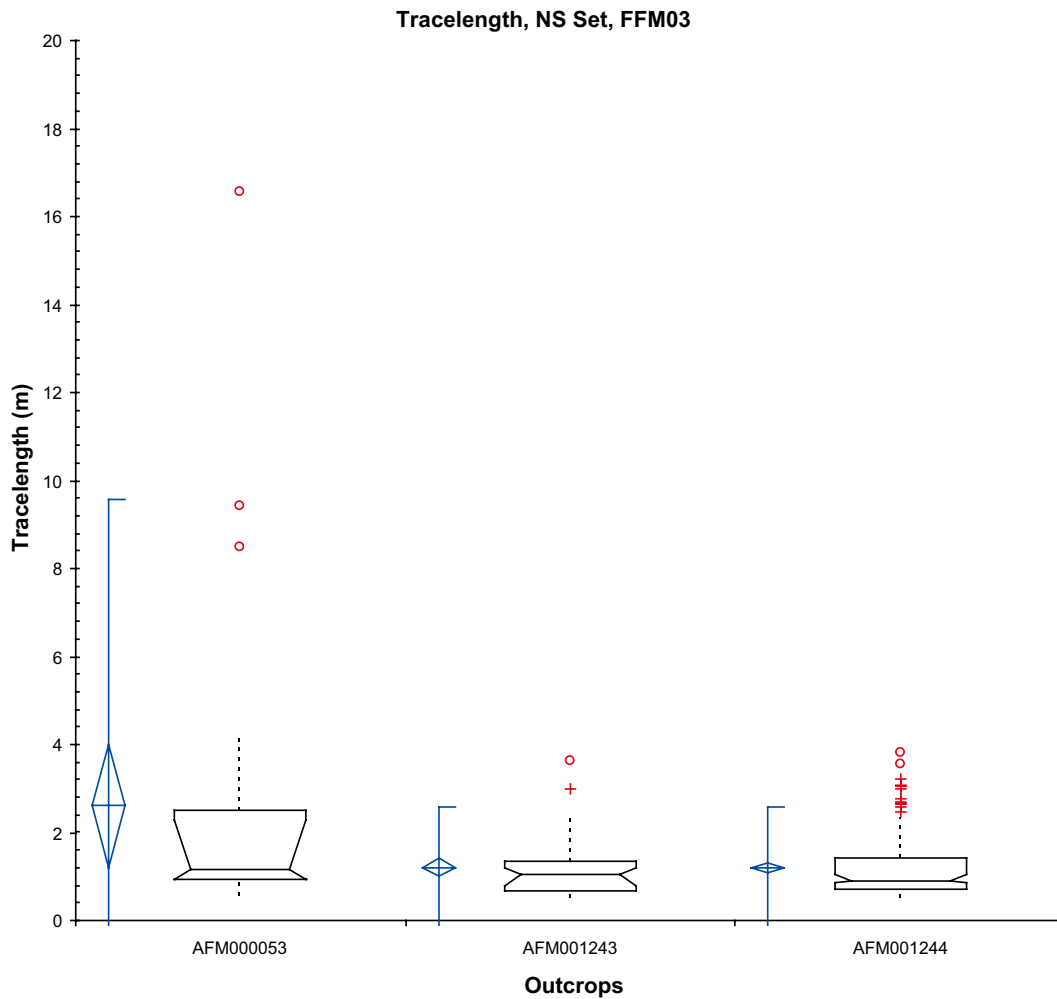
Figure 4-44. *Box and whisker plot, linked fractures, NS Set, Domain FFM03.*

Table 4-38. Comparative statistics and Kruskal-Wallis test results, linked fractures, NS Set, Domain FFM03.

Outcrop	# of fracs.	Mean	Std. Dev.	Std. Err.	95% CI of Mean		Median	IQR	95% CI of Median	
AFM000053	27	2.60	3.56	0.68	1.19	4.01	1.18	1.58	0.95	2.29
AFM001243	42	1.21	0.71	0.11	0.99	1.43	1.04	0.67	0.80	1.18
AFM001244	146	1.19	0.71	0.06	1.07	1.30	0.91	0.71	0.86	1.05

Outcrop	# of fracs.	Rank sum	Mean rank
AFM000053	27	3,592	133.019
AFM001243	42	4,522	107.667
AFM001244	146	15,107	103.469

Kruskal-Wallis statistic			5.143
Probability	0.076	(χ^2 approximation)	
Reject H0 at α = 0.05?		No	
Lump Outcrops?		Yes	

Figure 4-45. *Box and whisker plot, linked fractures, SH Set, Domain FFM03.*

Table 4-39. Comparative statistics and Kruskal-Wallis test results, linked fractures, SH Set, Domain FFM03.

Outcrop	# of fracs.	Mean	Std. Dev.	Std. Err.	95% CI of Mean		Median	IQR	95% CI of Median	
AFM000053	60	1.47	1.02	0.13	1.21	1.74	1.17	0.80	0.94	1.38
AFM001243	10	1.40	0.98	0.31	0.70	2.10	0.98	0.58	0.74	2.40
AFM001244	56	1.06	0.51	0.07	0.93	1.20	0.89	0.70	0.78	1.00

Outcrop	# of fracs.	Rank sum	Mean rank
AFM000053	60	4,306	71.767
AFM001243	10	654	65.400
AFM001244	56	3,041	54.304

Kruskal-Wallis statistic			6.654
Probability	0.036	(χ^2 approximation)	
Reject H0 at α = 0.05?		Yes	
Lump Outcrops?		No	

103

Outcrop scale size model

For the Outcrop Scale size model, the Kruskal-Wallis tests suggested that:

- In Domain FFM02, the NE and NW global sets could be lumped together across different outcrops into a single population for model parameterization;

- In Domain FFM03, it was only possible to lump together the NS global set across different outcrops.

For these outcrops, the traces were re-loaded into FracSys/FracSize, and the fracture radius distribution recomputed. In addition, the traces were combined to produce composite trace length scaling cumulative number plots. For the remainder of the outcrops, the Kruskal-Wallis tests indicated that the remaining global sets (SH, NS, and EW in FFM02, and NE, NW, EW, and SH in FFM03) represented different size distributions on different outcrops. As such, it was necessary to then choose which outcrop in a fracture domain would be used for the size model parameterization. As discussed in Chapter 3.2.3, a power-law (Pareto distribution) relationship was chosen to describe fracture sizes for all domains based on the trace length scaling plots presented in Appendix A. This decision was made largely to minimize simulation artifacts caused by fitting the large number of small traces after the power law distribution 'rolls over'. If the use of other size distributions besides power law is required, the FracSize fits can be utilized.

In Domain FFM02, outcrop AFM100201 was chosen to define the Outcrop Scale size distribution. The decision was based on the reduced potential for sample bias and censoring (when compared to AFM001264 and AFM001265), the larger physical area, the larger trace sample size, and the level of detail of the mapping.

In Domain FFM03, outcrop AFM000053 was chosen to define the Outcrop Scale size distribution. The other outcrops in the domain (AFM001243 and AFM001244) are long strip trenches constructed across known and postulated deformation zones. These trenches are both highly biased and censored, due to their aspect ratio. As such, AFM000053 provides a better estimate of an unbiased trace pattern.

For Domains FFM02 and FFM03, the minimum radius (r_0) and match point P_{32} represent the values at which the size model simultaneously matches both the detailed outcrop mapping data and the fracture record from the cored borehole data. For Domains FFM01 and FFM06, since no actual outcrop data is available for size matching, we assume that the size model for each set uses the same radius exponent (k_r) as Domain FFM02; see Chapter 3.2.3 for more details. The minimum radius (r_0) is set at the borehole radius, which, for NQ core, is approximately 0.0385 m. The P_{32} 'match' point associated with this size model for FFM01 and FFM06 represents the average (mean) P_{32}, as calculated from P_{10} values over 6-meter bin lengths using the Wang method.

Table 4-40 through Table 4-43 present the Outcrop Scale size model parameters. Note that the values in the tables below have NOT been truncated to lie within the parameter limits (r_{min} = 0.5 m, r_{max} = 564 m) of the SDM Forsmark 2.2 geological DFN model, as per the DFN memorandum /Munier 2006/. The appropriate truncated values are presented in the model summary tables in Chapter 7. Note that the values presented in the table for the power law scaling exponent are k_r (the radius exponent). If you will be simulating fractures in FracMan, you will need to use b, which is equal to $k_r + 1$, to specify the size exponent.

Table 4-40. Outcrop Scale size model, Domain FFM01.

Fracture domain	Fracture set	Set type	Size distribution	Min. radius r_0 (m)	Exponent (k_r)	Match P_{32}* r_0–∞ (1/m)
FFM01	NE	Global	Power Law	0.039	2.64	1.74
FFM01	NS	Global	Power Law	0.039	2.90	1.29
FFM01	NW	Global	Power Law	0.039	2.44	0.95
FFM01	SH	Global	Power Law	0.039	2.61	0.63
FFM01	ENE	Local	Power Law	0.039	2.20	2.74
FFM01	EW	Local	Power Law	0.039	3.06	1.12
FFM01	NNE	Local	Power Law	0.039	3.00	4.39
FFM01	SH2	Local	From SH	0.039	2.61	0.92
FFM01	SH3	Local	From SH	0.039	2.61	0.84

Table 4-41. Outcrop Scale size model, Domain FFM02.

Fracture domain	Fracture set	Set type	Size distribution	Min. radius r_0 (m)	Exponent (k_r)	Match P_{32} r_0–∞ (1/m)
FFM02	NE	Global	Power Law	0.10	2.64	3.31
FFM02	NS	Global	Power Law	0.06	2.90	1.61
FFM02	NW	Global	Power Law	0.04	2.44	2.12
FFM02	SH	Global	Power Law	0.07	2.61	2.78
FFM02	ENE	Global	Power Law	0.039*	2.20	3.65
FFM02	EW	Global	Power Law	0.15	3.06	1.19
FFM02	NNE	Local	Power Law	0.50	3.00	1.35
FFM02	NNW	Local	NA **			

* Not possible to simultaneously match borehole and outcrop data; minimum radius set at borehole radius.
** Impossible to parameterize; no trace data available (seen in boreholes only).

Table 4-42. Global fracture sets size models, Domain FFM03, Outcrop Scale Model.

Fracture domain	Fracture set	Set type	Size distribution	Min. radius r_0 (m)	Exponent (k_r)	Match P_{32} r_0–∞ (1/m)
FFM03	NE	Global	Power Law	0.07	2.62	2.91
FFM03	NS	Global	Power Law	0.05	2.63	1.49
FFM03	NW	Global	Power Law	0.36	2.59	1.46
FFM03	SH	Global	Power Law	0.12	2.57	0.96
FFM03	ENE	Local	Power Law	0.65	2.70	0.30
FFM03	EW	Local2	Power Law	1.03*	3.36	0.44

* Not possible to simultaneously match borehole and outcrop data; the surface appears to be more intensely fractured than the rock found in the cored boreholes.

Table 4-43. Global fracture sets size models, Domain FFM06, Outcrop Scale Model.

Fracture domain	Fracture set	Set type	Size distribution	Min. radius r_0 (m)	Exponent (k_r)	Match P_{32}* r_0–∞ (1/m)
FFM06	NE	Global	Power Law	0.039	2.64	3.30
FFM06	NS	Global	Power Law	0.039	2.90	2.15
FFM06	NW	Global	Power Law	0.039	2.44	1.61
FFM06	SH	Global	Power Law	0.039	2.61	0.64
FFM06	ENE	Local	Power Law	0.039	2.20	0.98
FFM06	SH2	Local	Power Law	0.039	2.61	1.03

Parameter variability

Parameter variability in the Outcrop Scale size model was addressed through two separate methods:

- Kruskal-Wallis analysis (previous section) tested the hypothesis that it was possible to lump together traces from the same set on different outcrops to construct a size distribution.

- The presentation of summary statistics, including means, percentiles, medians, and quartiles for each set in each fracture domain. These values allow for the stochastic simulation of variable fracture size distributions by downstream users, if so desired. Note that the DFN size-intensity models are anchored at single points (i.e. a 'match' P_{32}).

It should be noted that, for cases where the K-W test would not allow for the combination of trace sets that a judgment call was made as to which outcrop trace pattern most likely represented reality. However, if desired, it is possible to stochastically test alternative distributions by using the additional outcrop set fits presented in Table 4-28 and Table 4-29.

4.2.2   Tectonic fault model (TFM)

The Tectonic Fault Model (TFM) is a variant power-law scaling model that in practice is the polar opposite to the 'tectonic continuum' concept. It hypothesizes that the structures identified in both the DZ model and in the ground magnetic lineaments represent faults (Mode II and Mode III dislocations; minor and major deformation zones in the current site modeling parlance), while the structures identified on outcrops are primarily joints (Mode I dislocations). As such, it is likely that the two sets of features have different size and intensity distributions.

To completely parameterize a DFN using the TFM, it is necessary to use two different size distributions:

- The Outcrop Scale Model describes fracturing at the outcrop scale (joints). It is necessary to apply an upper truncation to both the size and intensity of the Outcrop Scale Model for each fracture set and fracture domain. Typically, the Outcrop Scale Model is used to describe the fracture pattern up to the onset of Euclidean scaling (0.5– ~30 m).

- The Tectonic Fault model then is used to describe the discontinuities (predominantly faults) at intermediate scales (~20–564 m) between the outcrop model and the DZ model.

The TFM is parameterized by fitting a power-law size-scaling exponent to trace data; only the ground magnetic lineaments and the deformation zone model traces are used. The TFM model assumes Euclidean size-intensity scaling; no mass fractal scaling alternative is produced. The trace length scaling plots used to parameterize the TFM are presented as Figure 9-1 through Figure 9-5 in Appendix A. Note that the SH Global set is not parameterized in the TFM model; no subhorizontal ground magnetic lineaments were noted in the data set. We recommend using the TCM model parameterization for the SH set, with the P_{32} recalculated based on a 28 m cutoff; these values have been included in the TFM model table.

A minimum radius cutoff (r_{min}) of 28 m was chosen for parameterization; this represents the effective radius of a square fracture with a 50 m trace length. The 28 m cutoff was chosen because:

1. Previous studies at sites in Sweden using length-transmissivity correlations /Dershowitz et al. 2003/ have suggested that a natural break in structure type occur at approximately 20 m–30 m scales. We hypothesize that this break represents the boundary between joint features and 'fault' features (joints reactivated and sheared, deformation zones, fracture swarms), which are of much grater interest for safety calculations for movements due to future earthquakes than the smaller-sized joints; and

2. The smallest trace mapped in the ground magnetic lineament data set is approximately 35 m long; the shortest traces for most other sets in the GML data are between 40 m and 50 m in length. It has been generally accepted, at least at Forsmark, that magnetic lineaments represent deformation zones or swarms of fractures (/Munier et al. 2003, Korhonen et al. 2004/). As such, it is appropriate to treat the ground magnetic lineament data set as faults.

The TFM model is not constrained to borehole data, although borehole data is used in the validation of the TFM model, because of the difficulty in determining what fracture set an MDZ delineated in the borehole data might belong to. MDZs exist as clusters of fractures; without additional information from borehole geophysics, hydraulic testing, or geometric modeling, it is not possible to assign the suspect MDZs in the borehole record to a specific 'fracture set'.

As the DFN model is built on orientation sets, the lack of set classifications for MDZ and DZ make them difficult to use in a DFN parameterization. As such, the TFM model is build solely from surface data. However, the borehole MDZ and DZ intersections are used as a validation exercise in Chapter 6 to build confidence in the model and to illustrate the results of using a 28 m radius cut-off in the TFM model. The TFM model parameters are presented below in Table 4-44.

4.2.3 Tectonic continuum size models

Past geological DFN models constructed for SKB site-descriptive models (SDM Forsmark 1.2, SDM Laxemar 1.2) have primarily used a coupled size-intensity scaling model built around the Pareto distribution ('power-law' scaling) to model outcrop and regional-scale fracturing. The Outcrop Scale size model described in the previous chapter does not use these size-intensity scaling relationships; it is built by extrapolating a size model for joints from the outcrop data alone.

Table 4-44. TFM parameters, all fracture domains.

Fracture domain	Fracture set	Set type	Size distribution	Min. radius r_0 (m)	Exponent (k_r)	Match P_{32} r_0–564 (1/m)
All Domains	NE	Global	Power Law	28	3	0.0285
All Domains	NS	Global	Power Law	28	2.2	0.0003
All Domains	NW	Global	Power Law	28	2.06	0.0003
All Domains	SH*	Global	Power Law	28	2.83	0.0286
All Domains	ENE	Global	Power Law	28	3.14	0.0871
All Domains	EW	Global	Power Law	28	2.85	0.0014

* SH set uses TCM radius exponent, but with P_{32} recalculated for new r_0.

However, it is still necessary to evaluate alternative size model hypotheses, such that the Forsmark 2.2 geological DFN is comparable to past models. As such, the parameterization of the version 2.2 Forsmark geological DFN includes two alternative size models that follow the tectonic continuum hypothesis: the Tectonic Continuum, Euclidean Scaling Model (TCM), and the Tectonic Continuum, Fractal Mass Scaling Model (TCMF). The methodology behind each alternative is described in great detail in Chapter 3.2.3.

Note that by their very nature, local sets are not accommodated for in the Tectonic Continuum models. The local sets do not have a visible component in either the ground magnetic lineament data or in the DZ models. As such, it is impossible to develop a coupled size-intensity relationship for them. For these sets, we recommend using the Outcrop Scale model parameters.

Basics of the tectonic continuum

The 'tectonic continuum' was a somewhat useful hypothesis postulated during SDM Laxemar 1.2. At its heart is the idea that both the size and intensity of fractures at multiple scales can be approximated through the use of a power-law relationship. The tectonic continuum model hypothesizes correlated size-intensity; it is not possible to change one without changing the other. These models describe how both the size and intensity of a given fracture set change with scale.

The tectonic continuum model is a useful concept because:

- It is fundamentally scale-invariant;

- It is consistent with current thinking about the nature of the large-scale deformation zones at Forsmark (that DZ are basically clusters of smaller fractures);

- Easy correlation between size and intensity for a (relatively) simple parameterization;

- Allows for the use of data at multiple scales (borehole, outcrop, regional geophysics) in the size parameterization; and

- Allows for the simulation of fractures in the critical size range between 50 m and 1,000 m (trace length) where there is a relative paucity of data.

However, the tectonic continuum hypothesis may not necessarily be geologically reasonable:

- Mechanical and rheological differences between faults and joints;

- The inherent implication that the exact-same stress patterns and stress history acted at both outcrop and regional scales; and

- The assumption of relative lithologic homogeneity (which was valid at Laxemar) may not be accurate for the Forsmark site, which has experienced very high levels of brittle and ductile deformation in the past.

The tectonic continuum model alternatives are based largely on surface fracture trace data at multiple scales. This makes for a difficult decision when developing a size model for domains FFM01 and FFM06. There are no outcrops available for these fracture domains; as such, assumptions have to be made as to how the size-intensity coupled scaling behaves in these domains. There are three basic options for modeling how the size-intensity couple behaves in under-sampled domains:

1. The model can be constrained by the P_{32} of the deformation zone fraction (as in the Laxemar 1.2 geological DFN). This requires that the DZ, which in the geometric model exist as rock volumes, be treated as single planar features, with additional assumptions made about their geometry and surface areas. A unique match point based on outcrop P_{21} and the radius exponent can then be generated, and compared to the borehole data intensity values to determine a final model fit. This alternative has the disadvantage that assumptions must be made about the intensity of the DZ in the subsurface, as well as the fact that it does not directly use the borehole intensity data for parameterization (the model is based solely on surface data).

2. The model can be constrained by the radius scaling exponent fit to one of the fracture domains that does posses outcrop size data (FFM02 and FFM03). Geologically, FFM01 appears very similar to FFM02, other than their differences in terms of the intensity of fracturing. The assumption is then made that FFM01 and FFM06 obey the same size/intensity scaling relationship as FFM02; this means that, when the coupled size-intensity models for FFM01 and FFM06 are fit to borehole intensity data, the radius exponent (k_r) and outcrop intensity match points (P_{32OC}) are the same as in FFM02. The only difference between the domains then becomes the final P_{32} match point, which is coupled to the borehole intensities (P_{32BH}), and the final minimum radius (r_0), i.e. adjusted to the lower P_{32} in FFM06.

3. The model can be constrained by fixing the minimum radius (r_0) for all distributions. By fixing r_0 and using the borehole fracture intensity (P_{32BH}), it would be possible to then calculate a range of radius exponents (k_r). As neither the true radius exponent nor the true minimum radius for FFM01 or FFM06 is known, this becomes a non-unique solution. It also lacks a physical basis on which to base the fracture size model.

The second alternative was chosen by the DFN modeling team for size-intensity parameterization in the tectonic continuum models. It was believed that this alternative best matched the site conceptualization; as the domains are lithologically similar, their patterns of breakage and fracturing should be the same. This is also in accordance with the current geological conceptualization of the site, where FFM01 and FFM02 are different largely in terms of intensity.

However, this choice does have a consequence: as the intensities in FFM01 are generally less than those in FFM02, to maintain the same size-intensity relation, it is necessary to, in some cases, increase the minimum radius (r_0) beyond that which fit the outcrops in FFM02. This situation suggests that the intensity of fracturing in outcrops in FFM02 is probably much greater than in FFM01, or that the scaling exponent for FFM01 for the set is smaller than the one for the set in FFM02. The impact of this uncertainty is examined in Section 5.

The only difference between the two tectonic continuum models (Euclidean and Fractal) are as to how intensity is hypothesized to change as a function of scale. In the Euclidean models, intensity scales linearly as a function of area. In the fractal models, areal intensity scaling follows the fractal mass dimension (see Chapter 3.2.4).

Parameterization of the tectonic continuum models

The mathematics behind the construction of the correlated size-intensity models is described in great detail in Chapter 3.2.3. A brief summary is presented here for review. The workflow for the parameterization of the tectonic continuum models is as follows:

1. Area-normalized cumulative number plots that describe the trace length/intensity scaling relationship. These plots are constructed by set for each fracture domain, and allow for the direct comparison of data from three different scales (outcrop mapping, high-resolution ground magnetic lineaments, and the 2.2 DZ model surface traces). The CCN plots for the TCM and TCMF alternatives are presented as Figure 9-6 through Figure 9-29 in Appendix A.

2. The radius exponent, k_r, was derived from the trace length scaling plots. An intensity value (P_{32OC}) at which simulated outcrop trace length intensities (P_{21}) matches observed outcrop trace lengths was calculated through simulation, assuming a fixed minimum radius (0.5 m).

3. The final size-intensity model parameters were constrained to borehole fracture intensity data (P_{32BH}) by changing the power law minimum radius value (r_0). In cases where it was not possible to simultaneously match borehole and outcrop data, the model defaults to matching borehole data.

The tectonic continuum size intensity models are summarized in Table 4-45 through Table 4-52. 'Match P_{32}' represents the correlated size-intensity value at which both the outcrop trace data and the borehole fracture intensity data are matched; i.e. the size-intensity model will simultaneously fit both scales. The associated area-normalized trace length scaling plots are presented in Appendix A.

Table 4-45. TCM size model, Domain FFM01.

Fracture domain	Fracture set	Set type	Size distribution	Min. Radius r_0 (m)	Exponent (k_r)	Match P_{32} $r_0-\infty$ (1/m)
FFM01	NE	Global	Power Law	0.66	3.02	1.74
FFM01	NS	Global	Power Law	0.06	2.78	1.29
FFM01	NW	Global	Power Law	0.59	2.85	0.95
FFM01	SH	Global	Power Law	0.82	2.85	0.63
FFM01	ENE	Local	Power Law	0.32	3.25	2.74
FFM01	EW	Local	Power Law	0.17	3.1	1.12
FFM01	NNE	Local	Use Size Model from Outcrop Scale Model			
FFM01	SH2	Local	Use Model for SH Set from Outcrop Scale Model			
FFM01	SH3	Local	Use Model for SH Set from Outcrop Scale Model			

Table 4-46. TCM size model, Domain FFM02.

Fracture domain	Fracture set	Set type	Size distribution	Min. radius r_0 (m)	Exponent (k_r)	Match P_{32} $r_0-\infty$ (1/m)
FFM02	NE	Global	Power Law	0.35	3.02	3.31
FFM02	NS	Global	Power Law	0.04	2.78	1.61
FFM02	NW	Global	Power Law	0.23	2.85	2.12
FFM02	SH	Global	Power Law	0.14	2.85	2.78
FFM02	ENE	Global	Power Law	0.26	3.25	3.65
FFM02	EW	Global	Power Law	0.16	3.1	1.19
FFM02	NNE	Local	Use Size Model from Outcrop Scale Model			
FFM02	NNW	Local	Use Size Model from Outcrop Scale Model			

Table 4-47. TCM size model, Domain FFM03.

Fracture domain	Fracture set	Set type	Size distribution	Min. Radius r_0 (m)	Exponent (k_r)	Match P_{32} $r_0-\infty$ (1/m)
FFM03	NE	Global	Power Law	0.24	2.95	2.91
FFM03	NS	Global	Power Law	0.36	2.93	1.49
FFM03	NW	Global	Power Law	0.59	2.90	1.46
FFM03	SH	Global	Power Law	0.20	2.81	0.96
FFM03	EW	Global	Power Law	0.93	3.24	0.44
FFM03	ENE	Local	Power Law	0.5	3.13	0.74*

* No borehole data; P_{32} and r_0 matched solely to outcrop data.

Table 4-48. TCM size model, Domain FFM06.

Fracture domain	Fracture set	Set type	Size distribution	Min. radius r_0 (m)	Exponent (k_r)	Match P_{32} r_0–∞ (1/m)
FFM06	NE	Global	Power Law	0.35	3.02	3.30
FFM06	NS	Global	Power Law	0.039*	2.78	2.15
FFM06	NW	Global	Power Law	0.32	2.85	1.61
FFM06	SH	Global	Power Law	0.79	2.85	0.64
FFM06	ENE	Local	Power Law	0.74	3.25	0.98
FFM06	SH2	Local	Use Model for SH Set from Outcrop Scale Model			

* Not possible to simultaneously match borehole and outcrop data; default to fitting borehole data.

Table 4-49. TCMF size model, Domain FFM01.

Fracture domain	Fracture set	Set type	Size distribution	Min. radius r_0 (m)	Exponent (k_r)	Match P_{32} r_0–∞ (1/m)
FFM01	NE	Global	Power Law	0.72	3.01	1.74
FFM01	NS	Global	Power Law	0.06	2.76	1.29
FFM01	NW	Global	Power Law	0.63	2.85	0.95
FFM01	SH	Global	Power Law	0.72	2.83	0.63
FFM01	ENE*	Local	Power Law	0.34	3.25	2.74
FFM01	EW	Local	Power Law	0.17	3.13	1.12
FFM01	NNE	Local	Use Size Model from Outcrop Scale Model			
FFM01	SH2	Local	Use Model for SH Set from Outcrop Scale Model			
FFM01	SH3	Local	Use Model for SH Set from Outcrop Scale Model			

* ENE set is labeled a local set in FFM01, but is simulated based on global set parameters from FFM02. ENE set is seen very strong in some FFM01 boreholes.

Table 4-50. TCMF size model, Domain FFM02.

Fracture domain	Fracture set	Set type	Size distribution	Min. radius r_0 (m)	Exponent (k_r)	Match P_{32} r_0–∞ (1/m)
FFM02	NE	Global	Power Law	0.38	3.01	3.31
FFM02	NS	Global	Power Law	0.05	2.76	1.61
FFM02	NW	Global	Power Law	0.24	2.85	2.12
FFM02	SH	Global	Power Law	0.12	2.83	2.78
FFM02	ENE	Global	Power Law	0.27	3.25	3.65
FFM02	EW	Global	Power Law	0.19	3.13	1.19
FFM02	NNE	Local	Use Size Model from Outcrop Scale Model			
FFM02	NNW	Local	Use Size Model from Outcrop Scale Model			

Table 4-51. TCMF size model, Domain FFM03.

Fracture Domain	Fracture Set	Set Type	Size Distribution	Min. Radius r_0 (m)	Exponent (k_r)	Match P_{32} r_0–∞ (1/m)
FFM03	NE	Global	Power Law	0.21	2.94	2.91
FFM03	NS	Global	Power Law	0.31	2.92	1.49
FFM03	NW	Global	Power Law	0.69	2.89	1.46
FFM03	SH	Global	Power Law	0.25	2.81	0.96
FFM03	EW	Global	Power Law	1.04	3.25	0.44
FFM03	ENE	Local	Use Size Model from Outcrop Scale Model*			

* ENE defined as a local set in FFM03.

Table 4-52. TCMF size model, Domain FFM06.

Fracture Domain	Fracture Set	Set Type	Size Distribution	Min. Radius r_0 (m)	Exponent (k_r)	Match P_{32} r_0–∞ (1/m)
FFM06	NE	Global	Power Law	0.38	3.01	3.30
FFM06	NS	Global	Power Law	0.039*	2.76	2.15
FFM06	NW	Global	Power Law	0.34	2.85	1.61
FFM06	SH	Global	Power Law	0.70	2.83	0.64
FFM06	ENE	Local	Power Law	0.78	3.25	0.98
FFM06	SH2	Local	Use Model for SH Set from Outcrop Scale Model			

* Not possible to simultaneously match borehole and outcrop data; default to fitting borehole data.

4.2.4 Evaluation of uncertainties

There are both conceptual and parameter uncertainties associated with the size model. The conceptual uncertainties associated with the size model come from the following sources:

* The "tectonic continuum" assumption;

* The uncertainty regarding to what extent ground based magnetic lineaments represent fracture traces;

* Whether the fracture intensity scales according to a fractal, a Euclidean or a composite scaling model over the scale ranges of interest for calculating the cumulative number/scaling plots;

* Whether linked or unlinked traces are the best representing of fracture lengths;

* The lack of constraints for the possible maximum size of subhorizontal fractures;

* The accuracy of the set definitions; and

* The scaling behavior of fracture intensity from the scale of outcrops to the scale of deformation zones.

There are also parameter uncertainties:

* For the OSM, there may be one or more probability distributions that show statistically significant fits to the measured data;

- Also, for a given parameterized size distribution in the OSM, the fit is not perfect, as measured by the test statistic; and

- For the tectonic continuum-based models, there is often more than one outcrop data set for the fracture domain, and the normalized cumulative size/number plots for the different outcrops may show some variability. This produces uncertainty in the fit of a line between the outcrop data and the deformation zone data sets; it is possible to obtain a different radius exponent (kr) by fitting the trace scaling relationship to a different outcrop. The current parameterization uses the outcrops judged to be most representative of the fracture domains as a whole.

4.3   Spatial model

4.3.1   Assumptions

The spatial model describes how many fractures occur in a specific volume of rock at a specific location in the modeling domain. As such, the model may depend upon the depth, the rock type, the influence of tectonic processes, the volume of interest and other geological factors. It may differ by fracture set as well. The derivation of the spatial is based on the assumptions that:

- Fracture set definitions are correct;

- DZ and MDZ are not part of the background fracture sets.

- Identification and delineation of deformation zones are correct;

- Outcrop data is relevant to the subsurface.

The derivation of the spatial model does not require knowledge of the fracture sizes, but it does depend upon the definition of the fracture sets and their associated orientation models. If the set definitions change, then the conceptual spatial model and its parameterization may also change.

The spatial model is intimately connected with fracture intensity. The intensity values are derived from outcrop and borehole data. In the SDM Forsmark version 2.2 geological DFN, fractures in boreholes and outcrops identified as belonging to DZ and MDZ were removed from the data used for derivation of the spatial model. If the spatial extent of the DZ and MDZ changes, or if MDZ are no longer viewed as a distinct from the background fracturing, then the underlying data used to develop the spatial model will change with unknown results.

A third important assumption is that the fracture data in outcrop is relevant to the subsurface, and can be integrated in some meaningful fashion with borehole fracture data. The possibility of this assumption not being true comes from the possibility that the surficial stress relief after the last glaciation produced some additional fracturing or fracture enhancement near the surface, especially in the subhorizontal fracture set that would be most favorably oriented for such enhancement. Data from the Forsmark nuclear power plant excavation provides quantitative data on depth to which this enhancement of subhorizontal fractures may have occurred, as well as providing some qualitative data on stress-relief effects on the subhorizontal fractures. If the post-glacial stress relief effects have significantly enhanced fracturing at the surface, then mixing outcrop and borehole fracture data may be problematic and lead to incorrect or highly uncertain results. For the purposes of the SDM Forsmark version 2.2 geological DFN, it was assumed that post-glacial stress relief impacted all fracturing down to some unknown depth. In reality, the data from the Forsmark nuclear power plant excavation /Carlsson 1979/ provides good evidence that the effects only impact the subhorizontal set, and there only to a depth of a few tens of meters.

4.3.2 Primary model

The spatial model addresses two related aspects of the variation in fracture intensity; how intensity may change with scale, and how intensity may change with geology. Many published studies have shown that even within a homogeneous geological environment consisting of the same lithology, alteration degree and tectonic history, fracture intensity changes according to a power law or other mathematical model as a function of scale. This aspect of the spatial model is important for predicting fracture intensity at scales of interest based on data measured at different scales.

Published studies have also shown how fracture intensity may vary based upon geological factors such as lithology. Thus it is important to know what geological factors might impact fracture intensity regardless of scale. The spatial model was derived through consideration of these two aspects.

Data used

The spatial model is based on analyses of outcrop and borehole fracture data; please refer to Section 2.1 for details on sources and extent of data utilized. The outcrop data used consists of linked and unlinked trace lengths, with the traces for each outcrop separated into the sets identified in Section 4.1. The borehole data used for analyses consists of the location in terms of measured depth (MD), with data from deformation and minor deformation zones excluded from the analysis. As in the case of the outcrops, the fractures in the each set identified were analyzed separately. Only fractures identified as "Visible in BIPS" were used.

Mass dimensions

Outcrop data

The results of the mass dimension calculations for the outcrop data are shown in Figure 10-1 through Figure 10-86, in Appendix B. Each figure represents the mass dimension of traces belonging to a specific fracture set and outcrop. The mass dimension plot consists of a series of points that represent the number of fractures within a circle of radius r for a randomly selected point on an existing fracture trace. This set of points is designated as the data "cloud". The plots also show the mean number of fractures for all randomly located circle centroids over a range of radii values; these calculations are shown as red filled circles and are referred to as the "locus of the mean" or the "mean locus". The line superimposed on the data cloud and mean locus represents a power law fit to the data. In most cases, this line was fit through non-linear regression using all of the points in the data cloud, since linear regression of log-transformed results produces a fit biased towards smaller values and misleading statistics In a few cases, the line was fit manually by user-specification of the parameters for the power law. This was required when the automatic fit was clearly not accurate due to data outliers, as is noted in the figure captions.

Data reported for each plot consists of the two parameters of the power law fit, that is, the slope and constant in the equation; the radius value corresponding to the onset of Euclidean scaling, estimated visually; and the fit statistics.

The tables (Table 4-53 and Table 4-54) show the parameters and fit statistics for the linked and unlinked data, further separated by outcrop and fracture set. Visual inspection of these tables suggests that the mass fractal dimension, D_m, appears to generally be in the 1.8 to 1.9 range, although there are some lower and higher values. A few of the sets and outcrops were such that the derived values are highly uncertain due to the outcrop shape or the small number of traces. These are noted as well. In particular, the values derived for outcrop AFM001265 and for the subhorizontal set in outcrop AFM001243 were difficult to determine. For this reason, analyses of the resulting mass dimension parameters were also carried out for two subsets: all of the data; and all of the data with the values from AFM001265 and the subhorizontal set from AFM001243 excluded.

Table 4-53. Fit parameters and fit statistics for mass dimension of traces in outcrop, unlinked traces. The "*"symbol indicates that the least-squares fit failed and the parameters were estimated by visually fitting a line. The "!" symbol indicates that the model was fitted to the meqan locus due to difficulties in fitting the data cloud.

Outcrop – unlinked traces		ρ	D_m	SSQ	SDE	
AFM000053	NE	3.68	1.83	6.98E+05	18.55	
AFM000053	NW	4.20	1.75	9.80E+05	22.01	
AFM000053	NS	0.35	1.91	3.30E+04	4.26	
AFM000053	SH	1.75	1.78	7.24E+05	19.68	*
AFM000053	ENE	1.05	1.98	1.98E+06	32.05	
AFM000053	WNW	4.50	1.87	4.25E+06	32.89	*
AFM000054	NE	5.19	1.89	8.93E+05	20.94	
AFM000054	NW	1.76	1.85	1.60E+05	9.07	
AFM000054	NS	1.83	1.89	6.87E+05	18.75	
AFM000054	SH	1.30	1.77	1.49E+05	8.67	
AFM000054	WNW	3.96	1.87	2.65E+06	36.31	
AFM001097	NE	15.20	1.93	1.09E+07	73.49	
AFM001097	NW	7.60	1.71	2.73E+06	36.83	
AFM001097	NS	2.30	1.93	6.00E+05	18.30	
AFM001097	SH	0.63	1.95	2.46E+05	11.72	
AFM001097	EW	4.10	1.77	6.20E+05	17.42	
AFM001098	NE	9.74	1.99	2.04E+06	31.82	
AFM001098	NW	2.86	2.02	1.96E+05	10.20	
AFM001098	SH	3.08	1.75	6.16E+05	18.17	
AFM001098	NNE	10.34	1.96	1.27E+07	81.34	
AFM001098	WNW	9.92	1.90	8.62E+05	20.76	
AFM001243	NE	18.29	2.15	1.07E+07	74.26	
AFM001243	NS	9.80	1.78	2.85E+06	27.19	
AFM001243	SH	5.51	0.98	3.76E+04	4.52	Bad Data
AFM001243	WNW	6.30	1.92	1.46E+06	28.31	
AFM001244	NE	20.00	1.80	2.82E+07	118.35	*
AFM001244	NW	12.00	1.80	1.05E+07	72.19	*
AFM001244	NS	9.54	1.77	1.36E+06	25.78	
AFM001244	SH	2.32	2.07	5.89E+05	17.34	
AFM001244	EW	4.80	1.80	2.13E+05	10.39	*
AFM001264	NE	7.52	1.94	6.46E+05	18.25	
AFM001264	NW	4.62	2.07	3.62E+05	13.61	
AFM001264	NS	5.02	1.54	8.70E+04	6.59	
AFM001264	ENE	6.02	1.81	3.56E+05	8.66	
AFM001264	WNW	5.89	1.82	1.35E+05	8.36	
AFM001265	NE	139.14	2.46	1.45E+03	1.22	!
AFM001265	NS/NNE					unable to fit
AFM001265	EW	73.00	2.31	1.37E+00	0.59	!
AFM100201	NE	16.37	1.85	7.10E+06	59.29	
AFM100201	NW	8.16	1.94	8.95E+06	87.36	
AFM100201	NS	3.90	1.80	6.81E+05	18.93	*
AFM100201	SH	3.69	1.98	3.50E+06	42.18	
AFM100201	EW	4.02	2.08	3.64E+06	43.37	

Table 4-54. Fit parameters and fit statistics for mass dimension of traces in outcrop, linked traces. The "*"symbol indicates that the least-squares fit failed and the parameters were estimated by visually fitting a line. The "!" symbol indicates that the model was fitted to the meqan locus due to difficulties in fitting the data cloud.

Outcrop – linked traces		r_0	D_m	SSQ	SDE	
AFM000053	NE	3.41	1.86	5.37E+05	16.27	
AFM000053	NW	4.21	1.75	1.21E+06	24.52	
AFM000053	NS	0.35	1.94	3.41E+04	4.39	
AFM000053	SH	1.80	1.72	5.44E+05	17.20	*
AFM000053	ENE	2.60	1.76	1.50E+06	28.54	*
AFM000053	WNW	3.57	1.93	1.36E+06	26.01	
AFM000054	NE	4.10	2.02	1.13E+06	23.38	
AFM000054	NW	1.12	2.04	2.38E+05	10.80	
AFM000054	NS	1.65	1.90	6.10E+05	17.66	
AFM000054	SH	1.32	1.73	1.63E+05	9.14	
AFM000054	WNW	4.11	1.86	3.07E+06	39.38	
AFM001097	NE	14.85	1.92	1.20E+07	77.35	
AFM001097	NW	5.40	1.87	3.22E+06	39.80	
AFM001097	NS	1.87	2.04	5.39E+05	16.71	
AFM001097	SH	0.70	1.87	2.72E+05	12.39	
AFM001097	EW	1.19	1.94	2.05E+05	10.13	
AFM001098	NE	7.47	2.09	1.49E+06	27.44	
AFM001098	NW	3.67	1.92	2.67E+05	11.61	
AFM001098	SH	3.07	1.81	6.78E+05	19.08	
AFM001098	NNE	11.72	1.91	1.48E+07	87.04	
AFM001098	WNW	7.86	1.98	1.03E+06	22.56	
AFM001243	NE	14.36	2.19	7.54E+06	62.70	
AFM001243	NS	3.45	2.24	7.63E+05	20.06	
AFM001243	SH	2.00	1.80	3.17E+04	4.08	*
AFM001243	WNW	4.40	2.04	1.54E+06	29.15	*
AFM001244	NE	16.91	1.76	2.55E+07	113.88	
AFM001244	NW	12.47	1.72	1.22E+07	77.57	*
AFM001244	NS	5.85	1.86	1.48E+06	27.17	
AFM001244	SH	2.49	1.98	8.22E+05	20.50	
AFM001244	EW	4.59	1.71	1.36E+05	8.33	
AFM001264	NE	7.97	1.86	2.48E+05	11.31	
AFM001264	NW	5.20	2.03	5.18E+05	16.24	*
AFM001264	NS	2.80	1.80	1.56E+04	2.86	*
AFM001264	ENE	6.39	1.84	2.44E+05	11.23	
AFM001264	WNW	5.88	1.73	1.64E+05	9.32	
AFM001265	NE	116.51	2.20	4.39E+05	21.08	*
AFM001265	NS/NNE	21.54	2.50	4.16E+00	1.02	
AFM001265	EW	47.63	1.89	2.55E+00	0.60	!
AFM100201	NE	14.84	1.89	8.07E+06	63.61	
AFM100201	NW	8.71	1.92	6.80E+06	58.96	
AFM100201	NS	2.62	1.97	1.23E+06	24.70	
AFM100201	SH	3.18	2.02	2.21E+06	33.79	
AFM100201	EW	5.55	1.93	2.05E+06	32.47	

A key question of the spatial modeling process was whether or not the mass dimensions differed by fracture set or by whether the data was linked or unlinked. These questions were addressed by calculating the Kruskal-Wallis /NIST 2007c/ and Wilcoxon Signed Rank Test /Wilcoxon 1945/, which are the non-parametric equivalent of the ANOVA and paired t-tests, respectively.

Do Mass Dimensions of Traces Differ by Set?

H0:   The mass dimensions do not differ by set

H1:   The mass dimensions do differ by set

Test: Calculate the Kruskal-Wallis (H) statistic for linked and unlinked data separately

Decision Rule: If $p(H) < 0.05$, reject H0, conclude they do differ by set

                If $p(H) \geq 0.05$, fail to reject H0, conclude they do not differ by set

Results of Test: The results of these two tests are shown in Table 4-55 and Table 4-56. In both cases, the probability $p(H)$ is substantially greater than 0.05, so the conclusion is that the mass dimensions do not differ by set.

Table 4-55. Kruskal-Wallis test results for testing differences of exponent by set, unlinked traces.

Test	**Kruskal-Wallis ANOVA**
Comparison	Dm - R2 by Set - R2: ENE, EW, NE, NS, NW, SH, WNW
Performed by	plapointe

n	41

Dm - R2 by Set - R2	n	Rank sum	Mean rank
ENE	2	47.5	23.75
EW	4	97.5	24.38
NE	9	241.5	26.83
NS	7	106.0	15.14
NW	7	139.5	19.93
SH	7	122.0	17.43
WNW	5	107.0	21.40

Kruskal-Wallis statistic	4.92
p	0.5536 (chisqr approximation, corrected for ties)

Table 4-56. Kruskal-Wallis test results for testing differences of exponent by set, linked traces.

Test	Kruskal-Wallis ANOVA
Comparison	Dm - R1 by Set - R1: ENE, EW, NE, NS, NW, SH, WNW
Performed by	plapointe

	n
n	41

Dm - R1 by Set - R1	n	Rank sum	Mean rank
ENE	2	19.5	9.75
EW	4	73.5	18.38
NE	9	228.5	25.39
NS	7	178.5	25.50
NW	7	142.0	20.29
SH	7	108.0	15.43
WNW	5	111.0	22.20

Kruskal-Wallis statistic	5.76
p	0.4512 (chisqr approximation, corrected for ties)

Do the Mass Dimensions of Traces Differ by Linkage?

H0:   The mass dimensions do not differ by linkage

H1:   The mass dimensions do differ by linkage

Test: Calculate the Wilcoxon Signed Rank (W) /Wilcoxon 1945/ statistic between the linked and unlinked data, pairing the data by outcrop and set.

Decision Rule: If p(W) < 0.05, reject H0, conclude they do differ by linkage

If p(W) ≥ 0.05, fail to reject H0, conclude they do not differ by linkage

Results of Test: The results of these two tests are shown in Table 4-57. The probability of W is substantially greater than 0.05, so the conclusions is that the mass dimensions do not differ by linkage.

Table 4-57. Wilcoxon Signed Rank test results for testing the mass dimension differences as a function of linkage model uncertainty.

Test	Wilcoxon signed ranks test		
Alternative hypothesis	Dm-Linked ≠ Dm-Unlinked		
Performed by	plapointe		

n	8		

Difference between pairs	n	Rank sum	Mean rank
Positive	5	24.0	4.80
Negative	3	12.0	4.00
Zero	0		

Difference between medians	0.033	
96.1% CI	-0.064 to 0.161	(exact)

Wilcoxon's W statistic	24	
2-tailed p	0.4609	(exact)

The implication of the conclusions for these two tests are that the mass dimensions for all sets and for linked and unlinked data can be combined in order to calculate a mass dimension scaling model for fracture traces. In order to interpret the distribution of dimensions for quantifying uncertainty, it is useful to determine if they conform to a normal probability distribution, or if another type of distribution may be more appropriate. For this reason, a series of tests on the linked, unlinked and combined mass dimensions were carried out to determine the distributional form. The results for normality testing are shown in Figure 4-46 through Figure 4-51.

The results show that, for the Shapiro-Wilk and Wilcoxon skewness tests, the distribution of the complete data sets are generally not normally distributed. However, when suspect data or extreme outliers have been removed, the data sets pass both normality tests. The statistical results, including confidence intervals, for the two data sets are shown in the figures.

The mean mass dimension for all of the data is 1.888, while the mean with the suspect data removed is 1.901. The 95% confidence intervals on both of these are ± 0.40 and ± 0.23, respectively. When the suspect data has been removed, the mass dimensions have a range of from -2σ to $+2\sigma$, or 1.64 to 2.16, which approximately represents a 95% coverage of the values, since they are normally distributed.

Since most of these outcrops are limited in extent, the mass dimensions calculated from the trace maps only apply to the scale of the outcrops, which if the outcrop area is approximated as a circle, then the maximum diameter would be approximately 30 m. Therefore, it is not possible to determine whether the scaling relations extend to scales greater than 30 m using the outcrop data.
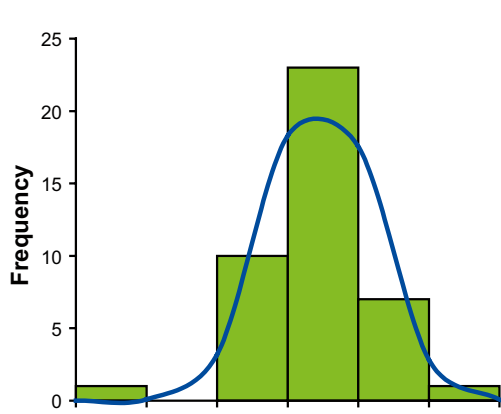
n	42
Mean	1.895
95% CI	1.849 to 1.942
Variance	0.0223
SD	0.1494
SE	0.0231
CV	8%
Median	1.900
95.6% CI	1.855 to 1.940
Range	0.94
IQR	0.17625
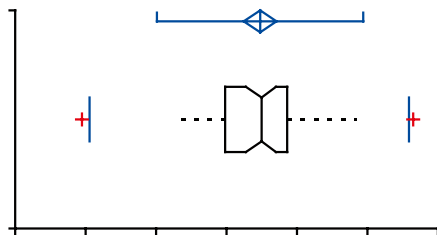
Percentile	
2.5th	1.411
25th	1.796
50th	1.900
75th	1.973
97.5th	2.318
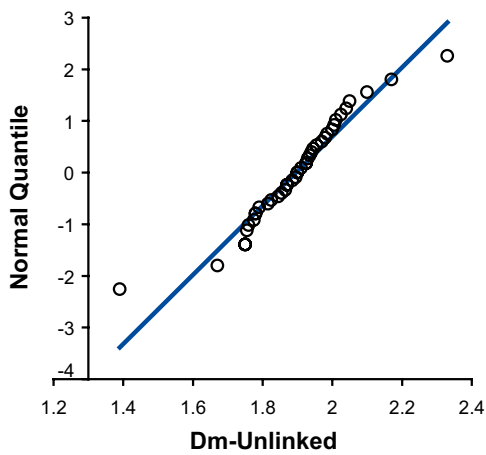
	Coefficient	p
Shapiro-Wilk	0.9414	0.0320
Skewness	-0.2724	0.4365
Kurtosis	3.3216	0.0060

Figure 4-46. *Results of normality testing on unlinked fracture trace mass dimensions.*

n	42
Mean	1.880
95% CI	1.814 to 1.947
Variance	0.0456
SD	0.2134
SE	0.0329
CV	11%
Median	1.880
95.6% CI	1.810 to 1.930
Range	1.48
IQR	0.1525

Percentile	
2.5th	1.022
25th	1.800
50th	1.880
75th	1.953
97.5th	2.449

	Coefficient	p
Shapiro-Wilk	0.8295	<0.0001
Skewness	-1.2220	0.0025
Kurtosis	8.0570	<0.0001
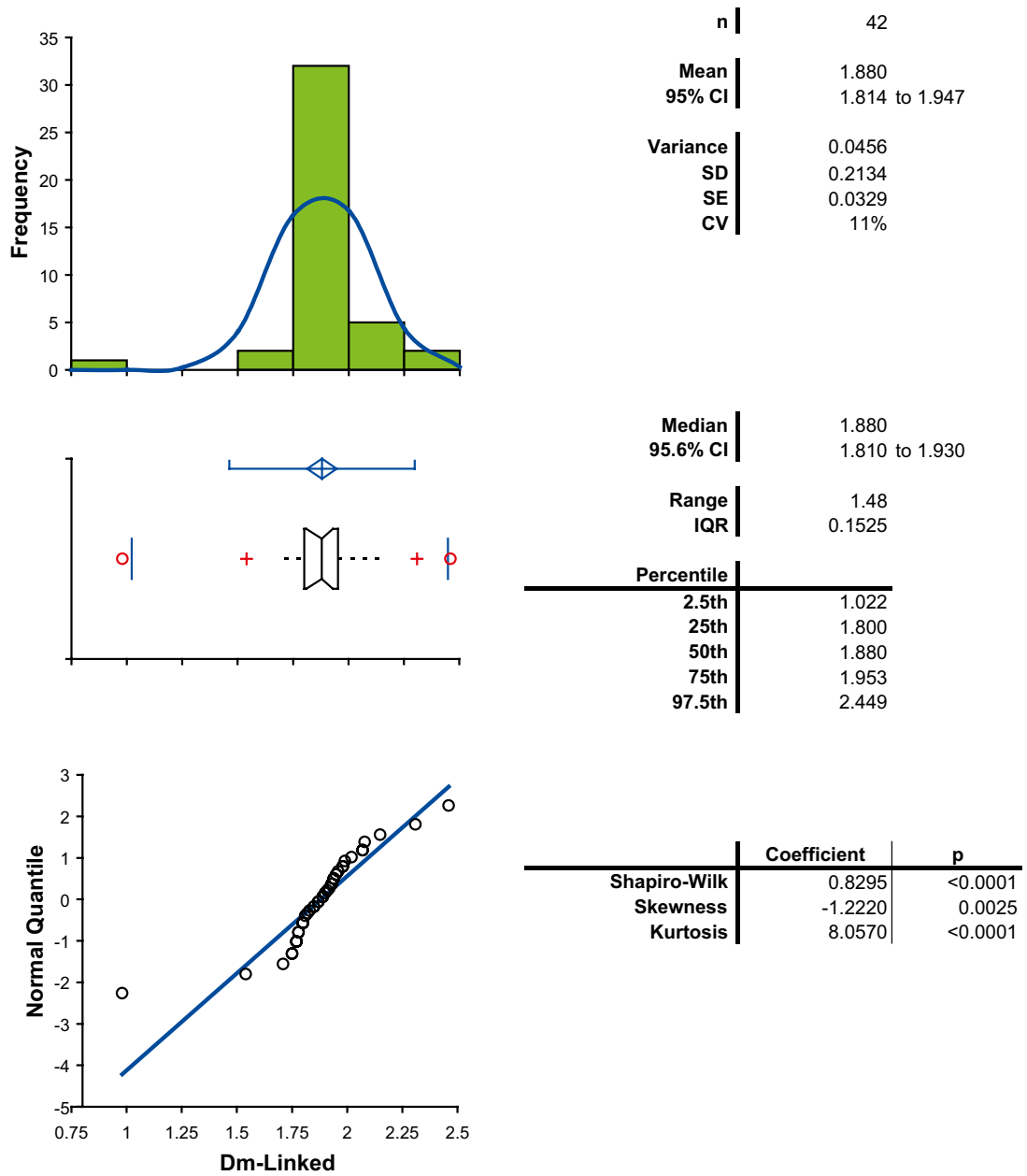
Figure 4-47. *Results of normality testing on linked fracture trace mass dimensions.*
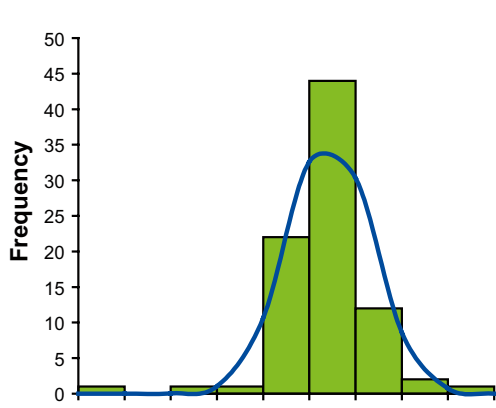
n	84
Mean	1.888
95% CI	1.848 to 1.928
Variance	0.0336
SD	0.1833
SE	0.0200
CV	10%
Median	1.893
96.2% CI	1.850 to 1.930
Range	1.48
IQR	0.18
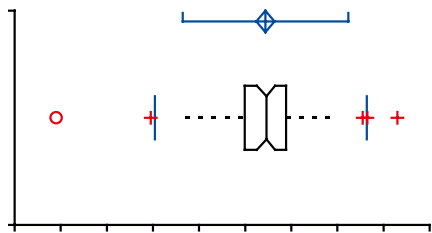
Percentile	
2.5th	1.409
25th	1.798
50th	1.893
75th	1.978
97.5th	2.328
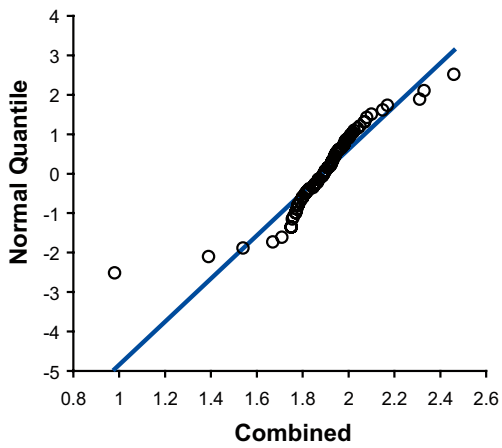
	Coefficient	p
Shapiro-Wilk	0.8651	<0.0001
Skewness	-1.0447	0.0004
Kurtosis	7.9023	<0.0001

Figure 4-48. *Results of normality testing on combined unlinked & linked fracture trace mass dimensions.*

n	39
Mean	1.892
95% CI	1.857 to 1.926
Variance	0.0113
SD	0.1062
SE	0.0170
CV	6%
Median	1.900
97.6% CI	1.845 to 1.940
Range	0.50
IQR	0.16

Percentile	
2.5th	1.670
25th	1.803
50th	1.900
75th	1.963
97.5th	2.170

	Coefficient	p
Shapiro-Wilk	0.9800	0.7026
Skewness	0.1696	0.6370
Kurtosis	-0.0854	0.9216
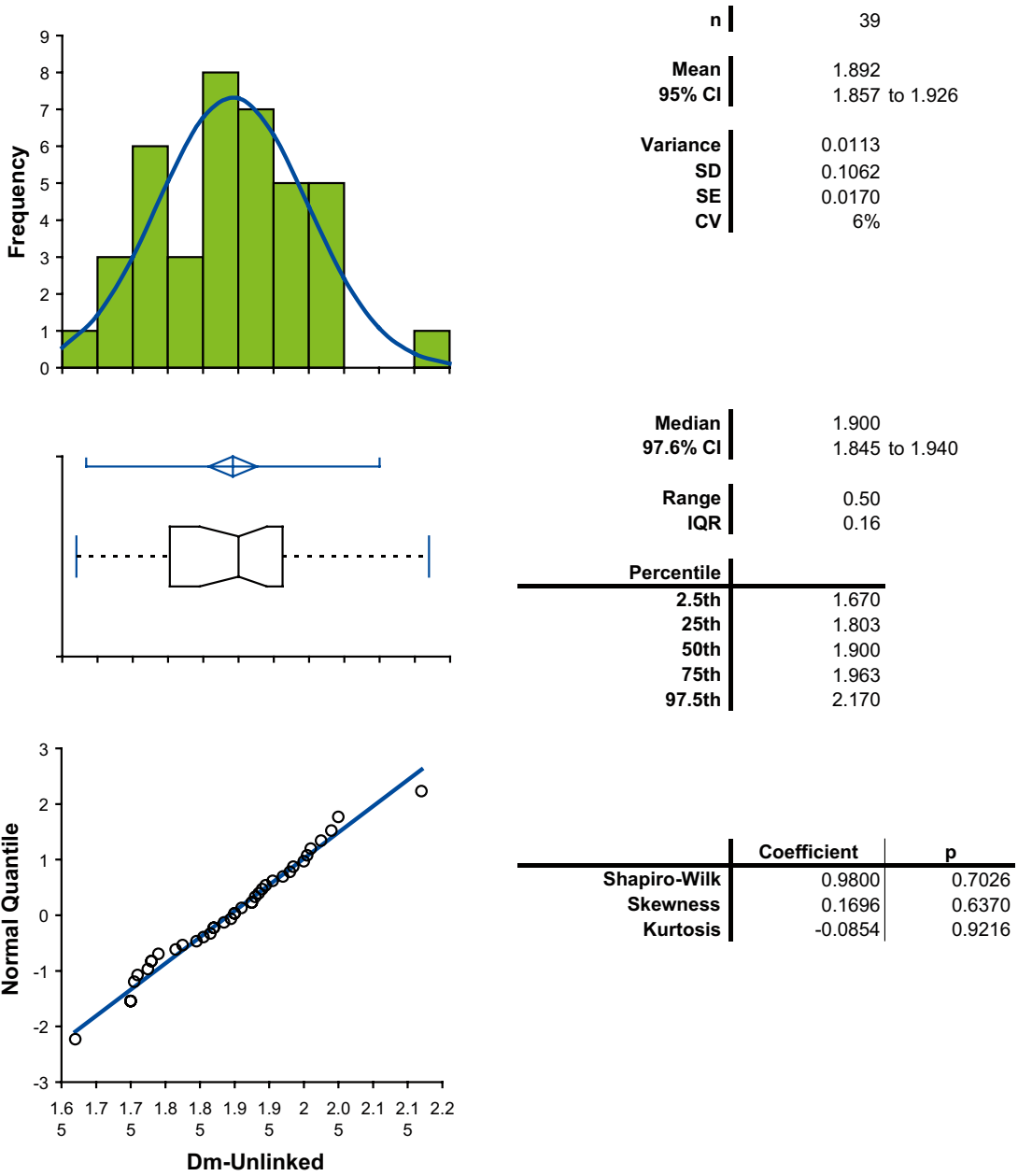
Figure 4-49. *Results of normality testing on unlinked fracture trace mass dimensions, suspect data removed.*

Frequency

16
14
12
10
8
6
4
2
0
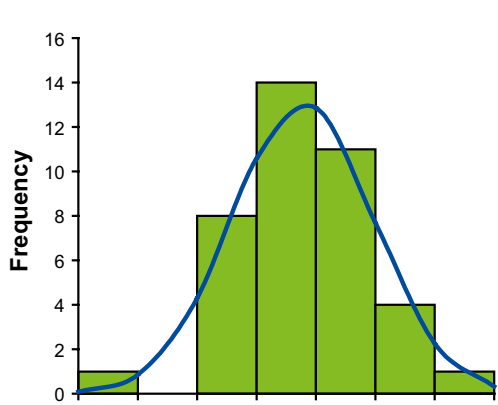
	n	39
	Mean	1.877
	95% CI	1.839 to 1.916
	Variance	0.0141
	SD	0.1188
	SE	0.0190
	CV	6%
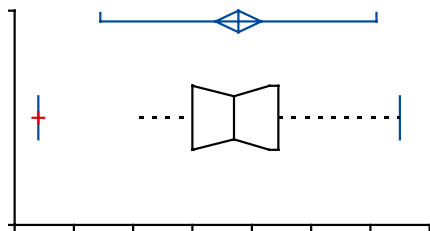
	Median	1.870
	97.6% CI	1.800 to 1.930
	Range	0.61
	IQR	0.15

Percentile	
2.5th	1.540
25th	1.800
50th	1.870
75th	1.945
97.5th	2.150

Normal Quantile

3
2
1
0
-1
-2
-3

1.5 1.6 1.7 1.8 1.9 2 2.1 2.2
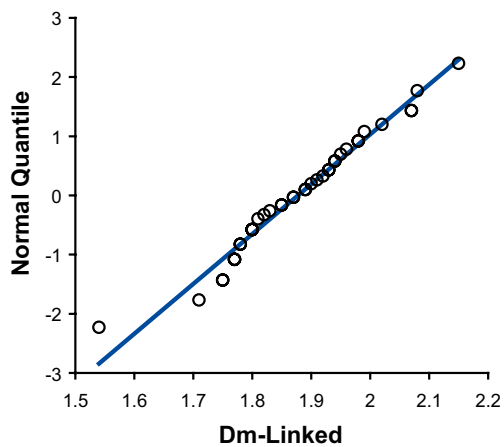
Dm-Linked

	Coefficient	p
Shapiro-Wilk	0.9739	0.4915
Skewness	-0.0687	0.8480
Kurtosis	0.7566	0.2626

Figure 4-50. *Results of normality testing on linked fracture trace mass dimensions, suspect data removed.*

n	83	
Mean	1.901	
95% CI	1.873 to 1.929	
Variance	0.0166	
SD	0.1287	
SE	0.0141	
CV	7%	

Median	1.900	
95.2% CI	1.865 to 1.930	
Range	0.79	
IQR	0.18	
Percentile		
2.5th	1.674	
25th	1.800	
50th	1.900	
75th	1.980	
97.5th	2.170	

	Coefficient	p
Shapiro-Wilk	0.9749	0.1043
Skewness	0.4514	0.0870
Kurtosis	0.9900	0.0961
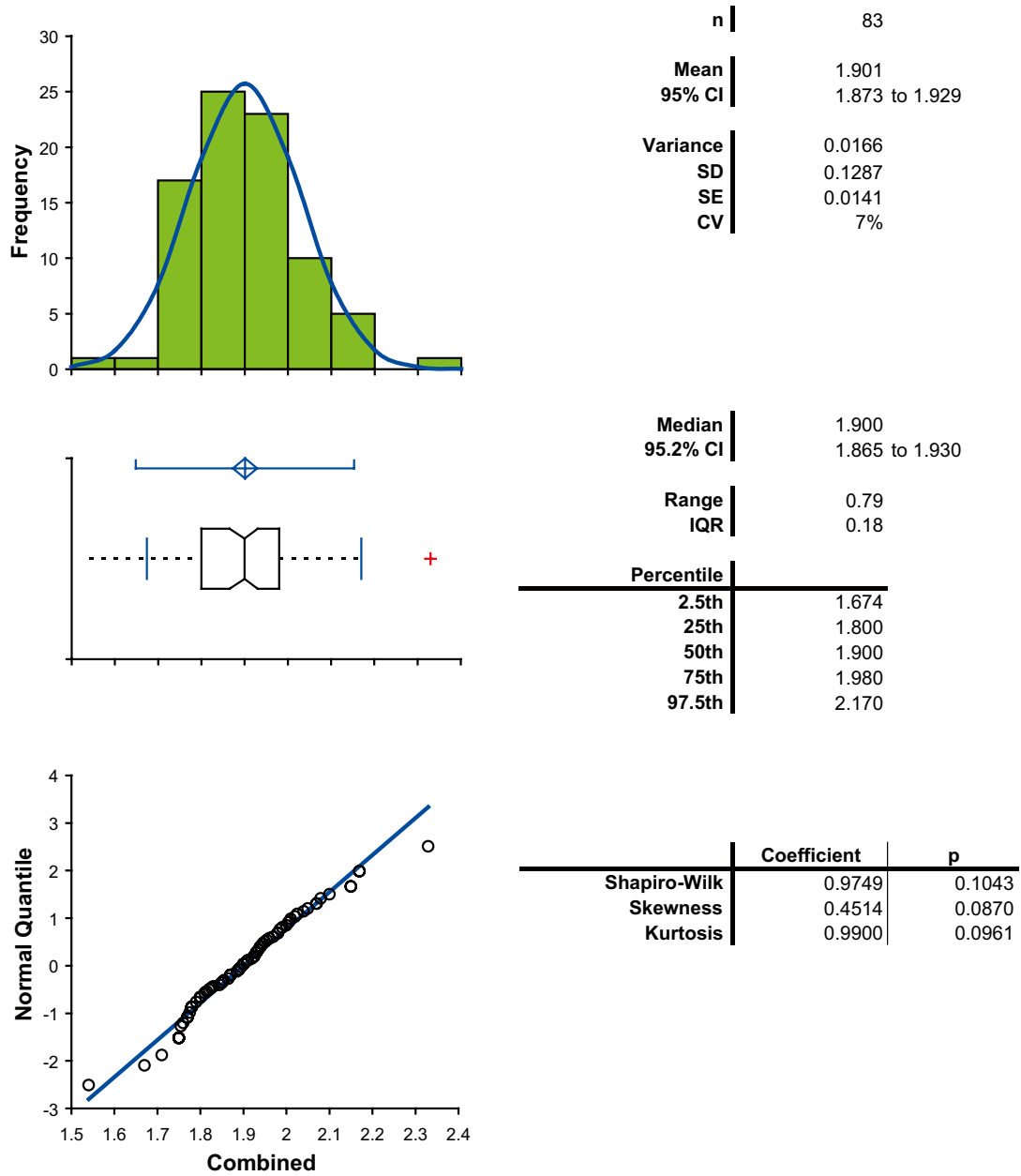
Figure 4-51. *Results of normality testing on combined unlinked and linked fracture trace mass dimensions, suspect data removed.*

Borehole data

The results of the mass dimension calculations for the borehole data are shown in Figure 10-87 through Figure 10-114 in Appendix B. Each figure represents a specific fracture set (NE, SH, NW, etc) and a specific borehole interval (defined as a length in meters), since most borehole data records were punctuated by deformation or minor deformation zones, rendering the mass dimension calculation over the entire data record inappropriate.

Each mass dimension plot consists of the mean locus as a function of interval size for a randomly selected fracture location. This differs from the display used for the outcrops for two reasons:

1. There are often a number of intervals in each borehole record, and there are more boreholes than outcrops. Displaying each set for each interval and for each borehole would produce a very large number of plots, making comparisons much more difficult;

2. Displaying the data clouds for multiple data sets on a single graph would completely obscure how the intensity varies with scale, because the graphs would be overwhelmed by a large number of disparate data points.

This for comparison purposes, each graph shows the results for all fracture sets within the specific borehole interval, and only the mean loci are displayed. In virtually all cases, the mean locus approximates Euclidean scaling at larger scales. Thus, the useful information that can be derived from each graph is the scale that denotes the onset of Euclidean scaling. It is worthwhile to note, in order to avoid confusion when interpreting these plots, that the calculation of the mass dimension for the borehole data covered scales that were sufficiently small so as to induce an artifact into the results. The fracture data recorded in the boreholes did not consist of micro-fractures and fractures that may have only partially cut the wellbore cylinder because of their small size /Stråhle et al. 2005/. Therefore, the number of fractures contained within an interval of a small size approaches 1.0 as the interval size shrinks to the typical fracture spacing value for that set in the interval. For interval sizes equal to the minimum fracture spacing, the mean value is exactly 1.0, and for interval values smaller, it is also exactly 1.0. For slightly larger intervals, the mean value is slightly larger than 1.0. This artifact leads to a slope approaching 0.0 for intervals at the scale of the mean fracture spacing, and a continuous increase in slope as the scales increase. The exact scale at which the artifact plays an insignificant role cannot be determined, but it clearly is not playing a significant role when the curve no longer continuously increases in slope. Thus, any inferences about the scaling behavior of the fracture intensity drawn at smaller scales in the plot where the slope is continuous changing may be obscured by this artifact. For this reason, the results from the borehole scaling analyses are only used to quantify the scale at which the onset of Euclidean scaling is observed. It *may* occur at smaller scales, but could be masked by the calculation artifact. Thus, the scale at which the data begin to approximate a straight line with slope 1.0 is more likely to be the *maximum* scale at which Euclidean scaling occurs. This same artifact occurs in the outcrop data as well, as the radius of the circle approaches the typical minimum spacing of the fracture traces.

Visual inspection of the borehole mass dimension plots show that the onset of Euclidean scaling is rarely greater than a few tens of meters. In fact, most sets and boreholes show an onset at scales below 30 m, which is the maximum outcrop scale. There are a few exceptions to this, but in general, Euclidean scaling is seen in almost every data set at a few tens of meters or less.

The mass dimension results are not inconsistent with the trace mass dimension results. The trace analyses suggested that the spatial pattern for each set was mildly fractal for scales up to the order of 25 m to 30 m, with a typical dimension of 1.90. The borehole mass dimensions show that in the majority of data sets, the scaling transitions to Euclidean by about 30 m. Thus, the two analyses together suggest two alternative mathematical implementations:

1. Combined Fractal/Euclidean Scaling Model

2. Fractal Scaling Model

The combined Fractal/Euclidean model is implemented by prescribing a fractal model for scales less than 30 m, and a Euclidean model for scales greater than 30 m. For this model, the fractal parameters and their statistics pertain to all sets and linkage models, independent of fracture domain or other category, at all scales less than 30 m. For scales greater than 30 m, the scaling is Euclidean.

For the fractal scaling model, the fractal parameterization is used to characterize the scaling behavior for all sets and linkage models, independent of fracture domain or other category, for all scales.

Geostatistical analysis

Semivariograms were calculated for the outcrop trace data to examine the spatial correlation of fracture intensity. Figure 11-1 through Figure 11-84 in Appendix C show the results for both unlinked and linked traces. In a few cases the raw semivariogram could not be calculated due the elongated shape of the outcrop, the paucity of trace data, or both. In an additional few cases, it was not possible to fit a semivariogram model to the raw semivariogram. Both of these instances are noted in Table 4-58, which summarizes the semivariogram model fit to the data for each set and outcrop. For each set and outcrop, the model shown in the figure and in the table represents the model with the smallest sum-of-squares deviation from the following suite of models: Spherical, Exponential, Gaussian, Power Law, and de Wijs.

The overall impression of the results of the geostatistical analysis is that many of the fracture sets do not show any consistent strongly spatially-correlated behavior over distances greater than 10 m. For example, the Global subhorizontal set fits a Power Law semivariogram for the unlinked traces on outcrop AFM100201 (Figure 11-41). The same set shows a slightly less correlated structure on outcrop AFM000054 (Figure 11-10), and shows very little spatial correlation on all other remaining outcrops.

The observation that there may be some degree of spatial correlation at distances less than 10 m may characterize some of the clustering observed in the fracture data. The fact that the spatial correlation is weak or absent at larger distances indicates that the spatial pattern of these clusters could be reasonably well approximated by a Poisson process rather than a spatially correlated model. From the standpoint of the "intended purpose" of the GeoDFN, which is to forecast fracture properties for earthquakes, construction and possibly hydrologic modeling, incorporating spatial correlation at the scale of a few meters is irrelevant. This is because the large features that are of importance for these purposes have spacings typically much greater than a few tens of meters, or the downstream modelling is done by averaging properties over blocks greater than a few meters in extent. Therefore, the possible spatial correlation that may exist at scales of a few meters is irrelevant for the intended purposes of the geological DFN models.

Thus, the semivariograms confirm the fractal results for outcrop and borehole, indicating that there are no strong spatial correlations in the data beyond 10 or so meters. Moreover, the apparent non-Euclidean behavior in the mass dimension plots for some of the data sets at scales less than 20–30 m, which could be due to artifacts in the calculation as much as to actual spatial structure, appear not to be strongly supported by the geostatistical analyses, which indicates an even smaller scale of fractal or spatially correlated structure. This further suggests that the Base Model, which includes Euclidean rather than fractal scaling, is most consistent with these results. Of the two alternative tectonic continuum models, the one based on Euclidean scaling would be consistent with the geostatistical results.

Table 4-58. Summary of geostatistical analyses. For all models except the Power Law, "a" indicates the Range, and "b" indicates the Sill. For the Power Law models, "a" indicates the prefactor and "b" indicates the exponent.

Unlinked	Set	Model	a	b	SSQ	Linked	Set	Model	a	b	SSQ
AFM000053	NE	Power	0.1850	0.301	0.0032	AFM000053	NE	Exponential	1.6517	0.323	0.0540
	NS	Power	0.0170	0.336	0.0044		NS	Power	0.0205	0.255	0.1690
	NW	Power	0.1990	0.076	0.0355		NW	Power	0.1994	0.076	0.0355
	SH	Spherical	4.3500	0.040	0.0878		SH	Exponential	1.8810	0.039	0.0263
	ENE	Power	0.0279	0.400	0.0535		ENE	Power	0.0278	0.401	0.0535
	WNW	Power	0.1850	0.092	0.0248		WNW	Power	0.1850	0.093	0.0248
AFM000054	NE	Power	0.2727	0.303	0.0347	AFM000054	NE	Exponential	2.9600	0.666	0.0649
	NS	Exponential	1.6830	0.449	0.1554		NS	Spherical	5.1866	0.406	0.1063
	NW	Power	0.0887	0.282	0.0791		NW	Spherical	7.3096	0.181	0.0841
	SH	Power	0.0465	0.301	0.1425		SH	Power	0.0494	0.278	0.2886
	WNW	Power	0.4690	0.369	0.0417		WNW	Power	0.4487	0.388	0.0834
AFM001097	NE	Exponential	7.9284	3.320	0.0282	AFM001097	NE	Spherical	12.9404	2.820	0.0393
	NS	Power	0.1295	0.313	0.0247		NS	Spherical	2.4488	0.276	0.4120
	NW	de Wijs	0.0928	0.172	0.0184		NW	Power	0.1759	0.312	0.0563
	SH	No Model Fitted					SH	Spherical	1.7602	0.023	0.7387
	EW	Nugget	0.0000	0.491	0.2359		EW	Exponential	1.1742	0.122	0.1802
AFM001098	NE	Spherical	13.0434	0.945	0.0162	AFM001098	NE	Power	0.3652	0.320	0.5606
	NW	Gaussian	1.5335	0.214	0.0932		NW	Exponential	1.5576	0.224	0.1460
	SH	Power	0.0671	0.162	0.1916		SH	Power	0.0698	0.149	0.3710
	NNE	Exponential	2.4090	1.193	0.1375		NNE	Exponential	2.5112	1.281	0.1012
	WNW	Exponential	2.4592	0.804	0.1163		WNW	Exponential	2.3961	0.784	0.2417
AFM001243	NE	Spherical	5.6959	0.723	0.1431	AFM001243	NE	Spherical	6.2333	0.617	0.2029
	NS	No Model Fitted					NS	No Model Fitted			
	SH	Exponential	1.3905	0.048	0.1414		SH	Exponential	1.3150	0.048	0.2831
	WNW	Exponential	1.9334	0.122	0.1392		WNW	Gaussian	1.4981	0.104	0.4582
AFM001244	NE	No Model Fitted				AFM001244	NE	No Model Fitted			
	NS	No Model Fitted					NS	No Model Fitted			
	NW	No Model Fitted					NW	No Model Fitted			
	SH	Spherical	7.3104	0.022	0.0291		SH	Spherical	3.0772	0.023	0.4533
	EW	No Model Fitted					EW	No Semivariogram Calculated			
AFM001264	NE	Power	0.1615	0.035	0.7093	AFM001264	NE	Power	0.1277	0.200	0.2077
	NS	No Semivariogram Calculated					NS	No Semivariogram Calculated			
	NW	Exponential	1.8234	0.341	0.0339		NW	Spherical	3.7694	0.239	0.4448
	SH	Exponential	2.1003	0.362	0.3399		SH				
	ENE	No Model Fitted					ENE	Spherical	2.5984	0.253	0.1033
	WNW	Exponential	1.6423	0.199	0.0555		WNW	Power	0.0917	0.377	0.0434
AFM001265	NE	No Model Fitted				AFM001265	NE	Exponential	1.2835	4.594	0.3166
	NS	No Semivariogram Calculated					NS	No Semivariogram Calculated			
	EW	Spherical	0.3894	11.948	0.3976		EW	Power	6.5542	0.049	0.2539
AFM100201	NE	Power	0.3314	0.269	0.0534	AFM100201	NE	Power	0.2884	0.276	0.1397
	NS	Power	0.0756	0.261	0.0911		NS	Power	0.0670	0.304	0.0636
	NW	Power	0.1162	0.275	0.1616		NW	Exponential	2.9109	0.226	0.1312
	SH	Power	0.1219	0.156	0.0520		SH	Power	0.1080	0.147	0.1165
	EW	Power	0.2689	0.111	0.0927		EW	Power	0.1079	0.237	0.2256

Multivariate statistical analyses

The multivariate statistical analyses are based upon the delineation of homogeneously fractured zones identified from the Cumulative Fracture Intensity (CFI) plots (Figure 4-52). Portions of each data set that approximate a constant slope indicate zones of homogeneous fracture intensity, and shallow slopes indicate higher intensity than steeper ones. The figure includes portions of the borehole that have been identified as deformation or minor deformation zones. These zones were not excluded at this stage in the development of the multivariate data set, but were excluded prior to analyses.

The percentage of each subcategory for each geological parameter was calculated over the homogeneously fractured layers. The resulting data set was used for subsequent statistical analyses. It contains a column that designates whether the layer was completely within a deformation zone ("Z" for deformation zone), partially within a deformation zone ("M" for mixed), or entirely outside of the identified deformation zones ("B" for background).

Preliminary exploratory data analysis

The Exploratory Data Analysis (EDA) was carried out to examine the correlation structure among the dependent fracture intensity variable and the independent geological variables. Non-parametric Spearman correlation coefficients and their statistical significance were calculated for the fracture intensity in each layer and the percentages of the various geological attributes. The results are presented as a series of tables showing the correlation and statistical significance of the correlation between P10 fracture intensity and the geological variables. Correlations that are significant at values of $\alpha = 0.05$ and 0.01 are indicated by '*' and '**', respectively.

The correlation matrices show that the correlations for the overall fracture P_{10} and the P_{10} of individual sets differ, although there are some commonalities. Review of the correlation with FRACTURE_MAPPED and FRACTURE_INTERP (Table 4-59) shows one anomaly; the NS set tends to behave in an opposite manner than the other sets. For example, most of the other
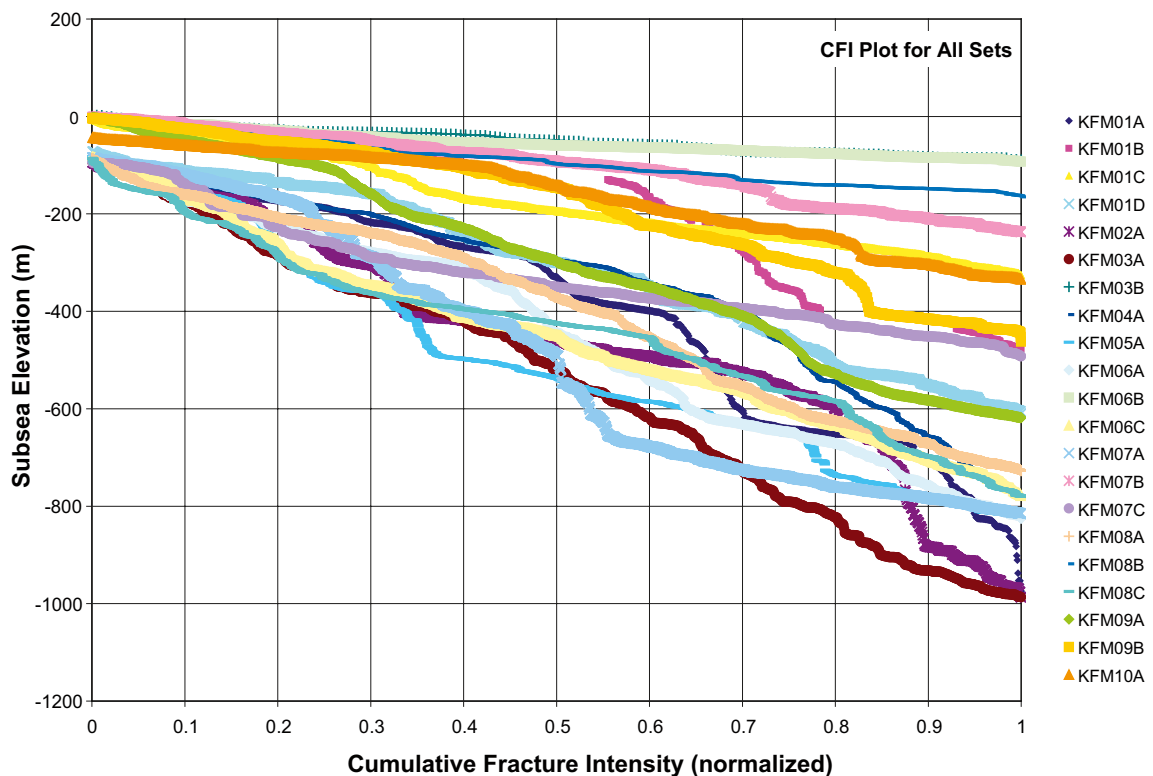
Figure 4-52. *CFI plot for all fracture sets inform all boreholes.*

Table 4-59. Spearman correlation coefficients between borehole P_{10} and FRACTURE_MAPPED, FRACTURE_INTERP & CONFIDENCE.

			Broken	Unbroken	Open	PartlyOpen	Sealed	Certain	Possible	Probable
Spearman's rho	P10	Correlation Coefficient	0.133	-0.133	-0.015	0.336	-0.085	-0.144	-0.053	0.117
		Sig. (2-tailed)	0.273	0.273	0.900	0.004	0.482	0.235	0.664	0.335
		N	70	70	70	70	70	70	70	70
	NWP10	Correlation Coefficient	0.036	-0.036	0.066	0.180	-0.088	-0.201	0.244	0.116
		Sig. (2-tailed)	0.767	0.767	0.586	0.135	0.470	0.095	0.042	0.338
		N	70	70	70	70	70	70	70	70
	ENEP10	Correlation Coefficient	-0.092	0.092	-0.023	-0.137	0.063	0.044	0.049	-0.050
		Sig. (2-tailed)	0.450	0.450	0.848	0.257	0.602	0.717	0.689	0.679
		N	70	70	70	70	70	70	70	70
	EWP10	Correlation Coefficient	-0.054	0.054	0.142	0.116	-0.156	0.136	0.047	-0.147
		Sig. (2-tailed)	0.655	0.655	0.241	0.337	0.196	0.261	0.698	0.226
		N	70	70	70	70	70	70	70	70
	NEP10	Correlation Coefficient	-0.192	0.192	-0.110	0.248	0.061	0.157	-0.017	-0.160
		Sig. (2-tailed)	0.111	0.111	0.365	0.039	0.616	0.194	0.886	0.186
		N	70	70	70	70	70	70	70	70
	NNEP10	Correlation Coefficient	-0.064	0.064	0.073	-0.186	-0.031	0.089	-0.020	-0.073
		Sig. (2-tailed)	0.596	0.596	0.547	0.124	0.799	0.465	0.867	0.549
		N	70	70	70	70	70	70	70	70
	NNWP10	Correlation Coefficient	0.131	-0.131	0.303	0.075	-0.296	-0.041	0.274	-0.106
		Sig. (2-tailed)	0.278	0.278	0.011	0.540	0.013	0.737	0.022	0.382
		N	70	70	70	70	70	70	70	70
	NSP10	Correlation Coefficient	-0.442	0.442	-0.369	0.072	0.341	0.340	-0.092	-0.361
		Sig. (2-tailed)	0.000	0.000	0.002	0.553	0.004	0.004	0.448	0.002
		N	70	70	70	70	70	70	70	70
	SHP10	Correlation Coefficient	0.482	-0.482	0.279	0.438	-0.387	-0.425	0.040	0.387
		Sig. (2-tailed)	0.000	0.000	0.019	0.000	0.001	0.000	0.744	0.001
		N	70	70	70	70	70	70	70	70

sets show a positive correlation between intensity and percentage of open or partially open fractures, and a negative correlation with sealed The NS set shows a tendency to be positively correlated with the percentage of sealed fractures and negatively or not correlated with the percentage of open and partially open fractures. The NS set also shows the only statistically significant positive correlation with the percentage of unbroken fractures.

With regards to MIN1 and MIN2 (Table 4-60 and Table 4-60), the most consistent statistically significant correlations are with the presence of calcite. Although not statistically significant in most instances, there is a negative correlation between fracture intensity and the percentage of feldspar-filled fractures. The presence of many of the refractory minerals, regardless of their type or classification, tends to be positively associated with increased intensity. Overall, there is not a single pattern that characterizes all fracture sets.

Inspection of the other correlation matrices (Table 4-61 through Table 4-64) do not reveal any strong patterns among the geological variables and the intensities of the fracture sets, though for certain variables, some sets seem to be more similar to one another than to others. This similarity can be more rigorously investigated through the calculation of a multinomial logistic regression model. In this approach, all of the parameter subcategory variables for each fracture are converted into binary variables indicating the presence or absence of the subcategory. For example, if a fracture was planar, then it would have a "1" in the planar subcategory or a "0" if it did not. The dependent variable is the fracture set. By examining the factors that can best predict the log-likelihoods of the dependent variable, the overall success in the prediction, and into which set or sets another set is typically misclassified, it is possible to determine which sets are more geologically similar, and what geological variables are most associated with each set.

The subcategory variables that were found to have significance for discriminating among the sets are shown in Table 4-65. An interesting result is that the sets designated as regional, NW, NS, NE and SH, are strongly negatively correlated with FFM02 and positively correlated with FFM03 (Table 4-66); no other sets show this association pattern. The result of the multinomial regression using these subcategory variables as independent variables is shown in Table 4-67. This table shows how the multinomial regression misclassified each set into other sets. If the assignment of sets were random, then the number assigned from, for example, the 1578 fractures from the ENE set would be in proportion to the overall percentage of each set. Table 4-67 shows how many fractures would be assigned to each set for a purely random assignment. Note that a random assignment would lead to approximately 95 fractures being correctly assigned, instead of the 436 actually correctly assigned by the multinomial regression. What is useful is to see where the regression miss-classifies the ENE set. Comparison between predicted and randomly assigned fractures show that the regression severely over-classifies some of the ENE fractures into the NNW: 290 versus the random 74. The regression has trouble distinguishing the NNW set from the ENE set, though it does not have that problem to the same extent with other sets. Likewise, the regression has difficulty in distinguishing between the NW and SH sets, and the NE, NNE and NS sets. The EW set has the least discernable pattern. It is interesting to note that the sets designated as global sets, which may be among the oldest, are the NW, NE, NS and SH, and that these sets seem to be more similar to themselves than to the other sets. Likewise the similarity of the ENE and NNW sets is interesting because they are approximately orthogonal, and it is common for joints that are orthogonal to have formed in a single stress field or deformation event. The reason for the greater geological independence of the EW set is not known, but a visual impression from the outcrop trace maps is that this set is highly variable in its geometry and termination relations from outcrop to outcrop, and may represent a more recent set.

Table 4-60. Spearman correlation coefficients for P_{10} vs. MIN1.

		P10	NWP10	ENEP10	EWP10	NEP10	NNEP10	NNWP10	NSP10	SHP10
MIN1 - Adularia	Correlation Coefficient	0.042	0.148	0.474	-0.127	0.081	0.240	-0.010	-0.072	-0.105
	Sig. (2-tailed)	0.732	0.222	**0.000**	0.295	0.503	0.045	0.933	0.552	0.388
	N	70	70	70	70	70	70	70	70	70
MIN1 - Asphalt	Correlation Coefficient	0.257	-0.019	0.010	0.171	0.249	-0.075	0.167	-0.113	0.274
	Sig. (2-tailed)	0.032	0.875	0.935	0.157	0.038	0.536	0.168	0.350	0.022
	N	70	70	70	70	70	70	70	70	70
MIN1 - Biotite	Correlation Coefficient	-0.182	0.144	0.051	-0.242	-0.178	-0.165	-0.149	-0.052	-0.075
	Sig. (2-tailed)	0.132	0.234	0.677	0.043	0.139	0.173	0.218	0.671	0.536
	N	70	70	70	70	70	70	70	70	70
MIN1 - Calcite	Correlation Coefficient	0.405	-0.285	0.011	0.411	0.500	0.105	0.232	0.181	0.298
	Sig. (2-tailed)	**0.001**	0.017	0.929	**0.000**	**0.000**	0.388	0.053	0.133	0.012
	N	70	70	70	70	70	70	70	70	70
MIN1 - Chlorite	Correlation Coefficient	0.115	0.107	0.025	-0.071	-0.221	-0.217	0.037	-0.389	0.376
	Sig. (2-tailed)	0.344	0.379	0.836	0.558	0.065	0.072	0.762	**0.001**	**0.001**
	N	70	70	70	70	70	70	70	70	70
MIN1 - ClayMinerals	Correlation Coefficient	0.116	0.276	-0.160	0.119	0.099	-0.116	0.008	-0.084	0.197
	Sig. (2-tailed)	0.337	0.021	0.185	0.327	0.415	0.338	0.946	0.488	0.102
	N	70	70	70	70	70	70	70	70	70
MIN1 - Epidote	Correlation Coefficient	0.015	0.029	0.213	-0.060	0.060	0.268	0.270	-0.084	-0.046
	Sig. (2-tailed)	0.901	0.810	0.076	0.624	0.622	0.025	0.024	0.490	0.707
	N	70	70	70	70	70	70	70	70	70
MIN1 - Fluorite	Correlation Coefficient	.	.	.	.	.	.	.	.	.
	Sig. (2-tailed)	.	.	.	.	.	.	.	.	.
	N	70	70	70	70	70	70	70	70	70
MIN1 - Galena	Correlation Coefficient	.	.	.	.	.	.	.	.	.
	Sig. (2-tailed)	.	.	.	.	.	.	.	.	.
	N	70	70	70	70	70	70	70	70	70
MIN1 - Goethite	Correlation Coefficient	-0.194	-0.045	-0.075	-0.072	-0.140	-0.037	-0.033	-0.045	-0.140
	Sig. (2-tailed)	0.108	0.709	0.539	0.552	0.248	0.762	0.784	0.709	0.248
	N	70	70	70	70	70	70	70	70	70
MIN1 - Hematite	Correlation Coefficient	-0.199	-0.098	-0.164	0.150	-0.134	-0.309	-0.215	0.240	-0.214
	Sig. (2-tailed)	0.098	0.421	0.176	0.215	0.270	**0.009**	0.074	0.045	0.076
	N	70	70	70	70	70	70	70	70	70
MIN1 - Kaolinite	Correlation Coefficient	0.063	0.058	-0.075	0.194	0.045	-0.037	-0.033	-0.145	0.140
	Sig. (2-tailed)	0.607	0.636	0.539	0.108	0.713	0.762	0.784	0.230	0.248
	N	70	70	70	70	70	70	70	70	70
MIN1 - Laumontite	Correlation Coefficient	0.026	0.327	-0.044	-0.099	0.167	0.024	-0.093	0.192	-0.044
	Sig. (2-tailed)	0.832	**0.006**	0.719	0.414	0.168	0.844	0.445	0.111	0.717
	N	70	70	70	70	70	70	70	70	70
MIN1 - NDR	Correlation Coefficient	-0.265	-0.040	-0.149	0.151	-0.165	-0.205	-0.132	0.017	-0.080
	Sig. (2-tailed)	0.026	0.741	0.220	0.212	0.172	0.089	0.277	0.886	0.509
	N	70	70	70	70	70	70	70	70	70
MIN1 - OxidizedWalls	Correlation Coefficient	-0.068	0.106	-0.003	0.022	0.254	0.045	-0.084	0.393	-0.304
	Sig. (2-tailed)	0.579	0.382	0.981	0.855	0.034	0.709	0.492	**0.001**	0.011
	N	70	70	70	70	70	70	70	70	70
MIN1 - PotashFeldspar	Correlation Coefficient	-0.063	0.003	-0.075	-0.072	-0.003	-0.037	-0.033	0.130	-0.104
	Sig. (2-tailed)	0.607	0.980	0.539	0.552	0.980	0.762	0.784	0.283	0.390
	N	70	70	70	70	70	70	70	70	70
MIN1 - Prehnite	Correlation Coefficient	0.069	0.237	0.023	0.061	0.164	-0.169	0.128	0.117	-0.041
	Sig. (2-tailed)	0.570	0.048	0.848	0.618	0.174	0.162	0.291	0.336	0.734
	N	70	70	70	70	70	70	70	70	70
MIN1 - Pyrite	Correlation Coefficient	0.244	0.165	-0.034	0.215	0.348	0.073	0.121	0.048	0.178
	Sig. (2-tailed)	0.042	0.173	0.779	0.074	**0.003**	0.546	0.318	0.692	0.141
	N	70	70	70	70	70	70	70	70	70
MIN1 - Pyrrhotite	Correlation Coefficient	-0.205	-0.007	0.126	-0.127	-0.075	-0.065	-0.059	-0.043	-0.169
	Sig. (2-tailed)	0.088	0.953	0.297	0.295	0.536	0.595	0.630	0.724	0.162
	N	70	70	70	70	70	70	70	70	70
MIN1 - Quartz	Correlation Coefficient	-0.073	0.199	0.128	0.011	0.033	0.181	0.164	-0.153	-0.189
	Sig. (2-tailed)	0.549	0.099	0.292	0.925	0.785	0.135	0.174	0.205	0.117
	N	70	70	70	70	70	70	70	70	70
MIN1 - RedFeldspar	Correlation Coefficient	-0.150	0.110	-0.131	0.106	-0.071	-0.065	-0.059	-0.015	-0.081
	Sig. (2-tailed)	0.216	0.364	0.279	0.384	0.560	0.595	0.630	0.904	0.503
	N	70	70	70	70	70	70	70	70	70
MIN1 - Sulfides	Correlation Coefficient	-0.106	0.209	-0.003	-0.007	-0.081	-0.065	-0.059	-0.140	-0.017
	Sig. (2-tailed)	0.383	0.082	0.980	0.956	0.507	0.595	0.630	0.247	0.886
	N	70	70	70	70	70	70	70	70	70
MIN1 - Unknownmineral	Correlation Coefficient	-0.033	0.037	-0.079	0.070	0.022	-0.005	0.197	0.072	-0.082
	Sig. (2-tailed)	0.783	0.760	0.518	0.567	0.855	0.970	0.102	0.552	0.502
	N	70	70	70	70	70	70	70	70	70
MIN1 - WhiteFeldspar	Correlation Coefficient	-0.080	0.135	-0.097	-0.061	-0.013	-0.094	-0.085	-0.072	-0.106
	Sig. (2-tailed)	0.511	0.265	0.426	0.616	0.918	0.441	0.486	0.552	0.381
	N	70	70	70	70	70	70	70	70	70
MIN1 - X1	Correlation Coefficient	0.149	-0.097	0.465	0.245	0.044	0.178	0.714	-0.262	0.096
	Sig. (2-tailed)	0.220	0.423	**0.000**	0.041	0.716	0.140	**0.000**	0.029	0.429
	N	70	70	70	70	70	70	70	70	70
MIN1 - X2	Correlation Coefficient	0.051	-0.070	0.228	0.186	0.092	0.374	0.407	-0.145	0.039
	Sig. (2-tailed)	0.677	0.567	0.058	0.122	0.447	**0.001**	**0.000**	0.230	0.750
	N	70	70	70	70	70	70	70	70	70
MIN1 - X3	Correlation Coefficient	0.208	-0.170	0.320	0.294	0.114	0.458	0.696	-0.216	0.127
	Sig. (2-tailed)	0.083	0.159	**0.007**	0.014	0.348	**0.000**	**0.000**	0.072	0.293
	N	70	70	70	70	70	70	70	70	70
MIN1 - X4	Correlation Coefficient	0.051	-0.070	0.228	0.186	0.092	0.374	0.407	-0.145	0.039
	Sig. (2-tailed)	0.677	0.567	0.058	0.122	0.447	**0.001**	**0.000**	0.230	0.750
	N	70	70	70	70	70	70	70	70	70
MIN1 - X5	Correlation Coefficient	0.033	0.100	-0.075	-0.072	0.098	-0.037	-0.033	0.015	0.069
	Sig. (2-tailed)	0.788	0.411	0.539	0.552	0.418	0.762	0.784	0.901	0.573
	N	70	70	70	70	70	70	70	70	70
MIN1 - X9	Correlation Coefficient	0.119	0.006	-0.131	-0.127	-0.087	-0.065	-0.059	0.064	0.152
	Sig. (2-tailed)	0.327	0.962	0.279	0.295	0.472	0.595	0.630	0.601	0.209
	N	70	70	70	70	70	70	70	70	70
MIN1 - Zeolites	Correlation Coefficient	0.039	0.197	-0.075	-0.072	0.015	-0.037	-0.033	0.118	0.009
	Sig. (2-tailed)	0.750	0.103	0.539	0.552	0.903	0.762	0.784	0.330	0.941
	N	70	70	70	70	70	70	70	70	70

Table 4-61. Spearman correlation coefficients for P_{10} vs. MIN2.

		P10	NWP10	ENEP10	EWP10	NEP10	NNEP10	NNWP10	NSP10	SHP10
MIN2 - Adularia	Correlation Coefficient	0.150	0.193	0.448	-0.021	0.214	0.249	0.141	-0.014	-0.049
	Sig. (2-tailed)	0.215	0.110	0.000	0.863	0.076	0.038	0.243	0.908	0.686
	N	70	70	70	70	70	70	70	70	70
MIN2 - Amphibole	Correlation Coefficient	0.114	-0.207	-0.106	0.336	0.187	-0.052	-0.048	0.224	-0.034
	Sig. (2-tailed)	0.345	0.086	0.380	0.004	0.121	0.666	0.696	0.062	0.778
	N	70	70	70	70	70	70	70	70	70
MIN2 - Asphalt	Correlation Coefficient	0.320	-0.089	0.114	0.363	0.233	-0.085	0.378	-0.192	0.362
	Sig. (2-tailed)	0.007	0.465	0.348	0.002	0.053	0.486	0.001	0.111	0.002
	N	70	70	70	70	70	70	70	70	70
MIN2 - Biotite	Correlation Coefficient	-0.148	0.123	-0.053	-0.010	-0.203	-0.110	-0.099	-0.160	-0.047
	Sig. (2-tailed)	0.222	0.312	0.664	0.936	0.092	0.367	0.413	0.186	0.699
	N	70	70	70	70	70	70	70	70	70
MIN2 - Calcite	Correlation Coefficient	0.272	0.095	0.168	-0.040	0.038	0.079	0.066	-0.274	0.373
	Sig. (2-tailed)	0.023	0.436	0.163	0.744	0.752	0.514	0.588	0.022	0.001
	N	70	70	70	70	70	70	70	70	70
MIN2 - Chalcopyrite	Correlation Coefficient	.	.	.	.	.	.	.	.	.
	Sig. (2-tailed)	.	.	.	.	.	.	.	.	.
	N	70	70	70	70	70	70	70	70	70
MIN2 - Chlorite	Correlation Coefficient	-0.008	-0.237	-0.081	0.086	0.187	0.125	-0.082	-0.019	0.011
	Sig. (2-tailed)	0.945	0.048	0.506	0.479	0.121	0.303	0.499	0.874	0.929
	N	70	70	70	70	70	70	70	70	70
MIN2 - ClayMinerals	Correlation Coefficient	0.147	0.263	0.040	0.079	0.193	-0.203	-0.053	0.025	0.182
	Sig. (2-tailed)	0.225	0.028	0.742	0.516	0.109	0.092	0.664	0.838	0.131
	N	70	70	70	70	70	70	70	70	70
MIN2 - Epidote	Correlation Coefficient	0.148	0.086	0.311	0.038	0.177	0.212	0.250	-0.088	0.077
	Sig. (2-tailed)	0.223	0.481	0.009	0.755	0.143	0.078	0.037	0.470	0.528
	N	70	70	70	70	70	70	70	70	70
MIN2 - Galena	Correlation Coefficient	0.152	-0.145	0.206	0.247	-0.021	-0.037	0.460	-0.145	0.188
	Sig. (2-tailed)	0.209	0.230	0.088	0.039	0.864	0.762	0.000	0.230	0.120
	N	70	70	70	70	70	70	70	70	70
MIN2 - Goethite	Correlation Coefficient	0.095	0.037	0.094	0.259	0.018	0.022	0.407	-0.255	0.219
	Sig. (2-tailed)	0.434	0.759	0.438	0.031	0.883	0.857	0.000	0.033	0.069
	N	70	70	70	70	70	70	70	70	70
MIN2 - Hematite	Correlation Coefficient	-0.054	-0.119	0.019	0.101	-0.120	-0.285	-0.096	0.012	-0.008
	Sig. (2-tailed)	0.659	0.325	0.873	0.405	0.322	0.017	0.430	0.920	0.950
	N	70	70	70	70	70	70	70	70	70
MIN2 - Hornblende	Correlation Coefficient	-0.110	-0.009	-0.075	-0.072	-0.057	-0.037	-0.033	-0.015	-0.033
	Sig. (2-tailed)	0.364	0.941	0.539	0.552	0.642	0.762	0.784	0.901	0.788
	N	70	70	70	70	70	70	70	70	70
MIN2 - Hypersthene	Correlation Coefficient	.	.	.	.	.	.	.	.	.
	Sig. (2-tailed)	.	.	.	.	.	.	.	.	.
	N	70	70	70	70	70	70	70	70	70
MIN2 - Laumontite	Correlation Coefficient	0.040	0.339	0.064	-0.096	0.213	0.102	-0.084	0.253	-0.124
	Sig. (2-tailed)	0.741	0.004	0.597	0.428	0.077	0.399	0.488	0.034	0.307
	N	70	70	70	70	70	70	70	70	70
MIN2 - Magnetite	Correlation Coefficient	0.128	0.185	-0.075	-0.072	0.033	-0.037	-0.033	-0.145	0.182
	Sig. (2-tailed)	0.291	0.126	0.539	0.552	0.788	0.762	0.784	0.230	0.132
	N	70	70	70	70	70	70	70	70	70
MIN2 - Muscovite	Correlation Coefficient	.	.	.	.	.	.	.	.	.
	Sig. (2-tailed)	.	.	.	.	.	.	.	.	.
	N	70	70	70	70	70	70	70	70	70
MIN2 - NDR	Correlation Coefficient	-0.231	-0.038	-0.136	0.043	-0.299	-0.197	0.150	0.011	-0.156
	Sig. (2-tailed)	0.054	0.755	0.262	0.725	0.012	0.103	0.215	0.929	0.196
	N	70	70	70	70	70	70	70	70	70
MIN2 - OxidizedWalls	Correlation Coefficient	-0.099	0.096	0.064	-0.029	0.163	0.035	-0.148	0.375	-0.372
	Sig. (2-tailed)	0.416	0.430	0.601	0.811	0.179	0.775	0.220	0.001	0.002
	N	70	70	70	70	70	70	70	70	70
MIN2 - PotashFeldspar	Correlation Coefficient	-0.146	0.038	-0.106	-0.103	-0.054	-0.052	-0.048	0.113	-0.211
	Sig. (2-tailed)	0.229	0.753	0.380	0.396	0.654	0.666	0.696	0.351	0.079
	N	70	70	70	70	70	70	70	70	70
MIN2 - Prehnite	Correlation Coefficient	0.136	0.202	0.097	0.103	0.147	-0.010	0.271	-0.010	0.127
	Sig. (2-tailed)	0.262	0.093	0.427	0.397	0.226	0.937	0.023	0.935	0.296
	N	70	70	70	70	70	70	70	70	70
MIN2 - Pyrite	Correlation Coefficient	0.244	0.047	-0.026	0.267	0.374	0.076	-0.010	0.050	0.265
	Sig. (2-tailed)	0.042	0.696	0.832	0.025	0.001	0.534	0.933	0.683	0.027
	N	70	70	70	70	70	70	70	70	70
MIN2 - Pyrrhotite	Correlation Coefficient	0.074	-0.145	-0.075	0.232	0.140	-0.037	-0.033	0.154	-0.039
	Sig. (2-tailed)	0.540	0.230	0.539	0.053	0.248	0.762	0.784	0.202	0.750
	N	70	70	70	70	70	70	70	70	70
MIN2 - Quartz	Correlation Coefficient	0.140	0.235	0.061	-0.042	0.302	0.396	-0.036	0.021	-0.012
	Sig. (2-tailed)	0.247	0.050	0.616	0.731	0.011	0.001	0.767	0.866	0.919
	N	70	70	70	70	70	70	70	70	70
MIN2 - RedFeldspar	Correlation Coefficient	-0.209	0.049	-0.131	-0.127	-0.074	-0.065	-0.059	0.027	-0.184
	Sig. (2-tailed)	0.082	0.689	0.279	0.295	0.542	0.595	0.630	0.822	0.127
	N	70	70	70	70	70	70	70	70	70
MIN2 - Sericite	Correlation Coefficient	.	.	.	.	.	.	.	.	.
	Sig. (2-tailed)	.	.	.	.	.	.	.	.	.
	N	70	70	70	70	70	70	70	70	70
MIN2 - Sulfides	Correlation Coefficient	0.177	-0.189	0.277	0.329	0.116	-0.075	0.444	-0.103	0.176
	Sig. (2-tailed)	0.143	0.118	0.020	0.005	0.339	0.536	0.000	0.395	0.146
	N	70	70	70	70	70	70	70	70	70
MIN2 - Unknownmineral	Correlation Coefficient	-0.047	0.121	-0.111	-0.088	-0.050	-0.110	0.098	0.072	0.019
	Sig. (2-tailed)	0.701	0.317	0.361	0.470	0.681	0.367	0.422	0.554	0.878
	N	70	70	70	70	70	70	70	70	70
MIN2 - WhiteFeldspar	Correlation Coefficient	-0.070	0.096	-0.063	-0.057	-0.115	-0.094	-0.085	-0.028	-0.029
	Sig. (2-tailed)	0.564	0.428	0.604	0.638	0.344	0.441	0.486	0.817	0.815
	N	70	70	70	70	70	70	70	70	70
MIN2 - X1	Correlation Coefficient	0.119	0.052	0.231	-0.009	0.029	0.214	0.273	-0.171	0.089
	Sig. (2-tailed)	0.326	0.670	0.054	0.938	0.810	0.075	0.022	0.157	0.465
	N	70	70	70	70	70	70	70	70	70
MIN2 - X2	Correlation Coefficient	.	.	.	.	.	.	.	.	.
	Sig. (2-tailed)	.	.	.	.	.	.	.	.	.
	N	70	70	70	70	70	70	70	70	70
MIN2 - X3	Correlation Coefficient	0.250	-0.099	0.232	0.239	0.115	0.197	0.520	-0.102	0.122
	Sig. (2-tailed)	0.037	0.417	0.053	0.046	0.343	0.102	0.000	0.401	0.312
	N	70	70	70	70	70	70	70	70	70
MIN2 - X4	Correlation Coefficient	.	.	.	.	.	.	.	.	.
	Sig. (2-tailed)	.	.	.	.	.	.	.	.	.
	N	70	70	70	70	70	70	70	70	70
MIN2 - X6	Correlation Coefficient	.	.	.	.	.	.	.	.	.
	Sig. (2-tailed)	.	.	.	.	.	.	.	.	.
	N	70	70	70	70	70	70	70	70	70
MIN2 - Zeolites	Correlation Coefficient	0.039	0.197	-0.075	-0.072	0.015	-0.037	-0.033	0.118	0.009
	Sig. (2-tailed)	0.750	0.103	0.539	0.552	0.903	0.762	0.784	0.330	0.941
	N	70	70	70	70	70	70	70	70	70

Table 4-62. Spearman correlation coefficients for P_{10} versus ROUGHNESS, SURFACE & JOINT ALTERATION.

		P10	NWP10	ENEP10	EWP10	NEP10	NNEP10	NNWP10	NSP10	SHP10
Irregular	Correlation Coefficient	0.058	0.165	0.041	-0.024	-0.169	-0.197	-0.144	-0.158	0.234
	Sig. (2-tailed)	0.633	0.172	0.735	0.841	0.163	0.102	0.233	0.192	0.052
	N	70	70	70	70	70	70	70	70	70
SNA	Correlation Coefficient	-0.133	-0.036	0.092	0.054	0.192	0.064	-0.131	0.442	-0.482
	Sig. (2-tailed)	0.273	0.767	0.450	0.655	0.111	0.596	0.278	**0.000**	**0.000**
	N	70	70	70	70	70	70	70	70	70
Planar	Correlation Coefficient	0.001	0.122	-0.303	-0.026	-0.085	-0.187	-0.244	-0.200	0.281
	Sig. (2-tailed)	0.995	0.315	**0.011**	0.833	0.484	0.120	**0.042**	0.097	**0.019**
	N	70	70	70	70	70	70	70	70	70
Stepped	Correlation Coefficient	0.155	0.090	-0.091	0.077	-0.018	0.069	0.246	-0.106	0.278
	Sig. (2-tailed)	0.201	0.461	0.452	0.528	0.882	0.569	**0.040**	0.384	**0.020**
	N	70	70	70	70	70	70	70	70	70
Undulating	Correlation Coefficient	0.170	0.058	0.153	0.033	0.062	0.269	0.412	-0.173	0.183
	Sig. (2-tailed)	0.158	0.635	0.205	0.785	0.610	**0.024**	**0.000**	0.152	0.129
	N	70	70	70	70	70	70	70	70	70
RNA	Correlation Coefficient	-0.133	-0.036	0.092	0.054	0.192	0.064	-0.131	0.442	-0.482
	Sig. (2-tailed)	0.273	0.767	0.450	0.655	0.111	0.596	0.278	**0.000**	**0.000**
	N	70	70	70	70	70	70	70	70	70
Rough	Correlation Coefficient	0.159	0.038	0.113	0.157	-0.147	-0.119	0.217	-0.386	0.398
	Sig. (2-tailed)	0.189	0.752	0.351	0.194	0.224	0.328	0.071	**0.001**	**0.001**
	N	70	70	70	70	70	70	70	70	70
Slickensided	Correlation Coefficient	0.067	0.152	0.221	0.082	0.039	-0.088	0.069	0.080	0.021
	Sig. (2-tailed)	0.582	0.210	0.066	0.499	0.751	0.469	0.570	0.512	0.860
	N	70	70	70	70	70	70	70	70	70
Smooth	Correlation Coefficient	-0.014	0.035	-0.166	-0.178	-0.106	0.010	0.046	-0.010	0.147
	Sig. (2-tailed)	0.910	0.777	0.170	0.141	0.381	0.936	0.706	0.937	0.224
	N	70	70	70	70	70	70	70	70	70
Fresh	Correlation Coefficient	-0.060	-0.079	-0.038	-0.115	0.004	-0.151	-0.388	0.181	-0.183
	Sig. (2-tailed)	0.623	0.516	0.758	0.342	0.976	0.213	**0.001**	0.133	0.130
	N	70	70	70	70	70	70	70	70	70
Gouge	Correlation Coefficient	-0.006	0.101	-0.106	-0.103	-0.012	-0.052	-0.048	0.127	-0.012
	Sig. (2-tailed)	0.958	0.407	0.380	0.396	0.923	0.666	0.696	0.294	0.920
	N	70	70	70	70	70	70	70	70	70
HighlyAltered	Correlation Coefficient	0.063	0.058	-0.075	0.194	0.045	-0.037	-0.033	-0.145	0.140
	Sig. (2-tailed)	0.607	0.636	0.539	0.108	0.713	0.762	0.784	0.230	0.248
	N	70	70	70	70	70	70	70	70	70
ModeratelyAltered	Correlation Coefficient	0.023	0.089	-0.045	0.104	0.111	-0.037	-0.155	0.060	0.061
	Sig. (2-tailed)	0.848	0.465	0.711	0.393	0.361	0.760	0.200	0.621	0.619
	N	70	70	70	70	70	70	70	70	70
SlightlyAltered	Correlation Coefficient	0.060	0.085	0.046	0.112	-0.011	0.149	0.388	-0.189	0.181
	Sig. (2-tailed)	0.624	0.485	0.705	0.357	0.929	0.219	**0.001**	0.117	0.134
	N	70	70	70	70	70	70	70	70	70
JA-0.75	Correlation Coefficient	0.265	-0.054	0.221	0.230	0.175	0.319	0.636	-0.109	0.208
	Sig. (2-tailed)	**0.028**	0.657	0.068	0.057	0.150	**0.008**	**0.000**	0.372	0.087
	N	69	69	69	69	69	69	69	69	69
JA-1	Correlation Coefficient	-0.195	-0.201	-0.163	-0.105	-0.200	-0.273	-0.349	0.047	-0.147
	Sig. (2-tailed)	0.108	0.097	0.180	0.388	0.100	**0.023**	**0.003**	0.702	0.229
	N	69	69	69	69	69	69	69	69	69
JA-1.5	Correlation Coefficient	0.352	-0.080	0.279	0.233	0.244	0.151	0.693	-0.081	0.284
	Sig. (2-tailed)	**0.003**	0.513	**0.020**	0.054	**0.043**	0.217	**0.000**	0.509	**0.018**
	N	69	69	69	69	69	69	69	69	69
JA-2	Correlation Coefficient	-0.076	0.288	-0.032	-0.050	0.033	-0.106	-0.315	0.050	-0.050
	Sig. (2-tailed)	0.534	**0.017**	0.792	0.685	0.788	0.385	**0.008**	0.682	0.682
	N	69	69	69	69	69	69	69	69	69
JA-3	Correlation Coefficient	0.050	0.336	-0.157	-0.171	0.062	-0.097	-0.285	0.059	0.064
	Sig. (2-tailed)	0.681	**0.005**	0.199	0.159	0.612	0.427	**0.017**	0.629	0.599
	N	69	69	69	69	69	69	69	69	69
JA-4	Correlation Coefficient	-0.048	0.142	-0.016	-0.018	0.044	-0.072	-0.169	0.120	-0.074
	Sig. (2-tailed)	0.696	0.243	0.894	0.881	0.723	0.555	0.165	0.324	0.548
	N	69	69	69	69	69	69	69	69	69
JA-5	Correlation Coefficient	0.079	0.105	0.152	-0.073	0.049	-0.037	-0.034	0.167	0.049
	Sig. (2-tailed)	0.518	0.391	0.213	0.548	0.691	0.760	0.782	0.170	0.691
	N	69	69	69	69	69	69	69	69	69
JA-6	Correlation Coefficient	0.079	-0.068	-0.017	0.259	0.136	-0.095	-0.086	0.209	0.025
	Sig. (2-tailed)	0.518	0.580	0.891	**0.032**	0.266	0.438	0.482	0.085	0.838
	N	69	69	69	69	69	69	69	69	69

Table 4-63. Spearman correlation coefficients for P_{10} vs. Best Rock Name (BRN).

		P10	NWP10	ENEP10	EWP10	NEP10	NNEP10	NNWP10	NSP10	SHP10
BRNAmphibolite	Correlation Coefficient	-0.003	0.188	0.138	0.085	0.139	-0.042	0.049	0.086	-0.079
	Sig. (2-tailed)	0.980	0.119	0.256	0.485	0.252	0.730	0.689	0.482	0.514
	N	70	70	70	70	70	70	70	70	70
BRNBreccia	Correlation Coefficient	0.123	0.155	0.054	0.056	0.145	-0.052	-0.048	0.215	0.076
	Sig. (2-tailed)	0.310	0.199	0.660	0.643	0.230	0.666	0.696	0.074	0.529
	N	70	70	70	70	70	70	70	70	70
BRNCalcsilicaterockskarn	Correlation Coefficient	-0.170	-0.021	0.112	-0.076	-0.167	-0.102	-0.092	-0.052	-0.114
	Sig. (2-tailed)	0.160	0.864	0.357	0.531	0.168	0.402	0.448	0.668	0.347
	N	70	70	70	70	70	70	70	70	70
BRNCarbonatedominatedhydrothermalveinsegregation	Correlation Coefficient	0.039	0.197	-0.075	-0.072	0.015	-0.037	-0.033	0.118	0.009
	Sig. (2-tailed)	0.750	0.103	0.539	0.552	0.903	0.762	0.784	0.330	0.941
	N	70	70	70	70	70	70	70	70	70
BRNDiorite_quartzdioriteandgabbro_metamorphic	Correlation Coefficient	-0.063	0.003	-0.075	-0.072	-0.003	-0.037	-0.033	0.130	-0.104
	Sig. (2-tailed)	0.607	0.980	0.539	0.552	0.980	0.762	0.784	0.283	0.390
	N	70	70	70	70	70	70	70	70	70
BRNFelsictointermediatevolcanicrock_metamorphic	Correlation Coefficient	-0.001	0.161	0.153	-0.080	0.100	-0.102	-0.092	0.199	-0.126
	Sig. (2-tailed)	0.991	0.183	0.206	0.510	0.411	0.402	0.448	0.099	0.298
	N	70	70	70	70	70	70	70	70	70
BRNGranite	Correlation Coefficient	0.128	0.185	-0.075	-0.072	0.033	-0.037	-0.033	-0.145	0.182
	Sig. (2-tailed)	0.291	0.126	0.539	0.552	0.788	0.762	0.784	0.230	0.132
	N	70	70	70	70	70	70	70	70	70
BRNGranitetogranodiorite_metamorphic_mediumgrained	Correlation Coefficient	0.040	-0.134	-0.134	0.337	0.246	0.125	-0.059	0.097	0.061
	Sig. (2-tailed)	0.743	0.269	0.270	0.004	0.040	0.302	0.625	0.425	0.615
	N	70	70	70	70	70	70	70	70	70
BRNGranite_finetomediumgrained	Correlation Coefficient	-0.173	0.239	0.067	-0.173	-0.091	-0.104	-0.080	0.046	-0.189
	Sig. (2-tailed)	0.151	0.046	0.579	0.152	0.456	0.394	0.513	0.707	0.117
	N	70	70	70	70	70	70	70	70	70
BRNGranite_granodioriteandtonalite_metamorphic_finetomediumgrain	Correlation Coefficient	-0.164	0.199	0.081	-0.174	-0.148	-0.095	0.089	-0.104	-0.160
	Sig. (2-tailed)	0.175	0.099	0.506	0.149	0.222	0.434	0.462	0.390	0.187
	N	70	70	70	70	70	70	70	70	70
BRNGranite_metamorphic_aplitic	Correlation Coefficient	0.080	0.069	0.204	0.079	0.260	0.041	-0.052	0.128	-0.013
	Sig. (2-tailed)	0.510	0.571	0.091	0.516	0.030	0.737	0.670	0.290	0.916
	N	70	70	70	70	70	70	70	70	70
BRNGranitoid_metamorphic	Correlation Coefficient	.	.	.	.	.	.	.	.	.
	Sig. (2-tailed)	.	.	.	.	.	.	.	.	.
	N	70	70	70	70	70	70	70	70	70
BRNGranodiorite	Correlation Coefficient	-0.146	0.189	0.131	-0.127	-0.152	-0.065	-0.059	-0.213	-0.138
	Sig. (2-tailed)	0.227	0.117	0.281	0.295	0.208	0.595	0.630	0.076	0.255
	N	70	70	70	70	70	70	70	70	70
BRNGranodiorite_metamorphic	Correlation Coefficient	0.021	0.203	0.168	-0.072	-0.069	-0.037	-0.033	-0.145	0.045
	Sig. (2-tailed)	0.864	0.092	0.164	0.552	0.573	0.762	0.784	0.230	0.713
	N	70	70	70	70	70	70	70	70	70
BRNHybridrock	Correlation Coefficient	.	.	.	.	.	.	.	.	.
	Sig. (2-tailed)	.	.	.	.	.	.	.	.	.
	N	70	70	70	70	70	70	70	70	70
BRNHydrothermalveinsegregation_unspecified	Correlation Coefficient	.	.	.	.	.	.	.	.	.
	Sig. (2-tailed)	.	.	.	.	.	.	.	.	.
	N	70	70	70	70	70	70	70	70	70
BRNPegmatite_pegmatiticgranite	Correlation Coefficient	0.006	0.034	-0.016	-0.290	-0.227	0.124	-0.126	-0.020	0.000
	Sig. (2-tailed)	0.964	0.781	0.897	0.015	0.059	0.308	0.299	0.869	0.997
	N	70	70	70	70	70	70	70	70	70
BRNQuartzdiorite	Correlation Coefficient	.	.	.	.	.	.	.	.	.
	Sig. (2-tailed)	.	.	.	.	.	.	.	.	.
	N	70	70	70	70	70	70	70	70	70
BRNQuartzdominatedhydrothermalveinsegregation	Correlation Coefficient	0.051	0.018	-0.108	0.060	0.050	-0.102	-0.092	0.165	0.014
	Sig. (2-tailed)	0.674	0.882	0.374	0.619	0.683	0.402	0.448	0.171	0.908
	N	70	70	70	70	70	70	70	70	70
BRNSedimentaryrock	Correlation Coefficient	-0.015	0.124	-0.075	0.133	-0.039	-0.037	-0.033	-0.039	0.080
	Sig. (2-tailed)	0.903	0.306	0.539	0.272	0.750	0.762	0.784	0.746	0.508
	N	70	70	70	70	70	70	70	70	70
BRNTonalite	Correlation Coefficient	.	.	.	.	.	.	.	.	.
	Sig. (2-tailed)	.	.	.	.	.	.	.	.	.
	N	70	70	70	70	70	70	70	70	70
BRNTonalitetogranodiorite_metamorphic	Correlation Coefficient	-0.104	0.039	-0.075	-0.072	0.003	-0.037	-0.033	0.033	-0.086
	Sig. (2-tailed)	0.390	0.746	0.539	0.552	0.980	0.762	0.784	0.784	0.477
	N	70	70	70	70	70	70	70	70	70

135

Table 4-64. Spearman correlation coefficients for P_{10} vs. Rock Name (RN).

		P10	NWP10	ENEP10	EWP10	NEP10	NNEP10	NNWP10	NSP10	SHP10
RNAmphibolite	Correlation Coefficient	0.049	0.137	0.039	-0.007	0.131	-0.202	-0.055	0.153	-0.003
	Sig. (2-tailed)	0.689	0.259	0.749	0.955	0.280	0.093	0.653	0.205	0.979
	N	70	70	70	70	70	70	70	70	70
RNCalcsilicaterockskarn	Correlation Coefficient	.	.	.	.	.	.	.	.	.
	Sig. (2-tailed)	.	.	.	.	.	.	.	.	.
	N	70	70	70	70	70	70	70	70	70
RNDiorite_quartzdioriteandgabbro_metamorphic	Correlation Coefficient	.	.	.	.	.	.	.	.	.
	Sig. (2-tailed)	.	.	.	.	.	.	.	.	.
	N	70	70	70	70	70	70	70	70	70
RNFelsictointermediatevolcanicrock_metamorphic	Correlation Coefficient	-0.032	0.149	0.061	-0.034	0.096	-0.085	-0.077	0.094	-0.152
	Sig. (2-tailed)	0.790	0.217	0.613	0.778	0.430	0.486	0.528	0.439	0.210
	N	70	70	70	70	70	70	70	70	70
RNGranitetogranodiorite_metamorphic_mediumg rained	Correlation Coefficient	0.028	-0.079	-0.120	0.350	0.234	0.064	-0.109	0.180	0.011
	Sig. (2-tailed)	0.821	0.518	0.323	**0.003**	0.051	0.599	0.371	0.135	0.927
	N	70	70	70	70	70	70	70	70	70
RNGranite_finetomediumgrained	Correlation Coefficient	-0.268	0.111	-0.125	-0.215	-0.228	-0.110	-0.099	0.021	-0.247
	Sig. (2-tailed)	**0.025**	0.361	0.302	0.074	0.057	0.367	0.413	0.861	0.039
	N	70	70	70	70	70	70	70	70	70
RNGranite_granodioriteandtonalite_metamorphic _finetomediumgraine	Correlation Coefficient	-0.131	0.130	-0.006	-0.122	-0.125	-0.063	0.117	-0.080	-0.149
	Sig. (2-tailed)	0.280	0.284	0.961	0.313	0.304	0.606	0.337	0.512	0.219
	N	70	70	70	70	70	70	70	70	70
RNGranite_metamorphic_aplitic	Correlation Coefficient	0.134	0.160	0.183	-0.072	0.146	-0.037	-0.033	0.203	-0.069
	Sig. (2-tailed)	0.269	0.185	0.129	0.552	0.228	0.762	0.784	0.092	0.573
	N	70	70	70	70	70	70	70	70	70
RNGranodiorite_metamorphic	Correlation Coefficient	.	.	.	.	.	.	.	.	.
	Sig. (2-tailed)	.	.	.	.	.	.	.	.	.
	N	70	70	70	70	70	70	70	70	70
RNPegmatite_pegmatiticgranite	Correlation Coefficient	0.069	0.070	0.177	-0.287	-0.077	0.162	-0.039	-0.096	0.037
	Sig. (2-tailed)	0.570	0.565	0.143	**0.016**	0.526	0.180	0.750	0.431	0.761
	N	70	70	70	70	70	70	70	70	70
RNTonalitetogranodiorite_metamorphic	Correlation Coefficient	-0.104	0.039	-0.075	-0.072	0.003	-0.037	-0.033	0.033	-0.086
	Sig. (2-tailed)	0.390	0.746	0.539	0.552	0.980	0.762	0.784	0.784	0.477
	N	70	70	70	70	70	70	70	70	70

Table 4-65. Subcategory variables with the most highly significant log-likelihoods for predicting fracture set membership likelihood.

Category	Chi-Square	Asymp. Sig.
Broken	156.87	1.4617E-30
Open	129.98	6.3394E-25
PartlyOpen	12.09	9.7587E-02
Sealed		
M1Adularia	85.20	1.1926E-15
M1Calcite	13.11	6.9469E-02
M1Chlorite	73.58	2.7806E-13
M1Epidote	16.56	2.0491E-02
M1Hematite	16.23	2.3065E-02
M1Laumontite	127.89	1.7302E-24
M1NDR	72.53	4.5392E-13
M1OxidizedWalls	20.05	5.4705E-03
M1Quartz	23.86	1.2073E-03
M2Adularia	36.65	5.4584E-06
M2Amphibole	45.67	1.0123E-07
M2Laumontite	24.62	8.8500E-04
M2NDR	112.96	2.2309E-21
M2OxidizedWalls	55.48	1.1983E-09
Planar	138.51	1.0411E-26
Stepped	30.99	6.2531E-05
Rough	90.10	1.1816E-16
Slickensided	15.70	2.8020E-02
Smooth	42.68	3.8378E-07
HighlyAltered	22.83	1.8283E-03
ModeratelyAltered	16.26	2.2882E-02
SlightlyAltered	59.38	2.0054E-10
Joint Alteration 1.0	89.60	1.4981E-16
Joint Alteration 1.5	32.23	3.6814E-05
Joint Alteration 2.0	24.84	8.0893E-04
BRNAmphibolite	30.22	8.6622E-05
BRNBreccia	16.75	1.9051E-02
BRN Diorite, quartzdiorite and gabbro metamorphic	19.54	6.6628E-03
BRN Granite, granodiorite and tonalite metamorphic, fine to medium grained	16.42	2.1562E-02
BRN Pegmatite, pegmatitic granite	19.27	7.3903E-03
FFM02	260.79	1.3939E-52
FFM03	44.21	1.9456E-07

Table 4-66. Logistic regression results for individual sets. The value of β ('B' in the SPSS output below) indicates the strength and sign of the correlation.

		B	Std. Error	Wald	df	Sig.	Exp(B)
EW	Intercept	12.121	4.030	9.047	1	0.003	
	[Broken=0]	-1.053	0.229	21.141	1	0.000	0.349
	[Broken=1]	0.000	.	.	0	.	.
	[Open=0]	-0.232	0.169	1.897	1	0.168	0.793
	[Open=1]	0.000	.	.	0	.	.
	[PartlyOpen=0]	-0.473	0.323	2.138	1	0.144	0.623
	[PartlyOpen=1]	0.000	.	.	0	.	.
	[M1Adularia=0]	0.438	0.239	3.352	1	0.067	1.550
	[M1Adularia=1]	0.000	.	.	0	.	.
	[M1Chlorite=0]	-0.318	0.122	6.725	1	0.010	0.728
	[M1Chlorite=1]	0.000	.	.	0	.	.
	[M1Epidote=0]	-0.016	0.574	0.001	1	0.977	0.984
	[M1Epidote=1]	0.000	.	.	0	.	.
	[M1Hematite=0]	-0.412	0.329	1.569	1	0.210	0.662
	[M1Hematite=1]	0.000	.	.	0	.	.
	[M1Laumontite=0]	1.038	0.155	44.740	1	0.000	2.824
	[M1Laumontite=1]	0.000	.	.	0	.	.
	[M1NDR=0]	-0.312	0.268	1.351	1	0.245	0.732
	[M1NDR=1]	0.000	.	.	0	.	.
	[M1OxidizedWalls=0]	0.279	0.193	2.095	1	0.148	1.322
	[M1OxidizedWalls=1]	0.000	.	.	0	.	.
	[M1Quartz=0]	0.024	0.242	0.010	1	0.920	1.025
	[M1Quartz=1]	0.000	.	.	0	.	.
	[M2Adularia=0]	-0.259	0.299	0.747	1	0.387	0.772
	[M2Adularia=1]	0.000	.	.	0	.	.
	[M2Amphibole=0]	-17.116	0.000	.	1	.	0.000
	[M2Amphibole=1]	0.000	.	.	0	.	.
	[M2Laumontite=0]	1.845	0.255	52.160	1	0.000	6.329
	[M2Laumontite=1]	0.000	.	.	0	.	.
	[M2NDR=0]	-0.893	0.123	52.892	1	0.000	0.410
	[M2NDR=1]	0.000	.	.	0	.	.
	[M2OxidizedWalls=0]	-0.072	0.142	0.262	1	0.609	0.930
	[M2OxidizedWalls=1]	0.000	.	.	0	.	.
	[Planar=0]	0.427	0.147	8.406	1	0.004	1.533
	[Planar=1]	0.000	.	.	0	.	.
	[Stepped=0]	0.982	0.265	13.791	1	0.000	2.671
	[Stepped=1]	0.000	.	.	0	.	.
	[Rough=0]	-0.553	0.165	11.185	1	0.001	0.575
	[Rough=1]	0.000	.	.	0	.	.
	[Slickensided=0]	-0.973	0.488	3.986	1	0.046	0.378
	[Slickensided=1]	0.000	.	.	0	.	.
	[Smooth=0]	0.000	.	.	0	.	.
	[Smooth=1]	0.000	.	.	0	.	.
	[HighlyAltered=0]	-1.763	1.978	0.795	1	0.373	0.171
	[HighlyAltered=1]	0.000	.	.	0	.	.
	[ModeratelyAltered=0]	-1.260	0.548	5.288	1	0.021	0.284
	[ModeratelyAltered=1]	0.000	.	.	0	.	.
	[SlightlyAltered=0]	-0.006	0.133	0.002	1	0.966	0.994
	[SlightlyAltered=1]	0.000	.	.	0	.	.
	[JA1=0]	0.549	0.202	7.415	1	0.006	1.732
	[JA1=1]	0.000	.	.	0	.	.
	[JA1.5=0]	0.812	0.313	6.737	1	0.009	2.251
	[JA1.5=1]	0.000	.	.	0	.	.
	[JA2=0]	0.361	0.219	2.720	1	0.099	1.435
	[JA2=1]	0.000	.	.	0	.	.
	[BRNAmphibolite=0]	0.060	0.158	0.141	1	0.707	1.061
	[BRNAmphibolite=1]	0.000	.	.	0	.	.
	[BRNBreccia=0]	2.563	2.912	0.775	1	0.379	12.978
	[BRNBreccia=1]	0.000	.	.	0	.	.
	[BRNDioritequartzdioriteandgabbrometamorphic=0]	-2.234	0.989	5.107	1	0.024	0.107
	[BRNDioritequartzdioriteandgabbrometamorphic=1]	0.000	.	.	0	.	.
	[BRNGranitegranodioriteandtonalitemetamorphicfinetomediumgrained=0]	1.299	0.261	24.770	1	0.000	3.665
	[BRNGranitegranodioriteandtonalitemetamorphicfinetomediumgrained=1]	0.000	.	.	0	.	.
	[BRNPegmatitepegmatiticgranite=0]	0.653	0.147	19.820	1	0.000	1.921
	[BRNPegmatitepegmatiticgranite=1]	0.000	.	.	0	.	.
	[FFM02=0]	3.166	0.146	469.440	1	0.000	23.710
	[FFM02=1]	0.000	.	.	0	.	.
	[FFM03=0]	1.057	0.229	21.322	1	0.000	2.876
	[FFM03=1]	0.000	.	.	0	.	.

Table 4-66 (continued)

		B	Std. Error	Wald	df	Sig.	Exp(B)
NS	Intercept	-1.741	3.099	0.316	1	0.574	
	[Broken=0]	0.165	0.208	0.628	1	0.428	1.179
	[Broken=1]	0.000	.	.	0	.	.
	[Open=0]	-0.612	0.144	17.939	1	0.000	0.543
	[Open=1]	0.000	.	.	0	.	.
	[PartlyOpen=0]	-0.254	0.238	1.141	1	0.285	0.776
	[PartlyOpen=1]	0.000	.	.	0	.	.
	[M1Adularia=0]	-0.159	0.149	1.139	1	0.286	0.853
	[M1Adularia=1]	0.000	.	.	0	.	.
	[M1Chlorite=0]	-0.006	0.097	0.004	1	0.948	0.994
	[M1Chlorite=1]	0.000	.	.	0	.	.
	[M1Epidote=0]	0.031	0.372	0.007	1	0.934	1.031
	[M1Epidote=1]	0.000	.	.	0	.	.
	[M1Hematite=0]	-0.749	0.238	9.913	1	0.002	0.473
	[M1Hematite=1]	0.000	.	.	0	.	.
	[M1Laumontite=0]	1.055	0.108	95.277	1	0.000	2.871
	[M1Laumontite=1]	0.000	.	.	0	.	.
	[M1NDR=0]	-0.161	0.248	0.424	1	0.515	0.851
	[M1NDR=1]	0.000	.	.	0	.	.
	[M1OxidizedWalls=0]	-0.688	0.152	20.586	1	0.000	0.503
	[M1OxidizedWalls=1]	0.000	.	.	0	.	.
	[M1Quartz=0]	-0.668	0.165	16.475	1	0.000	0.513
	[M1Quartz=1]	0.000	.	.	0	.	.
	[M2Adularia=0]	-0.396	0.212	3.479	1	0.062	0.673
	[M2Adularia=1]	0.000	.	.	0	.	.
	[M2Amphibole=0]	0.906	0.000	.	1	.	2.474
	[M2Amphibole=1]	0.000	.	.	0	.	.
	[M2Laumontite=0]	1.825	0.177	106.654	1	0.000	6.203
	[M2Laumontite=1]	0.000	.	.	0	.	.
	[M2NDR=0]	-0.291	0.103	7.905	1	0.005	0.748
	[M2NDR=1]	0.000	.	.	0	.	.
	[M2OxidizedWalls=0]	-0.569	0.095	35.778	1	0.000	0.566
	[M2OxidizedWalls=1]	0.000	.	.	0	.	.
	[Planar=0]	0.136	0.134	1.020	1	0.312	1.145
	[Planar=1]	0.000	.	.	0	.	.
	[Stepped=0]	0.297	0.211	1.989	1	0.158	1.346
	[Stepped=1]	0.000	.	.	0	.	.
	[Rough=0]	0.119	0.140	0.718	1	0.397	1.126
	[Rough=1]	0.000	.	.	0	.	.
	[Slickensided=0]	-1.549	0.440	12.372	1	0.000	0.212
	[Slickensided=1]	0.000	.	.	0	.	.
	[Smooth=0]	0.000	.	.	0	.	.
	[Smooth=1]	0.000	.	.	0	.	.
	[HighlyAltered=0]	-2.223	1.917	1.346	1	0.246	0.108
	[HighlyAltered=1]	0.000	.	.	0	.	.
	[ModeratelyAltered=0]	-0.477	0.568	0.704	1	0.401	0.621
	[ModeratelyAltered=1]	0.000	.	.	0	.	.
	[SlightlyAltered=0]	0.478	0.100	22.720	1	0.000	1.612
	[SlightlyAltered=1]	0.000	.	.	0	.	.
	[JA1=0]	-0.260	0.190	1.875	1	0.171	0.771
	[JA1=1]	0.000	.	.	0	.	.
	[JA1.5=0]	0.448	0.296	2.290	1	0.130	1.565
	[JA1.5=1]	0.000	.	.	0	.	.
	[JA2=0]	-0.187	0.207	0.814	1	0.367	0.830
	[JA2=1]	0.000	.	.	0	.	.
	[BRNAmphibolite=0]	0.110	0.128	0.739	1	0.390	1.116
	[BRNAmphibolite=1]	0.000	.	.	0	.	.
	[BRNBreccia=0]	1.564	1.506	1.078	1	0.299	4.777
	[BRNBreccia=1]	0.000	.	.	0	.	.
	[BRNDioritequartzdioriteandgabbrometamorphic=0]	1.419	1.342	1.118	1	0.290	4.133
	[BRNDioritequartzdioriteandgabbrometamorphic=1]	0.000	.	.	0	.	.
	[BRNGranitegranodioriteandtonalitemetamorphicfinetomediumgrained=0]	0.904	0.144	39.425	1	0.000	2.470
	[BRNGranitegranodioriteandtonalitemetamorphicfinetomediumgrained=1]	0.000	.	.	0	.	.
	[BRNPegmatitepegmatiticgranite=0]	0.466	0.104	20.068	1	0.000	1.593
	[BRNPegmatitepegmatiticgranite=1]	0.000	.	.	0	.	.
	[FFM02=0]	2.638	0.096	753.597	1	0.000	13.990
	[FFM02=1]	0.000	.	.	0	.	.
	[FFM03=0]	-0.539	0.151	12.825	1	0.000	0.583
	[FFM03=1]	0.000	.	.	0	.	.

Table 4-66 (continued)

NE	Intercept	-5.366	2.903	3.417	1	0.065	
	[Broken=0]	0.248	0.184	1.816	1	0.178	1.281
	[Broken=1]	0.000	.	.	0	.	.
	[Open=0]	-0.363	0.124	8.625	1	0.003	0.695
	[Open=1]	0.000	.	.	0	.	.
	[PartlyOpen=0]	-0.383	0.204	3.521	1	0.061	0.682
	[PartlyOpen=1]	0.000	.	.	0	.	.
	[M1Adularia=0]	0.571	0.147	15.083	1	0.000	1.771
	[M1Adularia=1]	0.000	.	.	0	.	.
	[M1Chlorite=0]	0.048	0.086	0.308	1	0.579	1.049
	[M1Chlorite=1]	0.000	.	.	0	.	.
	[M1Epidote=0]	0.033	0.342	0.009	1	0.924	1.033
	[M1Epidote=1]	0.000	.	.	0	.	.
	[M1Hematite=0]	-0.524	0.228	5.256	1	0.022	0.592
	[M1Hematite=1]	0.000	.	.	0	.	.
	[M1Laumontite=0]	0.560	0.089	39.237	1	0.000	1.750
	[M1Laumontite=1]	0.000	.	.	0	.	.
	[M1NDR=0]	0.073	0.223	0.106	1	0.744	1.076
	[M1NDR=1]	0.000	.	.	0	.	.
	[M1OxidizedWalls=0]	0.147	0.145	1.033	1	0.309	1.159
	[M1OxidizedWalls=1]	0.000	.	.	0	.	.
	[M1Quartz=0]	-0.007	0.162	0.002	1	0.968	0.993
	[M1Quartz=1]	0.000	.	.	0	.	.
	[M2Adularia=0]	0.130	0.201	0.422	1	0.516	1.139
	[M2Adularia=1]	0.000	.	.	0	.	.
	[M2Amphibole=0]	0.422	0.000	.	1	.	1.526
	[M2Amphibole=1]	0.000	.	.	0	.	.
	[M2Laumontite=0]	1.575	0.129	148.690	1	0.000	4.833
	[M2Laumontite=1]	0.000	.	.	0	.	.
	[M2NDR=0]	-0.088	0.092	0.923	1	0.337	0.915
	[M2NDR=1]	0.000	.	.	0	.	.
	[M2OxidizedWalls=0]	0.047	0.088	0.287	1	0.592	1.048
	[M2OxidizedWalls=1]	0.000	.	.	0	.	.
	[Planar=0]	0.110	0.113	0.957	1	0.328	1.117
	[Planar=1]	0.000	.	.	0	.	.
	[Stepped=0]	0.396	0.171	5.348	1	0.021	1.485
	[Stepped=1]	0.000	.	.	0	.	.
	[Rough=0]	-0.029	0.116	0.063	1	0.802	0.971
	[Rough=1]	0.000	.	.	0	.	.
	[Slickensided=0]	-0.283	0.471	0.363	1	0.547	0.753
	[Slickensided=1]	0.000	.	.	0	.	.
	[Smooth=0]	0.000	.	.	0	.	.
	[Smooth=1]	0.000	.	.	0	.	.
	[HighlyAltered=0]	-1.283	2.010	0.408	1	0.523	0.277
	[HighlyAltered=1]	0.000	.	.	0	.	.
	[ModeratelyAltered=0]	-0.386	0.531	0.527	1	0.468	0.680
	[ModeratelyAltered=1]	0.000	.	.	0	.	.
	[SlightlyAltered=0]	0.230	0.087	6.977	1	0.008	1.259
	[SlightlyAltered=1]	0.000	.	.	0	.	.
	[JA1=0]	-0.626	0.167	14.087	1	0.000	0.535
	[JA1=1]	0.000	.	.	0	.	.
	[JA1.5=0]	-0.115	0.224	0.264	1	0.607	0.891
	[JA1.5=1]	0.000	.	.	0	.	.
	[JA2=0]	-0.190	0.186	1.047	1	0.306	0.827
	[JA2=1]	0.000	.	.	0	.	.
	[BRNAmphibolite=0]	0.377	0.121	9.773	1	0.002	1.458
	[BRNAmphibolite=1]	0.000	.	.	0	.	.
	[BRNBreccia=0]	1.693	1.181	2.056	1	0.152	5.435
	[BRNBreccia=1]	0.000	.	.	0	.	.
	[BRNDioritequartzdioriteandgabbrometamorphic=0]	1.395	1.190	1.373	1	0.241	4.034
	[BRNDioritequartzdioriteandgabbrometamorphic=1]	0.000	.	.	0	.	.
	[BRNGranitegranodioriteandtonalitemetamorphicfinetomediumgrained=0]	0.718	0.126	32.463	1	0.000	2.050
	[BRNGranitegranodioriteandtonalitemetamorphicfinetomediumgrained=1]	0.000	.	.	0	.	.
	[BRNPegmatitepegmatiticgranite=0]	0.504	0.091	30.936	1	0.000	1.655
	[BRNPegmatitepegmatiticgranite=1]	0.000	.	.	0	.	.
	[FFM02=0]	2.926	0.082	######	1	0.000	18.647
	[FFM02=1]	0.000	.	.	0	.	.
	[FFM03=0]	-0.626	0.143	19.228	1	0.000	0.535
	[FFM03=1]	0.000	.	.	0	.	.

Table 4-66 (continued)

		B	Std. Error	Wald	df	Sig.	Exp(B)
NNW	Intercept	-0.998	8.694	0.013	1	0.909	
	[Broken=0]	0.421	0.336	1.569	1	0.210	1.524
	[Broken=1]	0.000	.	.	0	.	.
	[Open=0]	1.917	0.239	64.227	1	0.000	6.798
	[Open=1]	0.000	.	.	0	.	.
	[PartlyOpen=0]	0.297	0.257	1.343	1	0.247	1.346
	[PartlyOpen=1]	0.000	.	.	0	.	.
	[M1Adularia=0]	-0.396	0.262	2.284	1	0.131	0.673
	[M1Adularia=1]	0.000	.	.	0	.	.
	[M1Chlorite=0]	-0.538	0.136	15.576	1	0.000	0.584
	[M1Chlorite=1]	0.000	.	.	0	.	.
	[M1Epidote=0]	0.705	0.568	1.540	1	0.215	2.024
	[M1Epidote=1]	0.000	.	.	0	.	.
	[M1Hematite=0]	-0.337	0.485	0.483	1	0.487	0.714
	[M1Hematite=1]	0.000	.	.	0	.	.
	[M1Laumontite=0]	1.995	0.216	85.399	1	0.000	7.350
	[M1Laumontite=1]	0.000	.	.	0	.	.
	[M1NDR=0]	0.328	0.359	0.836	1	0.361	1.388
	[M1NDR=1]	0.000	.	.	0	.	.
	[M1OxidizedWalls=0]	-0.967	0.214	20.451	1	0.000	0.380
	[M1OxidizedWalls=1]	0.000	.	.	0	.	.
	[M1Quartz=0]	-2.225	0.230	93.697	1	0.000	0.108
	[M1Quartz=1]	0.000	.	.	0	.	.
	[M2Adularia=0]	-0.223	0.303	0.543	1	0.461	0.800
	[M2Adularia=1]	0.000	.	.	0	.	.
	[M2Amphibole=0]	1.169	0.000	.	1	.	3.218
	[M2Amphibole=1]	0.000	.	.	0	.	.
	[M2Laumontite=0]	3.245	0.434	55.984	1	0.000	25.669
	[M2Laumontite=1]	0.000	.	.	0	.	.
	[M2NDR=0]	-1.033	0.143	52.074	1	0.000	0.356
	[M2NDR=1]	0.000	.	.	0	.	.
	[M2OxidizedWalls=0]	-0.369	0.164	5.042	1	0.025	0.692
	[M2OxidizedWalls=1]	0.000	.	.	0	.	.
	[Planar=0]	0.989	0.192	26.479	1	0.000	2.689
	[Planar=1]	0.000	.	.	0	.	.
	[Stepped=0]	1.494	0.288	26.857	1	0.000	4.454
	[Stepped=1]	0.000	.	.	0	.	.
	[Rough=0]	0.264	0.188	1.968	1	0.161	1.303
	[Rough=1]	0.000	.	.	0	.	.
	[Slickensided=0]	-0.065	0.697	0.009	1	0.926	0.937
	[Slickensided=1]	0.000	.	.	0	.	.
	[Smooth=0]	0.000	.	.	0	.	.
	[Smooth=1]	0.000	.	.	0	.	.
	[HighlyAltered=0]	-2.823	4.408	0.410	1	0.522	0.059
	[HighlyAltered=1]	0.000	.	.	0	.	.
	[ModeratelyAltered=0]	-2.766	0.958	8.343	1	0.004	0.063
	[ModeratelyAltered=1]	0.000	.	.	0	.	.
	[SlightlyAltered=0]	-3.466	0.137	639.761	1	0.000	0.031
	[SlightlyAltered=1]	0.000	.	.	0	.	.
	[JA1=0]	-1.223	0.306	15.984	1	0.000	0.294
	[JA1=1]	0.000	.	.	0	.	.
	[JA1.5=0]	-1.191	0.326	13.336	1	0.000	0.304
	[JA1.5=1]	0.000	.	.	0	.	.
	[JA2=0]	-0.150	0.347	0.187	1	0.665	0.860
	[JA2=1]	0.000	.	.	0	.	.
	[BRNAmphibolite=0]	-0.730	0.171	18.254	1	0.000	0.482
	[BRNAmphibolite=1]	0.000	.	.	0	.	.
	[BRNBreccia=0]	3.863	5.144	0.564	1	0.453	47.615
	[BRNBreccia=1]	0.000	.	.	0	.	.
	[BRNDioritequartzdioriteandgabbrometamorphic=0]	0.134	4.972	0.001	1	0.978	1.144
	[BRNDioritequartzdioriteandgabbrometamorphic=1]	0.000	.	.	0	.	.
	[BRNGranitegranodioriteandtonalitemetamorphicfinetomediumgrained=0]	0.809	0.260	9.697	1	0.002	2.246
	[BRNGranitegranodioriteandtonalitemetamorphicfinetomediumgrained=1]	0.000	.	.	0	.	.
	[BRNPegmatitepegmatiticgranite=0]	0.395	0.160	6.142	1	0.013	1.485
	[BRNPegmatitepegmatiticgranite=1]	0.000	.	.	0	.	.
	[FFM02=0]	-2.718	0.164	273.389	1	0.000	0.066
	[FFM02=1]	0.000	.	.	0	.	.
	[FFM03=0]	-0.233	0.312	0.558	1	0.455	0.792
	[FFM03=1]	0.000	.	.	0	.	.

Table 4-66 (continued)

		B	Std. Error	Wald	df	Sig.	Exp(B)
NNE	Intercept	-6.021	4.442	1.837	1	0.175	
	[Broken=0]	0.220	0.322	0.466	1	0.495	1.246
	[Broken=1]	0.000	.	.	0	.	.
	[Open=0]	-0.737	0.215	11.713	1	0.001	0.478
	[Open=1]	0.000	.	.	0	.	.
	[PartlyOpen=0]	-0.185	0.347	0.285	1	0.593	0.831
	[PartlyOpen=1]	0.000	.	.	0	.	.
	[M1Adularia=0]	-2.125	0.155	187.021	1	0.000	0.119
	[M1Adularia=1]	0.000	.	.	0	.	.
	[M1Chlorite=0]	0.241	0.133	3.304	1	0.069	1.273
	[M1Chlorite=1]	0.000	.	.	0	.	.
	[M1Epidote=0]	0.149	0.491	0.092	1	0.761	1.161
	[M1Epidote=1]	0.000	.	.	0	.	.
	[M1Hematite=0]	0.218	0.375	0.337	1	0.561	1.244
	[M1Hematite=1]	0.000	.	.	0	.	.
	[M1Laumontite=0]	1.942	0.191	102.961	1	0.000	6.973
	[M1Laumontite=1]	0.000	.	.	0	.	.
	[M1NDR=0]	-0.064	0.356	0.032	1	0.858	0.938
	[M1NDR=1]	0.000	.	.	0	.	.
	[M1OxidizedWalls=0]	0.078	0.203	0.149	1	0.700	1.081
	[M1OxidizedWalls=1]	0.000	.	.	0	.	.
	[M1Quartz=0]	-0.672	0.191	12.351	1	0.000	0.511
	[M1Quartz=1]	0.000	.	.	0	.	.
	[M2Adularia=0]	-2.455	0.203	146.507	1	0.000	0.086
	[M2Adularia=1]	0.000	.	.	0	.	.
	[M2Amphibole=0]	1.005	0.000	.	1	.	2.732
	[M2Amphibole=1]	0.000	.	.	0	.	.
	[M2Laumontite=0]	2.244	0.285	61.986	1	0.000	9.435
	[M2Laumontite=1]	0.000	.	.	0	.	.
	[M2NDR=0]	-0.253	0.141	3.221	1	0.073	0.777
	[M2NDR=1]	0.000	.	.	0	.	.
	[M2OxidizedWalls=0]	0.222	0.118	3.536	1	0.060	1.248
	[M2OxidizedWalls=1]	0.000	.	.	0	.	.
	[Planar=0]	0.039	0.198	0.039	1	0.844	1.040
	[Planar=1]	0.000	.	.	0	.	.
	[Stepped=0]	0.236	0.310	0.581	1	0.446	1.267
	[Stepped=1]	0.000	.	.	0	.	.
	[Rough=0]	0.089	0.215	0.171	1	0.679	1.093
	[Rough=1]	0.000	.	.	0	.	.
	[Slickensided=0]	0.111	0.763	0.021	1	0.884	1.117
	[Slickensided=1]	0.000	.	.	0	.	.
	[Smooth=0]	0.000	.	.	0	.	.
	[Smooth=1]	0.000	.	.	0	.	.
	[HighlyAltered=0]	-0.248	2.902	0.007	1	0.932	0.780
	[HighlyAltered=1]	0.000	.	.	0	.	.
	[ModeratelyAltered=0]	-0.083	0.824	0.010	1	0.920	0.921
	[ModeratelyAltered=1]	0.000	.	.	0	.	.
	[SlightlyAltered=0]	0.286	0.140	4.147	1	0.042	1.331
	[SlightlyAltered=1]	0.000	.	.	0	.	.
	[JA1=0]	-0.095	0.295	0.103	1	0.748	0.910
	[JA1=1]	0.000	.	.	0	.	.
	[JA1.5=0]	0.144	0.440	0.107	1	0.744	1.155
	[JA1.5=1]	0.000	.	.	0	.	.
	[JA2=0]	-0.035	0.319	0.012	1	0.912	0.965
	[JA2=1]	0.000	.	.	0	.	.
	[BRNAmphibolite=0]	0.662	0.193	11.804	1	0.001	1.938
	[BRNAmphibolite=1]	0.000	.	.	0	.	.
	[BRNBreccia=0]	2.140	2.523	0.720	1	0.396	8.501
	[BRNBreccia=1]	0.000	.	.	0	.	.
	[BRNDioritequartzdioriteandgabbrometamorphic=0]	-2.805	0.981	8.176	1	0.004	0.060
	[BRNDioritequartzdioriteandgabbrometamorphic=1]	0.000	.	.	0	.	.
	[BRNGranitegranodioriteandtonalitemetamorphicfinetomediumgrained=0]	1.496	0.248	36.258	1	0.000	4.464
	[BRNGranitegranodioriteandtonalitemetamorphicfinetomediumgrained=1]	0.000	.	.	0	.	.
	[BRNPegmatitepegmatiticgranite=0]	0.243	0.124	3.846	1	0.050	1.276
	[BRNPegmatitepegmatiticgranite=1]	0.000	.	.	0	.	.
	[FFM02=0]	3.462	0.181	367.375	1	0.000	31.890
	[FFM02=1]	0.000	.	.	0	.	.
	[FFM03=0]	0.748	0.225	11.054	1	0.001	2.113
	[FFM03=1]	0.000	.	.	0	.	.

Table 4-66 (continued)

NW	Intercept	-1.403	3.359	0.174	1	0.676	
	[Broken=0]	-0.181	0.189	0.917	1	0.338	0.834
	[Broken=1]	0.000	.	.	0	.	.
	[Open=0]	-0.471	0.132	12.697	1	0.000	0.624
	[Open=1]	0.000	.	.	0	.	.
	[PartlyOpen=0]	-0.214	0.236	0.820	1	0.365	0.808
	[PartlyOpen=1]	0.000	.	.	0	.	.
	[M1Adularia=0]	0.343	0.173	3.917	1	0.048	1.409
	[M1Adularia=1]	0.000	.	.	0	.	.
	[M1Chlorite=0]	-0.304	0.096	10.135	1	0.001	0.738
	[M1Chlorite=1]	0.000	.	.	0	.	.
	[M1Epidote=0]	-1.801	0.313	33.195	1	0.000	0.165
	[M1Epidote=1]	0.000	.	.	0	.	.
	[M1Hematite=0]	-0.655	0.248	6.953	1	0.008	0.519
	[M1Hematite=1]	0.000	.	.	0	.	.
	[M1Laumontite=0]	0.904	0.111	66.605	1	0.000	2.468
	[M1Laumontite=1]	0.000	.	.	0	.	.
	[M1NDR=0]	0.012	0.229	0.003	1	0.957	1.012
	[M1NDR=1]	0.000	.	.	0	.	.
	[M1OxidizedWalls=0]	0.244	0.154	2.506	1	0.113	1.276
	[M1OxidizedWalls=1]	0.000	.	.	0	.	.
	[M1Quartz=0]	-0.194	0.180	1.158	1	0.282	0.824
	[M1Quartz=1]	0.000	.	.	0	.	.
	[M2Adularia=0]	0.347	0.252	1.894	1	0.169	1.414
	[M2Adularia=1]	0.000	.	.	0	.	.
	[M2Amphibole=0]	0.364	0.000	.	1	.	1.439
	[M2Amphibole=1]	0.000	.	.	0	.	.
	[M2Laumontite=0]	1.708	0.173	97.093	1	0.000	5.518
	[M2Laumontite=1]	0.000	.	.	0	.	.
	[M2NDR=0]	-0.907	0.097	87.889	1	0.000	0.404
	[M2NDR=1]	0.000	.	.	0	.	.
	[M2OxidizedWalls=0]	-0.123	0.103	1.415	1	0.234	0.885
	[M2OxidizedWalls=1]	0.000	.	.	0	.	.
	[Planar=0]	0.033	0.121	0.073	1	0.787	1.033
	[Planar=1]	0.000	.	.	0	.	.
	[Stepped=0]	0.238	0.185	1.665	1	0.197	1.269
	[Stepped=1]	0.000	.	.	0	.	.
	[Rough=0]	0.015	0.125	0.015	1	0.902	1.016
	[Rough=1]	0.000	.	.	0	.	.
	[Slickensided=0]	-0.805	0.442	3.325	1	0.068	0.447
	[Slickensided=1]	0.000	.	.	0	.	.
	[Smooth=0]	0.000	.	.	0	.	.
	[Smooth=1]	0.000	.	.	0	.	.
	[HighlyAltered=0]	-0.409	2.456	0.028	1	0.868	0.664
	[HighlyAltered=1]	0.000	.	.	0	.	.
	[ModeratelyAltered=0]	-0.539	0.544	0.981	1	0.322	0.583
	[ModeratelyAltered=1]	0.000	.	.	0	.	.
	[SlightlyAltered=0]	0.149	0.098	2.291	1	0.130	1.161
	[SlightlyAltered=1]	0.000	.	.	0	.	.
	[JA1=0]	-0.340	0.170	3.995	1	0.046	0.712
	[JA1=1]	0.000	.	.	0	.	.
	[JA1.5=0]	0.710	0.268	7.019	1	0.008	2.035
	[JA1.5=1]	0.000	.	.	0	.	.
	[JA2=0]	-0.238	0.187	1.631	1	0.202	0.788
	[JA2=1]	0.000	.	.	0	.	.
	[BRNAmphibolite=0]	-0.235	0.123	3.622	1	0.057	0.791
	[BRNAmphibolite=1]	0.000	.	.	0	.	.
	[BRNBreccia=0]	1.722	1.511	1.298	1	0.255	5.595
	[BRNBreccia=1]	0.000	.	.	0	.	.
	[BRNDioritequartzdioriteandgabbrometamorphic=0]	0.196	1.101	0.032	1	0.859	1.216
	[BRNDioritequartzdioriteandgabbrometamorphic=1]	0.000	.	.	0	.	.
	[BRNGranitegranodioriteandtonalitemetamorphicfinetomediumgrained=0]	0.344	0.138	6.209	1	0.013	1.410
	[BRNGranitegranodioriteandtonalitemetamorphicfinetomediumgrained=1]	0.000	.	.	0	.	.
	[BRNPegmatitepegmatiticgranite=0]	0.297	0.102	8.439	1	0.004	1.346
	[BRNPegmatitepegmatiticgranite=1]	0.000	.	.	0	.	.
	[FFM02=0]	2.523	0.092	754.677	1	0.000	12.468
	[FFM02=1]	0.000	.	.	0	.	.
	[FFM03=0]	-0.772	0.149	27.028	1	0.000	0.462
	[FFM03=1]	0.000	.	.	0	.	.

143

Table 4-66 (continued)

SH		B	Std. Error	Wald	df	Sig.	Exp(B)
SH	Intercept	4.171	2.552	2.671	1	0.102	
	[Broken=0]	0.385	0.170	5.143	1	0.023	1.469
	[Broken=1]	0.000	.	.	0	.	.
	[Open=0]	-1.036	0.116	80.346	1	0.000	0.355
	[Open=1]	0.000	.	.	0	.	.
	[PartlyOpen=0]	-0.725	0.190	14.582	1	0.000	0.484
	[PartlyOpen=1]	0.000	.	.	0	.	.
	[M1Adularia=0]	0.572	0.155	13.549	1	0.000	1.771
	[M1Adularia=1]	0.000	.	.	0	.	.
	[M1Chlorite=0]	-0.291	0.082	12.711	1	0.000	0.748
	[M1Chlorite=1]	0.000	.	.	0	.	.
	[M1Epidote=0]	-1.287	0.301	18.328	1	0.000	0.276
	[M1Epidote=1]	0.000	.	.	0	.	.
	[M1Hematite=0]	-0.312	0.233	1.788	1	0.181	0.732
	[M1Hematite=1]	0.000	.	.	0	.	.
	[M1Laumontite=0]	1.517	0.098	241.168	1	0.000	4.557
	[M1Laumontite=1]	0.000	.	.	0	.	.
	[M1NDR=0]	-0.955	0.193	24.423	1	0.000	0.385
	[M1NDR=1]	0.000	.	.	0	.	.
	[M1OxidizedWalls=0]	0.311	0.140	4.912	1	0.027	1.364
	[M1OxidizedWalls=1]	0.000	.	.	0	.	.
	[M1Quartz=0]	-0.026	0.165	0.024	1	0.877	0.975
	[M1Quartz=1]	0.000	.	.	0	.	.
	[M2Adularia=0]	0.116	0.207	0.315	1	0.575	1.123
	[M2Adularia=1]	0.000	.	.	0	.	.
	[M2Amphibole=0]	-0.926	0.000	.	1	.	0.396
	[M2Amphibole=1]	0.000	.	.	0	.	.
	[M2Laumontite=0]	2.457	0.157	246.520	1	0.000	11.674
	[M2Laumontite=1]	0.000	.	.	0	.	.
	[M2NDR=0]	-1.024	0.086	142.731	1	0.000	0.359
	[M2NDR=1]	0.000	.	.	0	.	.
	[M2OxidizedWalls=0]	-0.211	0.092	5.285	1	0.022	0.810
	[M2OxidizedWalls=1]	0.000	.	.	0	.	.
	[Planar=0]	-0.639	0.104	37.849	1	0.000	0.528
	[Planar=1]	0.000	.	.	0	.	.
	[Stepped=0]	-0.386	0.149	6.741	1	0.009	0.680
	[Stepped=1]	0.000	.	.	0	.	.
	[Rough=0]	0.229	0.105	4.742	1	0.029	1.257
	[Rough=1]	0.000	.	.	0	.	.
	[Slickensided=0]	0.425	0.434	0.957	1	0.328	1.529
	[Slickensided=1]	0.000	.	.	0	.	.
	[Smooth=0]	0.000	.	.	0	.	.
	[Smooth=1]	0.000	.	.	0	.	.
	[HighlyAltered=0]	-1.878	1.787	1.104	1	0.293	0.153
	[HighlyAltered=1]	0.000	.	.	0	.	.
	[ModeratelyAltered=0]	-1.297	0.464	7.812	1	0.005	0.273
	[ModeratelyAltered=1]	0.000	.	.	0	.	.
	[SlightlyAltered=0]	0.067	0.085	0.622	1	0.430	1.070
	[SlightlyAltered=1]	0.000	.	.	0	.	.
	[JA1=0]	-0.949	0.149	40.621	1	0.000	0.387
	[JA1=1]	0.000	.	.	0	.	.
	[JA1.5=0]	-0.254	0.195	1.708	1	0.191	0.775
	[JA1.5=1]	0.000	.	.	0	.	.
	[JA2=0]	-0.455	0.166	7.480	1	0.006	0.634
	[JA2=1]	0.000	.	.	0	.	.
	[BRNAmphibolite=0]	-0.270	0.111	5.898	1	0.015	0.763
	[BRNAmphibolite=1]	0.000	.	.	0	.	.
	[BRNBreccia=0]	1.849	0.972	3.619	1	0.057	6.354
	[BRNBreccia=1]	0.000	.	.	0	.	.
	[BRNDioritequartzdioriteandgabbrometamorphic=0]	-0.268	1.005	0.071	1	0.789	0.765
	[BRNDioritequartzdioriteandgabbrometamorphic=1]	0.000	.	.	0	.	.
	[BRNGranitegranodioriteandtonalitemetamorphicfinetomediumgrained=0]	0.631	0.124	26.046	1	0.000	1.879
	[BRNGranitegranodioriteandtonalitemetamorphicfinetomediumgrained=1]	0.000	.	.	0	.	.
	[BRNPegmatitepegmatiticgranite=0]	0.301	0.087	12.033	1	0.001	1.352
	[BRNPegmatitepegmatiticgranite=1]	0.000	.	.	0	.	.
	[FFM02=0]	1.842	0.069	709.141	1	0.000	6.309
	[FFM02=1]	0.000	.	.	0	.	.
	[FFM03=0]	-0.528	0.143	13.527	1	0.000	0.590
	[FFM03=1]	0.000	.	.	0	.	.

Table 4-67. Multinomial logistic regression classification results for predicting set membership from geological variables.

Classification										
	Predicted									
Observed	ENE	EW	NE	NNE	NNW	NS	NW	SH	Sum	Percent Correct
ENE	436	3	385	96	290	65	0	303	1578	27.60%
EW	23	19	261	66	28	94	4	360	855	2.20%
NE	201	15	2676	402	110	505	17	1278	5204	51.40%
NNE	4	2	210	265	0	96	0	133	710	37.30%
NNW	1	0	0	0	59	0	0	14	74	79.70%
NS	130	5	1089	413	54	560	14	618	2883	19.40%
NW	168	5	788	160	63	237	28	1316	2765	1.00%
SH	285	19	991	207	375	419	53	4393	6742	65.20%
Overall Percentage	6.00%	0.30%	30.80%	7.70%	4.70%	9.50%	0.60%	40.40%	20811	40.50%
Random										
	Predicted									
Observed	ENE	EW	NE	NNE	NNW	NS	NW	SH	Sums	
ENE	95	5	486	122	74	150	9	638	1578	
EW	51	3	263	66	40	81	5	345	855	
NE	312	16	1603	401	245	494	31	2102	5204	
NNE	43	2	219	55	33	67	4	287	710	
NNW	4	0	23	6	3	7	0	30	74	
NS	173	9	888	222	136	274	17	1165	2883	
NW	166	8	852	213	130	263	17	1117	2765	
SH	405	20	2077	519	317	640	40	2724	6742	
Overall Percentage	6.00%	0.30%	30.80%	7.70%	4.70%	9.50%	0.60%	40.40%	20811	

Overall, the multinomial regression results confirm that the sets designated as the older global sets have similar geological characteristics, including the subhorizontal fractures, while the local, probably more recent sets have slightly different geological characteristics. Because the fracture intensity is dominated by the older sets (approximately 85% of the fracture data in the non-deformation zones belongs to one of these four sets), it is not surprising that the mass dimensions for the fracture intensity among the different sets can be combined, since if 85% of the fractures formed under the same geological processes, they might be expected to have the same scaling behavior. Thus the multinomial results are consistent with the results from the mass dimension, and support the current set definitions. They also suggest that the current fracture domain definitions are useful from the standpoint of fracture modeling, and that it is mathematically justifiable to use the same parameters for spatial and scaling models for all of the global sets, or even all sets.

Adjustment for fractures not detected in BIPS

All of the statistical tests, regression modeling and other applications of the borehole data are based on fractures that were detected in the BIPS imagery. The final model, however, is based on compensating the borehole intensity values for the fractures not observed. If there are no statistically significant differences in the fractures that were observed and not observed in BIPS, then the resulting overall intensity can be obtained by multiplying the observed intensity by the ratio of (observed to not observed)/observed on an interval, borehole or domain-wide basis as appropriate for the application. Cross-tabulation and correlation analysis was used to test this hypothesis using the borehole data.

Table 4-68 shows the results of the cross-tabulations and six statistical measures of the association between the categorical geological variable and whether it was detected or not detected in BIPS. For each category, two numbers are reported: the value; and its approximate asymptotic significance. Significance values smaller than 0.05 indicate that there is an associated between the category and detection in BIPS. The value indicates the strength of the association and varies from –1.0 to 1.0 for the symmetrical measures, and .0 to 1.0 for the directional measures. For example, a test statistic value of 0.021 indicates that the error rate has only been reduced by 2.1% over what would be expected by random chance. This table shows that almost all the categorical variables do have a statistically significant association with BIPS detection, but that the impact on classifying the reading into Visible in BIPS is very insignificant, because all of the values are very close to 0.0. There is not a single variable that has a strong impact on the BIPS classification.

Table 4-69 and Figure 4-53 show the relation in another mathematical form; the percentages of each class of fractures as a function of rock type for a continuous variable (Table 4-69). As such, they can be compared using the Spearman correlation coefficient /Davis 2002/, which shows a very high linear correlation. This means that the percentage of fractures in each rock type category is statistically the same for fractures Visible and Not Visible in BIPS. Correlation analyses for other variables showed a similarly high degree of correlation. As a result, it is appropriate to compensate for the intensity for the fractures not visible in BIPS by adjusting the values for Visible in BIPS by the ratio.

Table 4-68. Cross-tabulation results for testing differences in fracture attributes among fracture domains.

	FRACT_MAPPED		FRACT_INTERPRET		CONFIDENCE	
Directional Measures	Value	Approx. Significance	Value	Approx. Significance	Value	Approx. Significance
Lambda	0.000	0.000	0.000	1.000	0.000	0.739
Goodman and Kruskal Tau	0.001	0.000	0.008	0.000	0.000	0.000
Uncertainty Coefficient	0.001	0.000	0.009	0.000	0.000	0.000
Symmetric Measures						
Phi	-0.032	0.000	0.088	0.000	0.020	0.000
Cramer's V	0.032	0.000	0.088	0.000	0.020	0.000
Contingency Coefficient	0.032	0.000	0.087	0.000	0.020	0.000
	SURFACE		**FRAC_ALTER_CODE**		**FRACT_ALTERATION**	
Directional Measures	Value	Approx. Significance	Value	Approx. Significance	Value	Approx. Significance
Lambda	0.000	0.000	0.000	0.000	0.000	0.000
Goodman and Kruskal Tau	0.006	0.000	0.001	0.000	0.001	0.000
Uncertainty Coefficient	0.009	0.000	0.002	0.000	0.002	0.000
Symmetric Measures						
Phi	0.081	0.000	0.038	0.000	0.038	0.000
Cramer's V	0.081	0.000	0.038	0.000	0.038	0.000
Contingency Coefficient	0.080	0.000	0.038	0.000	0.038	0.000
	MIN1		**MIN2**		**ROUGHNESS**	
Directional Measures	Value	Approx. Significance	Value	Approx. Significance	Value	Approx. Significance
Lambda	0.001	0.352	0.000	0.157	0.000	0.000
Goodman and Kruskal Tau	0.024	0.000	0.022	0.000	0.004	0.001
Uncertainty Coefficient	0.026	0.000	0.026	0.000	0.005	0.001
Symmetric Measures						
Phi	0.155	0.000	0.150	0.000	0.000	0.000
Cramer's V	0.155	0.000	0.150	0.000	0.004	0.001
Contingency Coefficient	0.155	0.000	0.148	0.000	0.004	0.001
	JOINT_ALTERATION		**BEST_ROCK_NAME**		**ROCK_NAME**	
Directional Measures	Value	Approx. Significance	Value	Approx. Significance	Value	Approx. Significance
Lambda	0.000	0.000	0.000	0.317	0.000	0.000
Goodman and Kruskal Tau	0.025	0.000	0.005	0.000	0.003	0.000
Uncertainty Coefficient	0.032	0.000	0.005	0.000	0.003	0.000
Symmetric Measures						
Phi	0.159	0.000	0.069	0.000	0.052	0.000
Cramer's V	0.159	0.000	0.069	0.000	0.052	0.000
Contingency Coefficient	0.157	0.000	0.069	0.000	0.052	0.000

Table 4-69. Percentages of fractures in categories Not Visible and Visible by Best Rock Name.

BEST_ROCK_NAME	Not Visible	Visible
Amphibolite	0.0932	0.0928
Aplite	0.0000	0.0001
Breccia	0.0007	0.0009
Calc-silicate rock (skarn)	0.0029	0.0020
Carbonate-dominated hydrothermal vein/segregation	0.0000	0.0000
Cataclastic rock	0.0000	0.0000
Diorite, quartz diorite and gabbro, metamorphic	0.0045	0.0020
Felsic to intermediate volcanic rock, metamorphic	0.0263	0.0177
Granite	0.0007	0.0002
Granite to granodiorite, metamorphic, medium-grained	0.6515	0.6174
Granite, fine- to medium-grained	0.0133	0.0146
Granite, granodiorite and tonalite, metamorphic, fine- to medium-grained	0.0361	0.0536
Granite, metamorphic, aplitic	0.0521	0.0703
Granitoid, metamorphic	0.0001	0.0004
Granodiorite	0.0008	0.0011
Granodiorite, metamorphic	0.0034	0.0093
Granodiorite-Granite	0.0001	0.0000
Hybrid rock	0.0000	0.0003
Hydrothermal vein/segregation, unspecified	0.0000	0.0000
Magnetite mineralization associated with calc-silicate rock (skarn)	0.0000	0.0000
Mylonite	0.0000	0.0001
Pegmatite, pegmatitic granite	0.1093	0.1119
Quartz diorite	0.0000	0.0002
Quartz-dominated hydrothermal vein/segregation	0.0031	0.0031
Sedimentary rock	0.0001	0.0002
Tonalite	0.0001	0.0001
Tonalite to granodiorite, metamorphic	0.0012	0.0012
Ultramafic rock, metamorphic	0.0007	0.0003

n	28 (cases excluded: 13 due to missing values)
rs statistic	0.93
95% CI	0.84 to 0.97
2-tailed p	<0.0001 (t approximation, corrected for ties)
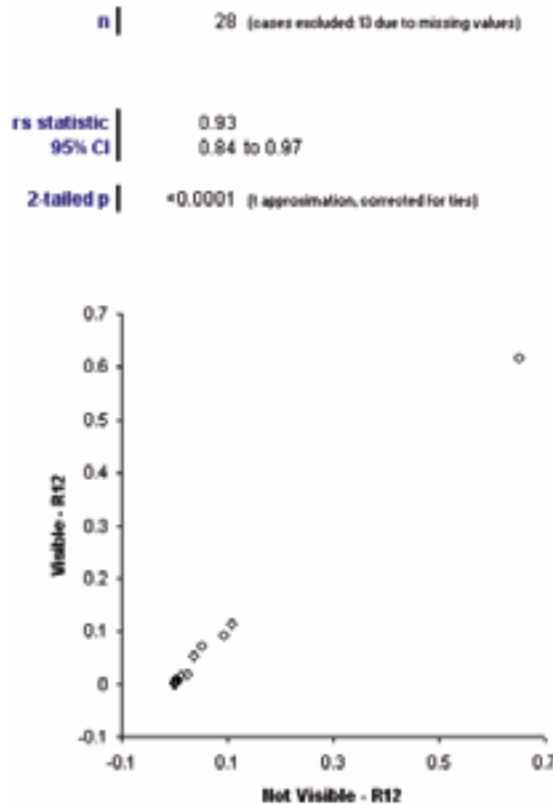
Figure 4-53. Cross-plot and Spearman correlation analysis for Best Rock Name.

Multivariate modeling & supporting calculations

The multivariate modeling was carried out to develop a predictive regression model, using one or more of the geological parameters to predict the borehole P10 fracture intensity. A statistically useful regression model must at least satisfy certain characteristics: the individual parameters should be statistically significant; the independent variables should not have a statistically significant amount of linear correlation; and the overall regression should be statistically significant. The significance of the individual parameter coefficients is typically measured through the significance of the t-statistic calculated for each coefficient; a threshold of $\alpha = 0.05$ is typically used for assessing the significance with probabilities less than this value considered as statistically significant. The degree of linear correlation is typically measured by the Variance inflation Factor, or VIF. Values of VIF greater than 2.0 are often considered as a threshold for collinearity problems. There are also some other collinearity tests, including the magnitude of the eigenvalues and the Condition Index. Eigenvalue magnitudes indicate how many independent factors are present; values that are close to 0.0 indicate collinearity. The Condition Index also measures collinearity; values greater than 15 are evidence of collinearity problems. The significance of the overall regression is measured through the significance of the F-test /Davis 2002/ applied to the ratio of variance related to the model and variance not related to the model. Values of $\alpha = 0.05$ indicate a typical threshold for assessing statistical significance, with probabilities below this α level taken as statistically significant. Analysis of the residuals can also indicate the predictive accuracy of the model, showing the magnitude of the mean residual, which is a measure of likely error, and the correspondence between the predicted minimum and maximum standardized value and the actual standardized values, which evaluates how well the residuals conform to a normal distribution.

Each regression model was derived through stepwise regression. Only models that satisfied the three conditions of statistical significance and lack of collinearity were considered further. The values for these three measures are reported for each regression model, and the final model with the highest r-square value was retained. The parameters that are reported for each model include the:

- values of the standardized and unstandardized coefficients and their significance;

- the VIF, Eigenvalue and Condition Index value for each coefficient;

- the magnitude of raw and predicted unstandardized and standardized residuals;

- the F-test results carried out on the overall regression model; and

- a plot of the actual vs. predicted P10 values in a standardized plot.

Regressions were developed for the overall P_{10} as well as the P_{10} values for each of the regional fracture sets. The regression results are shown in Figure 4-54 through Figure 4-58. The regressions were based on the only geological parameters that could be mapped over the repository volume and surrounding rock mass independent of the fracture themselves: the Best Rock Name (BRN) and Rock Name (RN).

For the overall combined P_{10} intensity, the best statistically significant model is comprised of rock types from the BRN parameter: amphibolite; breccia; granite to granodiorite, metamorphic, medium-grained; and granodiorite, metamorphic. All of these four rock types tend to promote enhanced lineal fracture intensity. In general, granites and finer grained siliceous rocks tend to have lower P_{10} values for most fracture sets, while the granodiorites, and especially the medium grained ones, seem to have the highest P_{10} intensities for most sets.

Although the regressions are statistically significant based on the criteria previously listed, the usefulness of them for assigning fracture intensity is less obvious. The adjusted R-square value for the regressions is generally 0.2 or less, the exception being the regression for the intensity of the NW set, with an adjusted R-square of 0.5. Overall, the low adjusted R-square values suggest

Model Summary[b]

Model	R	R Square	Adjusted R Square	Std. Error of the Estimate	Change Statistics				
					R Square Change	F Change	df1	df2	Sig. F Change
1	.488[a]	.238	.172	1.19710	.238	3.596	4	46	.012

a. Predictors: (Constant), BRNGranodiorite_metamorphic, BRNBreccia, BRNAmphibolite, BRNGranitetogranodiorite_metamorphic_mediumgrained

b. Dependent Variable: P10

Coefficients[a]

Model		Unstandardized Coefficients		Standardized Coefficients	t	Sig.	95% Confidence Interval for B		Correlations			Collinearity Statistics	
		B	Std. Error	Beta			Lower Bound	Upper Bound	Zero-order	Partial	Part	Tolerance	VIF
1	(Constant)	.248	.866		.286	.776	-1.494	1.990					
	BRNAmphibolite	4.570	1.857	.384	2.461	.018	.832	8.307	.196	.341	.317	.681	1.467
	BRNBreccia	169.547	68.625	.319	2.471	.017	31.412	307.682	.336	.342	.318	.991	1.009
	BRNGranitetogranodiorite_metamorphic_mediumgrained	2.153	1.084	.349	1.985	.053	-.030	4.335	.053	.281	.255	.534	1.871
	BRNGranodiorite_metamorphic	596.222	295.628	.314	2.017	.050	1.154	1191.289	.119	.285	.260	.682	1.465

a. Dependent Variable: P10

Collinearity Diagnostics[a]

Model	Dimension	Eigenvalue	Condition Index	Variance Proportions				
				(Constant)	BRNAmphibolite	BRNBreccia	BRNGranitetogranodiorite_metamorphic_mediumgrained	BRNGranodiorite_metamorphic
1	1	2.370	1.000	.01	.04	.01	.01	.00
	2	1.010	1.532	.00	.00	.11	.00	.58
	3	.956	1.575	.00	.02	.85	.00	.07
	4	.644	1.918	.00	.53	.03	.01	.00
	5	.020	10.802	.99	.40	.01	.98	.34

a. Dependent Variable: P10

Residuals Statistics[a]

	Minimum	Maximum	Mean	Std. Deviation	N
Predicted Value	.8014	5.2142	2.1978	.64206	51
Residual	-1.83044	2.93661	.00000	1.14822	51
Std. Predicted Value	-2.175	4.698	.000	1.000	51
Std. Residual	-1.529	2.453	.000	.959	51

a. Dependent Variable: P10
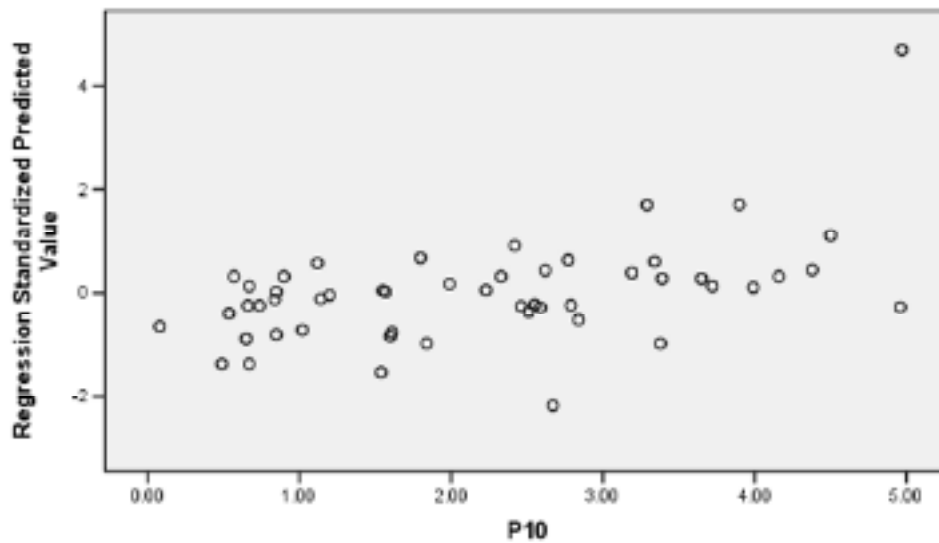
Figure 4-54. *Multivariate regression results for total P$_{10}$.*

Model Summary[b]

Model	R	R Square	Adjusted R Square	Std. Error of the Estimate	Change Statistics				
					R Square Change	F Change	df1	df2	Sig. F Change
1	.499[a]	.249	.201	.53992	.249	5.202	3	47	.003

a. Predictors: (Constant), BRNPegmatite_pegmatiticgranite, BRNBreccia, BRNGranite_finetomediumgrained

b. Dependent Variable: NEP10

Coefficients[a]

Model		Unstandardized Coefficients		Standardized Coefficients	t	Sig.	95% Confidence Interval for B		Correlations			Collinearity Statistics	
		B	Std. Error	Beta			Lower Bound	Upper Bound	Zero-order	Partial	Part	Tolerance	VIF
1	(Constant)	.820	.122		6.734	.000	.575	1.064					
	BRNBreccia	83.819	30.888	.344	2.714	.009	21.681	145.957	.364	.368	.343	.995	1.005
	BRNGranite_finetomediumgrained	-2.926	1.817	-.205	-1.610	.114	-6.581	.730	-.198	-.229	-.203	.987	1.013
	BRNPegmatite_pegmatiticgranite	-1.526	.658	-.295	-2.320	.025	-2.849	-.202	-.284	-.320	-.293	.990	1.010

a. Dependent Variable: NEP10

Collinearity Diagnostics[a]

Model	Dimension	Eigenvalue	Condition Index	Variance Proportions			
				(Constant)	BRNBreccia	BRNGranite_finetomediumgrained	BRNPegmatite_pegmatiticgranite
1	1	1.955	1.000	.09	.02	.06	.09
	2	1.000	1.398	.00	.79	.16	.00
	3	.816	1.547	.01	.18	.69	.09
	4	.229	2.923	.90	.02	.09	.82

a. Dependent Variable: NEP10

Residuals Statistics[a]

	Minimum	Maximum	Mean	Std. Deviation	N
Predicted Value	-.0657	2.1027	.6053	.30165	51
Residual	-.75004	1.75567	.00000	.52347	51
Std. Predicted Value	-2.224	4.964	.000	1.000	51
Std. Residual	-1.389	3.252	.000	.970	51

a. Dependent Variable: NEP10
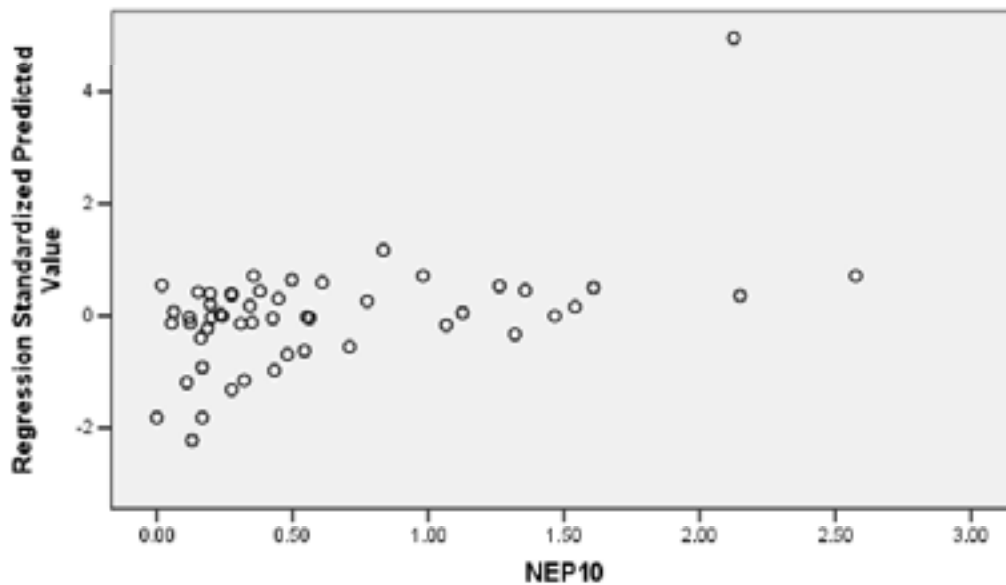
Figure 4-55. Multivariate regression results for NE P$_{10}$.

Model Summary[b]

Model	R	R Square	Adjusted R Square	Std. Error of the Estimate	Change Statistics				
					R Square Change	F Change	df1	df2	Sig. F Change
1	.740[a]	.547	.497	.24643	.547	10.881	5	45	.000

a. Predictors: (Constant), BRNQuartzdominatedhydrothermalveinsegregation, BRNGranodiorite_metamorphic, BRNBreccia, BRNAmphibolite, BRNCarbonatedominatedhydrothermalveinsegregation

b. Dependent Variable: NWP10

Coefficients[a]

Model		Unstandardized Coefficients		Standardized Coefficients	t	Sig.	95% Confidence Interval for B		Correlations			Collinearity Statistics	
		B	Std. Error	Beta			Lower Bound	Upper Bound	Zero-order	Partial	Part	Tolerance	VIF
1	(Constant)	.184	.043		4.309	.000	.098	.270					
	BRNBreccia	21.673	14.087	.155	1.539	.131	-6.700	50.046	.140	.224	.154	.997	1.003
	BRNAmphibolite	1.167	.329	.371	3.549	.001	.505	1.829	.324	.468	.356	.922	1.085
	BRNCarbonatedominated hydrothermalveinsegregat ion	720.438	199.620	.392	3.609	.001	318.383	1122.493	.342	.474	.362	.851	1.175
	BRNGranodiorite_ metamorphic	267.361	50.428	.533	5.302	.000	165.795	368.928	.506	.620	.532	.994	1.006
	BRNQuartzdominatedhydr othermalveinsegregation	-57.829	28.813	-.225	-2.007	.051	-115.861	.202	-.005	-.287	-.201	.801	1.248

a. Dependent Variable: NWP10

Collinearity Diagnostics[a]

Model	Dimension	Eigenvalue	Condition Index	Variance Proportions					
				(Constant)	BRNBreccia	BRNAmp hibolite	BRNCarbonat edominatedhy drothermalvei nsegregation	BRNGranodio rite_ metamorphic	BRNQuartzdo minatedhydrot hermalveinse gregation
1	1	2.028	1.000	.09	.01	.10	.06	.00	.09
	2	1.128	1.341	.07	.25	.01	.19	.15	.08
	3	1.002	1.422	.00	.32	.00	.00	.64	.00
	4	.875	1.522	.05	.38	.11	.27	.15	.01
	5	.548	1.924	.08	.02	.01	.47	.01	.78
	6	.419	2.199	.70	.02	.76	.00	.04	.03

a. Dependent Variable: NWP10

Residuals Statistics[a]

	Minimum	Maximum	Mean	Std. Deviation	N
Predicted Value	.0510	1.5310	.2991	.25705	51
Residual	-.29564	.73808	.00000	.23378	51
Std. Predicted Value	-.965	4.792	.000	1.000	51
Std. Residual	-1.200	2.995	.000	.949	51

a. Dependent Variable: NWP10
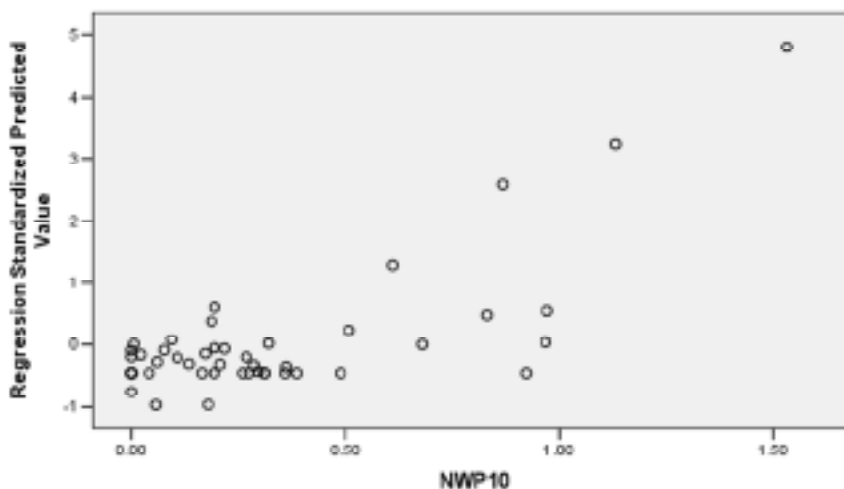
Figure 4-56. *Multivariate regression results for NW P_{10}.*

Model Summary[b]

Model	R	R Square	Adjusted R Square	Std. Error of the Estimate	Change Statistics				
					R Square Change	F Change	df1	df2	Sig. F Change
1	.511[a]	.261	.160	.40692	.261	2.591	6	44	.031

a. Predictors: (Constant), BRNGranite_metamorphic_aplitic, BRNQuartzdominatedhydrothermalveinsegregation, BRNFelsictointermediatevolcanicrock_metamorphic, BRNBreccia, BRNDiorite_quartzdioriteandgabbro_metamorphic, BRNGranite_finetomediumgrained

b. Dependent Variable: NSP10

Coefficients[a]

Model		Unstandardized Coefficients		Standardized Coefficients	t	Sig.	95% Confidence Interval for B		Correlations			Collinearity Statistics	
		B	Std. Error	Beta			Lower Bound	Upper Bound	Zero-order	Partial	Part	Tolerance	VIF
1	(Constant)	.214	.070		3.037	.004	.072	.356					
	BRNQuartzdominatedhydrothermalveinsegregation	83.636	42.856	.254	1.952	.057	-2.735	170.008	.214	.282	.253	.988	1.013
	BRNBreccia	52.197	23.319	.291	2.238	.030	5.201	99.193	.271	.320	.290	.992	1.008
	BRNDiorite_quartzdioriteandgabbro_metamorphic	50.273	29.734	.220	1.691	.098	-9.651	110.198	.192	.247	.219	.990	1.010
	BRNFelsictointermediatevolcanicrock_metamorphic	7.437	4.797	.220	1.550	.128	-2.231	17.105	.118	.228	.201	.832	1.202
	BRNGranite_finetomediumgrained	-1.889	1.505	-.180	-1.255	.216	-4.922	1.145	-.119	-.186	-.163	.817	1.224
	BRNGranite_metamorphic_aplitic	5.749	3.707	.202	1.551	.128	-1.722	13.220	.189	.228	.201	.985	1.015

a. Dependent Variable: NSP10

Collinearity Diagnostics[a]

Model	Dimension	Eigenvalue	Condition Index	Variance Proportions						
				(Constant)	BRNQuartzdominatedhydrothermalveinsegregation	BRNBreccia	BRNDiorite_quartzdioriteandgabbro_metamorphic	BRNFelsictointermediatevolcanicrock_metamorphic	BRNGranite_finetomediumgrained	BRNGranite_metamorphic_aplitic
1	1	1.962	1.000	.11	.05	.01	.00	.08	.09	.04
	2	1.164	1.298	.05	.02	.11	.05	.15	.12	.20
	3	1.007	1.396	.00	.03	.01	.86	.00	.00	.05
	4	.993	1.406	.00	.14	.73	.00	.02	.00	.05
	5	.886	1.488	.00	.58	.06	.00	.04	.00	.31
	6	.538	1.910	.10	.12	.01	.01	.68	.45	.03
	7	.451	2.085	.74	.06	.07	.07	.02	.33	.32

a. Dependent Variable: NSP10

Residuals Statistics[a]

	Minimum	Maximum	Mean	Std. Deviation	N
Predicted Value	-.2394	1.1296	.3162	.22691	51
Residual	-.73212	1.30213	.00000	.38172	51
Std. Predicted Value	-2.449	3.584	.000	1.000	51
Std. Residual	-1.799	3.200	.000	.938	51

a. Dependent Variable: NSP10
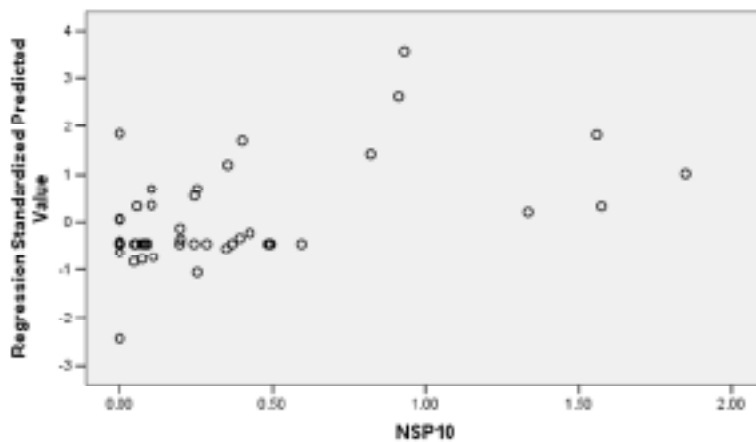
Figure 4-57. *Multivariate regression results for NS P_{10}.*

Coefficients[a]

Model		Unstandardized Coefficients		Standardized Coefficients	t	Sig.	95% Confidence Interval for B		Correlations			Collinearity Statistics	
		B	Std. Error	Beta			Lower Bound	Upper Bound	Zero-order	Partial	Part	Tolerance	VIF
1	(Constant)	.572	.116		4.946	.000	.339	.805					
	BRNQuartzdominatedhydrothermalveinsegregation	-116.273	66.998	-.250	-1.735	.090	-251.387	18.842	-.127	-.256	-.234	.879	1.138
	BRNGranite_metamorphic_aplitic	7.122	5.473	.177	1.301	.200	-3.914	18.159	.146	.195	.176	.983	1.017
	BRNAmphibolite	1.889	.807	.332	2.341	.024	.261	3.516	.238	.336	.316	.907	1.102
	BRNCalcsilicaterockskarn	14.616	10.966	.185	1.333	.190	-7.498	36.730	.127	.199	.180	.949	1.053
	BRNGranodiorite	-7.205	6.511	-.151	-1.107	.275	-20.336	5.926	-.141	-.166	-.149	.984	1.016
	BRNGranodiorite_metamorphic	107.876	123.191	.119	.876	.386	-140.561	356.314	.081	.132	.118	.988	1.013
	BRNSedimentaryrock	30.602	26.600	.156	1.150	.256	-23.042	84.247	.161	.173	.155	.990	1.010

a. Dependent Variable: SHP10

Model Summary[b]

Model	R	R Square	Adjusted R Square	Std. Error of the Estimate	Change Statistics				
					R Square Change	F Change	df1	df2	Sig. F Change
1	.465[a]	.216	.088	.60007	.216	1.693	7	43	.136

a. Predictors: (Constant), BRNSedimentaryrock, BRNGranodiorite_metamorphic, BRNGranodiorite, BRNQuartzdominatedhydrothermalveinsegregation, BRNGranite_metamorphic_aplitic, BRNCalcsilicaterockskarn, BRNAmphibolite

b. Dependent Variable: SHP10

Collinearity Diagnostics[a]

Model	Dimension	Eigenvalue	Condition Index	Variance Proportions							
				(Constant)	BRNQuartzdominatedhydrothermalveinsegregation	BRNGranite_metamorphic_aplitic	BRNAmphibolite	BRNCalcsilicaterockskarn	BRNGranodiorite	BRNGranodiorite_metamorphic	BRNSedimentaryrock
1	1	2.205	1.000	.08	.06	.04	.07	.05	.01	.00	.01
	2	1.105	1.413	.01	.08	.01	.00	.10	.32	.24	.07
	3	1.016	1.473	.00	.00	.00	.01	.02	.04	.16	.72
	4	.973	1.506	.01	.07	.37	.03	.00	.25	.15	.01
	5	.949	1.524	.00	.06	.27	.00	.05	.15	.38	.04
	6	.795	1.665	.00	.11	.00	.13	.64	.09	.00	.05
	7	.610	1.902	.08	.59	.13	.21	.02	.12	.01	.09
	8	.347	2.520	.82	.04	.19	.54	.12	.01	.05	.01

a. Dependent Variable: SHP10

Residuals Statistics[a]

	Minimum	Maximum	Mean	Std. Deviation	N
Predicted Value	.1211	1.8309	.7530	.29213	51
Residual	-.97302	2.06225	.00000	.55648	51
Std. Predicted Value	-2.163	3.690	.000	1.000	51
Std. Residual	-1.622	3.437	.000	.927	51

a. Dependent Variable: SHP10
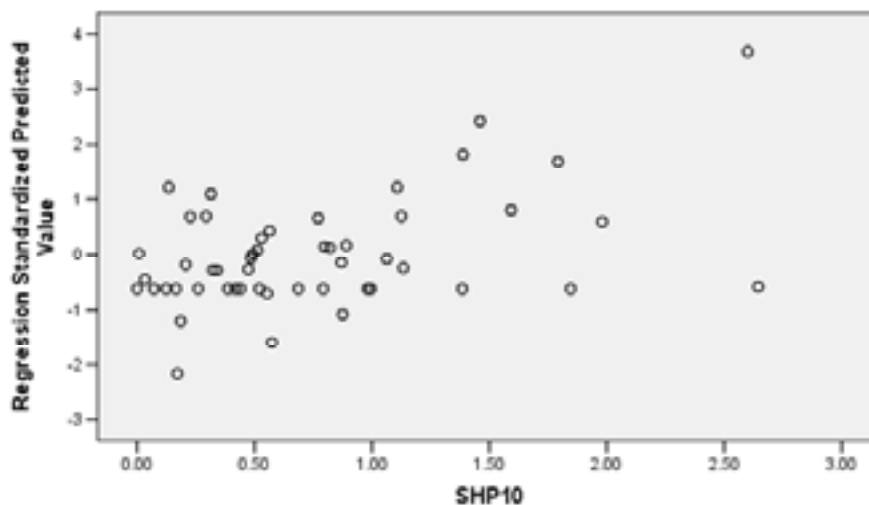
Figure 4-58. *Multivariate regression results for Subhorizontal (SH) P$_{10}$.*

that although there are some associations between certain rock types and fracture intensity, the ability to predict is fairly poor, because the variability in set intensity within a rock type does not differ much from the variability among rock types. Thus, it is not useful to develop individual intensity models for fracture sets as a function of rock type in order to reduce uncertainty.

The multivariate modeling also included analysis of fracture intensity as a function of individual geological parameters from the standpoint of reducing variance in the overall model. The Kruskal-Wallis test, the non-parametric equivalent of the more familiar parametric ANOVA procedure, was used to determine if the variation among subcategories of an individual parameter, such as lithology, was greater than the variations within the subcategories. If it were found that the variation within the subcategories was greater, then there is no benefit to having a separate intensity distribution for each subcategory. If on the other hand, the variation within subcategories is much less than the variation between them, then it is possible to reduce variance (and uncertainty) by specifying separate intensity models for each subcategory.

The Kruskal-Wallis ANOVA calculations are shown in Table 4-70. The results show very little dependence on the measured geological variables. Only variable with an asymptotic significance of 0.05 or less are considered to be significant. Of all the variables tested, only MIN1: hematite and sulfide; MIN2: asphalt; BRN: Granite-fine-to-medium grained; RN: amphibolite; and P_{10}: NE, SH have significances below 0.05. A Spearman correlation analysis of these factors and P_{10} (Table 4-71) shows that the overall fracture intensity increases as a function of the intensity of the NE and SH sets, and decreases as a function of the percentage of fractures that have hematite or sulfide mineralization, or are in fine to medium-grained granites. However, the overall Kruskal-Wallis results and the previous multinomial regression results together strongly indicate that stratifying the fracture intensities by the measured geological variables, including rock type, will do little to reduce overall model uncertainty.

One final series of investigations were carried out to evaluate ways to reduce model fracture intensity uncertainty: whether fracture domains could be combined or should remain separate. This was done using cross-tabulation tests for fracture domain vs. fracture set characteristics and relative set intensity. The results are shown in Table 4-72 and Table 4-73.

Table 4-72 shows that the geological characteristics of fractures are statistically different among fracture domains at a significant level. The relative abundance of the individual sets also differs significantly. The ranks are color-coded in Table 4-73 to visually indicate which sets are positively or negatively associated with the fracture domains. For example, Domain FFM03 has a positive association with the three sub-vertical global sets and the subhorizontal set. Domain FFM02 has a positive association with the subhorizontal set and a differentially greater abundance of the ENE and NNW sets. Domain FFM01 is the opposite of Domain FFM02, with a relative lack of abundance of the SH, ENE and NNW sets. It may be that the tectonic evolution of FFM03 was less intense than the other two domains, so that the older global sets were well developed, but the newer sets were not. FFM02, on the other hand, seems to also have an abundance of the orthogonal ENE and NNW sets and the subhorizontal sets, which might have arisen from greater tectonic deformation or impact of a later tectonic event that created the orthogonal ENE and NNW sets. FFM01, on the other hand, more closely resembles FFM03, but with a larger number of fracture sets.

The Kruskal-Wallis analysis indicates that the present division of the area into fracture domains delineates areas of different fracture intensities, and it is therefore useful in reducing model uncertainty to stratify the fracture model by the existing fracture domains.

Table 4-70. Kruskal-Wallis test results for quartile of fracture intensity vs. measured geological parameters for fractures.

Test Statistics [a,b]

	Broken	Unbroken
Chi-Square	.651	.651
df	3	3
Asymp. Sig.	.885	.885

a. Kruskal Wallis Test

b. Grouping Variable: NQ

Test Statistics [a,b]

	Open	PartlyOpen	Sealed
Chi-Square	6.850	.440	5.164
df	3	3	3
Asymp. Sig.	.077	.932	.160

a. Kruskal Wallis Test

b. Grouping Variable: NQ

Test Statistics [a,b]

	Irregular	SNA	Planar	Stepped	Undulating
Chi-Square	6.863	.651	3.945	5.328	3.578
df	3	3	3	3	3
Asymp. Sig.	.076	.885	.267	.149	.311

a. Kruskal Wallis Test

b. Grouping Variable: NQ

Test Statistics [a,b]

	RNA	Rough	Slickensided	Smooth
Chi-Square	.651	2.789	.418	5.227
df	3	3	3	3
Asymp. Sig.	.885	.425	.936	.156

a. Kruskal Wallis Test

b. Grouping Variable: NQ

Test Statistics [a,b]

	Fresh	Gouge	HighlyAltered	Moderately Altered	SlightlyAltered
Chi-Square	6.567	1.860	2.244	2.786	6.333
df	3	3	3	3	3
Asymp. Sig.	.087	.602	.523	.426	.096

a. Kruskal Wallis Test

b. Grouping Variable: NQ

Table 4-70. (continued).

Test Statistics [a,b]

	Chi-Square	df	Asymp. Sig.
M1Adularia	2.985	3	.394
M1Asphalt	6.529	3	.089
M1Biotite	6.368	3	.095
M1Calcite	2.925	3	.403
M1Chlorite	2.404	3	.493
M1Clay Minerals	1.176	3	.759
M1Epidote	1.377	3	.711
M1Fluorite	.000	3	1.000
M1Galena	.000	3	1.000
M1Goethite	2.159	3	.540
M1Hematite	18.515	3	.000
M1Kaolinite	2.778	3	.427
M1Laumontite	4.609	3	.203
M1NDR	17.899	3	.000
M1Oxidized Walls	.319	3	.956
M1Potash Feldspar	3.121	3	.373
M1Prehnite	.118	3	.990
M1Pyrite	4.372	3	.224
M1Pyrrhotite	1.079	3	.782
M1Quartz	5.118	3	.163
M1Red Feldspar	6.872	3	.076
M1Sulfides	12.765	3	.005
M1Unknownmineral	2.910	3	.406
M1White Feldspar	1.788	3	.618
M1X1	1.839	3	.606
M1X2	2.778	3	.427
M1X3	5.156	3	.161
M1X4	2.778	3	.427
M1X5	.199	3	.978
M1X9	2.382	3	.497
M1Zeolites	2.778	3	.427

a. Kruskal Wallis Test

b. Grouping Variable: NQ

Test Statistics [a,b]

	Chi-Square	df	Asymp. Sig.
M2Adularia	2.356	3	.502
M2Amphibole	5.597	3	.133
M2Asphalt	9.583	3	.022
M2Biotite	3.952	3	.267
M2Calcite	2.468	3	.481
M2Chalcopyrite	.000	3	1.000
M2Chlorite	.575	3	.902
M2Clay Minerals	.415	3	.937
M2Epidote	3.692	3	.297
M2Galena	2.579	3	.461
M2Goethite	.860	3	.835
M2Hematite	4.134	3	.247
M2Hornblende	3.121	3	.373
M2Hypersthene	3.690	3	.297
M2Laumontite	.320	3	.956
M2Magnetite	1.690	3	.639
M2Muscovite	6.289	3	.098
M2NDR	8.296	3	.040
M2Oxidized Walls	.252	3	.969
M2Potash Feldspar	2.419	3	.490
M2Prehnite	6.946	3	.074
M2Pyrite	1.767	3	.622
M2Pyrrhotite	2.285	3	.515
M2Quartz	4.406	3	.221
M2Red Feldspar	2.882	3	.410
M2Sericite	.000	3	1.000
M2Sulfides	.451	3	.930
M2Unknownmineral	4.454	3	.216
M2White Feldspar	2.978	3	.395
M2X1	2.860	3	.414
M2X2	.000	3	1.000
M2X3	3.073	3	.381
M2X4	.000	3	1.000
M2X6	.000	3	1.000
M2Zeolites	1.224	3	.747

a. Kruskal Wallis Test

b. Grouping Variable: NQ

156

Table 4-70. (continued).

Test Statistics [a,b]

	Chi-Square	df	Asymp. Sig.
RNAmphibolite	8.164	3	.043
RNCalcsilicaterockskarn	3.121	3	.373
RNDiorite_ quartzdioriteandgabbro_ metamorphic	.000	3	1.000
RNFelsictointermediatevo lcanicrock_metamorphic	4.827	3	.185
RNGranitetogranodiorite_ metamorphic_ mediumgrained	1.608	3	.658
RNGranite_ finetomediumgrained	4.221	3	.239
RNGranite_ granodioriteandtonalite_ metamorphic_ finetomediumgraine	5.048	3	.168
RNGranite_ metamorphic_aplitic	3.361	3	.339
RNGranodiorite_ metamorphic	2.142	3	.543
RNPegmatite_ pegmatiticgranite	2.823	3	.420
RNTonalitetogranodiorite _metamorphic	3.121	3	.373

a. Kruskal Wallis Test

b. Grouping Variable: NQ

Test Statistics [a,b]

	NWP10	ENEP10	EWP10	NEP10	NNEP10	NNWP10	NSP10	SHP10
Chi-Square	4.311	7.223	3.802	20.925	.075	3.124	1.928	31.379
df	3	3	3	3	3	3	3	3
Asymp. Sig.	.230	.065	.284	.000	.995	.373	.587	.000

a. Kruskal Wallis Test

b. Grouping Variable: NQ

Test Statistics [a,b]

	Ap0.75	Ap1	Ap1.5	Ap2	Ap3	Ap4	Ap5	Ap6
Chi-Square	6.988	1.819	7.811	.633	3.823	4.845	2.686	1.453
df	3	3	3	3	3	3	3	3
Asymp. Sig.	.072	.611	.050	.889	.281	.183	.443	.693

a. Kruskal Wallis Test

b. Grouping Variable: NQ

Table 4-70. (continued).

Test Statistics [a,b]

	Chi-Square	df	Asymp. Sig.
BRNAmphibolite	5.553	3	.136
BRNBreccia	5.597	3	.133
BRNCalcsilicaterockskarn	2.713	3	.438
BRNCarbonatedominated hydrothermalveinsegregation	2.778	3	.427
BRNDiorite_ quartzdioriteandgabbro_ metamorphic	3.121	3	.373
BRNFelsictointermediatevolcanicrock_metamorphic	5.264	3	.153
BRNGranite	1.690	3	.639
BRNGranitetogranodiorite _metamorphic_ mediumgrained	1.679	3	.642
BRNGranite_ finetomediumgrained	8.418	3	.038
BRNGranite_ granodioriteandtonalite_ metamorphic_ finetomediumgrain	5.343	3	.148
BRNGranite_ metamorphic_aplitic	3.060	3	.383
BRNGranitoid_ metamorphic	.000	3	1.000
BRNGranodiorite	.044	3	.998
BRNGranodiorite_ metamorphic	1.029	3	.794
BRNHybridrock	.000	3	1.000
BRNHydrothermalveinsegregation_unspecified	3.121	3	.373
BRNPegmatite_ pegmatiticgranite	4.890	3	.180
BRNQuartzdiorite	.000	3	1.000
BRNQuartzdominatedhydrothermalveinsegregation	3.162	3	.367
BRNSedimentaryrock	3.121	3	.373
BRNTonalite	3.690	3	.297
BRNTonalitetogranodiorite_metamorphic	3.121	3	.373

a. Kruskal Wallis Test

b. Grouping Variable: NQ

Table 4-71. Spearman correlation coefficients for fracture intensity and the significant regressors from the multinomial regression.

Correlations

			P10	M1Hematite	M1Sulfides	M2Asphalt	BRNGranite_finetomediumgrained	RNAmphibolite	NEP10	SHP10
Spearman's rho	P10	Correlation Coefficient	1.000	-.364**	-.146	.141	-.322**	-.085	.516**	.560**
		Sig. (2-tailed)	.	.000	.089	.102	.000	.323	.000	.000
		N	136	136	136	136	136	136	136	136
	M1Hematite	Correlation Coefficient	-.364**	1.000	.106	.064	.343**	.144	-.104	-.216*
		Sig. (2-tailed)	.000	.	.218	.460	.000	.095	.230	.012
		N	136	136	136	136	136	136	136	136
	M1Sulfides	Correlation Coefficient	-.146	.106	1.000	-.043	-.097	.060	-.086	-.051
		Sig. (2-tailed)	.089	.218	.	.615	.260	.488	.322	.557
		N	136	136	136	136	136	136	136	136
	M2Asphalt	Correlation Coefficient	.141	.064	-.043	1.000	.083	.069	.032	.251**
		Sig. (2-tailed)	.102	.460	.615	.	.335	.424	.710	.003
		N	136	136	136	136	136	136	136	136
	BRNGranite_finetomediumgrained	Correlation Coefficient	-.322**	.343**	-.097	.083	1.000	.273**	-.131	-.115
		Sig. (2-tailed)	.000	.000	.260	.335	.	.001	.129	.184
		N	136	136	136	136	136	136	136	136
	RNAmphibolite	Correlation Coefficient	-.085	.144	.060	.069	.273**	1.000	.063	-.047
		Sig. (2-tailed)	.323	.095	.488	.424	.001	.	.469	.587
		N	136	136	136	136	136	136	136	136
	NEP10	Correlation Coefficient	.516**	-.104	-.086	.032	-.131	.063	1.000	.051
		Sig. (2-tailed)	.000	.230	.322	.710	.129	.469	.	.552
		N	136	136	136	136	136	136	136	136
	SHP10	Correlation Coefficient	.560**	-.216*	-.051	.251**	-.115	-.047	.051	1.000
		Sig. (2-tailed)	.000	.012	.557	.003	.184	.587	.552	.
		N	136	136	136	136	136	136	136	136

**. Correlation is significant at the 0.01 level (2-tailed).

*. Correlation is significant at the 0.05 level (2-tailed).

Table 4-72. Cross tabulation results for assessing the relation between fracture domain and measured geological factors.

Directional Measures

			Value	Asymp. Std. Error [a]	Approx. T [b]	Approx. Sig.
Nominal by Nominal	Lambda	Symmetric	.014	.005	3.059	.002
		FRACTURE_DOMAIN Dependent	.000	.000	.[c]	.[c]
		FRACT_MAPPED Dependent	.026	.008	3.059	.002
	Goodman and Kruskal tau	FRACTURE_DOMAIN Dependent	.024	.002		.000[d]
		FRACT_MAPPED Dependent	.034	.003		.000[d]
	Uncertainty Coefficient	Symmetric	.023	.002	13.115	.000[e]
		FRACTURE_DOMAIN Dependent	.020	.002	13.115	.000[e]
		FRACT_MAPPED Dependent	.025	.002	13.115	.000[e]

a. Not assuming the null hypothesis.

b. Using the asymptotic standard error assuming the null hypothesis.

c. Cannot be computed because the asymptotic standard error equals zero.

d. Based on chi-square approximation

e. Likelihood ratio chi-square probability.

Symmetric Measures

		Value	Asymp. Std. Error [a]	Approx. T [b]	Approx. Sig.
Nominal by Nominal	Phi	.184			.000
	Cramer's V	.184			.000
	Contingency Coefficient	.181			.000
Ordinal by Ordinal	Kendall's tau-b	-.165	.007	-24.147	.000
N of Valid Cases		20814			

a. Not assuming the null hypothesis.

b. Using the asymptotic standard error assuming the null hypothesis.

Table 4-72. (continued).

Directional Measures

			Value	Asymp. Std. Error[a]	Approx. T[b]	Approx. Sig.
Nominal by Nominal	Lambda	Symmetric	.000	.000	.[c]	.[c]
		FRACTURE_DOMAIN Dependent	.000	.000	.[c]	.[c]
		FRACT_INTERPRET Dependent	.000	.000	.[c]	.[c]
	Goodman and Kruskal tau	FRACTURE_DOMAIN Dependent	.036	.002		.000[d]
		FRACT_INTERPRET Dependent	.045	.003		.000[d]
	Uncertainty Coefficient	Symmetric	.035	.002	15.849	.000[e]
		FRACTURE_DOMAIN Dependent	.031	.002	15.849	.000[e]
		FRACT_INTERPRET Dependent	.039	.002	15.849	.000[e]

a. Not assuming the null hypothesis.

b. Using the asymptotic standard error assuming the null hypothesis.

c. Cannot be computed because the asymptotic standard error equals zero.

Symmetric Measures

		Value	Asymp. Std. Error[a]	Approx. T[b]	Approx. Sig.
Nominal by Nominal	Phi	.234			.000
	Cramer's V	.165			.000
	Contingency Coefficient	.228			.000
Ordinal by Ordinal	Kendall's tau-b	-.155	.007	-22.529	.000
N of Valid Cases		20814			

a. Not assuming the null hypothesis.

b. Using the asymptotic standard error assuming the null hypothesis.

Table 4-72. (continued).

Directional Measures

			Value	Asymp. Std. Error[a]	Approx. T[b]	Approx. Sig.
Nominal by Nominal	Lambda	Symmetric	.006	.001	5.847	.000
		FRACTURE_DOMAIN Dependent	.020	.003	5.847	.000
		MIN1 Dependent	.000	.000	.[c]	.[c]
	Goodman and Kruskal tau	FRACTURE_DOMAIN Dependent	.055	.002		.000[d]
		MIN1 Dependent	.007	.000		.000[d]
	Uncertainty Coefficient	Symmetric	.030	.001	21.844	.000[e]
		FRACTURE_DOMAIN Dependent	.054	.002	21.844	.000[e]
		MIN1 Dependent	.021	.001	21.844	.000[e]

a. Not assuming the null hypothesis.

b. Using the asymptotic standard error assuming the null hypothesis.

c. Cannot be computed because the asymptotic standard error equals zero.

d. Based on chi-square approximation

e. Likelihood ratio chi-square probability.

Symmetric Measures

		Value	Asymp. Std. Error [a]	Approx. T[b]	Approx. Sig.
Nominal by Nominal	Phi	.311			.000
	Cramer's V	.220			.000
	Contingency Coefficient	.297			.000
Ordinal by Ordinal	Kendall's tau-b	-.013	.006	-2.239	.025
N of Valid Cases		20814			

a. Not assuming the null hypothesis.

b. Using the asymptotic standard error assuming the null hypothesis.

Table 4-72. (continued).

Directional Measures

			Value	Asymp. Std. Error[a]	Approx. T[b]	Approx. Sig.
Nominal by Nominal	Lambda	Symmetric	.003	.000	6.772	.000
		FRACTURE_DOMAIN Dependent	.010	.001	6.772	.000
		MIN2 Dependent	.000	.000	.[c]	.[c]
	Goodman and Kruskal tau	FRACTURE_DOMAIN Dependent	.028	.002		.000[d]
		MIN2 Dependent	.006	.001		.000[d]
	Uncertainty Coefficient	Symmetric	.017	.001	15.810	.000[e]
		FRACTURE_DOMAIN Dependent	.028	.002	15.810	.000[e]
		MIN2 Dependent	.012	.001	15.810	.000[e]

a. Not assuming the null hypothesis.

b. Using the asymptotic standard error assuming the null hypothesis.

c. Cannot be computed because the asymptotic standard error equals zero.

d. Based on chi-square approximation

e. Likelihood ratio chi-square probability.

Symmetric Measures

		Value	Asymp. Std. Error[a]	Approx. T[b]	Approx. Sig.
Nominal by Nominal	Phi	.218			.000
	Cramer's V	.154			.000
	Contingency Coefficient	.213			.000
Ordinal by Ordinal	Kendall's tau-b	-.028	.006	-4.712	.000
N of Valid Cases		20814			

a. Not assuming the null hypothesis.

b. Using the asymptotic standard error assuming the null hypothesis.

Table 4-72. (continued).

Directional Measures

			Value	Asymp. Std. Error[a]	Approx. T[b]	Approx. Sig.
Nominal by Nominal	Lambda	Symmetric	.000	.000	.[c]	.[c]
		FRACTURE_DOMAIN Dependent	.000	.000	.[c]	.[c]
		ROUGHNESS Dependent	.000	.000	.[c]	.[c]
	Goodman and Kruskal tau	FRACTURE_DOMAIN Dependent	.028	.002		.000[d]
		ROUGHNESS Dependent	.019	.001		.000[d]
	Uncertainty Coefficient	Symmetric	.021	.001	14.260	.000[e]
		FRACTURE_DOMAIN Dependent	.024	.002	14.260	.000[e]
		ROUGHNESS Dependent	.018	.001	14.260	.000[e]

a. Not assuming the null hypothesis.

b. Using the asymptotic standard error assuming the null hypothesis.

c. Cannot be computed because the asymptotic standard error equals zero.

d. Based on chi-square approximation

e. Likelihood ratio chi-square probability.

Symmetric Measures

		Value	Asymp. Std. Error[a]	Approx. T[b]	Approx. Sig.
Nominal by Nominal	Phi	.204			.000
	Cramer's V	.144			.000
	Contingency Coefficient	.199			.000
Ordinal by Ordinal	Kendall's tau-b	.135	.007	20.233	.000
N of Valid Cases		20814			

a. Not assuming the null hypothesis.

b. Using the asymptotic standard error assuming the null hypothesis.

Table 4-72. (continued).

Directional Measures

			Value	Asymp. Std. Error[a]	Approx. T[b]	Approx. Sig.
Nominal by Nominal	Lambda	Symmetric	.005	.001	7.028	.000
		FRACTURE_DOMAIN Dependent	.010	.001	7.028	.000
		BEST_ROCK_NAME Dependent	.000	.000	.[c]	.[c]
	Goodman and Kruskal tau	FRACTURE_DOMAIN Dependent	.016	.001		.000[d]
		BEST_ROCK_NAME Dependent	.003	.001		.000[d]
	Uncertainty Coefficient	Symmetric	.016	.001	13.566	.000[e]
		FRACTURE_DOMAIN Dependent	.019	.001	13.566	.000[e]
		BEST_ROCK_NAME Dependent	.014	.001	13.566	.000[e]

a. Not assuming the null hypothesis.

b. Using the asymptotic standard error assuming the null hypothesis.

c. Cannot be computed because the asymptotic standard error equals zero.

d. Based on chi-square approximation

e. Likelihood ratio chi-square probability.

Symmetric Measures

		Value	Asymp. Std. Error[a]	Approx. T[b]	Approx. Sig.
Nominal by Nominal	Phi	.197			.000
	Cramer's V	.140			.000
	Contingency Coefficient	.194			.000
Ordinal by Ordinal	Kendall's tau-b	.003	.007	.446	.656
N of Valid Cases		20814			

a. Not assuming the null hypothesis.

b. Using the asymptotic standard error assuming the null hypothesis.

Table 4-72. (continued).

Directional Measures

			Value	Asymp. Std. Error[a]	Approx. T[b]	Approx. Sig.
Nominal by Nominal	Lambda	Symmetric	.025	.005	5.151	.000
		FRACTURE_DOMAIN Dependent	.028	.006	4.533	.000
		Frac_Set_Name Dependent	.023	.006	3.619	.000
	Goodman and Kruskal tau	FRACTURE_DOMAIN Dependent	.085	.003		.000[c]
		Frac_Set_Name Dependent	.028	.001		.000[c]
	Uncertainty Coefficient	Symmetric	.061	.002	32.240	.000[d]
		FRACTURE_DOMAIN Dependent	.093	.003	32.240	.000[d]
		Frac_Set_Name Dependent	.045	.001	32.240	.000[d]

a. Not assuming the null hypothesis.

b. Using the asymptotic standard error assuming the null hypothesis.

c. Based on chi-square approximation

d. Likelihood ratio chi-square probability.

Symmetric Measures

		Value	Asymp. Std. Error[a]	Approx. T[b]	Approx. Sig.
Nominal by Nominal	Phi	.380			.000
	Cramer's V	.269			.000
	Contingency Coefficient	.355			.000
Ordinal by Ordinal	Kendall's tau-b	.108	.006	17.929	.000
N of Valid Cases		20814			

a. Not assuming the null hypothesis.

b. Using the asymptotic standard error assuming the null hypothesis.

Table 4-73. Kruskal-Wallis test results for evaluation of different set intensities as a function of fracture domain.

Test Statistics [a,b]

	FFM01	FFM02	FFM03
Chi-Square	2029.708	2988.194	473.066
df	7	7	7
Asymp. Sig.	.000	.000	.000

a. Kruskal Wallis Test

b. Grouping Variable: Set_ID

Ranks	Set_ID	N	Mean Rank
FFM01	NNE	710	13623
	EW	855	12576.36
	NS	2883	11551.28
	NE	5204	11503.51
	NW	2765	10454.31
	SH	6742	9117.86
	ENE	1578	7826.78
	NNW	74	3217.5
FFM02	NNW	74	18673.5
	ENE	1578	14064.22
	SH	6742	11549.24
	NW	2765	9867.399
	EW	855	9314.635
	NS	2883	9224.454
	NE	5204	9109.798
	NNE	710	8268
FFM03	NW	2765	10896.29
	NE	5204	10604.69
	SH	6742	10550.9
	NS	2883	10442.26
	NNE	710	9327
	NNW	74	9327
	EW	855	9327
	ENE	1578	9327

Verification of subhorizontal set size model

The size model for the subhorizontal set is the least constrained, as is much more difficult to detect horizontal deformation zone or fault lineaments. Likewise in outcrop, horizontal fractures are evident only if the outcrop is rough, and in that case, the trace of the horizontal fracture may be more a partial measure of its circumference than a true trace made by the intersection of a plane with a surface. To assess how useful the derived size model for subhorizontal fractures might be, a model was made for FFM03 using the orientation parameters for that fracture domain and the Euclidean size model. The fractures were generated over the depth range of 300 m to 900 m, which is the approximate depth range below which exfoliation effects do not appear to impact subhorizontal fracture intensity. The fractures were binned into 5 m bins and plotted on the intensity/depth plot (Figure 4-59). The red circles in this plot are the simulation results. Their scatter visually appears to conform to the measured data. A statistical test of the simulation results and the measured results over the interval 300 m to 900 m showed that the two populations have the same means and variance (Table 4-74).
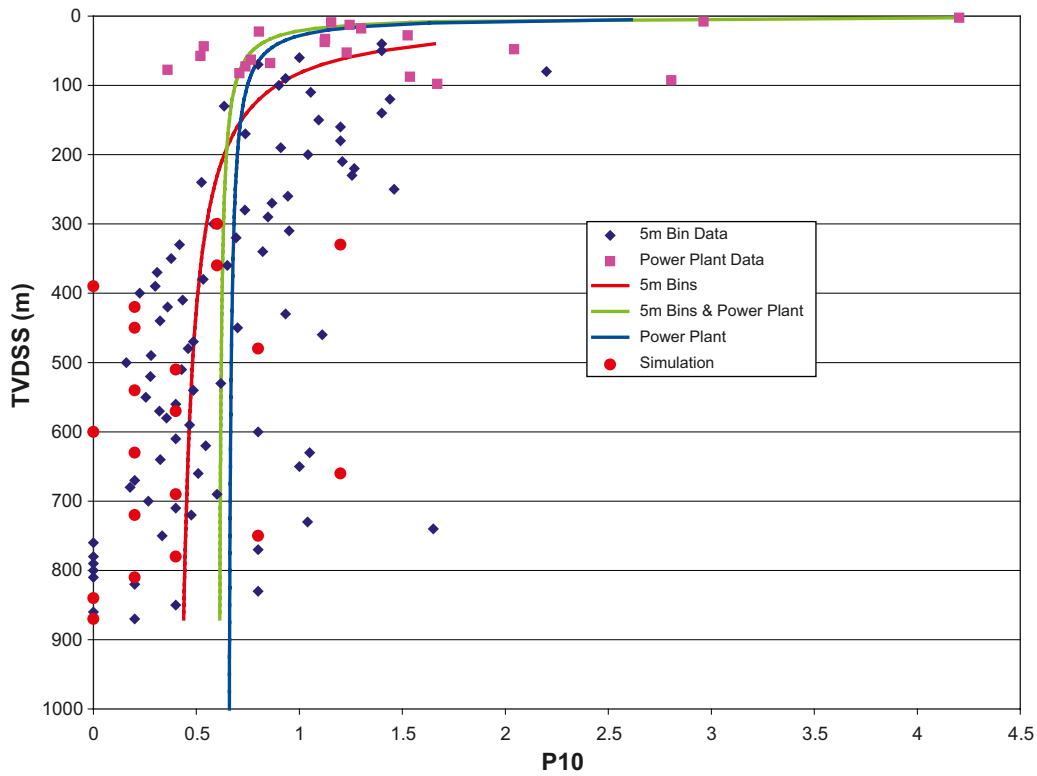
Figure 4-59. *Results of subhorizontal fracture simulation using the size and spatial model for the subhorizontal fracture sets.*

Table 4-74. Results of t-test and F-test for the simulated and measured data below 300 m.

n		78		

SH Intensity by Simulation	n	Mean	SD	SE
Measured	58	0.464	0.330	0.0433
Simulated	20	0.400	0.367	0.0821

Difference between means	0.064
95% CI	-0.126 to 0.253

t statistic	0.69
2-tailed p	0.4985 (Welch's approximation for unequal variances)

F statistic	0.81
95% CI	0.35 to 1.60

2-tailed p	0.5233

The results of these two tests indicating that the simulated subhorizontal fracture intensity and the measured subhorizontal fracture intensity are statistically the same below the zone of influence of any surface stress relief. The match also indicates that the depth-intensity relation inferred from the Forsmark power plant excavation data, the borehole data and the size model are internally consistent.

Multivariate statistical analysis of global Sets versus local sets

Whether the geological characteristics of the fracture sets designated as Local differed from those designated as Global was investigated through contingency table analysis, sometimes referred to as cross-tabulation. Only fractures in boreholes visible in BIPS were examined, since only fractures visible in BIPS could be reliably assigned to fracture orientation sets. Fractures within any type of deformation zone were also excluded.

The tests were carried out on all geological variables recorded that were nominal or ordinal variables (ordinal variable classes were treated as nominal variable classes for the sake of these tests). Several measures of Nominal association and their significance were used. These included: Lambda, Goodman and Kruskal Tau, and the Uncertainty Coefficient, explanations of which can be found in many statistical tests or at: http://www2.chass.ncsu.edu/garson/pa765/assocnominal.htm.

The tests were carried out on each of the four individual fracture domains separately, and also on all of the data combined across the four fracture domains.

An example of the cross tabulation for the openness of the fractures as a function of whether the fracture is part of a global or local set is shown in Table 4-75. All fracture domains have been combined in this cross tabulation. Note that the local sets tend to be less open or partly open than expected and more sealed. The global sets show the opposite relation, indicating that global sets tend to be slightly more open the local sets.

The results of the statistical tests are shown in Table 4-76. This table shows that the significance is approximately 0.0 for all of the tests, which indicates that the tests are highly significant. The reason that the tests are highly significant is the large amount of data, over seventeen thousand fractures, used in the tests. The column labeled "Value" is a measure of the association between openness classes and the global/local classes. A value close to zero means that there is no association between the two variables. In other words, knowing whether a fracture is global or local does not help in any useful way to assign it to the open, partly open or sealed classes, even though there is the slight tendency for local sets to be more often sealed.

Another example is the association between the global/local classification and the Best Rock Name variable. The cross tabulation is shown in Table 4-78. As this table shows, most of the rocks name classes have few fractures associated with them. Examination of the four dominant rock classes, amphibolite and the three granite and granodiorite classes, shows that there is an apparent tendency for the local sets to be found in amphibolites and a lesser tendency to be found in the main granite and granodiorite rock types. Perhaps the mechanical contrast between the amphibolites and the host rocks produced some additional fracture sets that had orientations reflecting both the regional stress field and the more local stresses created by the mechanical contrast. However, Table 4-77 shows that this association is very weak and not of use in assigning local or global sets preferentially to any particular host rock lithologies.

There were no cases in which there were any strong associations between a nominal or ordinal geological variable and whether the fracture was part of a local or global set. This was true whether the cross tabulations were restricted to an individual fracture domain or whether fractures were combined across all fracture domains. The consequence of this finding for purposes of building a DFN across the site is that procedures used to extrapolate or interpolate between measured data in boreholes used for global fracture sets are likely to be equally valid for local sets. Interpolation of the local fracture sets do not need to take into account any of the geological variables in a way that differs from the global sets, regardless of fracture domain.

Table 4-75. Cross tabulation of local versus global sets and whether they are open, partly open or sealed.

Crosstab

			FRACT_INTERPRET			
			Open	Partly open	Sealed	Total
SetType	Globa	Count	3612	389	11122	15123
		Expected Count	3457.1	360.5	11305.4	15123.0
		% within SetType	23.9%	2.6%	73.5%	100.0%
		% within FRACT_INTERPRET	89.5%	92.4%	84.2%	85.6%
		% of Total	20.5%	2.2%	63.0%	85.6%
	Local	Count	425	32	2080	2537
		Expected Count	579.9	60.5	1896.6	2537.0
		% within SetType	16.8%	1.3%	82.0%	100.0%
		% within FRACT_INTERPRET	10.5%	7.6%	15.8%	14.4%
		% of Total	2.4%	.2%	11.8%	14.4%
Total		Count	4037	421	13202	17660
		Expected Count	4037.0	421.0	13202.0	17660.0
		% within SetType	22.9%	2.4%	74.8%	100.0%
		% within FRACT_INTERPRET	100.0%	100.0%	100.0%	100.0%
		% of Total	22.9%	2.4%	74.8%	100.0%

Table 4-76. Statistical test results for the cross tabulation of fracture openness and whether it is part of a local or global set.

Directional Measures[f]

			Value	Asymp. Std. Error[a]	Approx. T[b]	Approx. Sig.
Nominal by Nominal	Lambda	Symmetric	.000	.000	.[c]	.[c]
		SetType Dependent	.000	.000	.[c]	.[c]
		FRACT_INTERPRET Dependent	.000	.000	.[c]	.[c]
	Goodman and Kruskal tau	SetType Dependent	.005	.001		.000[d]
		FRACT_INTERPRET Dependent	.004	.001		.000[d]
	Uncertainty Coefficient	Symmetric	.005	.001	4.976	.000[e]
		SetType Dependent	.006	.001	4.976	.000[e]
		FRACT_INTERPRET Dependent	.004	.001	4.976	.000[e]

a. Not assuming the null hypothesis.

b. Using the asymptotic standard error assuming the null hypothesis.

c. Cannot be computed because the asymptotic standard error equals zero.

d. Based on chi-square approximation

e. Likelihood ratio chi-square probability.

f. ETA statistics are available for numeric data only.

Table 4-77. Statistical test results for the cross tabulation of the host rock type and whether it is part of a local or global set.

Directional Measures[f]

			Value	Asymp. Std. Error[a]	Approx. T[b]	Approx. Sig.
Nominal by Nominal	Lambda	Symmetric	.000	.000	1.732	.083
		SetType Dependent	.001	.001	1.732	.083
		BEST_ROCK_ NAME Dependent	.000	.000	.[c]	.[c]
	Goodman and Kruskal tau	SetType Dependent	.007	.001		.000[d]
		BEST_ROCK_ NAME Dependent	.000	.000		.000[d]
	Uncertainty Coefficient	Symmetric	.004	.001	5.846	.000[e]
		SetType Dependent	.008	.001	5.846	.000[e]
		BEST_ROCK_ NAME Dependent	.003	.000	5.846	.000[e]

a. Not assuming the null hypothesis.

b. Using the asymptotic standard error assuming the null hypothesis.

c. Cannot be computed because the asymptotic standard error equals zero.

d. Based on chi-square approximation

e. Likelihood ratio chi-square probability.

f. ETA statistics are available for numeric data only.

Table 4-78. Cross tabulation of local vs. global sets and their host rock.

			Amphibolite	Breccia	Calc-silicate rock (skarn)	hydrothermal vein/segregation Carbonate-dominated	gabbro_ metamorphic Diorite_ quartz diorite and	rock_ metamorphic Felsic to intermediate volcanic	Granite	metamorphic_ medium-grained Granite to granodiorite_	medium-grained Granite_ fine- to	tonalite_ metamorphic_ fin Granite_ granodiorite and	Granite_ metamorphic_ aplitic	Granitoid_ metamorphic	Granodiorite	Granodiorite_ metamorphic	unspecified Hydrothermal vein/segregation_	Pegmatite_ pegmatitic granite	Quartz diorite	vein/segregation Quartz-dominated hydrothermal	Sedimentary rock	Tonalite	metamorphic Tonalite to granodiorite_	Total
SetType	Globa	Count	1429	7	23	1	44	99	3	9719	215	989	936	12	10	10	2	1534	1	36	3	0	50	15123
		Expected Count	1496.0	6.9	23.1	.9	59.9	113.9	2.6	9710.1	202.1	940.3	924.0	10.3	12.8	12.0	1.7	1520.9	.9	36.8	2.6	2.6	42.8	15123.0
		% within SetType	9.4%	.0%	.2%	.0%	.3%	.7%	.0%	64.3%	1.4%	6.5%	6.2%	.1%	.1%	.1%	.0%	10.1%	.0%	.2%	.0%	.0%	.3%	100.0%
		% within BEST_ ROCK_NAME	81.8%	87.5%	85.2%	100.0%	62.9%	74.4%	100.0%	85.7%	91.1%	90.1%	86.7%	100.0%	66.7%	71.4%	100.0%	86.4%	100.0%	83.7%	100.0%	.0%	100.0%	85.6%
		% of Total	8.1%	.0%	.1%	.0%	.2%	.6%	.0%	55.0%	1.2%	5.6%	5.3%	.1%	.1%	.1%	.0%	8.7%	.0%	.2%	.0%	.0%	.3%	85.6%
	Local	Count	318	1	4	0	26	34	0	1620	21	109	143	0	5	4	0	242	0	7	0	3	0	2537
		Expected Count	251.0	1.1	3.9	.1	10.1	19.1	.4	1628.9	33.9	157.7	155.0	1.7	2.2	2.0	.3	255.1	.1	6.2	.4	.4	7.2	2537.0
		% within SetType	12.5%	.0%	.2%	.0%	1.0%	1.3%	.0%	63.9%	.8%	4.3%	5.6%	.0%	.2%	.2%	.0%	9.5%	.0%	.3%	.0%	.1%	.0%	100.0%
		% within BEST_ ROCK_NAME	18.2%	12.5%	14.8%	.0%	37.1%	25.6%	.0%	14.3%	8.9%	9.9%	13.3%	.0%	33.3%	28.6%	.0%	13.6%	.0%	16.3%	.0%	100.0%	.0%	14.4%
		% of Total	1.8%	.0%	.0%	.0%	.1%	.2%	.0%	9.2%	.1%	.6%	.8%	.0%	.0%	.0%	.0%	1.4%	.0%	.0%	.0%	.0%	.0%	14.4%
Total		Count	1747	8	27	1	70	133	3	11339	236	1098	1079	12	15	14	2	1776	1	43	3	3	50	17660
		Expected Count	1747.0	8.0	27.0	1.0	70.0	133.0	3.0	11339.0	236.0	1098.0	1079.0	12.0	15.0	14.0	2.0	1776.0	1.0	43.0	3.0	3.0	50.0	17660.0
		% within SetType	9.9%	.0%	.2%	.0%	.4%	.8%	.0%	64.2%	1.3%	6.2%	6.1%	.1%	.1%	.1%	.0%	10.1%	.0%	.2%	.0%	.0%	.3%	100.0%
		% within BEST_ ROCK_NAME	100.0%	100.0%	100.0%	100.0%	100.0%	100.0%	100.0%	100.0%	100.0%	100.0%	100.0%	100.0%	100.0%	100.0%	100.0%	100.0%	100.0%	100.0%	100.0%	100.0%	100.0%	100.0%
		% of Total	9.9%	.0%	.2%	.0%	.4%	.8%	.0%	64.2%	1.3%	6.2%	6.1%	.1%	.1%	.1%	.0%	10.1%	.0%	.2%	.0%	.0%	.3%	100.0%

In terms of constructing a DFN model implementation that includes local fracture sets, we offer the following recommendations:

- If local-scale accuracy is required (i.e. for simulation of pump testing, grouting, fragmentation patterns, etc), we recommend using a composite DFN model. The model should include the Global fracture sets, as described in this report, as well as Local fracture sets simulated using spatial bootstrapping. Local set intensities and location models should be conditioned to match existing well data.

- If local-scale accuracy is not required, we recommend the use of conditional probability simulation as to the spatial occurrence of local fracture sets. The methodology for calculating the probability of occurrence, based on bin interval size, is detailed in Chapter 3.2.5. Table 4-79 presents the probabilities of occurrence, by set, fracture domain, and scale, for the Local sets.

Analysis of fracture termination relationships

A common reviewer comment, both from past SDMs and the early draft version of this geological DFN, has been that the models have not addressed the termination relationships between fracture sets. Terminations have the potential to affect both hydrologic and rock mechanical models; as such, it was deemed necessary to address terminations in the 2.2 version of the Forsmark geological DFN.

The termination study was performed inside ArcGIS after the linked outcrop fracture traces had been assigned to orientation sets. Each trace was assigned an 0.1 m thick buffer zone. Any trace with an endpoint inside the 0.1 m buffer zone was assumed to 'terminate' against that fracture. The assignment was based upon nodal endpoints, so as to not double-count terminator and terminatee.

The analysis was only peformed for outcrops inside domains FFM02 (AFM100201, AFM001264, and AFM001265) and FFM03; (AFM000053, AFM001243, and AFM001244); these are the only outcrops used in the DFN parameterization. Termination modeling was computed for all outcrops; however, like in the size modeling (Chapter 4.2), several of the outcrops in each domain were deemed to be too highly censored to offer accurate statistics. As such, the termination model is based upon the relationships in AFM100201 for domain FFM02, and on AFM000053 for domain FFM03. The results are presented below in . Note that there is no outcrop data for domains FFM01 and FFM06; we recommend using the termination matrix from FFM02 in the absence of any other data such as hydraulic data.

Table 4-79. Probability of occurrence of local sets as a function of domain and scale.

Fracture domain	Fracture set	Probability of occurrence at a given scale	
		6 m	30 m +
FFM01	ENE	0.09	0.17
FFM01	EW	0.15	0.20
FFM01	NNE	0.15	0.19
FFM01	SH2	0.09	0.15
FFM01	SH3	0.08	0.15
FFM02	NNE	NA	NA
FFM02	ENE	0.28	0.45
FFM02	NNW	0.12	0.18
FFM03	ENE	NA	NA
FFM03	EW	0.12	0.23
FFM06	ENE	0.20	0.15
FFM06	SH2	0.42	0.62

Table 4-80. Termination matrix for FFM02.

Relative set percentage					Total % termination
Fracture set	NE	NS	NW	EW	
NE terminates against	–	7.3%	19.5%	11.1%	38.0%
NS terminates against	26.9%	–	18.7%	12.7%	58.2%
NW terminates against	33.2%	5.9%	–	11.5%	50.7%
EW terminates against	35.1%	9.4%	19.5%	–	64.0%
Set History for Order of Generation					
Order	1	2	3	4	5
Set Name	NE	NW	EW	NS	SH?

Table 4-81. Termination matrix for FFM03.

Relative set percentage						Total % termination
Fracture set	NW	WNW	NE	NS	ENE	
NW terminates against	–	16.0%	19.1%	7.2%	10.9%	53.2%
WNW terminates against	24.2%	–	21.7%	4.5%	9.4%	59.8%
NE terminates against	23.1%	15.6%	–	5.0%	11.8%	55.5%
NS terminates against	25.9%	18.5%	16.7%	–	3.7%	64.8%
ENE terminates against	34.0%	17.0%	23.9%	6.9%	–	81.9%
Set history for order of generation						
Order	1		2	3	4	5	6
Set Name	NW		WNW	NE	NS	ENE	SH?

4.3.3 Recommendations for parameterization of the spatial model

The analyses indicate that the combined spatial/scaling/intensity model should be parameterized in the following manner:

1. Scaling: The Outcrop Scale model should scale according to a Mass Fractal Dimension of 1.9 for traces (2.9 for fractures in 3D) up to a scale of approximately 20–30 m. At scales greater than 30 m, the fractures and fracture traces should scale in a Euclidean manner. The scaling exponents are the same for all sets and fracture domains.

2. Spatial Controls on Fracture Intensity: The Outcrop Scale model has identified several geological factors that are related to fracture intensity. However, the only factor that appears useful for reducing intensity uncertainty is Fracture Domain. Therefore, fracture intensity models for each set should be specified only as a function of Fracture Domain.

3. Geostatistical analyses suggested no significant spatial correlations in fracture patterns at scales greater than 10 m. As such, we recommend using a Poisson point-process for locating fracture centers in 3D space (such as a Baecher model for fracture centers). The possible weak spatial correlation at scales less than 10 m might reflect some of the clustering observed in outcrop and boreholes outside of deformation zones, but the lack of spatial correlation at larger scales would indicate that the location of the zones is uncorrelated and that they could be modeled using a Poisson process.

4. Statistical analysis indicates no significant difference in terms of geologic or morphologic properties between Global fracture sets and Local fracture sets. As such, Local fracture sets are hypothesized to represent highly localized geologic or stress-field variations. We recommend either spatial bootstrapping or conditional probability for the description of these sets in a geological DFN.

5. Statistical analysis indicates no significant difference in terms of geologic or morphologic properties between fractures labeled 'Visible in BIPS' and 'Not Visible in BIPS'. As such, we recommend that fracture intensities (P_{32}) be corrected by set, by borehole and by fracture domain, for the percentage of fractures not visible in BIPS. This was done in all Forsmark 2.2 geological DFN modeling during the conversion of borehole P_{10} measurements to P_{32}.

4.4   Intensity model

Fracture intensity in the Forsmark 2.2 geological DFN model is closely linked to the size and spatial models; these cases have been extensively discussed in Chapters 4.2 and 4.3. The final intensity model is built atop the following assumptions:

- For Domains FFM01 and FFM06 in the Outcrop Scale Model, size-intensity match points are based on the mean P_{32} value (see Chapter 4.4.1) taken from the cored borehole data using the Wang solution, assuming the distribution minimum radius is equal to that of the borehole radius.

- For all other models (TFM, TCM, TCMF) and the other domains (FFM02 and FFM03) of the Outcrop Scale Model, size-intensity match points are build on simultaneously matching the mean P_{32} value taken from the cored boreholes with the P_{32} value that matches set P_{21} on the relevant surface outcrop.

- Where possible, variability in P_{32} is quantified. Though no strong depth dependence was noted, P_{32} does vary by lithology and by fracture domain. The non-spatial variability in P_{32} appears to vary as a Gamma distribution.

4.4.1   Fracture intensity from cored boreholes

The best source of information on the spatial variation of fracture intensity, as a function of fracture domain and set, is the composite core and BIPS mapping data from cored boreholes. As discussed in detail in Chapter 3.2.4, borehole fracture intersections were converted from line fracture frequency (P_{10}) to total fracture area per unit volume (P_{32}) using the Wang analytical solution. This conversion allows for the comparison of P_{32} across boreholes, sets, and domains, without worrying about orientation sampling biases.

The P_{32} values for each fracture set, in each borehole and each fracture domain, are computed over three different bin intervals: 6 m, 15 m, and 30 m. Box and whisker plots, along with frequency histograms for each set and domain are presented in Appendix E. Descriptive statistics, including means, deviations, and medians, are presented below, by fracture set and by fracture domain. Note that each table is broken out by "Affected by DZ" or "Not Affected by DZ"; the intensity difference in zones labeled 'Affected by DZ' is high enough to require special treatment. 'N' represents the number of bin intervals the statistic is based on.

The binned P_{32} values are used as inputs to the coupled size-intensity models, as well as in the spatial analysis of fracturing, the analysis of the effect of including 'Affected by DZ' zones in the final DFN model, and in the model uncertainty calculations.

Table 4-82. P_{32}, by set and 'affected by DZ' status, Domain FFM01, 6 m bins.

Fracture set	Aff. by DZ?	P_{32}						
		N	Mean	Median	Min.	Max.	Std. dev.	Skewness
ENE	No	83	2.74	1.52	0.31	15.30	2.87	2.15
	Yes	26	3.90	3.40	0.38	10.36	2.80	0.82
	Total	109	3.02	1.87	0.31	15.30	2.89	1.76
EW	No	134	1.12	0.75	0.22	4.84	0.94	1.82
	Yes	55	2.85	2.56	0.49	7.04	1.67	0.71
	Total	189	1.62	1.16	0.22	7.04	1.43	1.53
NE	No	860	1.73	0.77	0.00	25.52	2.76	3.38
	Yes	110	5.45	4.30	0.00	24.17	5.39	1.26
	Total	970	2.16	0.95	0.00	25.52	3.38	2.93
NNE	No	133	4.39	3.08	0.38	25.79	4.15	2.24
	Total	133	4.39	3.08	0.38	25.79	4.15	2.24
NS	No	687	1.29	0.49	0.00	22.27	2.15	3.36
	Yes	110	2.60	1.63	0.00	12.03	2.77	1.40
	Total	797	1.47	0.61	0.00	22.27	2.29	2.87
NW	No	868	0.95	0.47	0.00	10.24	1.31	2.27
	Yes	96	2.42	1.71	0.00	11.72	2.71	1.47
	Total	964	1.10	0.55	0.00	11.72	1.57	2.55
SH	No	747	0.63	0.27	0.00	8.36	0.90	2.73
	Yes	110	2.44	1.34	0.00	21.81	2.92:	3.30
	Total	857	0.86	0.43	0.00	21.81	1.47	5.41
SH2	No	141	0.92	0.41	0.00	18.03	1.82	6.35
	Total	141	0.92	0.41	0.00	18.03	1.82	6.35
SH3	No	137	0.84	0.25	0.00	9.27	1.64	3.12
	Yes	13	2.24	0.72	0.68	9.03	2.56	2.03
	Total	150	0.96	0.26	0.00	9.27	1.77	2.92
Total	No	3,790	1.29	0.54	0.00	25.79	2.17	4.02
	Yes	520	3.22	2.07	0.00	24.17	3.62	2.19
	Total	4,310	1.52	0.68	0.00	25.79	2.47	3.59

Table 4-83. P_{32}, by set and 'affected by DZ' status, Domain FFM02, 6 m bins.

Fracture set	Aff. by DZ	P_{32}						
		N	Mean	Median	Min.	Max.	Std. dev.	Skewness
ENE	No	46	3.65	2.91	0.00	14.75	3.80	1.40
	Yes	14	5.05	5.31	0.42	7.33	1.97	−1.01
	Total	60	3.98	3.44	0.00	14.75	3.50	1.13
EW	No	58	1.19	1.05	0.00	5.58	1.47	1.72
	Yes	2	0.18	0.18	0.00	0.36	0.26	NA
	Total	60	1.16	1.03	0.00	5.58	1.46	1.77
NE	No	119	3.31	1.84	0.00	18.40	3.70	1.84
	Yes	7	5.24	4.51	1.94	10.53	2.81	1.11
	Total	126	3.42	1.91	0.00	18.40	3.67	1.76
NNW	No	17	2.00	1.85	0.62	4.34	1.17	0.57
	Total	17	2.00	1.85	0.62	4.34	1.17	0.57
NS	No	70	1.61	0.76	0.00	11.24	2.45	2.13
	Yes	16	4.72	4.52	0.00	11.99	3.68	0.64
	Total	86	2.19	1.00	0.00	11.99	2.95	1.67
NW	No	120	2.12	1.12	0.00	13.52	2.57	2.05
	Yes	16	2.35	1.63	0.00	8.51	2.45	1.30
	Total	136	2.15	1.20	0.00	13.52	2.55	1.95
SH	No	144	2.78	2.46	0.00	11.50	2.13	1.48
	Yes	16	6.59	6.90	3.07	9.91	2.35	−0.06
	Total	160	3.17	2.68	0.00	11.50	2.43	1.22
Total	No	574	2.50	1.63	0.00	18.40	2.83	2.07
	Yes	71	4.60	4.59	0.00	11.99	3.08	0.29
	Total	645	2.73	1.82	0.00	18.40	2.93	1.76

Table 4-84. P_{32}, by set and 'affected by DZ' status, Domain FFM03, 6 m bins.

Fracture set	Aff. by DZ?	P_{32}						
		N	Mean	Median	Min.	Max.	Std. dev.	Skewness
EW	No	45	0.44	0.00	0.00	2.55	0.64	1.96
	Yes	4	0.41	0.21	0.00	1.24	0.58	1.41
	Total	49	0.44	0.00	0.00	2.55	0.63	1.91
NE	No	189	2.91	1.91	0.00	18.71	3.37	1.99
	Yes	4	4.52	4.25	3.19	6.38	1.59	0.38
	Total	193	2.94	1.93	0.00	18.71	3.35	1.96
NS	No	189	1.49	0.80	0.00	13.85	1.99	2.95
	Yes	4	0.00	0.00	0.00	0.00	0.00	0.00
	Total	193	1.46	0.80	0.00	13.85	1.98	2.97
NW	No	189	1.46	1.02	0.00	10.21	1.86	2.34
	Yes	4	1.15	0.95	0.00	2.68	1.13	0.95
	Total	193	1.45	1.02	0.00	10.21	1.84	2.35
SH	No	189	0.96	0.60	0.00	10.30	1.36	3.70
	Yes	4	2.48	2.47	1.81	3.17	0.59	0.08
	Total	193	1.00	0.60	0.00	10.30	1.36	3.55
Total	No	801	1.63	0.96	0.00	18.71	2.34	2.96
	Yes	20	1.71	1.19	0.00	6.38	1.88	1.07
	Total	821	1.64	0.96	0.00	18.71	2.33	2.94

Table 4-85. P_{32}, by set and 'affected by DZ' status, Domain FFM06, 6 m bins.

Fracture set	Aff. by DZ?	P_{32}						
		N	Mean	Median	Min.	Max.	Std. dev.	Skewness
ENE	No	5	0.98	0.78	0.15	2.38	0.86	1.31
NE	No	27	3.30	2.34	0.52	13.04	2.75	2.08
NS	No	27	2.15	2.02	0.26	5.25	1.27	0.91
NW	No	27	1.61	1.44	0.14	3.93	0.94	0.69
SH	No	27	0.64	0.39	0.00	2.49	0.66	1.62
SH2	No	17	1.03	0.59	0.12	4.42	1.06	2.22
Total	No	130	1.77	1.35	0.00	13.04	1.78	2.86

Table 4-86. P_{32}, by set and 'affected by DZ' status, Domain FFM01, 15 m bins.

Fracture set	Aff. by DZ?	P_{32}						
		N	Mean	Median	Min.	Max.	Std. dev.	Skewness
ENE	No	43	1.74	1.01	0.14	9.08	2.02	2.37
	Yes	10	3.68	3.18	0.31	8.23	2.40	0.47
	Total	53	2.10	1.38	0.14	9.08	2.21	1.71
EW	No	59	0.89	0.69	0.13	3.73	0.72	1.62
	Yes	23	2.63	2.34	0.28	5.63	1.61	0.37
	Total	82	1.37	0.97	0.13	5.63	1.30	1.57
NE	No	320	1.65	0.86	0.00	12.65	2.12	2.37
	Yes	41	5.76	4.81	0.00	17.90	4.94	0.86
	Total	361	2.12	1.04	0.00	17.90	2.90	2.49
NNE	No	67	3.24	1.99	0.00	13.40	3.22	1.26
	Total	67	3.24	1.99	0.00	13.40	3.22	1.26
NS	No	256	1.26	0.52	0.00	12.86	1.82	2.67
	Yes	41	2.70	1.55	0.00	9.63	2.43	1.11
	Total	297	1.46	0.73	0.00	12.86	1.97	2.27
NW	No	322	0.95	0.62	0.00	6.15	1.02	1.74
	Yes	36	2.36	1.92	0.00	8.27	2.27	1.13
	Total	358	1.09	0.70	0.00	8.27	1.27	2.24
SH	No	274	0.62	0.35	0.00	4.09	0.74	2.01
	Yes	41	2.46	1.51	0.00	12.88	2.52	2.33
	Total	315	0.86	0.44	0.00	12.88	1.29	4.34
SH2	No	54	0.90	0.59	0.00	6.61	1.16	2.77
	Total	54	0.90	0.59	0.00	6.61	1.16	2.77
SH3	No	54	0.82	0.21	0.00	5.13	1.34	2.02
	Yes	8	1.35	0.84	0.28	3.60	1.32	1.26
	Total	62	0.89	0.29	0.00	5.13	1.34	1.84
Total	No	1,449	1.22	0.61	0.00	13.40	1.72	3.00
	Yes	200	3.20	2.21	0.00	17.90	3.27	1.90
	Total	1,649	1.46	0.74	0.00	17.90	2.08	3.00

Table 4-87. P$_{32}$, by set and 'affected by DZ' status, Domain FFM02, 15 m bins.

Fracture set	Aff. by DZ?	P$_{32}$						
		N	Mean	Median	Min.	Max.	Std. dev.	Skewness
ENE	No	16	3.72	2.70	0.46	10.80	3.04	1.25
	Yes	3	4.62	5.49	2.88	5.50	1.51	−1.73
	Total	19	3.86	2.88	0.46	10.80	2.84	1.11
EW	No	18	1.36	1.11	0.20	3.92	1.09	1.44
	Total	18	1.36	1.11	0.20	3.92	1.09	1.44
NE	No	39	3.34	2.64	0.00	10.63	2.74	0.91
	Yes	1	4.57	4.57	4.57	4.57	NA	NA
	Total	40	3.37	2.65	0.00	10.63	2.71	0.88
NNW	No	8	1.43	1.50	0.74	2.23	0.51	−0.10
	Total	8	1.43	1.50	0.74	2.23	0.51	-0.10
NS	No	25	1.33	0.72	0.00	5.25	1.57	1.45
	Yes	3	5.87	7.09	3.31	7.23	2.22	−1.72
	Total	28	1.82	0.85	0.00	7.23	2.15	1.38
`NW	No	42	2.12	1.53	0.00	10.44	2.17	2.16
	Yes	2	1.29	1.29	1.11	1.46	0.25	NA
	Total	44	2.08	1.49	0.00	10.44	2.13	2.23
SH	No	50	2.56	2.38	0.00	7.54	1.55	1.03
	Yes	3	6.31	6.33	3.82	8.76	2.47	−0.05
	Total	53	2.77	2.47	0.00	8.76	1.80	1.24
Total	No	198	2.40	1.73	0.00	10.80	2.18	1.64
	Yes	12	4.80	5.03	1.11	8.76	2.37	−0.04
	Total	210	2.54	1.81	0.00	10.80	2.26	1.46

Table 4-88. P$_{32}$, by set and 'affected by DZ' status, Domain FFM03, 15 m bins.

Fracture set	Aff. by DZ?	P$_{32}$						
		N	Mean	Median	Min.	Max.	Std. dev.	Skewness
EW	No	17	0.43	0.21	0.00	2.23	0.53	2.71
NE	No	69	3.00	2.02	0.00	12.16	2.57	1.16
NS	No	70	1.54	0.97	0.00	8.33	1.66	2.23
NW	No	69	1.47	1.21	0.00	5.77	1.36	1.34
SH	No	69	0.97	0.68	0.00	5.25	0.96	2.67
Total	No	294	1.67	0.98	0.00	12.16	1.86	2.11

Table 4-89. P$_{32}$, by set and 'affected by DZ' status, Domain FFM06, 15 m bins.

Fracture set	Aff. by	P$_{32}$						
	DZ?	N	Mean	Median	Min.	Max.	Std. dev.	Skewness
ENE	No	5	0.98	0.78	0.15	2.38	0.86	1.31
NE	No	27	3.30	2.34	0.52	13.04	2.75	2.08
NS	No	27	2.15	2.02	0.26	5.25	1.27	0.91
NW	No	27	1.61	1.44	0.14	3.93	0.94	0.69
SH	No	27	0.64	0.39	0.00	2.49	0.66	1.62
SH2	No	17	1.03	0.59	0.12	4.42	1.06	2.22
Total	No	130	1.77	1.35	0.00	13.04	1.78	2.86

Table 4-90. P$_{32}$, by set and 'affected by DZ' status, Domain FFM01, 30 m bins.

Fracture set	Aff. by	P$_{32}$						
	DZ?	N	Mean	Median	Min.	Max.	Std. dev.	Skewness
ENE	No	28	1.62	1.08	0.07	6.37	1.67	1.43
	Yes	5	3.32	2.76	1.90	6.07	1.70	1.38
	Total	33	1.87	1.33	0.07	6.37	1.76	1.15
EW	No	33	0.78	0.64	0.06	2.26	0.56	0.96
	Yes	10	2.65	1.86	1.32	5.65	1.54	1.08
	Total	43	1.22	0.89	0.06	5.65	1.18	2.12
NE	No	164	1.68	1.06	0.00	11.68	1.91	2.20
	Yes	20	5.21	4.48	0.33	12.56	4.09	0.59
	Total	184	2.06	1.16	0.00	12.56	2.49	2.17
NNE	No	31	3.39	2.20	0.32	9.90	2.81	1.06
	Total	31	3.39	2.20	0.32	9.90	2.81	1.06
NS	No	127	1.29	0.66	0.00	9.42	1.66	2.35
	Yes	20	2.54	1.64	0.00	7.70	2.27	1.17
	Total	147	1.46	0.75	0.00	9.42	1.80	2.07
NW	No	161	0.93	0.78	0.00	4.47	0.82	1.50
	Yes	20	1.98	1.52	0.00	6.49	1.97	1.11
	Total	181	1.05	0.80	0.00	6.49	1.06	2.20
SH	No	138	0.64	0.43	0.00	4.10	0.66	1.97
	Yes	20	2.19	1.54	0.05	9.53	2.39	2.19
	Total	158	0.84	0.52	0.00	9.53	1.15	4.35
SH2	No	24	0.93	0.74	0.08	4.39	0.96	2.41
	Total	24	0.93	0.74	0.08	4.39	0.96	2.41
SH3	No	25	0.90	0.31	0.05	3.75	1.08	1.36
	Yes	4	1.03	0.77	0.28	2.30	0.92	1.21
	Total	29	0.92	0.42	0.05	3.75	1.04	1.30
Total	No	731	1.23	0.73	0.00	11.68	1.54	2.79
	Yes	99	2.89	1.90	0.00	12.56	2.83	1.61
	Total	830	1.43	0.83	0.00	12.56	1.82	2.72

Table 4-91. P$_{32}$, by set and 'affected by DZ' status, Domain FFM02, 30 m bins.

Fracture set	Aff. by							
	DZ?	N	Mean	Median	Min.	Max.	Std. dev.	Skewness
ENE	No	8	3.84	2.25	1.51	10.92	3.24	1.83
	Yes	1	6.08	6.08	6.08	6.08	NA	NA
	Total	9	4.09	2.56	1.51	10.92	3.12	1.48
EW	No	8	1.13	1.11	0.20	2.23	0.57	0.54
	Total	8	1.13	1.11	0.20	2.23	0.57	0.54
NE	No	18	3.32	2.54	0.46	9.15	2.49	1.12
	Yes	1	0.00	0.00	0.00	0.00	NA	NA
	Total	19	3.14	2.33	0.00	9.15	2.53	1.08
NNW	No	4	1.51	1.37	0.99	2.34	0.61	1.03
	Total	4	1.51	1.37	0.99	2.34	0.61	1.03
NS	No	10	1.17	0.77	0.00	3.31	1.12	0.75
	Yes	1	6.29	6.29	6.29	6.29	NA	NA
	Total	11	1.63	1.01	0.00	6.29	1.87	1.71
NW	No	18	2.30	1.85	0.20	9.45	2.14	2.38
	Yes	1	1.67	1.67	1.67	1.67	NA	NA
	Total	19	2.27	1.78	0.20	9.45	2.08	2.47
SH	No	22	2.47	2.26	0.61	5.44	1.31	1.18
	Yes	1	7.32	7.32	7.32	7.32	NA	NA
	Total	23	2.68	2.27	0.61	7.32	1.63	1.46
Total	No	88	2.42	1.90	0.00	10.92	2.06	2.03
	Yes	5	4.27	6.08	0.00	7.32	3.23	–0.66
	Total	93	2.52	1.91	0.00	10.92	2.16	1.77

Table 4-92. P$_{32}$, by set and 'affected by DZ' status, Domain FFM03, 30 m bins.

Fracture set	Aff. by							
	DZ?	N	Mean	Median	Min.	Max.	Std. dev.	Skewness
EW	No	8	0.42	0.30	0.09	1.13	0.35	1.40
NE	No	35	3.07	2.83	0.19	7.58	1.96	0.64
NS	No	35	1.52	1.07	0.44	6.22	1.29	2.08
NW	No	35	1.41	1.22	0.00	4.68	1.01	1.18
SH	No	35	0.97	0.69	0.12	4.73	0.89	2.91
Total	No	148	1.67	1.07	0.00	7.58	1.54	1.69

Table 4-93. P$_{32}$, by set and 'affected by DZ' status, Domain FFM06, 30 m bins.

Fracture set	Aff. By							
	DZ?	N	Mean	Median	Min.	Max.	Std. dev.	Skewness
NE	No	13	3.62	2.88	1.80	8.62	2.07	1.48
NS	No	13	2.23	1.80	0.77	4.57	1.16	1.10
NW	No	13	1.56	1.34	0.42	3.67	0.86	1.17
SH	No	13	0.79	0.63	0.10	2.37	0.66	1.32
Total	No	52	2.05	1.74	0.10	8.62	1.65	1.84

4.4.2 Analysis of zones labeled 'affected by DZ'

During the geologic modeling efforts at Forsmark, some sections of the cored boreholes were found to have anomalously high fracture frequencies when compared to the rest of the rock mass as a whole. Normally, higher fracture frequencies are indicative of deformation zones at Forsmark (Stephens, personal comm.). However, DZ intersections with the boreholes often contain additional indicators, such as geophysical anomalies, increased degrees of alteration, and the presence of evidence of previous ductile or brittle deformation. Sections of increased fracture frequency without other solid evidence of DZ or of a geometric match with other modeled structures were termed to be 'Affected by DZ', and were signaled out for special attention in the DFN modeling in the Fracture Domain report /Olofsson et al. 2007/.

The analysis of zones labeled 'Affected by DZ' at Forsmark consisted of the following efforts:

1. Do sections labeled 'Affected by DZ' follow a different set orientation pattern than the rest of the fractures in a given fracture domain? (Chapter 3.2.2)

2. Is the intensity pattern of 'Affected by DZ' fractures different than the intensity patterns of fractures 'Not Affected by DZ'? (Chapter 4.4.1)

3. Are fractures labeled 'Affected by DZ' different geologically or lithologically than fractures labeled 'Not Affected by DZ'? (this Chapter)

Previous sections have answered the first two questions: zones labeled 'Affected by DZ' can be parameterized using the same orientation models as fractures labeled ' Not Affected by DZ'. However, the analysis of binned fracture intensity data shows significant differences between the two populations. Fracture intensities in the zones labeled 'Affected by DZ' are generally much higher than intensities outside of these zones. A listing of the zones in cored boreholes labeled 'Affected by DZ' is presented as Table 4-94.

Table 4-94. Zones labeled 'affected by DZ' in the Forsmark 2.2 Geological Model.

Borehole IDCODE	ADJ_SECUP (Start) m	ADJ_SECLOW (End) m	Notes
KFM01C	48	62	
KFM01C	252	305	
KFM01C	330	450	
KFM02A	442	476	
KFM05A	616	685	
KFM05A	720	796	
KFM07A	422	507	
KFM07A	840	857	FFM05, not modeled in DFN
KFM08A	172	244	
KFM08A	315	342	
KFM09A	7.8	15	
KFM09A	40	86	
KFM09A	116	124	
KFM09A	754	758	included in DZ
KFM09A	758	770	FFM04, not modeled in DFN
KFM09B	43	59	
KFM09B	78	106	
KFM09B	132	283.6	
KFM09B	284.1	308	
KFM10A	449	478	

A final statistical analysis was conducted to determine if, geologically, morphologically, or lithologically, fractures in zones labeled 'Affected by DZ' were different than those outside of these zones. Nonparametric correlation analysis (Kendall's Tau) and cross-tabulation were completed using SPSS, in a fashion similar to the spatial analyses described in Chapter 4.3.2. Fracture data from SICADA table p_fract_core_eshi was used in the analysis. The results of the nonparametric correlation analysis, in SPSS output table format, are presented below as Table 4-95.

Table 4-95. Crosstabs analysis results: affected by DZ vs. Not Affected by DZ.

			ADJUSTED SECUP_m	APERTURE_ mm
Kendall's tau_b	ADJUSTEDSECUP_m	Correlation Coefficient	1.000	-.158**
		Sig. (2-tailed)	.	.000
		N	22582	22582
	APERTURE_mm	Correlation Coefficient	-.158**	1.000
		Sig. (2-tailed)	.000	.
		N	22582	22582
	CONFIDENCE_CODE	Correlation Coefficient	-.060**	.545**
		Sig. (2-tailed)	.000	.000
		N	22582	22582
	STRIKE_deg	Correlation Coefficient	.009*	-.063**
		Sig. (2-tailed)	.050	.000
		N	22582	22582
	DIP_deg	Correlation Coefficient	.134**	-.210**
		Sig. (2-tailed)	.000	.000
		N	22582	22582
	WIDTH_mm	Correlation Coefficient	-.023**	.272**
		Sig. (2-tailed)	.000	.000
		N	22582	22582
	JOINT_ALTERATION	Correlation Coefficient	-.095**	.599**
		Sig. (2-tailed)	.000	.000
		N	22582	22582
	NORTHING_ ADJUSTEDSECUP	Correlation Coefficient	-.013**	-.078**
		Sig. (2-tailed)	.004	.000
		N	22582	22582
	EASTING_ ADJUSTEDSECUP	Correlation Coefficient	.223**	.024**
		Sig. (2-tailed)	.000	.000
		N	22582	22582
	ELEVATION_ ADJUSTEDSECUP	Correlation Coefficient	-.937**	.156**
		Sig. (2-tailed)	.000	.000
		N	22582	22582
	Trend	Correlation Coefficient	-.005	-.024**
		Sig. (2-tailed)	.286	.000
		N	22582	22582
	Plunge	Correlation Coefficient	-.134**	.206**
		Sig. (2-tailed)	.000	.000
		N	22582	22582
	DZ_Class	Correlation Coefficient	-.134**	-.008
		Sig. (2-tailed)	.000	.248
		N	22582	22582

Table 4-95. Continued.

			CONFIDENCE_CODE	STRIKE_deg	DIP_deg
Kendall's tau_b	ADJUSTEDSECUP_m	Correlation Coefficient	-.060**	.009*	.134**
		Sig. (2-tailed)	.000	.050	.000
		N	22582	22582	22582
	APERTURE_mm	Correlation Coefficient	.545**	-.063**	-.210**
		Sig. (2-tailed)	.000	.000	.000
		N	22582	22582	22582
	CONFIDENCE_CODE	Correlation Coefficient	1.000	-.053**	-.132**
		Sig. (2-tailed)	.	.000	.000
		N	22582	22582	22582
	STRIKE_deg	Correlation Coefficient	-.053**	1.000	.063**
		Sig. (2-tailed)	.000	.	.000
		N	22582	22582	22582
	DIP_deg	Correlation Coefficient	-.132**	.063**	1.000
		Sig. (2-tailed)	.000	.000	.
		N	22582	22582	22582
	WIDTH_mm	Correlation Coefficient	.130**	-.040**	-.016**
		Sig. (2-tailed)	.000	.000	.002
		N	22582	22582	22582
	JOINT_ALTERATION	Correlation Coefficient	.899**	-.061**	-.186**
		Sig. (2-tailed)	.000	.000	.000
		N	22582	22582	22582
	NORTHING_ADJUSTEDSECUP	Correlation Coefficient	-.082**	.019**	.023**
		Sig. (2-tailed)	.000	.000	.000
		N	22582	22582	22582
	EASTING_ADJUSTEDSECUP	Correlation Coefficient	.053**	-.030**	.017**
		Sig. (2-tailed)	.000	.000	.000
		N	22582	22582	22582
	ELEVATION_ADJUSTEDSECUP	Correlation Coefficient	.055**	-.003	-.127**
		Sig. (2-tailed)	.000	.473	.000
		N	22582	22582	22582
	Trend	Correlation Coefficient	-.021**	.104**	.022**
		Sig. (2-tailed)	.000	.000	.000
		N	22582	22582	22582
	Plunge	Correlation Coefficient	.124**	-.060**	-.950**
		Sig. (2-tailed)	.000	.000	.000
		N	22582	22582	22582
	DZ_Class	Correlation Coefficient	-.009	.002	.024**
		Sig. (2-tailed)	.176	.718	.000
		N	22582	22582	22582

Table 4-95. Continued.

			WIDTH_mm	JOINT_ ALTERATION
Kendall's tau_b	ADJUSTEDSECUP_m	Correlation Coefficient	-.023**	-.095**
		Sig. (2-tailed)	.000	.000
		N	22582	22582
	APERTURE_mm	Correlation Coefficient	.272**	.599**
		Sig. (2-tailed)	.000	.000
		N	22582	22582
	CONFIDENCE_CODE	Correlation Coefficient	.130**	.699**
		Sig. (2-tailed)	.000	.000
		N	22582	22582
	STRIKE_deg	Correlation Coefficient	-.040**	-.061**
		Sig. (2-tailed)	.000	.000
		N	22582	22582
	DIP_deg	Correlation Coefficient	-.016**	-.186**
		Sig. (2-tailed)	.002	.000
		N	22582	22582
	WIDTH_mm	Correlation Coefficient	1.000	.221**
		Sig. (2-tailed)	.	.000
		N	22582	22582
	JOINT_ALTERATION	Correlation Coefficient	.221**	1.000
		Sig. (2-tailed)	.000	.
		N	22582	22582
	NORTHING_ ADJUSTEDSECUP	Correlation Coefficient	-.151**	-.091**
		Sig. (2-tailed)	.000	.000
		N	22582	22582
	EASTING_ ADJUSTEDSECUP	Correlation Coefficient	.102**	.067**
		Sig. (2-tailed)	.000	.000
		N	22582	22582
	ELEVATION_ ADJUSTEDSECUP	Correlation Coefficient	-.006	.090**
		Sig. (2-tailed)	.261	.000
		N	22582	22582
	Trend	Correlation Coefficient	.042**	-.029**
		Sig. (2-tailed)	.000	.000
		N	22582	22582
	Plunge	Correlation Coefficient	.017**	.176**
		Sig. (2-tailed)	.001	.000
		N	22582	22582
	DZ_Class	Correlation Coefficient	-.074**	-.002
		Sig. (2-tailed)	.000	.760
		N	22582	22582

Table 4-95. Continued.

			NORTHING_ADJUSTEDSECUP	EASTING_ADJUSTEDSECUP	ELEVATION_ADJUSTEDSECUP
Kendall's tau_b	ADJUSTEDSECUP_m	Correlation Coefficient	-.013**	.223**	-.937**
		Sig. (2-tailed)	.004	.000	.000
		N	22582	22582	22582
	APERTURE_mm	Correlation Coefficient	-.078**	.024**	.156**
		Sig. (2-tailed)	.000	.000	.000
		N	22582	22582	22582
	CONFIDENCE_CODE	Correlation Coefficient	-.082**	.053**	.055**
		Sig. (2-tailed)	.000	.000	.000
		N	22582	22582	22582
	STRIKE_deg	Correlation Coefficient	.019**	-.030**	-.003
		Sig. (2-tailed)	.000	.000	.473
		N	22582	22582	22582
	DIP_deg	Correlation Coefficient	.023**	.017**	-.127**
		Sig. (2-tailed)	.000	.000	.000
		N	22582	22582	22582
	WIDTH_mm	Correlation Coefficient	-.151**	.102**	-.006
		Sig. (2-tailed)	.000	.000	.261
		N	22582	22582	22582
	JOINT_ALTERATION	Correlation Coefficient	-.091**	.067**	.090**
		Sig. (2-tailed)	.000	.000	.000
		N	22582	22582	22582
	NORTHING_ADJUSTEDSECUP	Correlation Coefficient	1.000	-.315**	.011*
		Sig. (2-tailed)	.	.000	.015
		N	22582	22582	22582
	EASTING_ADJUSTEDSECUP	Correlation Coefficient	-.315**	1.000	-.224**
		Sig. (2-tailed)	.000	.	.000
		N	22582	22582	22582
	ELEVATION_ADJUSTEDSECUP	Correlation Coefficient	.011*	-.224**	1.000
		Sig. (2-tailed)	.015	.000	.
		N	22582	22582	22582
	Trend	Correlation Coefficient	-.003	-.023**	.000
		Sig. (2-tailed)	.515	.000	.974
		N	22582	22582	22582
	Plunge	Correlation Coefficient	-.023**	-.017**	.127**
		Sig. (2-tailed)	.000	.000	.000
		N	22582	22582	22582
	DZ_Class	Correlation Coefficient	-.076**	-.164**	.160**
		Sig. (2-tailed)	.000	.000	.000
		N	22582	22582	22582

Table 4-95. Continued.

			Trend	Plunge	DZ_Class
Kendall's tau_b	ADJUSTEDSECUP_m	Correlation Coefficient	-.005	-.134**	-.134**
		Sig. (2-tailed)	.286	.000	.000
		N	22582	22582	22582
	APERTURE_mm	Correlation Coefficient	-.024**	.206**	-.008
		Sig. (2-tailed)	.000	.000	.248
		N	22582	22582	22582
	CONFIDENCE_CODE	Correlation Coefficient	-.021**	.124**	-.009
		Sig. (2-tailed)	.000	.000	.176
		N	22582	22582	22582
	STRIKE_deg	Correlation Coefficient	.104**	-.060**	.002
		Sig. (2-tailed)	.000	.000	.718
		N	22582	22582	22582
	DIP_deg	Correlation Coefficient	.022**	-.950**	.024**
		Sig. (2-tailed)	.000	.000	.000
		N	22582	22582	22582
	WIDTH_mm	Correlation Coefficient	.042**	.017**	-.074**
		Sig. (2-tailed)	.000	.001	.000
		N	22582	22582	22582
	JOINT_ALTERATION	Correlation Coefficient	-.029**	.176**	-.002
		Sig. (2-tailed)	.000	.000	.760
		N	22582	22582	22582
	NORTHING_ADJUSTEDSECUP	Correlation Coefficient	-.003	-.023**	-.076**
		Sig. (2-tailed)	.515	.000	.000
		N	22582	22582	22582
	EASTING_ADJUSTEDSECUP	Correlation Coefficient	-.023**	-.017**	-.164**
		Sig. (2-tailed)	.000	.000	.000
		N	22582	22582	22582
	ELEVATION_ADJUSTEDSECUP	Correlation Coefficient	.000	.127**	.160**
		Sig. (2-tailed)	.974	.000	.000
		N	22582	22582	22582
	Trend	Correlation Coefficient	1.000	-.023**	.032**
		Sig. (2-tailed)	.	.000	.000
		N	22582	22582	22582
	Plunge	Correlation Coefficient	-.023**	1.000	-.024**
		Sig. (2-tailed)	.000	.	.000
		N	22582	22582	22582
	DZ_Class	Correlation Coefficient	.032**	-.024**	1.000
		Sig. (2-tailed)	.000	.000	.
		N	22582	22582	22582

**. Correlation is significant at the 0.01 level (2-tailed).

*. Correlation is significant at the 0.05 level (2-tailed).

The results of the SPSS analysis indicate that there are strong statistically-significant differences between the two groups ('Affected by DZ' and 'Not Affected by DZ') in terms of many of the class variables, like fracture set, fracture domain, roughness, and aperture, at a significance level of $\alpha = 0.05$. However, the differences in the relative set orientations have already been tested and found to make no significant difference in the orientation mode. There is no data available to determine if there is a difference in fracture sizes between the two classes, as there is no surface data mapped as 'Affected by DZ'. This leaves intensity as the only parameter for which an alternative parameterization was necessary; due to the relatively small sizes of most of these zones, they are assumed to follow the same spatial model as the rest of the geological DFN.

There are two alternatives for handling the zones labeled 'Affected by DZ' in DFN modeling:

1. Treat these zones as more highly fractured volumes of the rock mass, but identical in terms of other fracture parameters such as orientation, size, and the fracture location (spatial) model. The resulting intensity increase can be accommodated by adding a second fracture generation cycle within these volumes, such that the resulting fracture intensities match those presented in Table 4-82 through Table 4-93 for the sections labeled 'Affected by DZ'. This is the alternative recommended by the geological DFN team.

2. Treat these areas as separate model volumes, with independent parameterizations. Orientation (Chapter 4.1.3) and intensity (Chapter 4.4.1) distributions are given for these sections, by set and fracture domain, in the body of this report. If this option is chosen, we highly recommend spatial bootstrapping, such that the resulting outputs closely matches observations made in cored boreholes.

4.4.3 Fracture intensity as a gamma distribution

As discussed in Chapter 3.2.4, in addition to producing descriptive statistics and coupled size-intensity models for each fracture set in each fracture domain, an analysis was run to quantify the spatial variability in fracture intensity (P_{32}). The spatial variability of fracture intensity contains two components – a systematic variability, which is can be described by geostatistical trend and correlation analysis, and a random component of variability.

While a single value of fracture intensity P_{32} can be assigned to a single rock domain, this intensity variation increases as smaller and smaller sub-regions are considered. Theoretical analysis /Dershowitz 1984/ has demonstrated that the Gamma Distribution (Raiffa and Schlaiffer) is the appropriate distribution for variation of P_{32} as a function of the size of the sub-region being analysed. The gamma distribution applies because P_{32} is the analog of the Poisson distribution rate parameter nu, over a specified interval t, corresponding to the volume of the sub-region.

In the DFN spatial analysis, we have demonstrated that the assumption of spatial stationarity and uncorrelation at scales larger than 10 m is applicable to all fracture domains, and Euclidean scaling is applicable to all fracture domains at scales larger than 20 m–30 m. For these regions, the assumption of a Poisson distribution of fracture centers was found to be appropriate (Chapter 3.2.5). For these region, therefore, a gamma distribution was assumed to be appropriate. For regions and sets in which the Poisson assumption is appropriate, the Gamma distribution would be expected to provide a good model for spatial variability within sub-regions. For regions and sets for which the Poisson assumption is not appropriate, the gamma distribution may still provide a reasonable approximation for spatial variability of sub-regions.

This section describes an analysis of gamma distribution for sub-regions at scales between 6 m and 30 m. This analysis was based on binned borehole P_{32} data at scales of 6 m and 30 m. Alough 15 m scale binned data is available, it was not analysed due to budget and time constraints.

The procedure for simulating a Gamma distribution is documented in great detail in Chapter 3.2.4. The Kolmogorov-Smirnov (K-S) test was used to judge distribution goodness-of-fit. The fitted gamma distribution parameters are contained in Table 4-96. Figure 4-60 through Figure 4-66 illustrate the goodness of fit graphically between the observed fracture data and a simulated Gamma distribution for fracture domain FFM01.

Table 4-96. Gamma distribution parameters fit to fractures NOT affected by DZ.

Fracture domain	Fracture set	Set type	P$_{32}$ (6 m bins) –0.0385 m –564 m*					Gamma dist. params		Gamma scale
			Mean	Median	Std. dev.	Min	Max	Scale (θ)	Shape (κ)	(m)
FFM01	NE	Global	1.73	0.77	2.76	0.00	25.52	0.796	2.088	30 m
FFM01	NS	Global	1.29	0.49	2.15	0.00	22.27		No fit to gamma at tested scales	
FFM01	NW	Global	0.95	0.47	1.31	0.00	10.24	1.319	0.699	30 m
FFM01	SH	Global	0.63	0.27	0.90	0.00	8.36		No fit to gamma at tested scales	
FFM01	ENE	Local	2.74	1.52	2.87	0.31	15.30	0.765	2.055	30 m
FFM01	EW	Local	1.12	0.75	0.94	0.22	4.84	1.633	0.455	30 m
FFM01	NNE	Local	4.39	3.08	4.15	0.38	25.79	0.711	4.353	30 m
FFM01	SH2	Local	0.92	0.41	1.82	0.00	18.03	1.489	0.961	6 m
FFM01	SH3	Local	0.84	0.25	1.64	0.00	9.27	0.521	1.598	30 m
FFM02	NE	Global	3.31	1.84	3.70	0.00	18.40	1.047	2.541	30 m
FFM02	NS	Global	1.61	0.76	2.45	0.00	11.24		No fit to gamma at tested scales	
FFM02	NW	Global	2.12	1.12	2.57	0.00	13.52	1.036	1.676	30 m
FFM02	SH	Global	2.78	2.46	2.13	0.00	11.50	1.894	1.453	6 m
FFM02	ENE	Global	3.65	2.91	3.80	0.00	14.75	1.013	2.531	30 m
FFM02	EW	Global	1.19	1.05	1.47	0.00	5.58		No fit to gamma at tested scales	
FFM02	NNE	Local	Not found in borehole data							
FFM02	NNW	Local	2.00	1.85	1.17	0.62	4.34	2.166	0.913	6 m
FFM03	NE	Global	2.91	1.91	3.37	0.00	18.71	2.567	1.203	30 m
FFM03	NS	Global	1.49	0.80	1.99	0.00	13.85	1.475	0.989	30 m
FFM03	NW	Global	1.46	1.02	1.86	0.00	10.21	2.075	0.662	30 m
FFM03	SH	Global	0.96	0.60	1.36	0.00	10.30	2.429	0.335	30 m
FFM03	EW	Local2	0.44	0.00	0.64	0.00	2.55	0.919	0.346	30 m
FFM03	ENE	Local	Not found in borehole data							
FFM06	NE	Global	3.30	2.34	2.75	0.52	13.04	1.427	2.260	6 m
FFM06	NS	Global	2.15	2.02	1.27	0.26	5.25	1.667	1.140	6 m
FFM06	NW	Global	1.61	1.44	0.94	0.14	3.93	1.202	1.227	6 m
FFM06	SH	Global	0.64	0.39	0.66	0.00	2.49	1.338	0.531	30 m
FFM06	ENE	Local	0.98	0.78	0.86	0.15	2.38	2.368	0.460	6 m
FFM06	SH2	Local	1.03	0.59	1.06	0.12	4.42	1.402	0.913	6 m
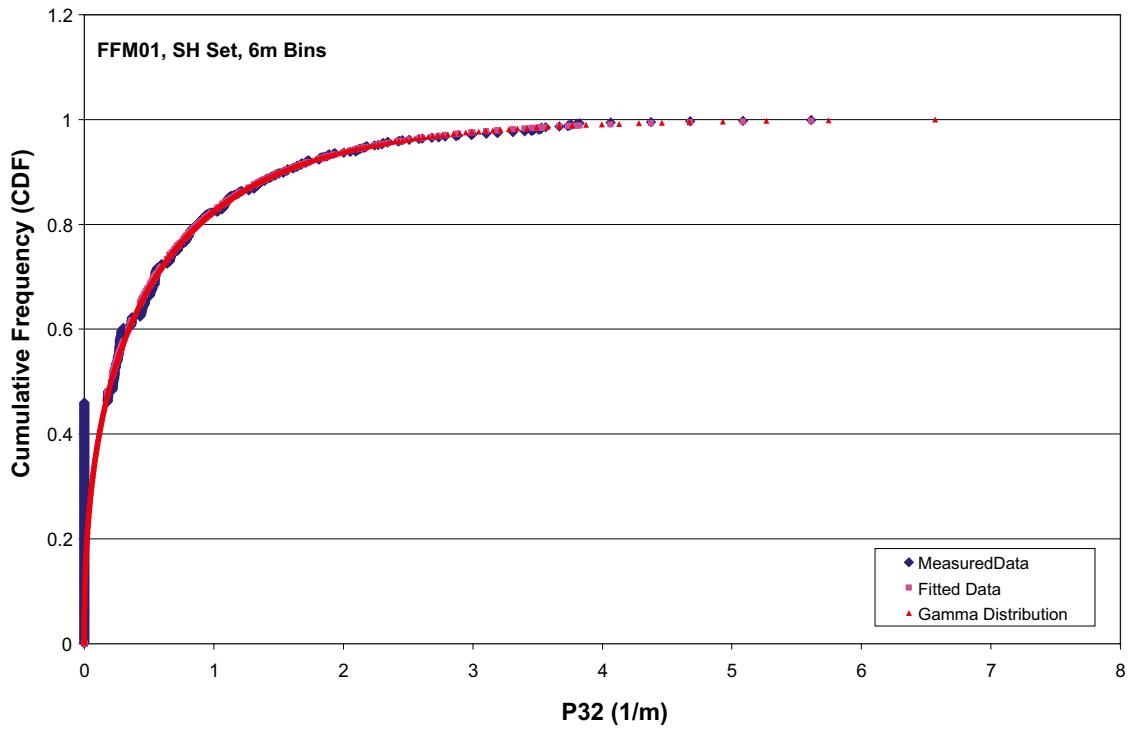
Figure 4-60. *CDF of measured P_{32} data from cored boreholes against an empirical CDF of a fitted Gamma distribution, SH set, Domain FFM01.*
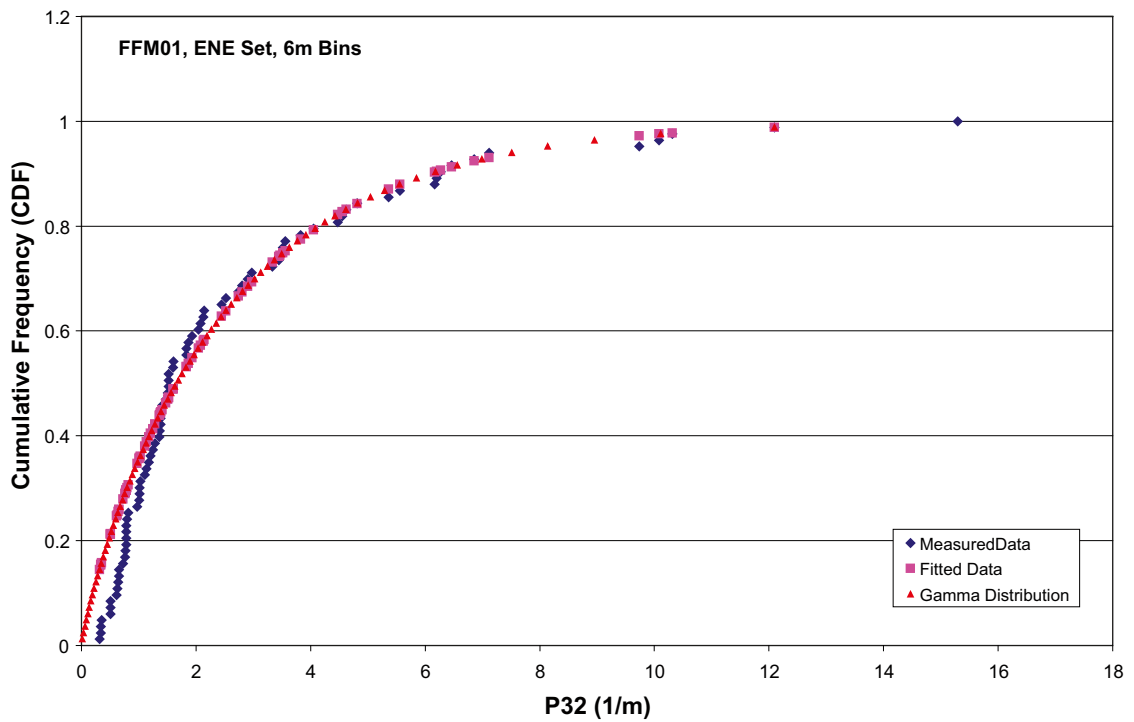
Figure 4-61. *CDF of measured P_{32} data from cored boreholes against an empirical CDF of a fitted Gamma distribution, ENE set, Domain FFM01.*
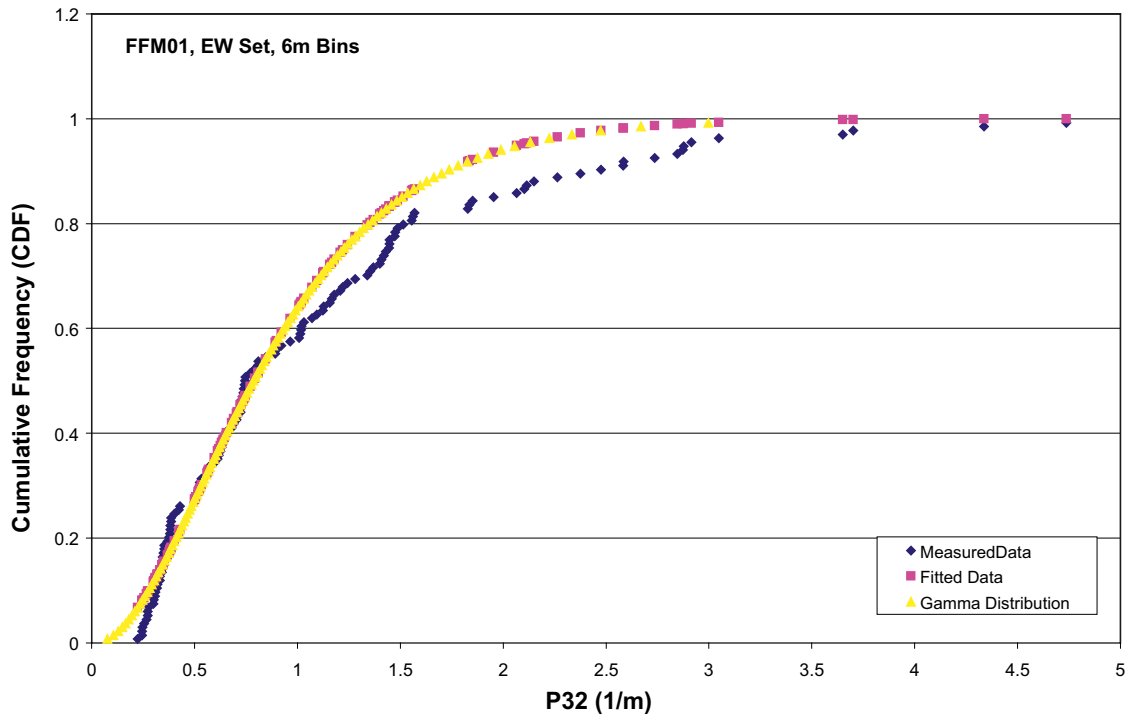
Figure 4-62. *CDF of measured P$_{32}$ data from cored boreholes against an empirical CDF of a fitted Gamma distribution, EW set, Domain FFM01.*
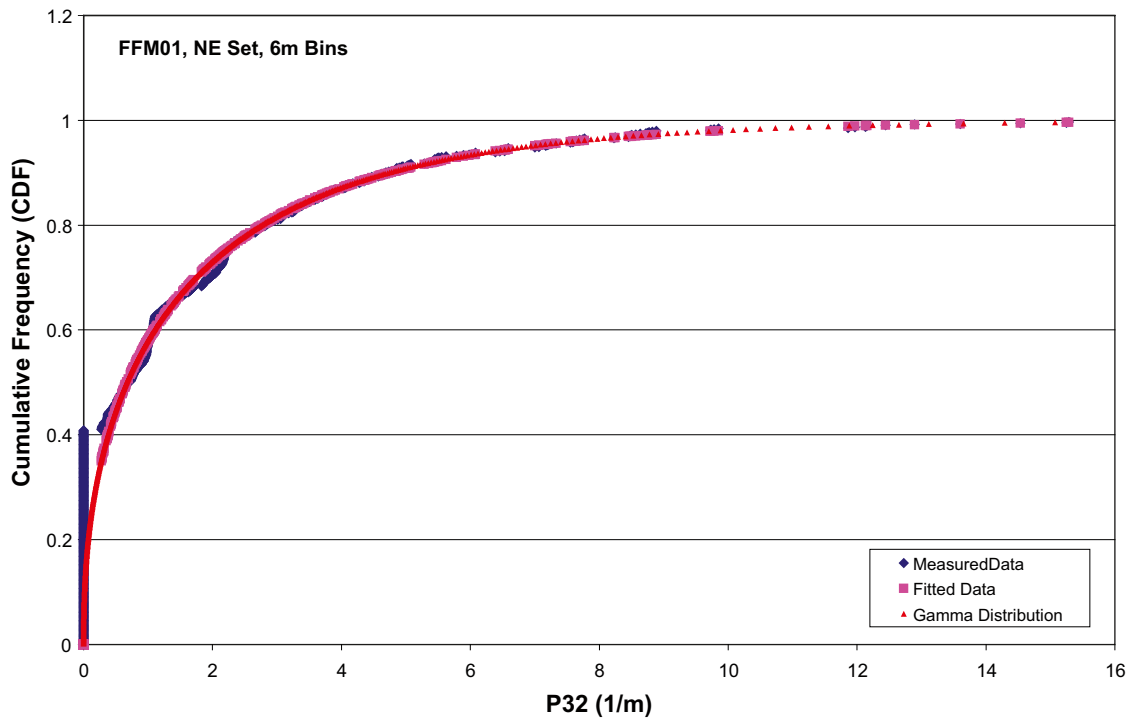
Figure 4-63. *CDF of measured P$_{32}$ data from cored boreholes against an empirical CDF of a fitted Gamma distribution, NE set, Domain FFM01.*
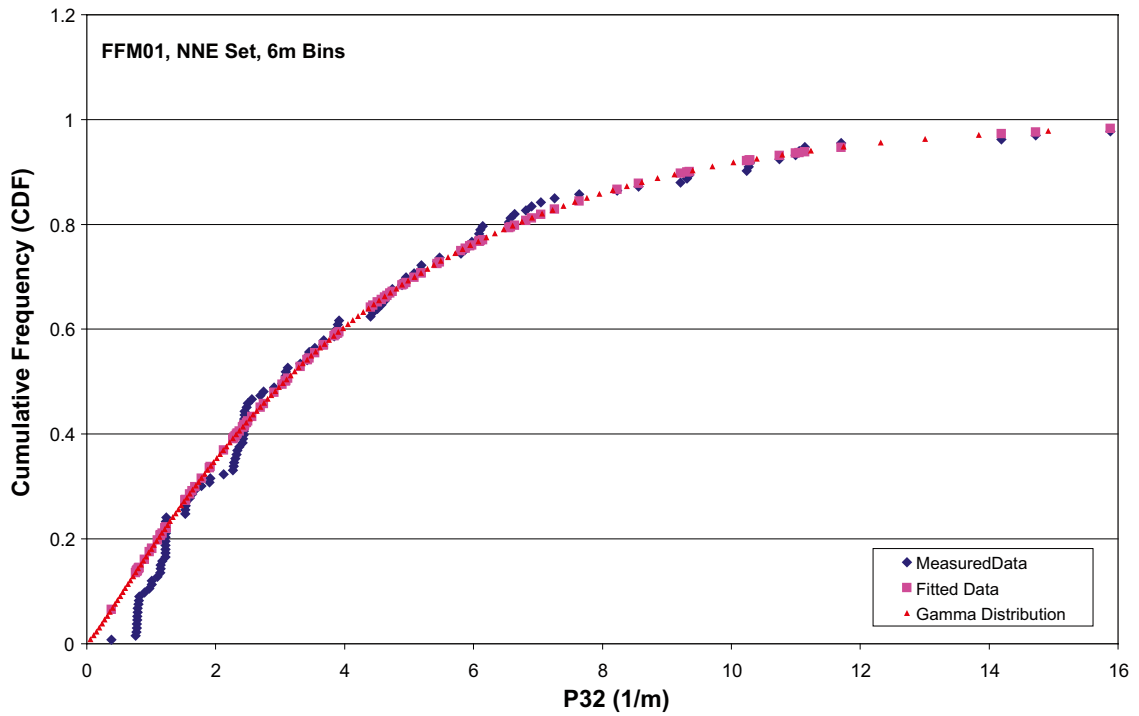
Figure 4-64. CDF of measured P$_{32}$ data from cored boreholes against an empirical CDF of a fitted Gamma distribution, NE set, Domain FFM01.
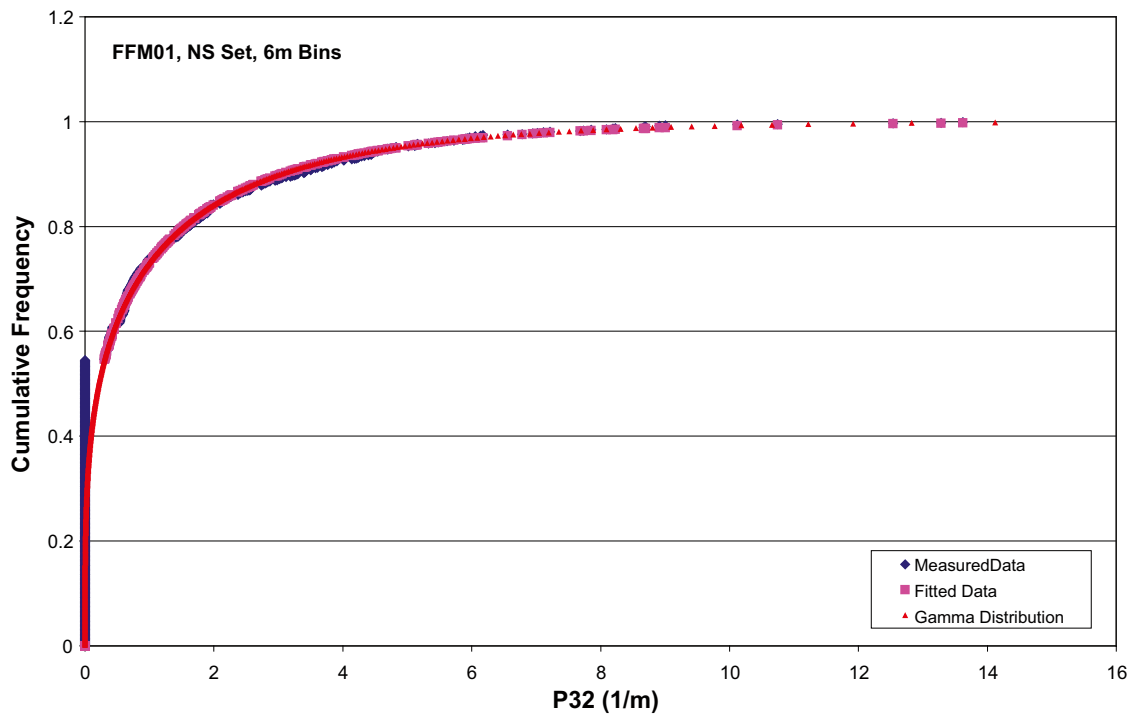
Figure 4-65. CDF of measured P$_{32}$ data from cored boreholes against an empirical CDF of a fitted Gamma distribution, NS set, Domain FFM01.
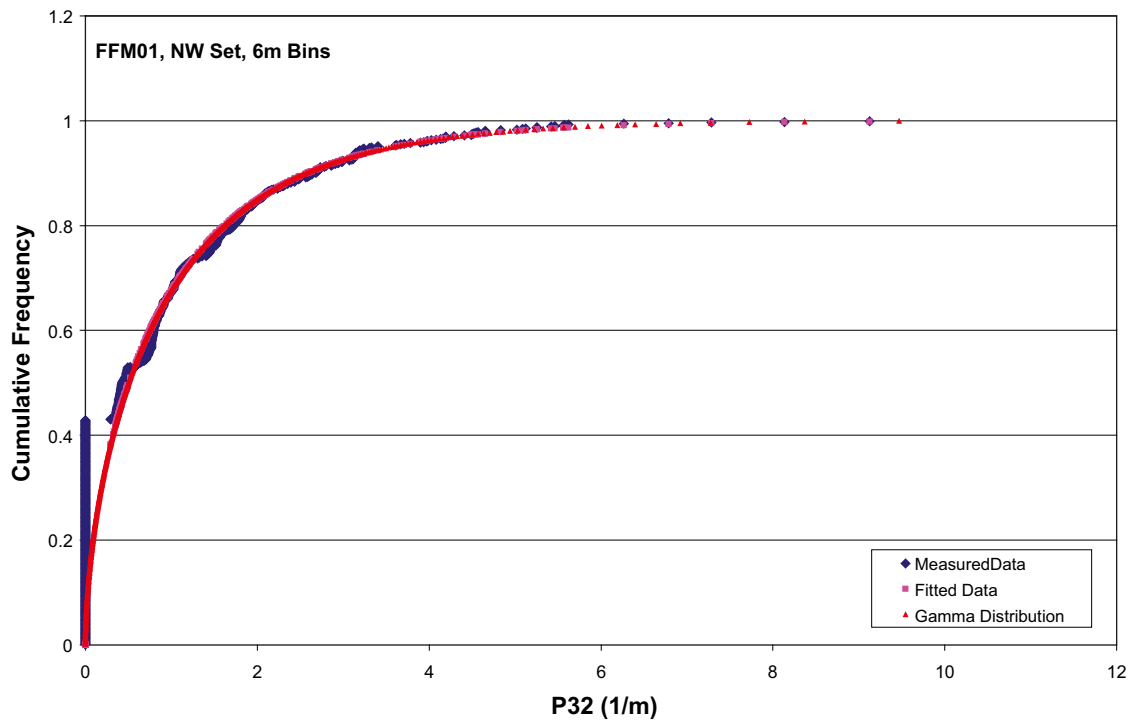
Figure 4-66. CDF of measured P_{32} data from cored boreholes against an empirical CDF of a fitted Gamma distribution, NW set, Domain FFM01.

The analysis results suggest, both graphically and statistically, that the intensity of nearly every fracture set in every fracture domain can be described as following a Gamma distribution at the scale of 30 m. At the smaller 6 m scale, fewer distributions pass the K-S goodness of fit test at $\alpha = 0.05$. It was not possible to fit a Gamma distribution to the NS fracture set in domains FFM01 or FFM02; it was also not possible to fit a Gamma distribution to the SH set in Domain FFM01 or the EW set in domain FFM02. It was possible to fit gamma distributions to all fracture sets in domains FFM03 and FFM06.

Even where the goodness of fit tests indicate that the assumption of a Gamma distribution does not pass at the 5% significance level, graphical comparison (Figure 4-60 through Figure 4-66) indicates that the gamma distribution is appropriate except for the zero-intensity intervals. These zero-intensity intervals are an artifact of analysis techniques used.

The results imply that the assumption of Poisson variability at the 6 m scale may not be appropriate, but that at scales on the order of 30 m, the assumption of a gamma distribution for intensity is a good one.

The CDF plots of the simulated Gamma distribution parameters versus the measured data illustrate graphically that, except for the large number of zero-cells, the gamma distribution is a reasonable distribution for describing fracture intensity variation in domain FFM01 for most fracture sets. Many of the fitted distributions fail to pass the goodness-of-fit test largely due to their numbers of zero-intersection segments; graphically, the fits appear quite good.

Note that the Gamma distributions presented in this chapter are referenced to the un-truncated P_{32} values from the borehole data; these data assume a fracture radius size range of 0.0385 m–~564 m. If a different size range is needed, we recommend using the following procedure:

Compute the new mean P_{32} value for the desired truncation range using :

$$P_{32}(r_{\min},r_{\max}) = \frac{[r_{\min}^{2-k_r} - r_{\max}^{2-k_r}]}{[r_0^{2-k_r} - r_1^{2-k_r}]} * P_{32}(r_0,r_1)$$
<div align="right">Equation 4-1</div>

where r_0 and r_1 are the current truncation limits and $P_{32}(r_0,r_1)$ is the fracture intensity associated with those limits, and r_{min} and r_{max} are the new truncation limits.

A rough estimate of the gamma distribution parameters can be made using the method of moments estimators /NIST 2007e/, according to the following equations:

$$\alpha = \left(\frac{\overline{x}}{s}\right)^2$$
<div align="right">Equation 4-2</div>

$$\beta = \left(\frac{s^2}{\overline{x}}\right)$$
<div align="right">Equation 4-3</div>

where $\overline{x}$ represents your target sample mean (the new mean P_{32} value) and s the standard deviation of the sample.

For a more robust estimate of the gamma distribution parameters, we recommend using a maximum-likelihood estimator for a population with an unknown variance (as the variance of the now truncated P_{32} distribution is not explicitly known). Various MLEs for the gamma distribution are described in /Evans et al. 2000/, or /Johnson et al. 1994/. The MLE should be based on the new set mean P_{32} value.

4.4.4 Variations in fracture intensity by lithology

The regression analysis and cross-tabulation results indicated that rock type could not be used to predict fracture intensity variations at the specified level of statistical significance. However, this does not imply that variations in intensity among the various rock types does not exist, nor that it might reduce the overall model uncertainty to specify intensity by rock type.

In order to evaluate how much the uncertainty might be reduced, P_{32} values as a function of rock type, fracture domain and fracture set were calculated (Table 4-97).The histograms for individual sets and all sets combined are shown in Figure 4-67 through Figure 4-75. This figure and the table show that the intensities differ by fracture domain and by rock type. Among all rock types listed, amphibolite tends to have the most consistently high fracture intensity. In terms of model parameterization, it is possible to lump all of the rock types together within a fracture domain, to model them all separately, or to combine some of the rock types. Clearly, combining amphibolite with other rock types will create higher uncertainty than estimating fracture intensity separately.

Table 4-97. P_{32} fracture intensity by rock type, fracture domain and set.

Fracturedomain Set & rock type	ALL Mean	FFM01 Mean	FFM02 Mean	FFM03 Mean	FFM06 Mean	ALL n	FFM01 n	FFM02 n	FFM03 n	FFM06 n
All by Rock Name - Amphibolite	10.210	7.249	14.716	17.043	8.083	78	49	12	14	3
All by Rock Name - Diorite, quartz diorite and gabbro, metamorphic	16.278	16.278				3	3			
All by Rock Name - Felsic to intermediate volcanic rock, metamorphic	11.722	11.722			14.596	10	8			2
All by Rock Name - Granite to granodiorite, metamorphic, medium-grained	5.262	4.594	8.642	4.821	6.135	366	245	58	56	7
All by Rock Name - Granite, fine- to medium-grained	6.535	6.641	9.889	4.808	1.827	34	20	9	4	1
All by Rock Name - Granite, granodiorite and tonalite, metamorphic, fine- to medium-grained	4.866	4.362	7.160	4.529	3.877	79	40	15	11	13
All by Rock Name - Granite, metamorphic, aplitic	6.863	5.787			4.551	36	12			24
All by Rock Name - Granodiorite, metamorphic	23.378					0				
All by Rock Name - Pegmatite, pegmatitic granite	4.877	4.489	7.036	4.384	3.697	154	100	22	23	9
All by Rock Name - Tonalite to granodiorite, metamorphic	5.825			5.825		7		7		
NW by Rock Name - Amphibolite	1.704	0.751	3.036	4.042	0.807	78	49	12	14	3
NW by Rock Name - Diorite, quartz diorite and gabbro, metamorphic	1.991	1.991				3	3			
NW by Rock Name - Felsic to intermediate volcanic rock, metamorphic	2.184	2.184			2.555	10	8			2
NW by Rock Name - Granite to granodiorite, metamorphic, medium-grained	0.971	0.816	1.588	1.030	0.798	366	245	58	56	7
NW by Rock Name - Granite, fine- to medium-grained	1.347	1.134	2.318	1.389		33	20	9	4	
NW by Rock Name - Granite, granodiorite and tonalite, metamorphic, fine- to medium-grained	1.006	1.042	0.937	0.959	0.908	79	40	15	11	13
NW by Rock Name - Granite, metamorphic, aplitic	0.911	0.805			0.798	36	12			24
NW by Rock Name - Granodiorite, metamorphic	3.352					0				
NW by Rock Name - Pegmatite, pegmatitic granite	0.819	0.751	0.932	1.009	0.878	154	100	22	23	9
NW by Rock Name - Tonalite to granodiorite, metamorphic	1.055			1.055		7		7		
NS by Rock Name - Amphibolite	2.365	0.842	3.830	6.875	1.167	78	49	12	14	3
NS by Rock Name - Diorite, quartz diorite and gabbro, metamorphic	3.267	3.267				3	3			
NS by Rock Name - Felsic to intermediate volcanic rock, metamorphic	3.538	3.538			0.818	10	8			2
NS by Rock Name - Granite to granodiorite, metamorphic, medium-grained	1.280	1.068	1.989	1.493	0.936	366	245	58	56	7
NS by Rock Name - Granite, fine- to medium-grained	1.308	0.874	3.541	1.283		33	20	9	4	
NS by Rock Name - Granite, granodiorite and tonalite, metamorphic, fine- to medium-grained	1.317	1.270	1.008	1.671	1.363	79	40	15	11	13
NS by Rock Name - Granite, metamorphic, aplitic	1.306	1.092			1.071	36	12			24
NS by Rock Name - Granodiorite, metamorphic	3.237					0				
NS by Rock Name - Pegmatite, pegmatitic granite	1.069	1.078	1.061	1.037	0.673	154	100	22	23	9

Fracturedomain Set & rock type	ALL Mean	FFM01 Mean	FFM02 Mean	FFM03 Mean	FFM06 Mean	ALL n	FFM01 n	FFM02 n	FFM03 n	FFM06 n
NS by Rock Name - Tonalite to granodiorite, metamorphic	1.050			1.050		7		7		
NE by Rock Name - Amphibolite	1.426	1.064	1.360	2.981	1.058	78	49	12	14	3
NE by Rock Name - Diorite, quartz diorite and gabbro, metamorphic	0.000	0.000				3	3			
NE by Rock Name - Felsic to intermediate volcanic rock, metamorphic	1.654	1.654			6.613	10	8			2
NE by Rock Name - Granite to granodiorite, metamorphic, medium-grained	1.033	0.966	1.067	1.284	3.848	366	245	58	56	7
NE by Rock Name - Granite, fine- to medium-grained	1.821	2.288	0.793	1.239		33	20	9	4	
NE by Rock Name - Granite, granodiorite and tonalite, metamorphic, fine- to medium-grained	1.086	1.003	0.911	1.436	1.491	79	40	15	11	13
NE by Rock Name - Granite, metamorphic, aplitic	2.066	1.906			1.774	36	12			24
NE by Rock Name - Granodiorite, metamorphic	8.411					0				
NE by Rock Name - Pegmatite, pegmatitic granite	0.819	0.795	0.624	1.133	1.878	154	100	22	23	9
NE by Rock Name - Tonalite to granodiorite, metamorphic	3.032			3.032		7		7		
SH_T by Rock Name - Amphibolite	3.747	3.597	4.791	3.144	5.051	78	49	12	14	3
SH_T by Rock Name - Diorite, quartz diorite and gabbro, metamorphic	3.783	3.783				3	3			
SH_T by Rock Name - Felsic to intermediate volcanic rock, metamorphic	3.939	3.939			4.610	10	8			2
SH_T by Rock Name - Granite to granodiorite, metamorphic, medium-grained	1.188	0.898	2.680	0.975	0.522	366	245	58	56	7
SH_T by Rock Name - Granite, fine- to medium-grained	1.099	1.106	1.520	0.898		33	20	9	4	
SH_T by Rock Name - Granite, granodiorite and tonalite, metamorphic, fine- to medium-grained	1.200	0.727	3.922	0.463	0.114	79	40	15	11	13
SH_T by Rock Name - Granite, metamorphic, aplitic	1.822	1.331			0.819	36	12			24
SH_T by Rock Name - Granodiorite, metamorphic	1.092					0				
SH_T by Rock Name - Pegmatite, pegmatitic granite	1.362	0.963	3.248	1.205	0.268	154	100	22	23	9
SH_T by Rock Name - Tonalite to granodiorite, metamorphic	0.689			0.689		7		7		
NNW by Rock Name - Amphibolite	0.080	0.000	0.430	0.000		75	49	12	14	
NNW by Rock Name - Diorite, quartz diorite and gabbro, metamorphic	0.000	0.000				3	3			
NNW by Rock Name - Felsic to intermediate volcanic rock, metamorphic	0.000	0.000				8	8			
NNW by Rock Name - Granite to granodiorite, metamorphic, medium-grained	0.026	0.003	0.154	0.000		359	245	58	56	
NNW by Rock Name - Granite, fine- to medium-grained	0.000	0.000	0.000	0.000		33	20	9	4	
NNW by Rock Name - Granite, granodiorite and tonalite, metamorphic, fine- to medium-grained	0.010	0.000	0.061	0.000		66	40	15	11	
NNW by Rock Name - Granite, metamorphic, aplitic	0.000	0.000				12	12			
NNW by Rock Name - Granodiorite, metamorphic	0.000					0				
NNW by Rock Name - Pegmatite, pegmatitic granite	0.041	0.000	0.260	0.000		145	100	22	23	
NNW by Rock Name - Tonalite to granodiorite, metamorphic	0.000			0.000		7		7		
ENE by Rock Name - Amphibolite	0.565	0.502	1.269	0.000	0.000	78	49	12	14	3

Fracturedomain Set & rock type	ALL Mean	FFM01 Mean	FFM02 Mean	FFM03 Mean	FFM06 Mean	ALL n	FFM01 n	FFM02 n	FFM03 n	FFM06 n
ENE by Rock Name - Diorite, quartz diorite and gabbro, metamorphic	0.000	0.000				3	3			
ENE by Rock Name - Felsic to intermediate volcanic rock, metamorphic	0.000	0.000			0.000	10	8			2
ENE by Rock Name - Granite to granodiorite, metamorphic, medium-grained	0.441	0.415	0.988	0.021	0.031	366	245	58	56	7
ENE by Rock Name - Granite, fine- to medium-grained	0.816	1.002	1.718	0.000		33	20	9	4	
ENE by Rock Name - Granite, granodiorite and tonalite, metamorphic, fine- to medium-grained	0.172	0.220	0.234	0.000	0.000	79	40	15	11	13
ENE by Rock Name - Granite, metamorphic, aplitic	0.157	0.000			0.089	36	12			24
ENE by Rock Name - Granodiorite, metamorphic	6.017					0				
ENE by Rock Name - Pegmatite, pegmatitic granite	0.327	0.299	0.760	0.000	0.000	154	100	22	23	9
ENE by Rock Name - Tonalite to granodiorite, metamorphic	0.000			0.000		7		7		
NNE by Rock Name - Amphibolite	0.007	0.011	0.000	0.000		75	49	12	14	
NNE by Rock Name - Diorite, quartz diorite and gabbro, metamorphic	5.432	5.432				3	3			
NNE by Rock Name - Felsic to intermediate volcanic rock, metamorphic	0.169	0.169				8	8			
NNE by Rock Name - Granite to granodiorite, metamorphic, medium-grained	0.116	0.170	0.000	0.003		359	245	58	56	
NNE by Rock Name - Granite, fine- to medium-grained	0.000	0.000	0.000	0.000		33	20	9	4	
NNE by Rock Name - Granite, granodiorite and tonalite, metamorphic, fine- to medium-grained	0.000	0.000	0.000	0.000		66	40	15	11	
NNE by Rock Name - Granite, metamorphic, aplitic	0.154	0.167				12	12			
NNE by Rock Name - Granodiorite, metamorphic	0.000					0				
NNE by Rock Name - Pegmatite, pegmatitic granite	0.187	0.271	0.000	0.000		145	100	22	23	
NNE by Rock Name - Tonalite to granodiorite, metamorphic	0.000			0.000		7		7		
EW by Rock Name - Amphibolite	0.315	0.482	0.000	0.000		75	49	12	14	
EW by Rock Name - Diorite, quartz diorite and gabbro, metamorphic	1.805	1.805				3	3			
EW by Rock Name - Felsic to intermediate volcanic rock, metamorphic	0.237	0.237				8	8			
EW by Rock Name - Granite to granodiorite, metamorphic, medium-grained	0.206	0.258	0.176	0.014		359	245	58	56	
EW by Rock Name - Granite, fine- to medium-grained	0.143	0.236	0.000	0.000		33	20	9	4	
EW by Rock Name - Granite, granodiorite and tonalite, metamorphic, fine- to medium-grained	0.074	0.099	0.086	0.000		66	40	15	11	
EW by Rock Name - Granite, metamorphic, aplitic	0.447	0.485				12	12			
EW by Rock Name - Granodiorite, metamorphic	1.270					0				
EW by Rock Name - Pegmatite, pegmatitic granite	0.253	0.332	0.149	0.000		145	100	22	23	
EW by Rock Name - Tonalite to granodiorite, metamorphic	0.000			0.000		7		7		
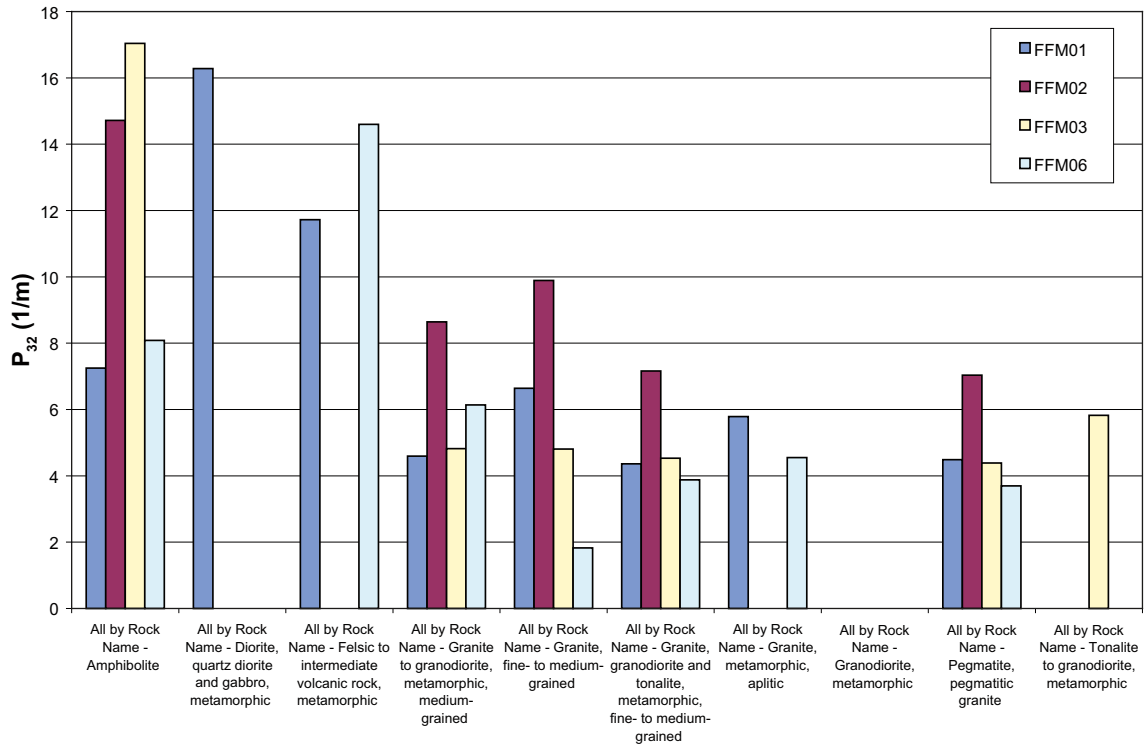
Figure 4-67. P_{32}, all sets combined, as a function of lithology and domain.
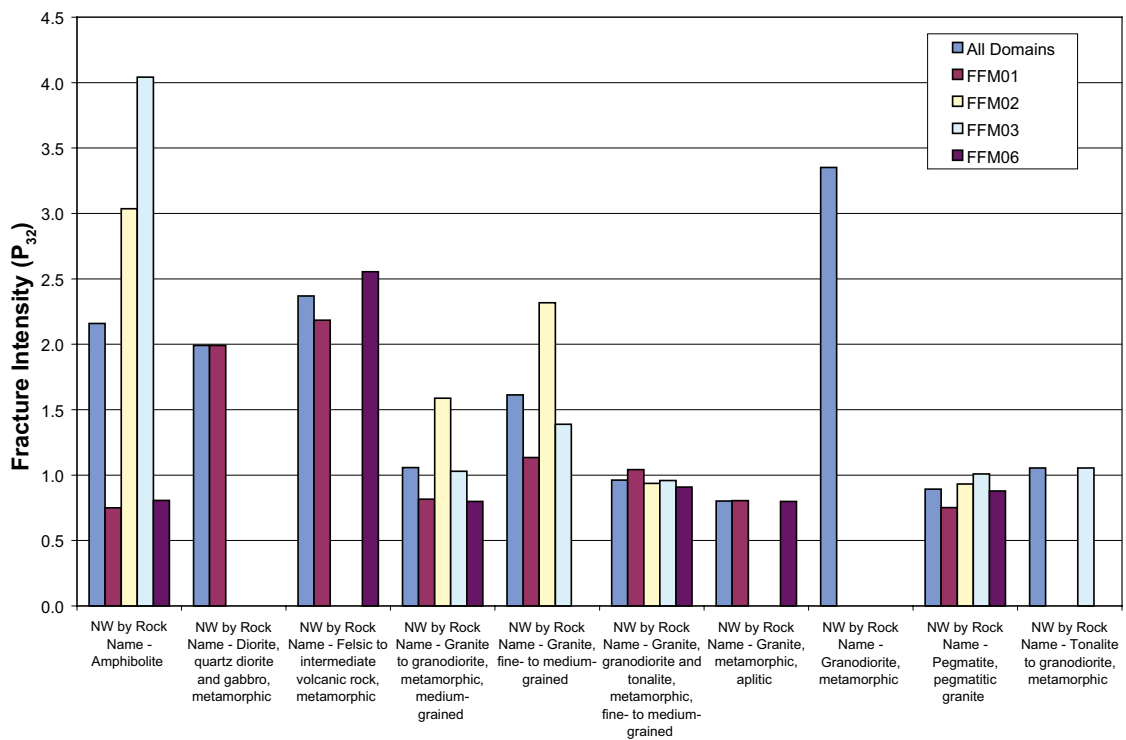
Figure 4-68. P_{32} of NW Set as a function of lithology and domain.
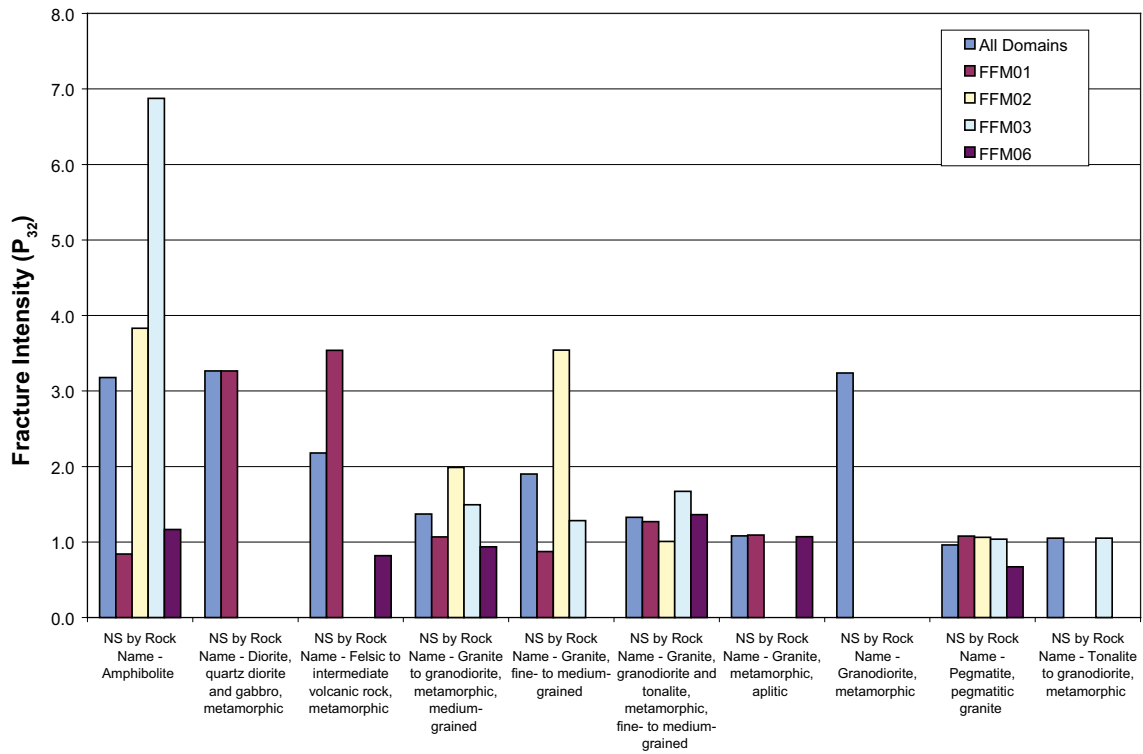
Figure 4-69. P_{32} of NS Set as a function of lithology and fracture domain.
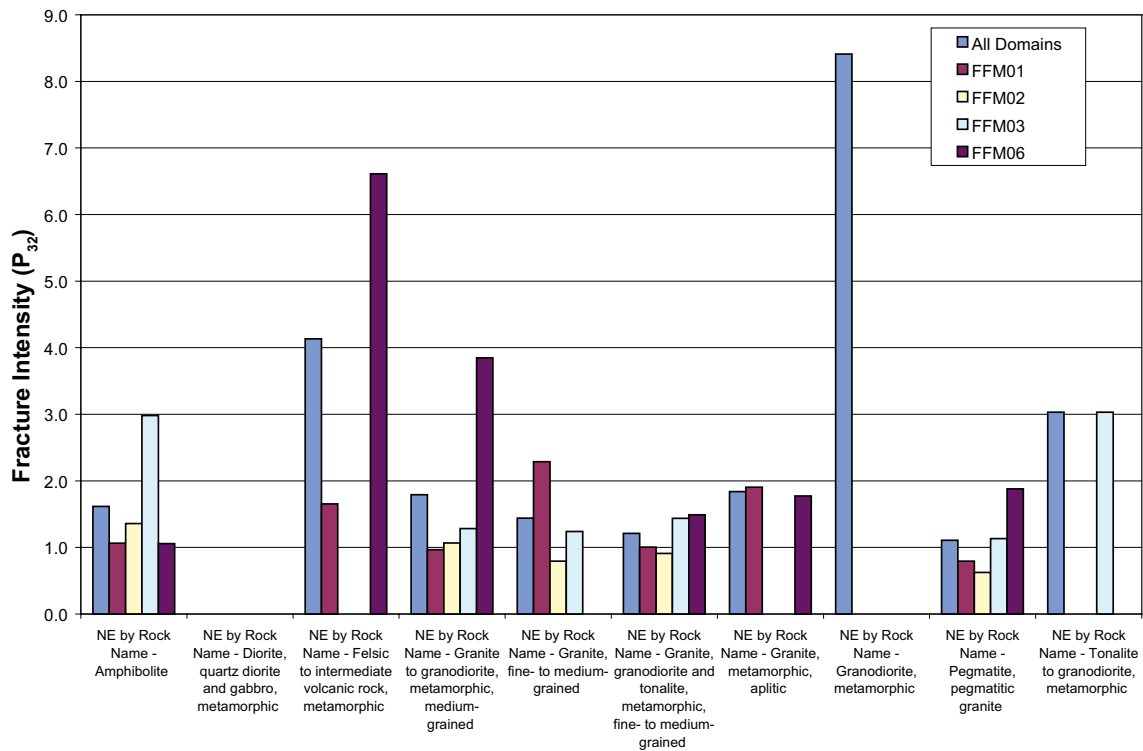
Figure 4-70. P_{32} of NE Set as a function of lithology and fracture domain.
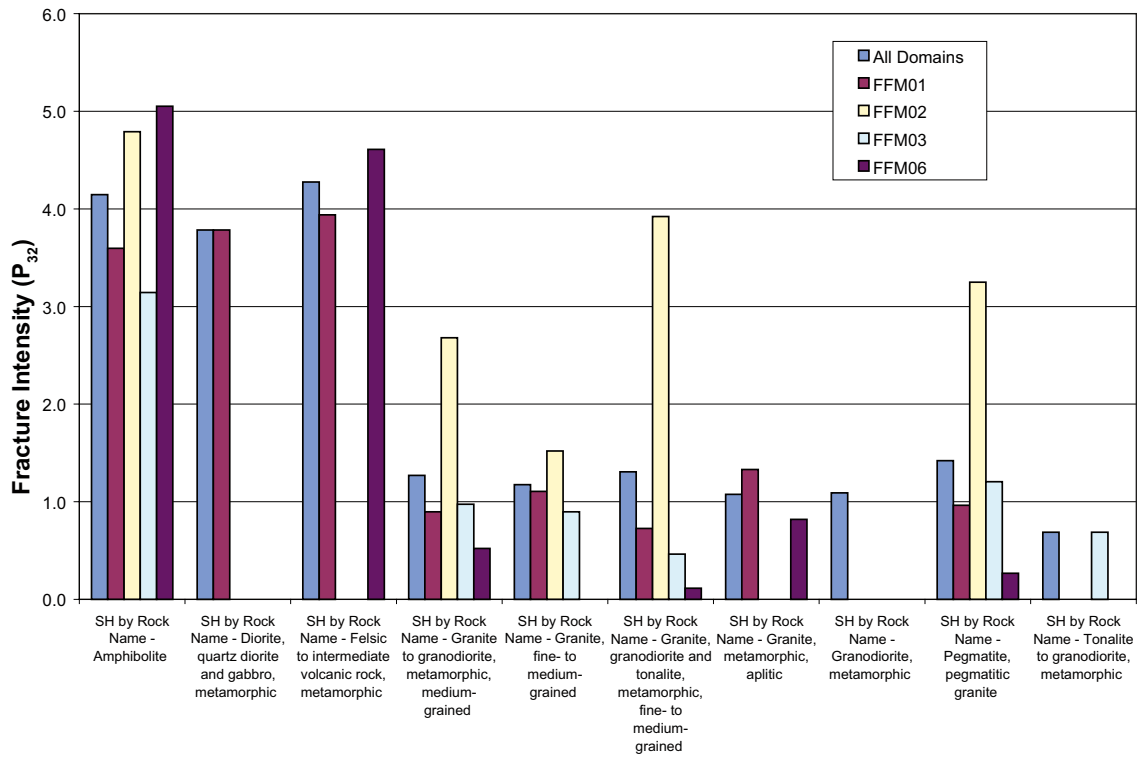
Figure 4-71. *P₃₂ of SH Set as a function of lithology and fracture domain.*
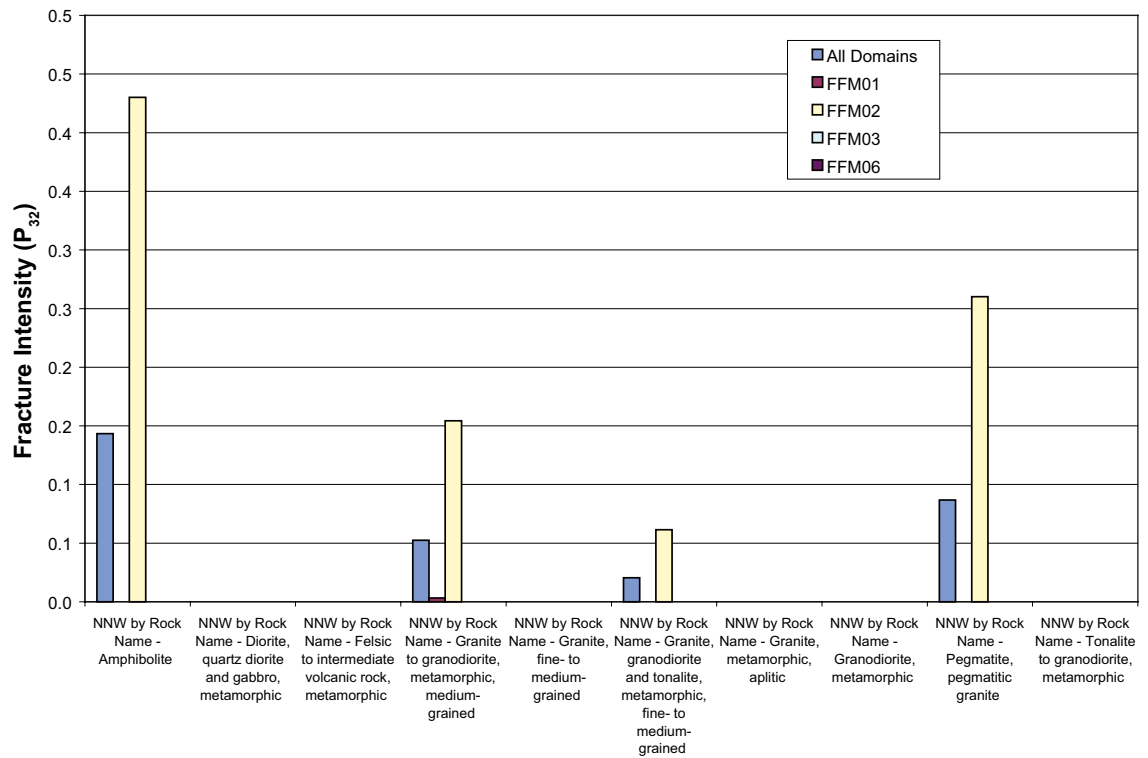
Figure 4-72. *P₃₂ of NNW Set as a function of lithology and fracture domain.*
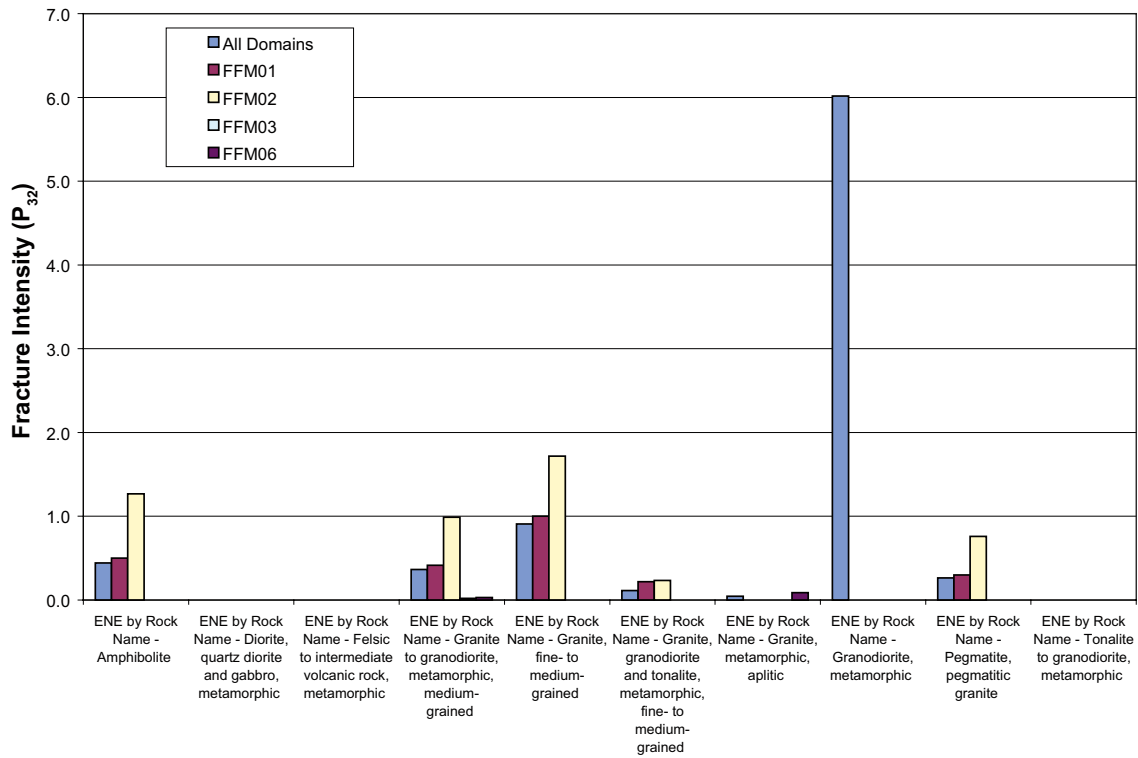
Figure 4-73. P_{32} *of ENE Set as a function of lithology and fracture domain.*
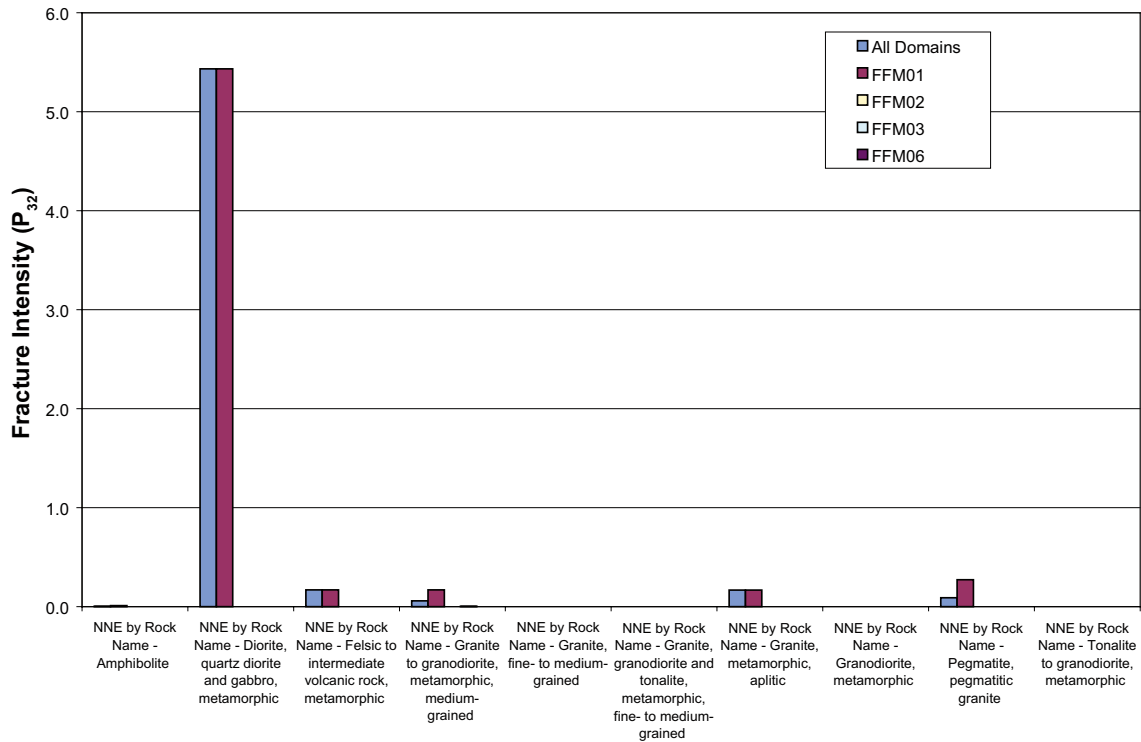
Figure 4-74. P_{32} *of NNE Set as a function of lithology and fracture domain.*

200
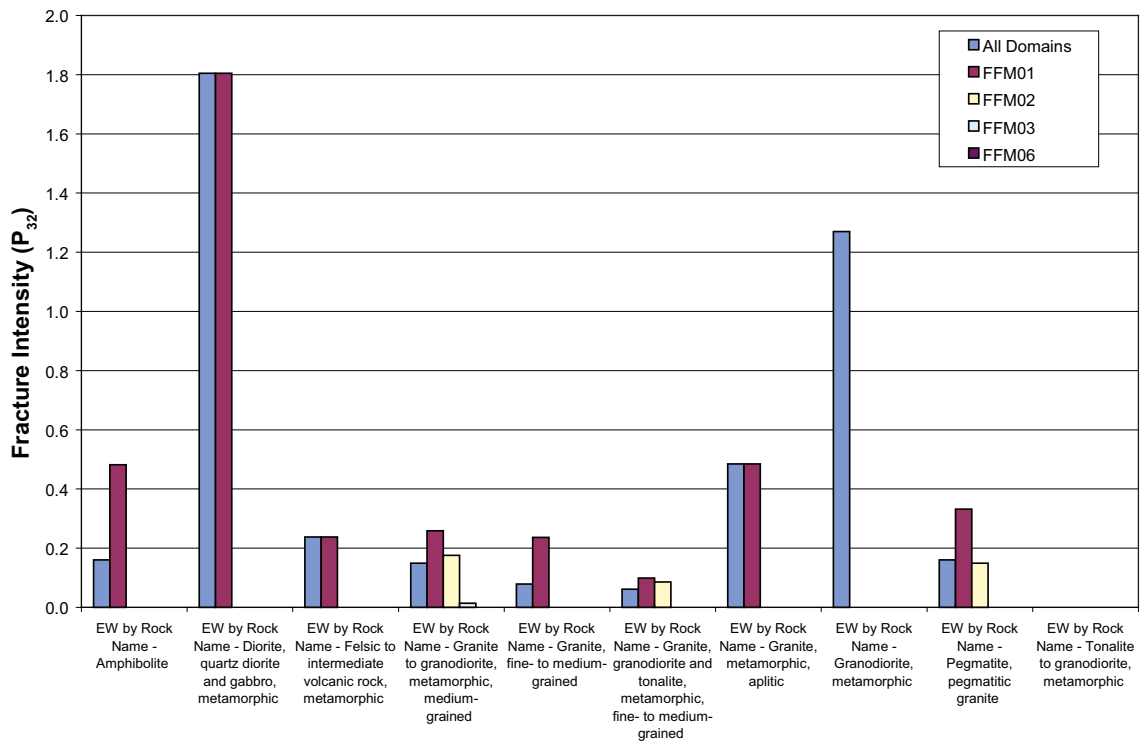
Figure 4-75. *P_{32} of EW Set as a function of lithology and fracture domain.*

Adjusting fracture intensity based on lithology

Methodology

Qualitative observation of fracturing in boreholes and outcrops suggests that fracture intensity varies among the various rock types with the proposed repository footprint. The coupled size/intensity models developed from outcrop traces and boreholes, and possibly including ground magnetic lineaments and deformation zone traces for the alternative models, are based on fracture data from many different lithologies present in each fracture domain. As a result, the coupled size/intensity models for each set are an "average" mode for each set in the domain. To account for variations among lithologies, the variation among the major rock types vs. the average intensity of the coupled size/intensity model was evaluated and quantified.

The first step was to summarize the average intensity (P_{32}) for the 6 m bins for each set and fracture domain. The way in which the average value was calculated differs for global and local sets. Global sets are presumed to occur everywhere throughout the fracture domain. If they are not found over an interval, then that interval is assigned an intensity value of 0.0. Unfractured or 0.0-intensity valued intervals are used in computing the average intensity. Local sets, in contrast, are not presumed to occur everywhere. Thus, an interval that does not contain a particular local set in that fracture domain is eliminated from the computation, rather than given a 0.0 value. Generation of the local sets is a two-step process rather than a one-step process, which is the case for the global sets. For local sets, the first step consists of deciding whether the local set exists in a particular volume of rock. If it is concluded that the local sets exists, then the intensity pertaining to that set is used to realize the set over the volume of interest.

The second step was to calculate the average intensity of each set as a function of lithology and fracture domain. This was done by selecting all portions of the boreholes that were unaffected by deformation zones. The mean value for each set was calculated by correcting the lineal fracture intensity (P_{10}) using Wang's method /Wang 2005/ to produce a volumetric fracture intensity (P_{32}). Since only fractures visible in BIPS could be reliably assigned to sets, the P_{10} values and the P_{32} values derived from them pertain only to the intensity of fractures visible in

201

BIPS. The intensity was then adjusted for this factor on a borehole by borehole basis, so that the final intensity for each set was compensated for borehole orientation as well as BIPS visibility.

The resulting mean intensity for each lithology group was divided by the mean intensity for all groups, to produce a lithology adjustment factor for each set, rock type and fracture domain. These factors can be used to adjust the intensity predicted using the "average" coupled size/intensity model for lithology.

Results

Table 4-98 shows the average values calculated from the 6 m bins as a function of fracture domain and set. In this table, sets that are global within a particular fracture domain are shaded in yellow; local sets are un-shaded. The blank cells in the local sets results from the case when no fractures of that set were found in the 6 m bin data.The deviation factors are shown in Table 4-99. The process for making the lithology adjustment can be illustrated with the following example.

- The OSM intensity model for the NE global fracture domain FFM02 specifies a mean P_{32} intensity of 1.14 m^2/m^3 in the size range of 0.5 m to 564 m. To adjust for lithology, the factors in Table 4-99 are used. For example, the adjustment factor for Amphibolite is 0.26. To adjust the average intensity for this rock type, the value of 1.14 m^2/m^3 would be multiplied by 0.26, to give the value of 0.296 m^2/m^3.to be used for simulating NE global set fractures, in domain FFM02, in volumes of rock identified as Amphibolite.

An adjustment factor value of 0.0 for a global set means that this set was not found in the data for this rock type outside of deformation zones or portions of the rock suspected of being affected by deformation zones. Thus, the data suggests that this global set is not present, or is only present with very low intensity, in this rock type. For the local sets, two additional designations occur: NFO and NBD. NFO implies that No Fracturing was Observed for this particular lithology and fracture domain, although the fracture set was present in other lithologies in the fracture domain. These may be taken as the equivalent of 0.0 values for the global sets. NBD means that this particular set was not observed in 6 m bins for the lithology and fracture domain. This is slightly different than the NFO designation, because it means that, although this fracture set might exist in the lithology, there were no contiguous intervals of this lithology of size 6 m that contained the set. In some cases, this is because the fracture set does not exist, while in others, it is because none of the fractured intervals covered an entire 6 m interval of borehole data. We recommend that cells with this designation be treated similarly to those designated by NFO, i.e. equivalent to 0.0.

Table 4-98. Average P_{32} values based on 6 m bins.

Domain	ENE Set	EW Set	NE Set	NNE Set	NNW Set	NS Set	NW Set	SH Set	SH2 Set	SH3 Set
FFM01	2.74	1.12	1.73	4.39		1.29	0.95	0.63	0.92	0.84
FFM02	3.65	1.19	3.31		2.00	1.61	2.12	2.78		
FFM03		0.44	2.91			1.49	1.46	0.96		
FFM06	0.98		3.30			2.15	1.61	0.64	1.03	

Table 4-99. P$_{32}$ intensity adjustment factors as a function of fracture domain, rock type and set.

ENE Set	EW Set	NE Set	NNE Set	NNW Set	NS Set	NW Set	SH Set	SH2 Set	SH3 Set	Domain	Rock Type
NFO	NFO	1.72	NFO	NFO	0.32	2.89	2.15	NFO	NFO	FFM01	Amphibolite Average
NFO	NFO	0.14	NFO	NFO	0.43	0.27	1.34	NFO	NFO	FFM01	Calc-silicate rock (skarn) Average
NFO	NFO	0.23	NFO	NFO	0.20	0.00	0.38	NFO	NFO	FFM01	Diorite_ quartz diorite and gabbro_ metamorphic Average
NFO	NFO	0.00	NFO	NFO	0.79	0.00	0.00	NFO	NFO	FFM01	Felsic to intermediate volcanic rock_ metamorphic Average
1.77	2.17	1.22	NFO	NFO	0.66	1.37	1.92	NFO	NFO	FFM01	Granite to granodiorite_ metamorphic_ medium-grained Average
NFO	1.69	1.44	NFO	NFO	0.52	0.25	0.53	NFO	NFO	FFM01	Granite_ fine- to medium-grained Average
0.33	1.12	1.38	NFO	NFO	0.42	1.01	0.49	NFO	NFO	FFM01	Granite_ granodiorite and tonalite_ metamorphic_ fine-medium grained Average
0.45	NFO	0.86	NFO	NFO	0.62	2.07	0.70	NFO	NFO	FFM01	Granite_ metamorphic_ aplitic Average
NFO	NFO	1.28	NFO	NFO	0.00	0.00	5.48	NFO	NFO	FFM01	Granodiorite_ metamorphic Average
1.36	2.35	0.88	1.11	NFO	0.64	1.07	2.69	1.94	NFO	FFM01	Pegmatite_ pegmatitic granite Average
1.20	0.00	0.26	NFO	NFO	0.17	0.07	0.27	NFO	NFO	FFM02	Amphibolite Average
0.36	0.17	0.49	NBD	1.52	0.24	0.36	0.46	NBD	NBD	FFM02	Granite to granodiorite_ metamorphic_ medium-grained Average
0.00	0.00	2.05	NBD	NFO	0.00	0.59	0.00	NBD	NFO	FFM02	Granite_ fine- to medium-grained Average
0.00	0.00	1.99	NBD	NFO	0.00	0.96	0.00	NBD	NFO	FFM02	Granite_ granodiorite and tonalite_ metamorphic_ fine-medium grained Average
0.00	0.02	1.08	NBD	NFO	0.10	0.87	0.15	NBD	NFO	FFM02	Pegmatite_ pegmatitic granite Average
NFO	1.74	0.94	NFO	NFO	1.48	0.16	1.03	NFO	NFO	FFM03	Amphibolite Average
NFO	0.87	0.72	NBD	NFO	1.39	0.78	0.60	NBD	NBD	FFM03	Granite to granodiorite_ metamorphic_ medium-grained Average
NFO	0.00	0.04	NBD	NFO	1.15	0.05	0.00	NBD	NBD	FFM03	Granite_ fine- to medium-grained Average
NFO	0.00	0.16	NBD	NFO	3.69	0.32	0.00	NBD	NBD	FFM03	Granite_ granodiorite and tonalite_ metamorphic_ fine-medium grained Average
NBD	0.00	0.92	NBD	NFO	0.82	1.12	0.62	NBD	NBD	FFM03	Pegmatite_ pegmatitic granite Average
NBD	0.00	0.70	NFO	NFO	0.00	0.67	1.15	NFO	NFO	FFM03	Tonalite to granodiorite_ metamorphic Average
2.28	NFO	0.41	NFO	NFO	0.00	1.47	0.61	NFO	NFO	FFM06	Amphibolite Average
NFO	NFO	0.00	NFO	NFO	0.00	0.00	0.00	NFO	NFO	FFM06	Felsic to intermediate volcanic rock_ metamorphic Average
1.28		0.08	NFO	NFO	0.19	0.30	0.18	NFO	NFO	FFM06	Granite to granodiorite_ metamorphic_ medium-grained Average
NFO	NBD	1.17	NFO	NFO	0.60	0.78	1.32	NFO	NFO	FFM06	Granite_ granodiorite and tonalite_ metamorphic_ fine-medium grained Average
NFO	NBD	0.69	NFO	NFO	1.44	1.20	3.88	NFO	NFO	FFM06	Granite_ metamorphic_ aplitic Average
NFO	NBD	0.31	NFO	NFO	0.35	0.04	0.82	NFO	NFO	FFM06	Pegmatite_ pegmatitic granite Average

Notes: NFO = No fractures of this local set were found for this lithology and fracture domain

NBD = No of this local set were found in 6m bins for this lithology and fracture domain in the data.

Global sets are shaded yellow

A value of 0.0 for a global set means that no data for this global set were found for this lithology and fracture domain

4.4.5 Fracture intensity as a function of depth

Although the evidence suggests /La Pointe et al. 2005/ that the global sets, including the subhorizontal set, are quite old, it is not unreasonable to hypothesize that the most recent glacial cycle could have enhanced or created new fractures parallel to the free surface as the weight of the ice was removed as the glaciers melted and retreated. /Stephansson and Ericcson 1975, Carlsson 1979/, and others have noted the existence of horizontal fractures near the surface in the gneissic bedrock in north-eastern Uppland that have wide apertures and are filled with unconsolidated sediments and rock fragments, while those further down do not have these characteristics. If this model for fracture intensity is correct, then there should be a zone extending down to some depth in which fracture intensity is greater and continuously decreases with depth until it reaches some characteristic value of the rock mass that is not affected by the stress relief. The change in intensity should be most evident in the intensity of subhorizontal fractures and less evident in the vertical fractures.

A series of plots (Figure 4-76 through Figure 4-79) describing how the unfractured intervals at Forsmark behave were created to visually evaluate possible trends in fracture intensity with depth below the surface. These plots show several characteristics:

1. There are zones in each fracture domain with higher and lower values of fracture intensity, whether expressed as the intensity of all fractures or only of open fractures;

2. The intensity does not show any obvious systematic trend with depth. There does appear to be, in a few cases, higher intensities within a few tens of meters of the surface, and lower intensities, particularly in FFM01 at depths below about 750 m; and

3. The zonation of high and low intensity differs among sets within a fracture domain, and also among fracture domains.
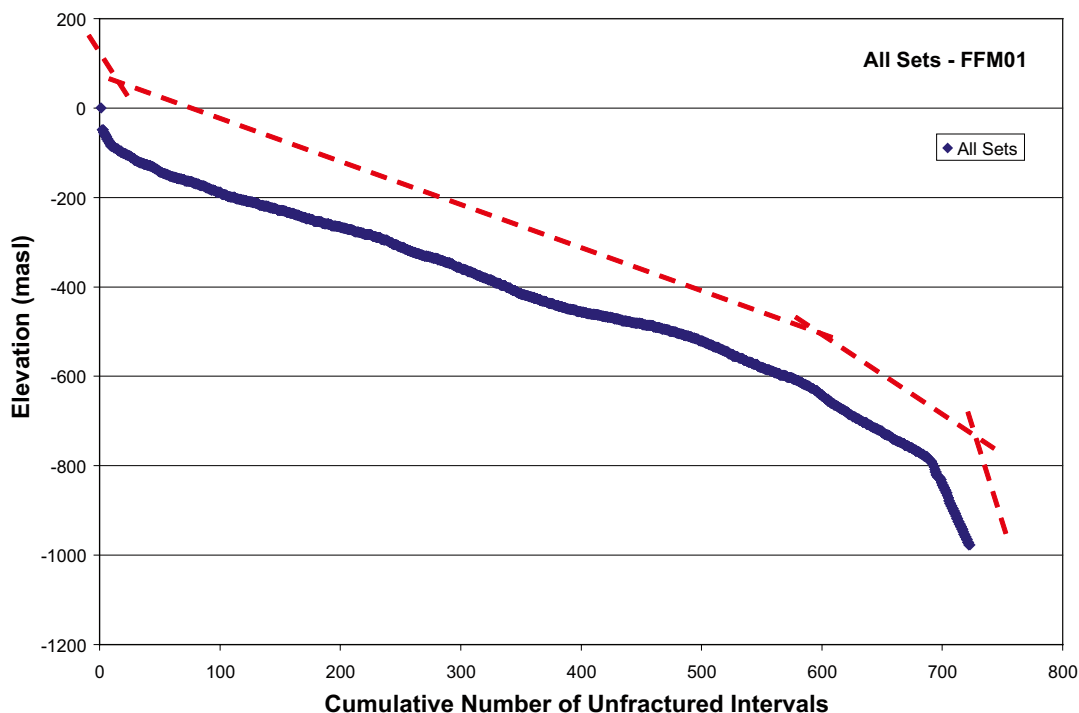
Figure 4-76. *Cumulative frequency plot of unfractured sections (zero-intervals) in FFM01.*
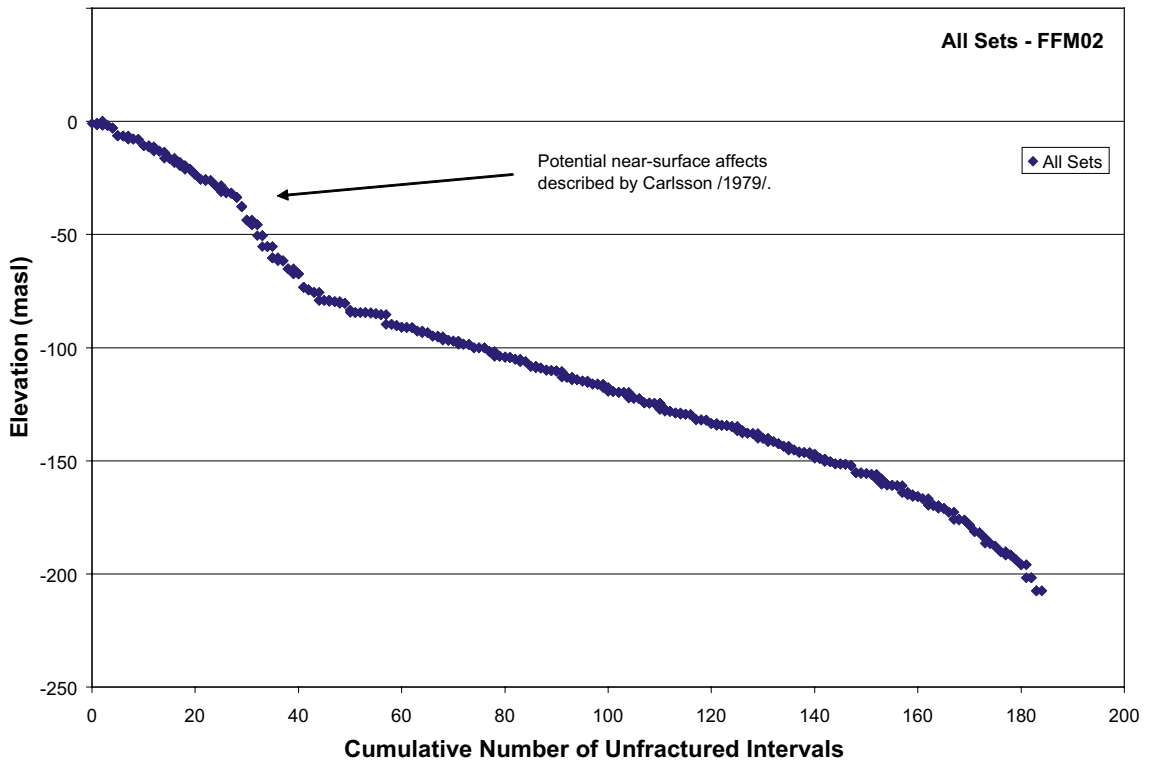
Figure 4-77. Cumulative frequency plot of unfractured sections (zero-intervals) in FFM02.
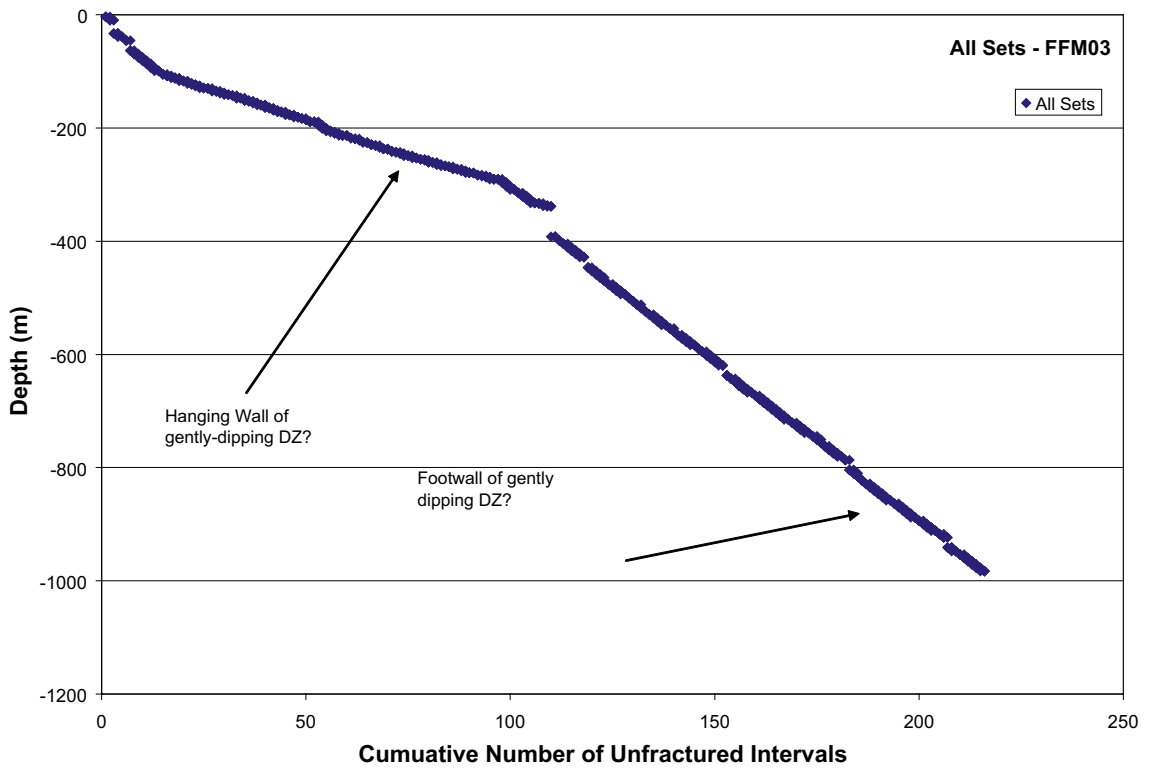
Figure 4-78. Cumulative frequency plot of unfractured sections (zero-intervals) in FFM03.
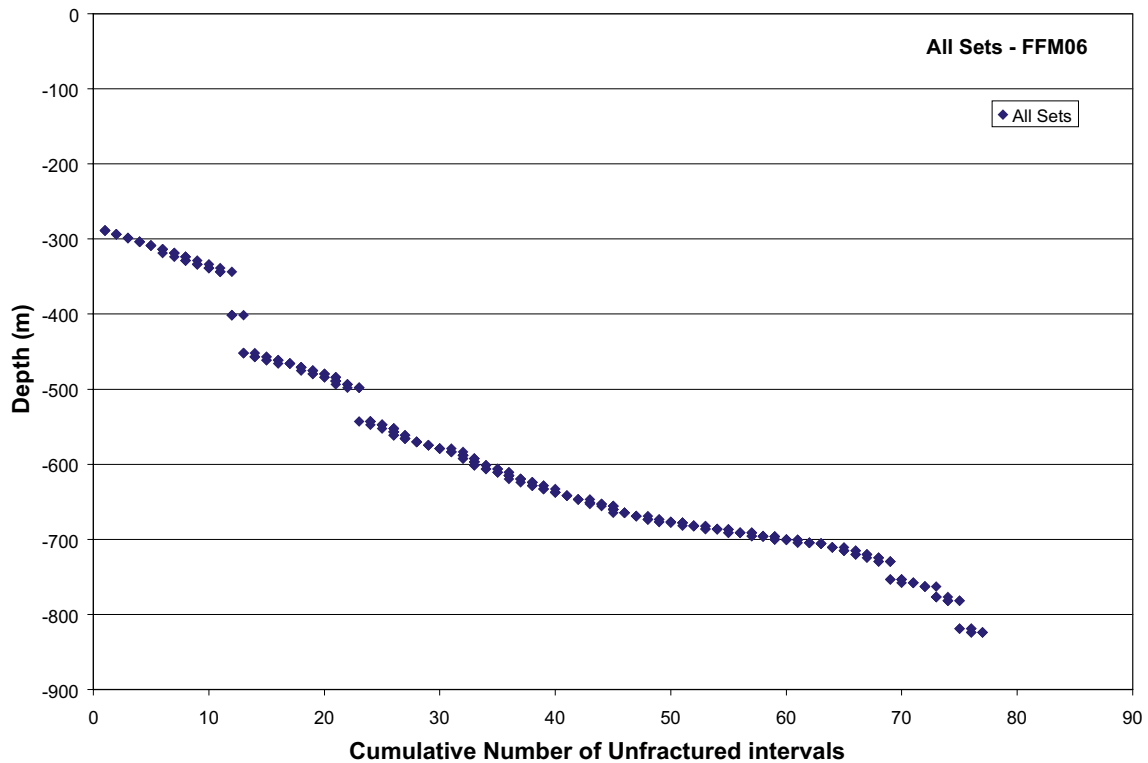
Figure 4-79. *Cumulative frequency plot of unfractured sections (zero-intervals) in FFM06.*

Figure 4-80 shows the percentage of 6 m intervals in FFM01 at a given depth that contain no fractures. If the percentage of unfractured rock increased with depth in a systematic way, there would be no vertical spread on the points for a given percentage on the x-axis, and the percentage would increase systematically with depth. The figure clearly shows that this is not the case.

Plots of borehole fracture intensity (P_{32}) as a function of fracture domain, fracture set, and depth are presented in Appendix E. These plots also indicate little to no regular patterns to overall fracture intensity as a function of depth, provided that non-fractured sections (zero-intervals) are taken into account. Within a given domain, some fracture sets may increase or decrease with depth slightly, but not in a globally predictable manner.

In other words, there are no strong trends of fracture intensity with depth, nor are the zones of higher and lower fracture intensity correlative across fracture domains. As such, we have not recommended a specific correction for fracture intensity as a function of depth below the ground surface.

4.4.6 Evaluation of uncertainties

The following uncertainties have been identified:

*   Fracture Intensity from Borehole Data: The size and intensity models are built upon the assumption that Wang's analytical solution for P_{32} as a function of P10 is an appropriate one. The Wang solution is only valid for Univariate Fisher distributions and line sampling; if either of these conditions is not met, then there can be significant uncertainty in the borehole intensity measurements.

All Sets-All Fractures FFM01
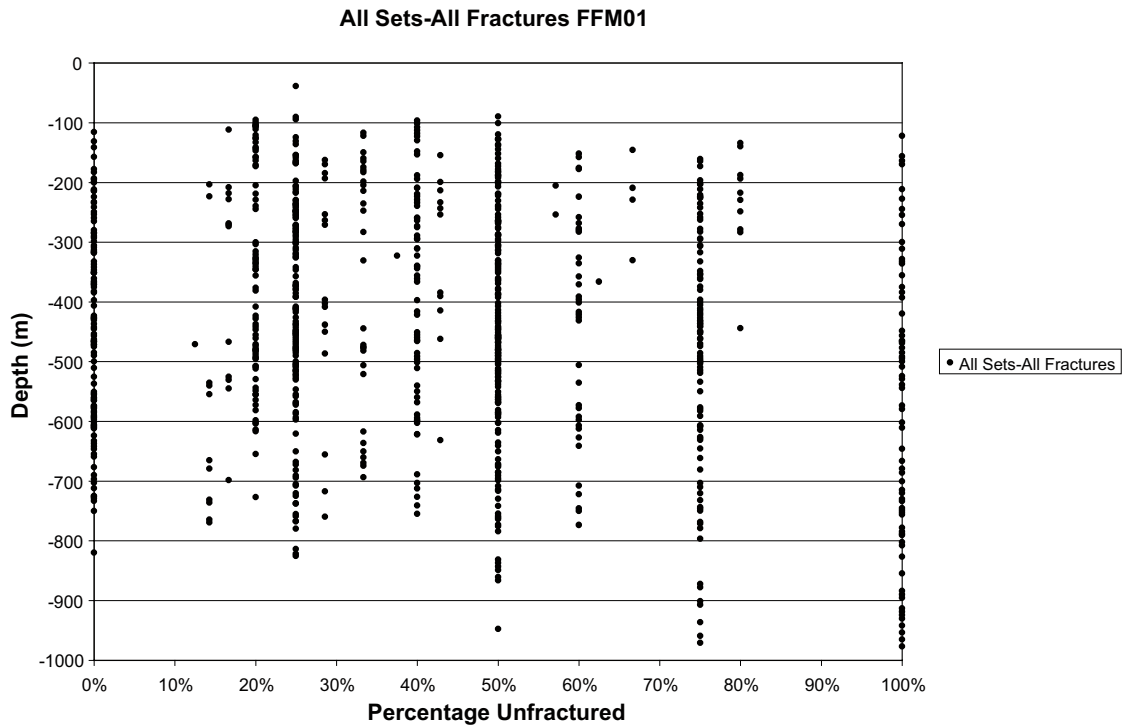
Figure 4-80. *Percentage of 6 m intervals at a given depth that contain no fractures, FFM01.*

4.4.7   Recommendations for parameterization of the intensity model

The aforementioned analyses suggest that the intensity models for the Forsmark geological DFN be simulated in accordance with the following recommendations:

1. Lithology. While lithology cannot be used to predict fracture intensity, fracture intensity does vary significantly by lithology. The intensities calculated for each set, rock type and fracture domain should be used, rather than combining the intensities for all sets or all rock types.

2. We recommend that the DFN model volume be first simulated, by fracture domain and fracture set, using the statistical model build for fractures labeled 'Not Affected by DZ'. Next, the zones labeled 'Affected by DZ' should be populated with additional fractures, using the same size and orientation models, up to the mean (or median) fracture intensities described in Chapter 4.4.1 for the 'Affected by DZ' zones. We recommend that the lateral extents and geometries of these zones be fully described by the geological modeling teams at SKB and SGU that originally postulated their extent prior to model construction.

5 Uncertainty analyses

5.1 Identification of uncertainties in the GeoDFN

There are several uncertainties in the GeoDFN model and its parameterization. These uncertainties are categorized by their type as to whether they are in the conceptual model, the mathematical implementation of the model, or in the data.

The primary impact of these uncertainties is on the number of large fractures that are likely to be intersected by canisters, which are vertical. The intensity of fracturing for larger fractures in the range 28 m to 564 m represents the component of fracturing that is of the greatest interest for these safety calculations, as they are large enough to have secondary slip during earthquakes that might impact safety, yet are small enough that they may be difficult to detect with 100% reliability during site reconnaissance and construction. The P_{32} intensity values for the various fracture sets, fracture domains and conceptual models are summarized in Table 5-1.

Table 5-1. Ratios of P_{32} intensity in the size range 28 m to 564 m for alternative fracture models.

Fracture domain	Fracture set	Set type	OSM+TFM 28 to 564 m	TCM 28 to 564 m	TCMF 28 m to 564 m	OSM+TFM vs TCM Ratio	OSM+TFM vs TCMF Ratio	TCM vs. TCMF Ratio
FFM01	NE	Global	0.0503	0.036	0.041	1.39	1.23	0.89
FFM01	NS	Global	0.0035	0.010	0.011	0.37	0.32	0.86
FFM01	NW	Global	0.0386	0.033	0.035	1.17	1.12	0.96
FFM01	SH	Global	0.0094	0.029	0.028	0.33	0.34	1.04
FFM01	ENE	Local	0.4186	0.010	0.011	41.04	38.62	0.94
FFM01	EW	Local	0.0024	0.004	0.003	0.61	0.70	1.16
FFM01	NNE	Local						
FFM01	SH2	Local						
FFM01	SH3	Local						
FFM02	NE	Global	0.1032	0.036	0.041	2.86	2.53	0.89
FFM02	NS	Global	0.0066	0.010	0.011	0.69	0.59	0.86
FFM02	NW	Global	0.0876	0.033	0.035	2.64	2.53	0.96
FFM02	SH	Global	0.0631	0.029	0.028	2.20	2.29	1.04
FFM02	ENE	Global	0.5283	0.010	0.011	51.80	48.75	0.94
FFM02	EW	Global	0.0058	0.004	0.004	1.50	1.43	0.96
FFM02	NNE	Local						
FFM02	NNW	Local						
FFM03	NE	Global	0.0894	0.030	0.028	3.00	3.22	1.07
FFM03	NS	Global	0.0235	0.024	0.022	0.96	1.07	1.11
FFM03	NW	Global	0.0929	0.042	0.050	2.19	1.84	0.84
FFM03	SH	Global	0.0361	0.016	0.019	2.29	1.88	0.82
FFM03	ENE	Local	0.1060	0.006	0.007	16.82	15.11	0.90
FFM03	EW	Local	0.0062	0.008				
FFM06	NE	Global	0.0700	0.036	0.041	1.94	1.72	0.89
FFM06	NS	Global	0.0057	0.012	0.013	0.49	0.43	0.88
FFM06	NW	Global	0.0653	0.033	0.035	1.97	1.88	0.96
FFM06	SH	Global	0.0097	0.029	0.028	0.34	0.35	1.04
FFM06	ENE	Local	0.2058	0.010	0.011	20.13	19.04	0.95
FFM06	SH2	Local						

5.1.1 Conceptual uncertainties

There are three main conceptual uncertainties in the Forsmark 2.2 geologic DFN model. These are:

- Are the fracture represented by deformation zones and ground magnetic lineaments part of the same fracture population represented by fractures in outcrop or measured in boreholes? The hypothesis that the fractures in outcrop and in boreholes are part of the same population as the larger fractures delineated through ground magnetic lineaments and deformation zones is referred to as the Tectonic Continuum Model or TCM. The conceptual model that treats the larger scale fracturing as a distinct population from the fractures in outcrop and boreholes is referred to as the OSM+TFM, where "OSM" is the Outcrop Scale Model representing the fractures measured in outcrops and boreholes, and "TFM" is the Tectonic Fault Model, representing the fractures identified through lineaments and deformation zones.

- Related to this uncertainty is the upper size limit for the OSM component of the combined model and the lower size limit for the TFM component. The current implementation of the OSM+TFM model does not place any size cut-offs on either component model, and as a result, most of the fracture intensity in the size range 28 m to 564 m is due to the OSM model. Conceptually, the OSM model represents joints and joints that have been re-activated as faults that can be represented as single surfaces. The TFM component consists of faults with finite width, or in essence, deformation zones. While is may be reasonable for the majority of large features to be re-activated joints, there is also some hydrologic evidence to suggest that there is a break in scale around 200 m /Dershowitz et al. 2003/ between single-plane features and deformation zones. As a result, there is uncertainty relative to placing an upper size limit on the single-plane features (the OSM component) and a lower limit on the deformation zone features (the TFM component) that could impact safety calculations related to future earthquakes.

- Does the fracture intensity scale in a Euclidean manner or according to a fractal model? This conceptual model impacts the TCM, since it covers a broad range of scales. The TCM is subdivided into the TCM proper, which assumes Euclidean scaling at all scales, and the TCMF, which assumes that the fracture intensity scales according to a fractal model.

- The fracturing in domains FFM01 and FFM06 is not expressed in outcrop, and so the size/intensity parameterization of fracturing in these domains is not constrained by outcrop data. As a result, there is no data to directly estimate fracture sizes for fracture sets in these two domains. The parameterization for fracture size thus was based on aspects of the FFM02 size/intensity model, such as the use of the same fracture size scaling exponent for each set, or alternatively, allowing the scaling exponent to vary but fixing other aspects of the model. These alternatives lead to increased uncertainty for the size/intensity parametrization of fracture sets in FFM01 and FFM06.

Tectonic continuum uncertainty

The basis for the TCM and its alternative, the OSM+TFM, derives from the uncertainty as to whether to conceptualize all of the fracturing into a single fracture population, or to break up the fracturing into outcrop and borehole fractures, which are largely joints, and lineaments and deformation zone fractures, which are likely to be faults. Since faults are likely to have different orientations than joints, and different geological characteristics, including size and intensity, the OSM+TFM represents this case. The TCM, on the other hand, does not distinguish between faults and joints. It is possible that the larger scale lineaments and deformation zones originated as joints, and developed into faults and shear zones as oblique stresses reactivated the joints. Size/intensity plots further suggest that many of the sets in many of the fracture domains show a consistent relation from outcrop to deformation zone scale, which is consistent with the TCM.

The difference in intensity for the TCM vs. the OSM+TFM models are shown in Table 5-1, in the column labeled "OSM+TFM vs. TCM". Since subhorizontal fractures are the set that will most frequently intersect a vertical canister deposition hole, the ratios and intensities associated with the global SH set are of greatest interest. The table shows that for fracture domains FFM02 and FFM03, the OSM_TFM model is about 2.2 to 2.3 times greater intensity in the 28 m to 564 m size range than the TCM model, and about 1.9 to 2.3 times greater than the TCMF model. A generalization is that the intensity for the OSM+TFM is about twice that of the TCM and TCMF for the subhorizontal fracture sets. In the other two fracture domains, the OSM+TFM combination produces lower fracture intensities. The table shows that the intensity for the subhorizontal set is almost exactly one-third the intensity in the TCM and TCMF alternatives.

Considering the other sets that are present in all three alternative models, the intensity, with the exception of the ENE set, the ratio between the OSM+TFM to the TCM and TCMF varies between 0.33 and 3.0. Thus, with the exception of the ENE set, the conceptual uncertainty spans a range of about a factor of three.

The reason that the ratio for the ENE set is high is due to the high OSM intensity for this set in FFM02, which propagates to the parameterization of FFM01 and FFM06. The ENE intensity for the OSM in FFM02 was based on an assumed minimum size corresponding to the borehole radius; it was the only set in FFM02 or FFM03 for which this was done. As a consequence, the calculated P_{32} may be less reliable than the calculations for the other sets in these two domains, and the ratios reported in Table 5-1 for the ENE set may be evidence that the P_{32} for the ENE set in FFM02 is not as reliable as the other values.

Upper size limit for single plane features and lower size limit for deformation zones

While various limits for a maximum upper limit for the OSM model and a minimum size limit for the TFM could be hypothesized, the uncertainty in selecting such limits can be investigated through the use of the 200 m threshold suggested by /Dershowitz et al. 2003/. In this investigation, the fracture intensity expressed as P_{32} was calculated for the OSM model from 28 m to 200 m, and for the TFM model from 200 m to 564 m (Table 5-2). This table also includes the previously calculated values for each model component over the 28 m to 564 m size range.

The intensity was calculated for various combinations:

- OSM and TFM over the size range 28 m to 564 m
- The OSM from 28 m to 200 m combined with the TFM from 28 m to 564 m
- The OSM from 28 m to 200 m combined with the TFM from 200 m to 564 m

Then the percentage of fracture intensity of the combined model with only an upper truncation on the OSM vs. the base model, in which both components extend over the entire 28 m to 564 m was calculated, as well as a second model in which the OSM extends up to 200 m, and the TFM has a lower limit of 200 m. These percentages are shown in the last two columns of the table. The results show that placing an upper limit of 200 m on the OSM model reduces the overall intensity to something on the order of 80% to 90% of the base model, with a mean and median of about 88%. Including a lower limit on the TFM model further reduces the overall fracture intensity, in some cases as low as 21%, with a median of around 72% and a mean of about 66%.

Euclidean vs. fractal scaling uncertainty

Table 5-1 also shows the ratio between the TCM and TCMF models for the fracture sets and fracture domains for the fracture sets that are global in at least one fracture domain. The ratios vary from a minimum of 0.82 for the SH set in FFM03 to 1.16 for the EW set in FFM01. The SH set varies from 0.82 in FFM03 to 1.04 in the other three domains. This suggests that the impact of assuming fractal or Euclidean scaling is not very large.

Table 5-2. Percent reduction in P_{32} for combined OSM/TFM model as a function of uncertainty in upper size limit for OSM and lower size limit for TFM.

Fracture Domain	Set	P_{32} For Individual model components as a function of Size Range				P_{32} for combined OSM and TFM Components			Percentage of P_{32} for Size-Limited OSM+TFM model vs. Full 28 m to 564 m range for both components	
		OSM (28–564 m)	OSM (28–200 m)	TFM (28–564 m)	TFM (200–564 m)	OSM (28–564 m) + TFM (28-564 m)	OSM (28–200 m) + TFM (28-564 m)	OSM (28–200 m) + OSM (200-564)	OSM (28-200) + TFM (28-564 m) vs Base	OSM (28–200) + TFM (200-564 m) vs Base
FFM01	NE	0.0218	0.0183	0.0285	0.0027	0.0503	0.0468	0.0210	93.00%	41.75%
FFM01	NS	0.0032	0.0029	0.0003	0.0001	0.0035	0.0032	0.0029	89.98%	83.10%
FFM01	NW	0.0384	0.0303	0.0003	0.0001	0.0386	0.0306	0.0304	79.11%	78.66%
FFM01	ENE	0.3315	0.2387	0.0871	0.0066	0.4186	0.3258	0.2454	77.83%	58.62%
FFM01	EW	0.0010	0.0009	0.0014	0.0002	0.0024	0.0023	0.0011	96.39%	45.10%
FFM02	NE	0.0747	0.0626	0.0285	0.0027	0.1032	0.0911	0.0653	88.32%	63.31%
FFM02	NS	0.0062	0.0055	0.0003	0.0001	0.0066	0.0059	0.0056	89.49%	85.78%
FFM02	NW	0.0873	0.0690	0.0003	0.0001	0.0876	0.0692	0.0690	79.03%	78.83%
FFM02	ENE	0.4413	0.3177	0.0871	0.0066	0.5283	0.4048	0.3244	76.62%	61.40%
FFM02	EW	0.0045	0.0041	0.0014	0.0002	0.0058	0.0055	0.0042	93.39%	72.55%
FFM03	NE	0.0609	0.0508	0.0285	0.0027	0.0894	0.0793	0.0535	88.70%	59.85%
FFM03	NS	0.0232	0.0194	0.0003	0.0001	0.0235	0.0197	0.0195	83.87%	82.83%
FFM03	NW	0.0926	0.0766	0.0003	0.0001	0.0929	0.0769	0.0767	82.76%	82.58%
FFM03	ENE	0.0189	0.0161	0.0871	0.0066	0.1060	0.1032	0.0227	97.35%	21.45%
FFM03	EW	0.0048	0.0046	0.0014	0.0002	0.0062	0.0060	0.0047	95.88%	76.31%
FFM06	NE	0.0415	0.0348	0.0285	0.0027	0.0700	0.0633	0.0375	90.43%	53.59%
FFM06	NS	0.0053	0.0047	0.0003	0.0001	0.0057	0.0051	0.0048	89.58%	85.28%
FFM06	NW	0.0650	0.0513	0.0003	0.0001	0.0653	0.0516	0.0514	79.05%	78.79%
FFM06	ENE	0.1187	0.0855	0.0871	0.0066	0.2058	0.1726	0.0921	83.85%	44.77%

Use of FFM02 models in parameterization Of FFM01 and FFM06

Since there are no outcrops in FFM01 and FFM06, the parameterization for these two domains relies in part on the outcrop data from FFM02. The model as presented in this report assumes that the slope of the line for the coupled size intensity plot for the TCM in FFM02 can be used for FFM01 and FFM06. This assumption would be reasonable if the breakage mechanism for rock in both domains was similar, which would imply that the lithologies are largely the same and the tectonic history is largely the same.

On the other hand, the lithologies may differ in their relative proportions, or the degree and type of tectonic deformation may differ. In this case, the slopes of the line for the TCM model may not be the same. The intensity for this second alternative can be calculated by fixing one end of the coupled size/intensity plot to the borehole intensity, assuming that the minimum size represented is the borehole diameter, and fixing the other end to the ground magnetic lineaments and deformation zone data. The scaling exponent, k_r, is varied until both the borehole P_{32} and the lineament/DZ P_{32} are matched.

The first step is to estimate the value of P_{32} in the TCM model for each set based on the parameterization in FFM02. This is done by determing the intensity of fracturing in the model greater than 564 m. To accomplish that, the P_{32} for the borehole and its minimum radius and scaling exponent are used to calculate the P_{32} for the deformation zones, $P_{32}(DZ)$, above r = 564 m:

$$P_{32}(DZ) = \frac{564^{2-k_r}}{r_0^{2-k_r}} P_{32}(borehole)$$

Equation 5-1

Recall that the borehole-adjusted P_{32} values were based on simulations in which no upper size limit was used; this is consistent with the geological conceptual model in the TCM that fractures range from the borehole diameter through the largest lineaments, although fractures with effective radii greater than 564 m are not included in the stochastic model.

The value of $P_{32}(borehole)$ is the mean value of the 6 m bins for the borehole fracture data, corrected for visibility in BIPS. The value of r_0 corresponds to the minimum size found to match the borehole fracture intensity.

The next step is to find the value of k_r that matches the 6 m binned borehole fracture intensity for sets in FFM01 or FFM06, and matches the $P_{32}(DZ)$. This is done by solving the equation:

$$k_r = 2 - \frac{\ln(P_{32}(borehole)/P_{32}(DZ))}{\ln(0.039/564)}$$

Equation 5-2

This new exponent can then be used to estimate the fracture intensity in the range of 28 m to 564 m. The results of applying Equations 5-1 and 5-2 are shown in Table 5-3 and Table 5-4.

These tables show that the intensity in the 28 m to 564 m size range is typically about one-third to two-thirds the intensity compared to the case using the same scaling exponent as in FFM02.

Table 5-3. Ratios in intensities for global land local fracture sets in FFM01 assuming and not assuming the same scaling exponent as FFM02.

| Fracture domain | Fracture set | Set type | Size distribution | Min. radius r_0 (m) | Exponent (k_r) | Match P_{32}* r_0 - ∞ (1/m) | P_{32} – Based on FFM02 | | | Estimated k_r not based on FFM02 | Ratio of exponents | P_{32} – Not Based on FFM02 28–564 | Ratio of intensities |
							28–564	>564	P_{32} 6 m bins				
FFM01	NE	Global	Power Law	0.66	3.02	1.74	0.0361	0.0018	1.6803	2.72	0.90	0.0134	0.37
FFM01	NS	Global	Power Law	0.06	2.78	1.29	0.0096	0.0010	1.0004	2.72	0.98	0.0078	0.82
FFM01	NW	Global	Power Law	0.59	2.85	0.95	0.0331	0.0028	0.9292	2.61	0.91	0.0145	0.44
FFM01	SH	Global	Power Law	0.82	2.85	0.63	0.0286	0.0024	0.5268	2.56	0.90	0.0107	0.37
FFM01	ENE	Local	Power Law	0.32	3.25	2.74	0.0102	0.0002	2.7427	2.97	0.91	0.0043	0.42
FFM01	EW	Local	Power Law	0.17	3.1	1.12	0.0039	0.0001	1.1174	2.93	0.95	0.0023	0.59

Table 5-4. Ratios in intensities for global land local fracture sets in FFM06 assuming and not assuming the same scaling exponent as FFM02.

| Fracture domain | Fracture set | Set type | Size distribution | Min. radius r_0 (m) | Exponent (k_r) | Match P_{32}* r_0 - ∞ (1/m) | P_{32} – Based on FFM02 | | | Estimated k_r Not Based on FFM02 | Ratio of exponents | P_{32} – Not based on FFM02 28-564 | Ratio of intensities |
							28–564	>564	P_{32} 6 m bins				
FFM06	NE	Global	Power Law	0.35	3.02	3.30	0.0361	0.0018	3.3268	2.7869	0.9228	0.0170	0.47
FFM06	NS	Global	Power Law	0.04	2.78	2.15	0.0115	0.0012	1.9333	2.7688	0.9960	0.0111	0.96
FFM06	NW	Global	Power Law	0.32	2.85	1.61	0.0331	0.0028	1.5492	2.6594	0.9331	0.0175	0.53
FFM06	SH	Global	Power Law	0.79	2.85	0.64	0.0286	0.0024	0.6490	2.5839	0.9066	0.0115	0.40
FFM06	ENE	Local	Power Law	0.74	3.25	0.98	0.0102	0.0002	1.1917	2.8861	0.8880	0.0033	0.32

5.1.2 Mathematical implementation uncertainties

Depth corrections

Analysis of the fracture intensity as a function of depth below the surface indicates that

1. Intensity is not constant with depth

2. The variation in intensity, with the exception of the upper few tens of meters, is not monotonic with depth; rather there are zones of higher and lower intensity that are not strongly depth-dependent.

Depth dependency, or even the existence of larger scale zones of higher and lower intensity that are not monotonic functions of depth, can impact the parameterization of the model fracture intensity. The coupled size/intensity relations that have been developed for each set and domain are in part anchored to the mean borehole fracture intensity. The calculation of the mean intensity can be somewhat biased due to the combination of zonation and the fact that not all boreholes penetrate to the same depth. For example, if there is a zone of higher fracture intensity from 200 m to 300 m below the surface in a fracture domain, and a zone of lower than average intensity from 800 m to 1,000 m, there will be more borehole penetrations of the upper intense zone than the lower less intense zone. A straight average of the data will tend to skew the calculated mean towards the more abundant measurements in the upper intense zone. In this situation, it would be more accurate to average the fracture intensity over the 200 to 300 m zone, and also over any other zones, and then calculate the mean and other statistics by depth zone, rather than ignoring the zonation. However, there is no good evidence at Forsmark to suggest that the zones seen in one borehole are laterally correlative across the site. In this case, the straight arithmetic average of all the data would be more accurate.

It is possible that fracture intensity might show a different pattern with depth were the open fractures analyzes separately. However, the GeoDFN guidance document /Munier 2006/ specifically restricts the parameterization to a model in which fractures designated as "open" or "sealed" are combined. As a consequence, the behavior of open or sealed fracture intensity as a function of depth is outside the scope of the GeoDFN.

Since it is not clear which method is correct, there is uncertainty arising as to whether the mean borehole intensity should be based on depth zonation or straight arithmetic averaging. The base case model for the GeoDFN has assumed that straight arithmetic averaging is appropriate, because the zones cannot be correlated across the fracture domains from borehole to borehole with any certainty. To examine the magnitude of this mathematical implementation assumption, the borehole intensities were average by 100 m depth zone for all sets and fracture domains, and compared to the intensity calculated through straight arithmetic averaging. The results are shown in Table 5-5.

The percent difference is the amount of deviation from the base case in which the fracture intensity is calculated through straight arithmetic averaging. The differences vary by fracture set and domain, but for the most part, are 10% or less. The difference is biased as well; it is much more common for the depth-interval weighted fracture intensity to be lower than the arithmetic averaged value. This is probably because of the slightly higher fracture intensity in the upper few hundred meters of many boreholes, and the lower intensity seen below 700–800 m in some boreholes.

Table 5-5. Uncertainty due to depth correction for fracture intensity. Yellow shaded cells indicate global sets.

FFM01	ENE	EW	NE	NNE	NS	NW	SH	SH2	SH3	SUM
Weighted	2.54	0.98	1.49	4.23	1.05	0.71	0.52	1.57	1.44	14.52
Unweighted	2.74	1.12	1.68	4.39	1.00	0.93	0.53	1.64	1.61	15.65
Difference	−0.20	−0.14	−0.19	−0.17	0.05	−0.22	−0.01	−0.07	−0.17	−1.12
% Difference	−7.47%	−12.69%	−11.23%	−3.82%	5.09%	−23.49%	−2.18%	−4.22%	−10.51%	−7.16%
FFM02										
Weighted	1.13	0.52	2.67	1.88	0.82	1.71	2.93			11.66
Unweighted	1.17	0.48	2.74	2.00	0.78	1.76	2.78			11.72
Difference	−0.04	0.04	−0.06	−0.13	0.04	−0.06	0.15			−0.06
%Difference	−3.24%	8.47%	−2.24%	−6.34%	4.49%	−3.19%	5.29%			−0.50%
FFM03										
Weighted		0.05	2.82		1.36	1.45	0.88			6.56
Unweighted		0.10	2.91		1.49	1.46	0.96			6.92
Difference		−0.05	−0.09		−0.13	−0.01	−0.09			−0.37
%Difference		−49.59%	−3.05%		−8.58%	−0.74%	−8.96%			−5.28%
FFM06										
Weighted	0.82		3.81		1.61	1.39	0.48	1.16		9.26
Unweighted	1.19		3.33		1.93	1.55	0.65	1.34		9.99
Difference	−0.37		0.48		−0.32	−0.16	−0.17	−0.18		−0.73
%Difference	−31.33%		14.38%		−16.73%	−10.48%	−25.89%	−13.59%		−7.32%

Lithology corrections

The intensity model may be implemented with or without consideration of how fracture intensity varies by lithology. In the previous section, the lithology adjustment factors (Table 4-99) were calculated. These factors represent how much less or greater the intensity for a particular lithology is relative to the average lithology for the fracture domain and set of interest. Perusal of this table indicates that the greatest underestimate in fracture intensity is for the subhorizontal set in the Granodiorite_Metamorphic lithology in FFM01, which has approximately 5 times the intensity as the average value for this set in FFM01. Several other sets would have an overestimate. For the more pervasive rock types, the differences are much less extreme.

Affected by DZ

Fractures that are not in mapped deformation zones, but have geological characteristics that suggest that they were affected by deformation zones, have been separated from the background fracturing in the parameterization. The identification of the extent of these zones in which background fractures may have been affected by deformation zones is uncertain, and errors may be made in delineating the extent of these zones. As a consequence, some background fractures not enhanced by later deformation may have been assigned to these zones, while other fractures that were enhanced have been included in the background fracturing, despite considerable effort to properly assign the fractures. Since there is no way to determine an independent size/number scaling exponent for the fractures affected by deformation zones, the ratios of their borehole intensities can be compared to derive a coarse estimate of the possible error in assignment. It is presumed that the fracture measured in borehole have a minimum size equal to the borehole radius, and that any fractures greater than 1,000 m in horizontal trace length will have been identified and assigned to the deformation zone class. Table 5-6 illustrates the results of these uncertainty calculations.

Table 5-6. Ratios of P_{32} for fractures affected by deformation zones to fractures not affected by deformation zones.

Fracture domain	Fracture set	Set type	Mean P_{32} ratios (0.5–564 m)		
			OSM	TCM	TCMF
FFM01	NE	Global	3.14	3.14	2.89
FFM01	NS	Global	2.01	2.01	1.86
FFM01	NW	Global	2.54	2.54	2.43
FFM01	SH	Global	3.89	3.89	4.35
FFM01	ENE	Local	1.42	1.42	1.34
FFM01	EW	Local	2.55	2.55	2.62
FFM01	NNE	Local	0.00	NA	NA
FFM01	SH2	Local	0.00	NA	NA
FFM01	SH3	Local	2.67	NA	NA
FFM02	NE	Global	1.58	1.58	1.58
FFM02	NS	Global	2.93	2.93	2.93
FFM02	NW	Global	1.11	1.11	1.11
FFM02	SH	Global	2.37	2.37	2.37
FFM02	ENE	Global	1.38	1.38	1.38
FFM02	EW	Global	0.15	0.15	0.15
FFM02	NNE	Local	0.00	NA	NA
FFM02	NNW	Local	NA	NA	NA
FFM03	NE	Global	6.08	1.55	1.55
FFM03	NS	Global	0.00	0.00	0.00
FFM03	NW	Global	1.26	0.79	0.79
FFM03	SH	Global	5.22	2.57	2.57
FFM03	ENE	Local	0.00	NA	NA
FFM03	EW	Local	0.61	0.94	0.94
FFM06	NE	Global	0.00	0.00	0.00
FFM06	NS	Global	0.00	0.00	0.00
FFM06	NW	Global	0.00	0.00	0.00
FFM06	SH	Global	0.00	0.00	0.00
FFM06	ENE	Local	0.00	0.00	0.00
FFM06	SH2	Local	0.00	NA	NA

The table suggests that the intensity in the regions impacted by deformation zones is two to three times greater than the regions not affected. Values of 0.0 on the table, such as are found in FFM06, indicate that none of the areas affected by deformation zones contained this fracture set for the fracture domain.

5.2 Recommendations for uncertainty propagation to downstream models

Table 5-7 summarizes the impact of the key uncertainties described in Section 5.1. The uncertainty with the greatest impact is in the parameterization of the size/intensity for FFM01 and FFM06. The uncertainty derives from the fact that there were no outcrops for these two fracture domains, and as such, either an assumption must be made that FFM02 is analogous, so its size/ scaling parameters can be used, or that the domains are different, but less constrained due to lack of outcrop data. The next most significant uncertainty is whether fracture sets are part of a single population that extends from fracture with radii 0.039 m up to sizes of kilometers, or whether there are distinct joint and fault populations.

Table 5-7. Summary of key uncertainties and their expected impacts on downstream modeling.

Uncertainty	Magnitude	Comments
Tectonic Continuum	0.3 to 3.0	Varies significantly by domain and fracture set.
Upper Size Limit on OSM; Lower Size Limit on TFM	0.6 to 0.9	For the combined OSM+TFM model, the specification of am upper size limit for the OSM and/or a lower size limit for the TFM reduces the fracture intensity by about a third. The impact does vary, with the greatest reduction about 0.21.
Euclidean vs. Fractal	0.82 to 1.16	Fairly minor impact, especially on subhorizontal fractures.
Use of FFM02 for parameterization of Size/Intensity for FFM01 & FFM06	0.3–0.7	If FFM02 scaling exponent is not used, predicted intensities in the 28 m to 564 m size range are about 1/3 to 2/3 greater.
Rock Type	A maximum of about 5 times the average intensity; typical values are from 0.5 to 2	Varies by fracture domain and set; Variation is greatest for minor rock types like amphibolite or pegmatite.
Depth	On the order of 10% or less	Varies by fracture set and fracture domain; tends to be biased such that ignoring depth dependence slightly increases reported mean fracture intensities.
Affected by DZ	2 to 3	Fracture intensities in regions identified as being affected by deformation zones are two to three times greater than those outside of identified zones.

The results shown in Table 5-7 show that the best way to reduce uncertainty in downstream models is to:

- Model each fracture domain separately;

- Model each fracture set within each fracture domain separately;

- Assign intensities by rock type; many major rock types can be combined, but the amphibolite group and the fine- to medium-grained granite differ substantially from average domain intensities and should be modeled separately if adjustments by lithology are incorporated; and

- Minimize the scale difference between the scale over which fracture data is collected and the scale to which it is applied. Extrapolating outcrop data to 100 m simulation grid cells produces less uncertainty than extrapolating to 500 m grid cells.

Downstream users of this data must decide upon whether the uncertainty relative to the Tectonic Continuum hypothesis creates unacceptably large uncertainties in the hydraulic or mechanical properties of the rock. If the uncertainties are too large for a particular use, then additional effort should be addressed to justifying either the Outcrop Scale model or one of the Tectonic Continuum alternatives.

6 Verification of the Forsmark 2.2 geological DFN models

6.1 Objectives

The purpose of verification is to build confidence during model development and to establish the scientific basis and accuracy of the model for its intended scope of use. This chapter concentrates on verification of the model parameters after development of the model by using tables presented in the summary chapter of this report (Chapter 7). The verification cases consist of:

- Verification of the orientation model using boreholes in domain FFM01 and FFM06 (Chapter 6.1.1).

- Verification of the fracture size model through a comparison of simulated trace planes to observed trace planes within the limits of the size model fits (Chapter 6.1.2).

- Verification of the mean fracture intensities, by fracture set and domain (Chapter 6.1.3). The following cases were tested:
  - Verification of the intensity of the MDZ size fraction (r > 28 m). These structures are of particular importance to geologic and hydrologic modelers.
  - Verification of the intensity models as compared to analytical benchmarks, as described in the DFN memorandum /Munier 2006/.

- Verification of the model performance on a data set that was not used in the development of DFN parameters. This verification uses the Boremap/BIPS information from borehole KFM08D, which has not been included in the Forsmark 2.2 geological modeling efforts, but has a single-hole interpretation completed.

The verification cases were built on the parameter tables given in Chapter 7. Analyses were performed on observed outcrops in fracture domains FFM02 and FFM03, from cored boreholes in FFM01 (KFM04A) and FFM06 (KFM08C), and from observed data from KFM08D which penetrate fracture domains FFM01, FFM02, and FFM06. The approach has been to systematically visualize simulated exploration results compared to corresponding field data and evaluate and discuss results based on visual comparison.

6.1.1 Verification of orientation model

The verification of the orientation model focuses on the data from the cored borehole array; as the orientation model was built directly from the outcrop trace data, it makes little sense to verify the model against the outcrop data if alternatives are available. As such, we focus on domains FFM01 and FFM06. The goal of this exercise is to determine if the derived model parameters will produce stereonets that are reasonably similar to those observed in selected boreholes.

The orientation models for FFM01 and FFM06 are used in conjunction with the combined Outcrop Scale and Tectonic Fault models (OSM+TFM), assuming a Poissonian location model and Euclidean scaling. Borehole KFM04A is used in for comparision in domain FFM01, while KFM08C is used for comparison in domain FFM06. As we are primarily concerned about orientations and relative set intensity (P_{10}), the match point values for fracture size (r_0) and intensity (P_{32}) from Table 7-2 were used to build the verification simulations.

The Outcrop Scale model fits tend to combine relatively high P_{32} values with small values for r_0; as such, untruncated simulations produce a very large number of fractures, even in small simulation volumes. For this reason, the verification DFN models were generated in a limited

volume (40 m x 40 m x 40 m) so as to be able to complete the simulations within a reasonable time frame. Once the DFN models were completed, they were sampled using an array of short borehole segments that, when added together, completely duplicate the trajectory of the target borehole at the selected scale (15 m long segments). A schematic cartoon of the model set up is presented below as Figure 6-1.

FracMan ORS files, containing the trend, plunge, and measured depth (ADJ_SECUP) of the fractures intersected by the simulated boreholes, were imported into DIPS. Next, stereoplots for both the measured boreholes and the simulated boreholes were constructed. These stereonets are presented, by fracture set and fracture domain, as Figure 6-2 and Figure 6-3.

The visual similarities are quite good for domain FFM01; the sole exception is for the NW Global set. It appears rotated approximately 10° clockwise in KFM04A relative to the set mean pole specified for the NW set in FFM01. For all other sets in FFM01, the degree of rotation between simulation and reality appears to be much less.

The fits for domain FFM06 appear slightly better than for FFM01; the mean poles of the simulated sets appear to be in roughly the correct positions, but the spread and shapes of the pole clusters appear quite different. This is largely due to the limited amount of borehole data (3 cored boreholes, all drilled in different directions) available for paramterization in domain FFM06. It should also be noted that the overall dispersion of the fracture orientation data from cored boreholes in FFM06 is higher than in other domains; the 95% confidence interval on the mean for FFM06 (Table 4-21) is almost twice as large as the 95% confidence interval on the mean for FFM01 (Table 4-15). As such, it is expected that the mean pole orientation fit will be slightly weaker for FFM06 than FFM01. Statistically, the worst fit is to the subhorizontal set; the mean trend of the subhorizontal fractures in KFM08C seems to be substantially different from the other boreholes in FFM06.

Figure 6-1. *40 x 40 x 40 m model volume and example borehole used for orientation verification simulations.*

KFM04A observed NE set	KFM04A simulated NE set
KFM04A observed NS set	KFM04A simulated NS set

KFM04A observed NW set	KFM04A simulated NW set
KFM04A observed SH set	KFM04A simulated SH set

Figure 6-2. *Comparative stereonets for Domain FFM01. Data observed in KFM04A are presented on the left; the results of the DFN verification simulations are presented on the right.*

KFM08C observed NE set	KFM08C simulated NE set
KFM08C observed NS set	KFM08C simulated NS set

KFM08C observed NW set	KFM08C simulated NW set
KFM08C observed SH set	KFM08C simulated SH set

Figure 6-3. *Comparative stereonets for Domain FFM06. Data observed in KFM08C are presented on the left; the results of the DFN verification simulations are presented on the right.*

The differences between the mean poles of the simulated fracture sets versus the core data were quantified using FracSys/ISIS /Dershowitz et al. 1998/. A single hard-sector search was run on each orientation set to obtain the univariate Fisher distribution parameters. The results are presented in Table 6-1 and Table 6-2; the 95% confidence interval of the mean from the Orientation Model chapter are presented as general guides to the goodness-of-fit.

6.1.2 Verification of size model

The goal of the verification of the size model is to address how well the final model product is able to reproduce the trace patterns seen in outcrop. Trace data from outcrops AFM100201 (FFM02) and AFM000053 (FFM03) are compared to trace maps created through stochastic simulation using the Tectonic Continuum, Euclidean scaling models. The OSM+TFM, TCMF and TCM alternatives exhibit essentially the same size/intensity relation at the outcrop scale, so only the TCM was evaluated in these analyses.

Two different surfaces were evaluated for each set; one a horizontal 100 m by 100 m surface; the other a portion of the 100 m by 100 m surface that approximated the footprint of the detailed outcrop mapping limits. The former surface will have different censoring and truncation effects than the actual outcrop or the second sampling plane, but offers the advantage of providing a more statistically robust result due to the much greater number of trace intersections.

Table 6-1. Comparision of Fisher statistics for simulated FFM01 fracture sets versus observations in KFM04A.

Fracture set name	Trend (°)	Plunge (°)	Dispersion fisher κ	Solid angle (°)	95% C.I. of mean (°)
KFM04_sim_NE	318	6	14.9	5.4	4.7
KFM04_obs_NE	315	1	20.9		
KFM04_sim_NS	85	0	24.5	7.95	5.1
KFM04_obs_NS	270	5	21.3		
KFM04_sim_NW	50	0	8.9	4.7	5.8
KFM04_obs_NW	230	5	15.7		
KFM04_sim_SH	357	85	16.6	1.8	4.5
KFM04_obs_SH	1	87	17.4		

Table 6-2. Comparision of Fisher statistics for simulated FFM06 fracture sets versus observations in KFM08C.

Fracture set name	Trend (°)	Plunge (°)	Dispersion fisher κ	Solid angle (°)	95% C.I. of mean (°)
KFM08C_sim_NE	124	15	49.6	5.2	10.9
KFM08C_obs_NE	126	10	45.1		
KFM08C_sim_NS	86	1	21.6	6.2	8.1
KFM08C_obs_NS	91	4	19.5		
KFM08C_sim_NW	36	2	14.3	4.5	8.1
KFM08C_obs_NW	218	3	22.4		
KFM08C_sim_SH	78	66	17.1	37.8	8.1
KFM08C_obs_SH	308	72	10.8		
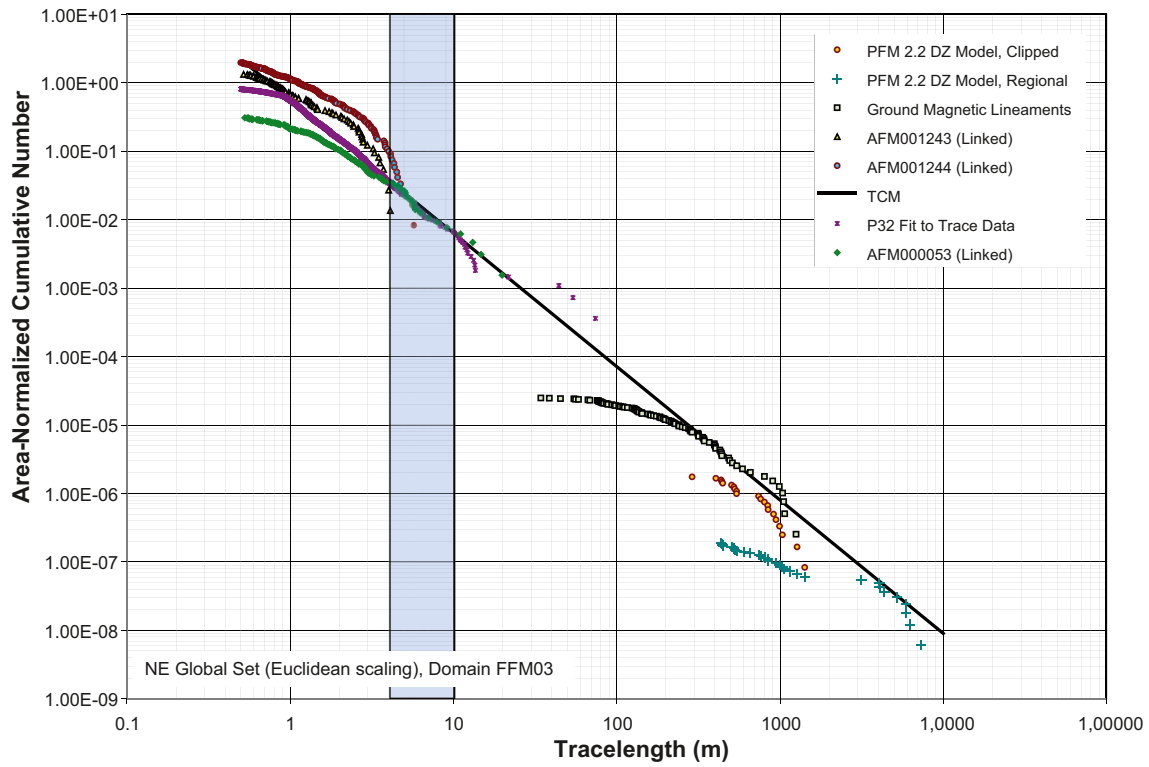
Figure 6-4. *Extent of size verification range, NE Set, Domain FFM03. Verification statistics refer to traces with lengths in the interval of 4 m–10 m.*
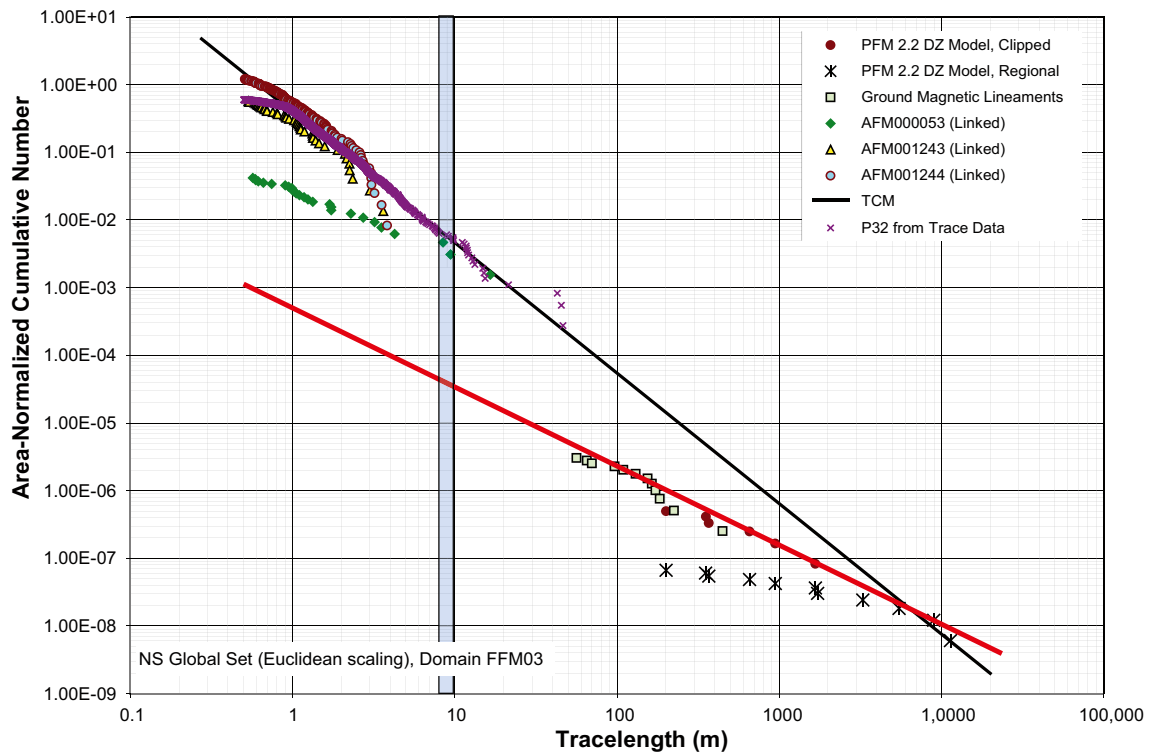
Figure 6-5. *Extent of size verification range, NS Set, Domain FFM03. Verification statistics refer to traces with lengths in the interval of 8 m–10 m.*
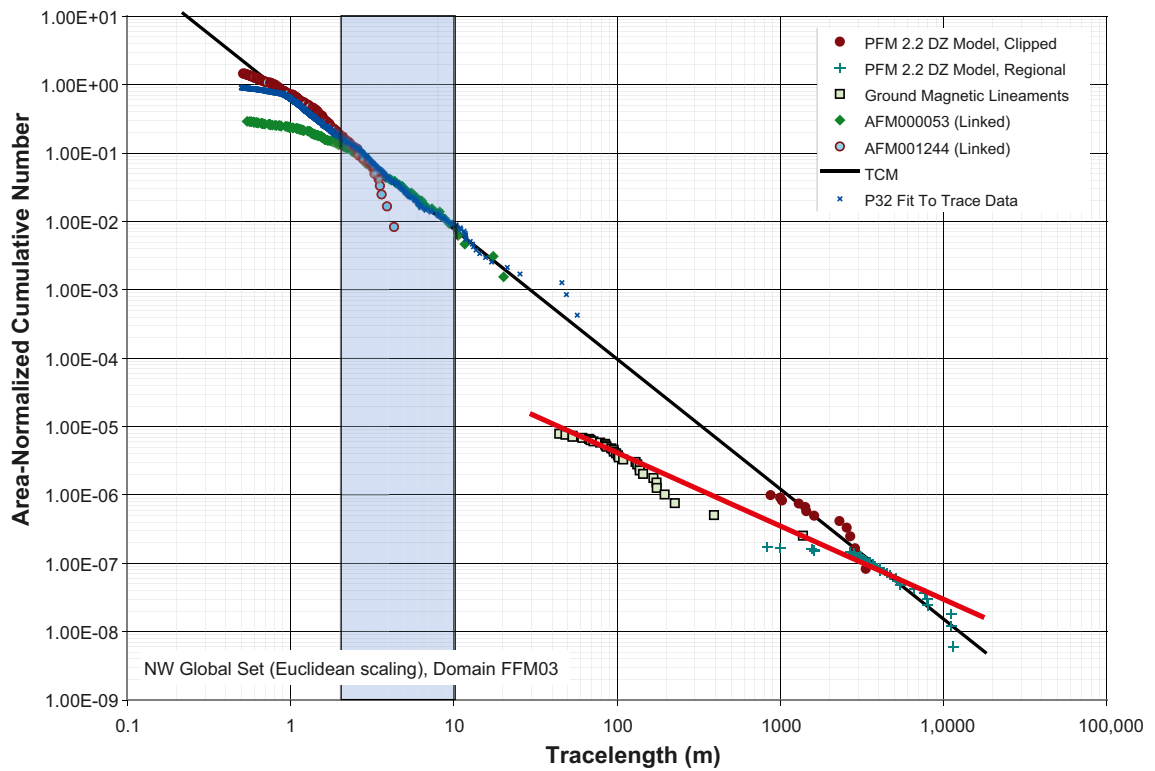
Figure 6-6. *Extent of size verification range, NW Set, Domain FFM03. Verification statistics refer to traces with lengths in the interval of 2 m–10 m.*
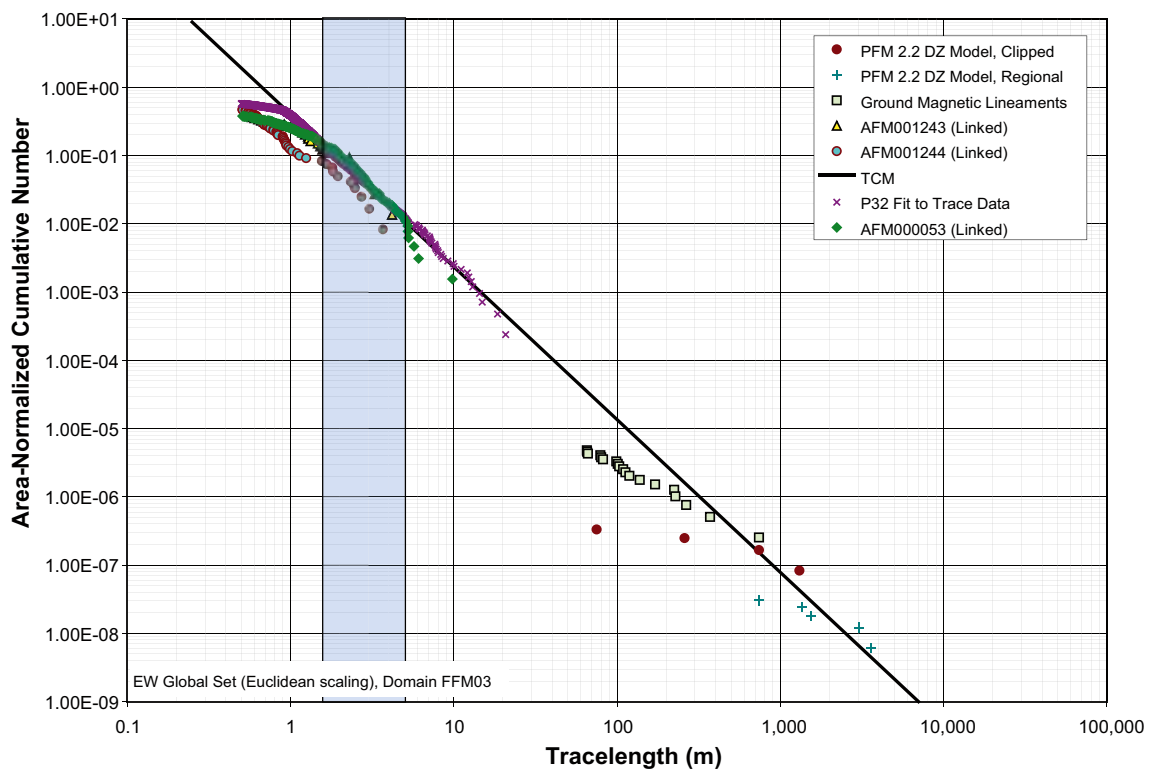
Figure 6-7. *Extent of size verification range, EW Set, Domain FFM03. Verification statistics refer to traces with lengths in the interval of 1.5 m–5 m.*
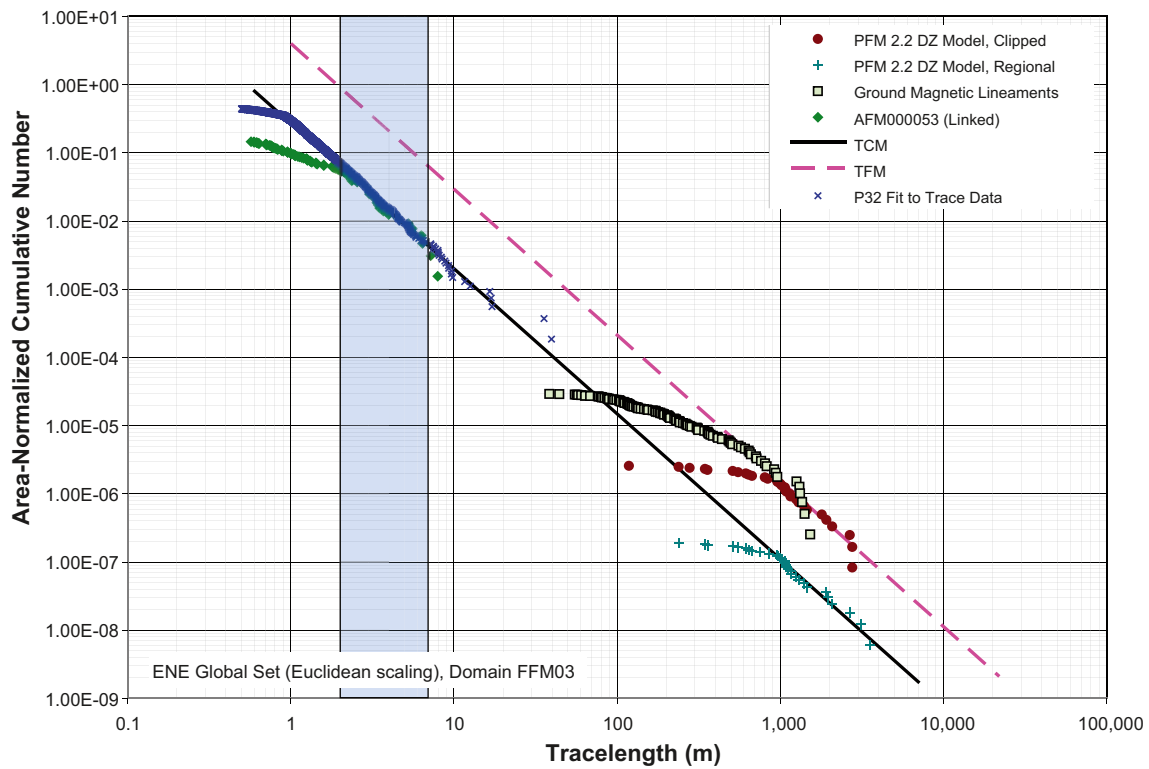
Figure 6-8. *Extent of size verification range, ENE Set, Domain FFM03. Verification statistics refer to traces with lengths in the interval of 2 m–7 m.*
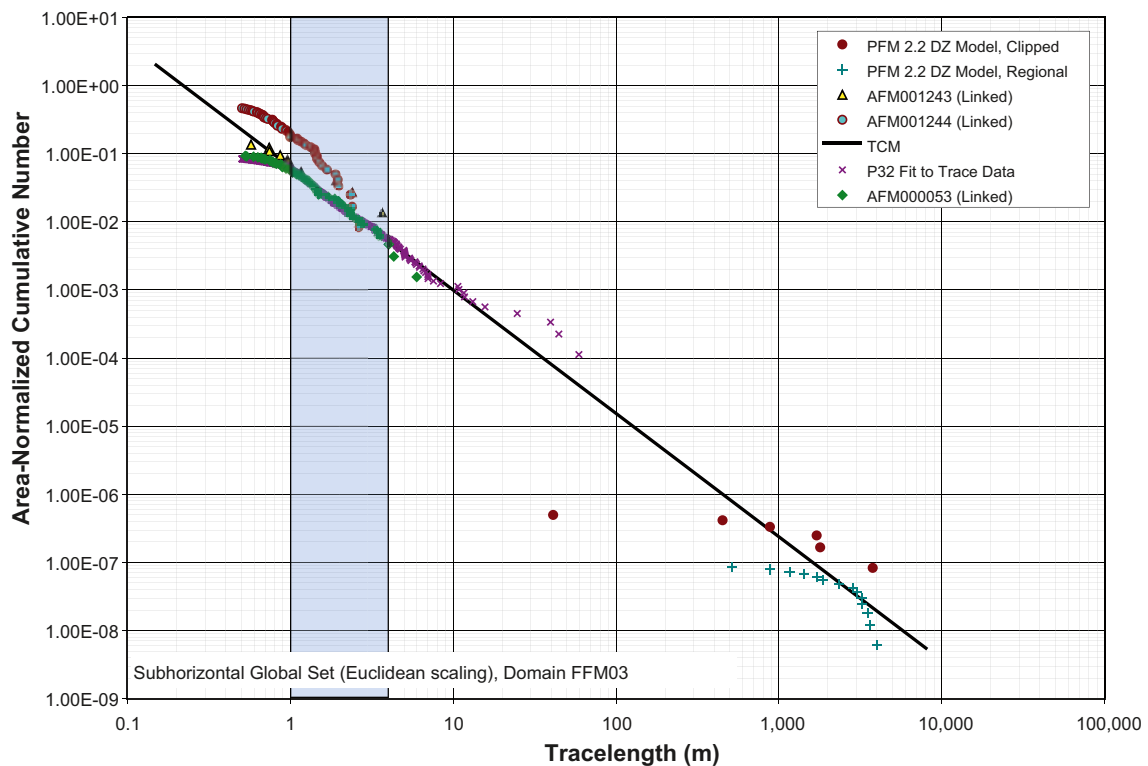
Figure 6-9. *Extent of size verification range, SH Set, Domain FFM03. Verification statistics refer to traces with lengths in the interval of 1 m–4 m.*
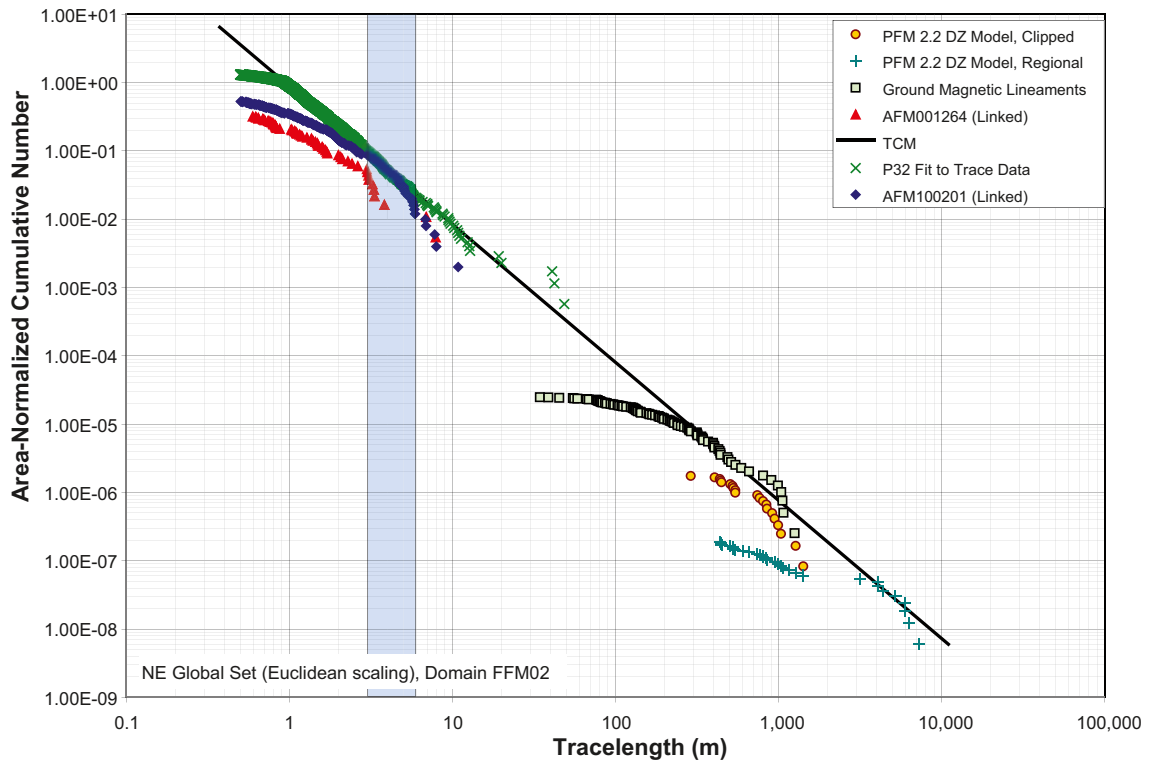
Figure 6-10. *Extent of size verification range, NE Set, Domain FFM02. Verification statistics refer to traces with lengths in the interval of 3 m–6 m.*
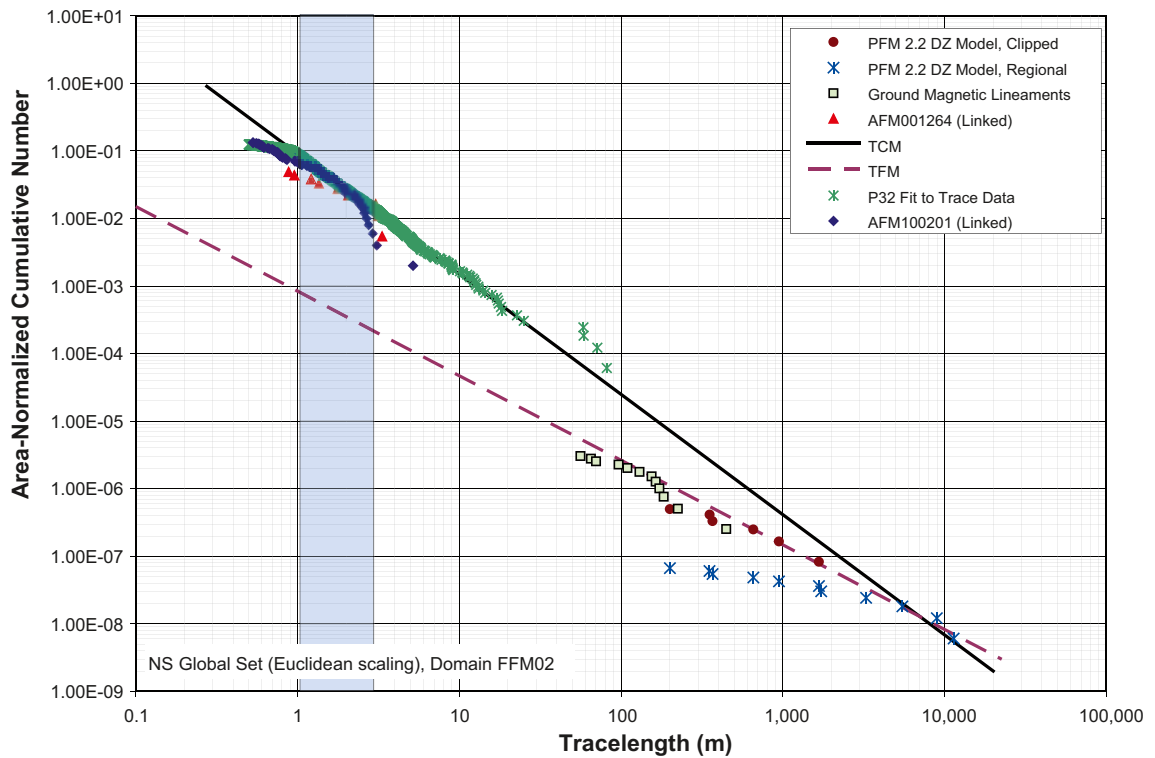
Figure 6-11. *Extent of size verification range, NS Set, Domain FFM02. Verification statistics refer to traces with lengths in the interval of 1 m–3 m.*
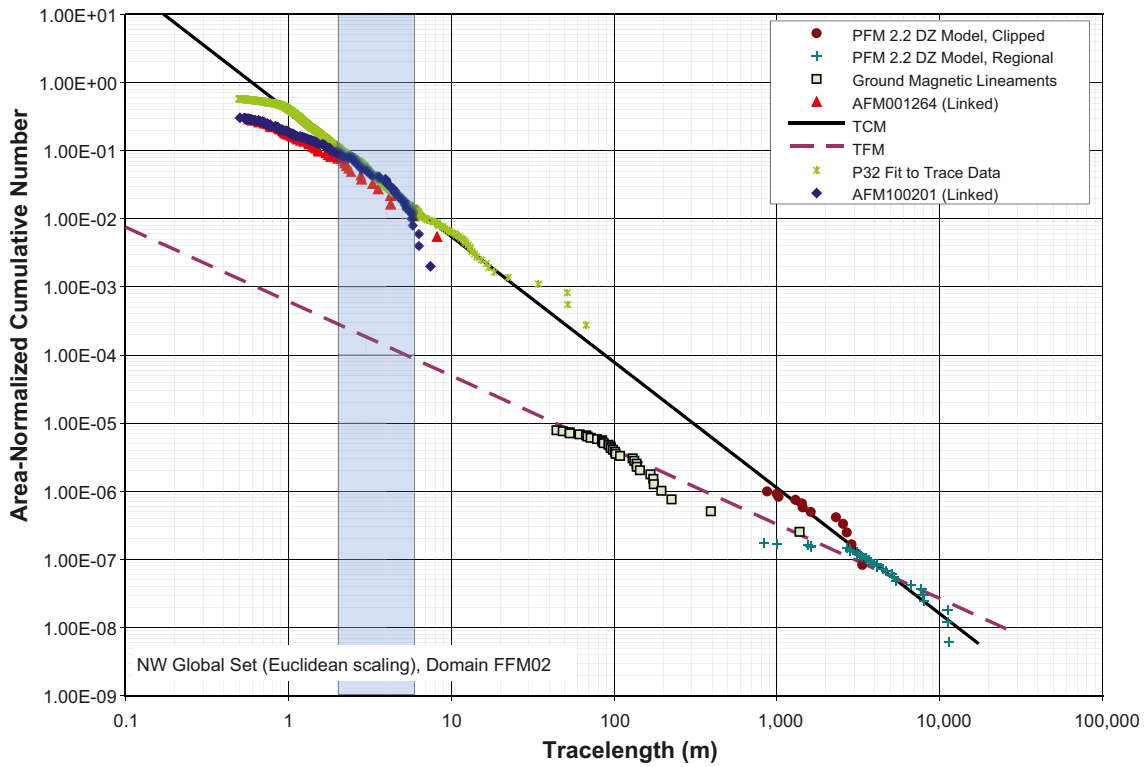
Figure 6-12. *Extent of size verification range, NW Set, Domain FFM02. Verification statistics refer to traces with lengths in the interval of 2 m–6 m.*
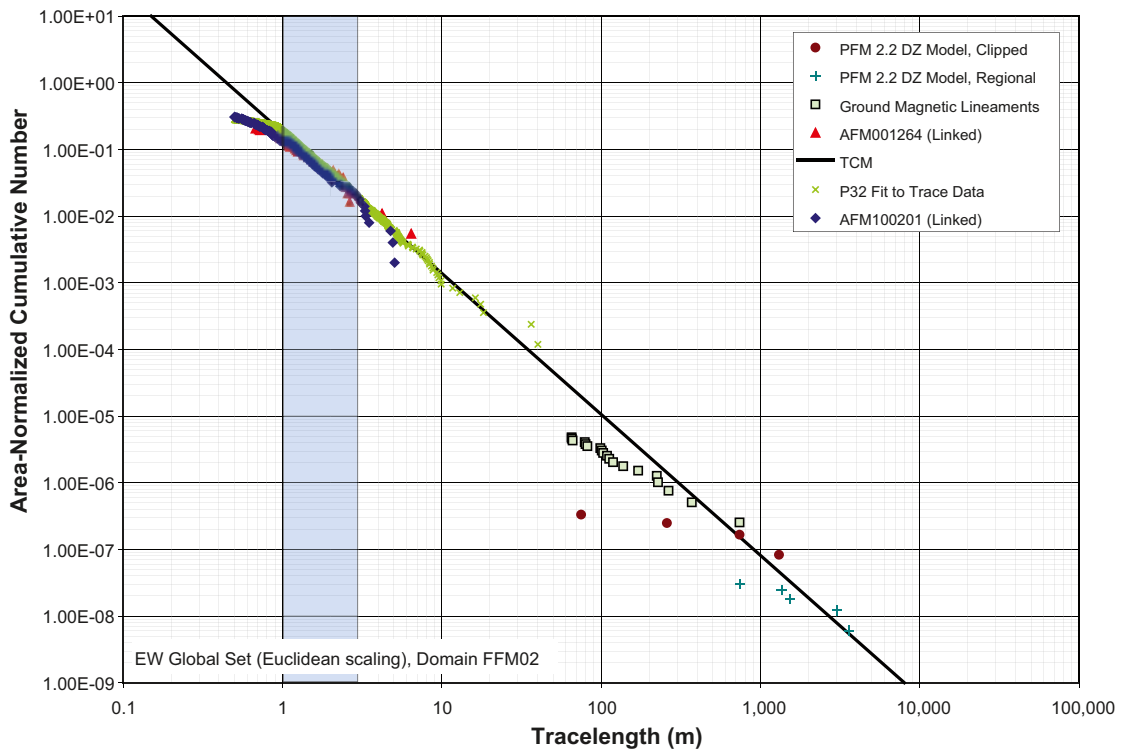
Figure 6-13. *Extent of size verification range, EW Set, Domain FFM02. Verification statistics refer to traces with lengths in the interval of 1 m–3 m.*
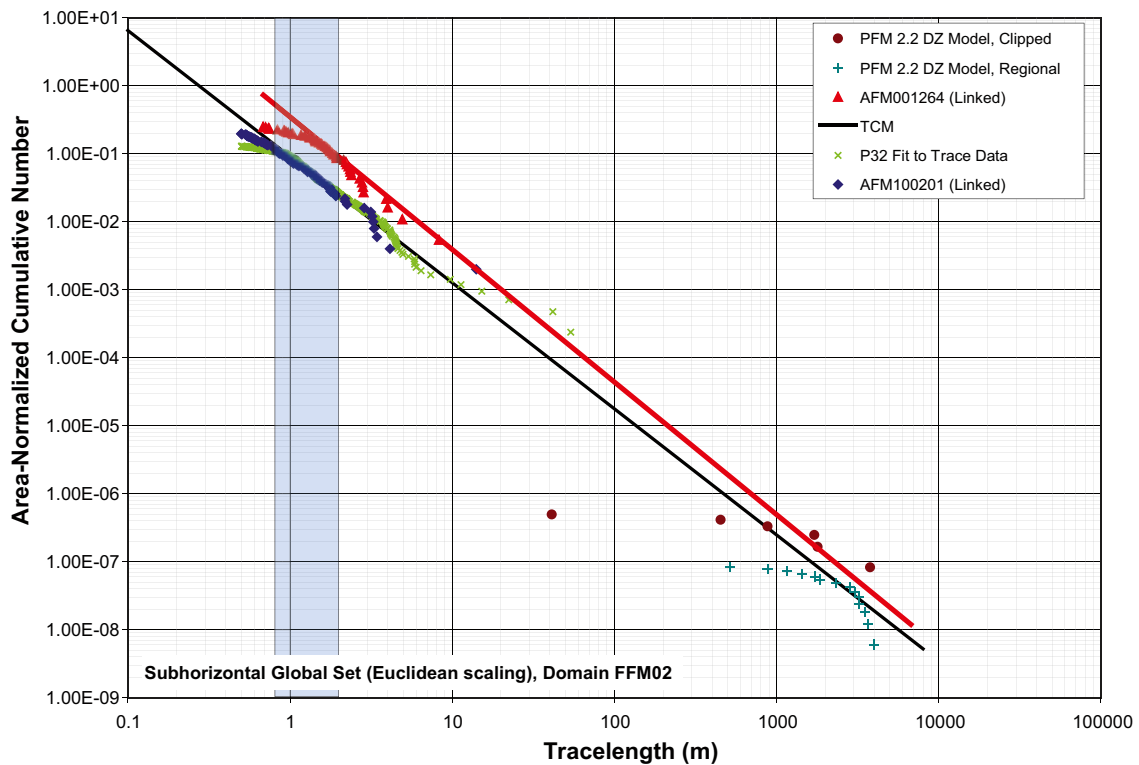
Figure 6-14. *Extent of size verification range, SH Set, Domain FFM02. Verification statistics refer to traces with lengths in the interval of 0.8 m–2 m.*

The size model verification was completed by constructing stochastic DFN realizations for each fracture domain in a 100 m x 100 m x 100 m simulation volume. Fracture set orientations were taken from Table 7-1. As previously described, the TCM model (Table 7-4) with an r_{min} of 0.5 m and a P_{32} calibrated to that minimum radius (Table 7-6) was used for these simulations. A Poisson point process was used to describe fracture centers (Enhanced Baecher model /Dershowitz et al. 1998/). For each fracture domain, the stochastic DFN models were sampled using two separate trace planes; a 100 m x 100 m square traceplane centered at the middle of the model volume, and a smaller, irregular polygon surface representing the mapped extent of the target outcrop. This second trace plane takes into account the orientation sample bias and truncation effects of the original data source.

A visualization of the traces produced by the FFM03 stochastic DFN simulations is presented as Figure 6-15. Figure 6-16 shows a comparison of the observed traces to the simulated traces on outcrop AFM000053. Note that, with the exception of the termination relationships, the simulated fracture patterns look extremely similar to the natural outcrop.

Finally, a numerical comparision of the goodness-of-fit of the simulated trace planes to observed data in FFM03 is presented in Table 6-3. The comparison is done in terms of fracture P_{21} (intensity) within the specified size range. If the size model is adequate (i.e. the size model is accurately simulating the frequency of fractures of a given size), the P_{21} intensities should be fairly similar.
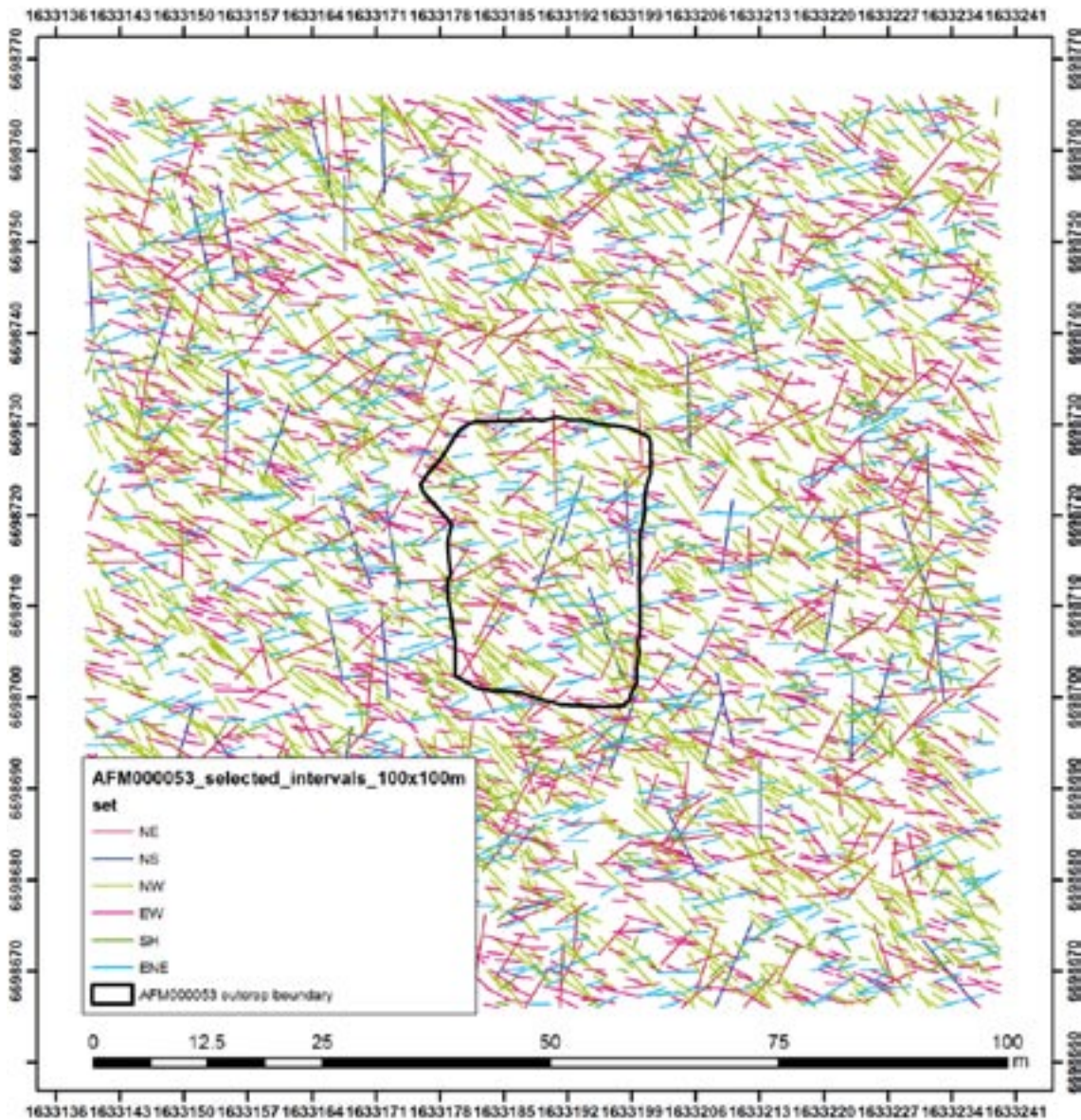
Figure 6-15. *Results of trace plane sampling of stochastic DFN, TCM model, Domain FFM03.*

Table 6-3. Comparison of simulated P_{21} to observed P_{21}, AFM000053 in domain FFM03.

Fracture set	Trace length Interval		P_{21}		Percent
	Lower (m)	Upper (m)	Observed	Simulated	difference
NE	4	10	0.16	0.16	3%
NS	8	10	0.03	0.04	18%*
NW	2	10	0.48	0.6	26%
EW	1.5	5	0.36	0.35	–2%
ENE	2	7	0.16	0.2	24%
SH	1	4	0.09	0.09	1%

* NS set in AFM000053 is a very small sample size.
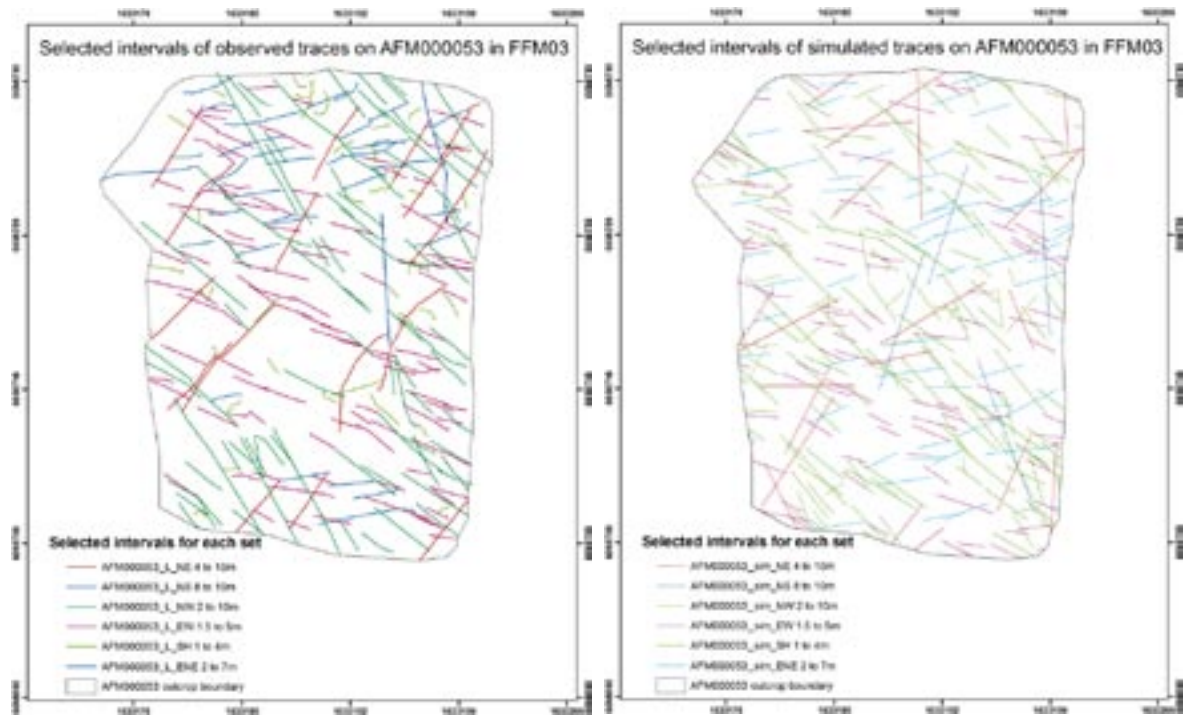
Figure 6-16. Observed (left) and Simulated (right) traces in selected size ranges, AFM000053 in domain FFM03.

The results for FFM03 suggest that the TCM models may over-estimate outcrop fracture intensities in the NW and ENE sets, but will perform fairly well for all other sets. The somewhat higher model result is most likely due to the fact that the intensity model in the TCM is conditioned not only to outcrop data, but also to borehole data. As such, it represents an average for the entire domain.

A visualization of the traces produced by the FFM02 stochastic DFN simulations is presented as Figure 6-17. Figure 6-18 show a comparison of the observed traces to the simulated traces on outcrop AFM100201. Note that, with the exception of the termination relationships, the simulated fracture patterns look extremely similar to the natural outcrop. Finally, a numerical comparision of the goodness-of-fit of the simulated trace planes to observed data in FFM02 is presented in Table 6-4.

Table 6-4. Comparison of simulated P_{21} to observed P_{21}, AFM100201 in domain FFM02.

Fracture set	Trace length Interval		P_{21}		Percent
	Lower (m)	Upper (m)	Observed	Simulated	difference
NE	3	6	0.33	0.32	-4.4%
NS	1	3	0.11	0.13	10.5%
NW	2	6	0.29	0.33	12.7%
EW	1	3	0.17	0.19	10.1%
SH	0.8	2	0.11	0.12	6.7%
Total			1.03	1.09	5.8%
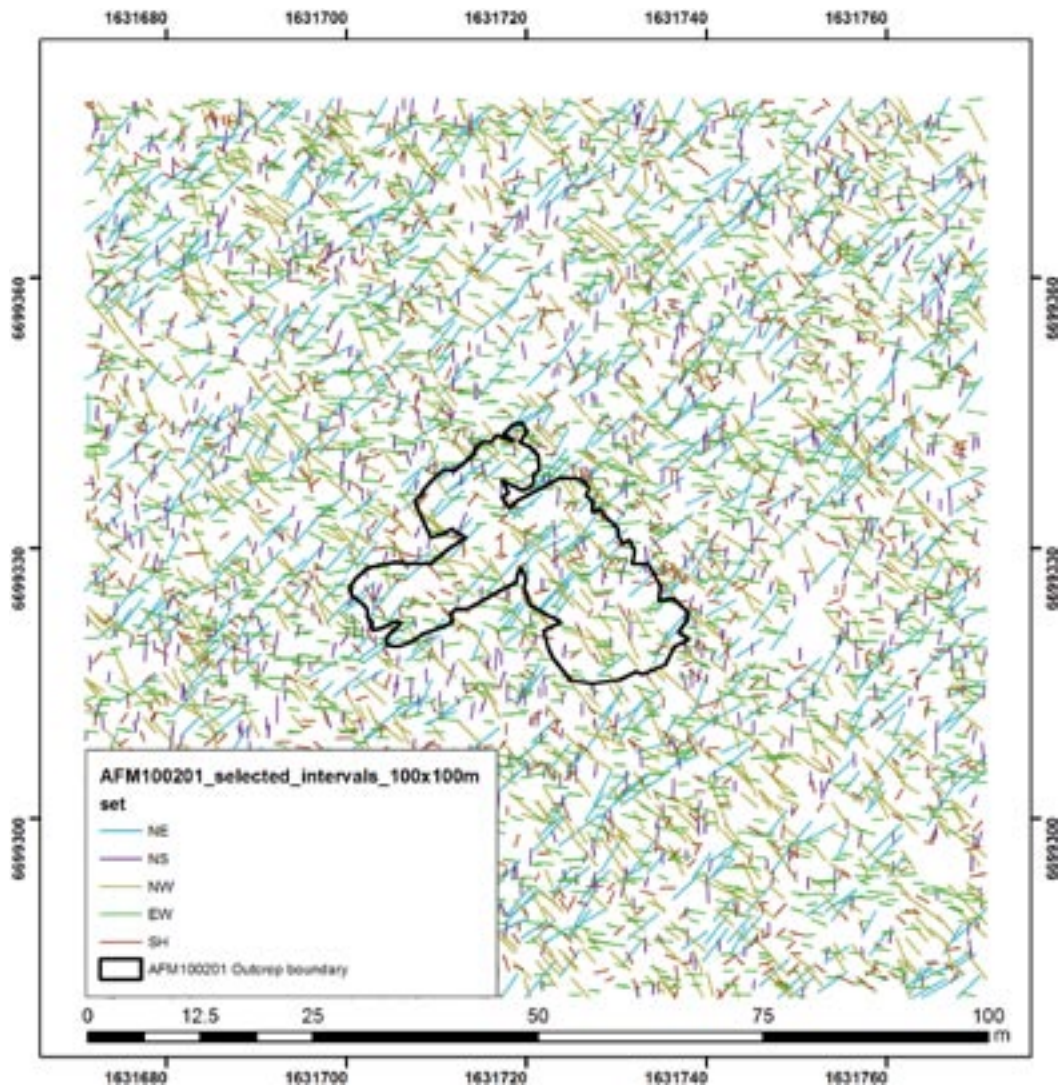
Figure 6-17. *Results of trace plane sampling of stochastic DFN, TCM model, Domain FFM02.*
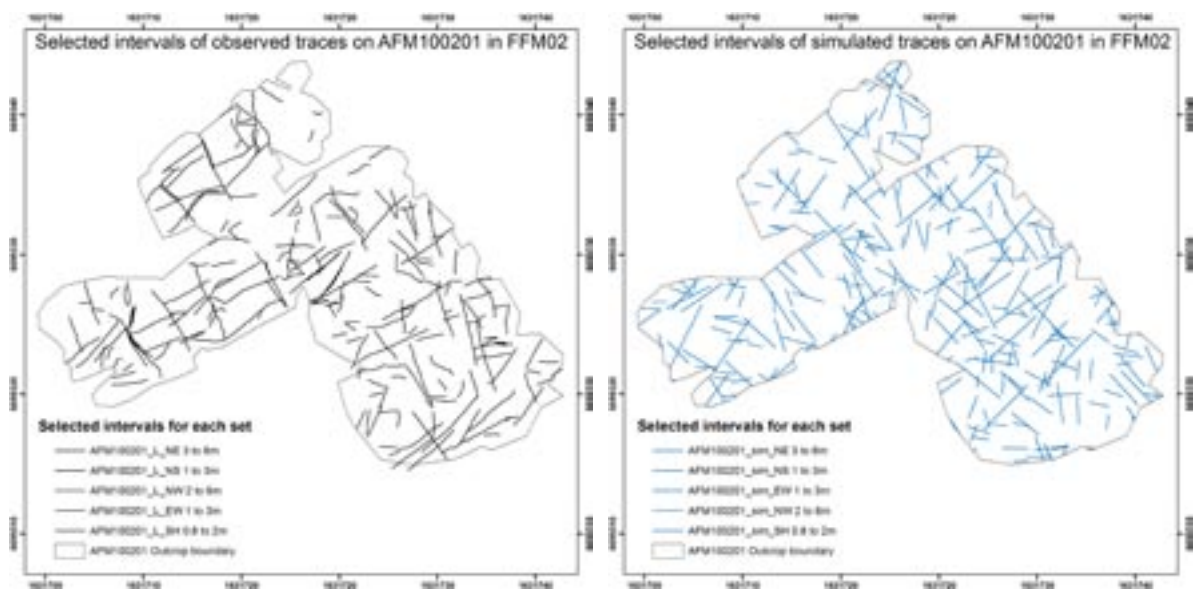
Figure 6-18. *Observed (left) and simulated (right) traces in selected size ranges, AFM100201 in domain FFM02.*

The results for FFM02 suggest that the TCM models may slightly over-estimate outcrop fracture intensities in all sets, but still performs fairly well overall, with only a 6% difference between total P_{21} values. The model's slightly higher intensity is most likely due to the fact that the intensity model in the TCM is conditioned not only to outcrop data, but also to borehole data. As such, it represents an average for the entire domain; it seems possible that the outcrop intensities may not be representative of the domain as a whole.

6.1.3 Verification of intensity model

The verification analyses described in the previous chapter focused on the coupled size/intensity relation for the TCM mode at the outcrop scale. A further test of this model is to assess how well it predicts intensity in the subsurface, and to include the OSM+TFM alternative as well as the TCM. This requires comparisons to borehole fracture intensities rather than trace intensities in surface outcrops.

Verifying fracture intensity parameterizations was conducted in much the same manner as the orientation and size models. Stochastic realizations were completed, sampled using simulated boreholes, and compared to 6 m binned P_{10} data from the Forsmark site. Note that zero-radius boreholes (line sampling) were used in the verification; this is in accordance with how fracture intensities were calibrated in the Forsmark 2.2 GeoDFN model using the Wang solution. Borehole KFM04A was chosen as a representative borehole for domain FFM01, while Borehole KFM08C was chosen as a representative borehole for domain FFM06. Intensity verifications of FFM02 and FFM03 are included in the discussion of the size model verification in Chapter 6.1.2.

For each conceptual model alternative (OSM+TFM and TCM), stochastic DFNs of the Global fracture sets were created in a 40 m x 40 m x 40 model volume, following the model summary tables presented in Chapter 7. Note that the 'match point' values of r_0 and P_{32} were used for the simulations, which is appropriate for carrying out borehole comparisons. The mean P_{10} value was calculated for each simulated borehole in each fracture domain, and then compared to real site observations in Table 6-5.

The verification suggests that, with the exception of the NS Global set, the tectonic continuum models do an excellent job of reproducing average P_{10} values in both FFM01 and FFM06. Both models tend to slightly over-estimate subhorizontal fracture intensity. The NS Global set is somewhat problematic; its parameterization is largely derived from a single outcrop (AFM100201) in domains FFM01, FFM02, and FFM03. That specific outcrop features a relatively low P_{21} intensity of the NS Global set; in addition, the traces mapped on this outcrop appear fairly short when compared to the other sets. However, borehole data in all three domains suggests a higher P_{32} value (when calculated from P_{10}) then would be expected from the outcrop data.

The TCM alternative assumes coupled size-intensity scaling based on surface trace data; a low surface intensity for the NS Global set coupled with a high borehole intensity results in a fracture population heavily skewed towards very small (< 1 m) fractures. It is likely that, in the case of the NS Global set, AFM100201 is not representative of FFM01 and FFM02. The Outcrop-Scale Model, which pins intensity to the borehole P_{10}, produces much more reasonable numbers in the boreholes, giving credence to this hypothesis.

Table 6-5. Comparison of observed P10 to simulated P10 in domains FFM01 and FFM06.

FFM01 Fracture set	Mean P10 KFM04A	OSM+TFM	TCM
NE	0.50	0.29	0.48
NS	0.47	0.40	2.05
NW	0.65	0.45	0.64
SH	0.49	0.49	0.52
Total	2.11	1.63	3.69

FFM06 Fracture set	Mean P10 KFM08C	OSM+TFM	TCM
NE	1.57	0.80	1.21
NS	1.04	1.00	2.10
NW	0.89	0.71	0.97
SH	0.22	0.59	0.49
Total	3.72	3.10	4.77
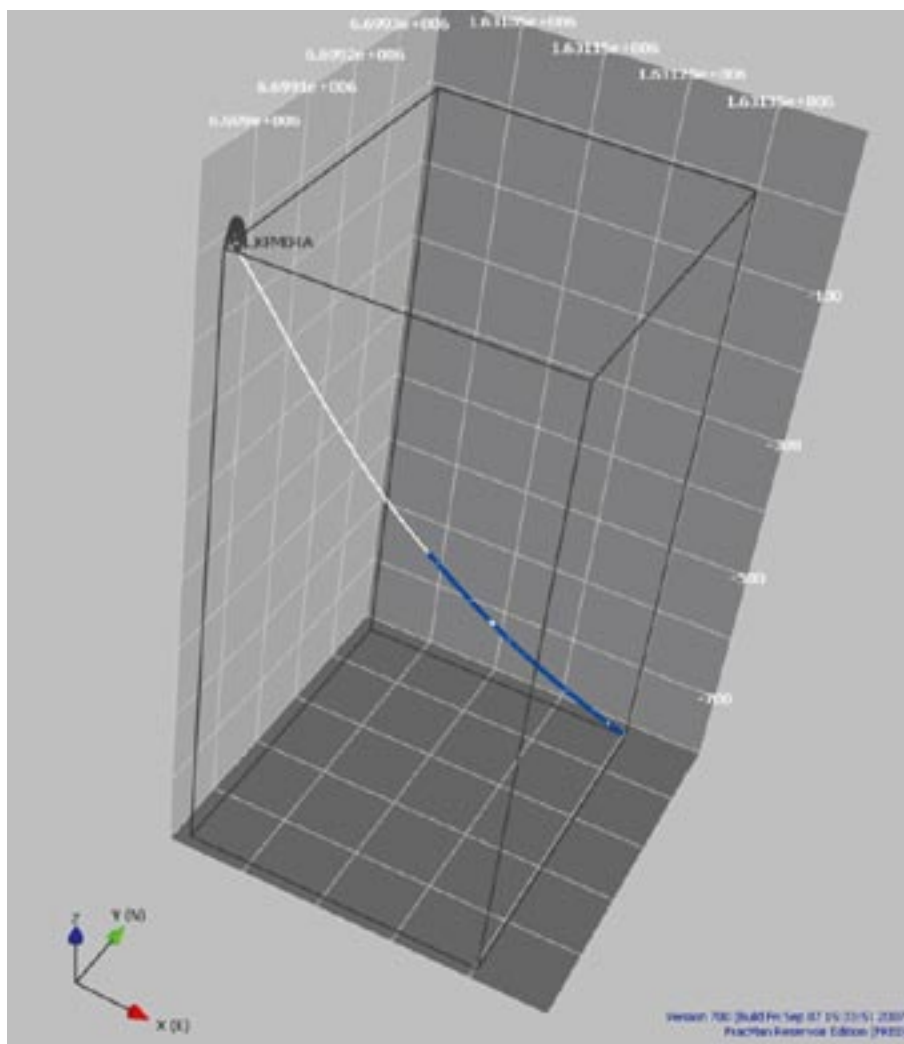
Figure 6-19. P_{10} intervals (blue(in KFM04A, domain FFM01. Gaps represent sections affected by DZ or containing DZ that are removed from the calculations.

234
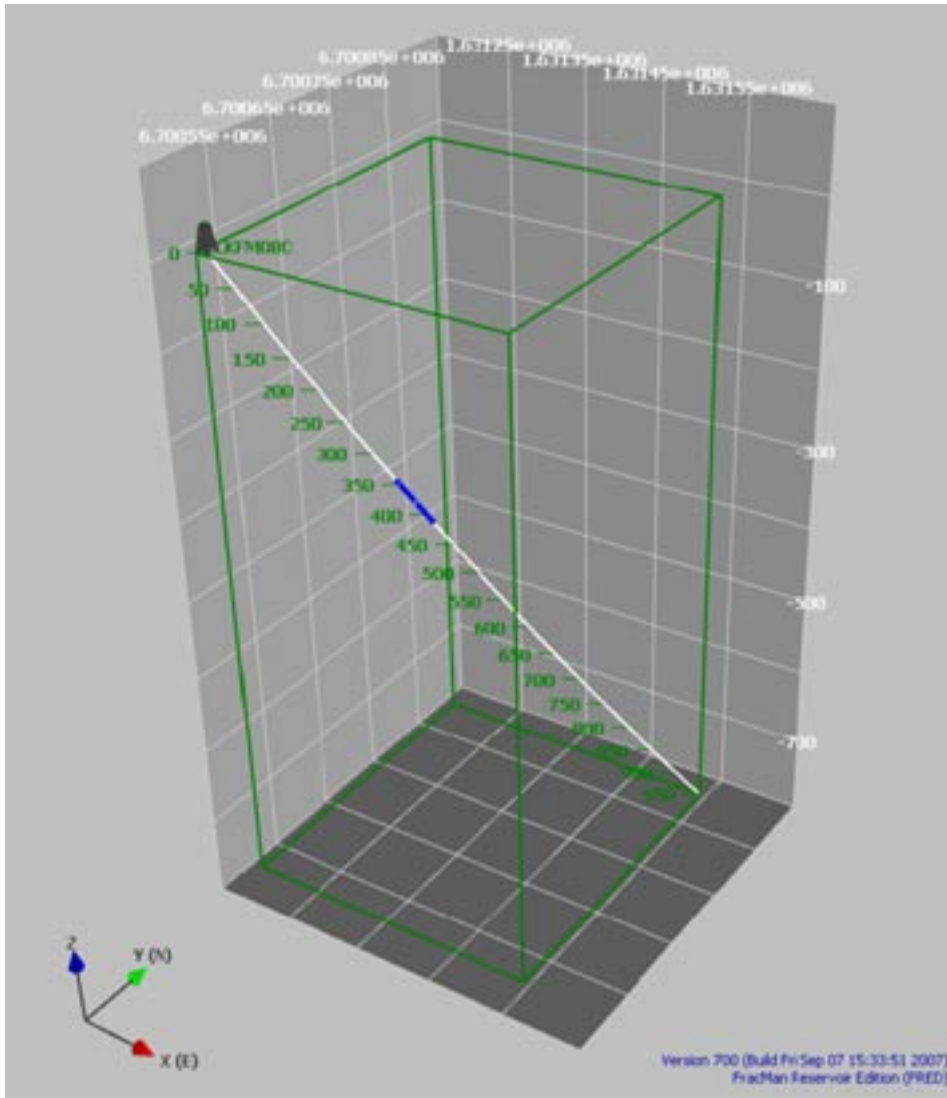
Figure 6-20. *P_{10} intervals (blue(in KFM08C, domain FFM06. Gaps represent sections affected by DZ or containing DZ that are removed from the calculations.*

Comparison of P_{32} to semi-analytical solution

Preliminary discussions during the planning phases for Forsmark 2.2 in /Munier 2006/ suggested that a useful verification case for the final geological DFN models would be to compare the P_{32} values assigned to each set to those that could be expected based on semi-analytical solutions. The planning document /Munier 2006/ lists the following analytical benchmarks (derived from /Dershowitz et al. 1998/) to be completed as a 'back of the envelope' check of the Forsmark geological DFN parameterizations.

$$P_{32} = 2 \cdot P_{10}$$ Equation 6-1

$$P_{32} = \frac{4}{\pi} \cdot P_{21}$$

The comparison was done by taking the fitted P_{32} values (the P_{32} to which the size model was fit, and not the P_{32} relative to the 0.5 m r_{min} cut-off) for each model alternative in each model domain, and comparing them to the analytical estimate, based on the observed mean P_{10} values in the borehole array. The results are presented in Table 6-6 and Table 6-7.

Table 6-6. Comparison of P_{32} values from DFN parameterization for Global fracture sets to analytical solution based on borehole P_{10}.

Fracture domain	Mean P_{10} (data)	P_{32} (at $r_{min} = r_0$) Benchmark	TCM	OSM+TFM
FFM01	1.45	2.89	4.61	4.65
FFM06	3.72	7.44	7.7	7.76

Table 6-7. Comparison of P_{32} values from DFN parameterization for Global fracture sets to analytical solution based on outcrop P_{21} from AFM100201.

Fracture domain	P_{21} data	P_{32t} (r_{min} of 0.5 m) Benchmark	TCM	OSM+TFM
FFM02	2.48	3.16	6.53	3.62
FFM03	2.06	2.62	4.7	2.81

* Uses data from AFM001264, since no ENE Set on AFM100201.

The benchmark calculations suggest that the P_{32}s for the Outcrop Scale Model derived from P_{21} intensities correspond fairly well with the values derived from the analytical solution. This is not surprising, as that data was directly used in the parametization. The method does not work, however, for the tectonic continuum alternatives, as it is not possible to directly compare the P_{21} values measured at different scales due to resolution issues and the requirement of area normalization.

The benchmark calculations also suggest that the P_{32}s for both the OSM and the TCM models in domain FFM06 are fairly reasonable. However, the goodness-of-fit is much less apparent for domain FFM01; the analytical benchmark under-estimates P_{32} relative to the geological DFN. This is at odds, however, with the conclusions in the previous section (Table 6-5) where, with the exception of the NS Set in the tectonic continuum models, the P_{32} values in the Forsmark 2.2 geological DFN produce very reasonable mean borehole P_{10} values.

The analytical benchmarks presented as Equation 6-1 also assume a completely random orientation distribution (i.e. Fisher $\kappa = 0$). The benchmark calculations also assume a uniform density of orientations. Neither case is strictly true of data derived from Forsmark cored boreholes; there is a clear subdivision of fractures into horizontal and vertical sets, with a relative dearth of moderately-dipping (30°–60°) fractures. In fact, the orientation distributions are highly non-uniform.

It should be noted that these are approximations only; the analytical solutions in Equation 6-1 do not take the orientations of the boreholes relative to the fracture sets into account. As such, this equation will under-estimate P_{32} for steeply-dipping boreholes orthogonal to the fracture set mean pole. As a majority of the fracture sets at Forsmark are steeply dipping, the analytical equation will tend to under-estimate the P_{32} values of the subvertical sets. In the same vein, for a vertical or near-vertical borehole, the porportionality constant (C13) for P_{10} of subhorizontally-oriented boreholes is fairly close to 1. A C13 of 2 will over-estimate the intensity of the subhorizontal set.

Verification of TCM/TFM model intensity in the MDZ size range

Recent site characterization efforts have focused on detecting and quantifying the size and intensity of 'minor deformation zones', or MDZ. These features are geologic structures hypothesized to exist in the size range between outcrop fractures ($r \sim 10$ m) and the start of the deterministic size deformation zone (DZ) models ($r = 564$ m). These structures are of critical importance to site characterization; they are features of a scale that directly affects repository layouts, tunnel and shaft stability, local hydraulic conditions, and have the potential to undergo slip in an earthquake.

As such, a verification exercise was performed to determine how well the Forsmark 2.2 geological DFN was able to characterize the intensity of MDZ structures. There is little information from this size range (10 m–1,000 m, in terms of surface trace length); the majority of the data we have come from ground magnetic lineaments with limited areal coverage, and the few MDZ intercepts found in cored boreholes. As a result, there is moderately high uncertainty in the parameters derived from the measured data. However, even if an exact match is not obtained, there should not be significantly more or significantly fewer MDZ in the simulations than in the measured data.

It is important to note that there are structures in the Forsmark 2.2 DZ model that are shorter than 1,000 m in trace length ($r = 564$ m). There were 40 such structures mapped in the Forsmark 2.2 DZ model; of these, 28 were not included in the final RVS block model. These structures were included in the geologic modeling because the data density was such that it was possible to trace them between multiple boreholes and map their areal extents accurately. Even though these structures will ultimately be simulated deterministically, we have included their intercepts in the validation of the TFM and TCM models, as they exist in the size range that, at least at depth, will be simulated stochastically. A list of the MDZ structures used in this verification exercise is presented below as Table 6-8.

The simulation process used in the MDZ verification is as follows:

- A simulation volume of 6,000 m x 6,000 m x 1,500 m, encompassing the entire candidate volume at Forsmark, is used for the simulations. A schematic cartoon of the simulation volume is included as Figure 6-21. Five stochastic realizations of the TCM and TFM models are generated within this volume. These models assume a lower radius cut-off value (rmin) of 28 m, as specified in the geoDFN parameter tables. A realization is performed for each fracture domain (FFM01, FFM02, FFM03, and FFM06).

- A total of four borheoles are chosen for sampling and verification. Three of these are within domain FFM01, while the fourth is within FFM06. Domains FFM02 and FFM03 were omitted from the verification due to a paucity of available MDZ data for comparison. The boreholes are placed in the model according to their actual trajectories, with total P_{10} calculated over the full length of the domain intersection (including DZ lengths) in a given fracture domain.

- For each borehole, the number of simulated intersections is compared to observations from Forsmark cored boreholes. As it is not possible to divide the MDZ population recorded in cored boreholes into orientation sets, it is necessary to cast the verification in terms of total MDZ intensity (P_{32}). Though simulations were performed on a set-by-set basis, the resulting output tables only consider total MDZ intensity.

The results of the MDZ verification are presented in Table 6-9; the results are classified by fracture domain and by borehole.

Table 6-8. List of MDZ (and short DZ) included in TCM/TFM verification exercise.

Borehole IDCODE	Structure type	ADJ_SECUP m	ADJ_SECLOW m	Fracture domain
KFM01B	ZFMNNW0404	415	454	FFM01
KFM01D	DZ not modelled	176	184	FFM02
KFM01D	DZ not modelled	411	421	FFM01
KFM01D	DZ not modelled	488	496	FFM01
KFM01D	DZ not modelled	771	774	FFM01
KFM02A	DZ not modelled	520	600	FFM01
KFM02A	DZ not modelled	922	925	FFM01
KFM02A	DZ not modelled	976	982	FFM01
KFM03A	DZ not modelled	942	949	FFM03
KFM03B	DZ not modelled	62	67	FFM03
KFM03B	DZ not modelled	953	956	FFM03
KFM04A	ZFMNE1188	290	370	FFM04
KFM04A	ZFMNE1188	412	462	FFM04
KFM05A	ZFMENE0401B	590	616	FFM01
KFM05A	ZFMENE2383	936	992	FFM01
KFM05A	ZFMNE2282	395	436	FFM01
KFM06A	DZ not modelled	128	146	FFM02
KFM06A	DZ not modelled	652	656	FFM01
KFM06A	DZ not modelled	882	905	FFM06
KFM06A	DZ not modelled	925	933	FFM06
KFM06A	ZFMNNE2255	619	624	FFM01
KFM06A	ZFMNNE2273	518	545	FFM01
KFM06C	DZ not modelled	102	169	FFM01
KFM06C	DZ not modelled	623	677	FFM06
KFM06C	ZFMWNW0044	502	555	FFM06
KFM06C	ZFMNNE2008	283	306	FFM01
KFM07A	DZ not modelled	196	205	FFM01
KFM07B	DZ not modelled	51	58	FFM02
KFM07B	DZ not modelled	119	135	FFM02
KFM07B	ZFM1203	93	102	FFM02
KFM07C	ZFM1203	92	103	FFM02
KFM08A	DZ not modelled	528	557	FFM01
KFM08A	DZ not modelled	623.6	624.1	FFM01
KFM08A	DZ not modelled	672	693	FFM01
KFM08A	DZ not modelled	915	925	FFM01
KFM08A	DZ not modelled	925	946	FFM01
KFM08A	DZ not modelled	967	976	FFM01
KFM08A	ZFMNNW1204	479	496	FFM01
KFM08B	ZFMENE2403	275	283.7	FFM01
KFM08B	ZFMNNW1205	133	140	FFM01
KFM08B	ZFMNNW1205	167	185	FFM01
KFM08C	DZ not modelled	161	191	FFM01
KFM08C	DZ not modelled	666	667	FFM01
KFM08C	DZ not modelled	283.6	284.1	FFM01
KFM09B	DZ not modelled	308	340	FFM01
KFM09B	ZFMENE2325A	520	550	FFM01

Table 6-9. Comparison of TFM and TCM models to observed data for fractures in the MDZ size range.

TFM Model Borehole IDCODE	Fracture domain	Fracture domain Limits ADJSECUP	ADJSECLOW	# of simulated MDZ intersections 1	2	3	4	5	Mean	# of MDZ intersections Observed
KFM01D	FFM01	191	800	15	17	24	20	18	19	3
KFM05A	FFM01	237	1,000	24	24	29	27	33	27	3
KFM08A	FFM01	102	843	46	30	36	28	32	34	6
KFM08A	FFM01	946	1,001	3	4	0	2	1	2	1
KFM06A	FFM06	740	998	14	9	10	12	10	11	2

TCM Model Borehole IDCODE		Fracture domain limits ADJSECUP	ADJSECLOW	# of simulated MDZ intersections 1	2	3	4	5	Mean	# of MDZ Intersections observed
KFM01D	FFM01	191	800	22	38	45	46	27	36	3
KFM05A	FFM01	237	1,000	36	50	39	51	45	44	3
KFM08A	FFM01	102	843	43	57	48	70	37	51	6
KFM08A	FFM01	946	1,001	0	6	1	3	2	2	1
KFM06A	FFM06	740	998	18	20	16	13	15	16	2
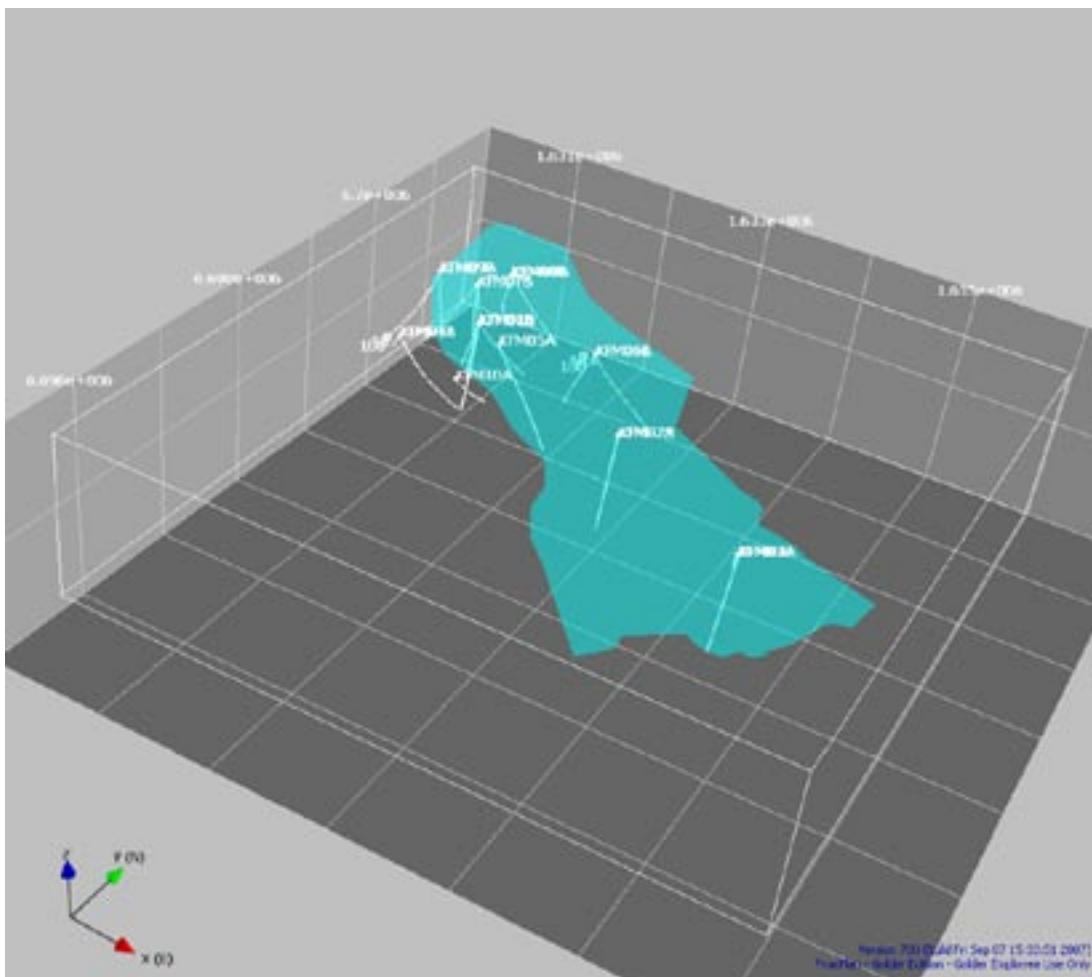
Figure 6-21. Simulation region used for verification of TCM/TFM in MDZ size range.
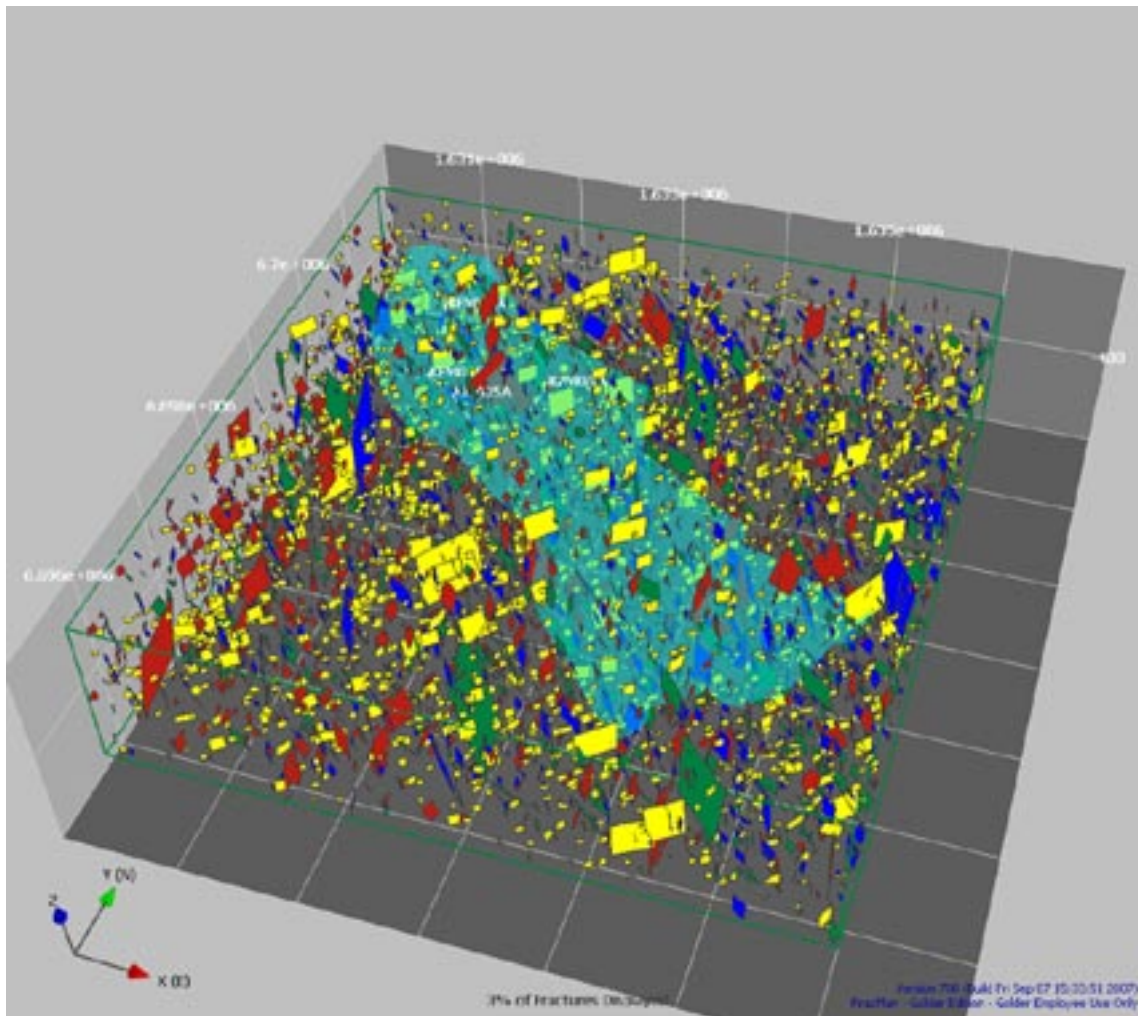
Figure 6-22. *Example realization of NS, NW, and SH sets, TFM. Note that due to the set's high intensity in the TFM, only 1% of the NE Global set is displayed. The remaining sets are presented at 100%.*

In general, simulation results show much higher MDZ intensities than observed in cored boreholes; there are generally no more than 3–4 MDZ per borehole, per fracture domain. However, the simulation results show anywhere from 10–70 MDZ, per hole, per domain. This suggests that the arbitrary minimum radius of 28 m may be too small. If we believe the borehole data, accept that every feature mapped as a DZ but not included in the DZ model is truly a deformation zone, and believe our TCM and TFM models are accurate, then we are left with the possibility that the MDZ mapped in the holes represent much larger structures (on the order of 100 m or larger) in terms of fracture radius. Another possibility is that there is a lower size cutoff for the TFM model. Results obtained in the course of the uncertainty analyses shows that there is often a reduction of about one order of magnitude in the intensity when the lower 28 m cutoff is increased to 200 m (Chapter 5.1.1).

Figure 6-23 illustrates a sample realization of the simulations for FFM06; note that most of the intersections in this section come from subhorizontally-oriented MDZ. The subhorizontal Global set, in both the TFM and the TCM model alternatives, is the one with the least amount of data. There are no observations for this set in the ground-magnetic lineament data, and only a few large, shallowly-dipping DZ in the Forsmark 2.2 DZ model. As such, both the size and intensity of MDZ in the subhorizontal set is highly uncertain.
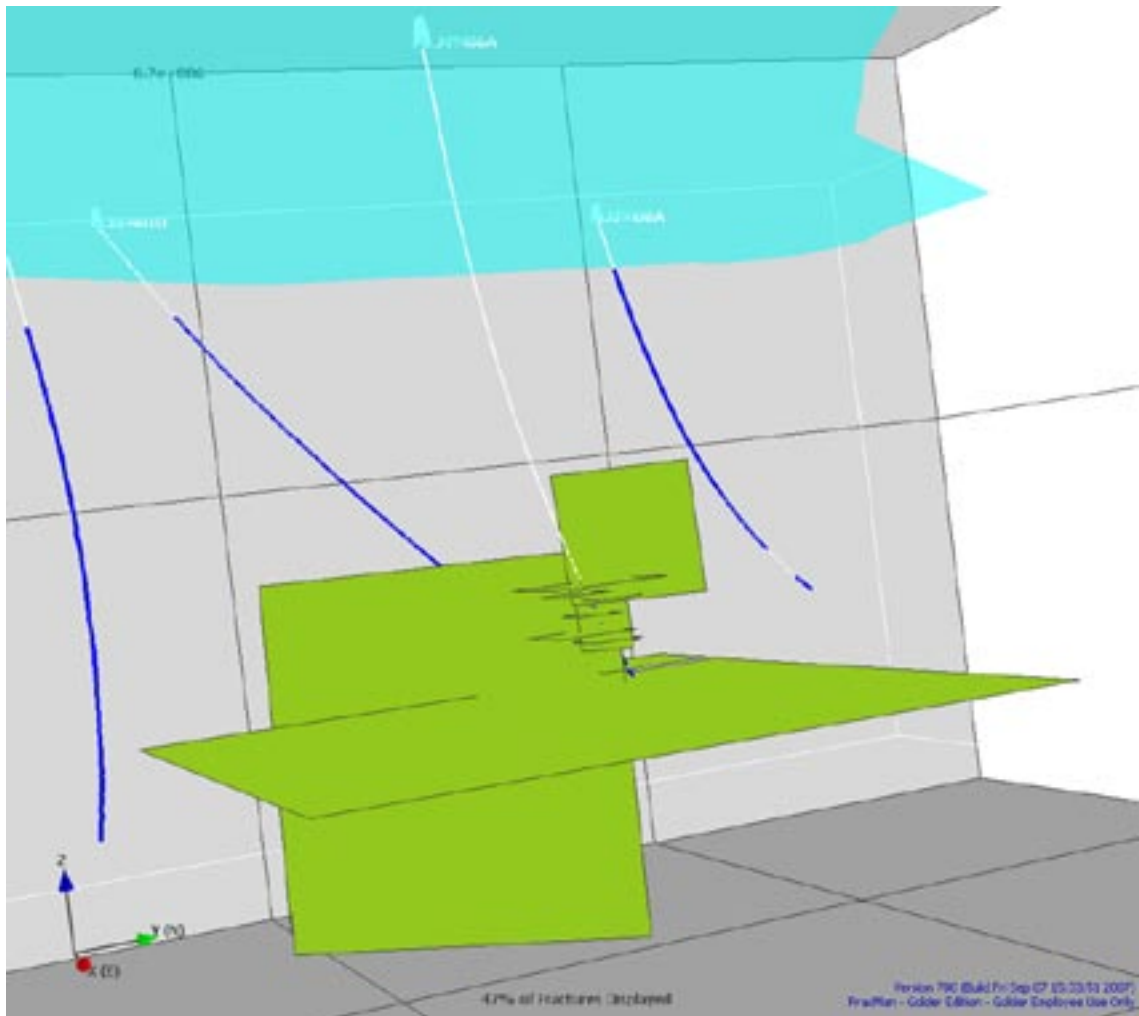
Figure 6-23. Screenshot of TFM MDZ intersections, KFM06A in FFM06. Note that the SH MDZ dominate; this suggests that the rmin value of 28 m is too low for SH MDZ.

To clarify the effects that the uncertainty in the SH Global set might have on the final DFN parameters, a second set of simulations was run excluding this set. The results are presented in Table 6-10. Simulation results seem to suggest that, in the current model, the subhorizontal DZ fraction is substantially overstated; in all validation cases, it represents more than one-half the intersected intensity.

The logical solution to the intensity problem is to increase the minimum radius cutoff used in the DFN intensity model. A problem arises, however, with attempting to base a minimum-radius cutoff for MDZ from borehole intersection data. The data set is highly scattered; some boreholes show no MDZ, while others show five or more MDZ. In addition, there is no hard data as to exactly where the MDZ – large joint/background fracture transition actually is. In reality, the boundary is likely very fuzzy, with some larger joints exhibiting shear offset or reactivation in the brittle regime, and with some structures that would be mapped as joints actually representing faults without a well-developed damage zone.

The problem is further exacerbated by the fact that we can only compare total intensity statistics; it is difficult to come to any concrete conclusions about which particular orientation set is over- or under-estimated. The lack of orientation data for the MDZ population in the cored borehole data makes any intensity parameterization fit to borehole data a fundamentally non-unique solution.

241

Table 6-10. Comparison of TFM and TCM models to observed data for fractures in the MDZ size range, with the SH Global set excluded.

TFM Model, No Subhorizontal MDZ										# of MDZ
Borehole	Fracture	Fracture domain limits		# of simulated MDZ intersections						Intersections
IDCODE	domain	ADJSECUP	ADJSECLOW	1	2	3	4	5	Mean	observed
KFM01D	FFM01	191	800	7	4	1	3	1	3	3
KFM05A	FFM01	237	1,000	12	7	9	11	13	10	3
KFM08A	FFM01	102	843	18	9	17	12	15	14	6
KFM08A	FFM01	946	1,001	3	1	0	1	0	1	1
KFM06A	FFM06	740	998	3	2	2	1	3	2.2	2

TCM Model, No Subhorizontal MDZ										# of MDZ
Borehole	Fracture	Fracture Domain Limits		# of simulated MDZ intersections						Intersections
IDCODE	Domain	ADJSECUP	ADJSECLOW	1	2	3	4	5	Mean	Observed
KFM01D	FFM01	191	800	14	17	25	29	18	21	3
KFM05A	FFM01	237	1,000	27	22	18	27	21	23	3
KFM08A	FFM01	102	843	26	31	24	43	24	30	6
KFM08A	FFM01	946	1,001	0	5	1	2	0	2	1
KFM06A	FFM06	740	998	8	8	11	8	9	8.8	2

Based on the results of this verification, we suggest that, if and where possible, additional work be performed, either through hydraulic testing or additional surface/underground mapping, to determine what the actual size range of MDZ is, and where the transition line should be drawn. Until additional information is gathered, coming to any solid conclusions regarding the MDZ/ joint cut-off is not possible.

6.1.4   Verification: prediction of cored borehole KFM08D

A final exercise in the verification of the Forsmark 2.2 geological DFN was the prediction of the patterns of fracturing in a borehole not used in the model parameterization. Cored borehole KFM08D, which is located near the center of the northern half of the Forsmark candidate region, was used for this exercise. KFM08D dips roughly east-west at an approximately 53 degree angle, and crosses through the northern half of the candidate volume. Figure 6-24 shows the trajectory of KFM08D relative to the fracture domains FFM01 and FFM06.

Data sources used in this verification case include:

- p_fract_core (dated 20070411).

- p_object_location (dated 20070411).

- A draft version of the KFM08D single-hole interpretation /Carlsten et al. 2007/, dated April 2007.

- RVS-computed intercepts of Fracture Domain and Forsmark 2.2 DZ model features. The RVS intercepts were performed by Ingemar Markstrom of Golder Associates, AB, in August 2007. No formal data delivery or reference is available; however, the relevant project emails and data tables are available upon request.

The results of the preliminary single-hole interpretation /Carlsten et al. 2007/ is summarized below in Table 6-11. Since the single-hole interpretation does not include intercepts with modeled structures in the Forsmark 2.2 DZ model nor the fracture domains in the 2.2 fracture zones, hypothetical intercepts for both classes of data were computed using RVS; these intercepts are presented below in Table 6-12. Both the fracture domain and DZ model intercepts are highly
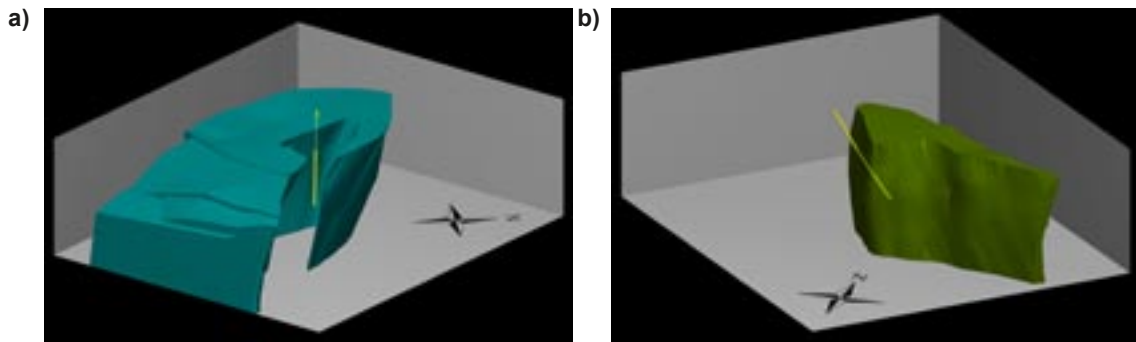
Figure 6-24. *Path of KFM08D relative to Local Model volume and fracture domains FFM01 (a) and FFM06 (b).*

uncertain; additional geologic modeling work done during stage 2.3 may make an update to this analysis required. Note that a tentative effort has been made (Table 6-11) to match possible DZ listed in the SHI to named structures in the 2.2 DZ (Table 6-12); this is based solely on proximity to the RVS intercepts and does not include any examination of the rock core or BIPS imagery.

Table 6-11. Preliminary results of single-hole interpretation (SHI) for borehole KFM08D.

Rock units			Possible DZ			
MD_Start	MD_End	Rock Unit	number	MD_Start	MD_End	Potential match to 2.2 DZ
59	395.65	RU1	DZ1	184	210	MDZ
395.65	569.76	RU2a	DZ2	318	324	ZFMENE0159A
569.76	597	RU3a	DZ3	371	396	ZFMENE0159B
597	651.37	RU4a	DZ4	496	506	MDZ
651.37	841.61	RU2b	DZ5	546	571	MDZ
841.61	876.71	RU5	DZ6	582	609	ZFMNNE2308
876.71	896.66	RU4b	DZ7	621	634	MDZ
896.66	928.52	RU3b	DZ8	644	689	ZFMENE2320
928.52	941.75	RU2c	DZ9	737	749	ZFMNNE2293
			DZ10	770	777	MDZ
			DZ11	819	842	MDZ
			DZ12	903	941.75	ZFNWNW2225

Table 6-12. KFM08D intercepts with fracture domains and Forsmark 2.2 DZ model structures from August 2007 RVS model.

Fracture domains			DZ intersected, local model			
MD_Start	MD_End	Domain	name	MD_Start	MD_End	Map to SHI DZ?
3.1	60.1	FFM02	ZFMENE0159A	304.1	344.7	DZ2
60.1	403.4	FFM01	ZFMENE0159B	373.2	389.7	DZ3
403.4	942.3	FFM06	ZFMENE2320	667	740	DZ8?
			ZFMNNE2293	717.7	739.1	DZ9?
			ZFMNNE2308	601.8	623.1	DZ6
			ZFMWNW2225	905.6	942.3	DZ12

The methodology for the prediction of borehole KFM08D is as follows:

1. Using preliminary data from the drilling of KFM08D, which fracture domains KFM08D intersects (Table 6-12) was determined.

2. The preliminary BIPS/Boremap data (SICADA table p_fract_core) was then processed to classify fractures in terms of fracture domain, presence inside or outside of deformation zones, and visibility in BIPS.

3. The fracture data from KFM08D was assigned to the orientation sets used in the Forsmark 2.2 geological DFN model. FracSys/ISIS was used to divide the fractures into sets using an initial hard-sector search, combined with a sector preconditioning refinement /Dershowitz et al. 1998/. The orientation assignment was done only for fractures visible in BIPS and outside of mapped (preliminary SHI) deformation zones. Stereonets of the fracture sets are visible below as Figure 6-25 and Figure 6-26. Though domain FFM02 was encountered in the upper part of KFM08D in the RVS intercepts, no data inside that domain exists in the cored borehole record (p_fract_core). As such, no formal verification against FFM02 in KFM08D was performed.
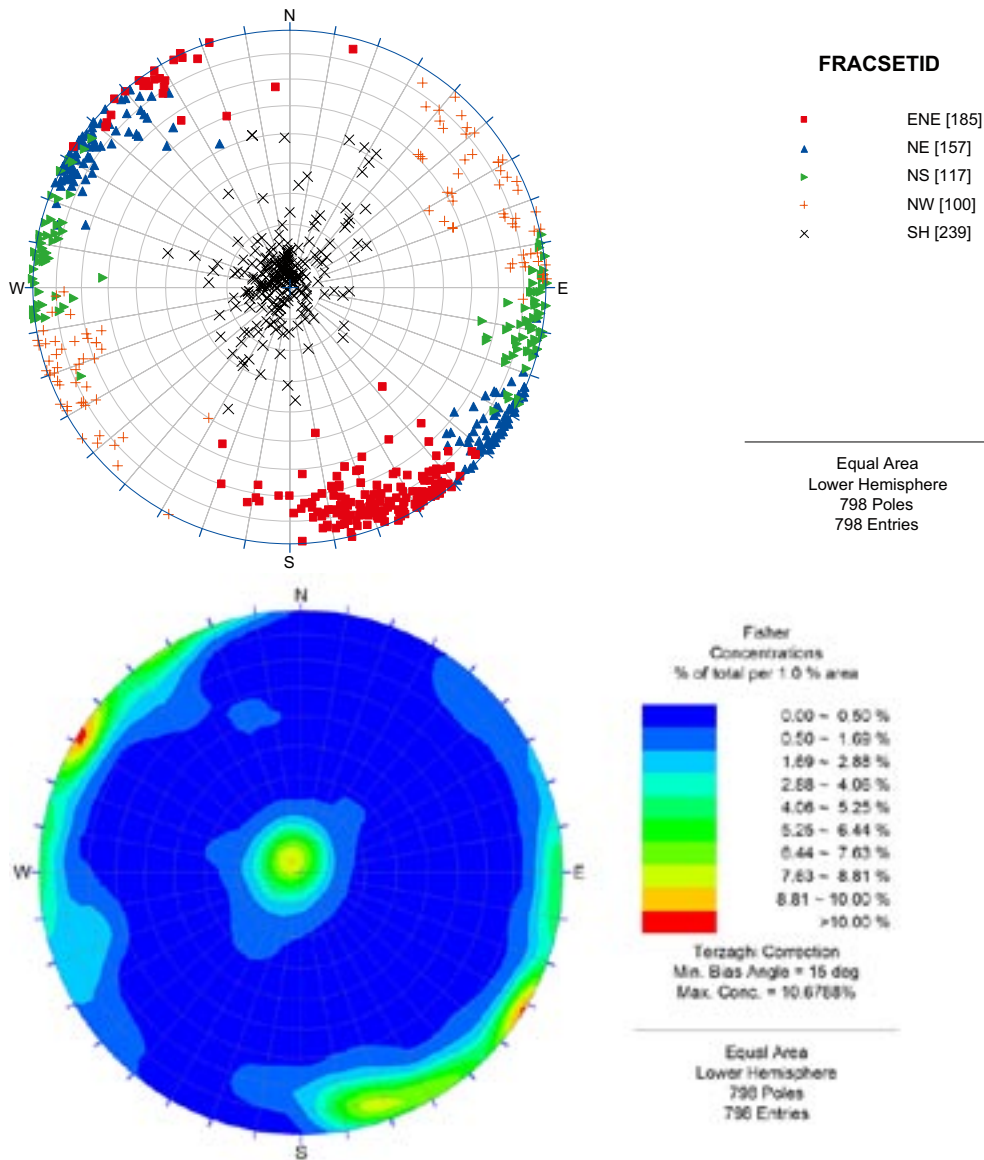
Figure 6-25. *KFM08D fracture sets, Domain FFM01, fractures outside mapped DZ and visible in BIPS.*
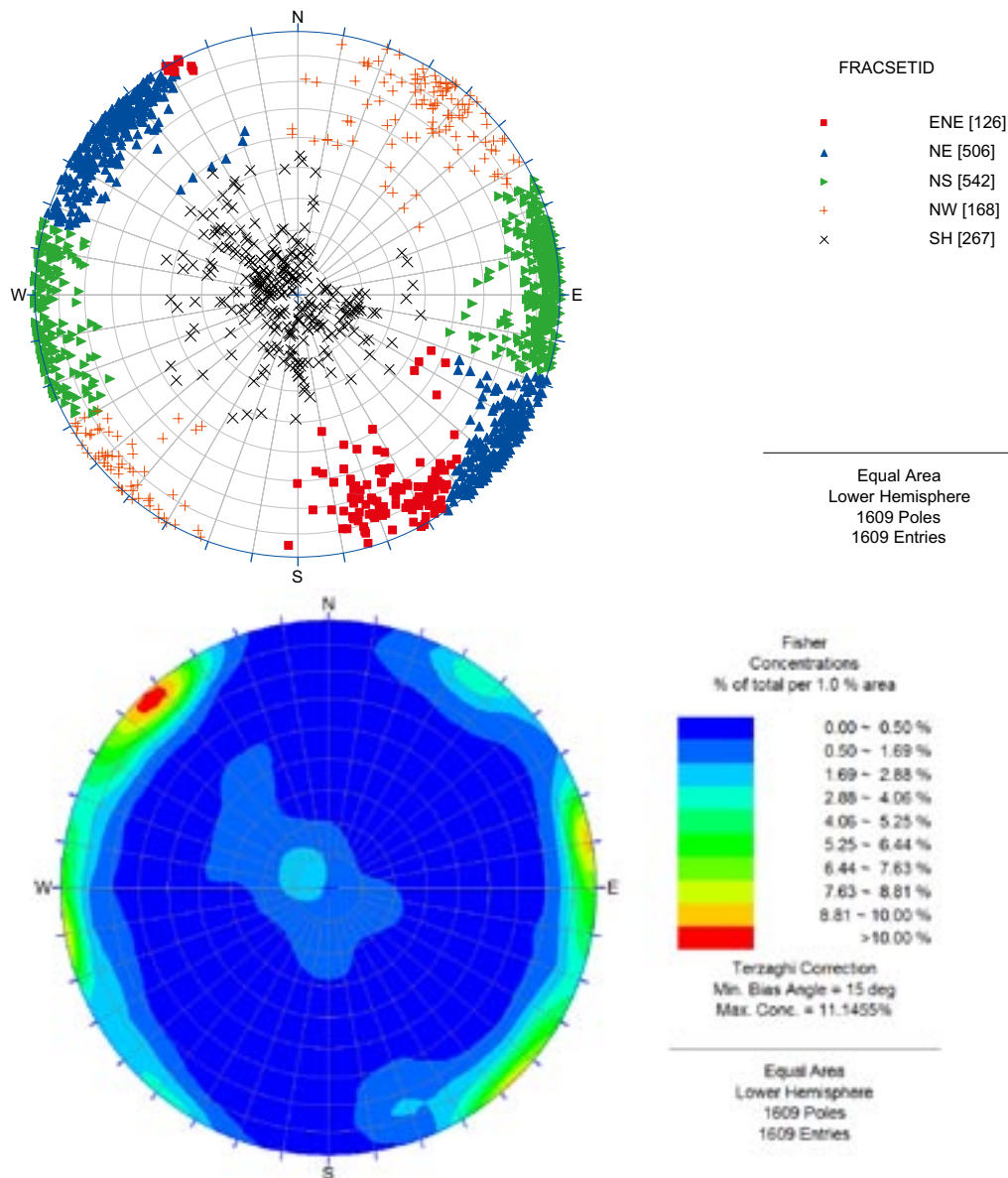
Figure 6-26. *KFM08D fracture orientations and sets, Domain FFM06, fractures outside mapped DZ and visible in BIPS.*

4. Fracture intensity measurements were computed for both the full KFM08D record (for segments outside mapped DZ) and for only fractures visible in BIPS. P_{10} was computed for all intervals assuming 30 m section lengths. P_{10} values for observed data are presented below as Table 6-13 and Table 6-14.

5. Using the property tables contained in Chapter 7 of this report, a single DFN realization for both the OSM+TFM and TCM model alternatives was constructed using FracMan /Dershowitz et al. 1998/. The models were constructed in a similar fashion to the intensity simulations described in Chapter 6.1.3; they exist in a 40 m x 40 m x 40 m volume. A summary, with links to the appropriate tables in Chapter 7, of the properties used to generate the KFM08D DFNs is presented below.. Initially, only the Global sets present in each domain were simulated. However, an examination of the KFM08D fracture data indicated the presence of the ENE Local set in domains FFM01 and FFM06. The models were re-run, including the ENE set, at full intensity throughout the simulation volume.

Table 6-13. Measured fracture intensity (P_{10}) for domain FFM01, borehole KFM08D.

FFM01 Bin Size	Visible in BIPS Interval	SECUP (m)	SECLOW (m)	P_{10}	# of Fractures
30 m	1	60	90	1.87	56
30 m	2	90	120	2.27	68
30 m	3	120	150	2.93	88
30 m	4	150	180	2.90	87
30 m	5	210	240	5.43	163
30 m	6	240	270	4.10	123
30 m	7	270	300	3.73	112
30 m	8	324	354	0.13	4

Summary statistics					
	Mean	Std Dev	Median	Max	Min
Total	2.92	1.59	2.92	5.43	0.13

FFM01 Bin Size	All fractures interval	SECUP (m)	SECLOW (m)	P_{10}	# of fractures
30 m	1	60	90	2.33	70
30 m	2	90	120	2.63	79
30 m	3	120	150	3.83	115
30 m	4	150	180	6.13	184
30 m	5	210	240	7.93	238
30 m	6	240	270	5.63	169
30 m	7	270	300	5.77	173
30 m	8	324	354	0.27	8

Summary statistics					
	Mean	Std Dev	Median	Max	Min
Total	4.32	2.50	4.73	7.93	0.27

Table 6-14. Measured fracture intensity (P$_{10}$) for domain FFM06, borehole KFM08D.

FFM06 Bin size	Visible in BIPS interval	SECUP (m)	SECLOW (m)	P$_{10}$	# of Fractures
30 m	9	403	433	4.90	147
30 m	10	433	463	2.90	87
30 m	11	463	493	1.80	54
30 m	12	506	536	4.67	140
30 m	13	689	719	8.80	264
30 m	14	777	807	7.80	234
30 m	15	842	872	3.73	112
30 m	16	872	902	2.10	63

Summary statistics

	Mean	Std dev	Median	Max	Min
Total	4.59	2.56	4.20	8.80	1.80

FFM06 Bin size	All Fractures interval	SECUP (m)	SECLOW (m)	P$_{10}$	# of Fractures
30 m	9	403	433	6.17	185
30 m	10	433	463	3.93	118
30 m	11	463	493	2.37	71
30 m	12	506	536	4.93	148
30 m	13	689	719	10.80	324
30 m	14	777	807	8.70	261
30 m	15	842	872	5.97	179
30 m	16	872	902	3.53	106

Summary statistics

	Mean	Std dev	Median	Max	Min
Total	5.80	2.80	5.45	10.80	2.37

The following DFN properties were used in generation of KFM08D stochastic simulations:

OSM+TFM Realization

- Sets included: NE, NS, NW and SH (FFM01 and FFM06) Global sets, ENE Local set.
- Orientation Model(s): Table 7-1, used mean value for Fisher κ, by domain.
- Size Model(s): Table 7-2 and 7-3, by domain.
- Spatial model: Poissonian (Enhanced Baecher model for fracture centers).
- Intensity Model(s): Used Match P$_{32}$, kr, and r0 from the size model (Table 7-2 and 7-3). P$_{32}$ taken as mean P$_{32}$ for domain (not simulated as a gamma distribution.

TCM Realization

- Sets included: NE, NS, NW and SH (FFM01 and FFM06) Global sets, ENE Local set.

- Orientation Model(s): Table 7-1, used mean value for Fisher κ, by domain.

- Size Model(s): Table 7-4, by domain. The TCM model alternative was used.

- Spatial model: Poissonian (Enhanced Baecher model for fracture centers).

- Intensity Model(s): Used Match P_{32}, kr, and r_0 from the size model (Table 7-2 and 7-3). P_{32} taken as mean P_{32} for domain (not simulated as a gamma distribution .

As each fracture set was modeled separately, terminations were not included in the simulations. In addition, as this was designed to be a 'blind' prediction of in-situ fracturing and not a model calibration or formal model realization, lithology corrections were not used in the simulations.

6. The resulting DFN models were sampled using an array of simulated boreholes to represent KFM08D. The drill path data for KFM08D (p_object_location) was used to get the orientation of the borehole in terms of 30 m segments. Then, the start point of the 30 m segment was chosen using a semi-random Cartesian location inside the model domain, such that the entire borehole was inside the simulation volume and that the borehole's actual orientation (in terms of trend and plunge) was respected.

7. Simulated sampling was carried out using the borehole array. The orientations of fractures in specific sets were directly compared to the orientations of the sets fitted to the actual KFM08D data. The verification compares a) the location of the simulated versus actual set mean poles, and b) the relative set intensities.

8. Fracture intensities were validated by directly comparing simulated mean P_{10} values outside of deformation zones to mean P_{10} values computed from the BIPS/Boremap data for KFM08D. The comparison is made in terms of total fracture intensity (both Visible in BIPS and not Visible in BIPS) so as to accurately evaluate the DFN parameterization.

Verification of KFM08D fracture orientations

The comparison of predicted fracture orientations versus actual fracture orientations for KFM08D consisted of two components: a numeric comparison of the mean pole vector locations for each fracture set, and a comparision of the relative set intensities. To compare the mean pole locations, the solid angle between the set mean pole fit to KFM08D data and the mean pole proscribed for that fracture set in a given domain was calculated. Goodness of fit is judged using the 95% confidence intervals on the mean pole vector and on the distribution of the Fisher κ (as described in Chapter 3.2.2).

Table 6-15 illustrates the results of the blind prediction of fracture set orientations in KFM08D. In FFM01, the mean pole vector fit to the SH and ENE sets in KFM08D fell inside the 95% confidence cone around the mean pole. This suggests an excellent fit between the data and the model. For all other fracture sets in FFM01, the results were slightly poorer. The fitted mean poles fell outside the 95% confidence interval on the mean pole, but, with the exception of the NW set, all fell well inside the 95% confidence interval for the Fisher distribution of set mean poles. This builds confidence that the hypothesis that, though the set mean pole varies spatially, the variation itself is accurately simulated using a Fisher distribution.

In FFM06, only the NS set fell inside 95% confidence cone surrounding the set mean pole. However, the NS, NE, and NW sets still showed a good fit; they are inside the 95% confidence interval for the Fisher distribution of set mean poles, and are fairly close (within 3-4 degrees) of the 95% cone of confidence on the set mean pole. The SH set is the only anomaly in domain FFM06; it falls well outside both confidence intervals. This suggests that, if the specific orientations of subhorizontal fractures inside FFM06 are of concern to downstream models, additional testing should be considered, or a bootstrap approach to subhorizontally-dipping fracture orientations be taken.

A direct comparison of contoured stereonets (Figure 6-27 and Figure 6-28) offers some interesting insights. For FFM01, the OSM+TFM model performs well. It tends to under-predict the intensity of the subhorizontal fracture set encountered in KFM08D slightly, and slightly over-predicts (Table 6-16) the intensity of the Local ENE set (at the expense of the Global NE set). Visually, the OSM+TFM model performs well; it appears quite similar to the data recorded in KFM08D. The TCM model performed somewhat worse at predicting KFM08D; it tended to underestimate the relative intensity of all sets in FFM01 relative to the NE Global set.

Table 6-15. Comparison of fitted set mean poles to KFM08D fracture data and the Forsmark 2.2 geological DFN orientation model.

FFM01 set	2.2 DFN Model trend	Plunge	KFM08D Trend	Plunge	Solid angle	95% CI Mean pole	95% C.I. Fisher K
NE	314.9	1.3	304.8	1.0	10.1	4.7	20.5
NS	270.1	5.3	98.2	1.2	10.4	5.1	20.6
NW	230.1	4.6	67.0	2.0	18.1	5.8	24.9
SH	0.8	87.3	329.0	86.0	2.2	4.5	20.2
ENE	157.5	3.1	157.0	8.8	5.7	5.7	14.1

FFM06 set	2.2 DFN Model Trend	Plunge	KFM08D Trend	Plunge	Solid angle	95% CI Mean	95% C.I. Fisher K
NE	125.7	10.1	309.1	1.5	12.1	10.9	19.1
NS	91.0	4.1	86.3	2.5	5.0	8.1	14.1
NW	34.1	0.8	39.2	7.2	8.2	8.1	14.1
SH	84.3	71.3	273.9	85.4	23.2	8.1	14.1
ENE	155.4	8.3	153.8	15.9	7.8	4.2	31.1

Table 6-16. Comparison of relative set intensity, domain FFM01, KFM08D versus verification simulations.

FFM01 Fracture set	KFM08D, Fitted sets # of fractures	Relative Intensity	TCM Model # of fractures	Relative intensity	OSM+TFM Model # of fractures	Relative intensity
NE	157	19.7%	234	25.8%	243	25.1%
NS	117	14.7%	210	23.1%	207	21.3%
NW	100	12.5%	67	7.4%	103	10.6%
SH	239	29.9%	98	10.8%	147	15.2%
ENE	185	23.2%	299	32.9%	270	27.8%
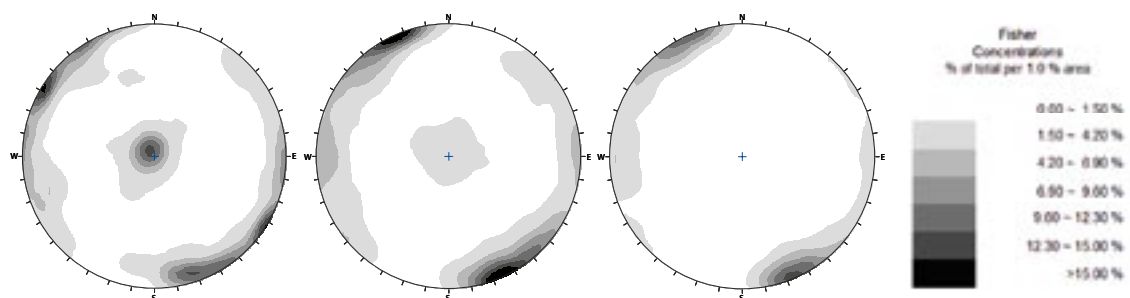
Figure 6-27. Domain FFM01, Comparison of measured and simulated stereoplots: KFM08D (left), OSM+TFM (middle), and TCM (right). Data has been Terzaghi-corrected, with a maximum correction factor of 7.
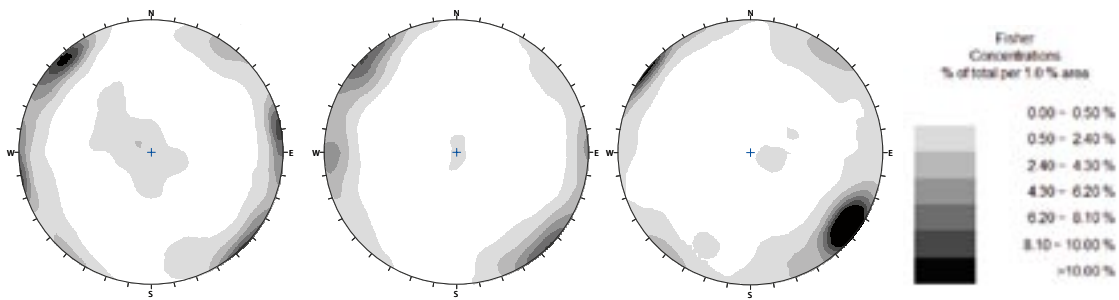
Figure 6-28. *Domain FFM06, Comparison of measured and simulated stereoplots: KFM08D (left), OSM+TFM (middle), and TCM (right). Data has been Terzaghi-corrected, with a maximum correction factor of 7.*

For domain FFM06, the OSM+TFM model again shows (Table 6-17) the best predicted relative intensities with respect to the data from KFM08D. There are slight variabilities (< 10%) in many of the sets, but, overall the stereonet comparison appears quite reasonable. Again, the TCM model does not perform quite as well as the OSM+TFM model; it tends to over-estimate the intensity of the NE Global set, relative to all other sets. Neither model was able to predict the complexity of the subhorizontal orientation set observed in KFM08D. The pattern of multiple potential subhorizontal sets (a Global set and a Local set) is seen in several other Forsmark cored borehoes; however, as the orientation of the Local subhorizontal set is highly variable (see Chapter 4.1.3 for more details), accurate prediction of this secondary subhorizontal set is difficult.

Verification of KFM08D fracture intensities

The verification of the Forsmark 2.2 geological DFN intensity model through a blind prediction of KFM08D fracturing involved a comparison of the observed mean fracture frequency (P_{10}) versus results from simulated models using the OSM+TFM and TCM model alternatives. The comparison was done on the total fracture intensity outside of mapped deformation zone, and included both fractures Visible in BIPS and Not Visibile in BIPS. As such, it is not possible to directly compare the intensity results to the relative intensity figures in the previous sub-chapter. Table 6-18 illustrates the percentage of fractures outside of mapped deformation zones in each fracture domain.

Table 6-17. Comparison of relative set intensity, domain FFM06, KFM08D versus verification simulations.

FFM06	KFM08D, Fitted Sets		TCM Model		OSM+TFM Model	
Fracture set	# of fractures	Relative intensity	# of fractures	Relative intensity	# of fractures	Relative intensity
NE	506	31.4%	926	57.5%	759	38.8%
NS	542	33.7%	116	7.2%	537	27.5%
NW	168	10.4%	212	13.2%	247	12.6%
SH	267	16.6%	158	9.8%	215	11.0%
ENE	126	7.8%	198	12.3%	198	10.1%

Table 6-18. Percentage of fractures visible in BIPS, KFM08D.

Fracture domain	FFM01	FFM06
Number of fractures visible In BIPS	798	1,609
Number of open fracs visible In BIPS	249	339
Total number of fractures	1,164	2,062
% of Open fractures Visible in BIPS	31.20%	21.07%
% of Fractures Visible in BIPS	68.56%	78.03%

A comparison of the measured fracture intensities and distributions by fracture domain presented below as Table 6-19. It is not possible to directly compare the intensity of the simulated KFM08D fracture sets versus the recorded KFM08D fracture sets individually; KFM08D fractures were divided into sets using only fractures labeled Visible in BIPS. This means that the orientation sets created from the KFM08D data do not represent the full fracture intensity.

However, the geological DFN parameterizations used to build the simulated KFM08D DFNs specify fracture intensity in terms of all fractures (both Visible and Not Visible in BIPS). As such, the intensity of the resulting DFNs includes both Visible in Bips AND Not Visible in BIPS. The comparisons of borehole fracture intensity described below reflect both Visible in BIPS fractures and Not Visible in BIPS fractures.

The average P_{10} intensity (in both simulated boreholes and in the KFM08D raw data) is still a good guide to the overall performance of the blind prediction of KFM08D. Note that the total number of fractures is NOT a good guide to model performance; the blind prediction simulations used ALL 30 m bin intervals for building model statistics, while the KFM08D statistics come only from intervals outside of mapped deformation zones.

The most significant conclusion invoked by Table 6-19 is that both the OSM+TFM and TCM models underpredict the *mean* fracture intensity recorded by borehole KFM08D by approximately 30%. The reason for the under-prediction is unknown at this time. However, we suspect that the under-prediction could be due to a large number of higher-intensity intervals recorded in KFM0D in between or near deformation zones. In other site boreholes, these zones have been labeled 'Affected by DZ' and modeled separately as zones of higher intensity. As KFM08D has not yet been formally included in the Forsmark site geologic model (it falls outside the data freeze date for revision 2.2 of the SDM), it is not possible to test this hypothesis at this time.

The verification simulations utilized the mean fracture intensity values for each domain and fracture set given in Table 7-6. As such, the variation (deviation, maximum and minimum values) recorded in Table 6-19 represent stochastic variability rather than true spatial variability.

Table 6-19. Comparison of blind prediction results of total fracture intensity (P_{10}) for KFM08D, all sets, by domain.

Domain FFM01	Mean	Standard deviation	Median	Max.	Min.	Number of fractures
KFM08D	4.32	2.50	4.73	7.93	0.27	1,036
OSM+TFM	3.13	0.29	3.10	3.63	2.77	939
TCM	3.14	0.39	3.13	3.70	2.57	943

Domain FFM06	Mean	Standard deviation	Median	Max.	Min.	Number of fractures
KFM08D	5.80	2.80	5.45	10.80	2.37	1,392
OSM+TFM	4.09	0.39	4.07	4.80	3.20	2,210
TCM	4.02	0.19	3.95	4.43	3.80	2,152

6.2   Conclusions

In general this verification analysis shows that:

- In terms of the orientation models, the Forsmark 2.2 geological DFN adequately character-izes mean fracture set orientations in domains FFM01 and FFM06. Visually and statistically, the models are quite close.

- In terms of the size model, it is clear that, given the available surface trace data, it is only possible to accurately re-create portions of the trace distributions using the TCM model. Alternative size models, such as as lognormal or exponential distribution of fracture radii, might produce better overall matches to the trace data in some cases. The improvement in the size matches, however, are likely to be completely offset by the loss of the ability to simulate fracture sizes within other size ranges (i.e. MDZ and joints > 10 m in trace length) provided by the power-law scaling relationships.

- The fits of the intensity model to measured data are generally quite good, with the exception of the NS Global set in Domains FFM01, FFM02, and FFM06. Though exact matches were not possible, both the analytical benchmarks and the data comparisons indicate that the geological DFN model will produce reasonable fracture intensities.

- The verification of fracture intensity in the MDZ size range showed that the DFN models over-predicted the borehole intensity, especially for the subhorizontal case. The mismatch, however, may be due to the fact that there is little to no information on the size range for which the comparison should be made. We have chosen an arbitrary cut-off based on a func-tional definition of MDZ (structures with a trace length larger than 50 m, or 28 m equivalent radius). A larger minium size could greatly improve the match, and the uncertainty studies with a minimum size of 200 m would reduce the P_{32} to values that would be fairly close matches in many cases.

- The blind prediction of borehole KFM08D suggests that, in terms of fracture orientation and relative set intensities, the OSM+TFM model may perform slightly better than the TCM model. However, the blind prediction results underpredict the total mean fracture intensity in KFM08D by approximately 30%. We believe this is likely due to unmapped zones that, if included in the revision 2.2 geological model, would be labeled 'Affected by DZ'.

- The NS fracture set generally shows the poorest matches. There is very little data for that particular set in Domain FFM02; the NS set has a very low P21 in AFM100201, with a resulting low match P_{32} to the outcrop data (a match P_{32} of 0.245 m²/m³, for a size range of 0.5 m to ~ 10 m, based on outcrop truncations). However, the P10 values from the borehole record in FFM01, FFM02, and FFM06 (and the resulting P_{32} values computed using Wang's C13) are significantly higher. This suggests that the outcrop used to parameterize the NS Global Set in FFM02 is highly non-representative of the rock mass as a whole.

This potential affects all size/intensity models, but impacts the tectonic continuum alternatives especially hard. The TCM and TCMF are coupled size-intensity models, the same size-intensity scaling relationship from FFM02 is used in both FFM01 and FFM06. This means that the lack of outcrop trace data in FFM02 affects nearly all the fracture domains in the DFN model. This is a fundamental limitation of the tectonic continuum approach.

Without additional outcrop data, it is not possible to further reduce the uncertainty in the size-intensity matches for the NS Global set. Another option would be the use of trace data from other outcrops (AFM001097, AFM001098) for the NS set as proxies. A final option is to use the Outcrop Scale + Tectonic Fault Model alternative to describe the NS set in stochastic site models.

7 Geological DFN model summary tables, conclusions and recommendations

This section presents brief summary tables of the SDM Forsmark 2.2 geological DFN; no new data or analyses are presented in this section. Note that the fracture sets are divided into Global and Local sets; please see Chapter 3.2.2 for a discussion on the limitations of the Local fracture sets. The exponent presented for all power-law fracture size models is k_r (the radius distribution exponent). If you are generating stochastic models in FracMan, you will need to use the b exponent, which is equivalent to $k_r + 1$.

Also note that the minimum radius value given is (r_{min}), a truncation limit, and not r_0 (the minimum size parameter of the probability distribution). As such, all P_{32} values presented in the Intensity Model tables represent truncated P_{32}, as per the recommendations provided in the DFN memorandum /Munier et al. 2006/. P_{32} values presented alongside the size models are given as match points to the size distribution; they extend from the 'true' minimum radius to an r_{max} of 564 m.

7.1 Summary tables: Orientation model

The orientation model is common to all model alternatives.

The orientation model can be used two ways:

- As single static values representing global averages for each set. To use the model in this fashion, use the mean pole vector given for each fracture set (φ, θ), and use the average Fisher concentration parameter (κ) for each fracture set in each domain.

- As a spatially-varying parameter in a stochastic simulation. To use the model in this fashion, use the mean pole vector given (φ, θ) for each fracture set in each fracture domain as a starting point. The location of the mean pole vector of a fracture set can then be given as a univariate Fisher distribution using the set means concentration parameter (κmp). Once, for a given cell, volume, or realization, the mean pole vector is located, the concentration parameter (κ) for the actual distribution of fracture orientations can be taken as a random draw from a normal distribution, given the values in Table 7-1.

7.2 Summary tables: Size model

The size model for the Forsmark 2.2 geological DFN consists of two alternative models; one build on coupled size-intensity relationships (TCM/TCMF) derived largely from outcrop data at the surface, and a second model (OSM+TFM) built with size information primarily from surface outcrops, but with intensity parameterized largely from borehole data and not directly coupled to fracture size.

The GeoDFN team recommends the 'Tectonic Continuum' models as the preferred model alternative, based on ease of use and applicability to a wide range of scales.

7.2.1 Outcrop scale and tectonic fault model (OSM+TFM)

It should be noted that it is not possible to use either model without the other, if a complete population of fractures over the designated DFN size range (0.5 m–564 m) is desired.

Table 7-1. PFM 2.2 Orientation model.

Fracture domain	Fracture set	Set type	Probability distribution	Mean pole trend	Plunge	κ_{mp}*	Distribution of Fisher κ Mean	Std. Dev.	Median
FFM01	NE	Global	Univariate Fisher	314.9	1.3	47.4	20.9	9.4	17.8
FFM01	NS	Global	Univariate Fisher	270.1	5.3	47.0	21.3	13.2	20.3
FFM01	NW	Global	Univariate Fisher	230.1	4.6	32.3	15.7	8.1	12.6
FFM01	SH	Global	Univariate Fisher	0.8	87.3	48.9	17.4	7.1	14.4
FFM01	ENE	Local	Univariate Fisher	157.5	3.1	100.0	34.1	17.0	34.1
FFM01	EW	Local	Univariate Fisher	0.4	11.9	30.0	13.9	5.6	13.5
FFM01	NNE	Local	Univariate Fisher	293.8	0.0	33.1	21.8	0.9	NA
FFM01	SH2	Local	Univariate Fisher	164.0	52.6	NA	35.43	NA	NA
FFM01	SH3	Local	Univariate Fisher	337.9	52.9	10.2	17.1	0.1	NA
FFM02	NE	Global	Univariate Fisher	315.3	1.8	33.8	27.0	24.0	22.9
FFM02	NS	Global	Univariate Fisher	92.7	1.2	24.1	30.7	27.1	19.2
FFM02	NW	Global	Univariate Fisher	47.6	4.4	18.6	19.7	22.9	13.9
FFM02	SH	Global	Univariate Fisher	347.4	85.6	87.8	23.2	8.8	20.4
FFM02	ENE	Global	Univariate Fisher	157.9	4.0	100.0	53.2	35.1	47.6
FFM02	EW	Global	Univariate Fisher	186.3	4.3	46.5	34.2	20.6	33.2
FFM02	NNE	Local	Univariate Fisher	107.2	1.8	NA	45.3	NA	NA
FFM02	NNW**	Local	Univariate Fisher	73.0	5.6	NA	11.6	NA	NA
FFM03	NE	Global	Univariate Fisher	311.1	2.7	81.3	25.9	9.8	24.7
FFM03	NS	Global	Univariate Fisher	270.2	6.9	91.4	19.7	10.8	18.2
FFM03	NW	Global	Univariate Fisher	42.4	2.8	84.8	18.4	7.3	17.4
FFM03	SH	Global	Univariate Fisher	348.8	81.0	77.3	13.1	5.7	11.8
FFM03	ENE	Local	Univariate Fisher	164.8	1.2	NA	44.0	NA	NA
FFM03	EW	Local2	Univariate Fisher	196.5	7.3	50.7	27.2	17.6	22.7
FFM06	NE	Global	Univariate Fisher	125.7	10.1	54.6	45.1	21.5	53.3
FFM06	NS	Global	Univariate Fisher	91.0	4.1	100.0	19.5	7.8	15.2
FFM06	NW	Global	Univariate Fisher	34.1	0.8	100.0	16.1	6.1	15.9
FFM06	SH	Global	Univariate Fisher	84.3	71.3	100.0	10.8	5.1	10.8
FFM06	ENE	Local	Univariate Fisher	155.4	8.3	NA	20.8	NA	NA
FFM06	SH2	Local	Univariate Fisher	0.0	47.5	NA	12.7	NA	NA

* κ_{mp} represents the Fisher concentration parameter of the distribution of the fitted mean poles (i.e the mean pole of the mean poles). See Chapter 3.2.2 for more information.

** Note that no size or intensity model exists for the NNW set in domain FFM02.

Table 7-2. Fracture sizes, outcrop scale model (OSM).

Fracture domain	Fracture set	Set type	Size distribution	Min. radius r_0 (m)	Exponent (k_r)	Match P_{32} r_0–∞ (1/m)
FFM01	NE	Global	Power Law	0.039	2.64	1.74
FFM01	NS	Global	Power Law	0.039	2.90	1.29
FFM01	NW	Global	Power Law	0.039	2.44	0.95
FFM01	SH	Global	Power Law	0.039	2.61	0.63
FFM01	ENE	Local	Power Law	0.039	2.20	2.74
FFM01	EW	Local	Power Law	0.039	3.06	1.12
FFM01	NNE	Local	Power Law	0.039	3.00	4.39
FFM01	SH2	Local	From SH	0.039	2.61	0.92
FFM01	SH3	Local	From SH	0.039	2.61	0.84
FFM02	NE	Global	Power Law	0.10	2.64	3.31
FFM02	NS	Global	Power Law	0.06	2.90	1.61
FFM02	NW	Global	Power Law	0.04	2.44	2.12
FFM02	SH	Global	Power Law	0.07	2.61	2.78
FFM02	ENE	Global	Power Law	0.039*	2.20	3.65
FFM02	EW	Global	Power Law	0.15	3.06	1.19
FFM02	NNE	Local	Power Law	0.5	3.00	1.35
FFM02	NNW	Local	Impossible to Parameterize; no size data available			
FFM03	NE	Global	Power Law	0.07	2.62	2.91
FFM03	NS	Global	Power Law	0.05	2.63	1.49
FFM03	NW	Global	Power Law	0.36	2.59	1.46
FFM03	SH	Global	Power Law	0.12	2.57	0.96
FFM03	ENE	Local	Power Law	0.65	2.70	0.30
FFM03	EW	Local2	Power Law	1.03**	3.36	0.44
FFM06	NE	Global	Power Law	0.039	2.64	3.30
FFM06	NS	Global	Power Law	0.039	2.90	2.15
FFM06	NW	Global	Power Law	0.039	2.44	1.61
FFM06	SH	Global	Power Law	0.039	2.61	0.64
FFM06	ENE	Local	Power Law	0.039	2.20	0.98
FFM06	SH2	Local	Power Law	0.039	2.61	1.03

* Not possible to simultaneously match borehole and outcrop data; size model fit defaults to radius of borehole as minimum radius of distribution.

** Not possible to simultaneously match borehole and outcrop data; the surface data for this set in FFM03 appears much more intense than the cored borehole data.

7.2.2 Summary tables: Tectonic continuum models (TCM/TCMF)

The only difference between the tectonic continuum model alternatives is the assumption of Euclidean (TCM) or Fractal Mass (TCMF) size-intensity scaling.

Table 7-3. Fracture sizes, Tectonic Fault Model (TFM).

Fracture domain	Fracture set	Set type	Size distribution	Min. radius r_0 (m)	Exponent (k_r)	Match P_{32} r_0–564 (1/m)
All Domains	NE	Global	Power Law	28	3	0.0285
All Domains	NS	Global	Power Law	28	2.2	0.0003
All Domains	NW	Global	Power Law	28	2.06	0.0003
All Domains	SH*	Global	Power Law	28	2.83	0.0286
All Domains	ENE	Global	Power Law	28	3.14	0.0871
All Domains	EW	Global	Power Law	28	2.85	0.0014

* SH set uses TCM radius exponent, but with P_{32} recalculated for new r_0.

Table 7-4. Fracture sizes, TCM.

Fracture domain	Fracture set	Set type	Size distribution	Min. radius r_0 (m)	Exponent (k_r)	Match P_{32} r_0–∞ (1/m)
FFM01	NE	Global	Power Law	0.66	3.02	1.74
FFM01	NS	Global	Power Law	0.06	2.78	1.29
FFM01	NW	Global	Power Law	0.59	2.85	0.95
FFM01	SH	Global	Power Law	0.82	2.85	0.63
FFM01	ENE	Local	Power Law	0.32	3.25	2.74
FFM01	EW	Local	Power Law	0.17	3.1	1.12
FFM01	NNE	Local	Use Sizes from Outcrop Scale Model			
FFM01	SH2	Local	Use Sizes for SH Set from Outcrop Scale Model			
FFM01	SH3	Local	Use Sizes for SH Set from Outcrop Scale Model			
FFM02	NE	Global	Power Law	0.35	3.02	3.31
FFM02	NS	Global	Power Law	0.04	2.78	1.61
FFM02	NW	Global	Power Law	0.23	2.85	2.12
FFM02	SH	Global	Power Law	0.14	2.85	2.78
FFM02	ENE	Global	Power Law	0.26	3.25	3.65
FFM02	EW	Global	Power Law	0.16	3.1	1.19
FFM02	NNE	Local	Use Sizes from Outcrop Scale Model			
FFM02	NNW	Local	Use Sizes from Outcrop Scale Model			
FFM03	NE	Global	Power Law	0.24	2.95	2.91
FFM03	NS	Global	Power Law	0.36	2.93	1.49
FFM03	NW	Global	Power Law	0.59	2.90	1.46
FFM03	SH	Global	Power Law	0.20	2.81	0.96
FFM03	EW	Global	Power Law	0.93	3.24	0.44
FFM03	ENE	Local	Power Law	0.5	3.13	0.74
FFM06	NE	Global	Power Law	0.35	3.02	3.30
FFM06	NS	Global	Power Law	0.039*	2.78	2.15
FFM06	NW	Global	Power Law	0.32	2.85	1.61
FFM06	SH	Global	Power Law	0.79	2.85	0.64
FFM06	ENE	Local	Power Law	0.74	3.25	0.98
FFM06	SH2	Local	Use Sizes for SH set from Outcrop Scale Model			

* Not possible to simultaneously match borehole and outcrop data; size model fit defaults to radius of borehole as minimum radius of distribution.

Table 7-5. Fracture sizes, TCMF.

Fracture domain	Fracture set	Set type	Size distribution	Min. radius r_0 (m)	Exponent (k_r)	Match P_{32} r_0–∞ (1/m)
FFM01	NE	Global	Power Law	0.72	3.01	1.74
FFM01	NS	Global	Power Law	0.06	2.76	1.29
FFM01	NW	Global	Power Law	0.63	2.85	0.95
FFM01	SH	Global	Power Law	0.72	2.83	0.63
FFM01	ENE	Local	Power Law	0.34	3.25	2.74
FFM01	EW	Local	Power Law	0.17	3.13	1.12
FFM01	NNE	Local	Use Sizes from Outcrop Scale Model			
FFM01	SH2	Local	Use Sizes for SH Set from Outcrop Scale Model			
FFM01	SH3	Local	Use Sizes for SH Set from Outcrop Scale Model			
FFM02	NE	Global	Power Law	0.38	3.01	3.31
FFM02	NS	Global	Power Law	0.05	2.76	1.61
FFM02	NW	Global	Power Law	0.24	2.85	2.12
FFM02	SH	Global	Power Law	0.12	2.83	2.78
FFM02	ENE	Global	Power Law	0.27	3.25	3.65
FFM02	EW	Global	Power Law	0.19	3.13	1.19
FFM02	NNE	Local	Use Sizes from Outcrop Scale Model			
FFM02	NNW	Local	Use Sizes from Outcrop Scale Model			
FFM03	NE	Global	Power Law	0.21	2.94	2.91
FFM03	NS	Global	Power Law	0.31	2.92	1.49
FFM03	NW	Global	Power Law	0.69	2.89	1.46
FFM03	SH	Global	Power Law	0.25	2.81	0.96
FFM03	EW	Local	Power Law	1.04	3.25	0.44
FFM03	ENE	Local	Use Sizes from Outcrop Scale Model			
FFM06	NE	Global	Power Law	0.38	3.01	3.30
FFM06	NS	Global	Power Law	0.039*	2.76	2.15
FFM06	NW	Global	Power Law	0.34	2.85	1.61
FFM06	SH	Global	Power Law	0.70	2.83	0.64
FFM06	ENE	Local	Power Law	0.78	3.25	0.98
FFM06	SH2	Local	Use Sizes for SH set from Outcrop Scale			

* Not possible to simultaneously match borehole and outcrop data; size model fit defaults to radius of borehole as minimum radius of distribution.

7.3 Summary tables: Intensity model

The values presented in the Intensity Model tables represent truncated P_{32} values between 0.5 m and 564 m. If different values are desired, use the P_{32} match points and r_0 values from the Size Model tables in conjunction with Equation 3-11 to re-scale P_{32}. Also note that the TFM model is only valid when paired with fractures NOT affected by DZ.

Table 7-6. Mean P_{32} intensity, fractures NOT affected by DZ.

Fracture domain	Fracture set	Set type	Mean P_{32} (0.5–564 m)			(28–564 m)
			OSM	TCM	TCMF	TFM
FFM01	NE	Global	0.33	2.30	2.50	0.0285
FFM01	NS	Global	0.13	0.24	0.26	0.0003
FFM01	NW	Global	0.29	1.10	1.15	0.0003
FFM01	SH	Global	0.13	0.95	0.85	0.0286
FFM01	ENE	Local	1.24	1.60	1.70	0.0871
FFM01	EW	Local	0.07	0.34	0.33	0.0014
FFM01	NNE	Local	0.34	Use OSM	Use OSM	NA
FFM01	SH2	Local	0.19	Use OSM	Use OSM	NA
FFM01	SH3	Local	0.17	Use OSM	Use OSM	NA
FFM02	NE	Global	1.14	2.30	2.50	0.0285
FFM02	NS	Global	0.25	0.24	0.26	0.0003
FFM02	NW	Global	0.67	1.10	1.15	0.0003
FFM02	SH	Global	0.86	0.95	0.85	0.0286
FFM02	ENE	Global	1.65	1.60	1.70	0.0871
FFM02	EW	Global	0.34	0.34	0.40	0.0014
FFM02	NNE	Local	1.35	Use OSM	Use OSM	NA
FFM02	NNW	Local	Impossible to parameterize; no size data			
FFM03	NE	Global	0.86	1.45	1.30	0.0285
FFM03	NS	Global	0.34	1.10	0.95	0.0003
FFM03	NW	Global	1.18	1.70	1.95	0.0003
FFM03	SH	Global	0.43	0.45	0.55	0.0286
FFM03	ENE	Local	0.36	0.74	0.80	0.0871
FFM03	EW	Local	1.17	0.95	1.10	0.0014
FFM06	NE	Global	0.63	2.30	2.50	0.0285
FFM06	NS	Global	0.21	0.29	0.31	0.0003
FFM06	NW	Global	0.50	1.10	1.15	0.0003
FFM06	SH	Global	0.13	0.95	0.85	0.0286
FFM06	ENE	Local	0.44	1.60	1.70	0.0900
FFM06	SH2	Local	0.21	Use OSM	Use OSM	NA

Table 7-7. Mean P$_{32}$ intensity, fractures affected by DZ.

Fracture domain	Fracture set	Set type	Mean P$_{32}$ r_0–∞	Mean P$_{32}$ (0.5–564 m)		
				OSM	TCM	TCMF
FFM01	NE	Global	5.45	1.04	7.22*	7.22*
FFM01	NS	Global	2.60	0.26	0.49	0.49
FFM01	NW	Global	2.42	0.75	2.79*	2.79*
FFM01	SH	Global	2.44	0.50	3.69*	3.69*
FFM01	ENE	Local	3.90	1.76	2.27	2.27
FFM01	EW	Local	2.85	0.19	0.87	0.87
FFM01	NNE	Local	0.00	0.00	0.00	0.00
FFM01	SH2	Local	0.00	0.00	0.00	0.00
FFM01	SH3	Local	2.24	0.46	Use OSM	Use OSM
FFM02	NE	Global	5.24	1.80	3.64	3.95
FFM02	NS	Global	4.72	0.73	0.71	0.77
FFM02	NW	Global	2.35	0.74	1.22	1.27
FFM02	SH	Global	6.59	2.04	2.24	2.01
FFM02	ENE	Global	5.05	0.50	2.21	2.35
FFM02	EW	Global	0.18	0.05	0.05	0.06
FFM02	NNE	Local	0.00	0.00	0.00	0.00
FFM02	NNW	Local	0.00	0.00	0.00	0.00
FFM03	NE	Global	4.52	5.25	2.25	2.02
FFM03	NS	Global	0.00	0.00	0.00	0.00
FFM03	NW	Global	1.15	1.49	1.34	1.53
FFM03	SH	Global	2.48	2.24	1.15	1.41
FFM03	ENE	Local	0.00	0.00	0.00	0.00
FFM03	EW	Global	0.41	0.72	0.89	1.03
FFM06	NE	Global	0.00	0.00	0.00	0.00
FFM06	NS	Global	0.00	0.00	0.00	0.00
FFM06	NW	Global	0.00	0.00	0.00	0.00
FFM06	SH	Global	0.00	0.00	0.00	0.00
FFM06	ENE	Local	0.00	0.00	0.00	0.00
FFM06	SH2	Local	0.00	0.00	0.00	0.00

* r_0 fit to set in FFM01 is larger than r_{min} (0.5 m); as such, P$_{32}$ is increased.

7.4   Summary: Spatial model

For the Global fracture sets in the Forsmark 2.2 geological DFN, we recommend that fracture locations are simulated according to a Poisson point process (such as an Enhanced Baecher model for fracture centers /Dershowitz et al. 1998/). Euclidean scaling can be assumed at all model scales 30 m and larger.

Mild fractal clustering (mean D of 1.9) is observed at scales less than 30 m. However, the 95% confidence interval surrounding D is ± 0.23; this suggests that it may be difficult to distinguish between the natural variability inherent in a Poisson model following Euclidean scaling and a fractally-clustered model. As such, we recommend assuming Euclidean scaling (TCM) at all scales.

With respect to the Local fracture sets in the Forsmark 2.2 geological DFN, no significant geologic or morphologic trends were noted. These sets are hypothesized to represent highly local variations in the past stress fields and rock properties. As such, we recommend the use of either a bootstrap model based on local borehole conditioning of fracture intensity or a probabilistic approach based on the intersection probability calculated from the 6 m binned borehole data record. A summary of these probabilities is presented below in Table 7-8.

Table 7-8. Probability of occurrence of local sets as a function of domain and scale.

Fracture domain	Fracture set	Probability of occurrence at a given scale	
		6 m	30 m +
FFM01	ENE	0.09	0.17
FFM01	EW	0.15	0.20
FFM01	NNE	0.15	0.19
FFM01	SH2	0.09	0.15
FFM01	SH3	0.08	0.15
FFM02	NNE	NA	NA
FFM02	ENE	0.28	0.45
FFM02	NNW	0.12	0.18
FFM03	ENE	NA	NA
FFM03	EW	0.12	0.23
FFM06	ENE	0.20	0.15
FFM06	SH2	0.42	0.62

Table 7-9. Termination matrix for FFM02.

Relative set percentage					Total %
Fracture set	NE	NS	NW	EW	termination
NE terminates against	0.0%	7.3%	19.5%	11.1%	38.0%
NS terminates against	26.9%	0.0%	18.7%	12.7%	58.2%
NW terminates against	33.2%	5.9%	0.0%	11.5%	50.7%
EW terminates against	35.1%	9.4%	19.5%	0.0%	64.0%
Set history for order of generation					
Order	1	2	3	4	5
Set name	NE	NW	EW	NS	SH?

Table 7-10. Termination matrix for FFM03.

Relative set percentage						Total %
Fracture set	NW	WNW	NE	NS	ENE	termination
NW	0.0%	16.0%	19.1%	7.2%	10.9%	53.2%
WNW	24.2%	0.0%	21.7%	4.5%	9.4%	59.8%
NE	23.1%	15.6%	0.0%	5.0%	11.8%	55.5%
NS	25.9%	18.5%	16.7%	0.0%	3.7%	64.8%
ENE	34.0%	17.0%	23.9%	6.9%	0.0%	81.9%
Set history for order of generation						
Order	1	2	3	4	5	6
Set name	NW	WNW	NE	NS	ENE	SH?

The DFN models described in the above sections are independent of geologic controls other than the fracture domains. However, the results of the exploratory data analysis and DFN modeling parameterization (Section 4) have suggested that it is possible to compensate for spatial variations in fracture intensity by applying corrections based on lithology.

7.4.1 Adjusting the fractal dimension

The fractal scaling correction is based on the mass dimension, Dm. The number of fractures per unit area or volume varies as a function of a constant term ρ, the scale, r, and the mass dimension, Dm:

$$P_{21}(r_1) = \frac{\rho r_1^{D_m}}{C r_1^2} * \mu$$

The mass dimension may be estimated from the traces in outcrop, borehole or rock volume. If the dimension is to be used in a different dimensional space than which it is estimated, the appropriate correction needs to be made, for example, if the dimension is estimated from traces and is to be used for volumes, then the value of 1.0 should be added.

If the trace density, P_{21}, for an outcrop of scale r_0, is:

$$P_{21}(r_0) = \frac{\rho r_0^{D_m}}{C r_0^2} * \mu$$

where C is some factor such as π, and μ is the mean trace area, then at a different scale, r1,

$$P_{21}(r_1) = \frac{\rho r_1^{D_m}}{C r_1^2} * \mu$$

The ratio of these two values is:

$$\frac{P_{21}(r_0)}{P_{21}(r_1)} = \frac{r_0^{D_m-2}}{r_1^{D_m-2}}$$

7.4.2 Adjusting the P_{32} of any of the models for lithology

The statistical analysis of fracture intensity has suggested that fracture intensity can at least be partially controlled by subsurface lithology. The correlations were not particularly strong, save for amphibolite, but it was possible to develop a series of correction factors to P_{32} to allow end-users to locally adjust intensity to subsurface geology. The details of this method and the lithology adjustment table are discussed in Chapter 4.4.4.

7.5 Modeling conclusions

7.5.1 Limitations

The limitations of the SDM 2.2 geological fracture model derive primarily from the constraints of the available data and the specified intended uses of the model. The SDM 2.2 model is based upon the data listed in Section 2; and new or additional data was not part of the analyses and may lead to changes in the results.

The coupled size-intensity models for each set, whether in reference to the Outcrop Scale or Alternative models, are based on surface data from outcrops and interpreted lineaments. There is no direct use of subsurface borehole intensity information in the development of the probability distributions that describe size, nor is the intensity associated with the size derived from borehole data. Borehole intensity data is used to assess uncertainty as a function of tock type, and to determine the functional form of the variation of intensity with depth and rock type. Therefore, the accuracy to which the coupled model can predict the subsurface fracture intensity is limited by the extent to which the surface fracture sizes and intensity differ from the subsurface, after adjustments are made for depth and lithology.

The SDM Forsmark 2.2 geological DFN model is based on fractures identified as being outside of deformation zones. Thus, the model is limited to describing only fractures outside of deformation zones, and does not apply to describing the orientation, size or intensity of major deformation zones. Minor deformation zones are assumed to be those smaller than 1,000 m in trace length, and are included as part of the stochastic fracture model.

The data available from surface outcrops lies entirely within fracture domains FFM02 and FFM03. Borehole data comes from both these two domains and from Domain FFM01 and Domain FFM06. Since the coupled size/intensity models for the Outcrop Scale and the Alternative Models are based all or in part on outcrop data, the model has the least uncertainty when applied to these two fracture domains. Application to FFM01 is more uncertain, as there is no surface data to calculate a size model, although there is borehole data for quantifying relations between intensity, rock type and depth. The limited volume of data from Domain FFM06 has NOT been used in the uncertainty analysis. As a result, the application of the model to FFM01 has a much higher uncertainty than to the application of the model to FFM02 or FFM03. Application to FFM06 is uncertain to a degree that could not be quantified with the data available.

The Tectonic Fault model (TFM), which is calibrated in part from the ground magnetic lineament data, has a higher degree of uncertainty than other models. The detection reliability of the method has not been quantified; the plots of the outcrop, deformation zone and magnetic lineament data suggests that for at least some sets, the detection probability is substantially less than 100% as an alternative explanation to the possibility that there are simply not as many fractures of this size at the scale of the magnetic lineament data. Therefore, the detection reliability of the magnetic lineament data and the TFM alternative model based on them should be carefully assessed by any user.

The model is only valid within the boundaries of fracture domains FFM01, FFM02, FFM03, and FFM06, to a depth of 1,000 m. It is not valid for deeper depths or for locations outside the site domain boundaries.

The predictive accuracy is no greater than the bounds determined from the uncertainty calculations. For purposes of validation or prediction, the uncertainty limits quantify the resolution. The actual limits may be greater, as not every possible uncertainty has been quantified, but the limits should not be less.

The model is not a hydrologic or mechanical model, although a hydrologic or mechanical model can be in part derived from it. No considerations of flow or transport, safety or construction were made in developing this model.

7.5.2   Key uncertainties

The identification and impact of key uncertainties has been summarized in Table 5-7 and discussed in detail in Chapter 5. The following is a summary:

The key identified uncertainties are:

- Does the tectonic continuum exist, allowing for the development of a single model to encompass borehole, outcrop, ground magnetic lineament and deformation zone data?

- If the tectonic continuum does not exist, and there are distinct populations of joints and reactivated joints that differ from a fault/deformation zone related fractures, then is there an upper size limit to the joints or a lower size limit to the deformation zones?

- Does the fracture intensity scale as a Euclidean, fractal or other type of model from borehole/ outcrop scale to repository scale?

- What is the impact of fracture intensity variations by rock type? Can intensities for rock types be combined, and if so, what magnitude of uncertainty does this produce?

- How does fracture intensity vary as a function of depth? If depth dependency is ignored, what is the magnitude of the possible error?

- Does the mean pole of a fracture set vary spatially within a fracture domain? If so, what uncertainty is likely if a constant mean orientation is used for each set within each fracture domain?

- How does the uncertainty regarding the orientations of each fracture observation impact the results?

The magnitude of these uncertainties were evaluated by comparing the intensity of fracturing in the 28 m to 564 m effective radius size range.

Based on the quantification of possible impacts on permeability and mechanical deformation, the uncertainty with the greatest impacts is whether a 'tectonic continuum' between outcrop and deformation zone structures exists or not. Current evidence suggests that fractures measured in outcrop and borehole may be a distinct population from the kilometer-scale deformation zones and the fractures represented by ground magnetic lineaments. The possible impact is approximately one (1) order of magnitude for fracture intensity. This has a direct impact of approximately an order of magnitude on the permeability of the rock mass.

A related uncertainty pertains to the alternative model (OSM+TFM) in which joints and fault zones are treated as separate populations. It is uncertain what the upper size limit for the joints may be, or what a lower size limit for the deformation zones may be. Based on one possible limit indicated by hydrotests –200 m – the impact may be on the order of a reduction in intensity from 0.66 to 0.9 times the intensity for no truncation limits. The 200 m upper limit on the OSM has a fairly negligible impact, leading to a median reduction of about 0.9 of the untruncated intensity. Inclusion of an additional lower limit to the TFM component reduces the total intensity to a median of about 0.7 times the untruncated intensity.

If the tectonic continuum model is adopted, then the next most important uncertainty is the uncertainty about the scaling behavior at scales greater than a few tens of meters, as it impacts the scaling model for the tectonic continuum models. The possible impact is approximately one-half (0.5) an order of magnitude on intensity, with a corresponding effect on the permeability of the rock mass.

For the Outcrop Scale, where the size models come strictly from outcrop data, the impact of uncertainty is far smaller; a maximum of about 1.6 times for the mean mass dimension and the extrapolation of the outcrop intensity data to the entire repository domain. In this case, the uncertainty produced through combining fracture data from different rock types would create the greatest impact. If the data are combined but a few unique rock types with very different fracture intensities, such as amphibolite, are modeled separately for each domain, then the impact can be reduced.

Since there were no fracture trace data from outcrops to parameterize the models for FFM01 and FFM06, two alternative strategies were devised to develop the coupled size-intensity parameterization in the TCM models. This uncertainty is on the order of 2 to 3.

Intensity was found to vary by lithology, fracture set and domain. If lithology is not known or if domain averages are used for each set, then the maximum possible uncertainty approximately a factor of 5; more typical values are about a factor of 2.

When the depth-dependency was evaluated, it was found that fracture intensity varies by fracture set and domain. Other than the uppermost hundred meters or so, there appears to be no systematic change in fracture intensity with depth, nor can the zones of higher and lower intensity at depth be correlated to other boreholes. Other than in the near surface environment, the intensity variations are not systematic functions of depth. The variation can be modeled as a Gamma distribution. If depth dependency is ignored in calculating average intensities for each set and domain, then there will be a tendency to slightly (about 10%) overestimate the mean intensity.

Uncertainties regarding orientations of fracturing play only an insignificant role in fracture intensity, a the only possible impact is in the set classification, which could possibly impact the coupled size/intensity parameter values in that the are anchored in part to the borehole fracture intensity. However, the other uncertainties in the coupled size/intensity calculations for the TCM and OSM are much greater.

Statistical analysis of the fractures visible and not visible in BIPS indicates that there are no statistically significant differences in the geological attributes of these two groups. Therefore, no additional uncertainty is expected. The Forsmark version 2.2 geological DFN model was based on scaling up the borehole P_{32} values according to the ratios of the observed and unobserved fractures; if only the intensity values associated with the visible fractures is used, then the uncertainty related to this assumption with regards to permeability magnitude is in direct proportion to the ratio of (observed + unobserved)/observed.

7.6　Recommendations

To the extent that the quantified uncertainty is too large for downstream users of this data, additional effort needs to be employed to reduce the uncertainty. It is recommended that hydrologic, safety analysis and engineering teams assess whether the uncertainty limits are adequate for their needs, and to provide feedback to the geological modeling team.

To the extent that lack of data, specifically fracture size data, in Domains FFM01 and FFM06 produce too great uncertainty, it is recommended that additional fracture size data, such as traces derived from tunnel or drilled shaft walls, be collected in these fracture domains if and where possible.

All users of the models developed in this study should evaluate for themselves the adequacy of the parameterization of the model for their specific needs and requirements.

8   References

Carlsson, A, 1979. Characteristic features of a superficial rock mass in southern central Sweden – horizontal and subhorizontal fractures and filling materials. Striae, Vol. 11, 79 p.

Carlsten S, Gustafasson J, Samuelsson E, Stephens M, Thunehed H, 2007. Geological single-hole interpretation of KFM08D, Forsmark site investigation. Draft of SKB P-report, dated 042007. Svensk Kärnbränslehantering AB.

Davis J, 2002. Statistics and Data Analysis in Geology, Third Edition. John Wiley and Sons, New York, New York, USA.

Danielsson P, Forssberg O, Larsson N Å, 2006. Method description for detailed fracture mapping of rock outcrops. MD 132.003e, version 3.0, dated 20061103, Svensk Kärnbränslehantering AB.

Dershowitz W, 1984. Rock Joint Systems, Doctoral dissertation, Massachusetts Institute of Technology, Cambridge, MA, USA.

Dershowitz W, Lee G, Geier J, Foxford T, La Pointe P, Thomas A, 1998. FRACMAN, Interactive discrete feature data analysis, geometric modeling and exploration simulation. User documentation, version 2.6. Golder Associates, Inc., Redmond, Washington, USA.

Dershowitz W, Doe T, Uchida M, Hermanson J, 2003. Correlations between Fracture Size, Transmissivity, and Aperture, in Proceedings Volume 1, Soil and Rock America 2003, 12th Panamerican Conference on Soil Mechanics and Geotechnical Engineering, Verlag Glückauf GMBH, Essen, Germany.

Evans M, Hastings N, Peacock B, 2000. Statistical Distributions, 3rd Edition, John Wiley and Sons, New York, New York, USA.

Fisher N, Lewis T, Embleton B, 1987. Statistical analysis of spherical data, Cambridge University Press, Cambridge, UK.

Fox A, Hermanson J, 2006. Identification of additional possible minor deformation zones at Forsmark through a review of data from cored boreholes. Forsmark site investigation, SKB P-06-293, Svensk Kärnbränslehantering AB.

Isaksson H, 2003. Interpretation of topographic lineaments. Forsmark site investigation, SKB P-03-40, Svensk Kärnbränslehantering AB.

Isaksson H, Pitkänen T, Thunehed H, 2006a. Ground magnetic survey and lineament interpretation in an area northwest of Bolundsfjärden. Forsmark site investigation, SKB P-06-85, Svensk Kärnbränslehantering AB.

Isaksson H, Thunehed H, Pitkänen T, Keisu M, 2006b. Detailed ground and marine magnetic survey and lineament interpretation in the Forsmark area – 2006, Forsmark site investigation, SKB P-06-261, Svensk Kärnbränslehantering AB.

Johansson R, Isaksson H, 2006. Assessment of inferred lineaments in the north-western part of the Forsmark site investigation area. Present knowledge and recommendations for further investigations. Forsmark site investigation, Report SKB P-05-261, Svensk Kärnbränslehantering AB.

Johnson N, Kotz S, Balakrishnan N, 1994. Continuous Univariate Distributions, Volume I and II, 2nd Edition, John Wiley and Sons, New York, New York, USA.

Korhonen K, Paananen M, Paulamäki S, 2004. Interpretation of lineaments from airborne geophysical and topographic data. An alternative model within version 1.2 of the Forsmark modeling project, SKB P-04-241, Svensk Kärnbränslehantering AB.

La Pointe P R, Cladouhos T, Follin S, 1999. Calculation of displacement on fractures intersecting canisters induced by earthquakes: Aberg, Beberg and Ceberg examples. SKB TR-99-03, Svensk Kärnbränslehantering AB.

La Pointe P R, Olofsson I, Hermanson J, 2005. Statistical model of fractures and deformation zones for Forsmark: Preliminary site description Forsmark area – version 1.2. SKB R-05-26, Svensk Kärnbränslehantering AB.

Munier R, Stenberg L, Stanfors R, Milnes A G, Hermanson J, Triumf C A, 2003. Geological Site Descriptive Model; A strategy for the model development during site investigations, SKB R-03-07, Svensk Kärnbränslehantering AB.

Munier R, 2004. Statistical analysis of fracture data, adapted for modelling Discrete Fracture Networks-Version 2. SKB R-04-66, Svensk Kärnbränslehantering AB.

Munier R, 2006. DFN related modeling issues to consider during 2.2 modeling. Project memorandum, distributed 20060608, Svensk Kärnbränslehantering AB.

Munier R, Stigsson M, 2007. *in prep*. Implementation of uncertainties in borehole geometries and geological orientation data in SICADA. SKB R-07-19, Svensk Kärnbränslehantering AB.

NIST, 2007a. Box plot. Chapter 1.3.3.7, NIST/SEMATECH e-Handbook of Statistical Methods, National Institute of Standards and Technology, United States Department of Commerce, Washington D.C., USA.
http://www.itl.nist.gov/div898/handbook/eda/section3/boxplot.htm
Last accessed 20070903.

NIST, 2007b. Anderson-Darling and Shapiro-Wilk tests, Chapter 7.2.1.3,

NIST/SEMATECH e-Handbook of Statistical Methods, National Institute of Standards and Technology, United States Department of Commerce, Washington D.C., USA.
http://www.itl.nist.gov/div898/handbook/prc/section2/prc213.htm
Last accessed 20070903.

NIST, 2007c. How can we compare several populations with unknown distributions (the Kruskal-Wallis test)?. Chapter 7.4.1, NIST/SEMATECH e-Handbook of Statistical Methods, National Institute of Standards and Technology, United States Department of Commerce, Washington D.C., USA.
http://www.itl.nist.gov/div898/handbook/prc/section4/prc41.htm
Last accessed 20070903.

NIST, 2007d. Kolmogorov-Smirnov Goodness-of-Fit Test, Chapter 1.3.5.16, NIST/SEMATECH e-Handbook of Statistical Methods, National Institute of Standards and Technology, United States Department of Commerce, Washington D.C., USA.
http://www.itl.nist.gov/div898/handbook/eda/section3/eda35g.htm
Last accessed 20070903.

NIST, 2007e. Gamma distribution, Chapter 1.3.6.11, NIST/SEMATECH e-Handbook of Statistical Methods, National Institute of Standards and Technology, United States Department of Commerce, Washington D.C., USA.
http://www.itl.nist.gov/div898/handbook/eda/section3/eda366b.htm
Last accessed 20070903.

Olofsson I, Simeonov A, Stigsson M, Stephens M, Follin S, Nilsson A C, Röshoff K, Lindberg U, Lanaro F, Fredriksson L, 2007. (In press), A fracture domain concept as a basis for the statistical modelling of fractures and minor deformation zones, and interdisciplinary coordination. Site descriptive modeling Forsmark, stage 2.2, SKB R-07-15, Svensk Kärnbränslehantering AB.

Press W, Flannery B, Teukolsky S, Vetterling W, 1992. Numerical Recipes in C: The Art of Scientific Computing. Cambridge University Press, Cambridge, UK.

Stephansson O, Ericsson B, 1975. Pre-Holocene joint fillings at Forsmark, Uppland, Sweden. Geologiska Föreningens i Stockholm Förhandlingar 97, 91–95.

Stephens M, Forssberg O, 2006. Rock types and ductile structures on a rock domain basis, and fracture orientation and mineralogy on a deformation zone basis. Preliminary site description Forsmark area – version 1.2. SKB R-06-78, Svensk Kärnbränslehantering AB.

Stråhle A, Larsson N Å, 2005. Metodbeskrivning Boremap-Kartering, MD 143.006, version 2.0, dated 20051103, Svensk Kärnbränslehantering AB.

Schlaifer H, Raiffa R, 1972. Applied Statistical Decision Theory, MIT Press, Cambridge, Massachusetts, USA.

Triumf C A, 2003. Identification of lineaments in the Simpevarp area by the interpretation of topographical data. Oskarshamn site investigation, SKB P-03-99, Svensk Kärnbränslehantering AB.

Triumf C A, 2004. Joint interpretation of lineaments in the eastern part of the site descriptive model area. Oskarshamn site investigation, SKB P-04-37, Svensk Kärnbränslehantering AB.

Wang X, 2005. Stereological Interpretation of Rock Fracture Traces on Borehole Walls and Other Cylindrical Surfaces, Virginia Polytechnic Institute and State University, doctoral dissertation.

Wilcoxon F, 1945. Individual comparisons by ranking methods. Biometrics, 1, 80–83.

Öhman J, Hermanson J, Fox A, La Pointe P, 2007. *in press*. Linking of fracture traces from detailed outcrop maps at Forsmark. Forsmark site investigation, SKB P-XX-XXX, Svensk Kärnbränslehantering AB.

ERRATUM

While finalising the main report of the Forsmark Site Description /SKB 2008/, errors were discovered in Table 5-3 and Table 5-4 (p. 214) of the Forsmark stage 2.2 geological DFN summary report /Fox et al. 2007/. These errors do not affect the parameterisation of the reported DFN models nor of downstream models based on them. The errors are in the parameterisation presented in tables documenting a specific uncertainty case. This uncertainty case was later presented as a model alternative ("r_0-fixed") in the Forsmark Site Description /SKB 2008/.

This erratum is judged to be of interest to readers wishing to follow or examine the logic behind the derivation of the "r_0-fixed" DFN model alternative described in the main report of the Forsmark Site Description /SKB 2008/. To aid the reader in placing this erratum in its proper context, we provide below a short description of how Tables 5-3 and 5-4 in /Fox et al. 2007, p. 214/ relate to the "r_0-fixed" model /Table 5-8 in SKB 2008/ and clarify the key assumptions and limitations of its derivation.

In the Forsmark 2.2 Geological DFN report /R-07-46/, there are two alternative models (OSM + TFM and TCM/TCMF) that rely on the length/intensity of the deterministically-modelled deformation zones as a component of their parameterisation. The traces of deformation zones in the Forsmark 2.2 DZ model and the lineaments identified in the high-resolution ground-magnetic surveys were divided into orientation sets, and their trace lengths were plotted on complementary cumulative number (CCN) plots, with lengths normalised by observation area (or pseudo-area, for the fractal scaling case). It is important to note that in the CCN plots, the lineaments and DZ traces were not subdivided by fracture domain; the only subdivision was by orientation set. In addition, neither the intensity (P_{32}) of MDZ in cored boreholes nor the intensity of the deterministic deformation zones were used at all in the development of the radius scaling exponent k_r. The estimation of k_r was based wholly on the trace lengths of structures observed on detail-mapped fracture outcrops, on MDZ-sized lineaments derived from high-resolution ground magnetic surveys, and on the surface traces of deterministically-modelled deformation zones.

The rationale for the treatment of magnetic lineaments and DZ traces was the following:

1. The coverage of the lineament data set is very limited. Even inside the Forsmark local model area, the lineament coverage is somewhat incomplete. If lineament traces from across all fracture domains had not been used in the model parameterisation, there would not have been sufficient data for some domains to compute a size-intensity relationship across the complete scale of the geological DFN model.

2. Second, if lineaments and DZ had been divided into fracture domains at the surface, severe truncation effects, mass defects, and biased sampling would have been introduced into the trace length data set. Clipping lineaments to only the lengths that lie inside a fracture domain seriously biases the trace length distribution, which directly affects the size-intensity model (changes k_r).

Therefore, to limit the potential censoring effects/sampling bias and to ensure an adequate number of lineaments / DZ traces for parameterisation, the CCN plots, and therefore the radius scaling exponent (k_r) are based on the lengths of DZ and lineaments inside the entire local model area, and not inside domains. What this means is that, effectively, one end of the CCN plot was fixed as a pivot point and was not free to move. Differences in the radius scaling exponent k_r between domains FFM02 and FFM03 (at the surface) were accounted for using only the outcrop trace length data; the same lineaments and DZ traces were used to fit k_r for both domain FFM02 and domain FFM03.

This is an appropriate assumption if both the density of lineaments and the relative intensity of each orientation set are roughly set are roughly uniform over the local model area, and does not differ significantly between fracture domains. However, at Forsmark the relative intensity of NW-striking lineaments is much higher outside of domain FFM02 (and hence also outside domain FFM01, which lies underneath FFM02) than it is on the inside. In other words, there is significant anisotropy in the density of certain lineament sets. It is possible that if the lineaments had been clipped such that only the segments inside FFM02/FFM01 were used in the CCN plots for FFM02/FFM01 that it might not have been possible at all to fit a straight line on the CCN plots between outcrops, MDZ-sized lineaments, and surface traces of deterministic DZ; i.e. the assumption of tectonic continuum would be completely invalidated. However, the spatial anisotropy of aspect of MDZ-sized lineaments and DZ surface traces was not explored during the Forsmark 2.2 geological DFN modelling.

What is the effect of this assumption on the geological DFN parameterisation? Effectively, the radius scaling exponent (k_r) is biased towards an average value (i.e. the average over the entire Forsmark local model domain) with respect to lineaments and DZ traces. If the density of NW-striking lineaments and DZ traces in a particular fracture domain (FFM02. for example) is significantly less than the 'average' value for the entire local model domain, then the TCM, TCMF, and TMF models will most likely not produce an estimate of k_r that is accurate for MDZ-sized structures in that domain and orientation set. The consequence is that, at MDZ scales and larger, the TCM, TCMF, and TFM models overestimate the intensity of the MDZ and DZ sized features with a NW strike.

In short, the following assumptions were made:

1 In the TCM models for domain FFM01 in Forsmark 2.2, both the Euclidean and Fractal cases, k_r was specified from outcrop and lineament trace data and that the P_{32} specified was a "match" P_{32}. The match P_{32} was calculated by:

   a Calculating k_t from trace length scaling plots.

   b Calculating k_r from k_t using $k_r = k_t + 1$

   c Calculating the P_{32} of the outcrop traces in FFM02 (P_{32OC}) using $r_{min} = 0.5$ m, $r_{max} = \infty$ ($1 \cdot 10^{31}$ m in DFN simulations). The goal here was to calculate a P_{32} intensity that, when sampled, will produce traces that when plotted on a CCN plot fall on the same fitted k_t line.

   d P_{32OC} is now compared to P_{32} calculated from 6 m borehole intervals (bins) (P_{32BH}):

   • If $P_{32OC} > P_{32BH}$, the minimum radius is reduced, and P_{32BH} becomes $P_{32match}$. This is the case for domain FFM02; the P_{32} in the boreholes is higher than the P_{32} in outcrop. We are saying that the borehole P_{32} is higher because it encounters smaller fractures than those mapped in the outcrops.

   • If $P_{32OC} < P_{32BH}$, the minimum radius is increased. This means that the borehole contains larger fractures than the outcrop. This is the case for domain FFM01 for the TCM and TCMF models, where we do not have trace length data from outcrops (as the domain is not exposed at the ground surface), and instead use the k_r and P_{32OC} from FFM02. FFM01 has, on average, a lower intensity than FFM02. Therefore, if P_{32} is lower, k_r is fixed, and the match point for P_{32OC} is fixed, r_0 must change for the power law equation to be valid. The TCM models assume that domain FFM01 and FFM06 are functionally equivalent to domain FFM02 (i.e. the k_r value for FFM02 can be used to characterise sizes in these domains).

2 The tables 5-3 and 5-4 of the geological DFN summary report /R-07-46/ / present the result of an uncertainty case that tests the assumption that the k_r values in FFM01 are different than the k_r values in FFM02. The P_{32} values labelled "P_{32}-6 m bins" *are incorrect* in these tables. Those P_{32} values were calculated using too many borehole segments. Basically, for boreholes in FFM01 where one regional fracture set was not present (i.e. the NS set is not present in KFM01D), the average value calculation did not delete the 'extra' empty borehole sections from the analysis. This meant that a number of sections with no fractures crept into the calculation, and reduced the average P_{32}. This does, however, not affect the DFN model parameterisation of the other model variants (OSM+TFM and TCMF/TCM). The only

thing it affects is the content of Tables 5-3 and 5-4 in the uncertainty analysis section of the geological DFN summary report /R-07-46/. The corrected tables are provided below.

3 The 'r_0-fixed' (called 'k_r-scaled' model in previous reports) calculation makes the following assumptions:

   a. $r_1 = 0.039$ m

   b. $r_2 = \infty$ ($1 \cdot 10^{31}$ m)

   c. $r_3 = 564$ m

   d. $r_4 = \infty$ ($1 \cdot 10^{31}$ m)

   e. $P_{32}(r_1, r_2)$ = arithmetic average of P_{32} calculated over 6 m long borehole lengths. Also, for the recalculation, we ***assume*** that the P_{32} of DZ (structures > 564 m radius) is the same in FFM01 and FFM06 as it is in FFM02. This allowed us to fix both sides of Equation 3-11 (p.41, R-07-46) and solve for k_r.

4 The match point P_{32} in all size models is labelled as going from r_0 to ∞. *Technically*, since we excluded all DZ from the calculation, *and* we are making the assumption that all fractures > 564 m are DZ *and* are captured in the deterministic model, the P_{32} match point should actually be considered as valid for fractures with radii between r_0 and 564 m. For most of the size-intensity models, this makes a slight difference in the 3rd or 4th decimal place, which, given that the uncertainties in the geological DFN model parameterisation are within the range of one order of magnitude, is inconsequential.

Referens

Fox A, La Pointe P, Hermanson J, Öhman J, 2007. Statistical geological discrete fracture network model. Forsmark modelling stage 2.2. SKB R-07-46, Svensk Kärnbränslehantering AB.

Table 5-3. Intensity ratios in FFM01 for model cases assuming domain independence of scaling exponent ('r_0-fixed' model) versus domain dependence of scaling exponent (k_r of FFM01 = k_r of FFM02).

Fracture Domain	Fracture Set	Set Type	Min. Radius r_0 (m)	TCM – Based on k_r derived from FFM02				TCM – k_r in FFM01 not equal to k_r in FFM02				
				k_r	P_{32} (m²/m³)			r_0*	k_r*	Ratio k_r*/ k_r	P_{32} (28–564 m)	Ratio of P_{32} (28–564 m)
					$r_0 - \infty$	(> 564 m)	(28–564 m)					
FFM01	NE	Global	0.66	3.02	1.74	0.0018	0.0361	0.039	2.72	0.90	0.0136	0.38
FFM01	NS	Global	0.06	2.78	1.29	0.0010	0.0096	0.039	2.75	0.99	0.0086	0.89
FFM01	NW	Global	0.59	2.85	0.95	0.0028	0.0331	0.039	2.61	0.92	0.0146	0.44
FFM01	SH	Global	0.82	2.85	0.63	0.0024	0.0286	0.039	2.58	0.91	0.0114	0.40
FFM01	ENE	Local	0.32	3.25	2.74	0.0002	0.0102	0.039	2.97	0.91	0.0043	0.42
FFM01	EW	Local	0.17	3.10	1.12	0.0001	0.0039	0.039	2.93	0.95	0.0023	0.59

Table 5-4. Intensity ratios in FFM06 for model cases assuming domain independence of scaling exponent ('r_0-fixed' model) versus domain dependence of scaling exponent (k_r of FFM06 = k_r of FFM02).

Fracture Domain	Fracture Set	Set Type	Min. Radius r_0 (m)	TCM – k_r in FFM06 equal to k_r in FFM02				TCM – k_r in FFM06 not equal to k_r in FFM02				
				k_r	P_{32} (m²/m³)			r_0*	k_r*	Ratio k_r*/ k_r	P_{32} (28–564 m)	Ratio of P_{32} (28–564 m)
					$r_0 - \infty$	(> 564 m)	(28–564 m)					
FFM06	NE	Global	0.35	3.02	3.30	0.0018	0.0361	0.039	2.79	0.92	0.0170	0.47
FFM06	NS	Global	0.04	2.78	2.15	0.0012	0.0114	0.039	2.78	1.00	0.0114	1.00
FFM06	NW	Global	0.32	2.85	1.61	0.0028	0.0331	0.039	2.66	0.93	0.0177	0.54
FFM06	SH	Global	0.79	2.85	0.64	0.0024	0.0286	0.039	2.58	0.91	0.0115	0.40
FFM06	ENE	Local	0.74	3.25	0.98	0.0002	0.0102	0.039	2.87	0.88	0.0031	0.30

* Minimum radius (r_0) and scaling exponent (k_r) calculated for 'r_0-fixed' model.

Area-normalized trace length scaling plots
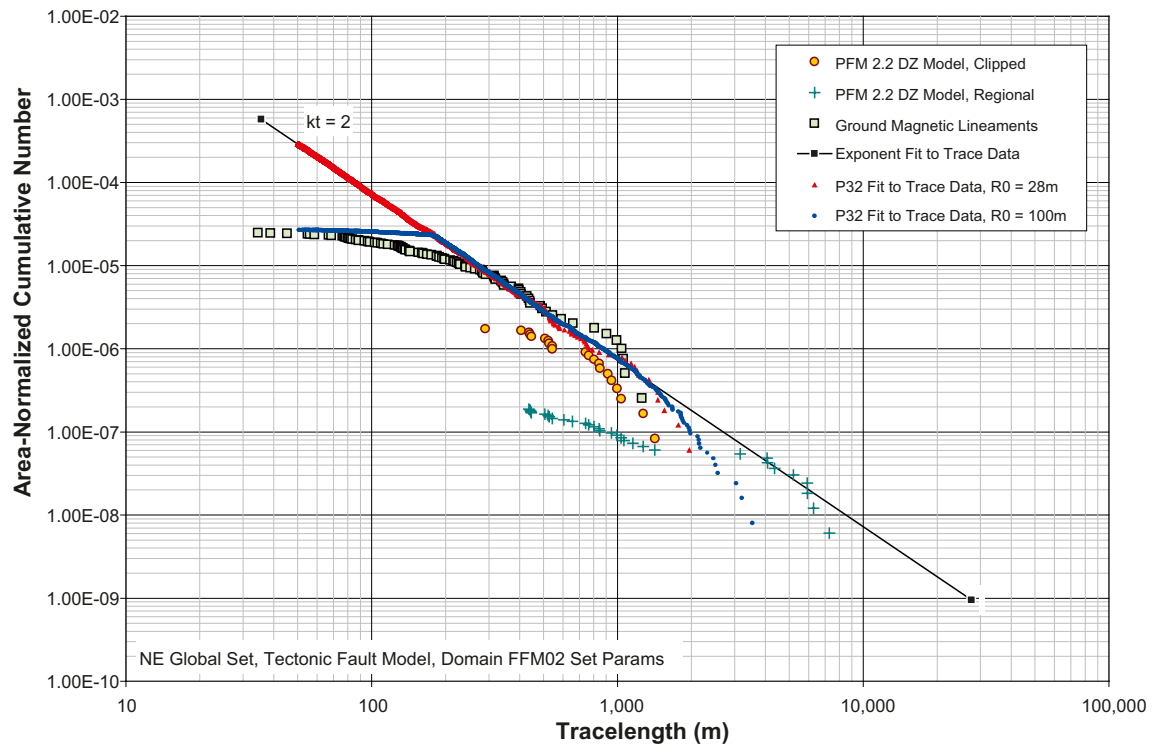
Figure 9-1. *NE Global set, Tectonic Fault Model (TFM) using domain FFM02 orientation parameters.*
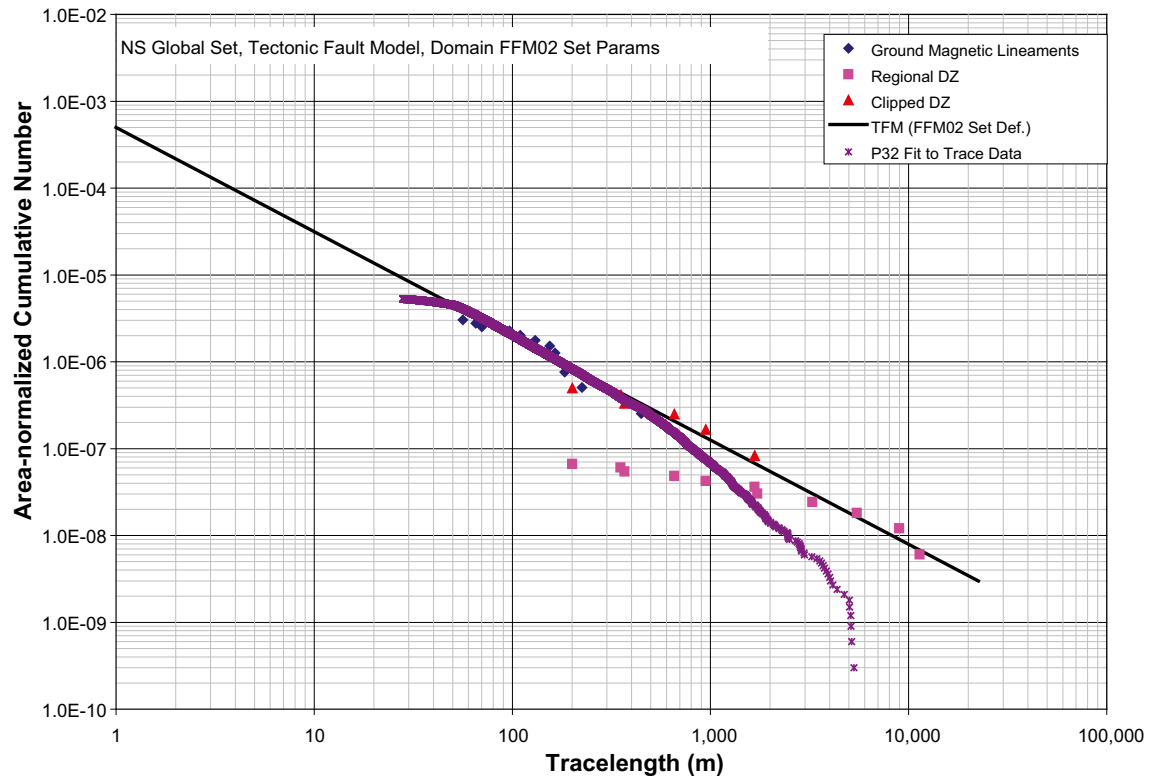
Figure 9-2. *NS Global set, Tectonic Fault Model (TFM) using domain FFM02 orientation parameters.*
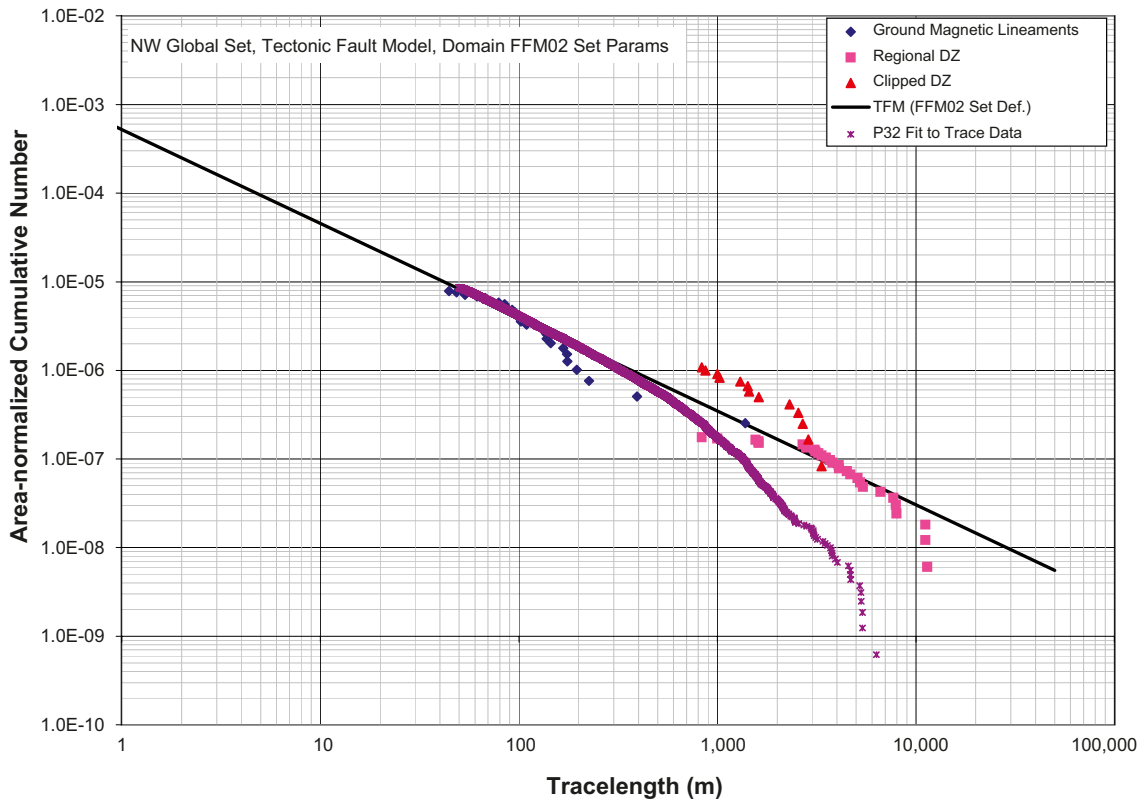
Figure 9-3. *NW Global set, Tectonic Fault Model (TFM) using domain FFM02 orientation parameters.*
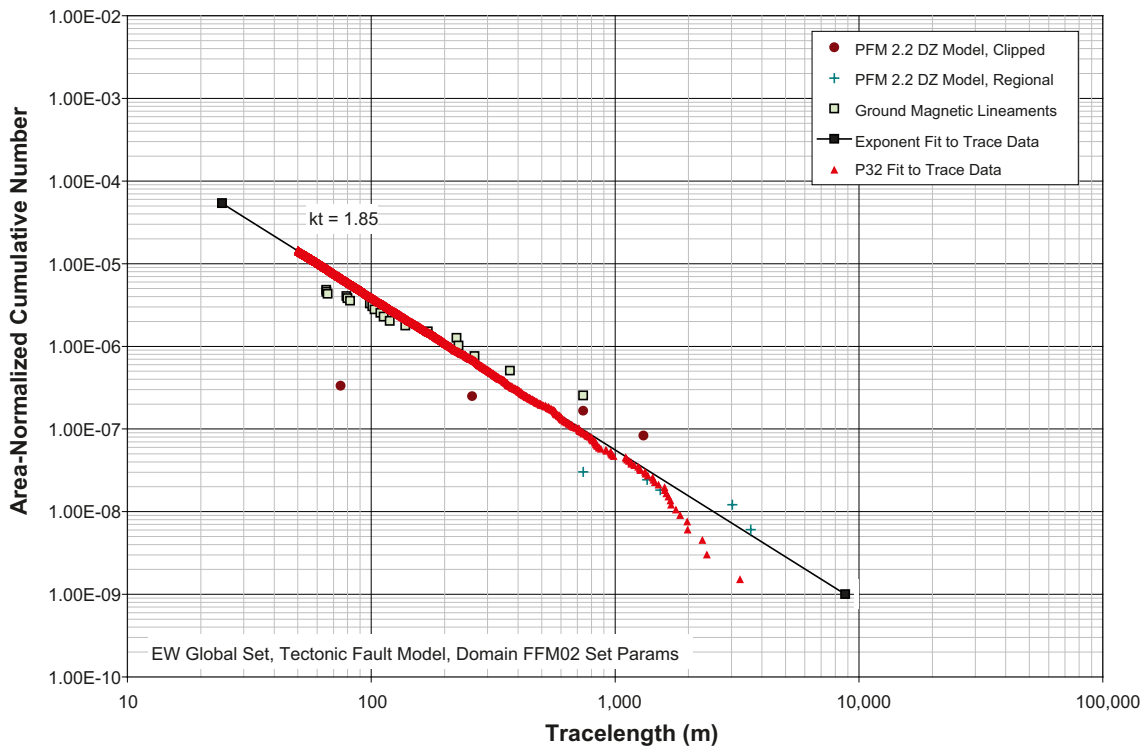
Figure 9-4. *EW Global set, Tectonic Fault Model (TFM) using domain FFM02 orientation parameters.*
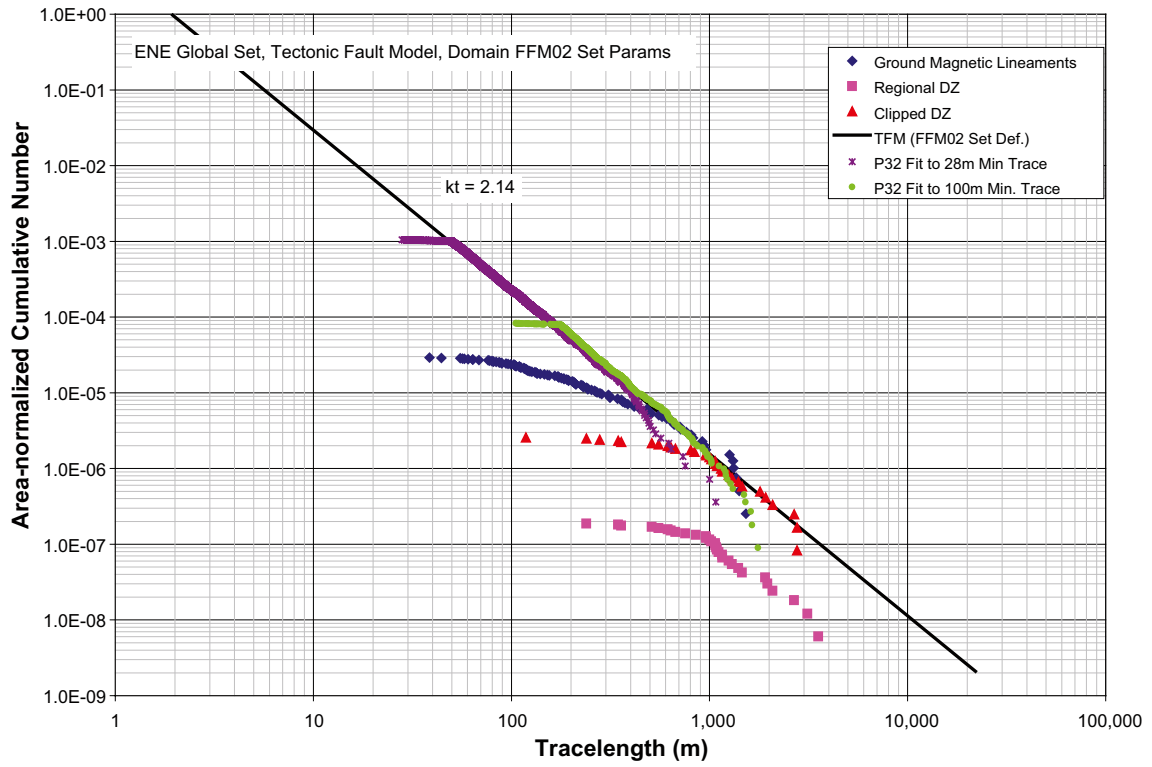
Figure 9-5. *ENE Global set, Tectonic Fault Model (TFM) using domain FFM02 orientation parameters.*
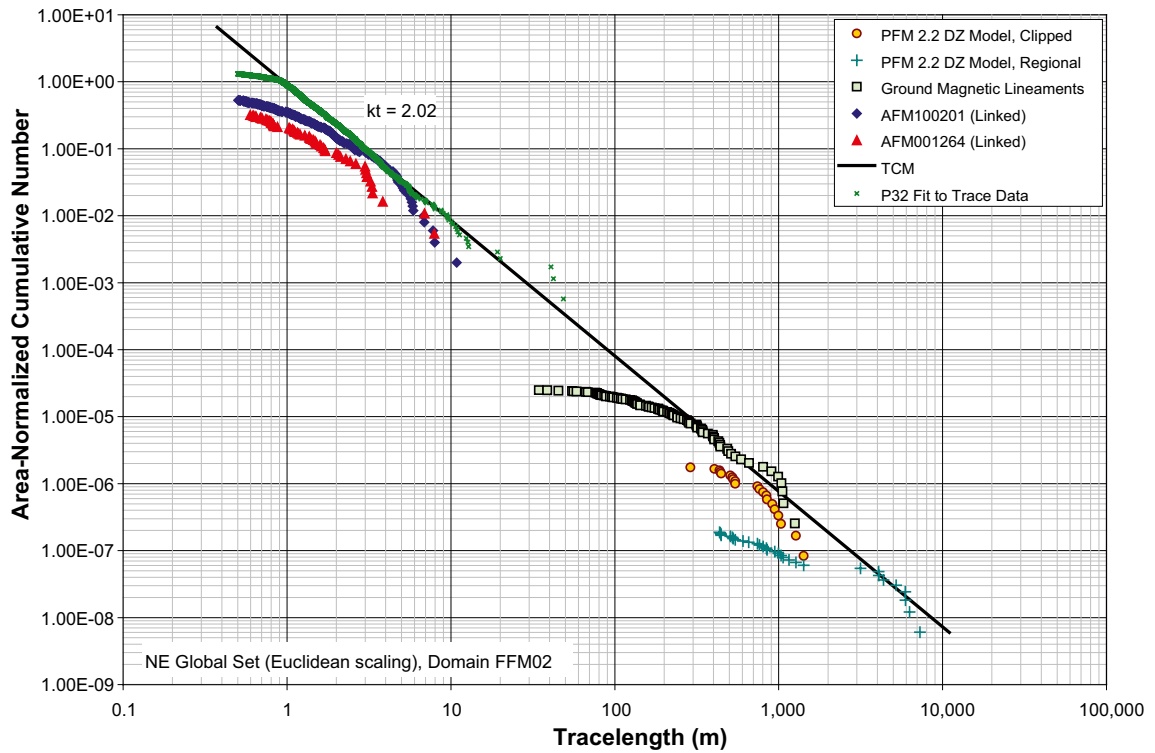
Figure 9-6. *NE Global set, Euclidean scaling (TCM), Domain FFM02.*

3
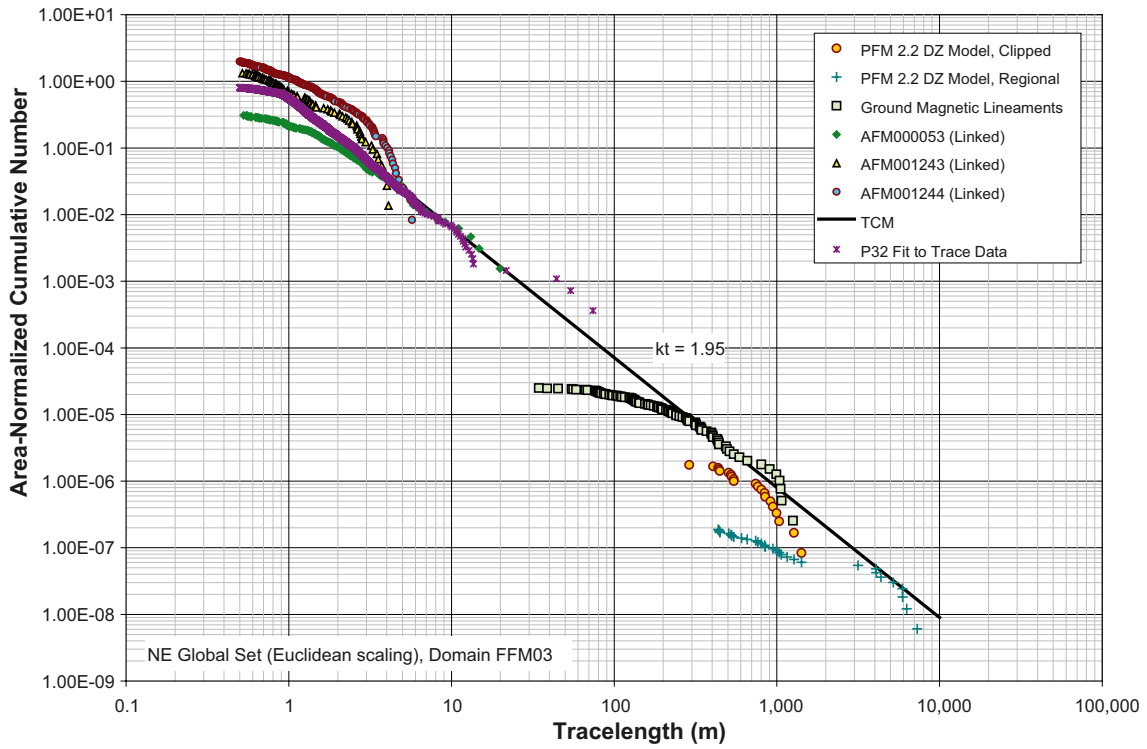
Figure 9-7. *NE Global set, Euclidean scaling (TCM), Domain FFM03.*
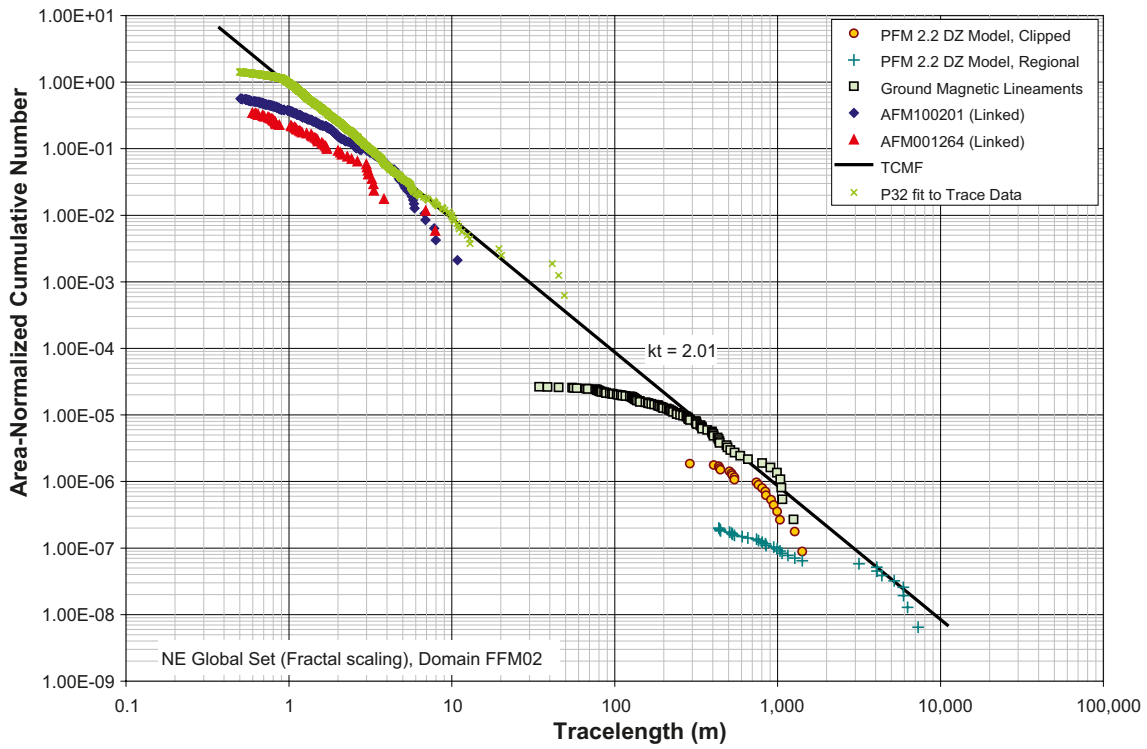
Figure 9-8. *NE Global set, Fractal mass scaling (TCMF), Domain FFM02.*
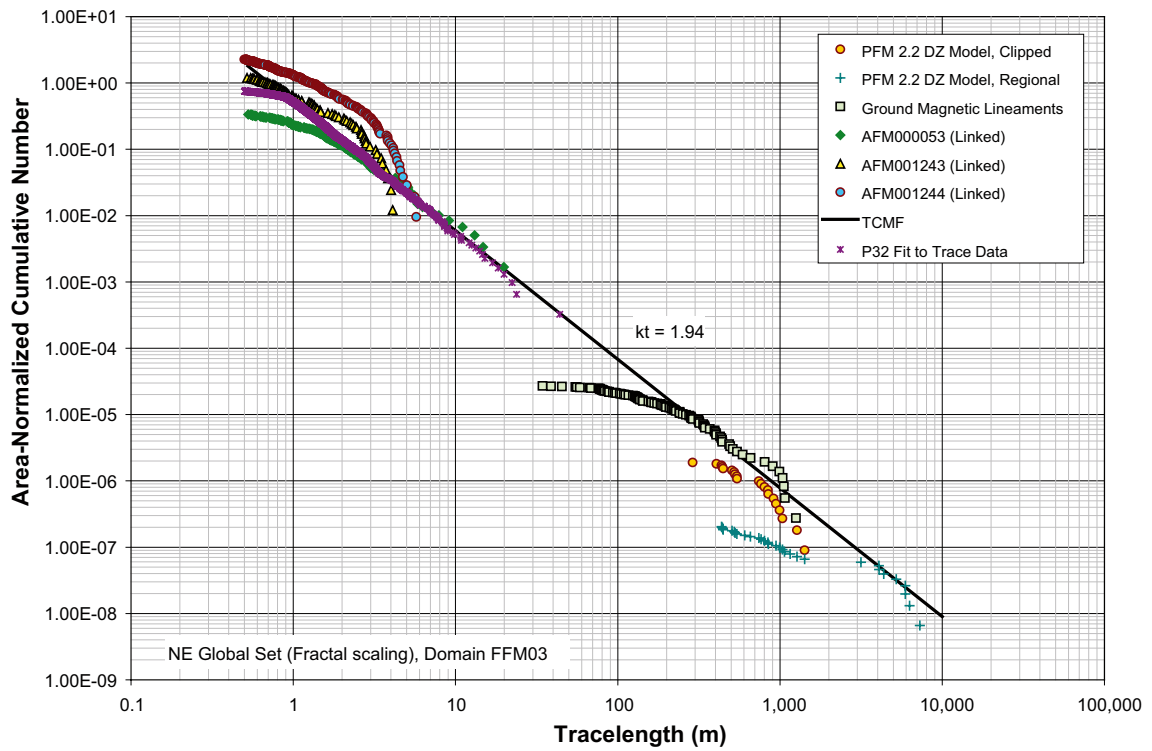
Figure 9-9. *NE Global set, Fractal mass scaling (TCMF), Domain FFM03.*
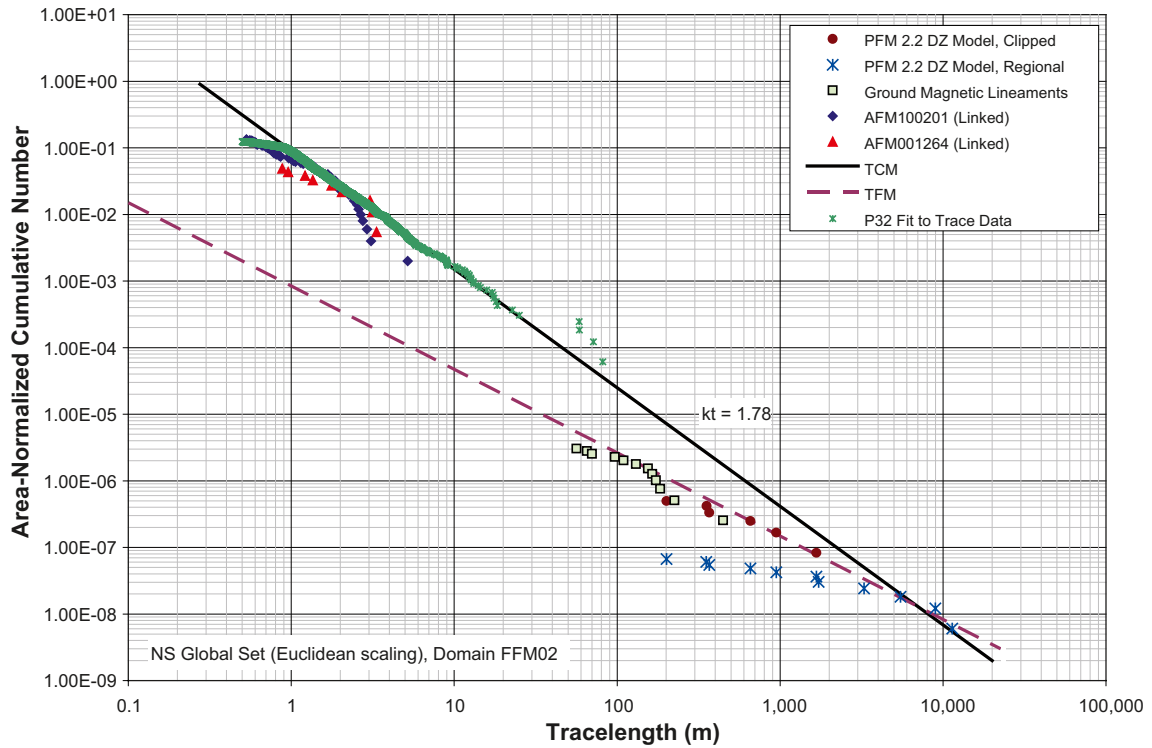
Figure 9-10. *NS Global set, Euclidean scaling (TCM), Domain FFM02.*

5
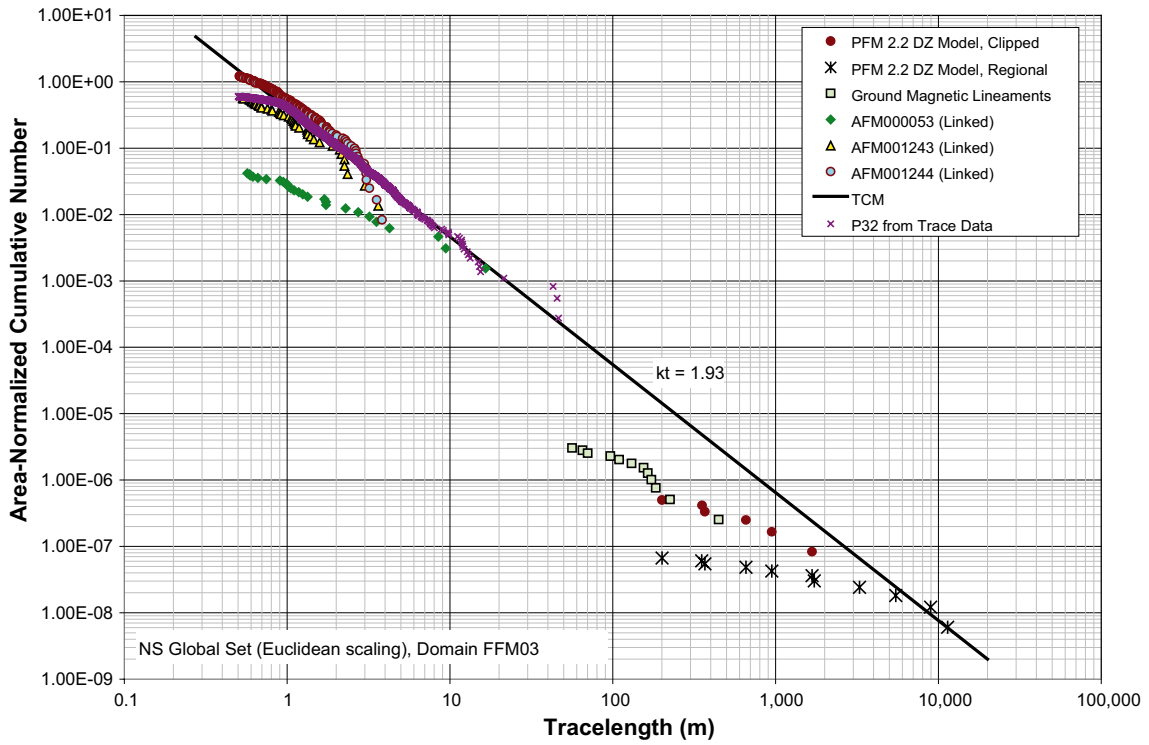
Figure 9-11. *NS Global set, Euclidean scaling (TCM), Domain FFM03.*
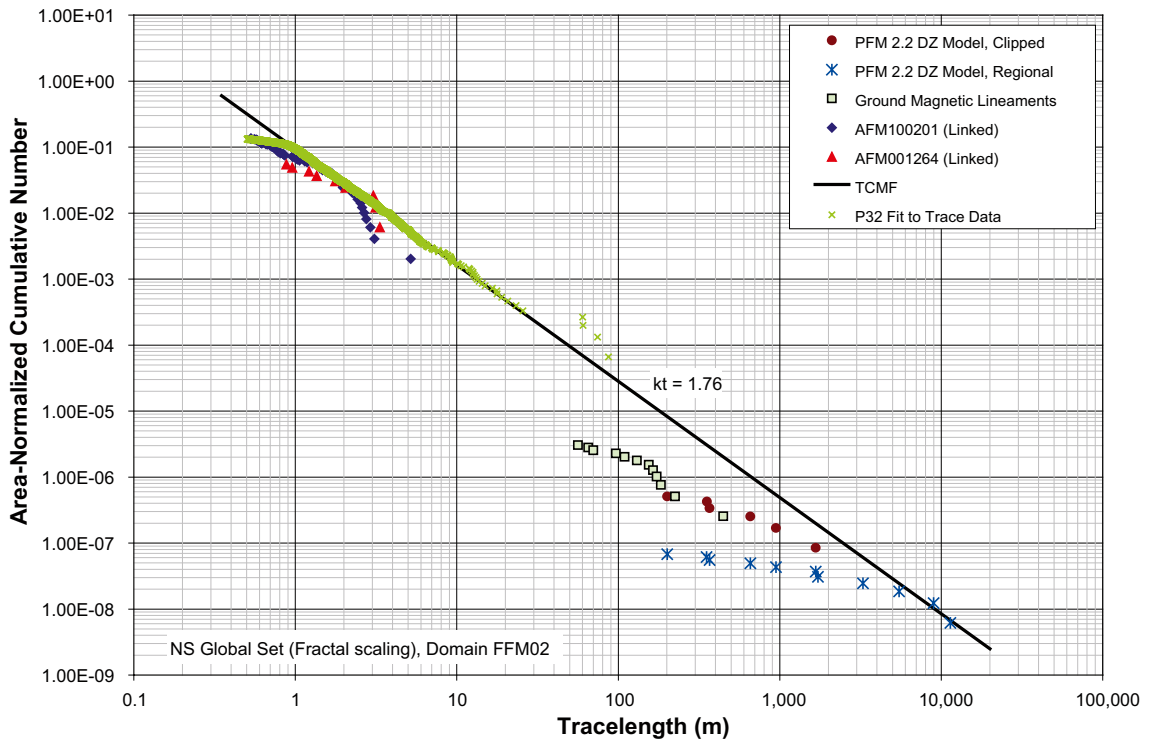
Figure 9-12. *NS Global set, Fractal mass (TCMF) scaling, Domain FFM02.*

6
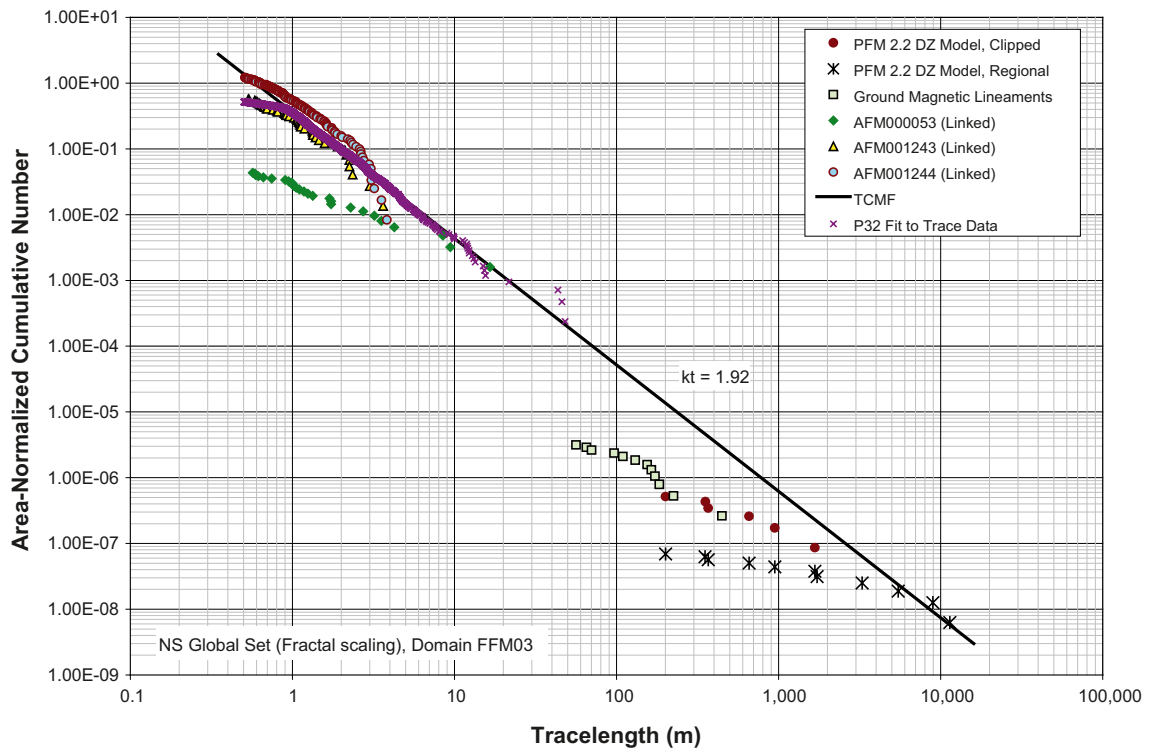
Figure 9-13. *NS Global set, Fractal mass (TCMF) scaling, Domain FFM03.*
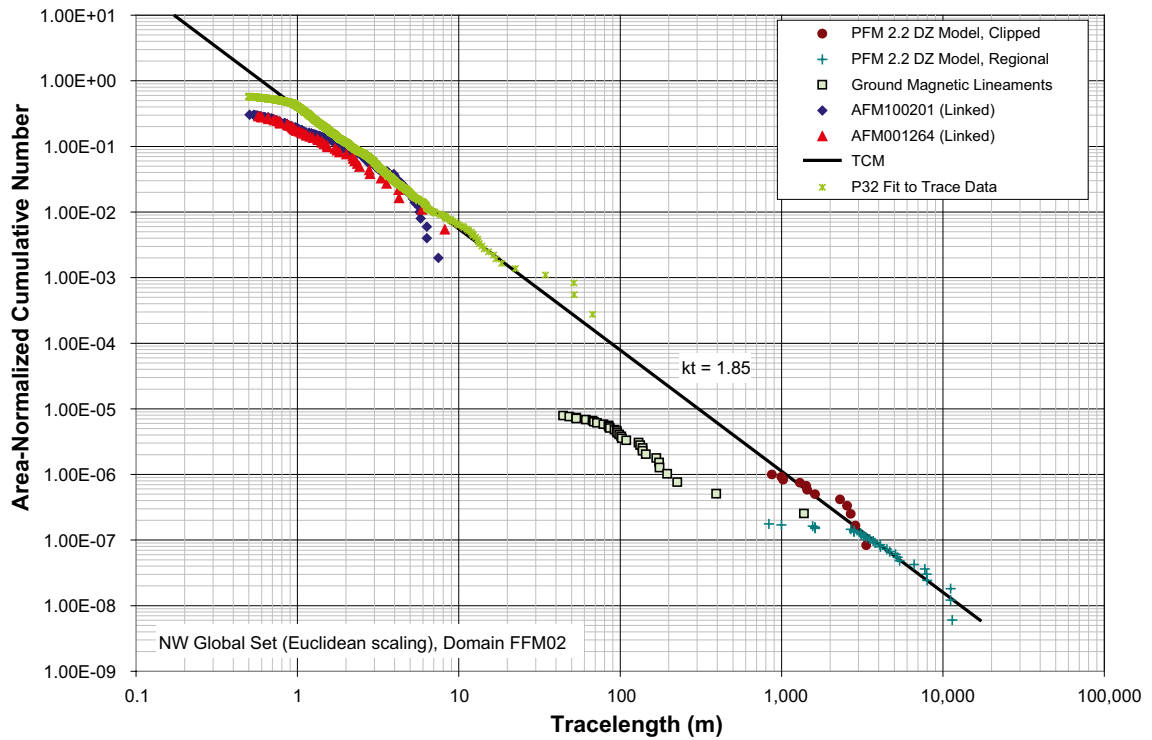
Figure 9-14. *NW Global set, Euclidean scaling (TCM), Domain FFM02.*
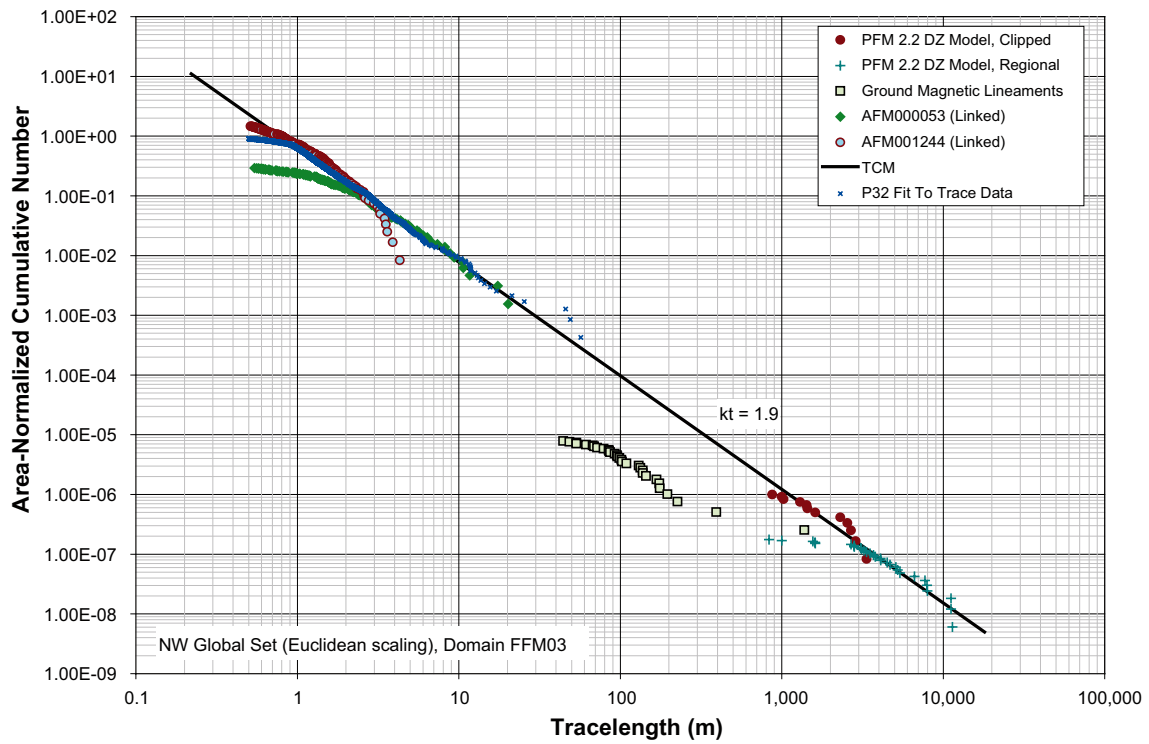
Figure 9-15. *NW Global set, Euclidean scaling (TCM), Domain FFM03.*
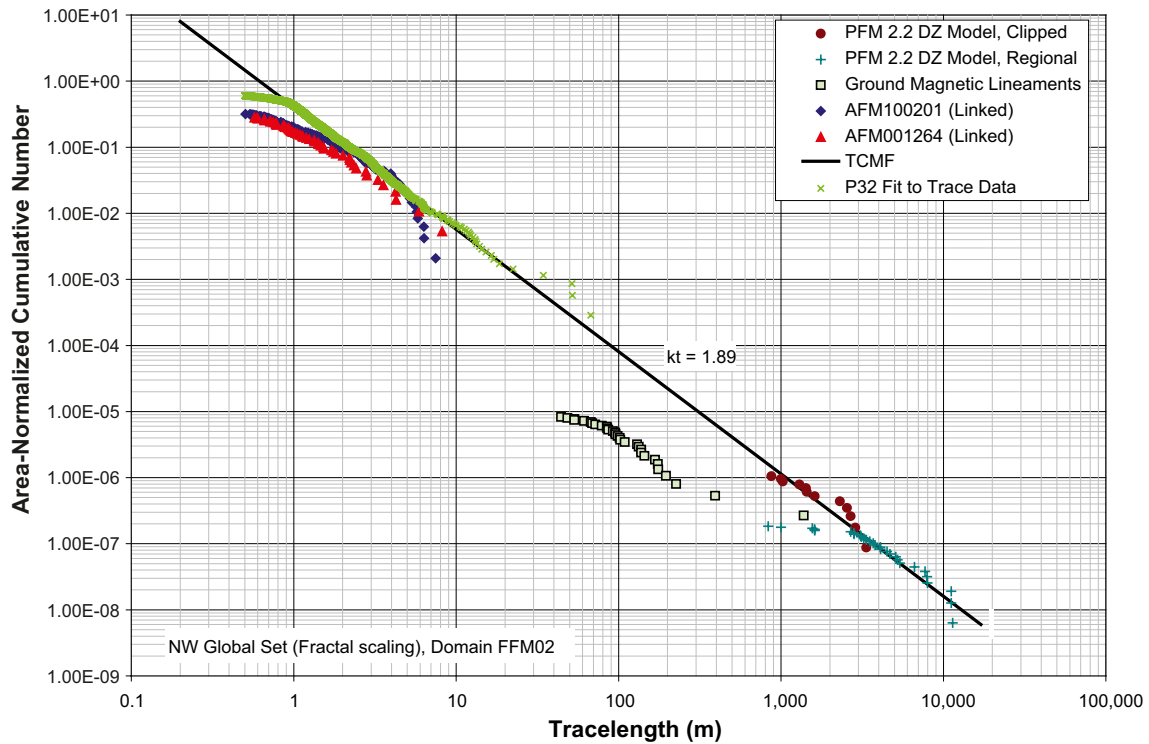
Figure 9-16. *NW Global set, Fractal mass scaling (TCMF), Domain FFM02.*
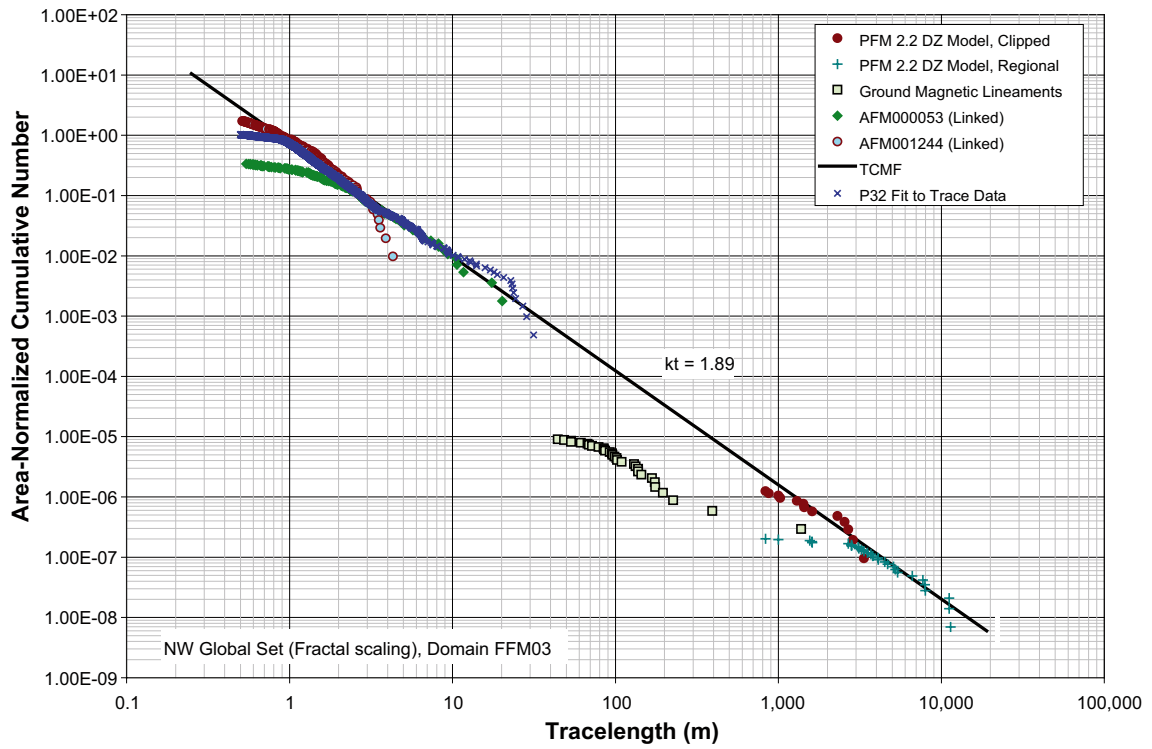
Figure 9-17. *NW Global set, Fractal mass scaling (TCMF), Domain FFM03.*
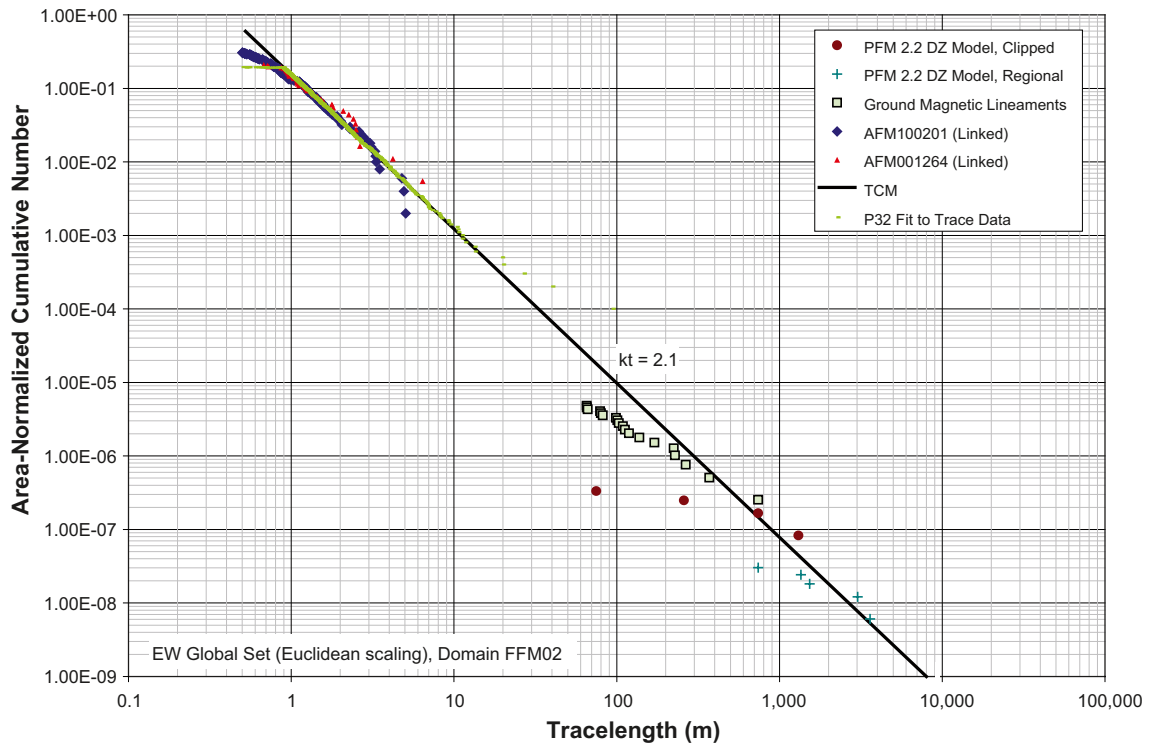
Figure 9-18. *EW Global set, Euclidean scaling (TCM), Domain FFM02.*
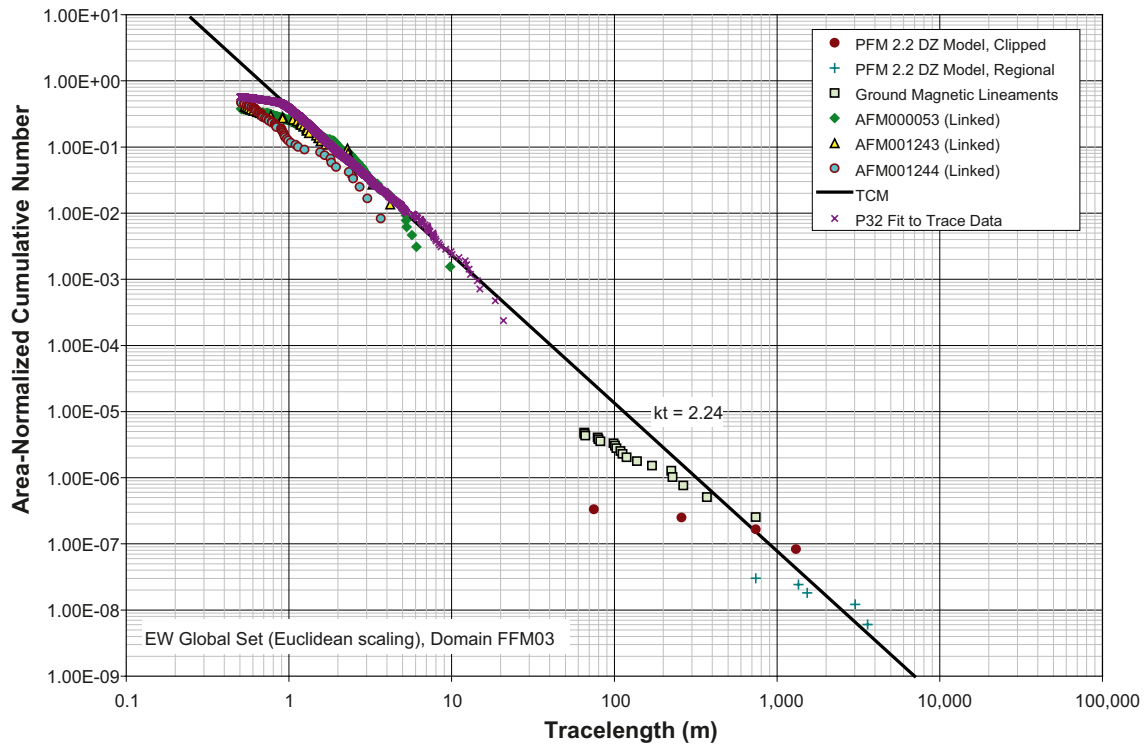
Figure 9-19. *EW Global set, Euclidean scaling (TCM), Domain FFM03.*
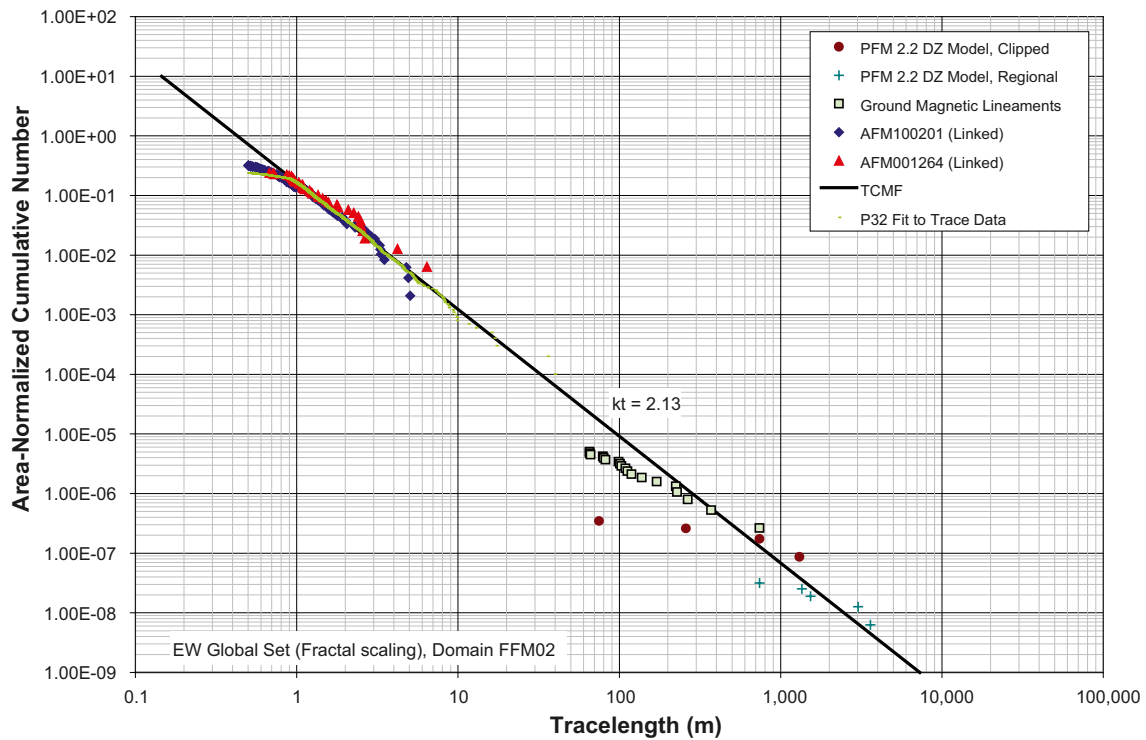
Figure 9-20. *EW Global set, Fractal mass scaling (TCMF), Domain FFM02.*
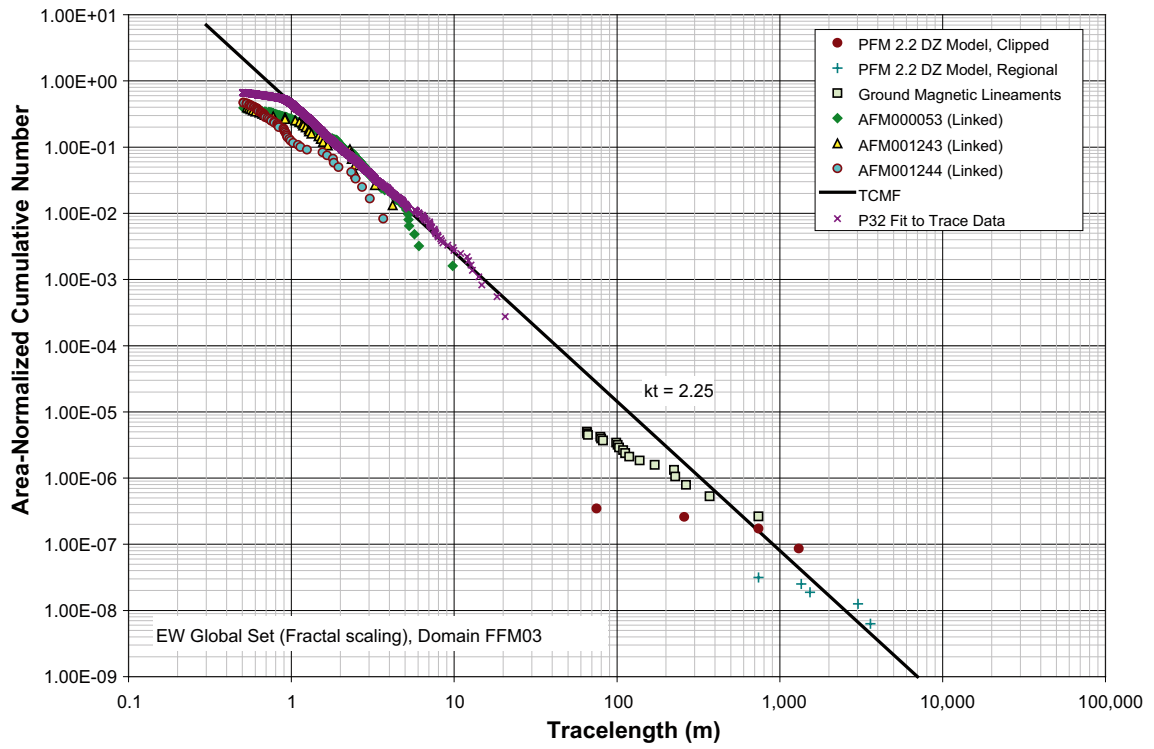
Figure 9-21. *EW Global set, Fractal mass scaling (TCMF), Domain FFM03.*
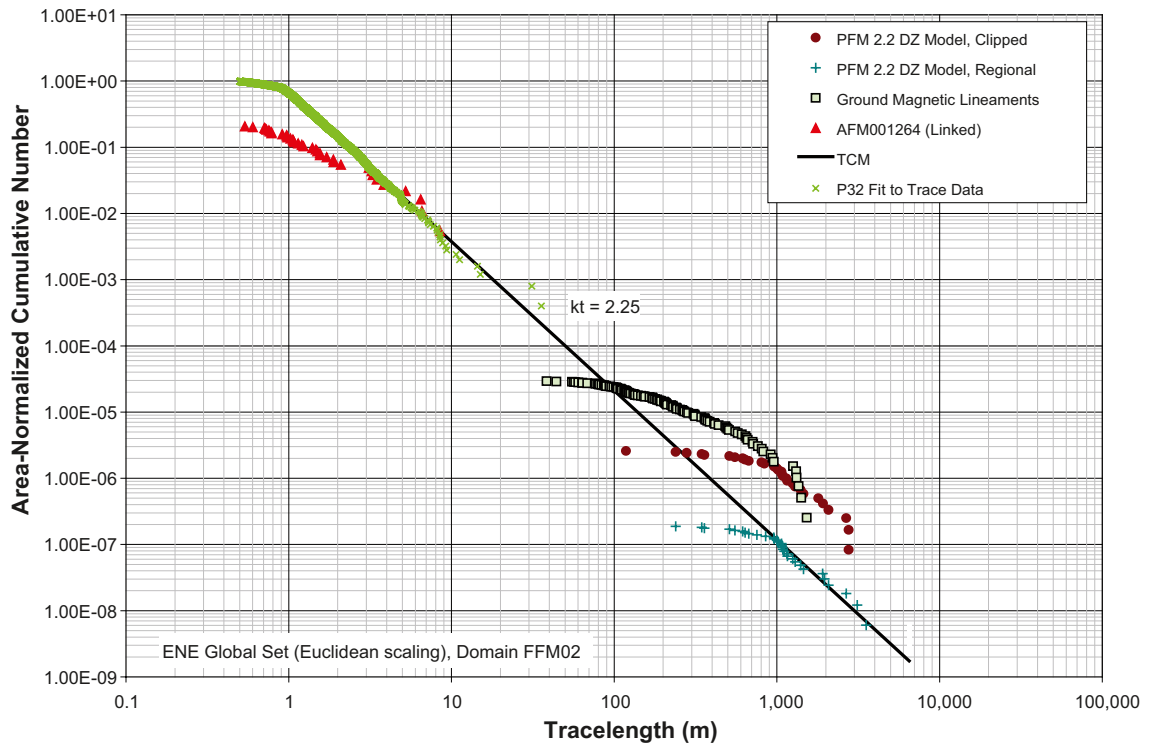
Figure 9-22. *ENE Global set, Euclidean scaling (TCM), Domain FFM02.*
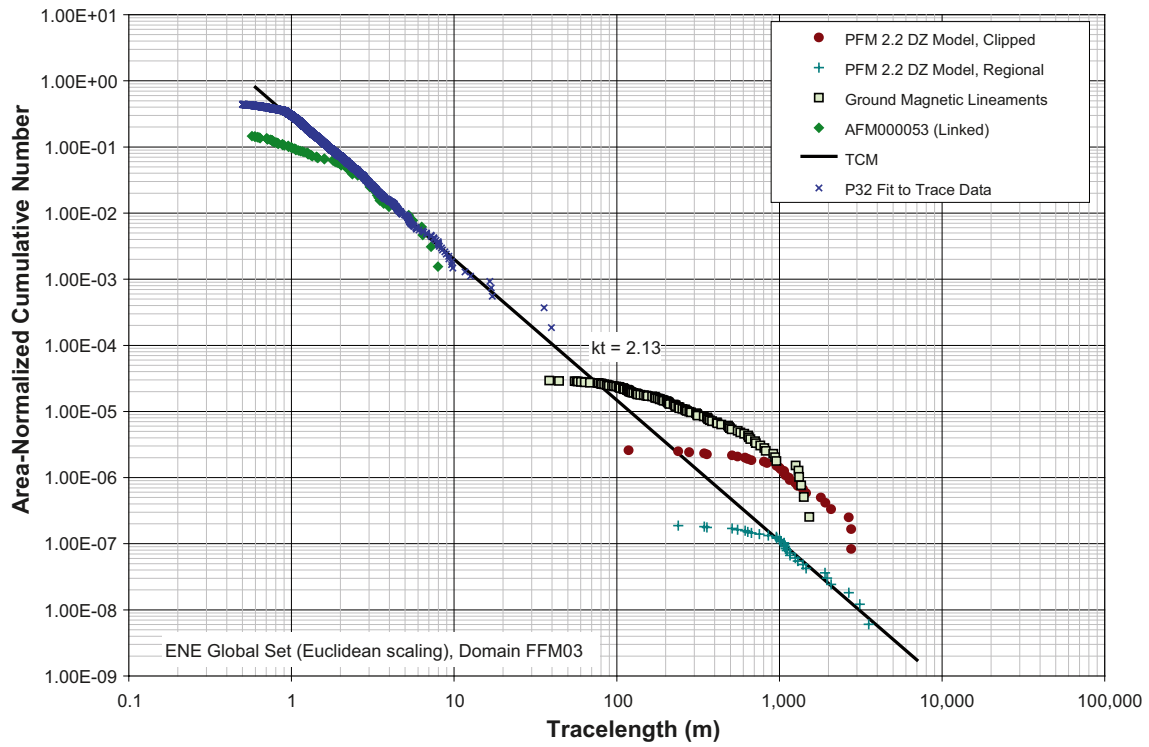
Figure 9-23. *ENE Global set, Euclidean scaling (TCM), Domain FFM03.*
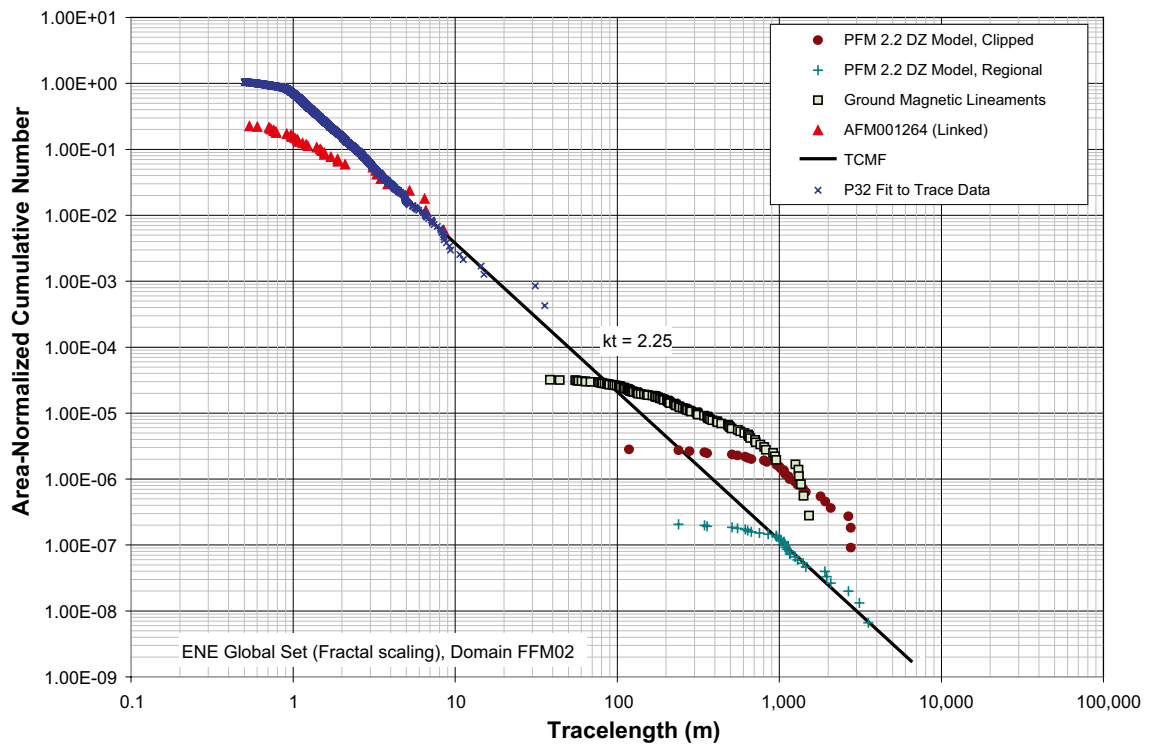
Figure 9-24. *ENE Global set, Fractal mass scaling (TCMF), Domain FFM02.*
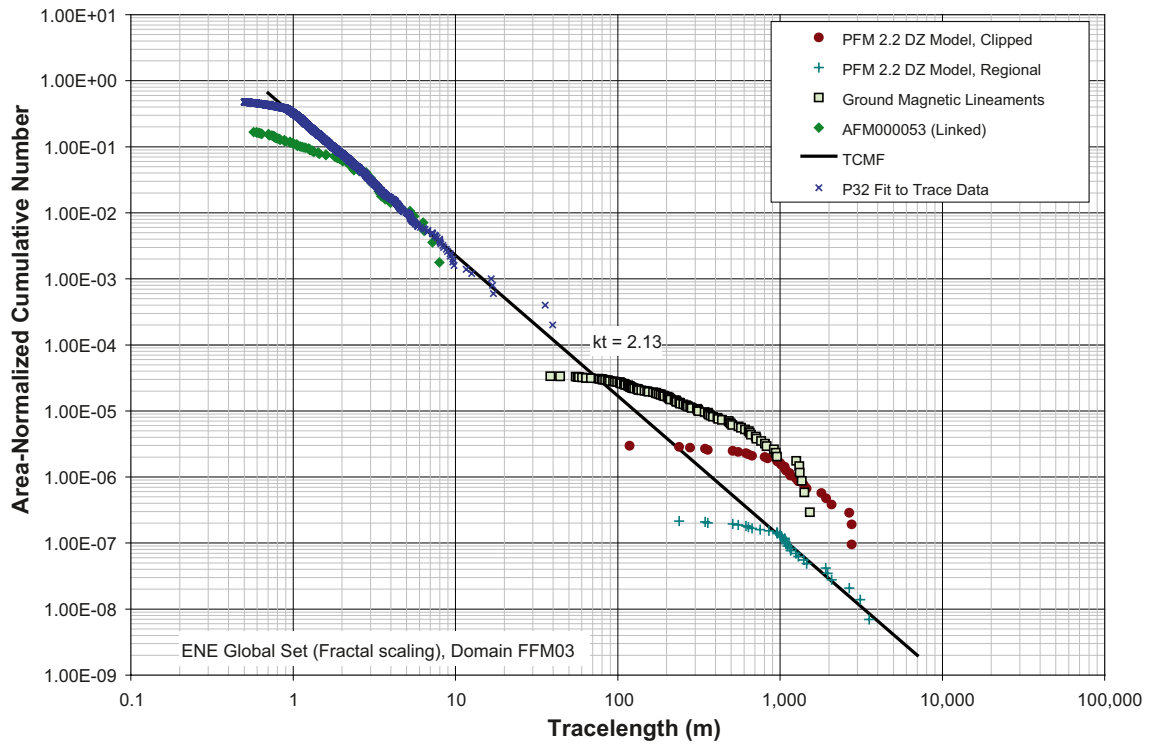
Figure 9-25. *ENE Global set, Fractal mass scaling (TCMF), Domain FFM03.*
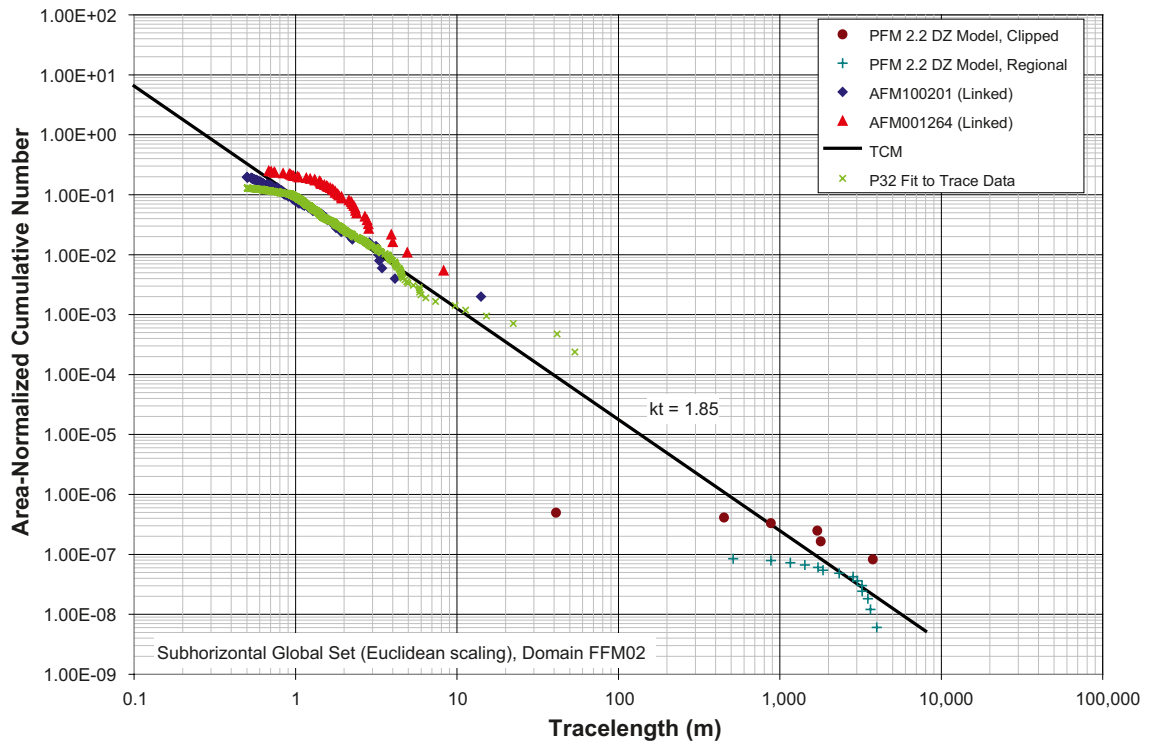
Figure 9-26. *SH Global set, Euclidean scaling (TCM), Domain FFM02.*

13
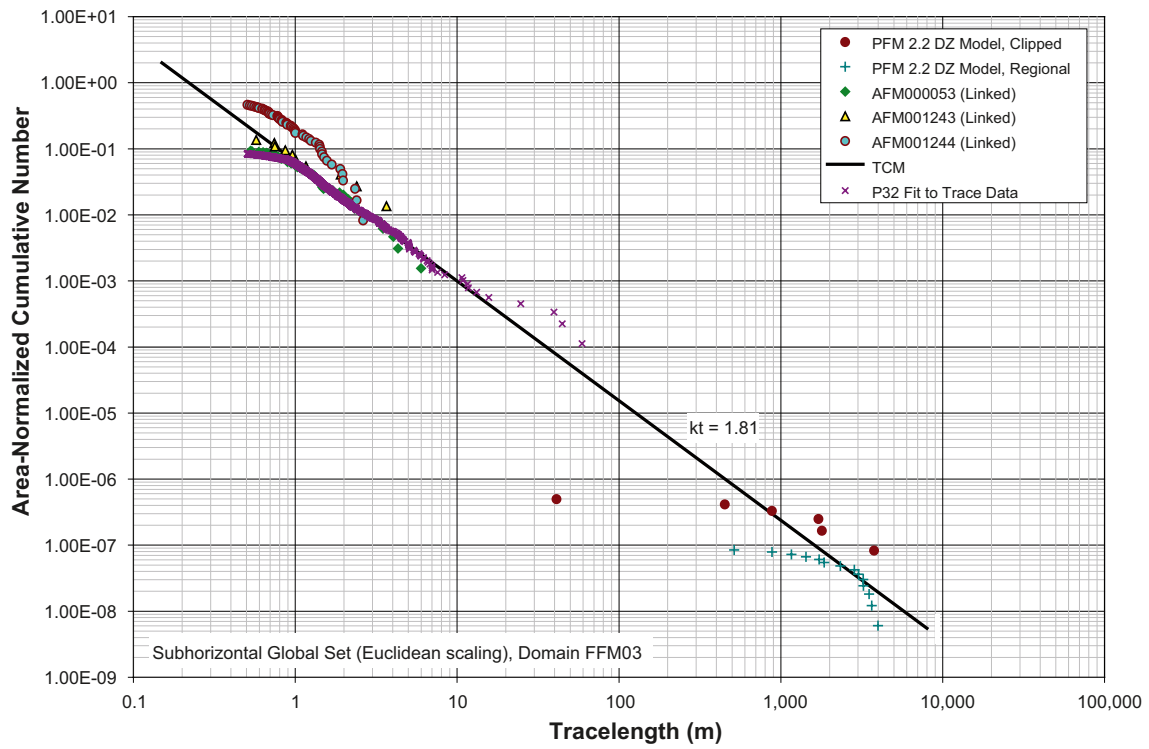
Figure 9-27. *SH Global set, Euclidean scaling (TCM), Domain FFM03.*
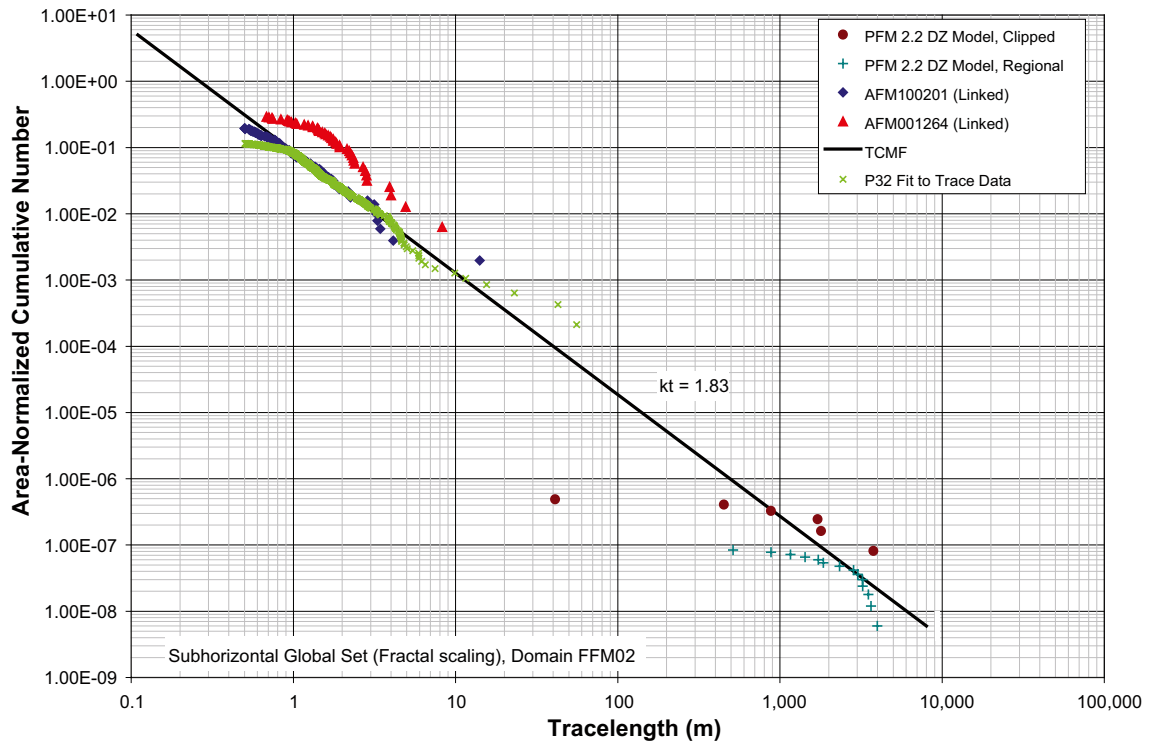
Figure 9-28. *SH Global set, Fractal mass scaling (TCMF), Domain FFM02.*
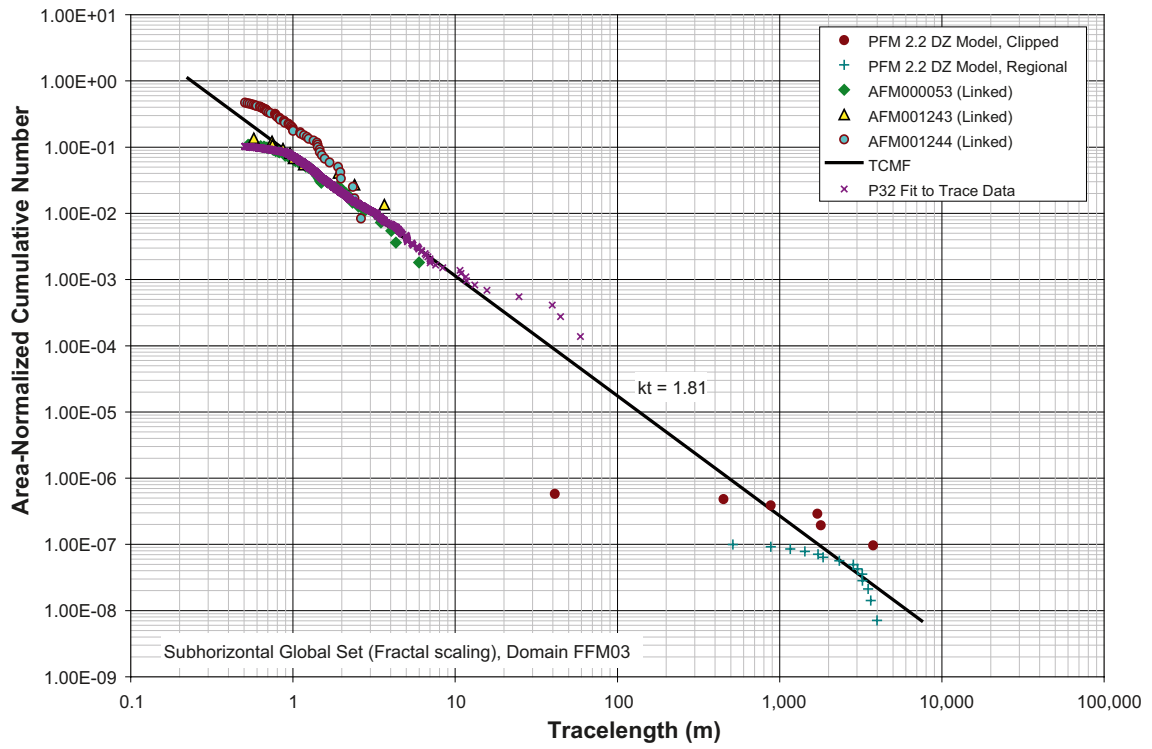
Figure 9-29. *SH Global set, Fractal mass scaling (TCMF), Domain FFM03.*
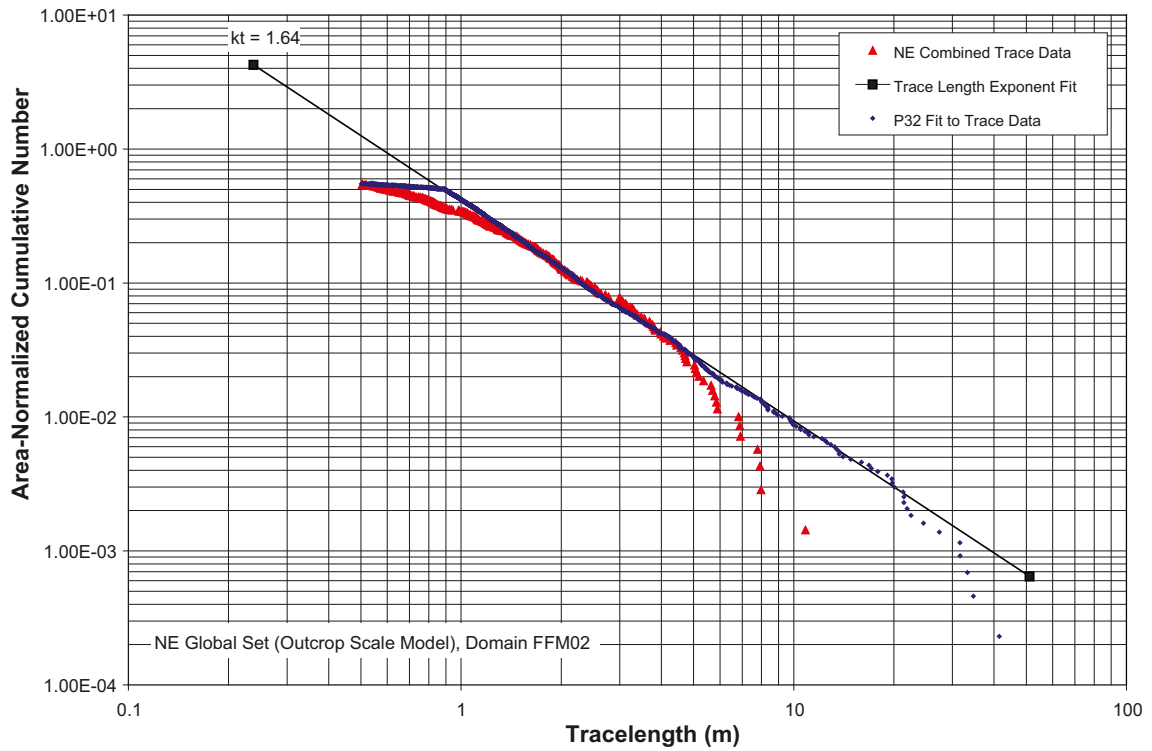
Figure 9-30. *NE Global set, Outcrop-scale model (OSM), Domain FFM02.*
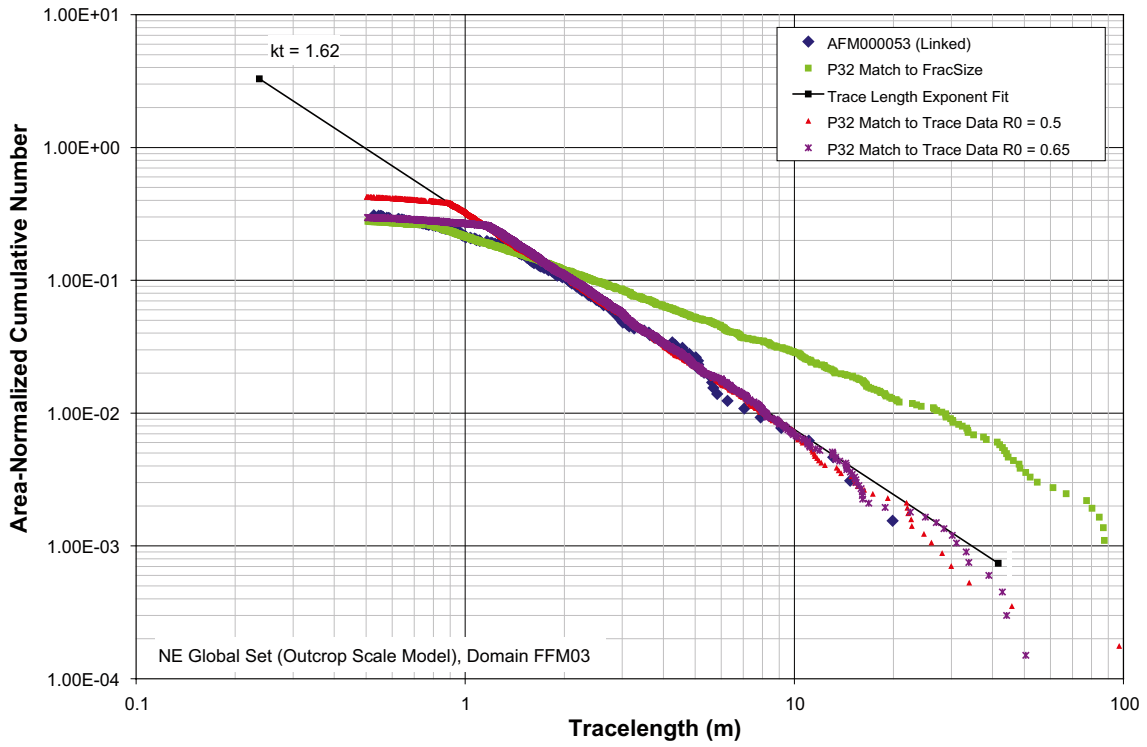
Figure 9-31. *NE Global set, Outcrop-scale model (OSM), Domain FFM03.*
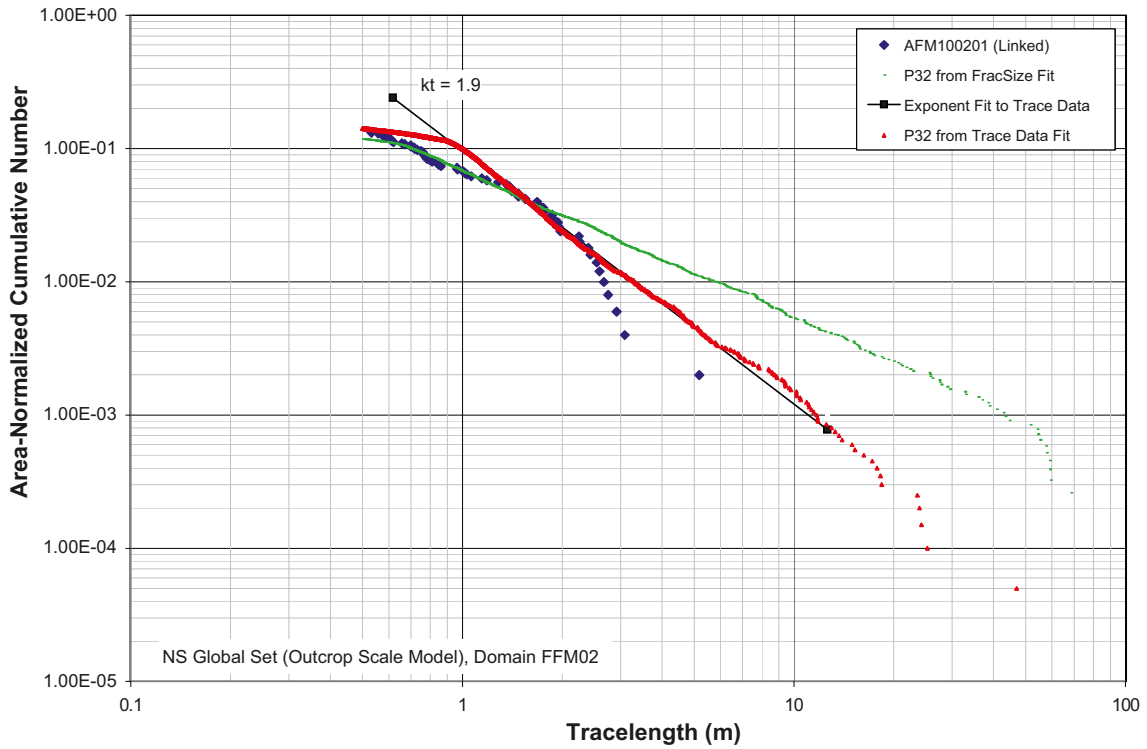
Figure 9-32. *NS Global set, Outcrop-scale model (OSM), Domain FFM02.*

16
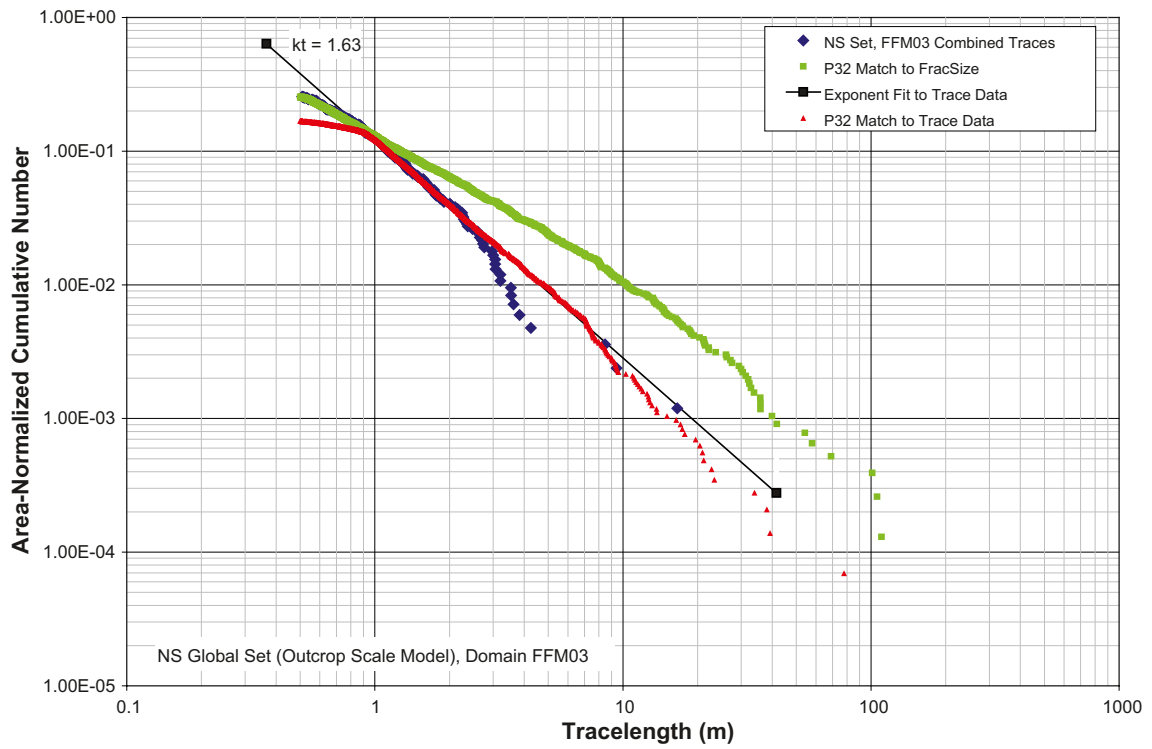
Figure 9-33. *NS Global set, Outcrop-scale model (OSM), Domain FFM03.*
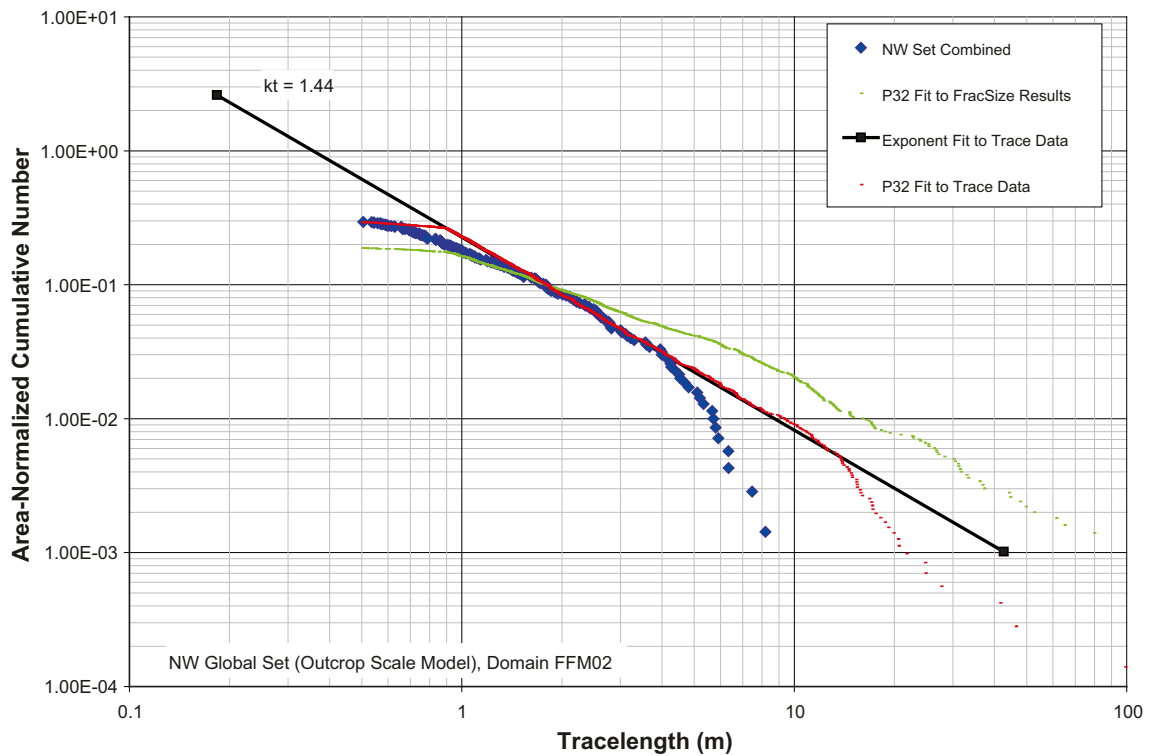
Figure 9-34. *NW Global set, Outcrop-scale model (OSM), Domain FFM02.*

17
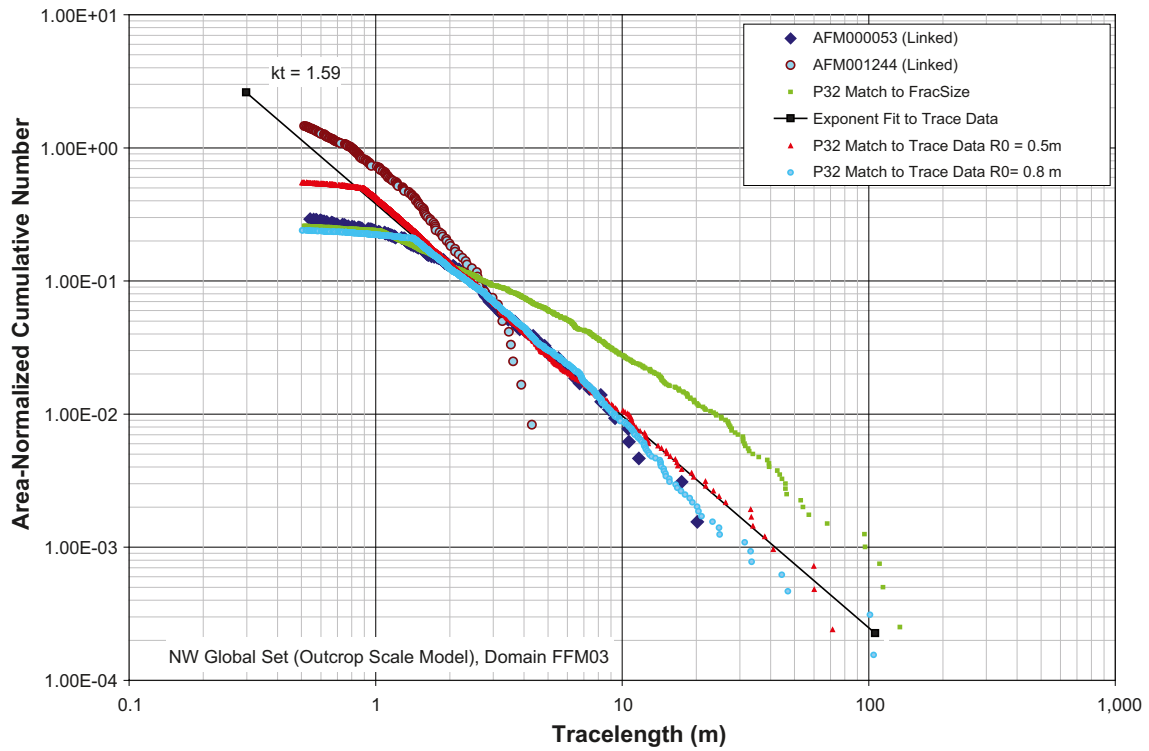
Figure 9-35. *NW Global set, Outcrop-scale model (OSM), Domain FFM03.*
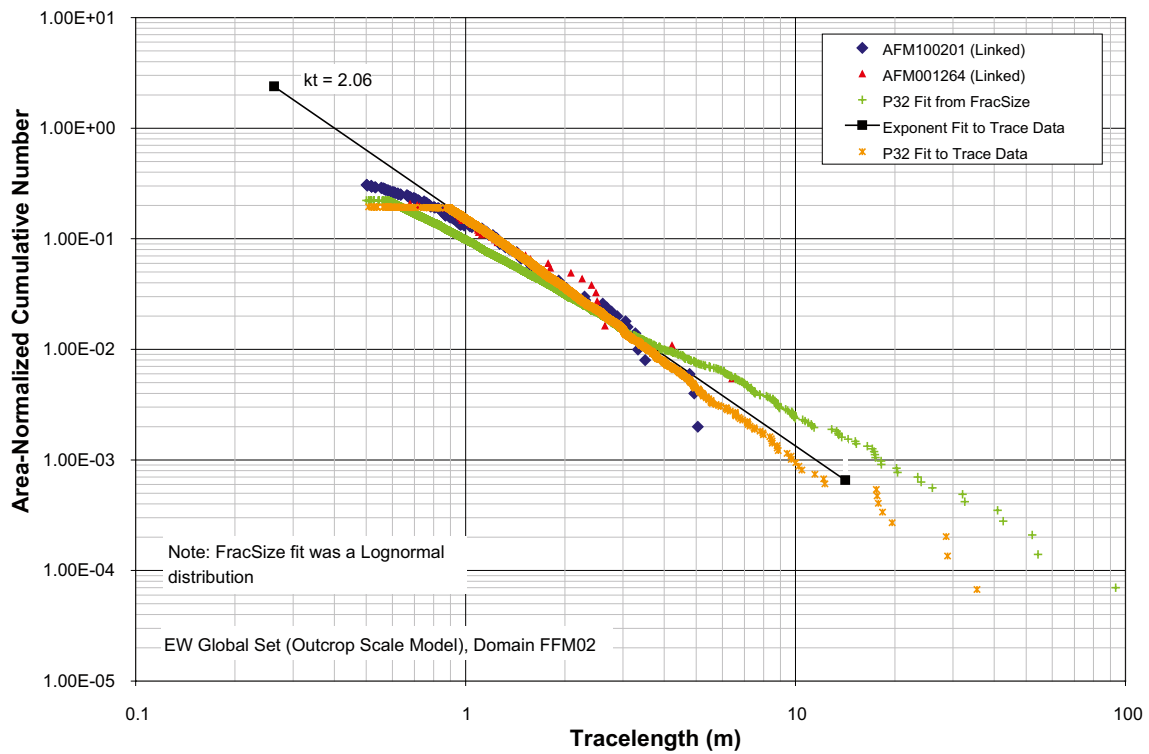
Figure 9-36. *EW Global set, Outcrop-scale model (OSM), Domain FFM02.*

18
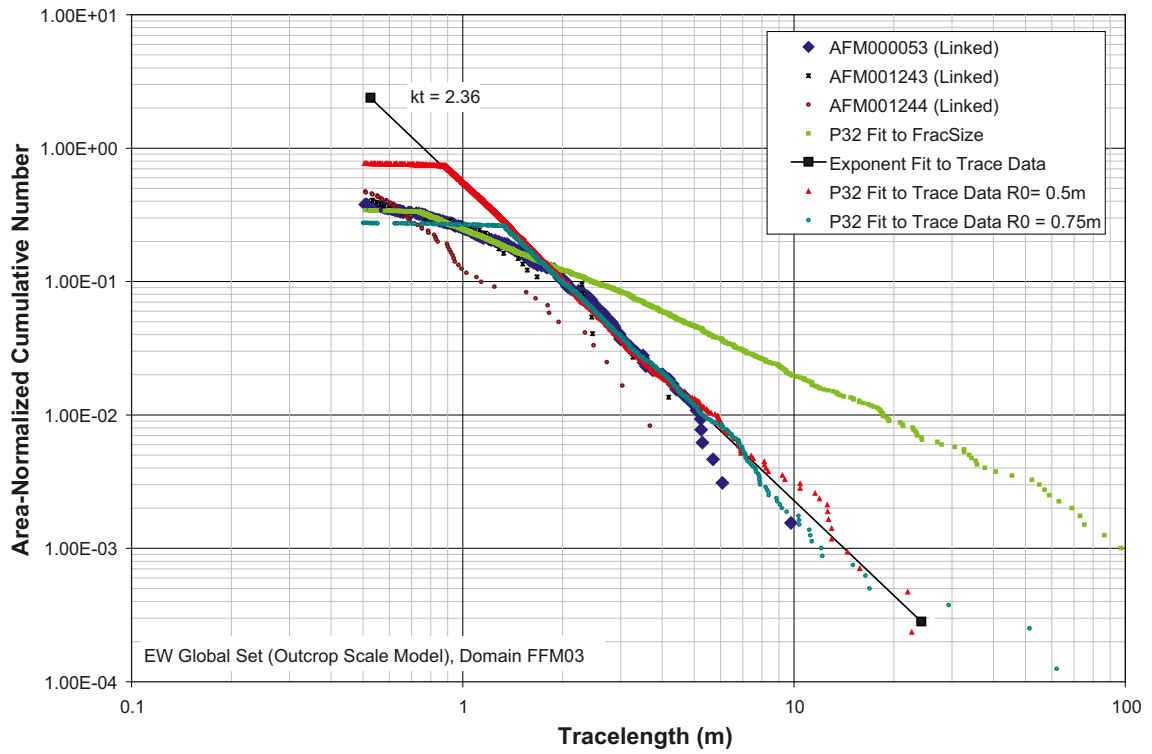
Figure 9-37. *EW Global set, Outcrop-scale model (OSM), Domain FFM03.*
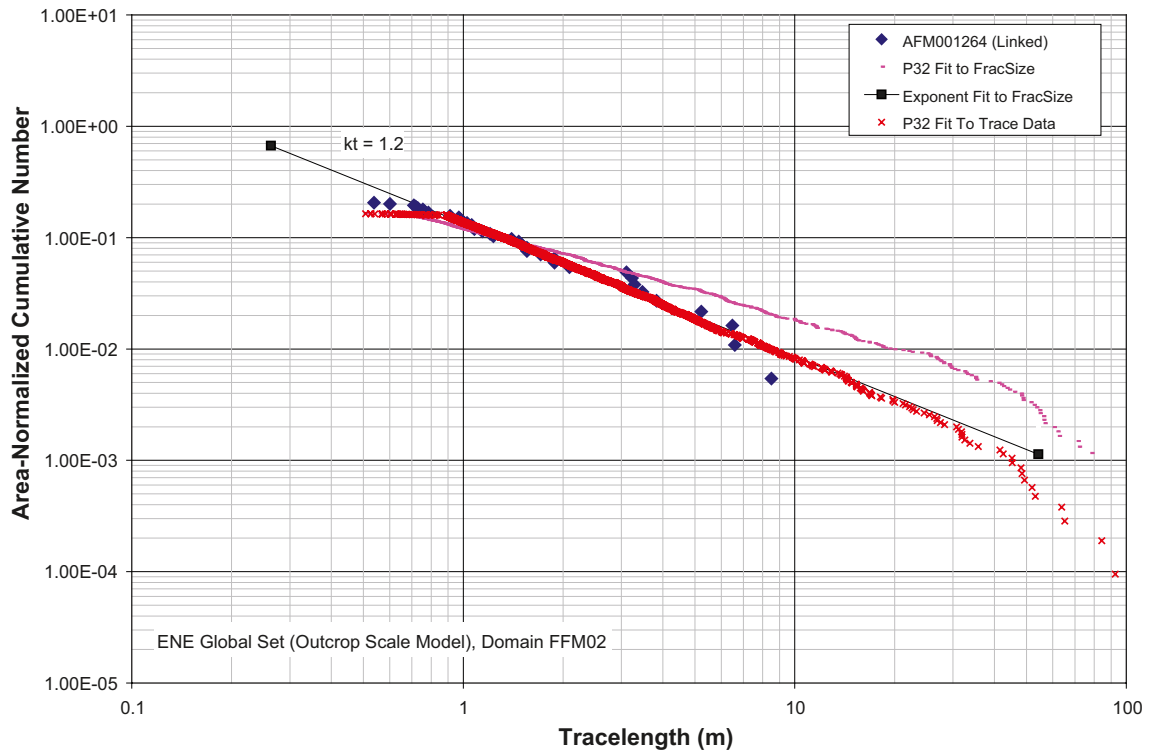
Figure 9-38. *ENE Globa/Locall set, Outcrop-scale model (OSM), Domain FFM02.*
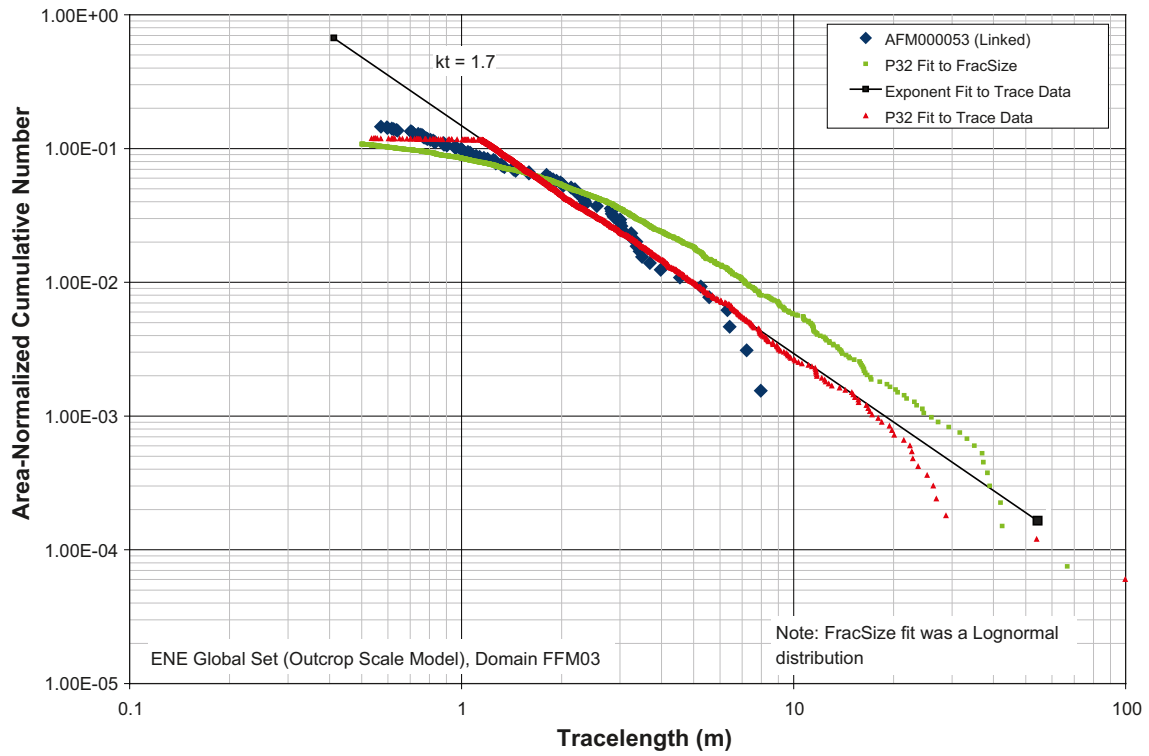
Figure 9-39. *ENE Global/Local set, Outcrop-scale model (OSM), Domain FFM03.*
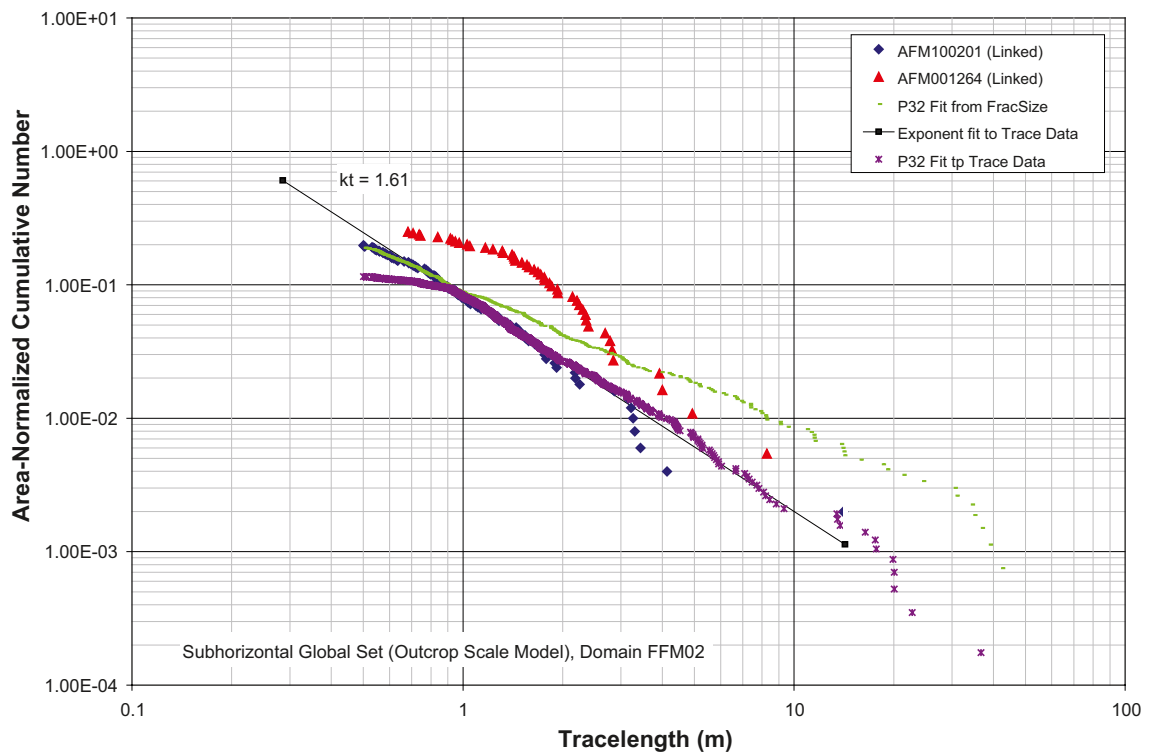
Figure 9-40. *SH Global set, Outcrop-scale model (OSM), Domain FFM02.*
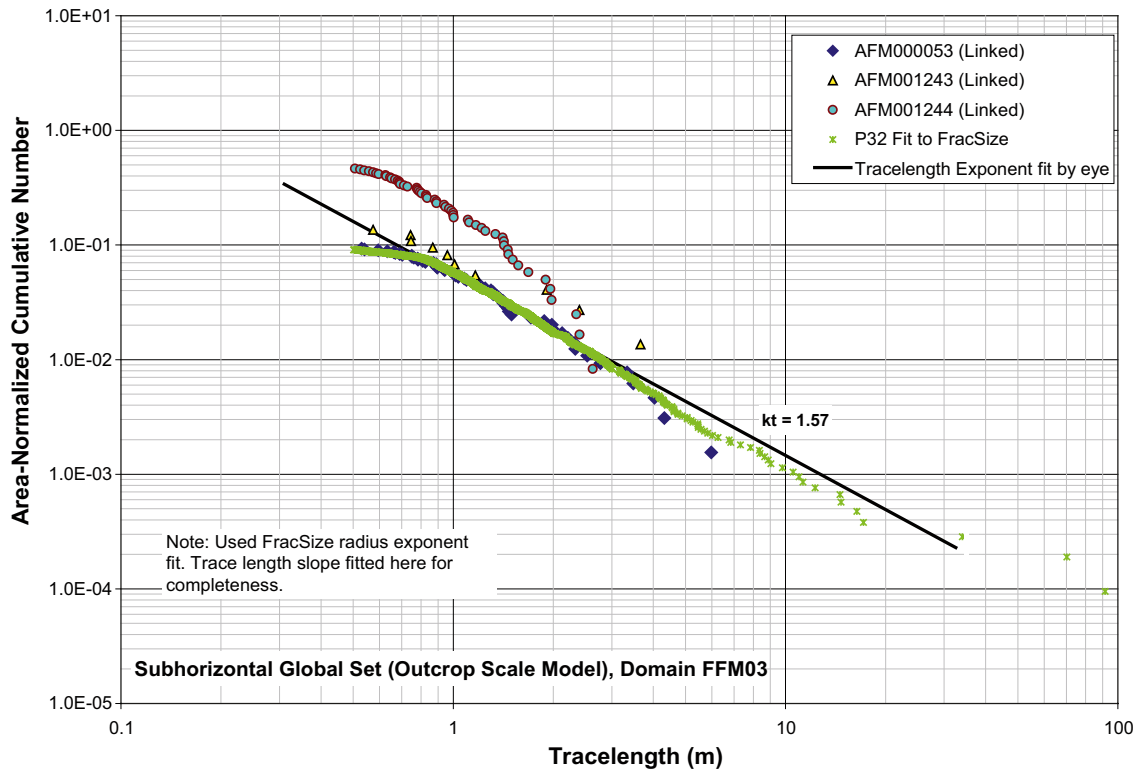
Figure 9-41. *SH Global set, Outcrop-scale model (OSM), Domain FFM03.*
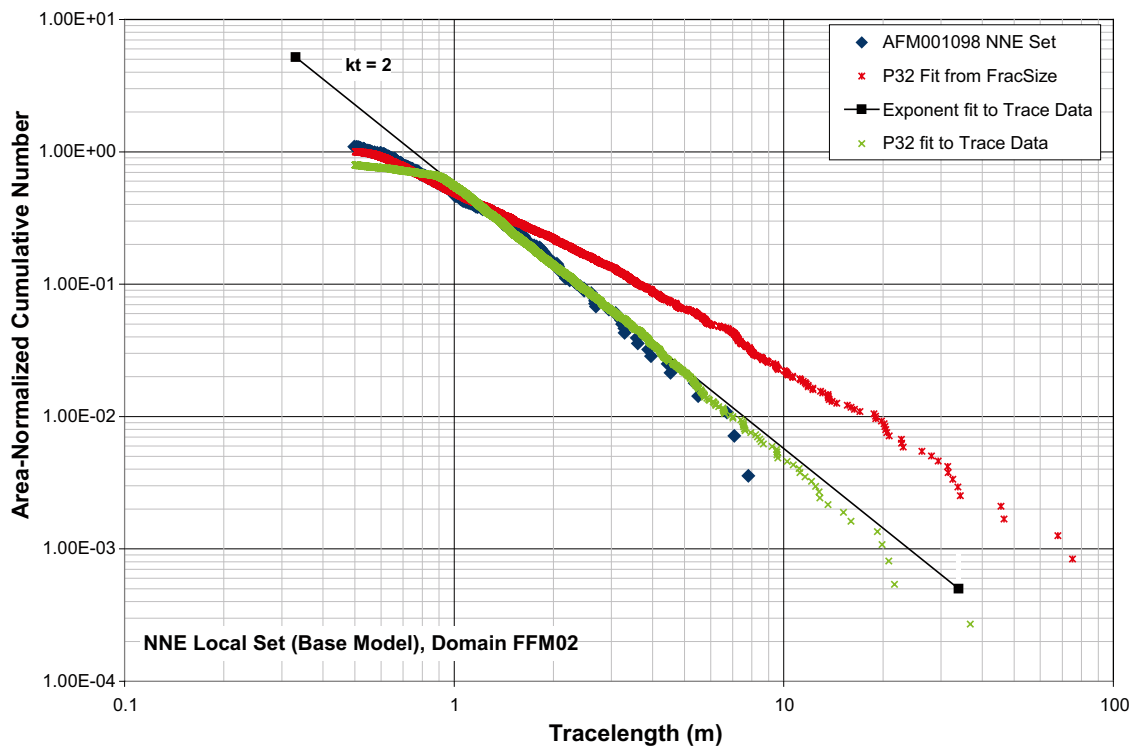
Figure 9-42. *NNE Local set, Outcrop-scale model (OSM), Domain FFM02.*

21

Outcrop and borehole mass dimension plots

Mass Fractal Analysis
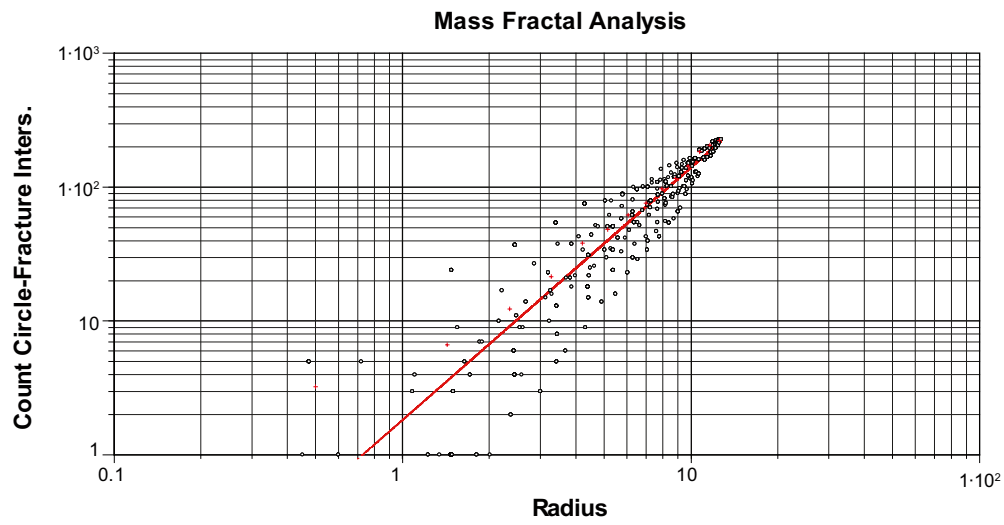
Figure 10-1. *Mass dimension plot for AFM000053, NE unlinked set.*

Mass Fractal Analysis
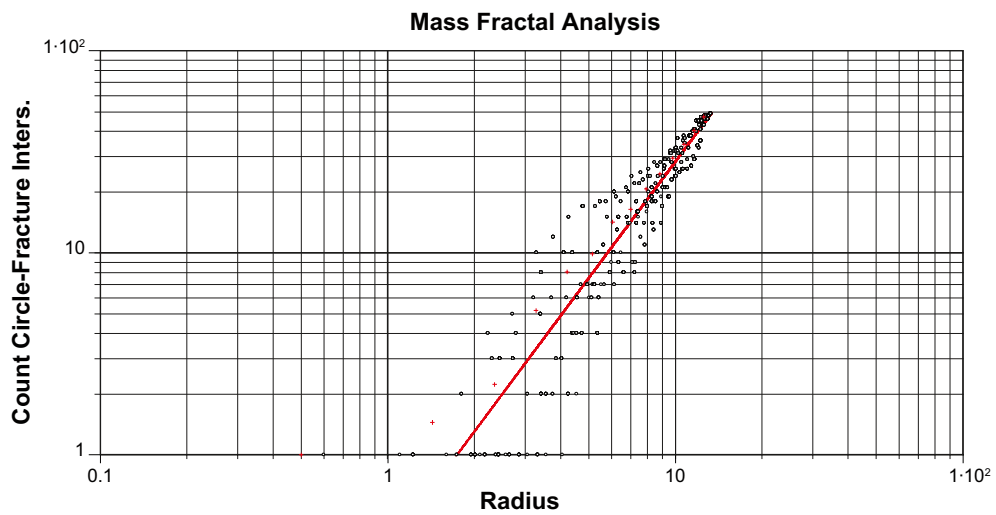
Figure 10-2. *Mass dimension plot for AFM000053, NS unlinked set.*
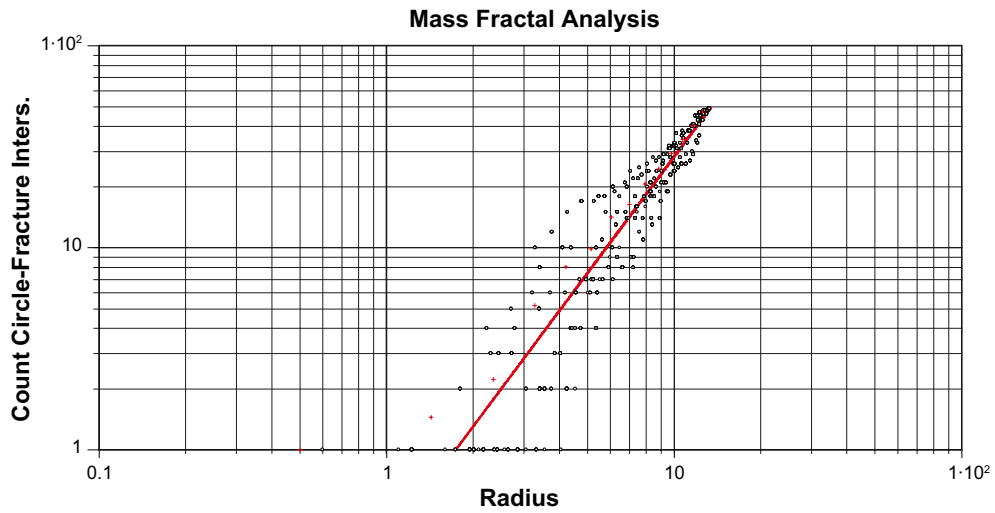
Figure 10-3. *Mass dimension plot for AFM000053, NW unlinked set.*
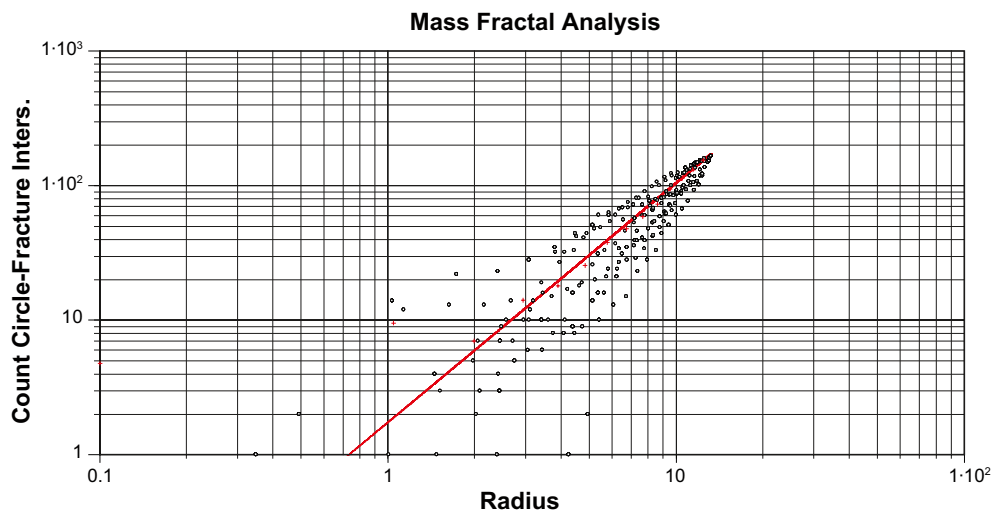
Figure 10-4. *Mass dimension plot for AFM000053, SH unlinked set.*
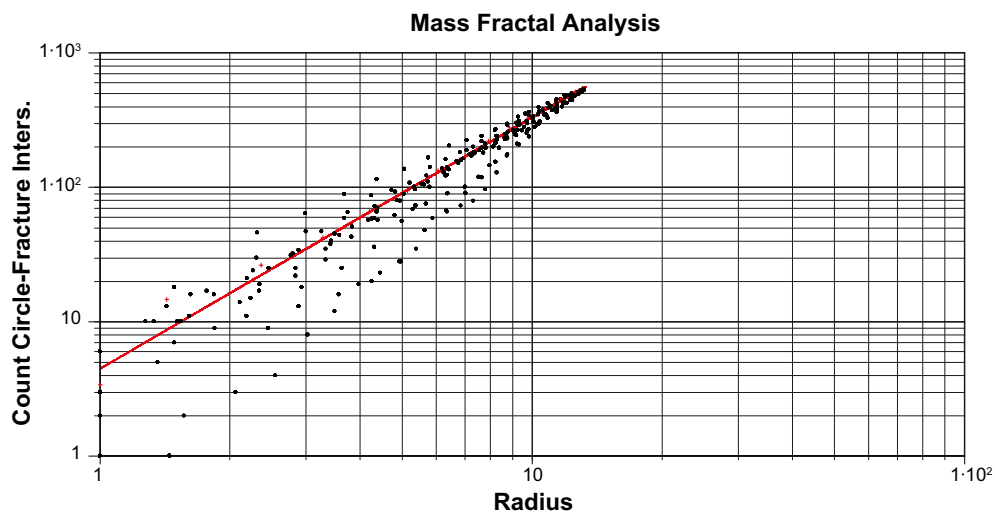
Figure 10-5. *Mass dimension plot for AFM000053, WNW unlinked set.*

24

Mass Fractal Analysis
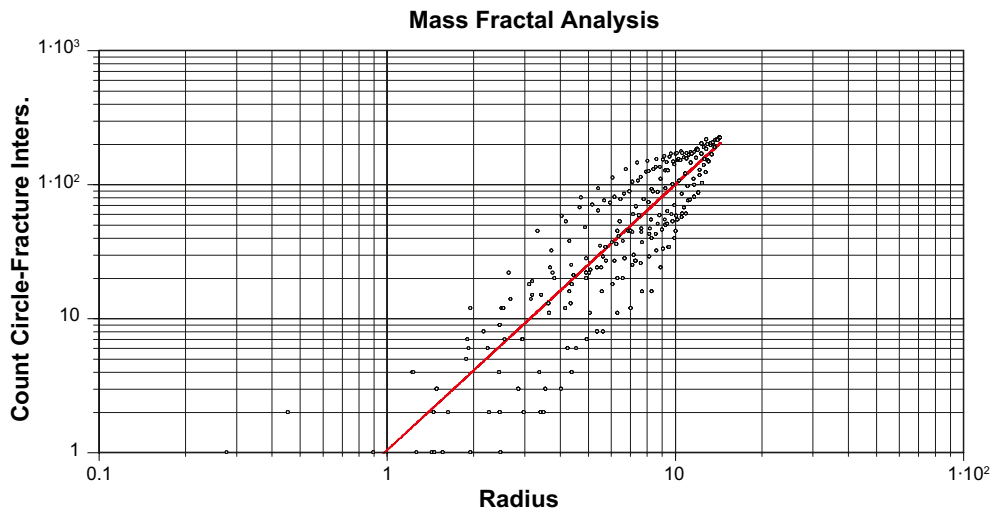
Figure 10-6. Mass dimension plot for AFM000053, ENE unlinked set.

Mass Fractal Analysis
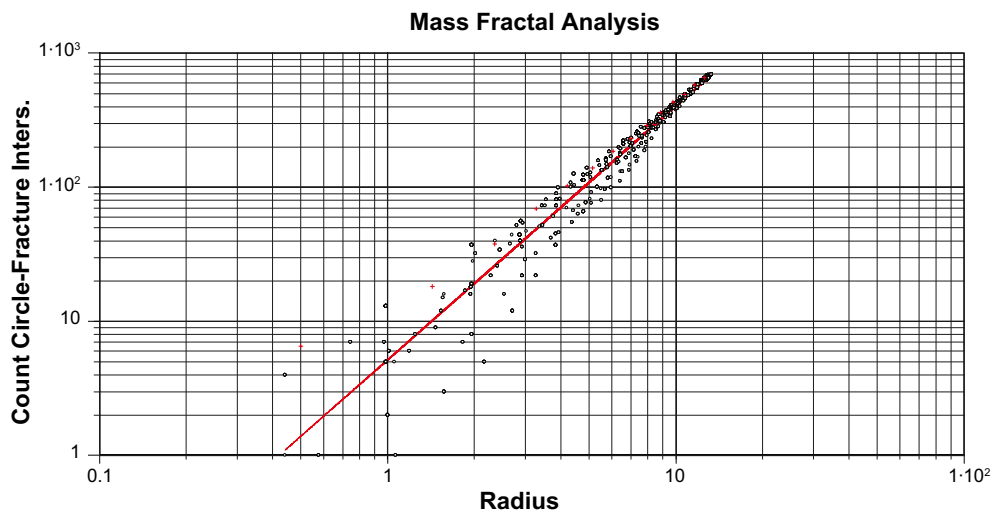
Figure 10-7. Mass dimension plot for AFM000054, NE unlinked set.

Mass Fractal Analysis
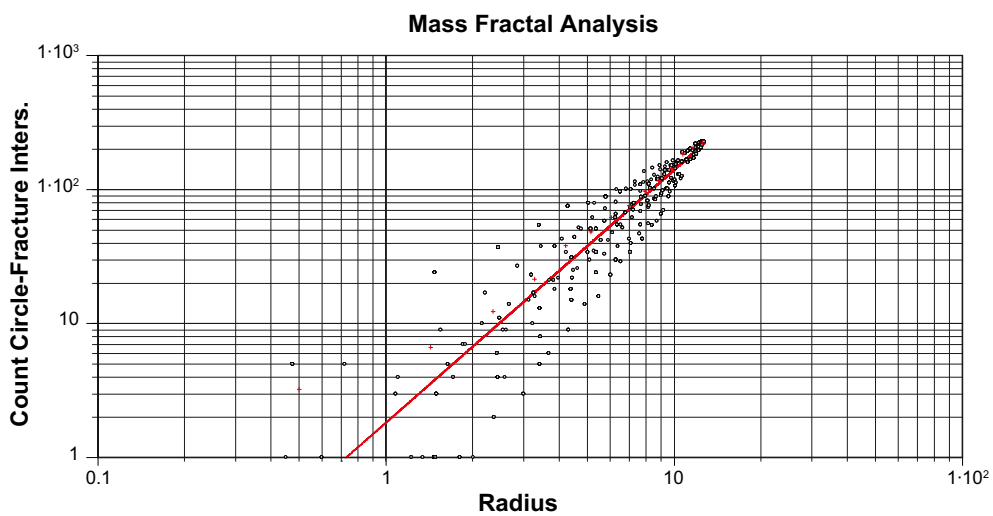
Figure 10-8. Mass dimension plot for AFM000054, NS unlinked set.

Mass Fractal Analysis
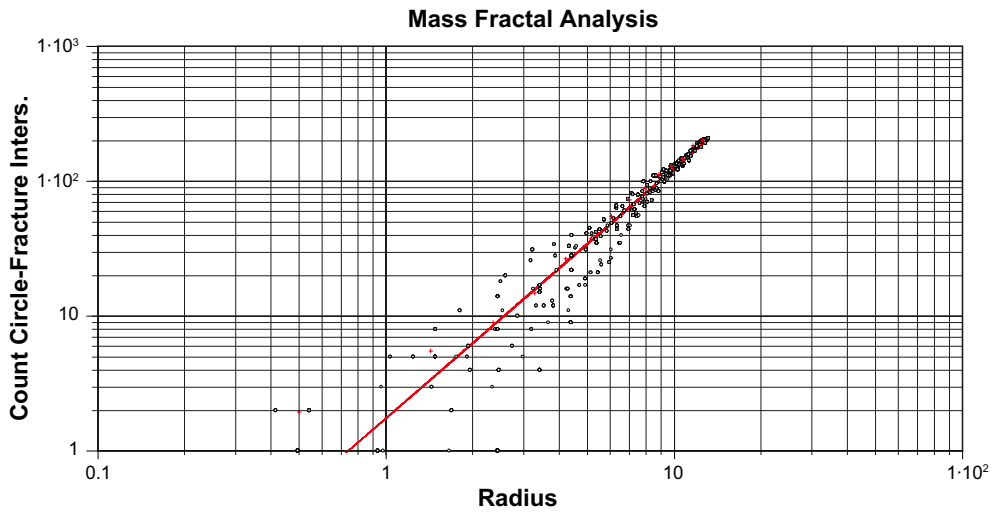
Figure 10-9. Mass dimension plot for AFM000054, NW unlinked set.

Mass Fractal Analysis
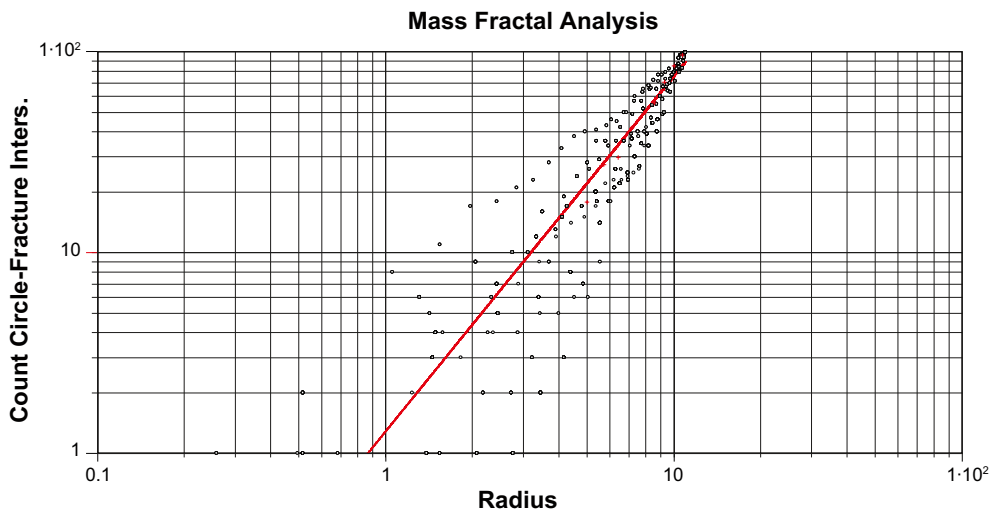
Figure 10-10. Mass dimension plot for AFM000054, SH unlinked set.

Mass Fractal Analysis
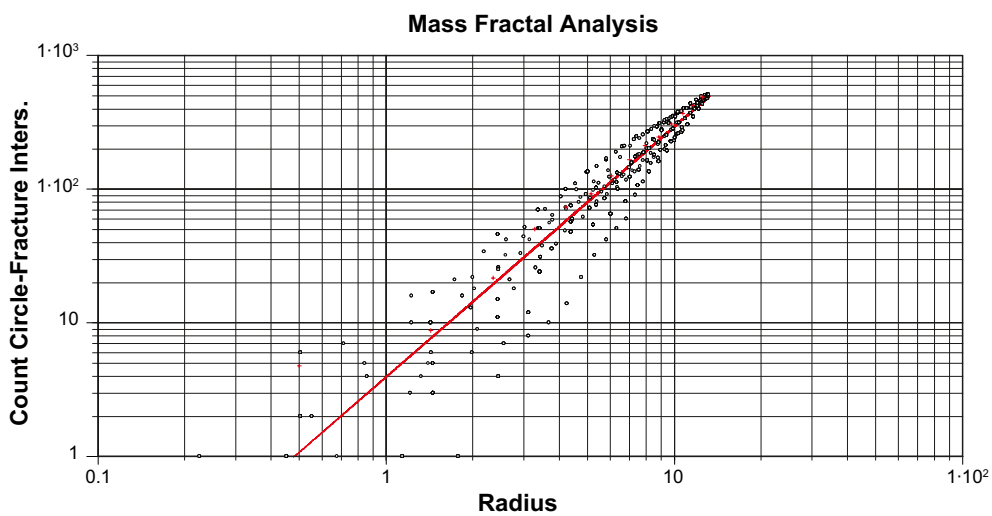
Figure 10-11. Mass dimension plot for AFM000054, WNW unlinked set.
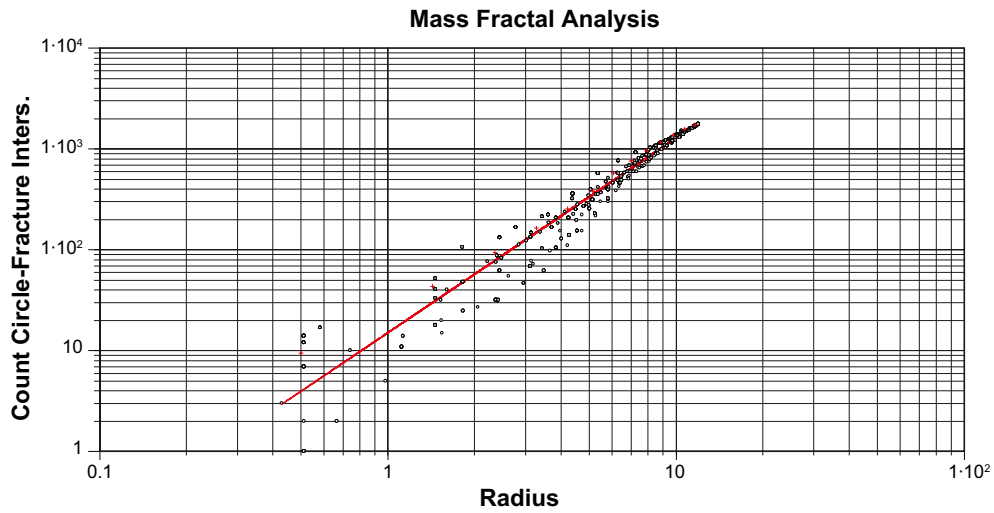
Figure 10-12. *Mass dimension plot for AFM001097, NE unlinked set.*
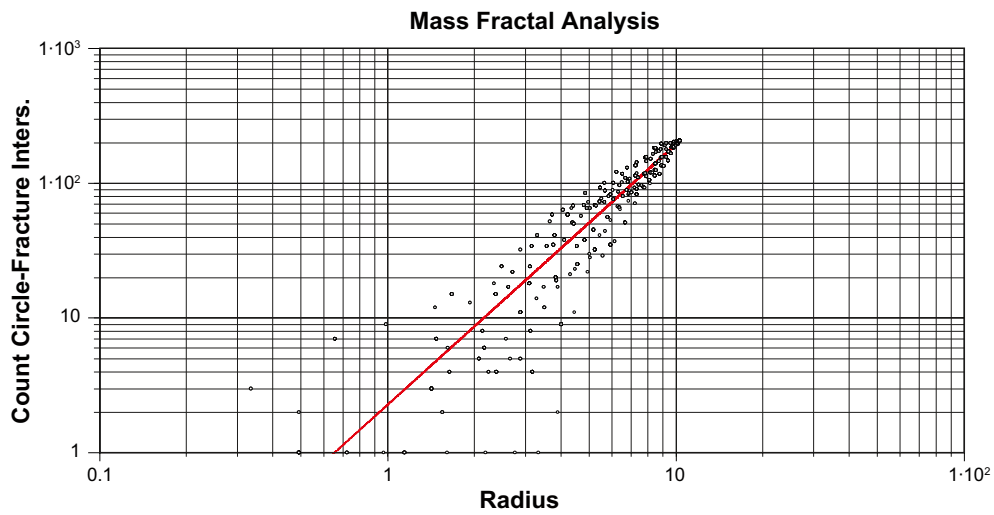
Figure 10-13. *Mass dimension plot for AFM001097, NS unlinked set.*
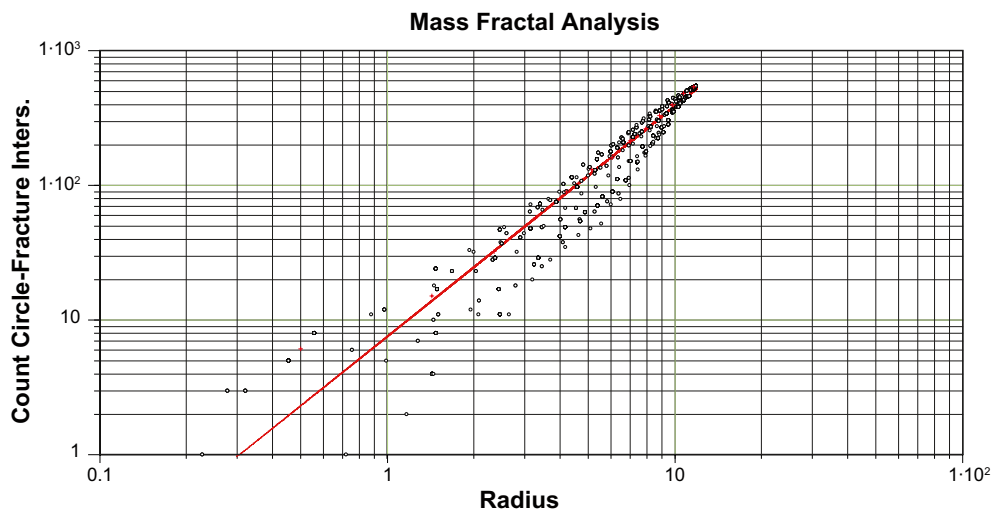
Figure 10-14. *Mass dimension plot for AFM001097, NW unlinked set.*
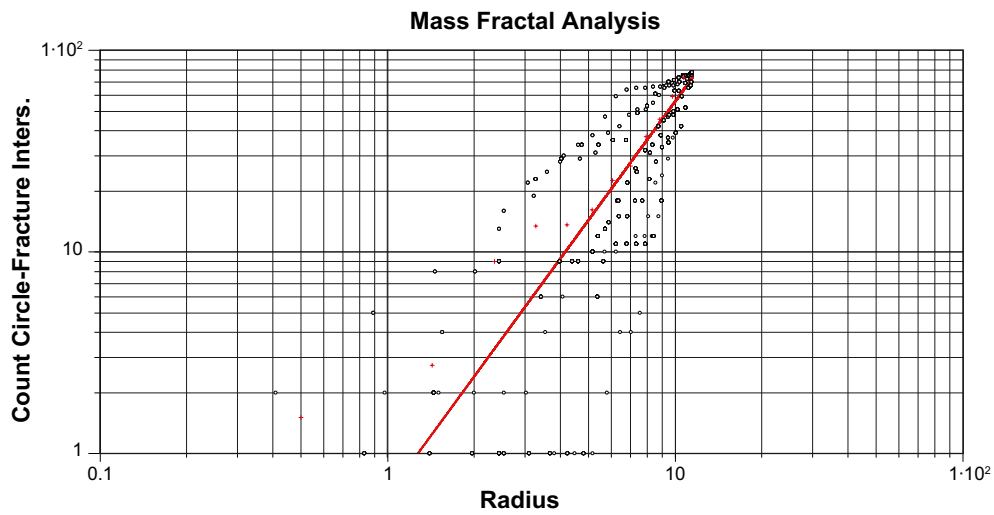
Figure 10-15. *Mass dimension plot for AFM001097, SH unlinked set.*
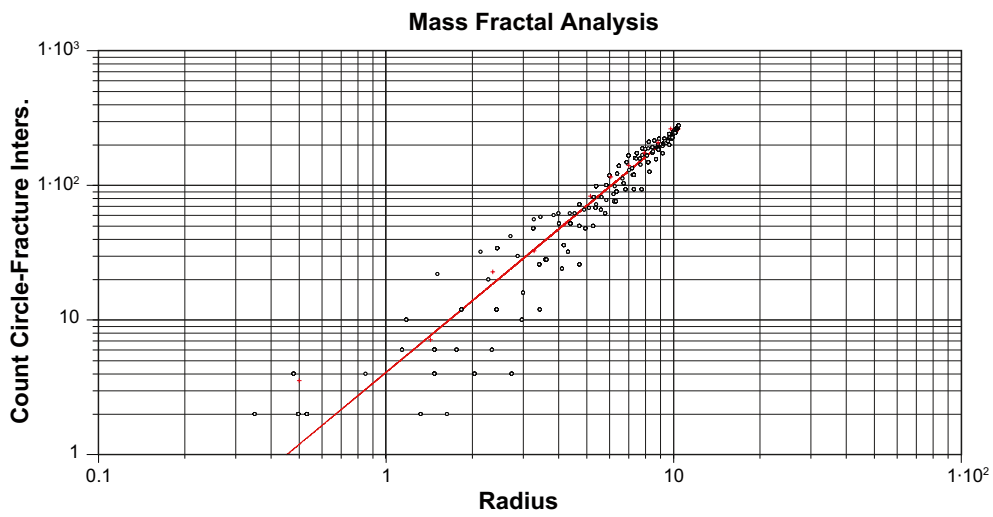
Figure 10-16. *Mass dimension plot for AFM001097, EW unlinked set.*
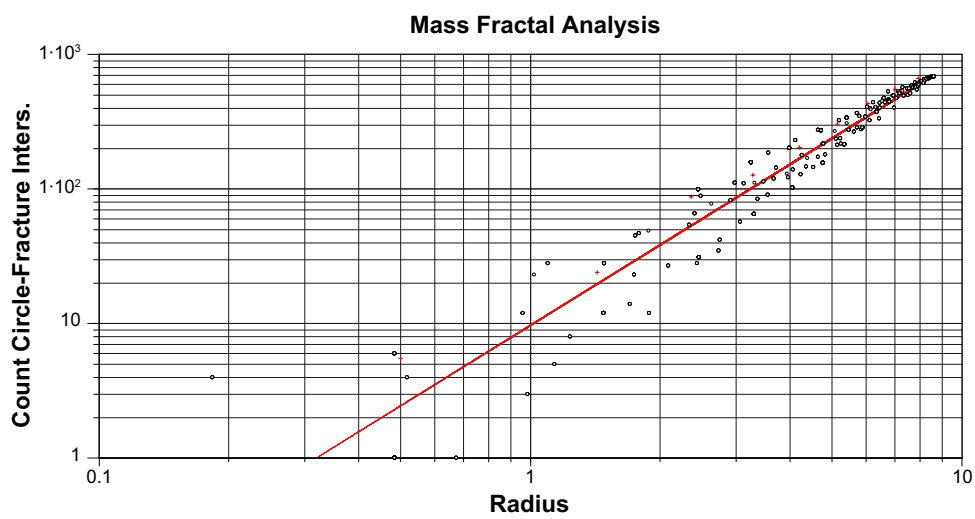
Figure 10-17. *Mass dimension plot for AFM001098, NE unlinked set.*
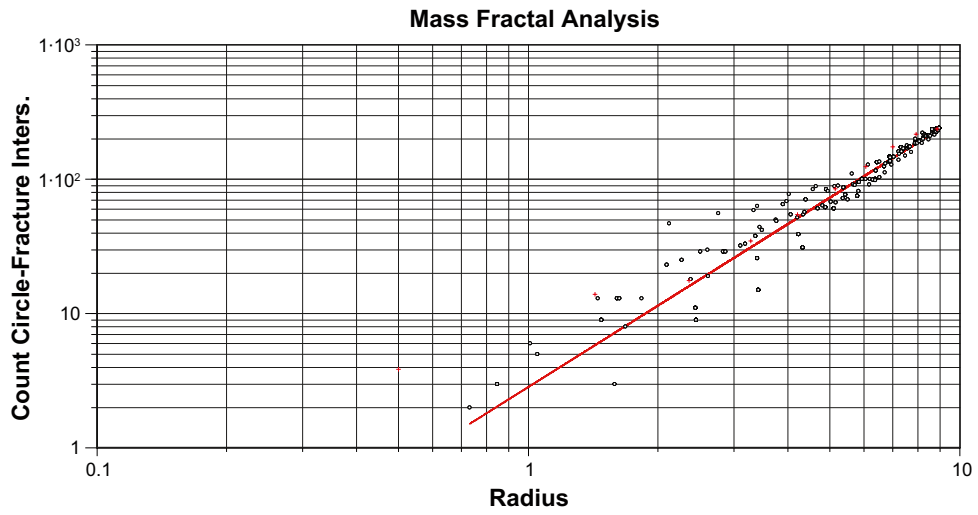
Figure 10-18. *Mass dimension plot for AFM001098, NW unlinked set.*
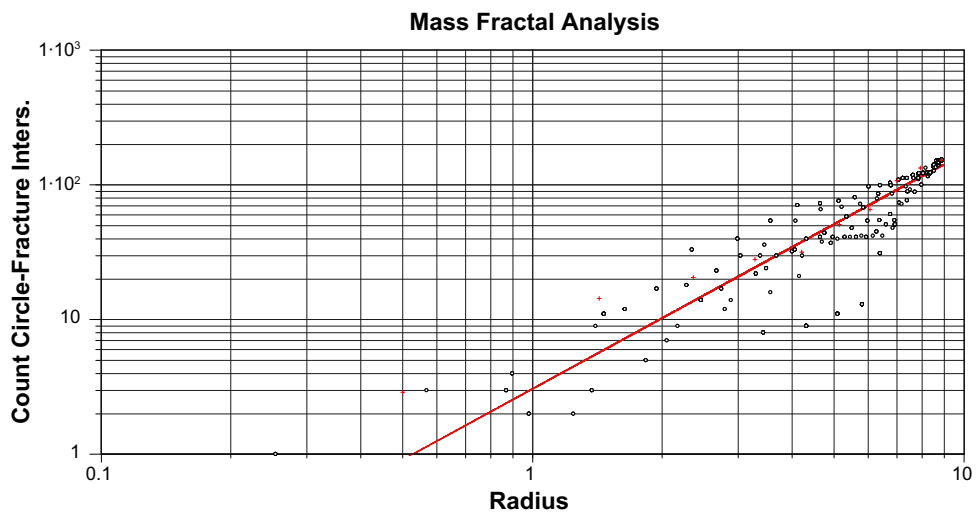
Figure 10-19. *Mass dimension plot for AFM001098, SH unlinked set.*
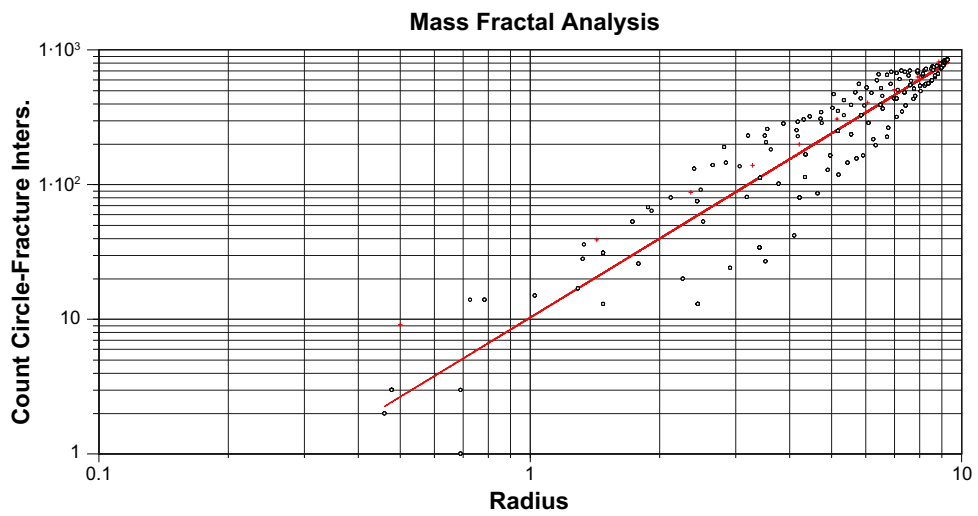
Figure 10-20. *Mass dimension plot for AFM001098, NNE unlinked set.*
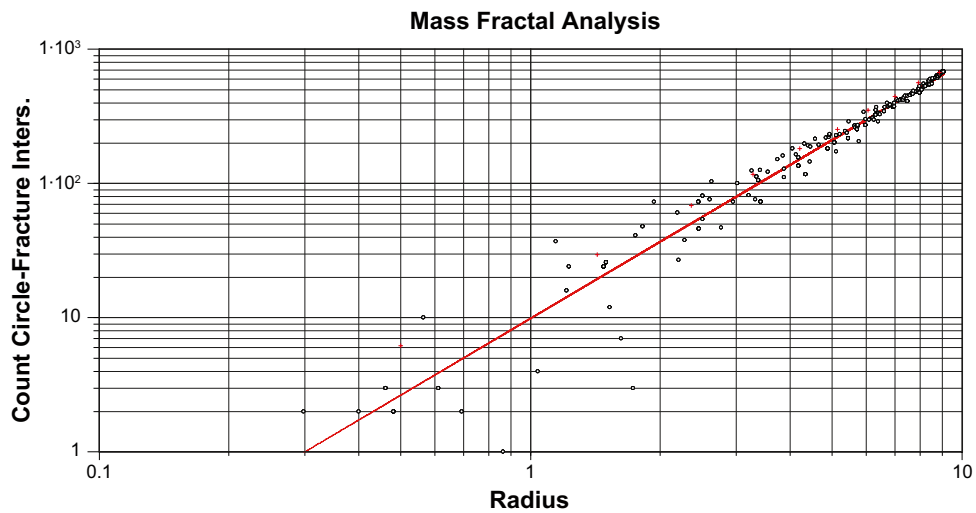
Figure 10-21. *Mass dimension plot for AFM001098, WNW unlinked set.*
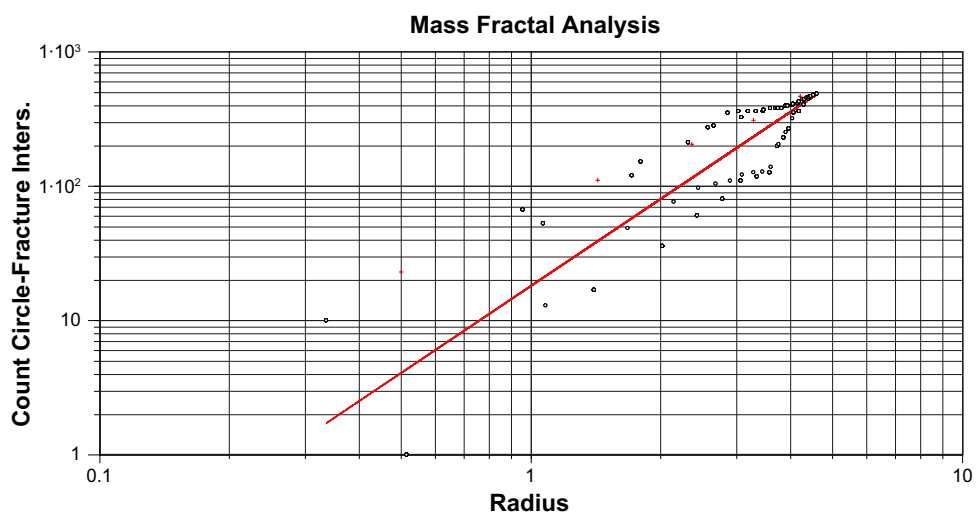
Figure 10-22. *Mass dimension plot for AFM001243, NE unlinked set.*
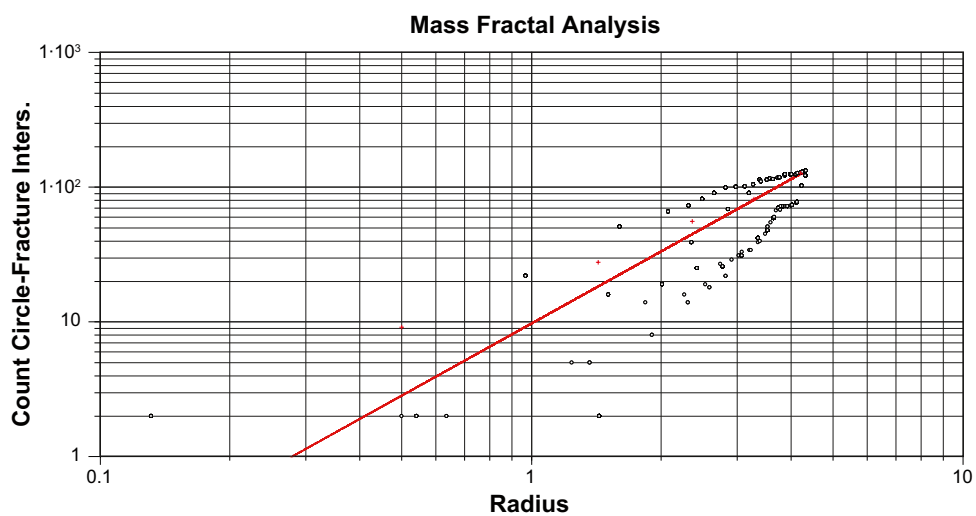
Figure 10-23. *Mass dimension plot for AFM001243, NS unlinked set.*
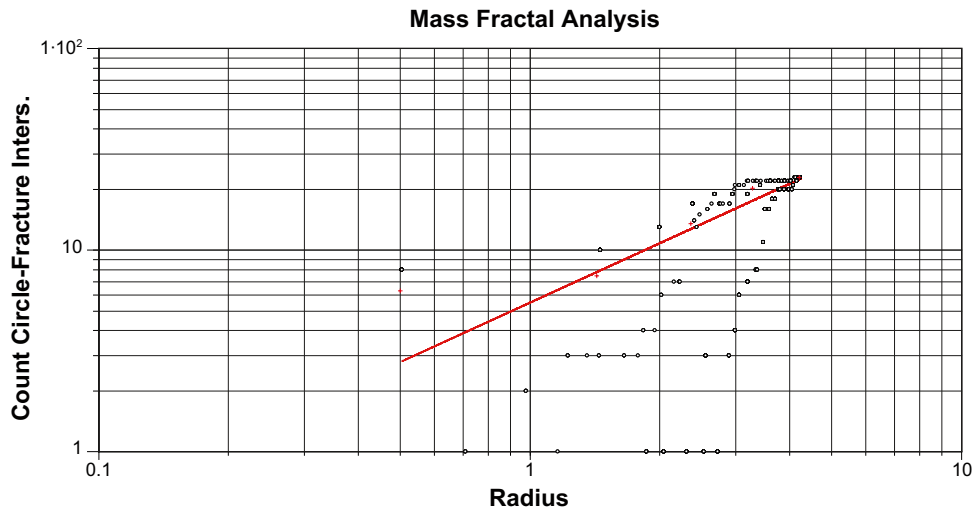
Figure 10-24. *Mass dimension plot for AFM001243, SH unlinked set.*
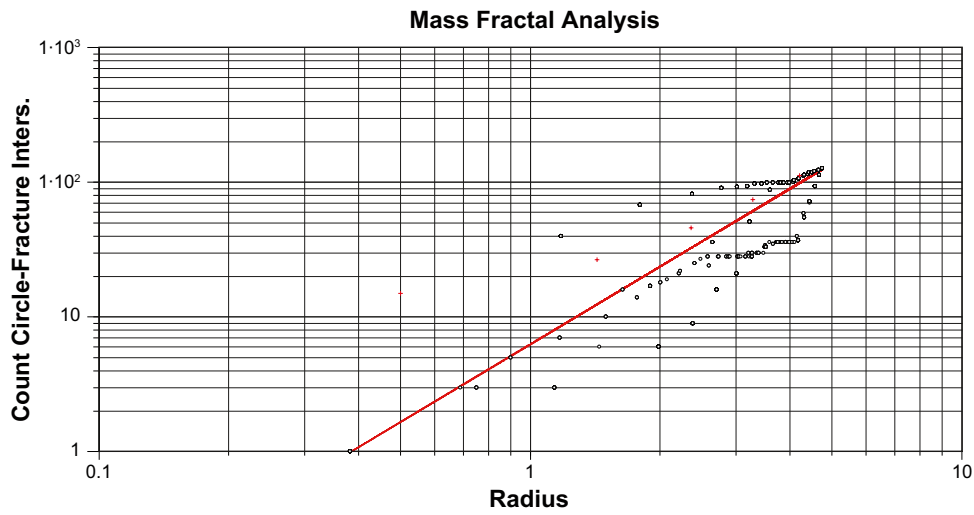
Figure 10-25. *Mass dimension plot for AFM001243, WNW unlinked set.*
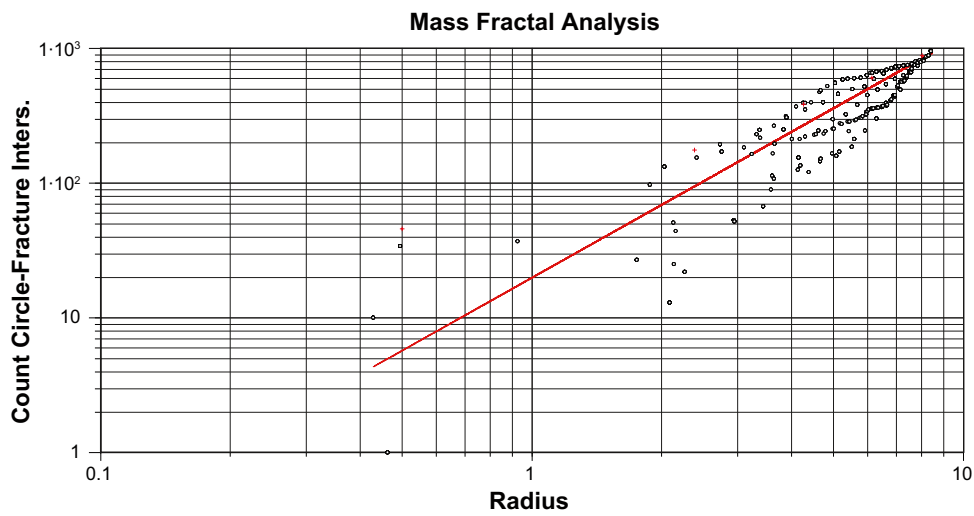
Figure 10-26. *Mass dimension plot for AFM001244, NE unlinked set.*

Mass Fractal Analysis
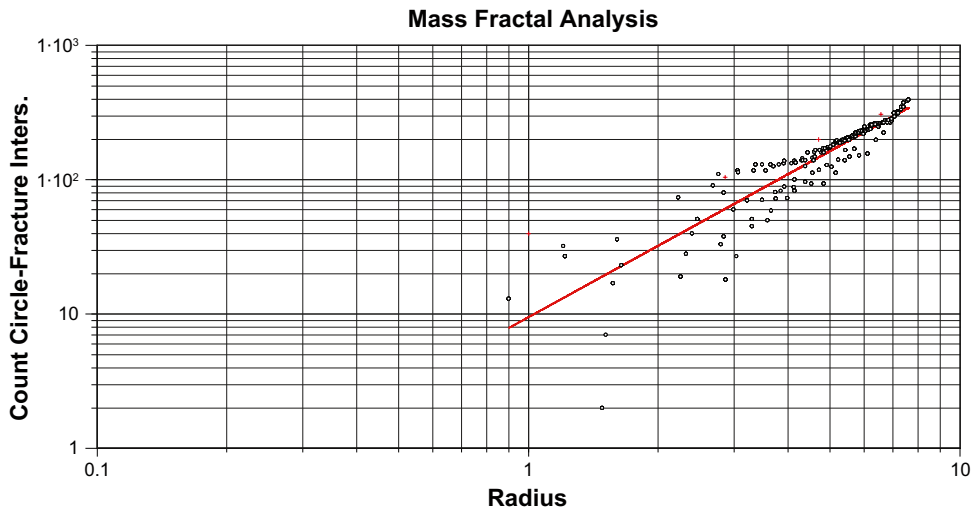
Figure 10-27. Mass dimension plot for AFM001244, NS unlinked set.

Mass Fractal Analysis
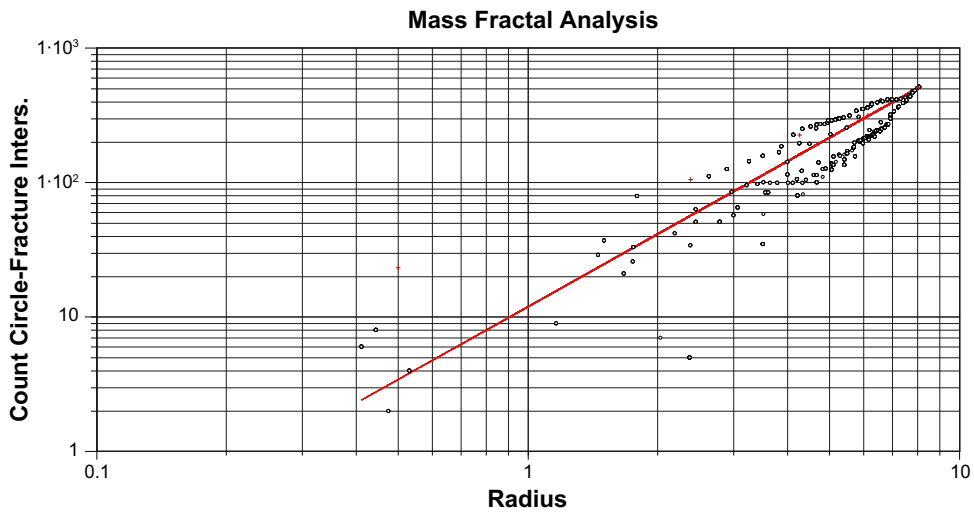
Figure 10-28. Mass dimension plot for AFM001244, NW unlinked set.

Mass Fractal Analysis
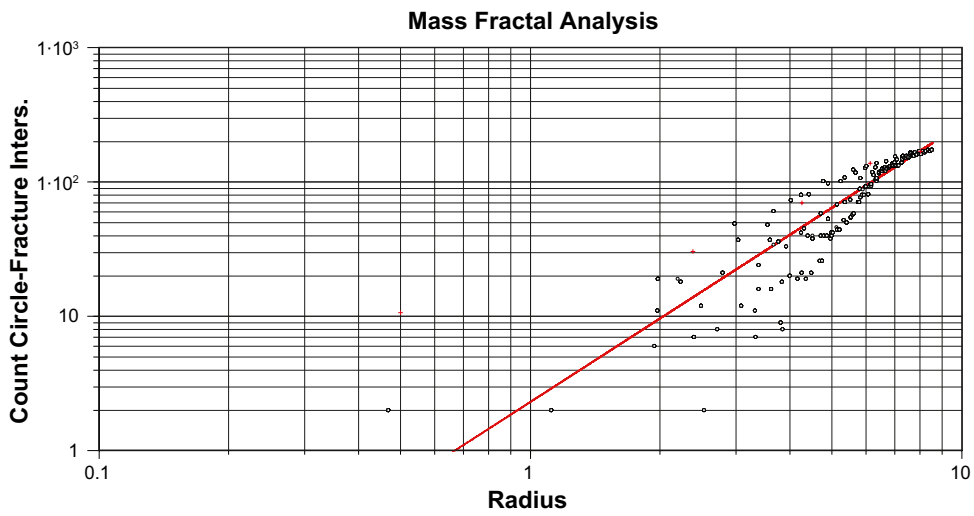
Figure 10-29. Mass dimension plot for AFM001244, SH unlinked set.
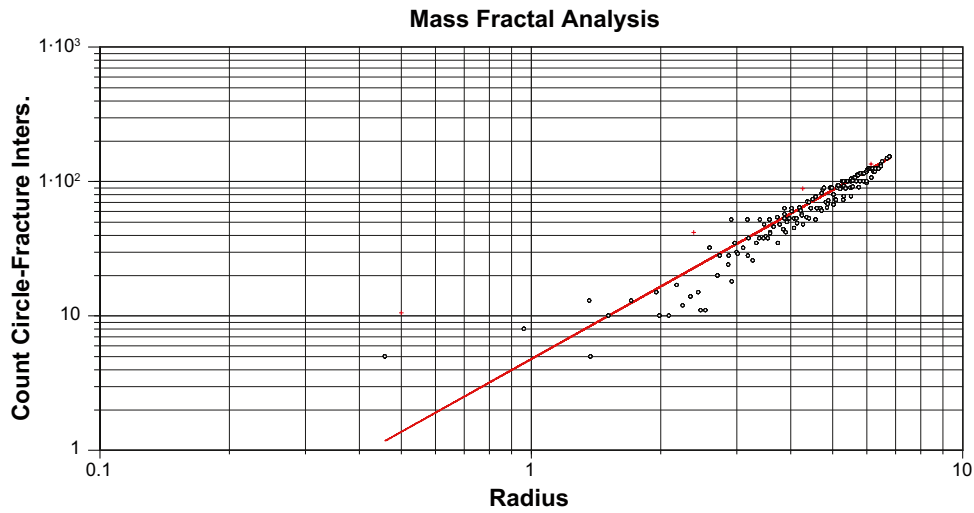
Figure 10-30. *Mass dimension plot for AFM001244, EW unlinked set.*
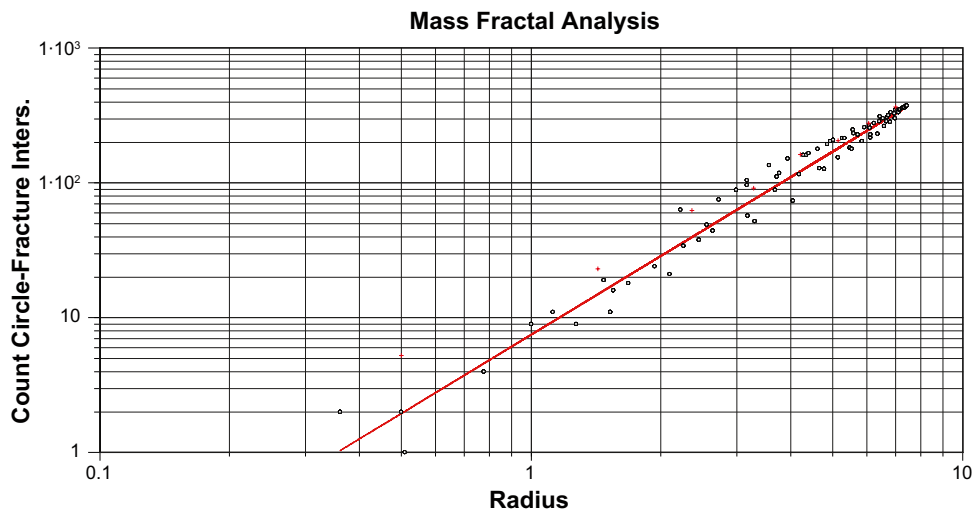
Figure 10-31. *Mass dimension plot for AFM001264, NE unlinked set.*
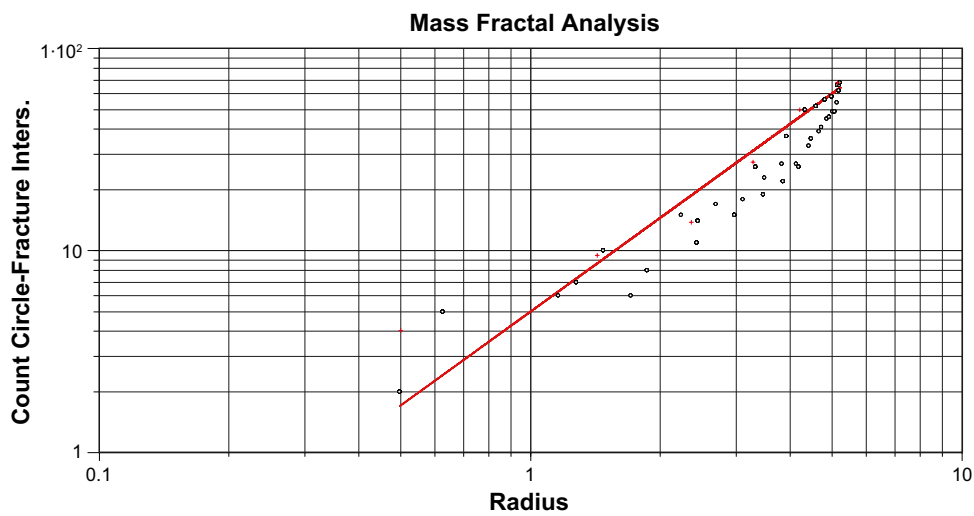
Figure 10-32. *Mass dimension plot for AFM001264, NS unlinked set.*

Mass Fractal Analysis
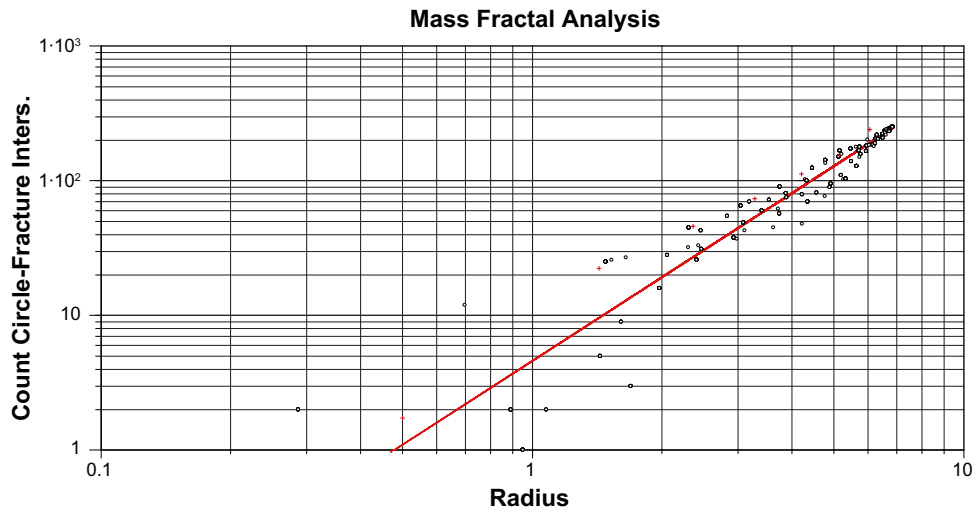
Figure 10-33. *Mass dimension plot for AFM001264, NW unlinked set.*

Mass Fractal Analysis
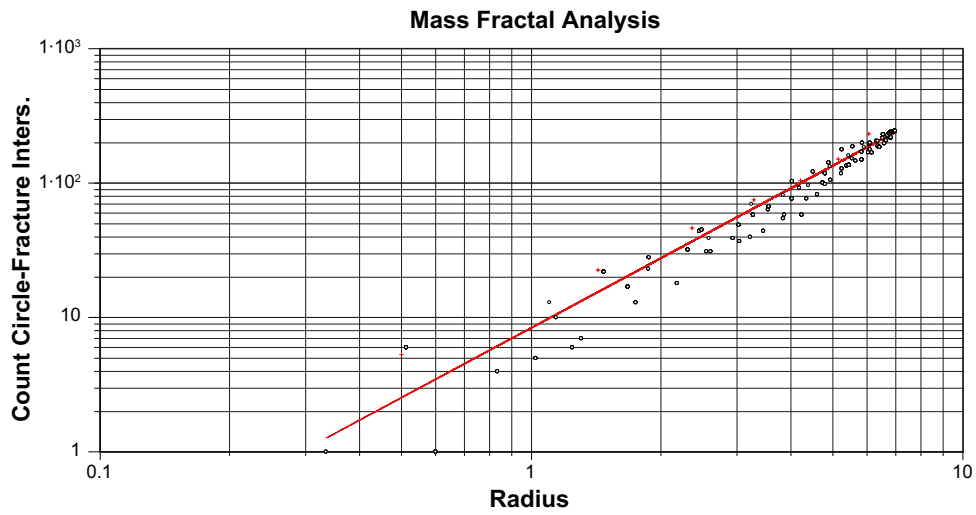
Figure 10-34. *Mass dimension plot for AFM001264, SH unlinked set.*

Mass Fractal Analysis
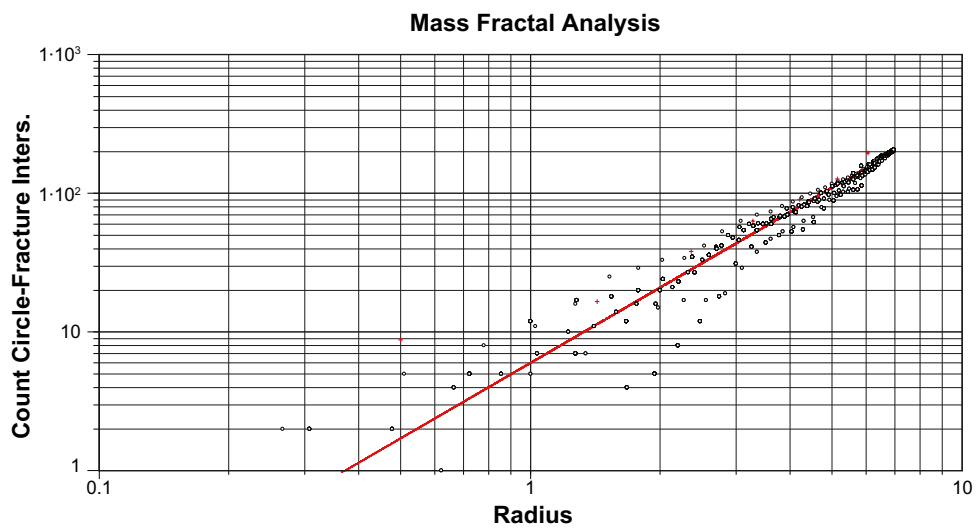
Figure 10-35. *Mass dimension plot for AFM001264, ENE unlinked set.*
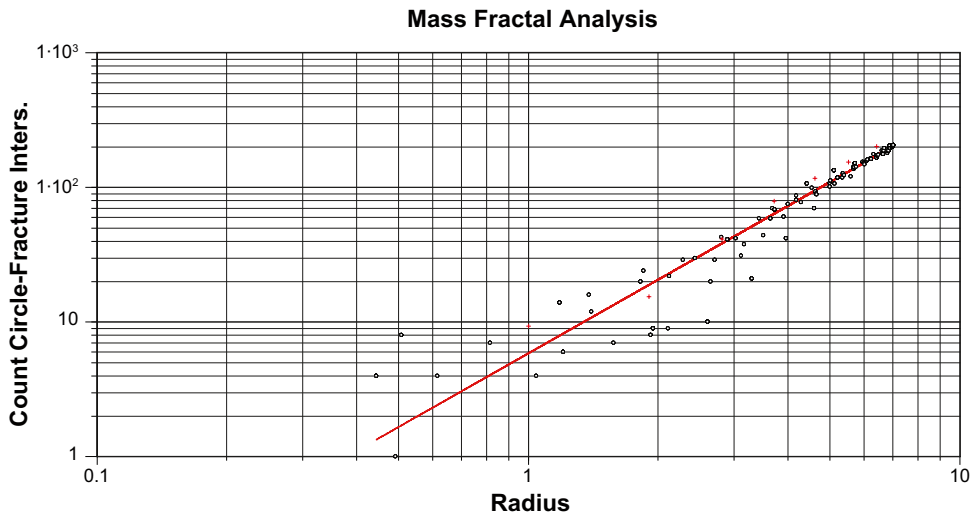
Figure 10-36. *Mass dimension plot for AFM001264, WNW unlinked set.*
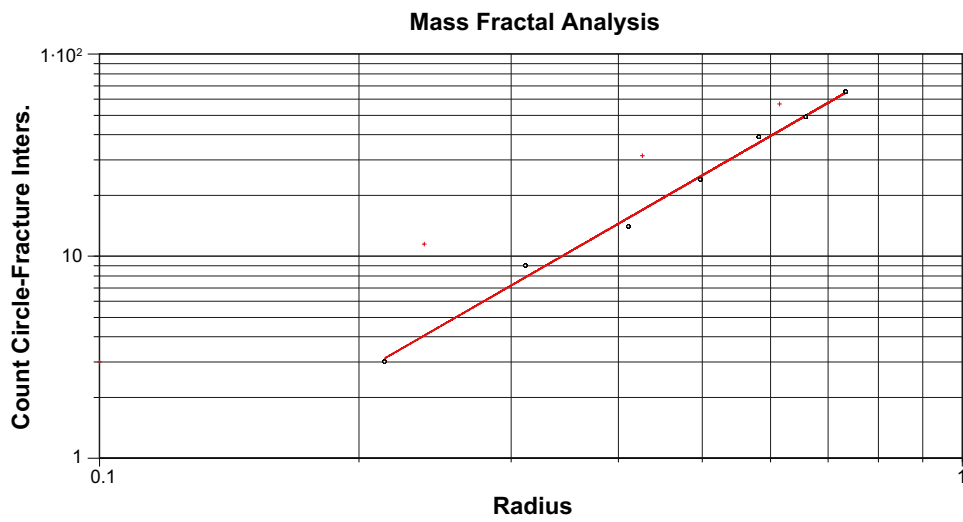
Figure 10-37. *Mass dimension plot for AFM001265, NE unlinked set.*
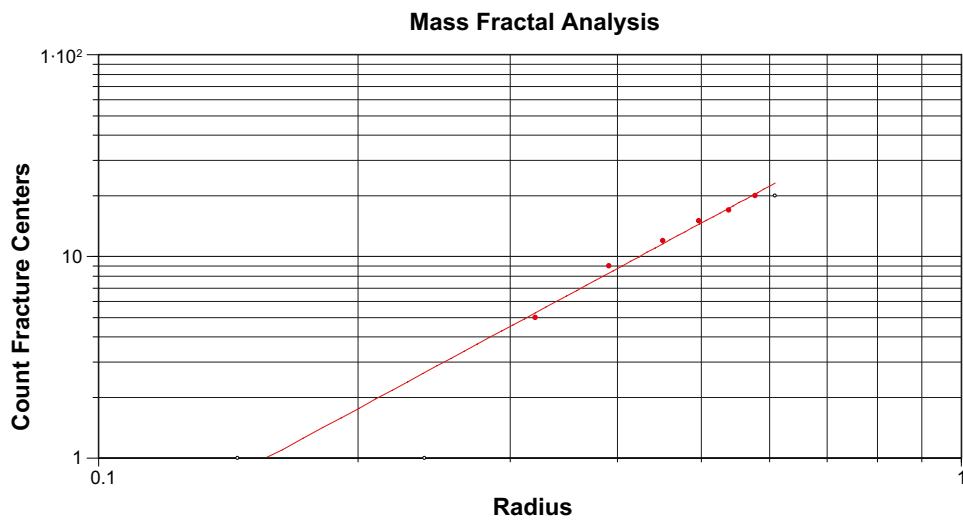
Figure 10-38. *Mass dimension plot for AFM001265, EW unlinked set.*

Mass Fractal Analysis
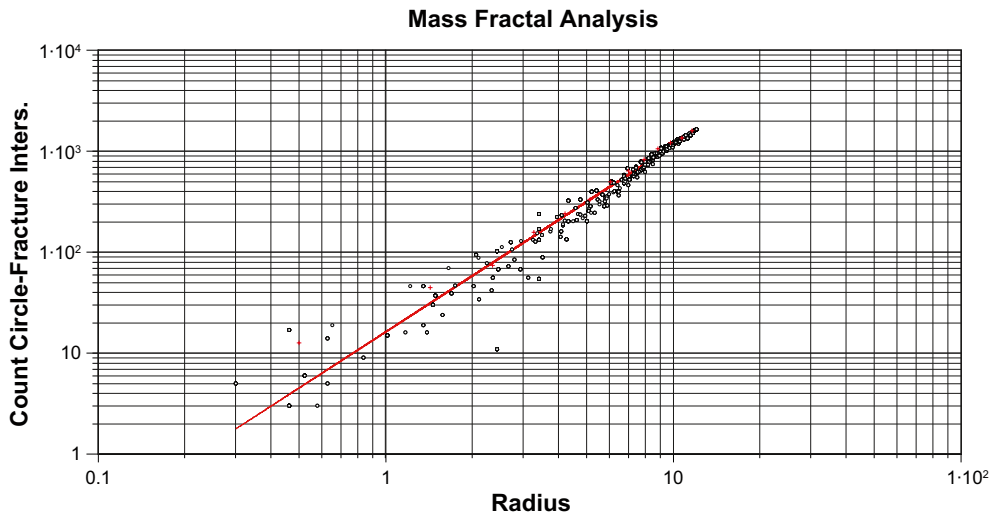
Figure 10-39. Mass dimension plot for AFM100201, NE unlinked set.

Mass Fractal Analysis
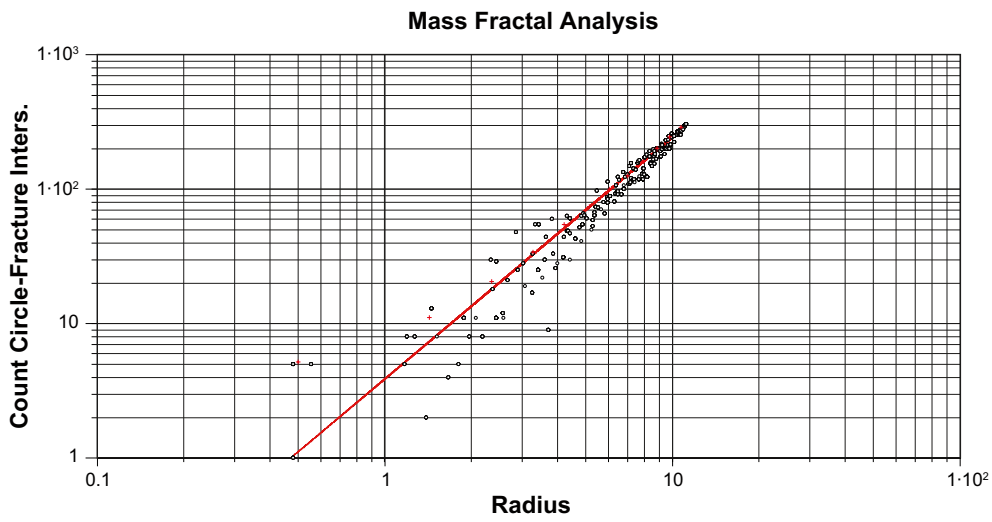
Figure 10-40. Mass dimension plot for AFM100201, NS unlinked set.

Mass Fractal Analysis
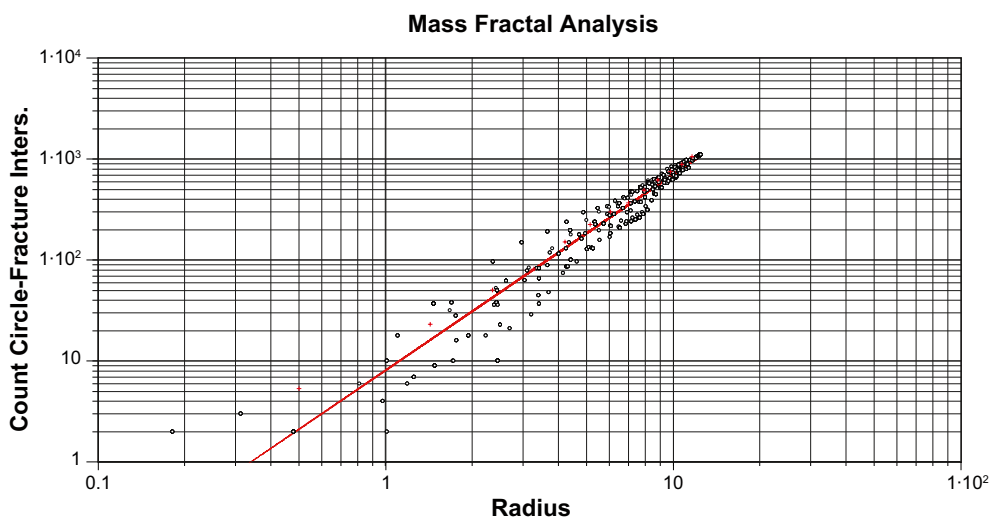
Figure 10-41. Mass dimension plot for AFM100201, NW unlinked set.

Mass Fractal Analysis
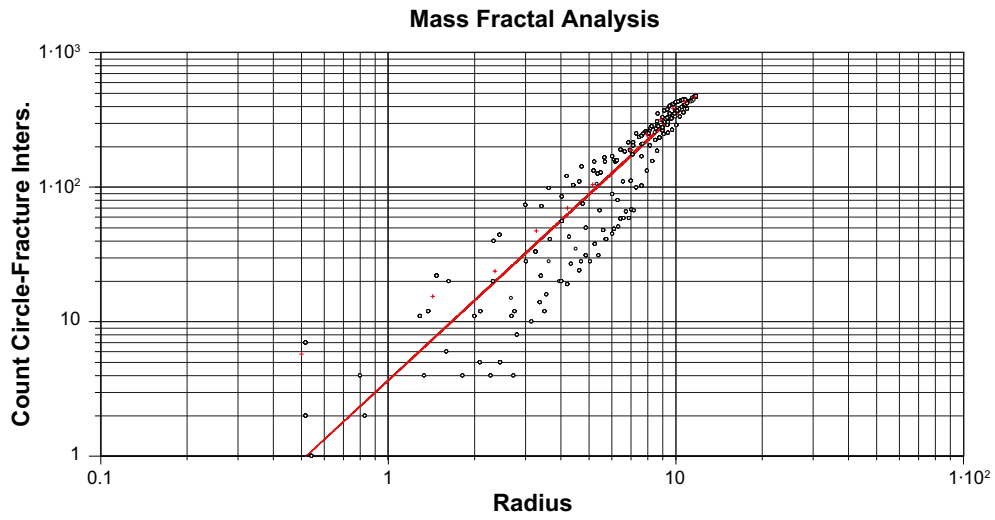
Figure 10-42. *Mass dimension plot for AFM100201, SH unlinked set.*

Mass Fractal Analysis
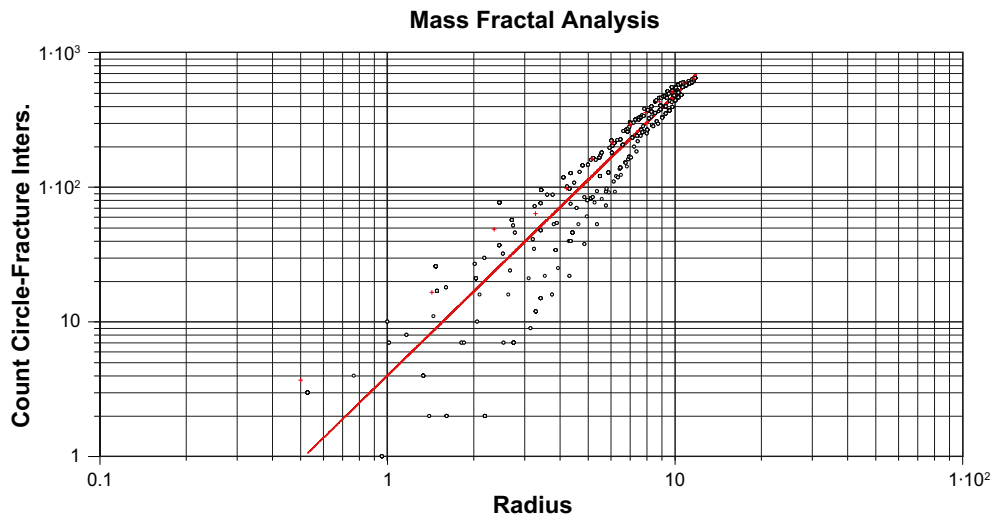
Figure 10-43. *Mass dimension plot for AFM100201, EW unlinked set.*

Mass Fractal Analysis
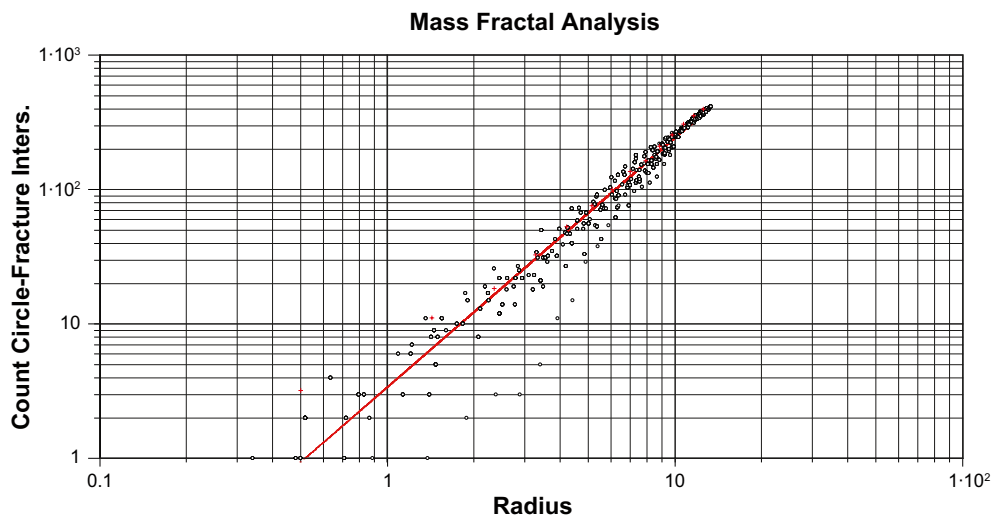
Figure 10-44. *Mass dimension plot for AFM000053, NE linked set.*

Mass Fractal Analysis
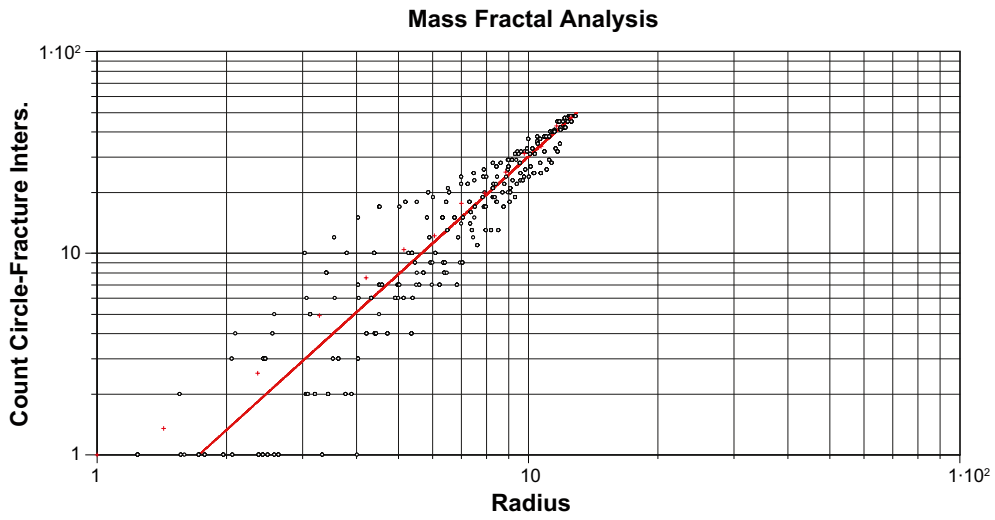
Figure 10-45. *Mass dimension plot for AFM000053, NS linked set.*

Mass Fractal Analysis
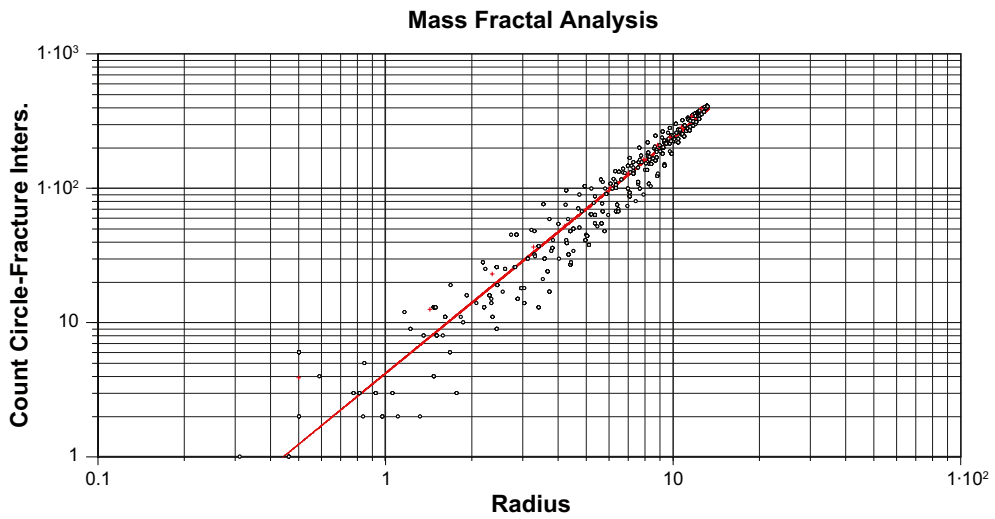
Figure 10-46. *Mass dimension plot for AFM000053, NW linked set.*

Mass Fractal Analysis
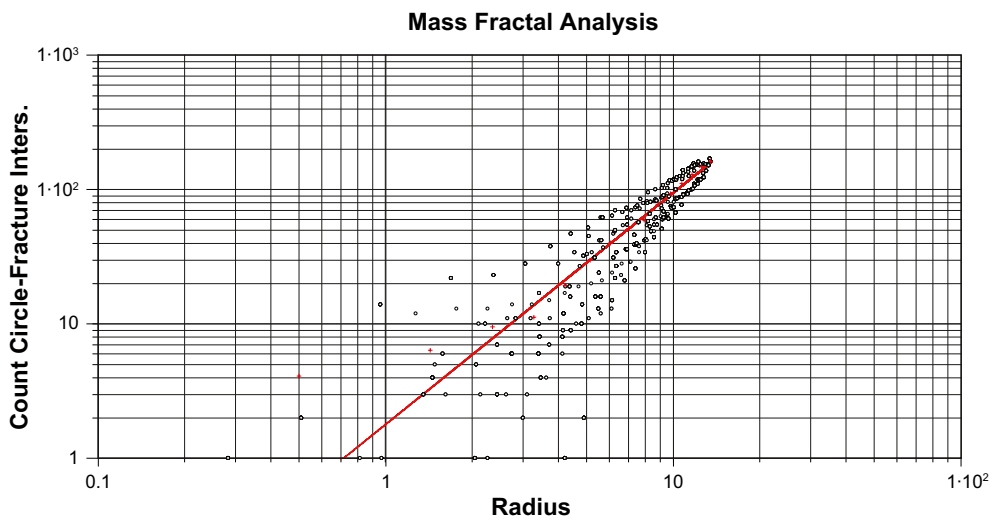
Figure 10-47. *Mass dimension plot for AFM000053, SH linked set.*
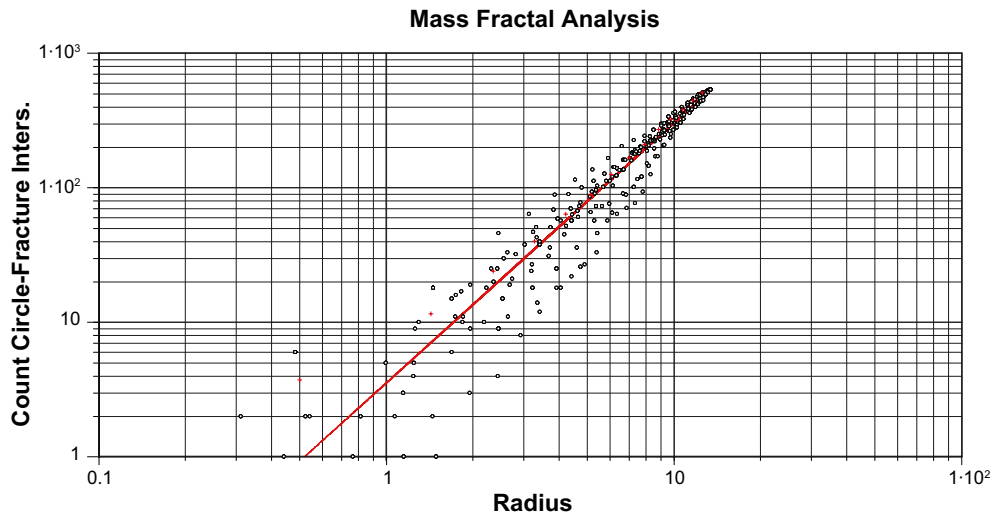
Figure 10-48. *Mass dimension plot for AFM000053, WNW linked set.*
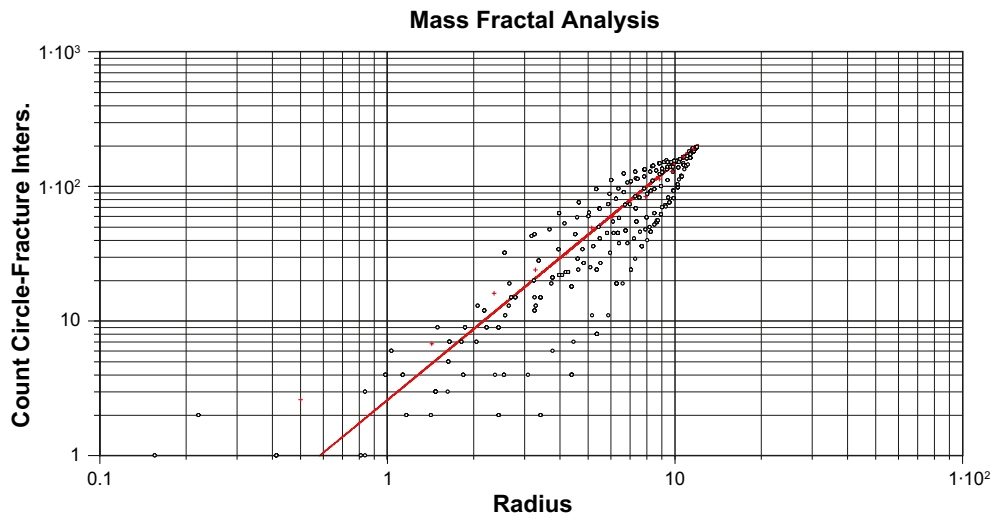
Figure 10-49. *Mass dimension plot for AFM000053, ENE linked set.*
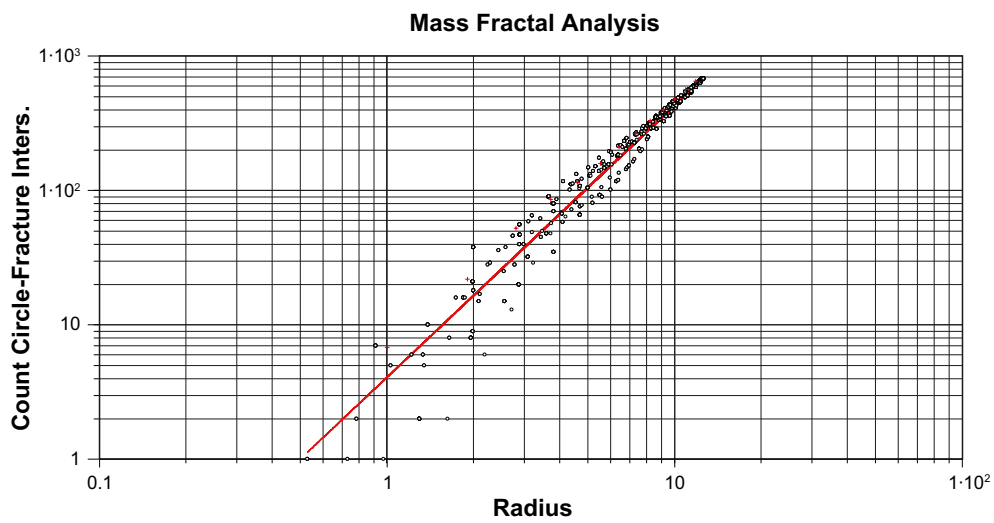
Figure 10-50. *Mass dimension plot for AFM000054, NE linked set.*

Mass Fractal Analysis
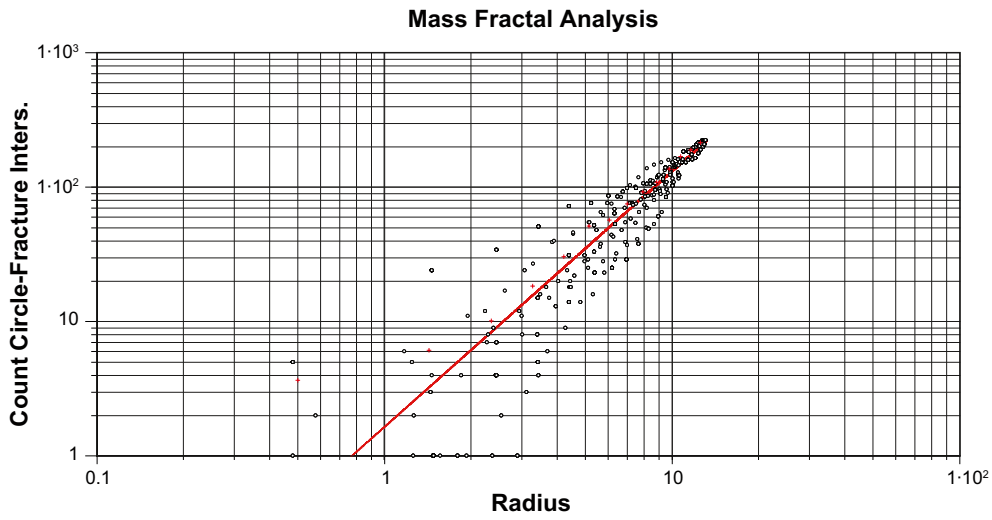
Figure 10-51. Mass dimension plot for AFM000054, NS linked set.

Mass Fractal Analysis
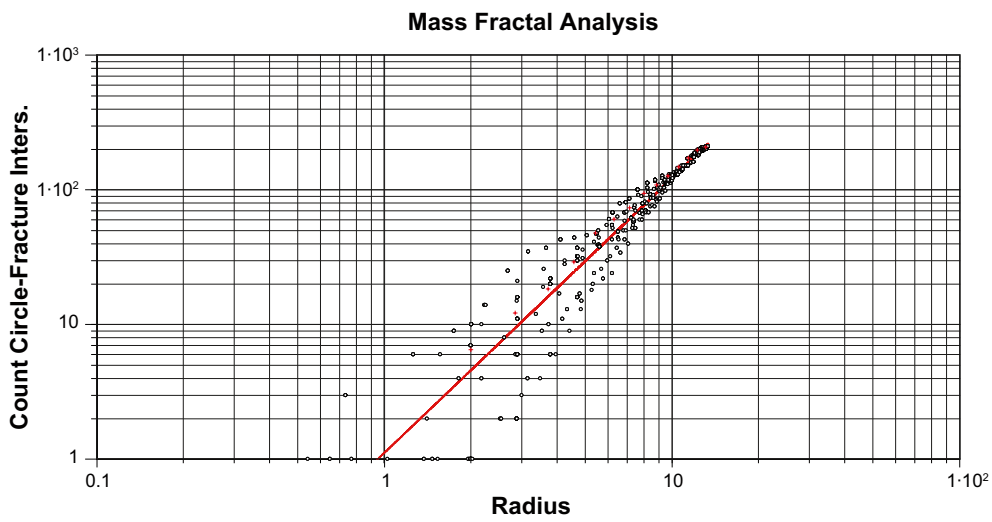
Figure 10-52. Mass dimension plot for AFM000054, NW linked set.

Mass Fractal Analysis
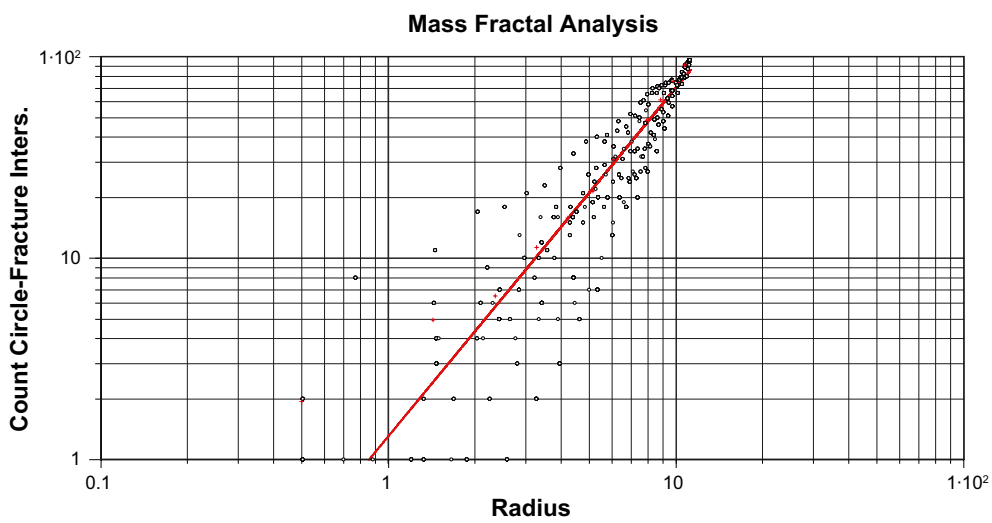
Figure 10-53. Mass dimension plot for AFM000054, SH linked set.
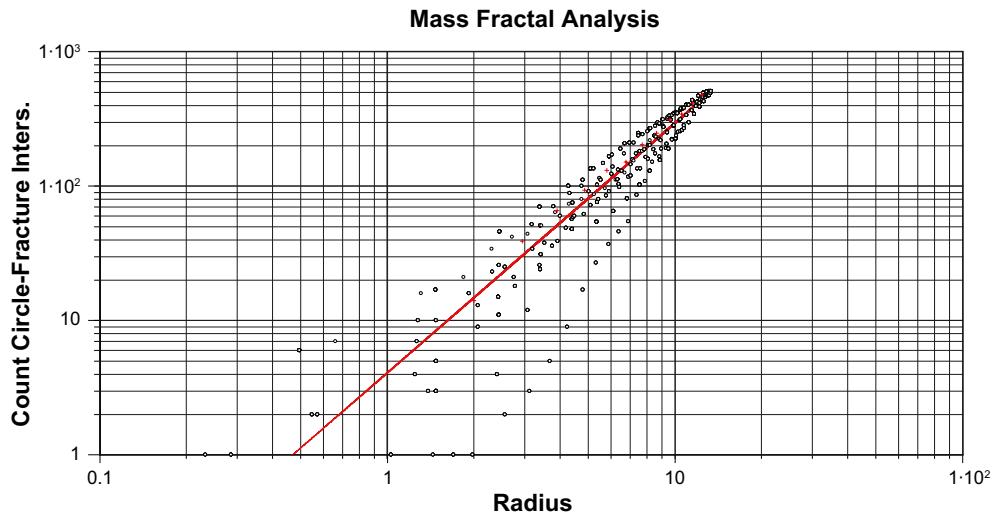
Figure 10-54. *Mass dimension plot for AFM000054, WNW linked set.*
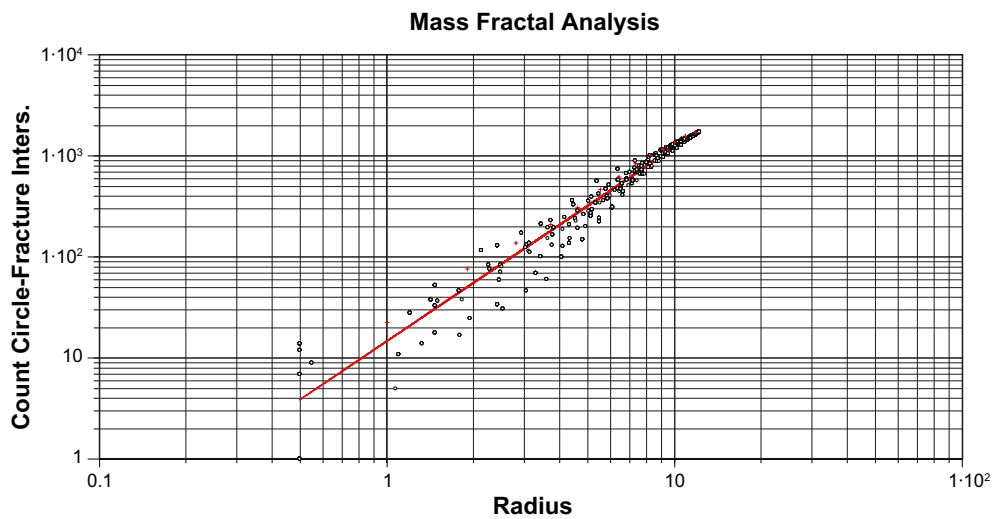
Figure 10-55. *Mass dimension plot for AFM001097, NE linked set.*
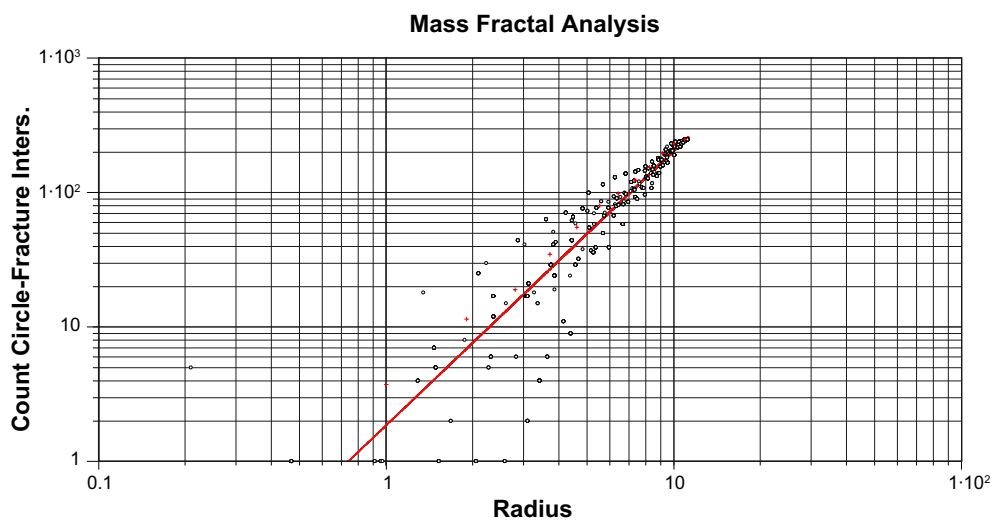
Figure 10-56. *Mass dimension plot for AFM001097, NS linked set.*
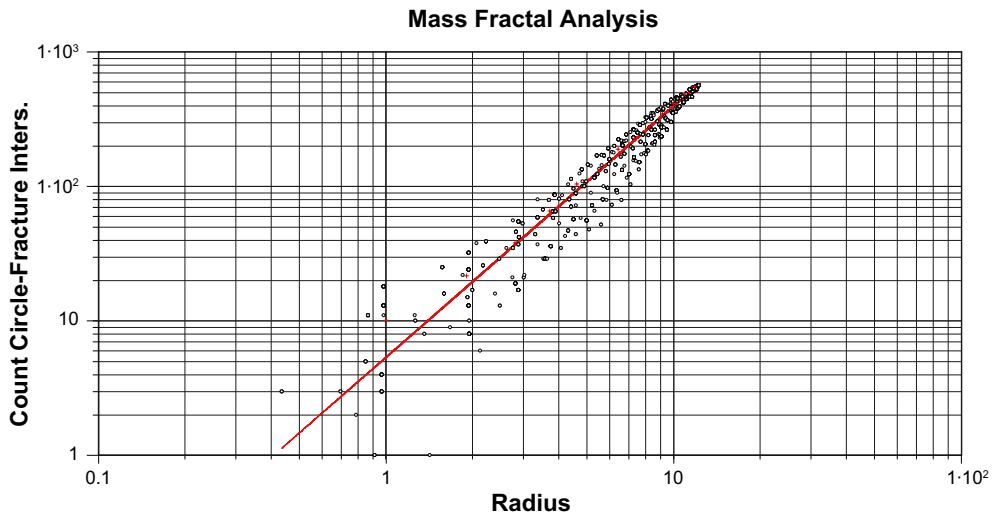
Figure 10-57. *Mass dimension plot for AFM001097, NS linked set.*
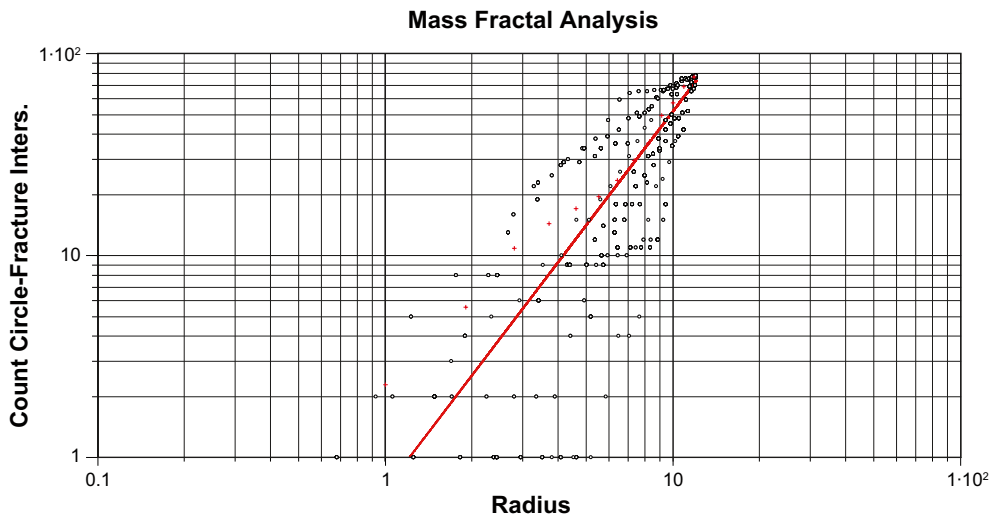
Figure 10-58. *Mass dimension plot for AFM001097, SH linked set.*
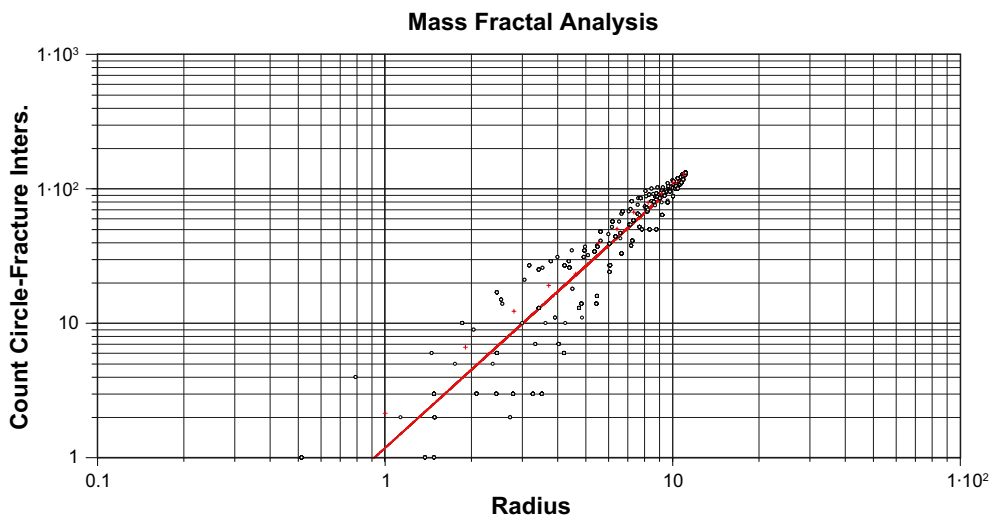
Figure 10-59. *Mass dimension plot for AFM001097, EW linked set.*
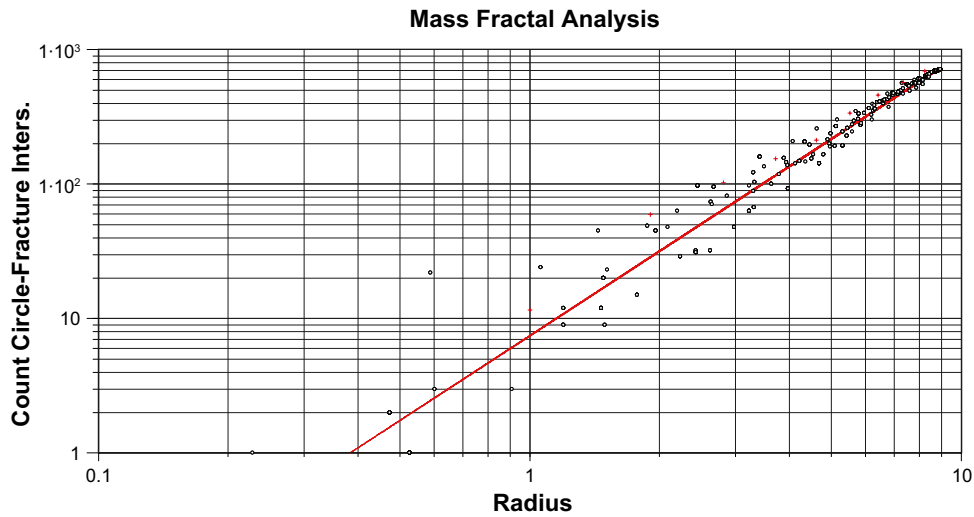
Figure 10-60. *Mass dimension plot for AFM001098, NE linked set.*
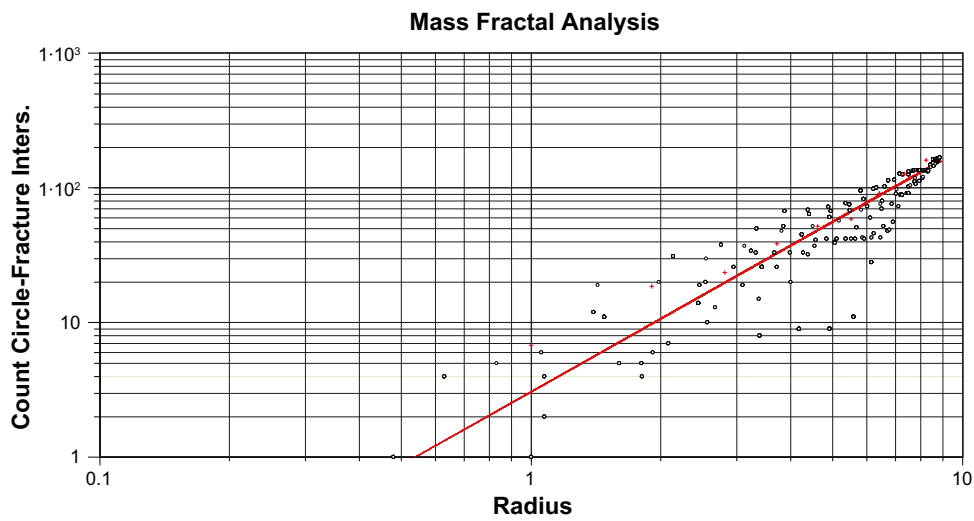
Figure 10-61. *Mass dimension plot for AFM001098, NW linked set.*
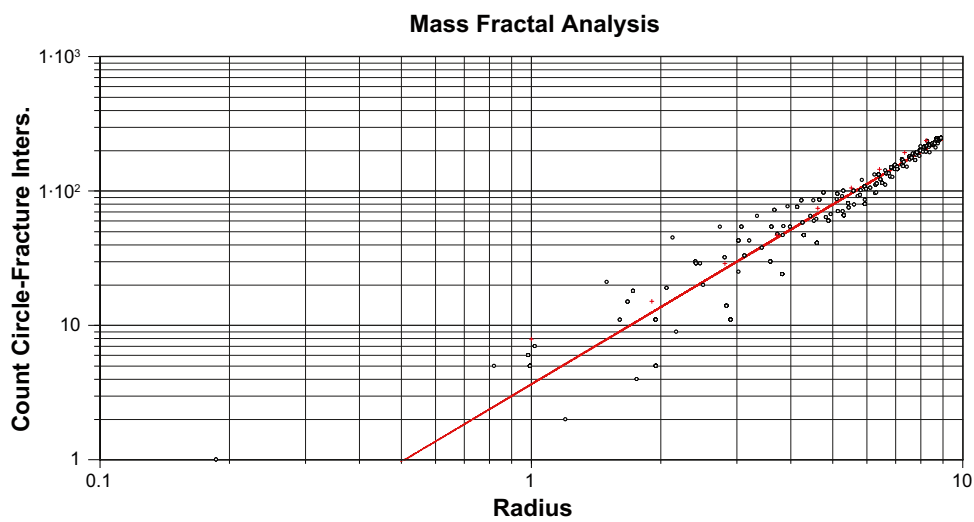
Figure 10-62. *Mass dimension plot for AFM001098, SH linked set.*
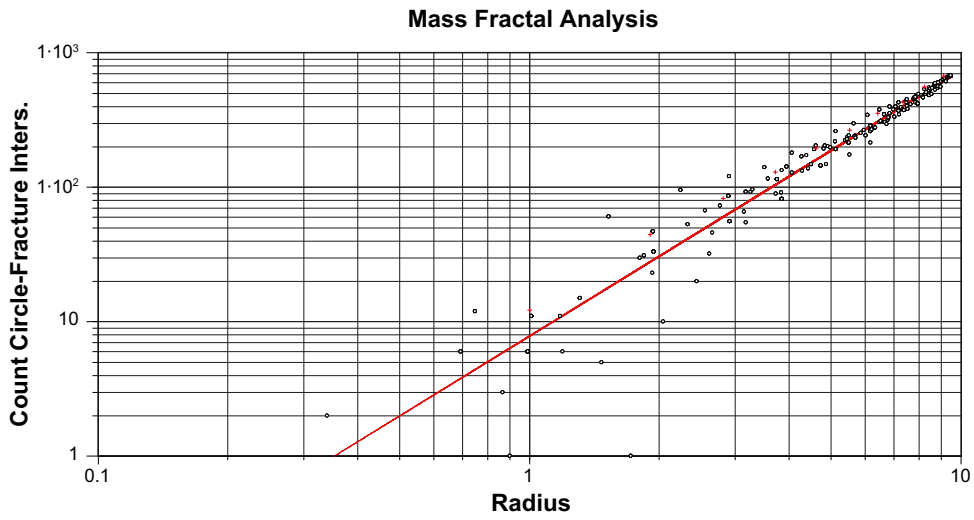
Figure 10-63. *Mass dimension plot for AFM001098, WNW linked set.*
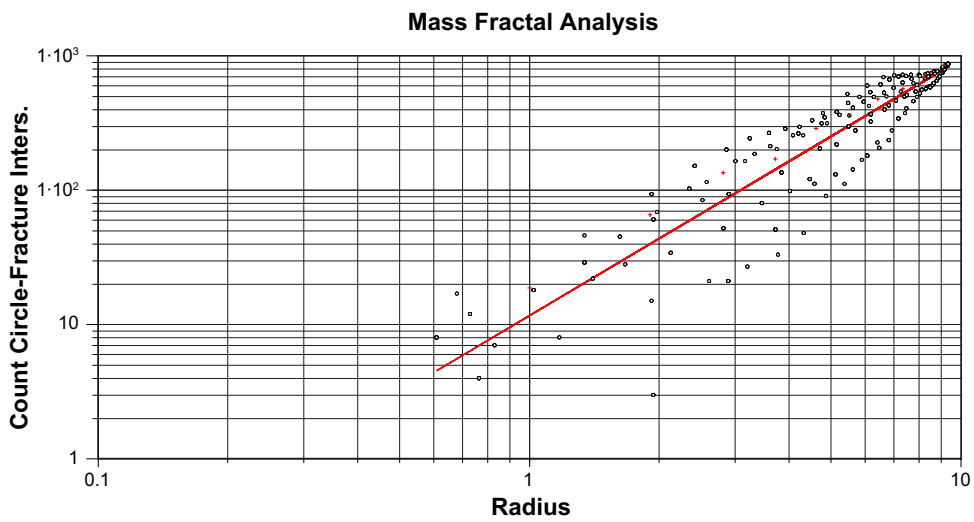
Figure 10-64. *Mass dimension plot for AFM001098, NNE linked set.*
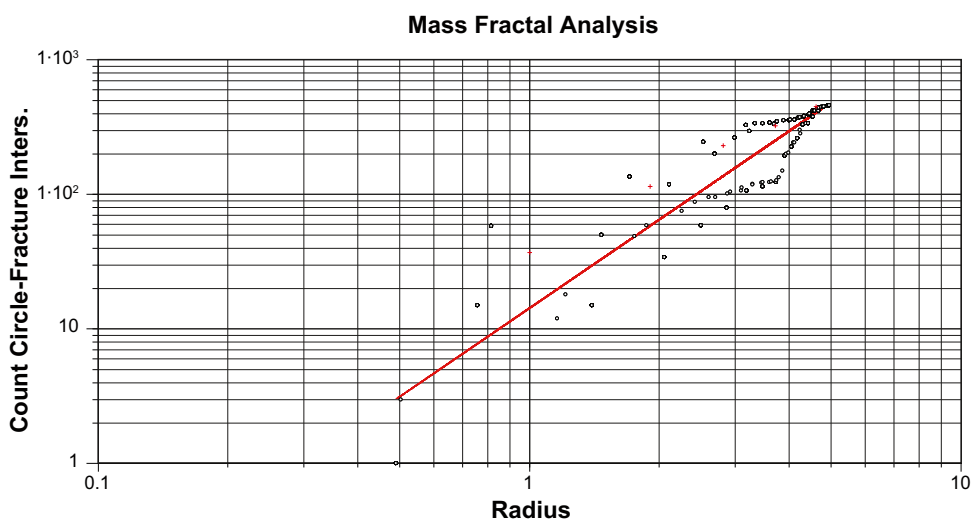
Figure 10-65. *Mass dimension plot for AFM001243, NE linked set.*

44
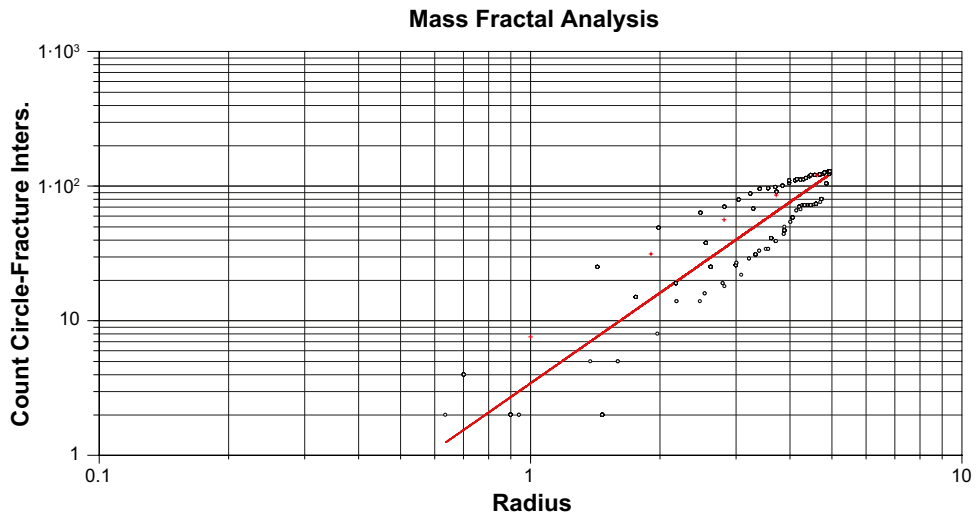
Figure 10-66. *Mass dimension plot for AFM001243, NS linked set.*
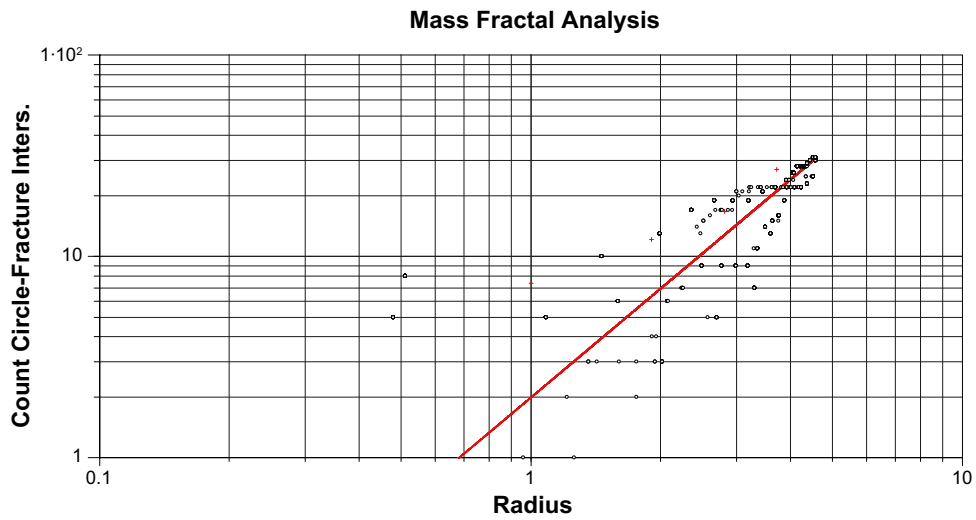
Figure 10-67. *Mass dimension plot for AFM001243, SH linked set.*
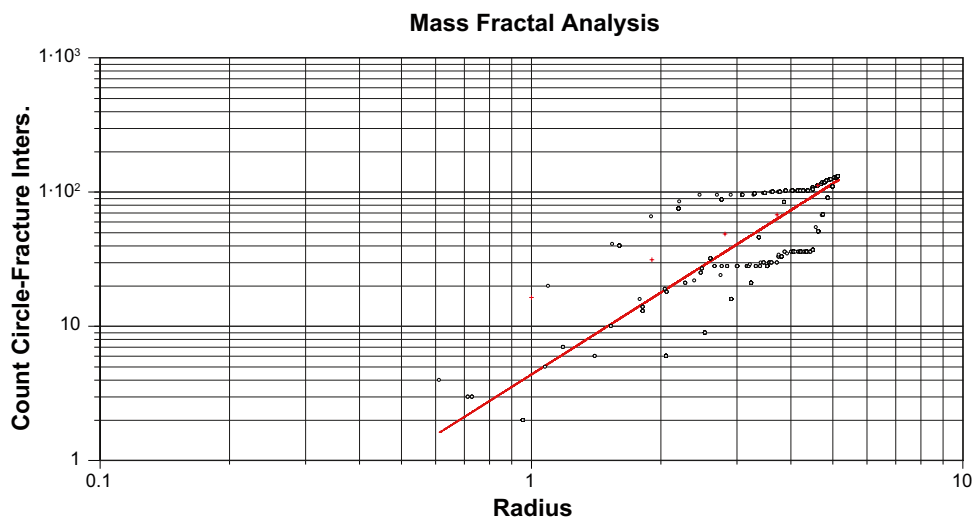
Figure 10-68. *Mass dimension plot for AFM001243, WNW linked set.*

Mass Fractal Analysis
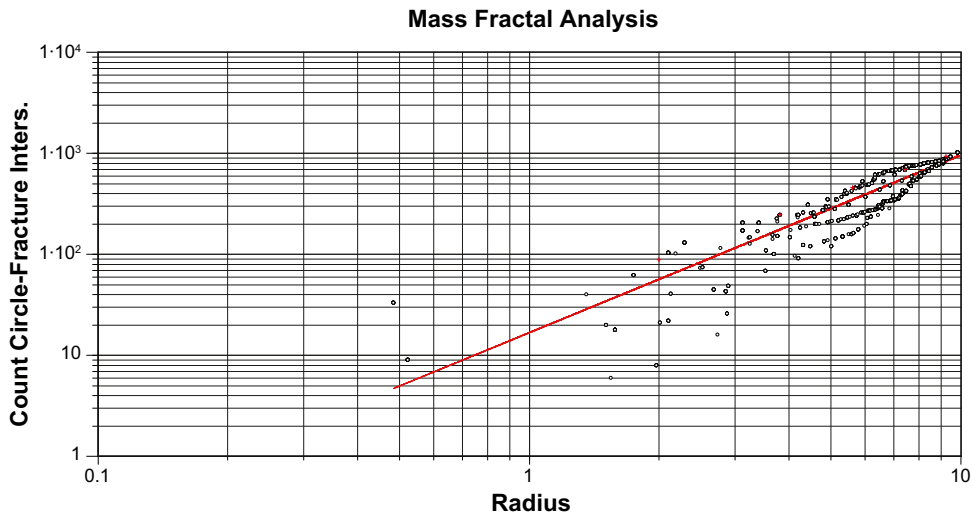
Figure 10-69. *Mass dimension plot for AFM001244, NE linked set.*

Mass Fractal Analysis
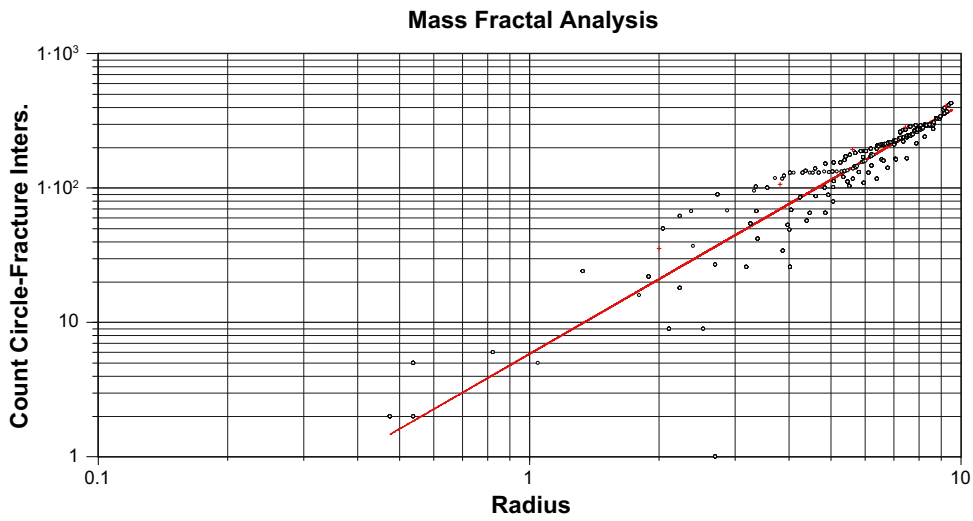
Figure 10-70. *Mass dimension plot for AFM001244, NS linked set.*

Mass Fractal Analysis
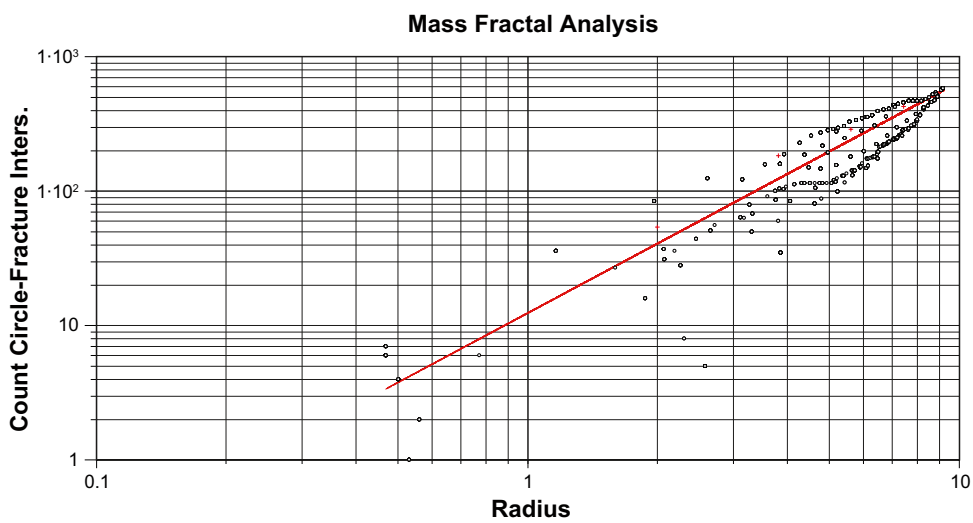
Figure 10-71. *Mass dimension plot for AFM001244, NW linked set.*
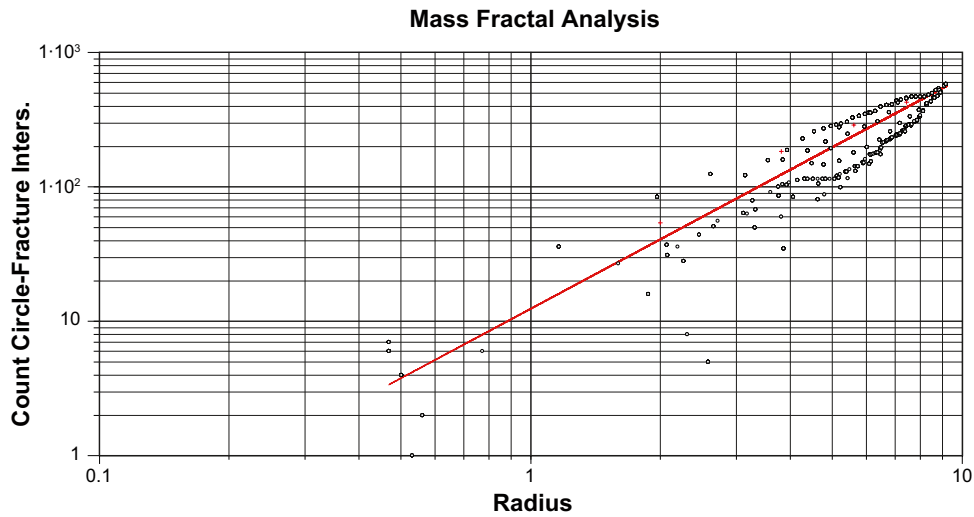
Figure 10-72. *Mass dimension plot for AFM001244, SH linked set.*
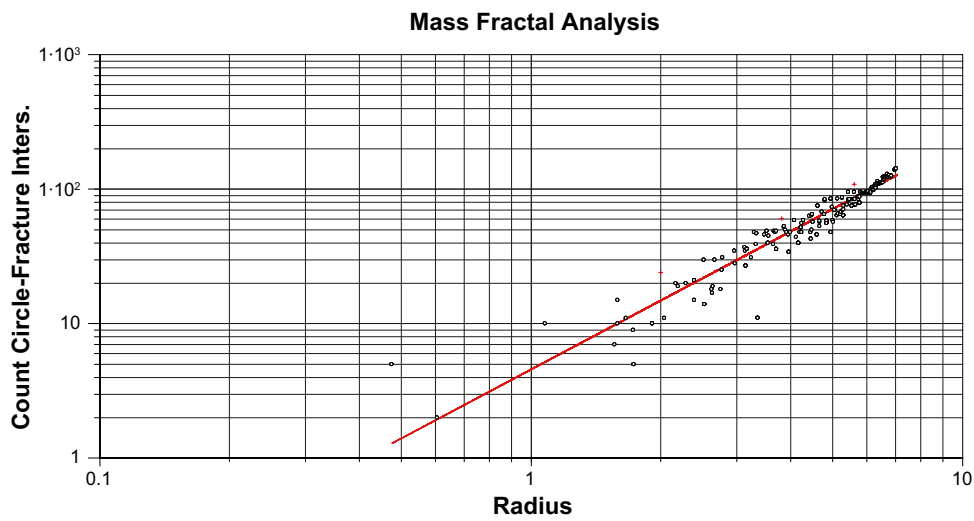
Figure 10-73. *Mass dimension plot for AFM001244, EW linked set.*
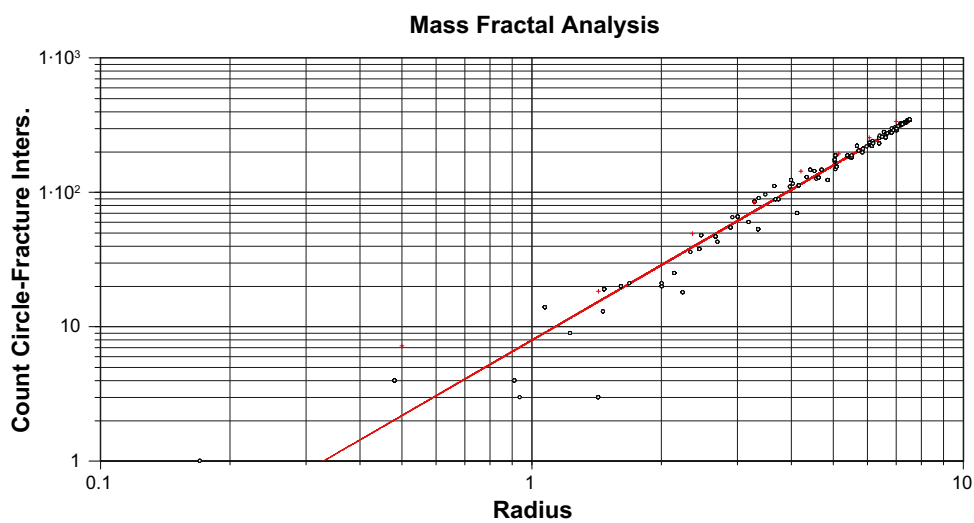
Figure 10-74. *Mass dimension plot for AFM001264, NE linked set.*
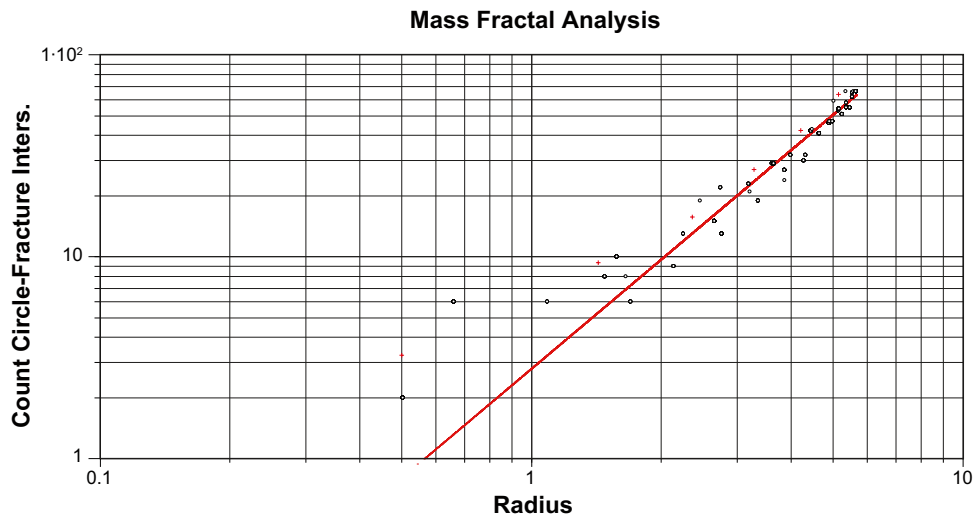
Figure 10-75. *Mass dimension plot for AFM001264, NS linked set.*
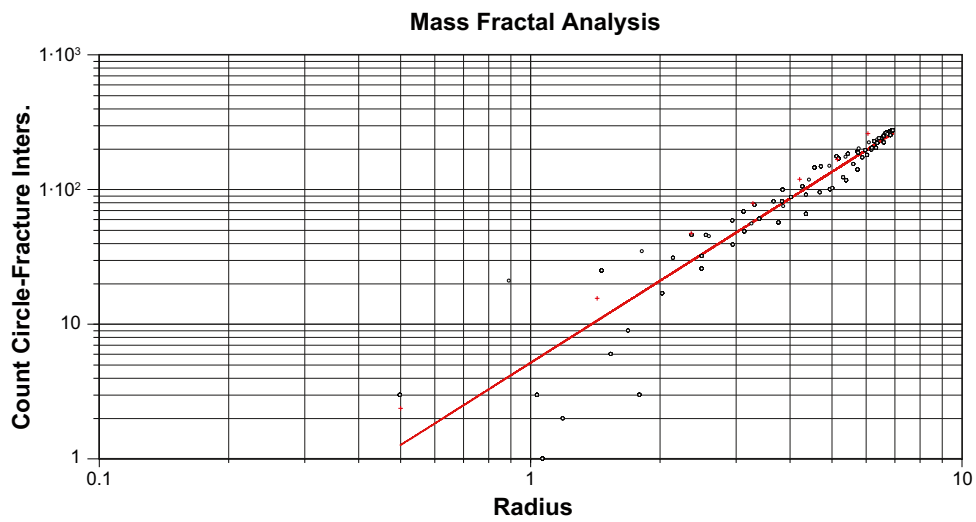
Figure 10-76. *Mass dimension plot for AFM001264, NW linked set.*
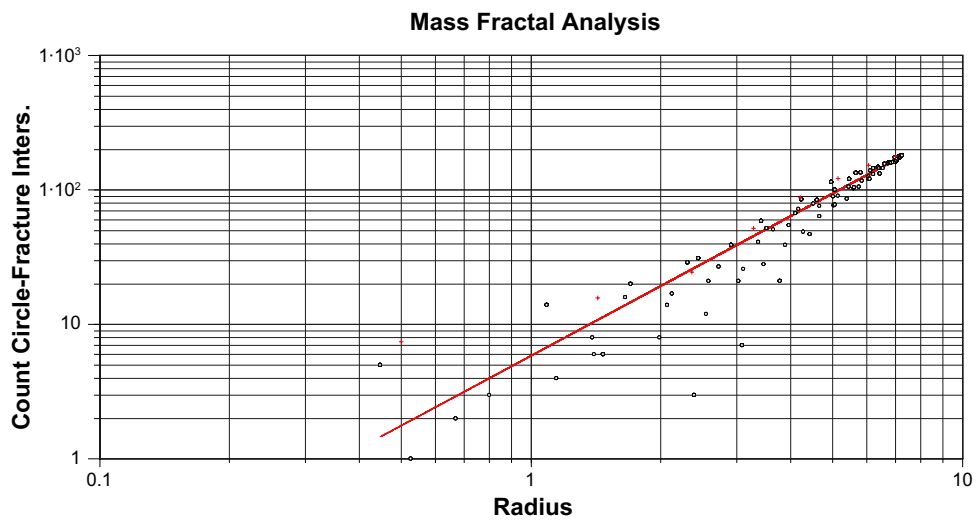
Figure 10-77. *Mass dimension plot for AFM001264, WNW linked set.*
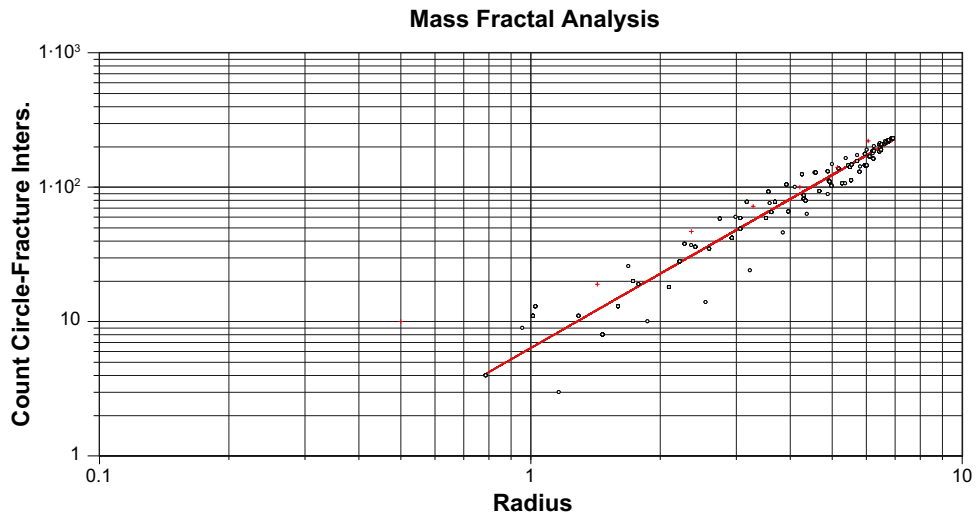
Figure 10-78. *Mass dimension plot for AFM001264, ENE linked set.*
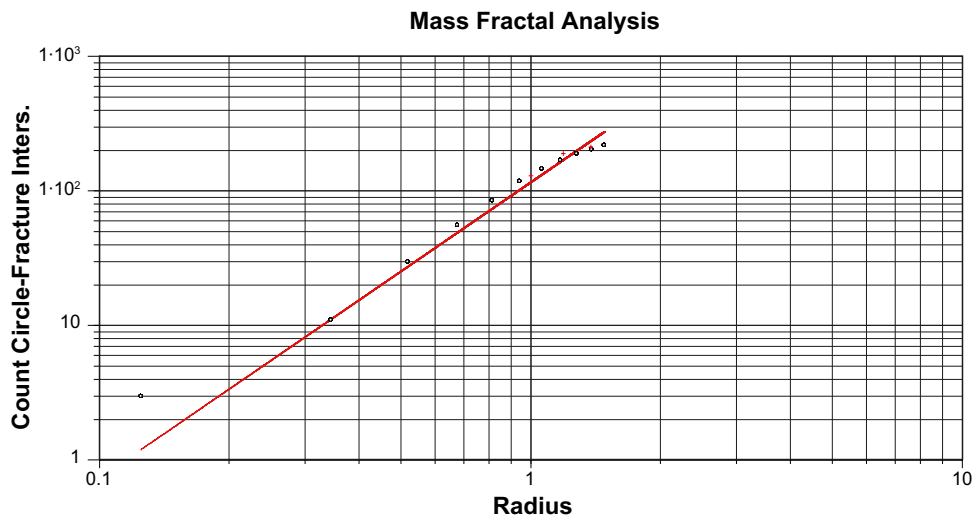
Figure 10-79. *Mass dimension plot for AFM001265, NE linked set.*
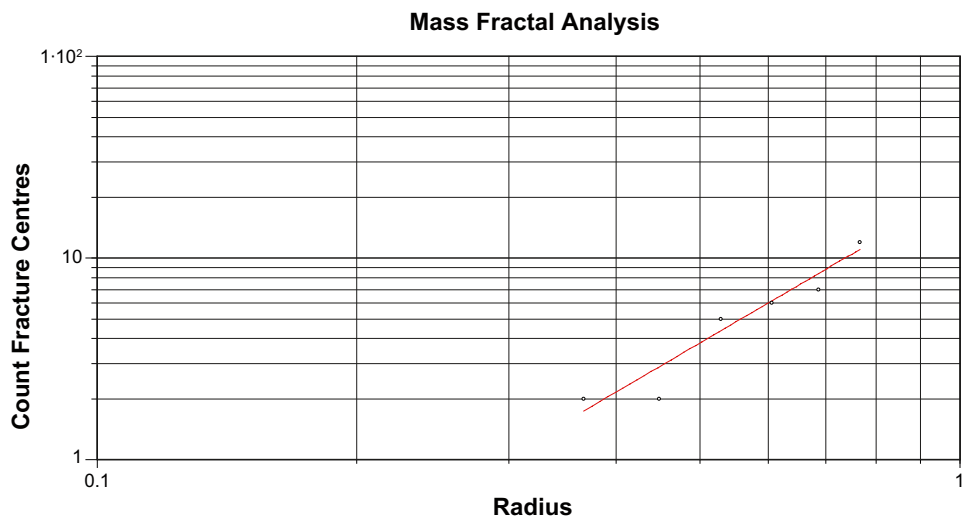
Figure 10-80. *Mass dimension plot for AFM001265, NS-NNE linked set.*

Mass Fractal Analysis
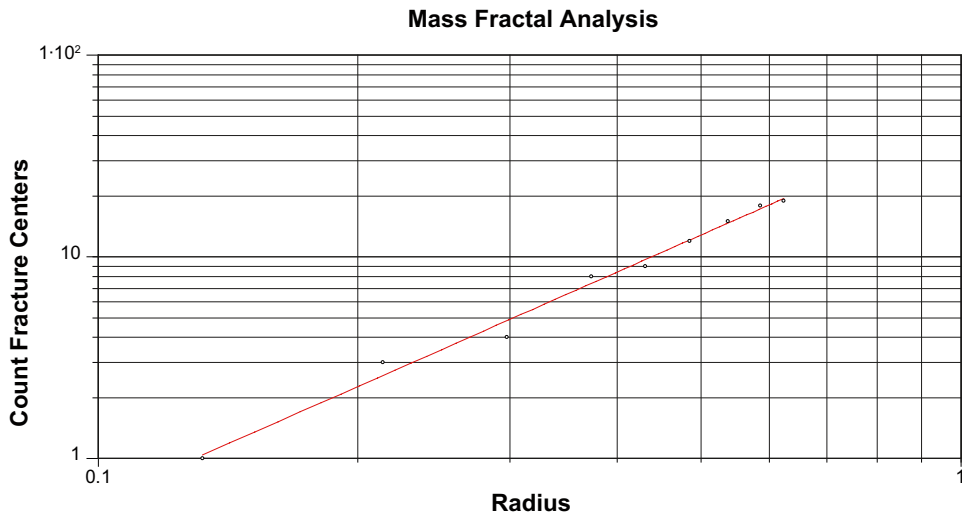
Figure 10-81. *Mass dimension plot for AFM001265, EW linked set.*

Mass Fractal Analysis
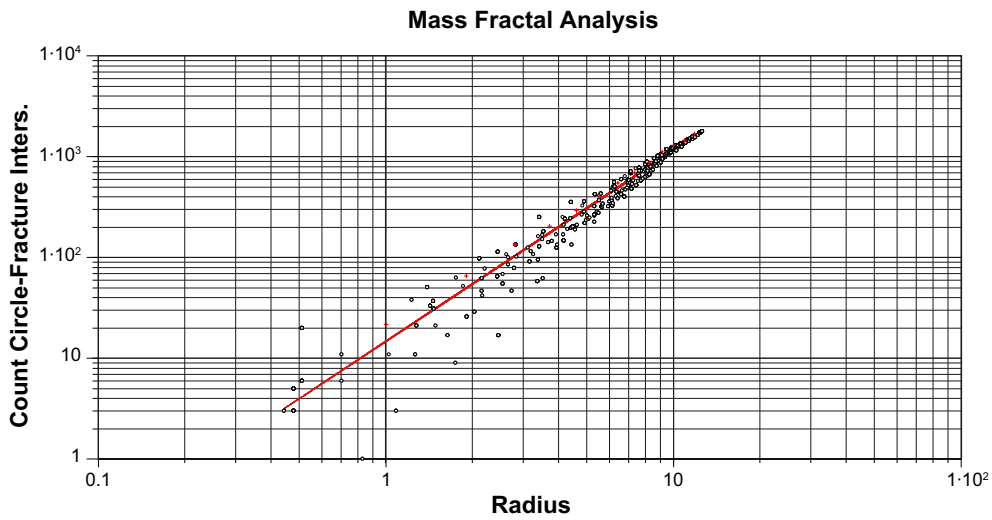
Figure 10-82. *Mass dimension plot for AFM100201, NE linked set.*

Mass Fractal Analysis
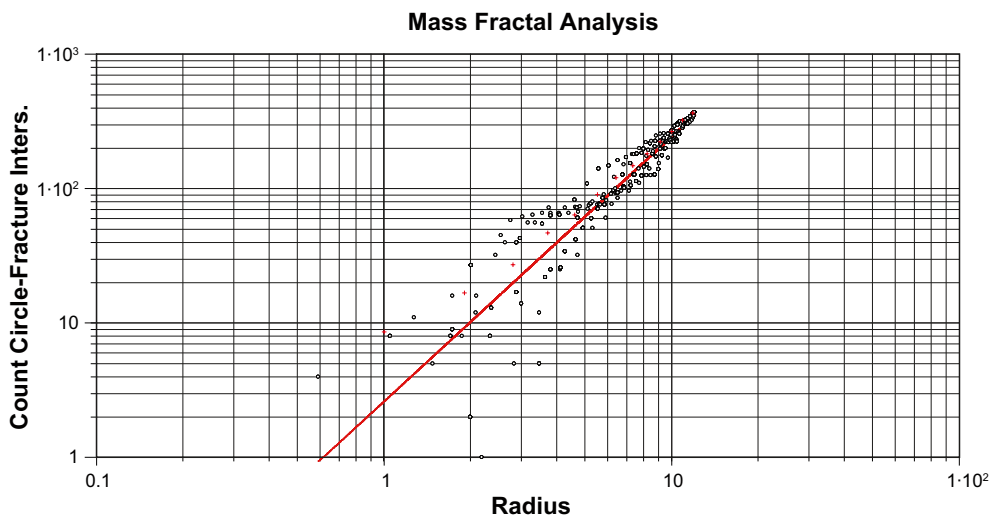
Figure 10-83. *Mass dimension plot for AFM100201, NS linked set.*
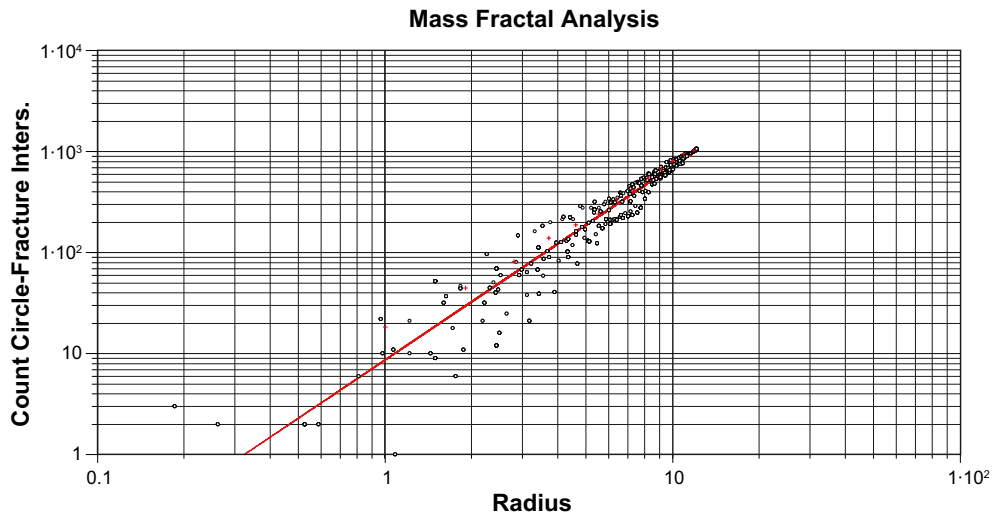
Figure 10-84. *Mass dimension plot for AFM100201, NW linked set.*
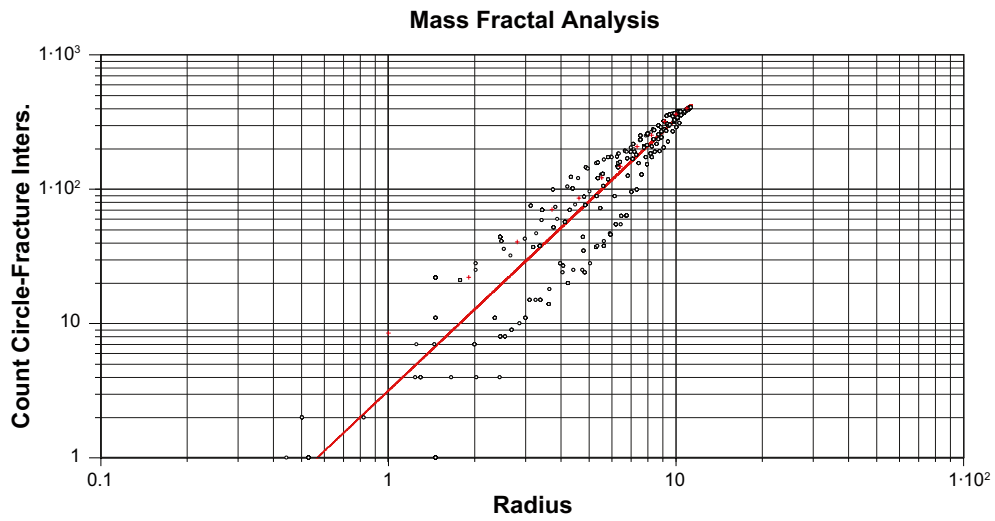
Figure 10-85. *Mass dimension plot for A FM100201, SH linked set.*
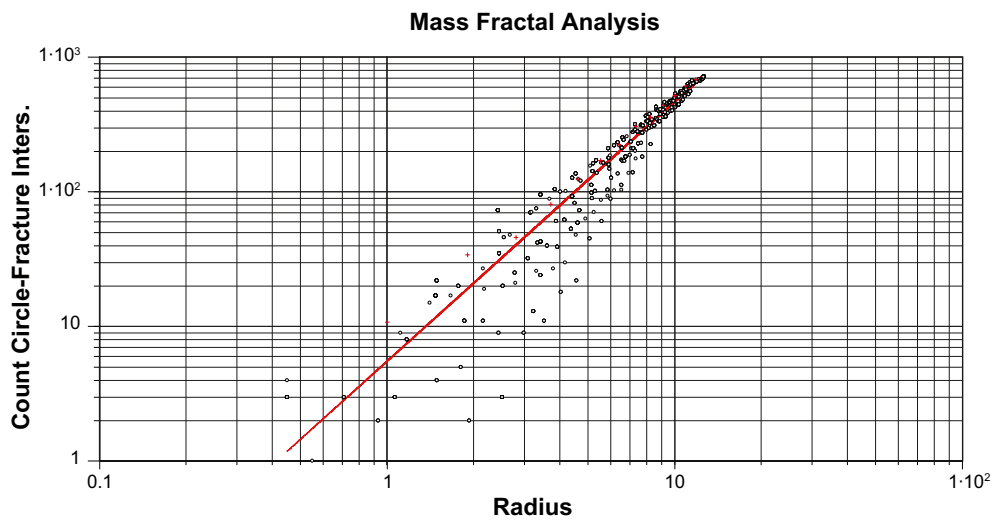
Figure 10-86. *Mass dimension plot for A FM100201, EW linked set.*

51
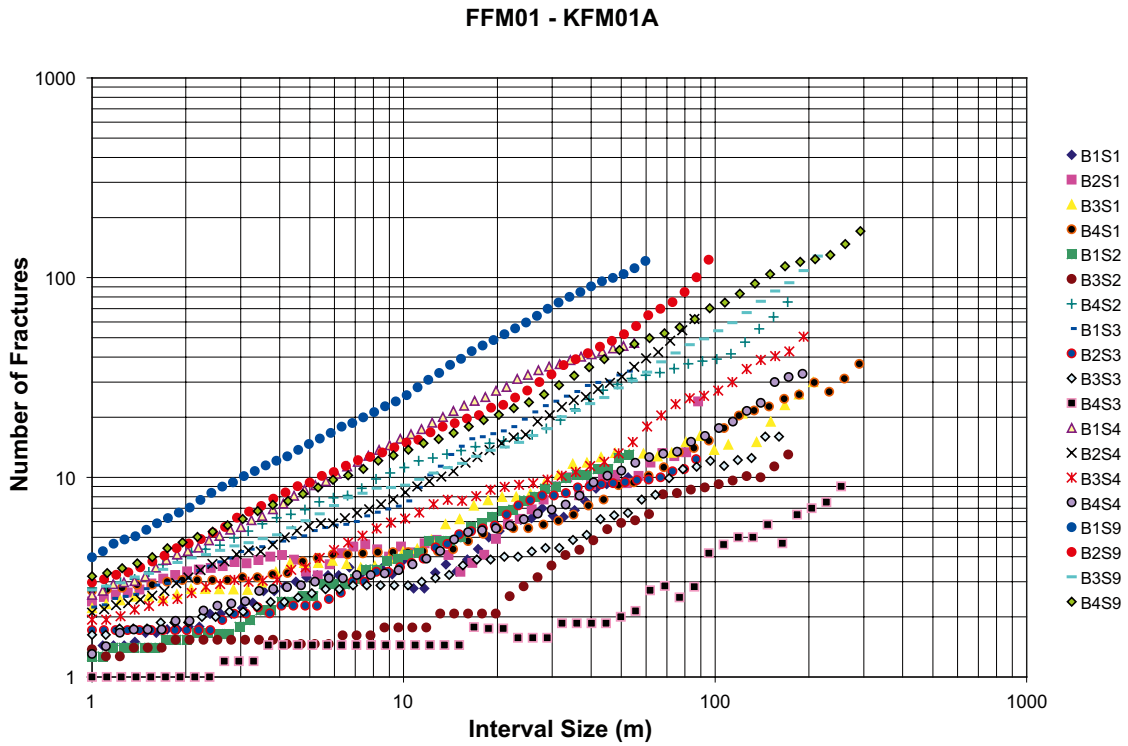
Figure 10-87. *Mass dimension plot for fracture data from KFM01A, Domain FFM01.*
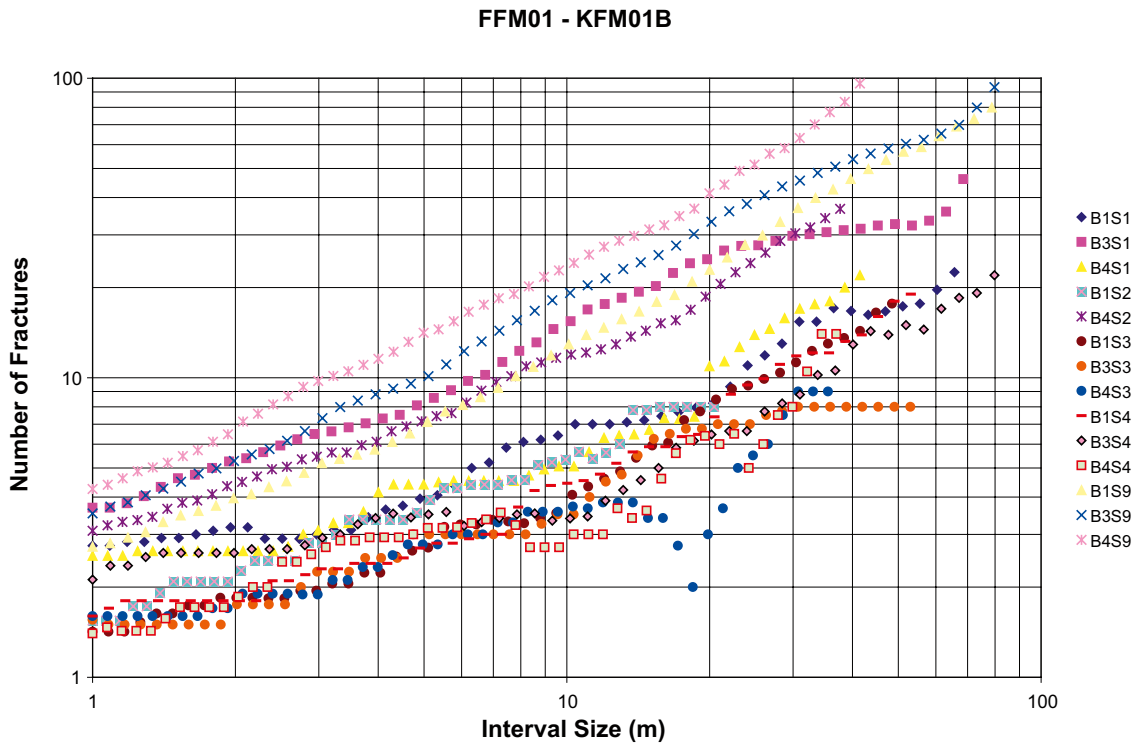
Figure 10-88. *Mass dimension plot for fracture data from KFM01B, Domain FFM01.*
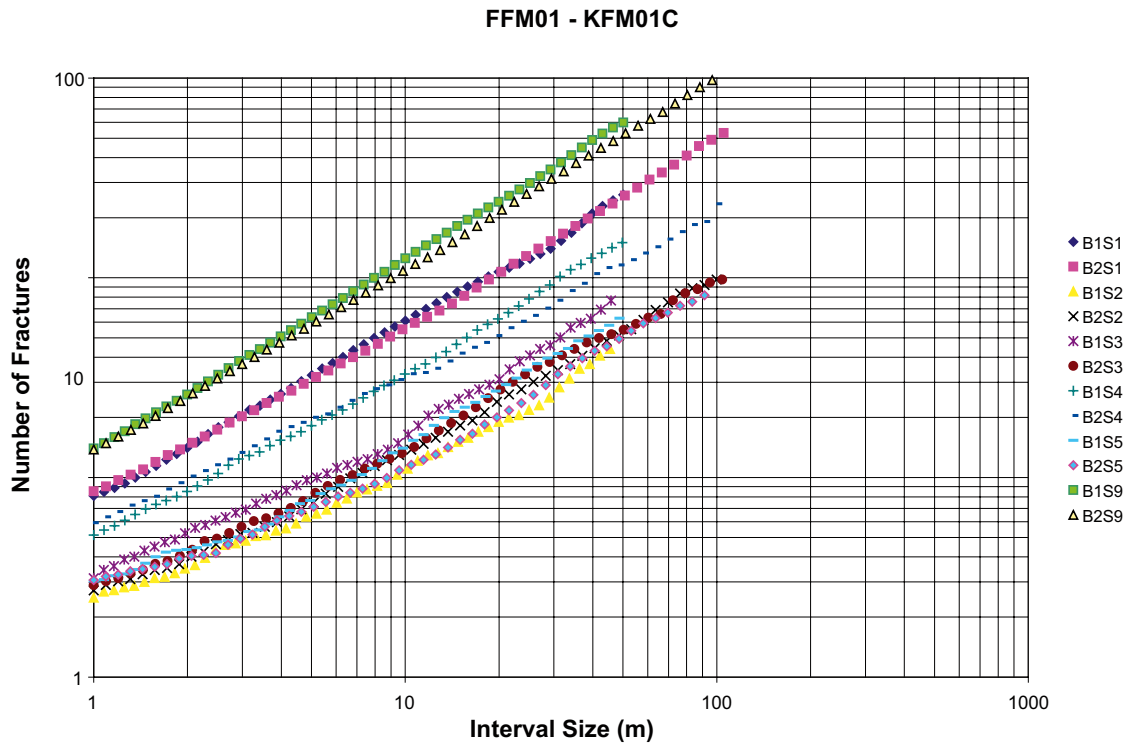
FFM01 - KFM01C

Figure 10-89. *Mass dimension plot for fracture data from KFM01C, Domain FFM01.*
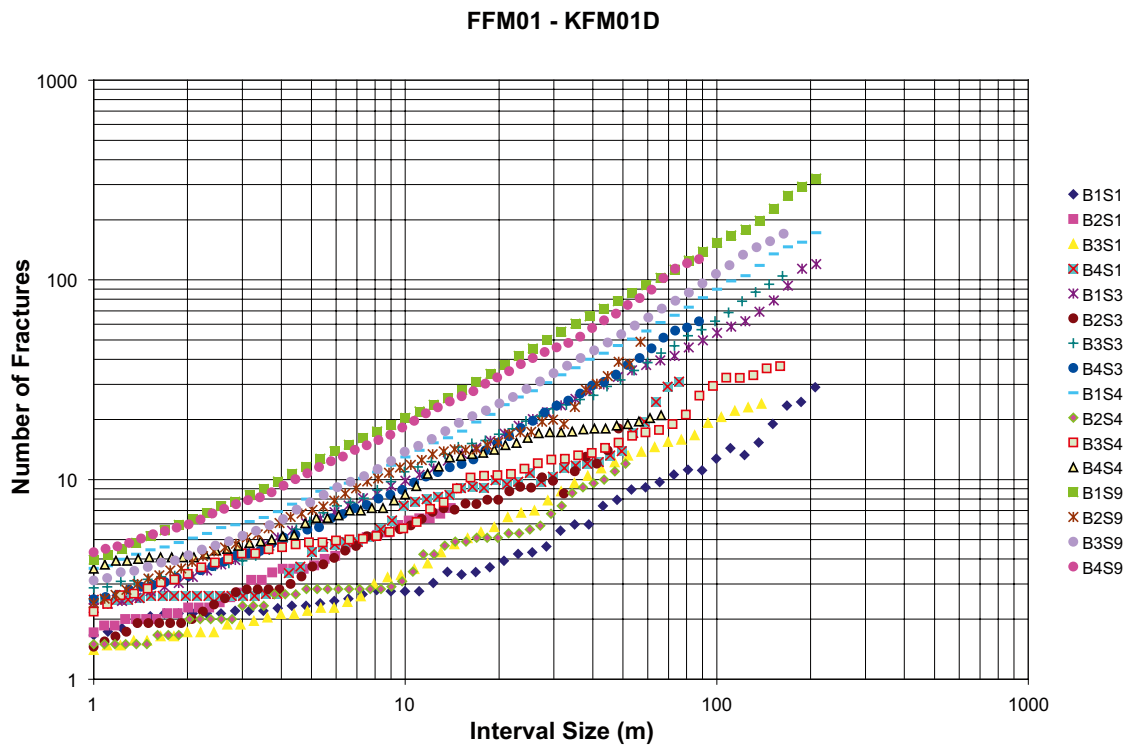
FFM01 - KFM01D

Figure 10-90. *Mass dimension plot for fracture data from KFM01D, Domain FFM01.*

53
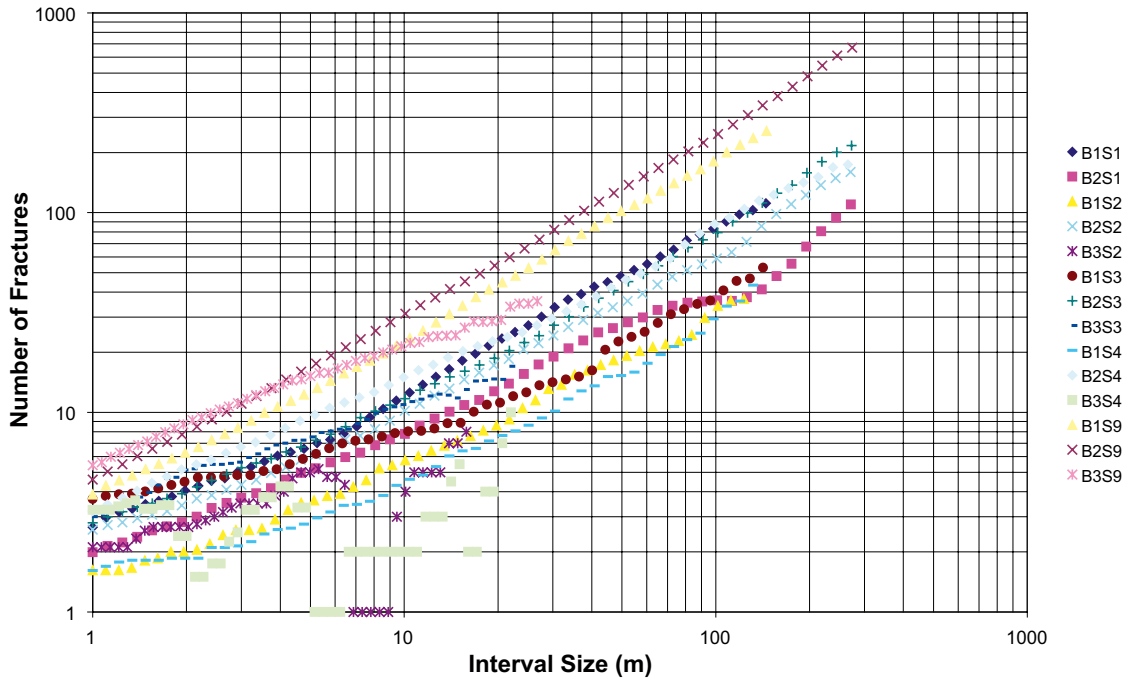
FFM01 - KFM04A

Figure 10-91. Mass dimension plot for fracture data from KFM04A, Domain FFM01.

FFM01 - KFM05A
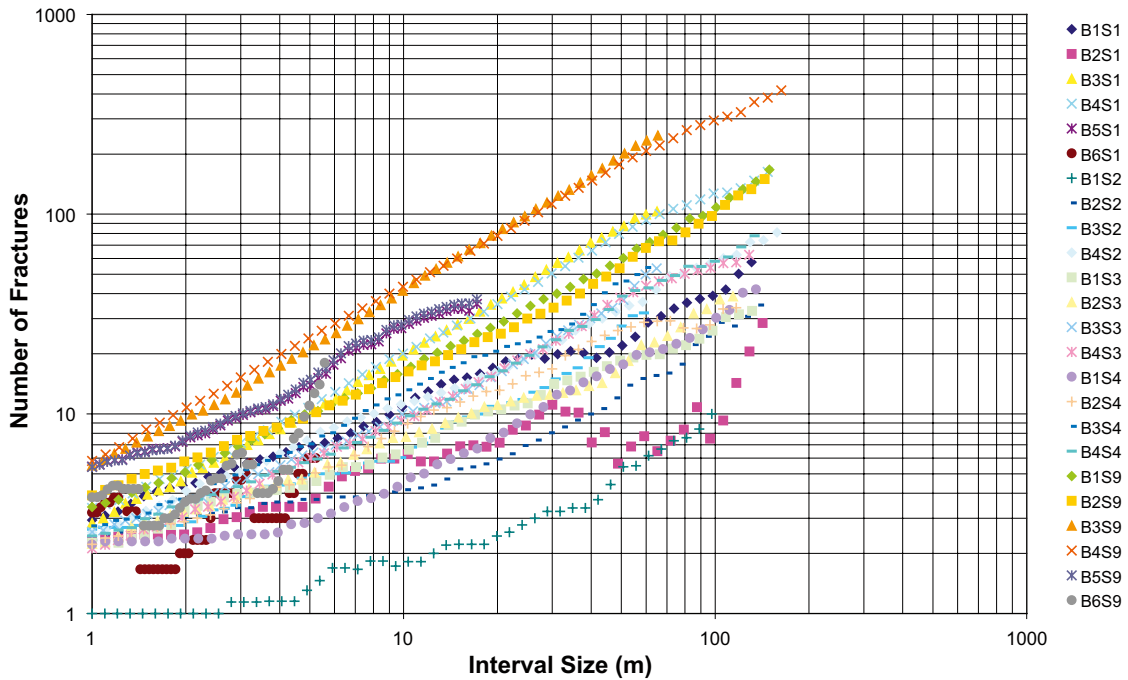
Figure 10-92. Mass dimension plot for fracture data from KFM05A, Domain FFM01.

FFM01 - KFM06A
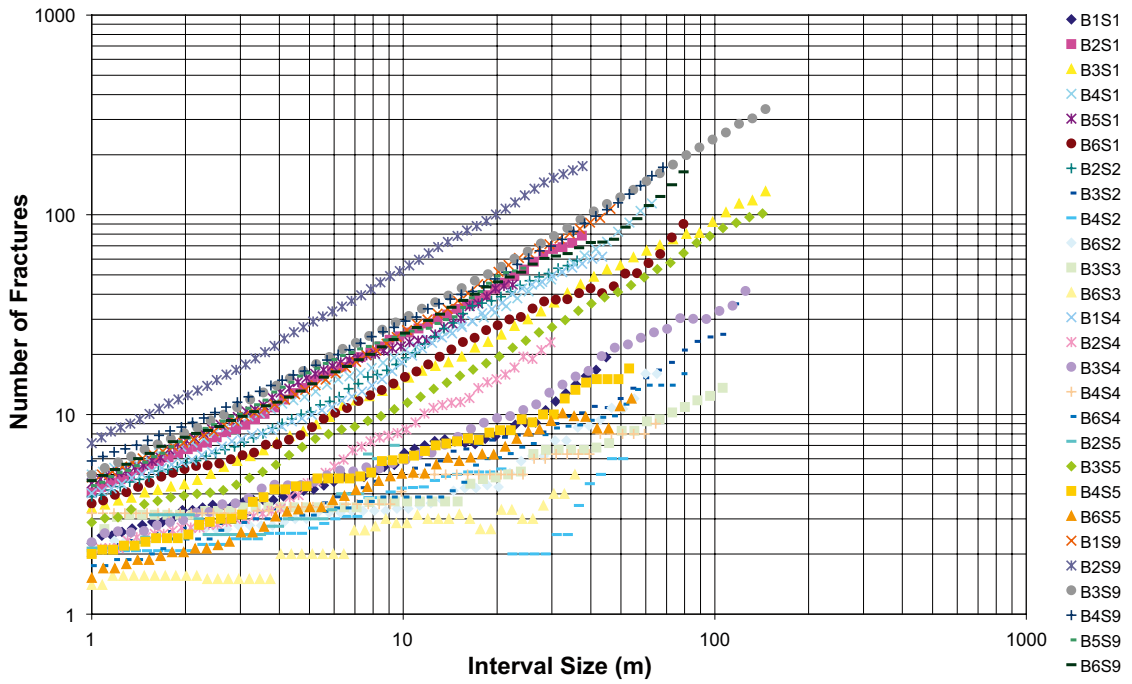
Figure 10-93. *Mass dimension plot for fracture data from KFM06A, Domain FFM01.*

FFM01 - KFM06C
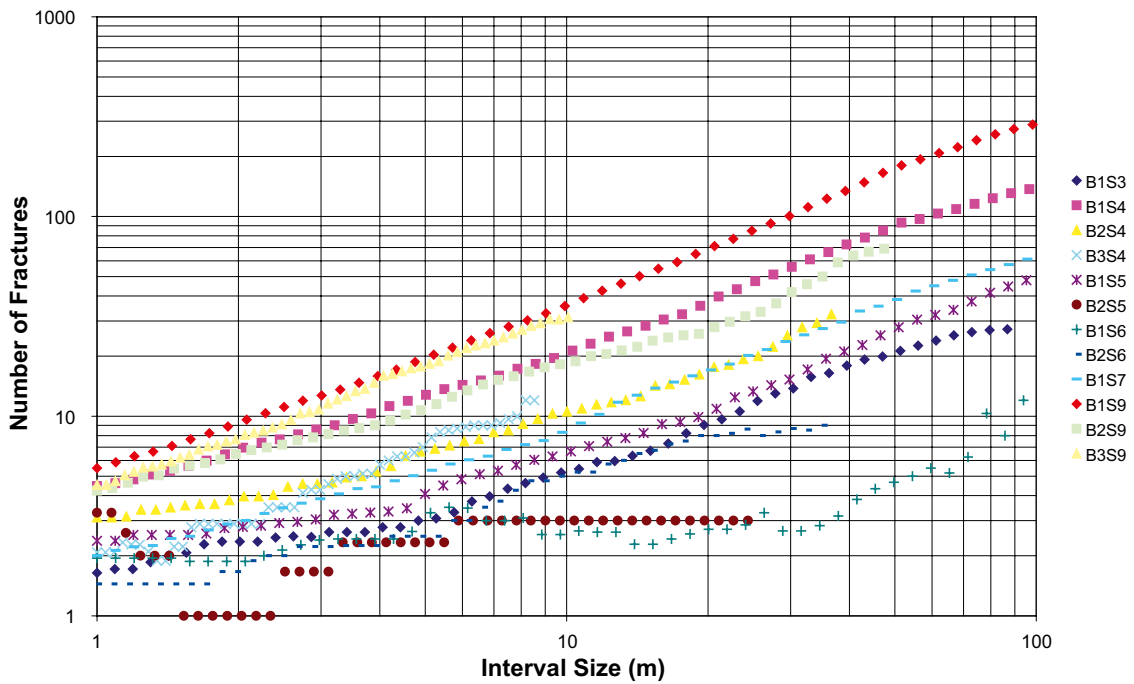
Figure 10-94. *Mass dimension plot for fracture data from KFM06C, Domain FFM01.*

FFM01 - KFM07A
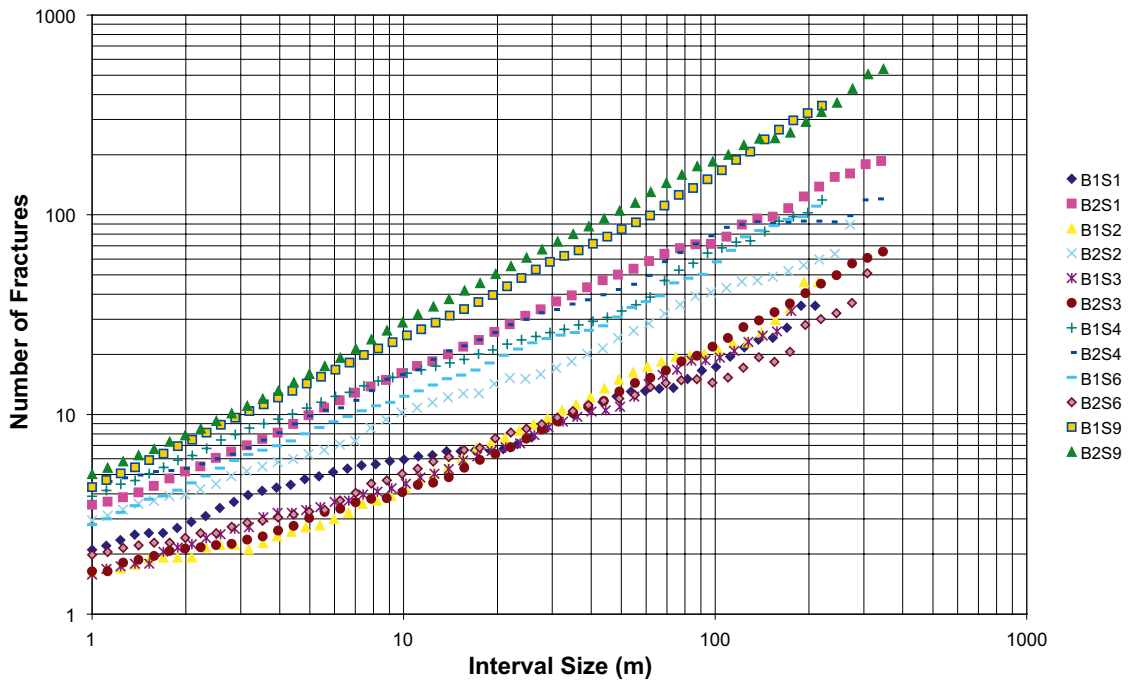
Figure 10-95. Mass dimension plot for fracture data from KFM07A, Domain FFM01.

FFM01 - KFM07B
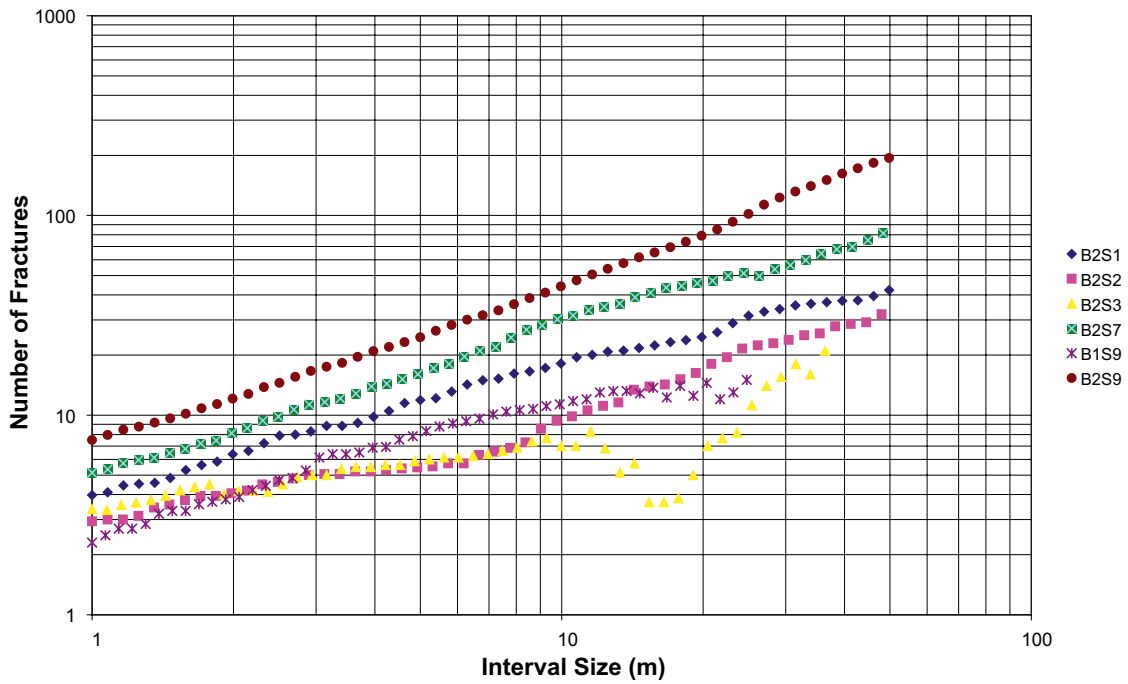
Figure 10-96. Mass dimension plot for fracture data from KFM07B, Domain FFM01.

FFM01 - KFM08A
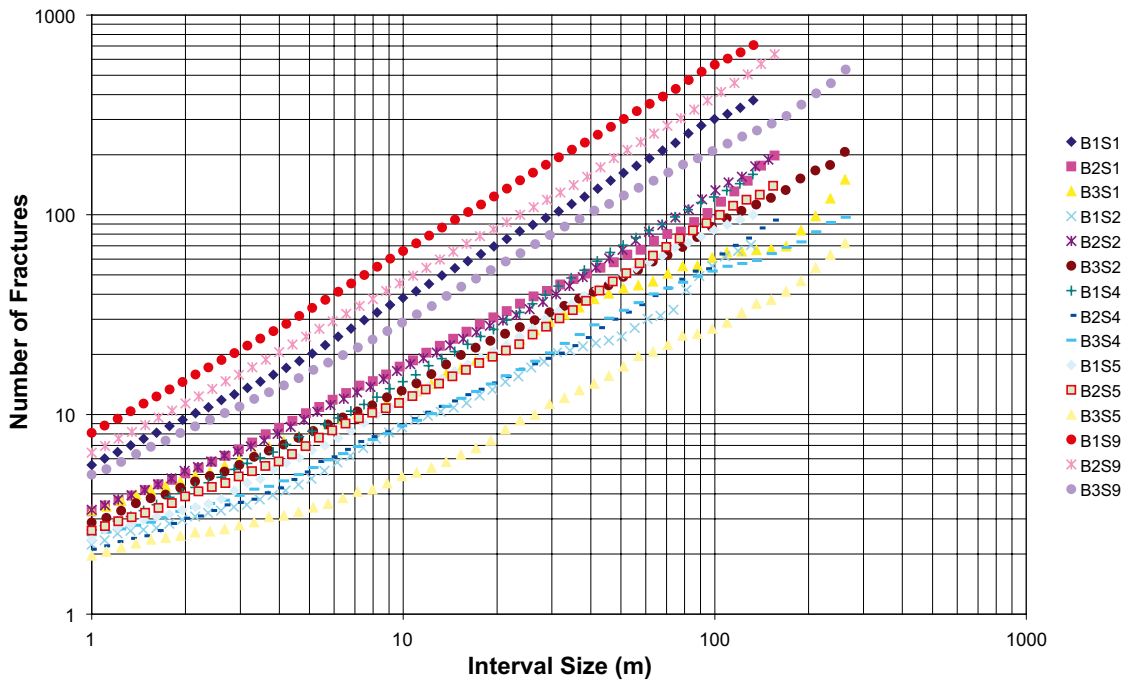
Figure 10-97. *Mass dimension plot for fracture data from KFM08A, Domain FFM01.*

FFM01 - KFM08B
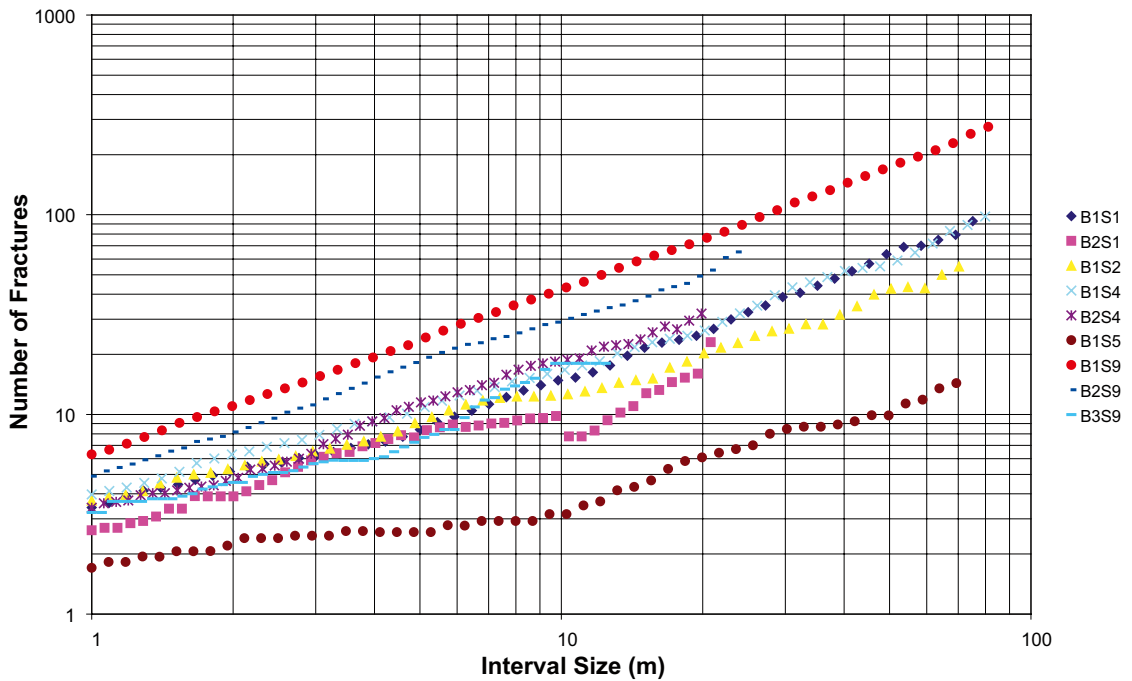
Figure 10-98. *Mass dimension plot for fracture data from KFM08B, Domain FFM01.*

FFM01 - KFM08C
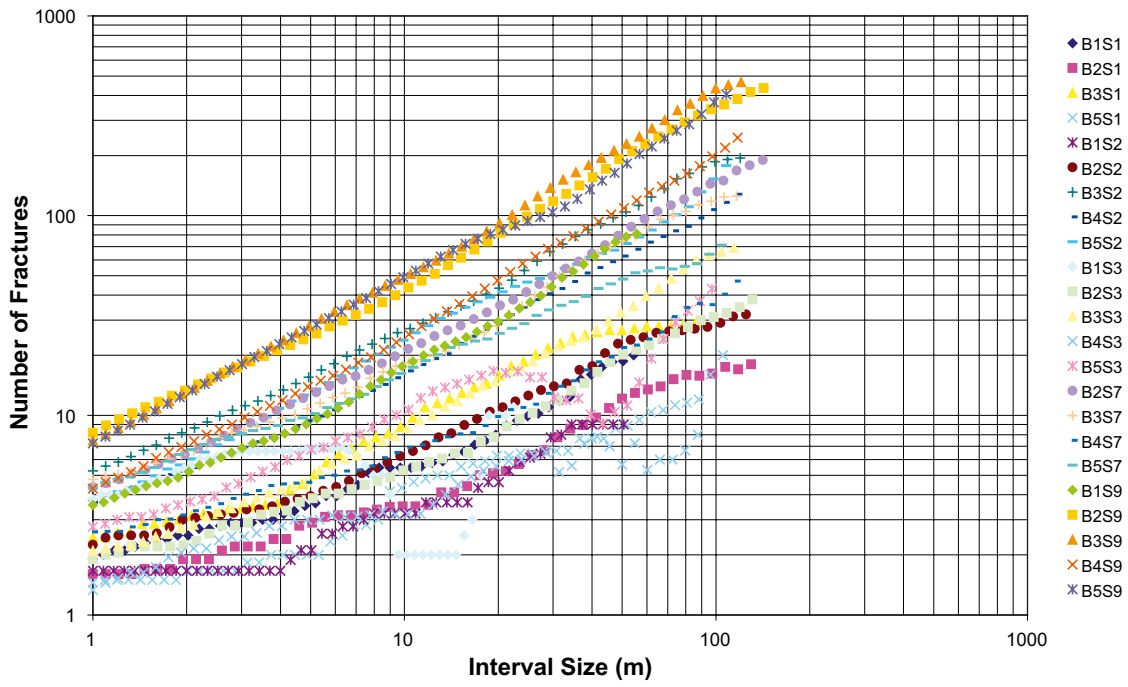
Figure 10-99. Mass dimension plot for fracture data from KFM08C, Domain FFM01.

FFM01 - KFM09A
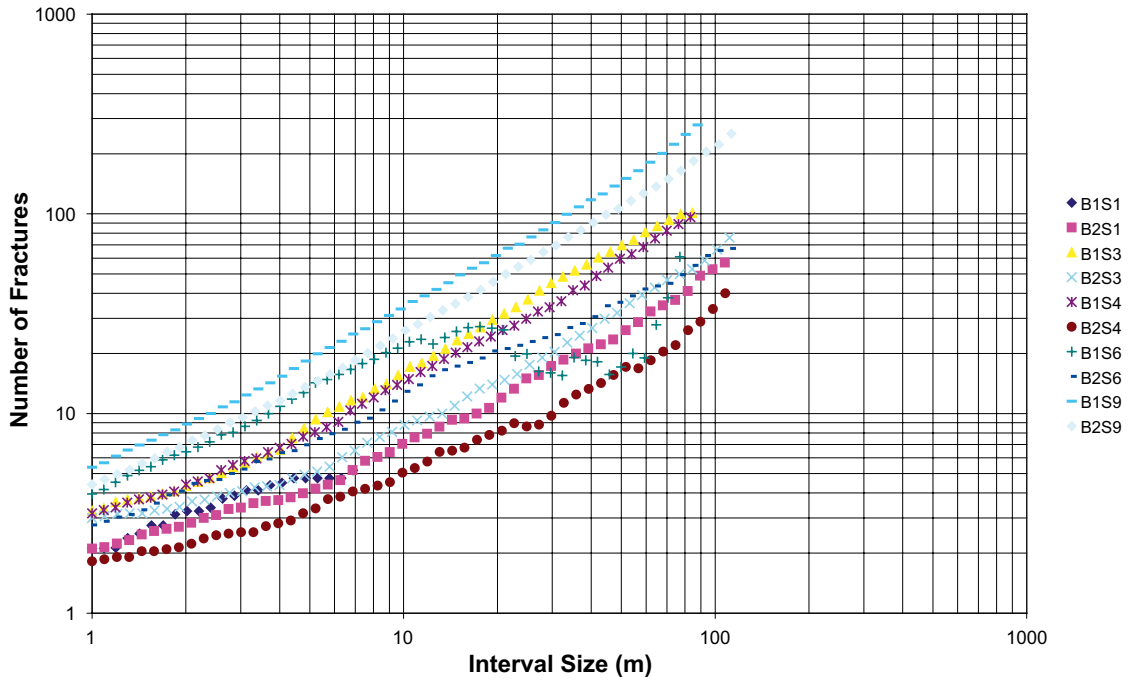
Figure 10-100. Mass dimension plot for fracture data from KFM09A, Domain FFM01.

58
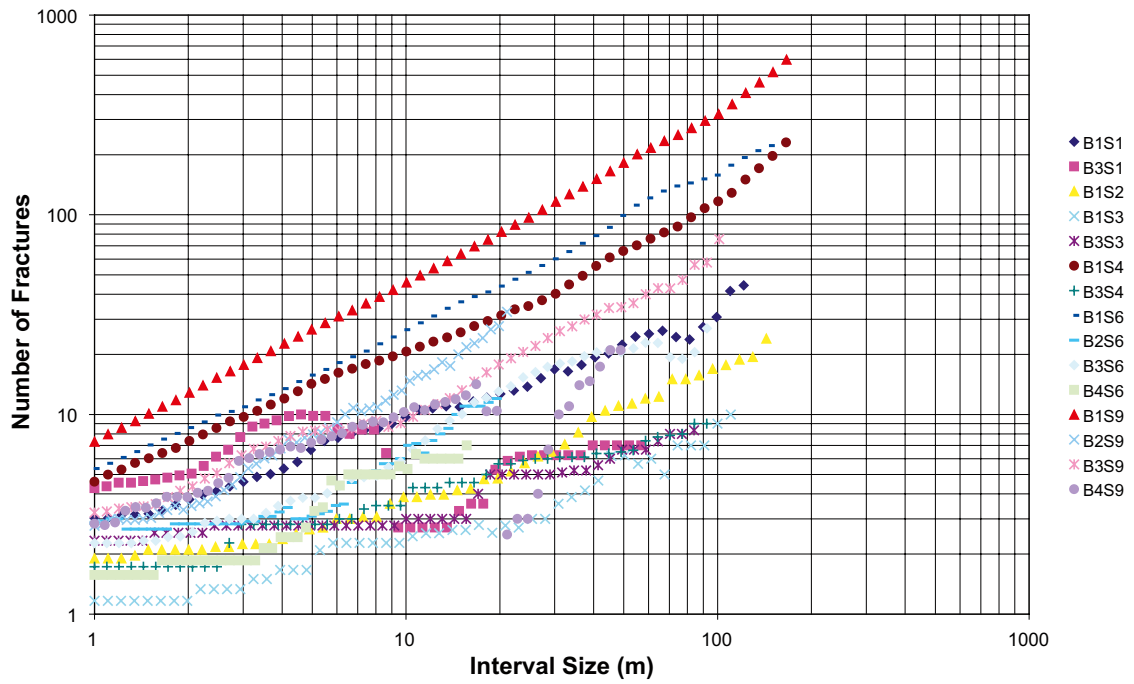
FFM01 - KFM09B

Figure 10-101. Mass dimension plot for fracture data from KFM09B, Domain FFM01.

FFM02 - KFM01A
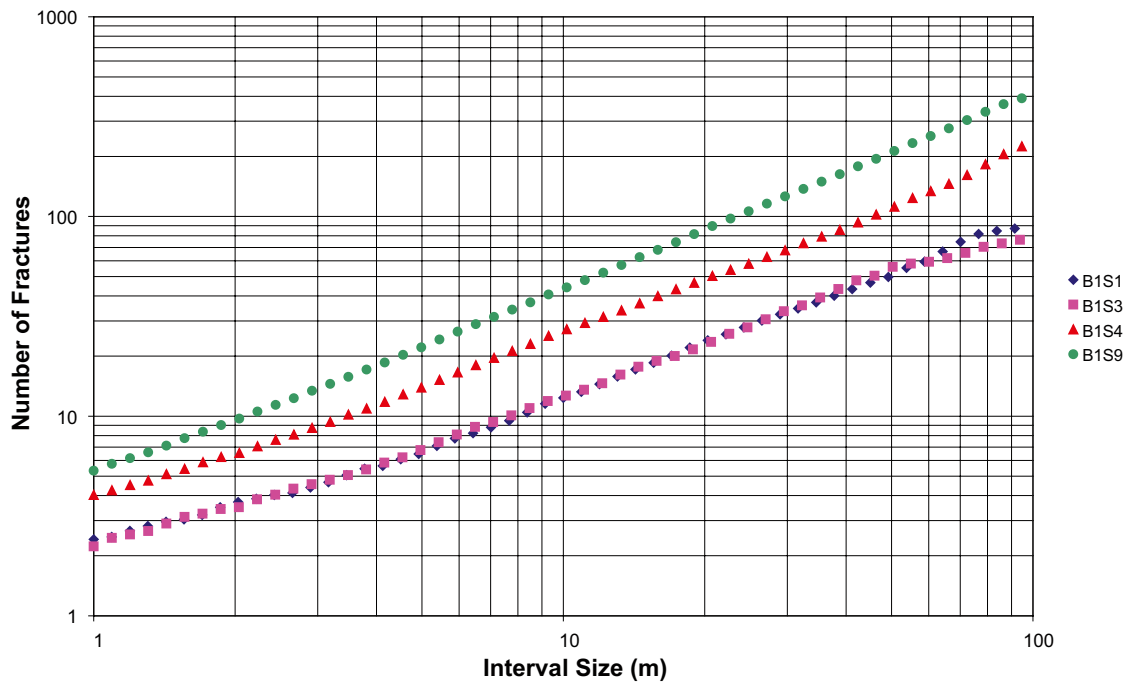
Figure 10-102. Mass dimension plot for fracture data from KFM01A, Domain FFM02.
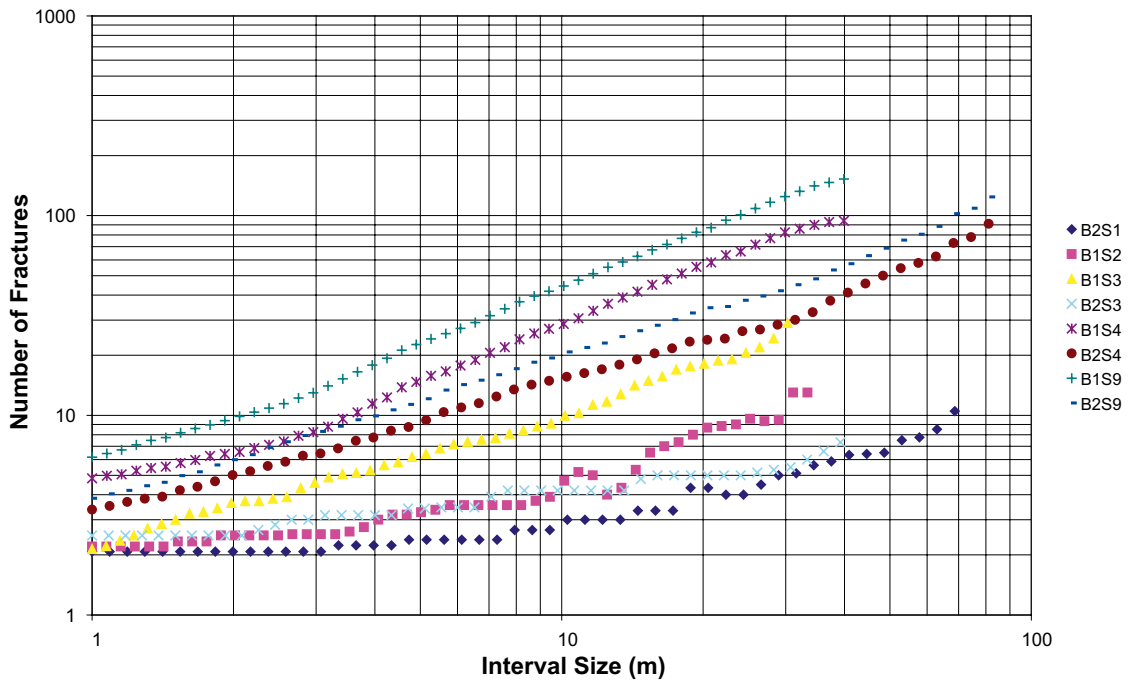
Figure 10-103. *Mass dimension plot for fracture data from KFM01B, Domain FFM02.*
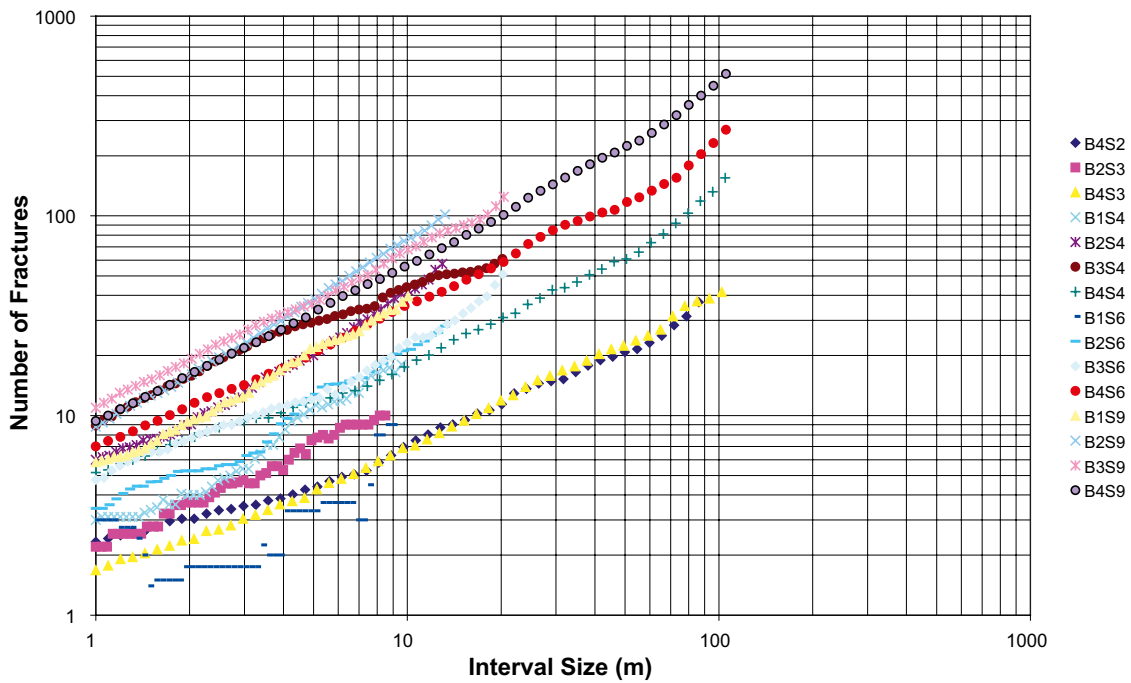
Figure 10-104. *Mass dimension plot for fracture data from KFM01C, Domain FFM02.*
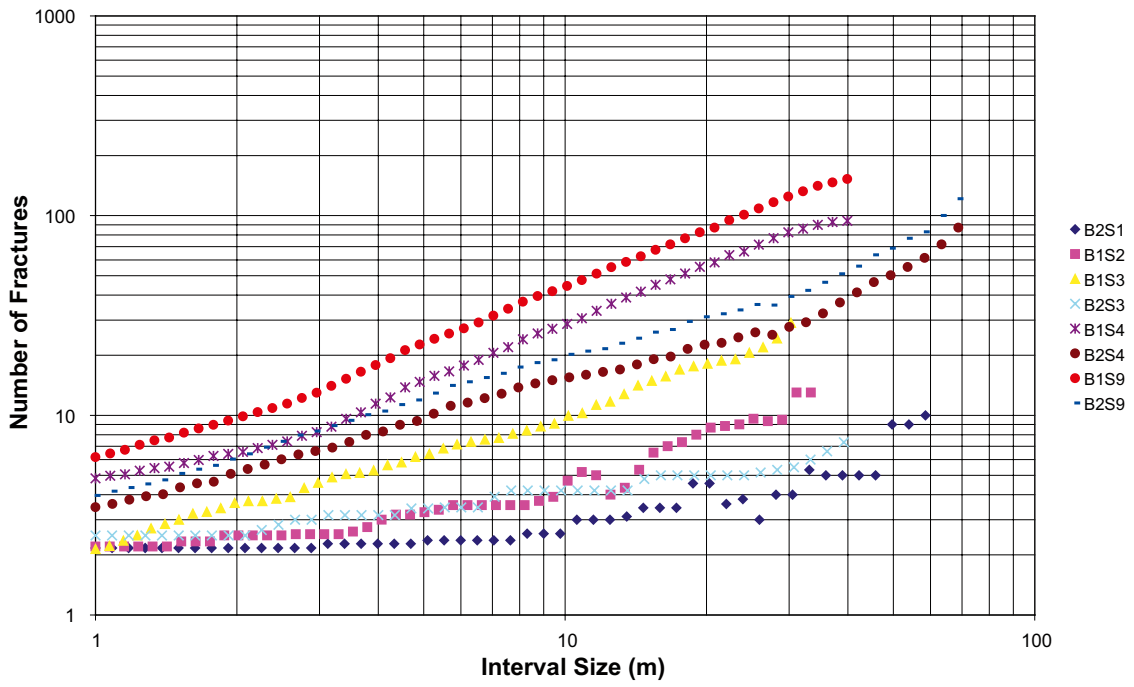
Figure 10-105. *Mass dimension plot for fracture data from KFM01D, Domain FFM02.*
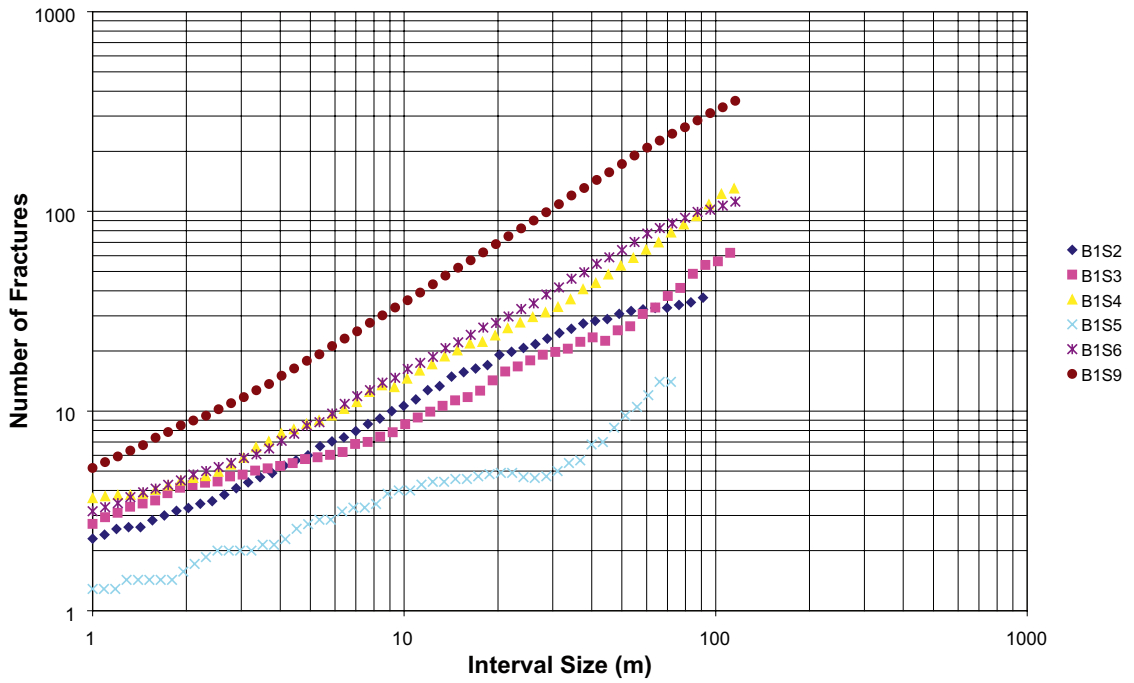
Figure 10-106. *Mass dimension plot for fracture data from KFM05A, Domain FFM02.*
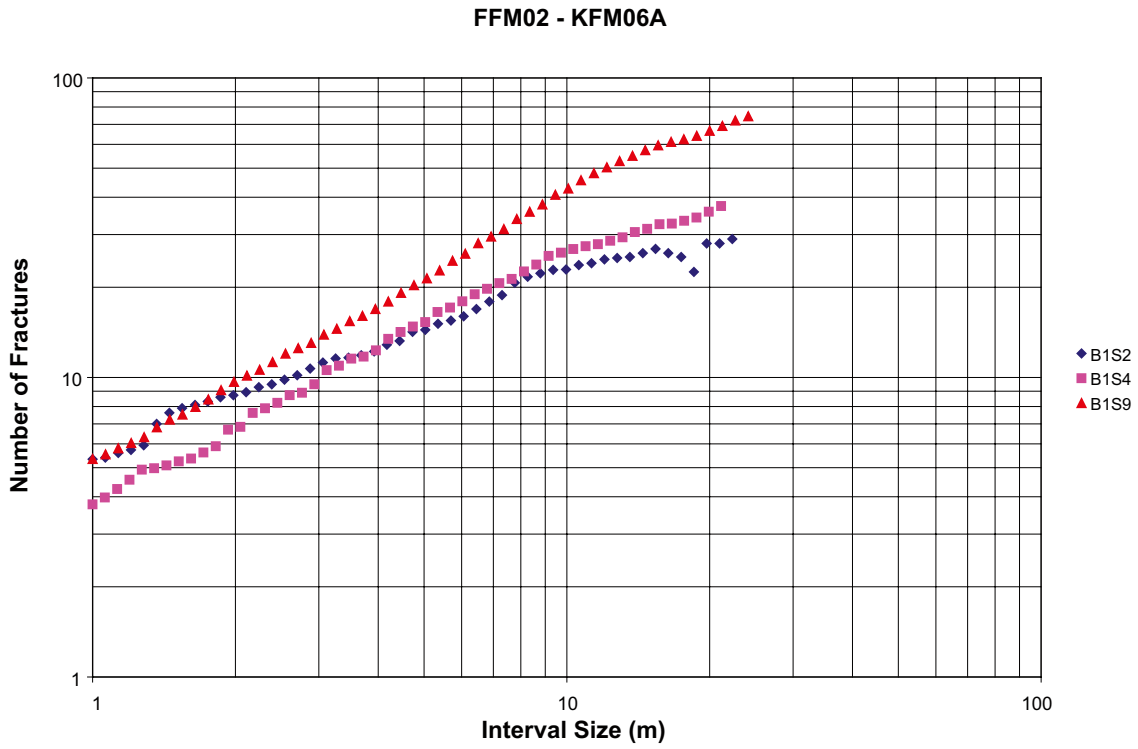
FFM02 - KFM06A

Figure 10-107. Mass dimension plot for fracture data from KFM06A, Domain FFM02.
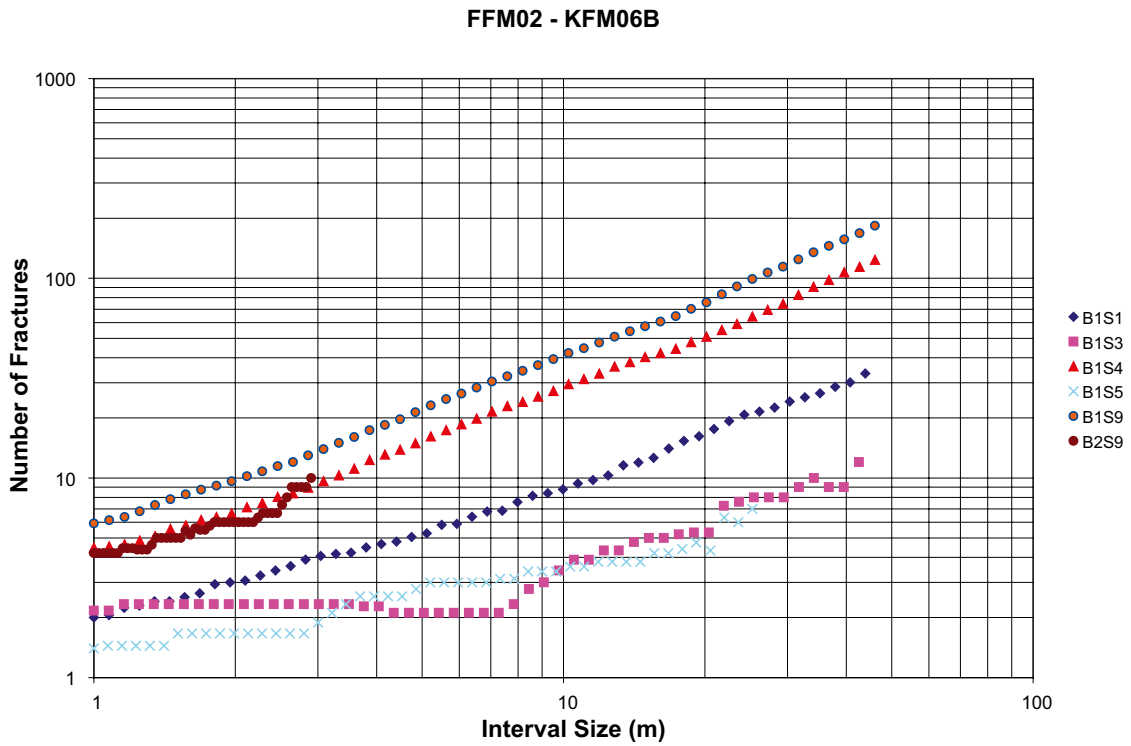
FFM02 - KFM06B

Figure 10-108. Mass dimension plot for fracture data from KFM06B, Domain FFM02.

FFM02 - KFM07B
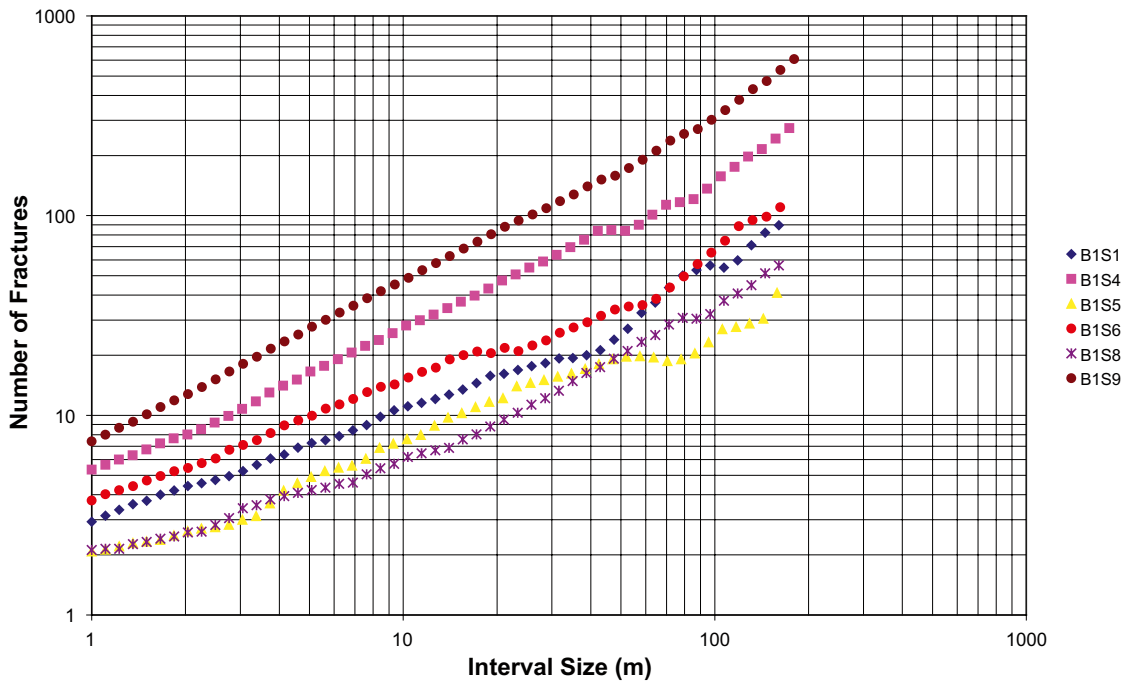
Figure 10-109. Mass dimension plot for fracture data from KFM07B, Domain FFM02.

FFM02 - KFM08B
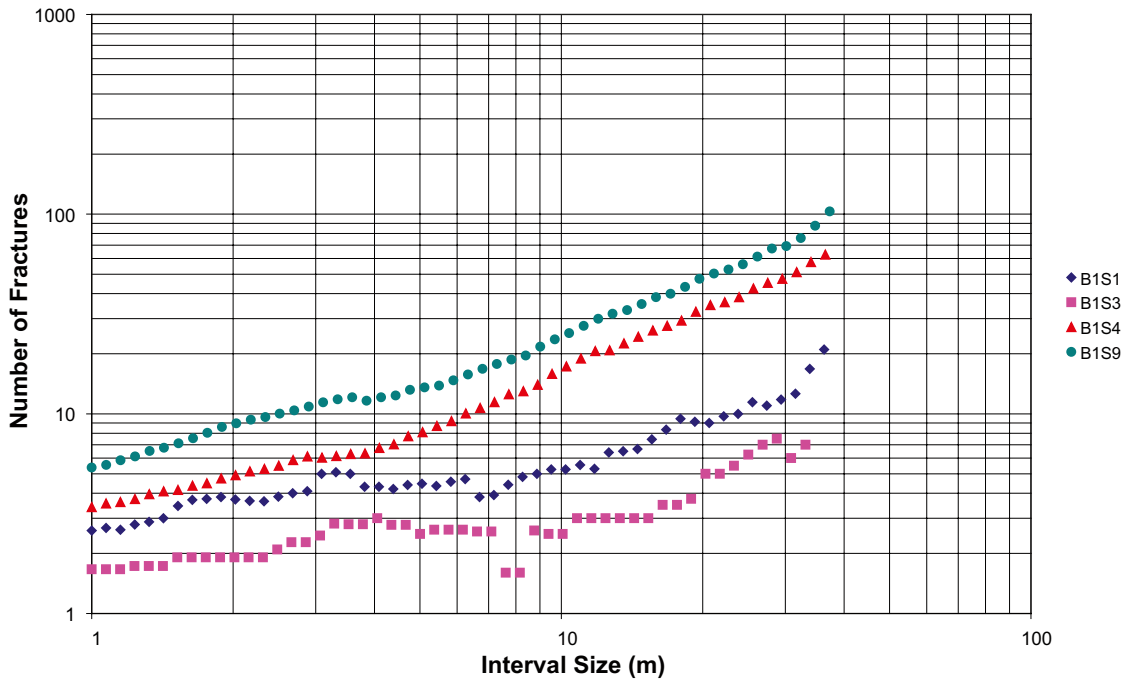
Figure 10-110. Mass dimension plot for fracture data from KFM08B, Domain FFM02.

FFM02 - KFM09A
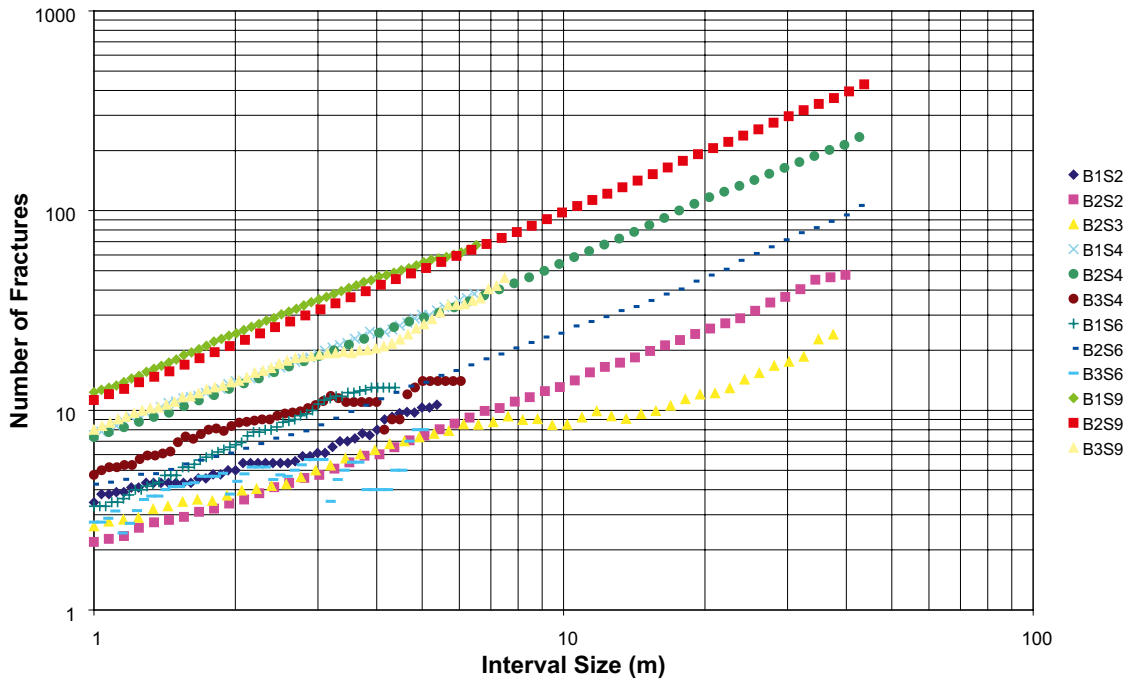
Figure 10-111. Mass dimension plot for fracture data from KFM09A, Domain FFM02.

FFM02 - KFM09B
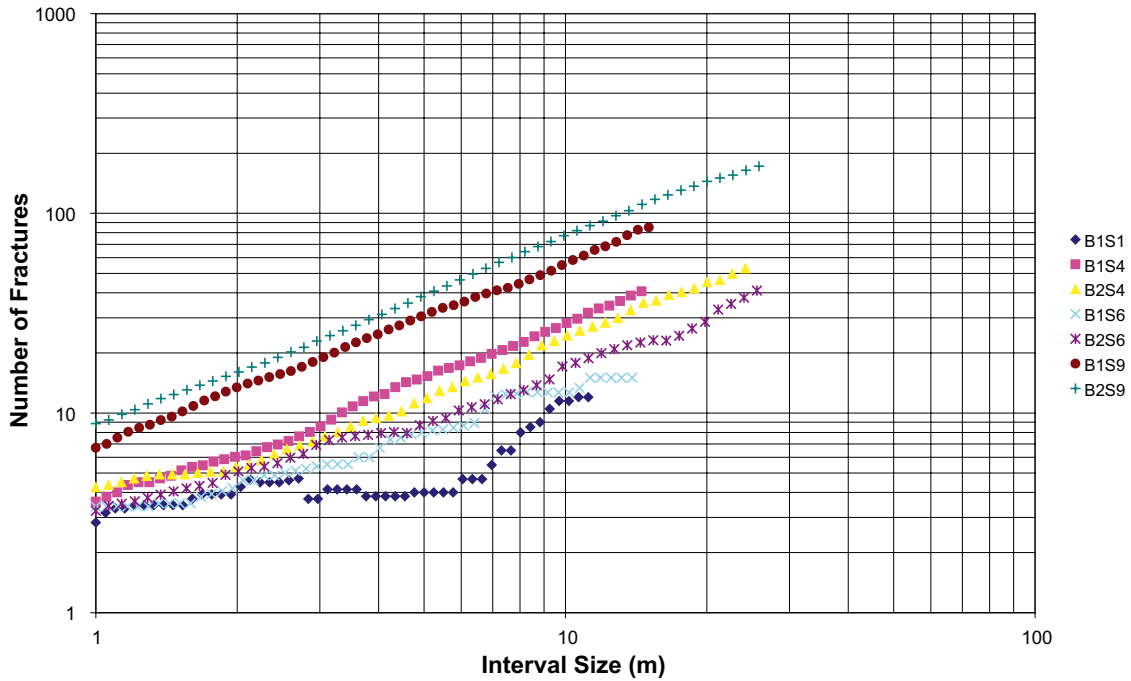
Figure 10-112. Mass dimension plot for fracture data from KFM09B, Domain FFM02.
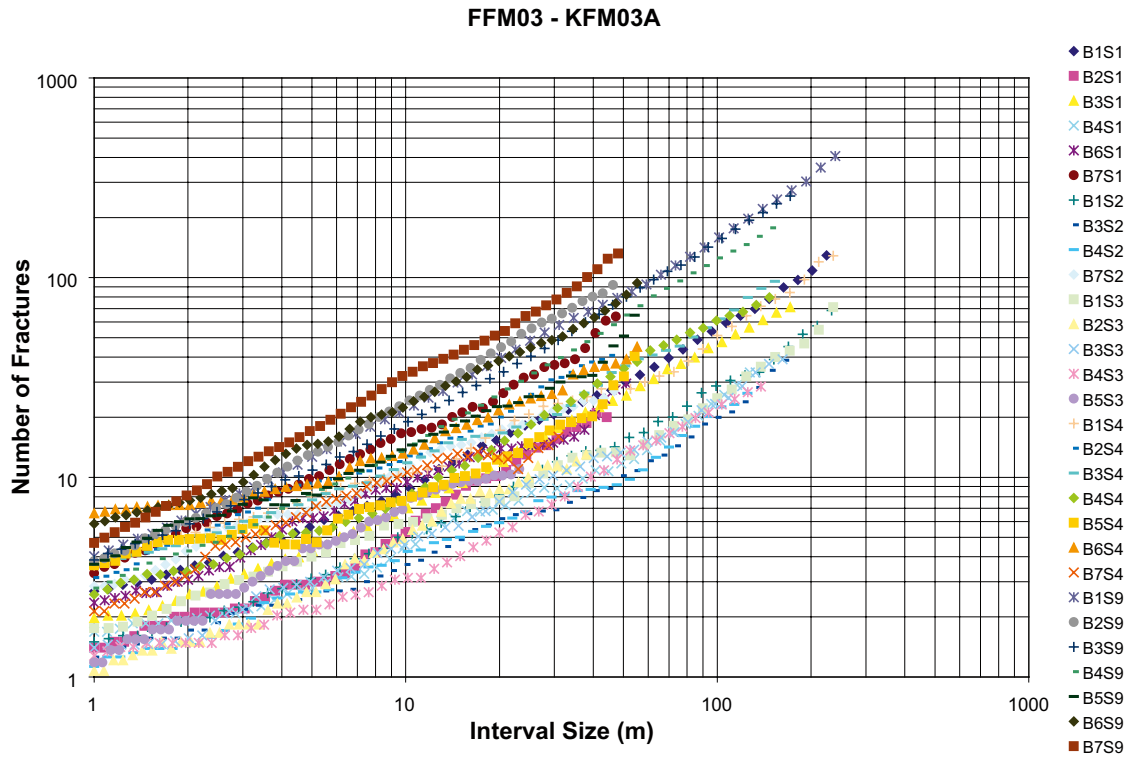
Figure 10-113. *Mass dimension plot for fracture data from KFM03A, Domain FFM03.*
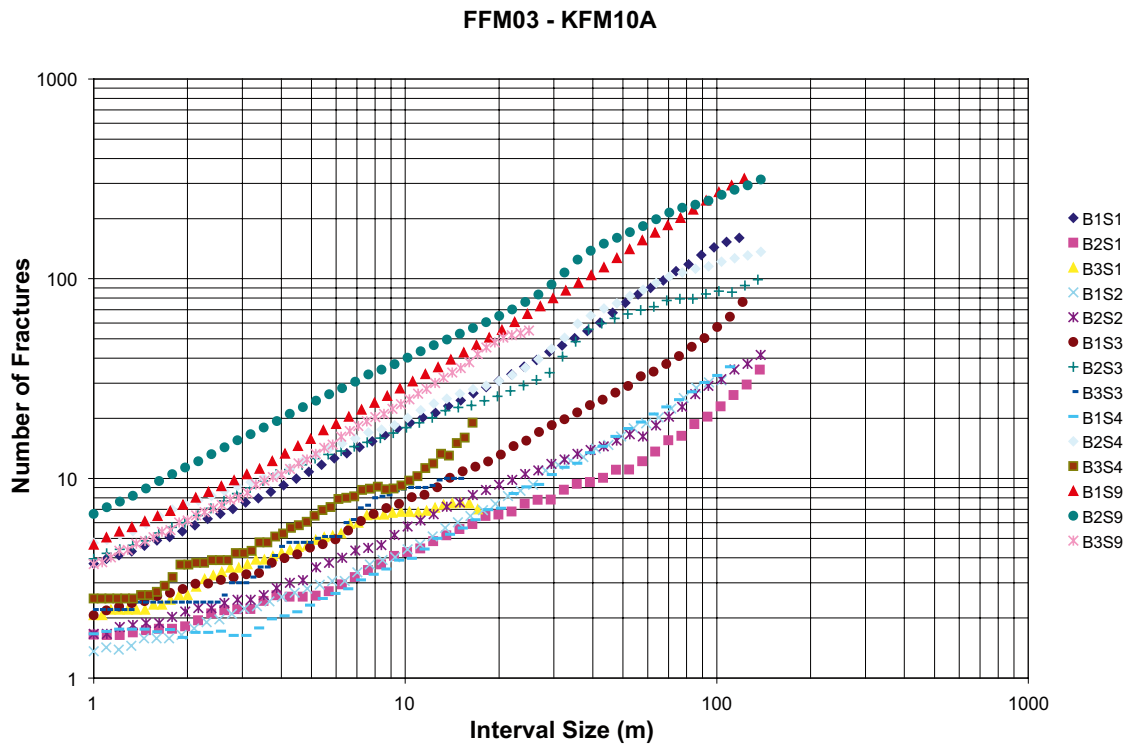
Figure 10-114. *Mass dimension plot for fracture data from KFM10A, Domain FFM03.*

Semivariograms for spatial analysis
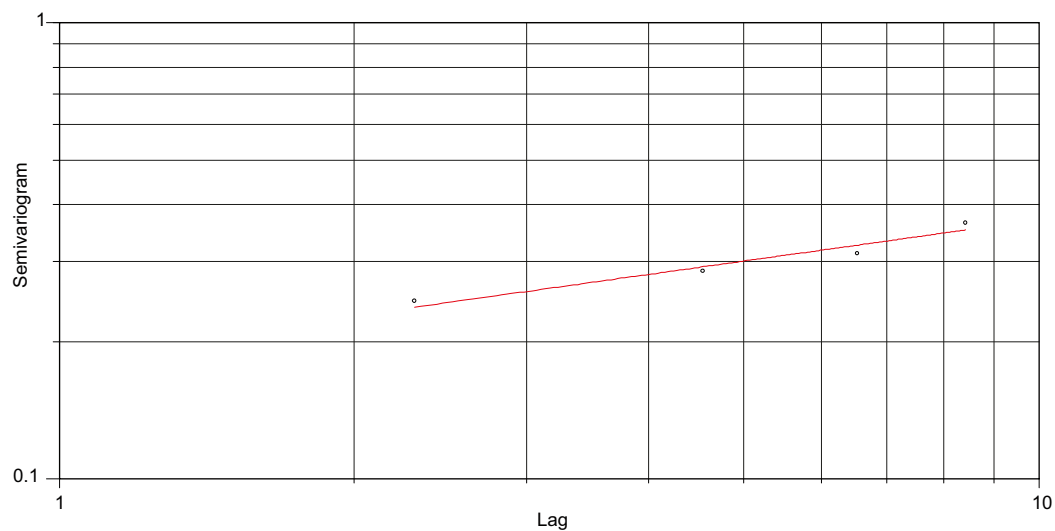
Figure 11-1. *Semivariogram for fracture intensity, AFM000053, NE Set, unlinked traces.*
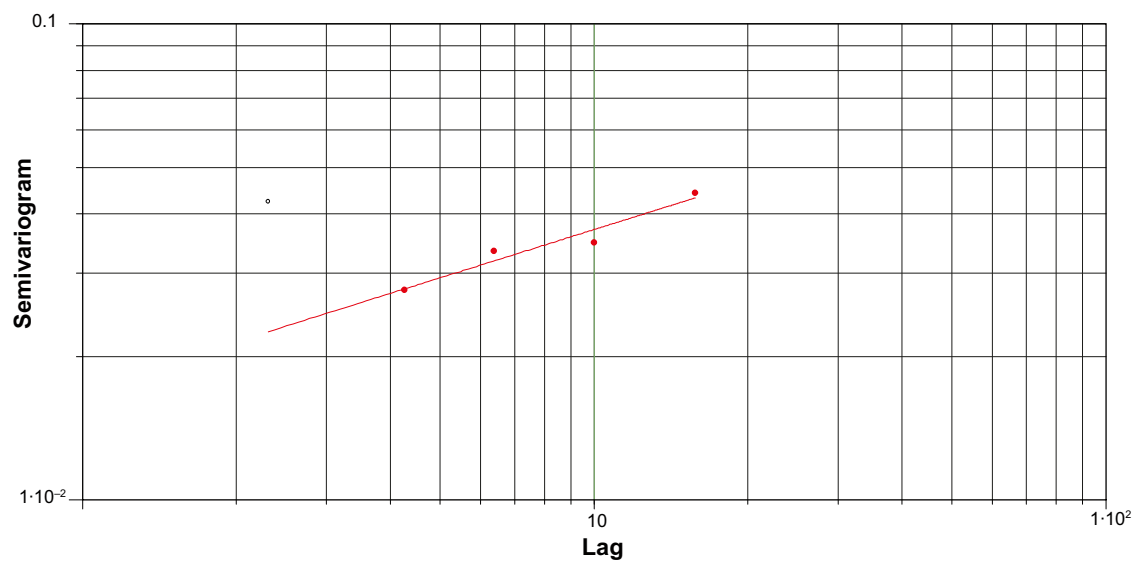
Figure 11-2. *Semivariogram for fracture intensity, AFM000053, NS Set, unlinked traces.*
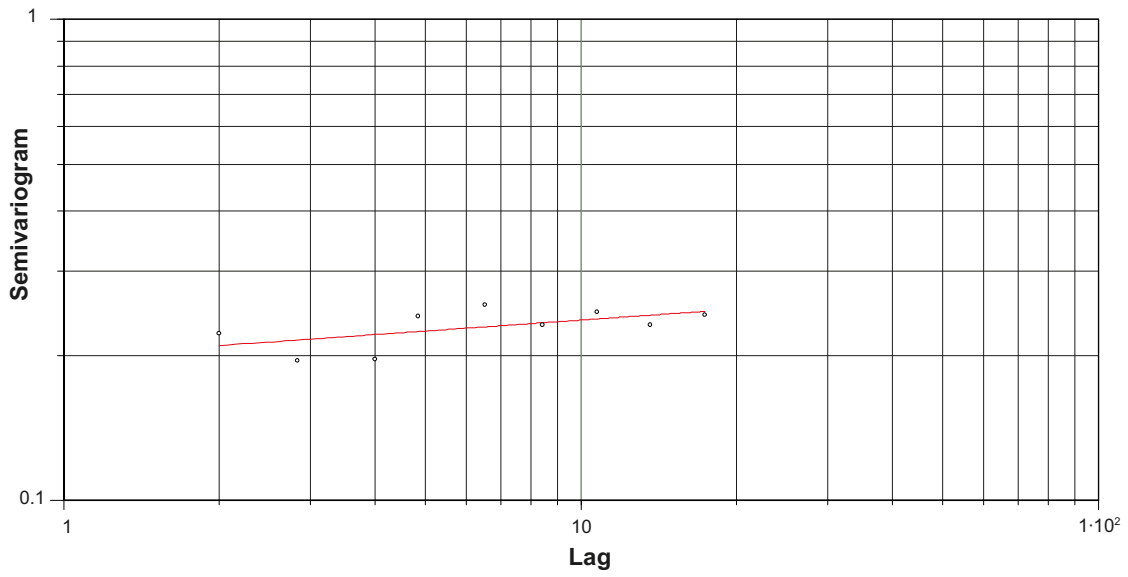
Figure 11-3. *Semivariogram for fracture intensity, AFM000053, NW Set, unlinked traces.*
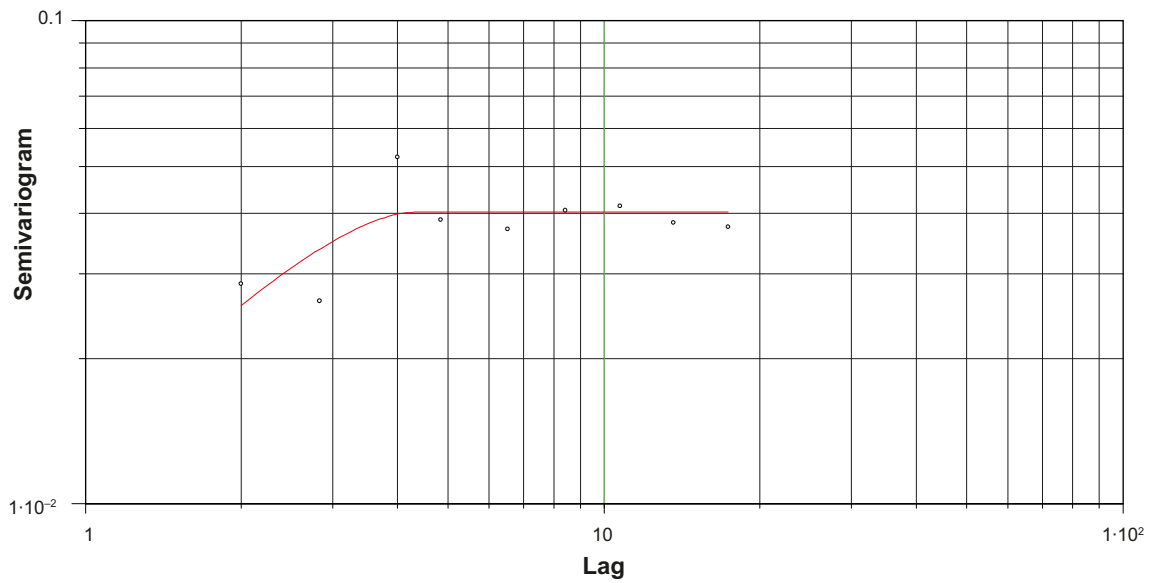
Figure 11-4. *Semivariogram for fracture intensity, AFM000053, SH Set, unlinked traces.*
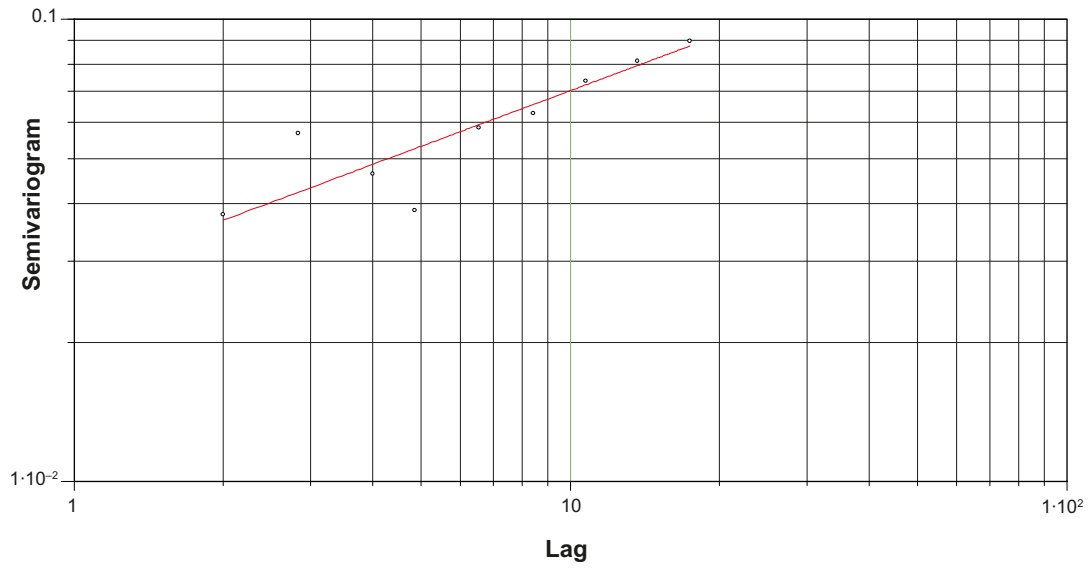
Figure 11-5. *Semivariogram for fracture intensity, AFM000053, ENE Set, unlinked traces.*
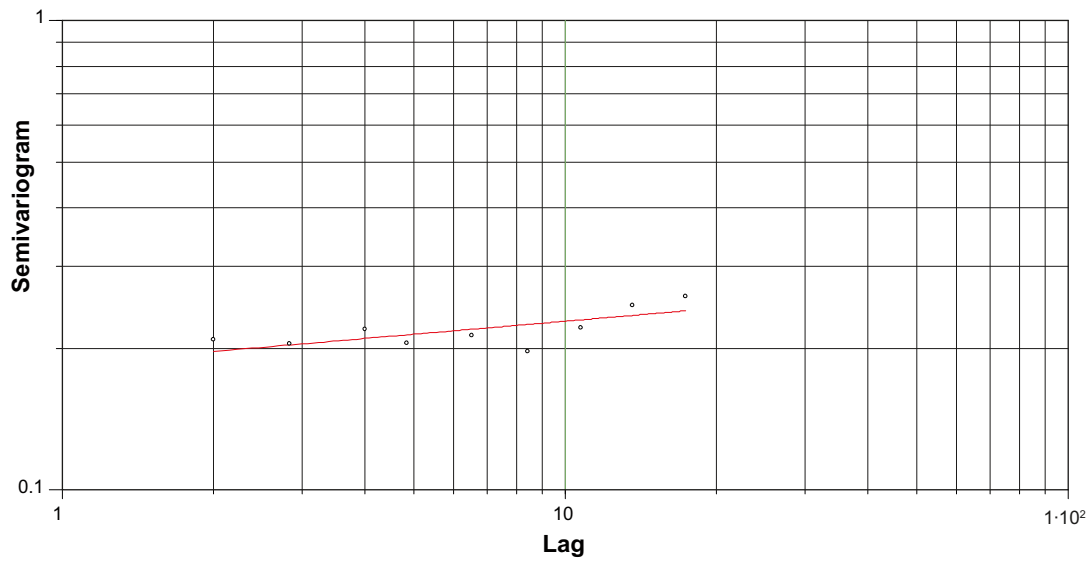
Figure 11-6. *Semivariogram for fracture intensity, AFM000053, WNW Set, unlinked traces.*
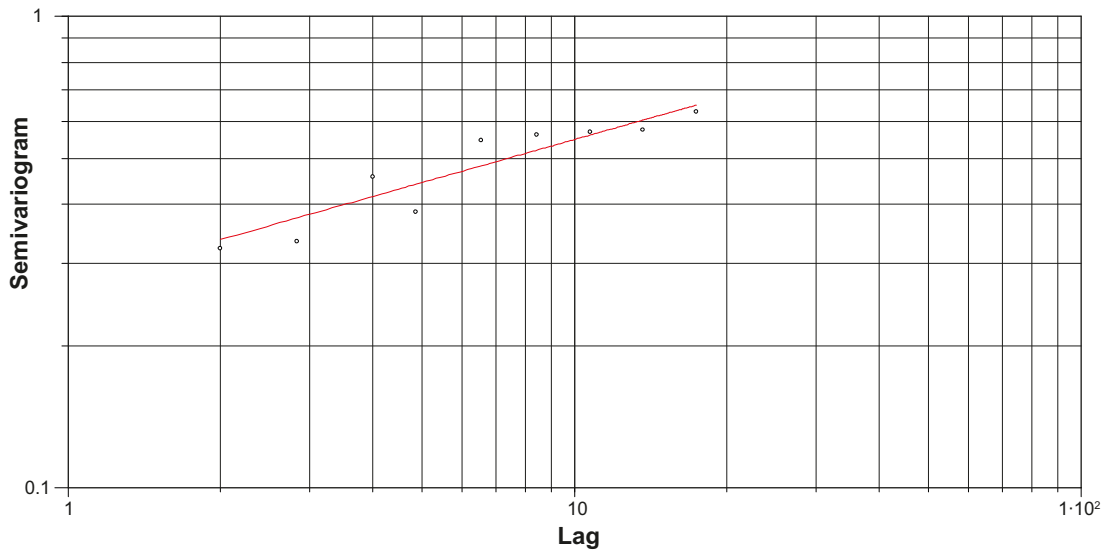
Figure 11-7. *Semivariogram for fracture intensity, AFM000054, NE Set, unlinked traces.*
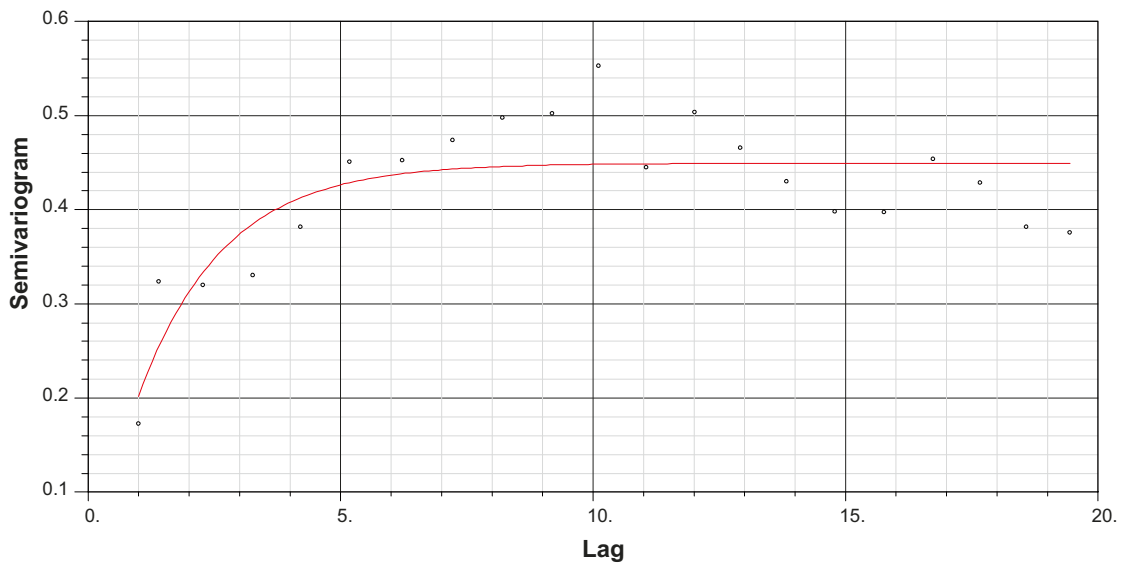
Figure 11-8. *Semivariogram for fracture intensity, AFM000054, NS Set, unlinked traces.*
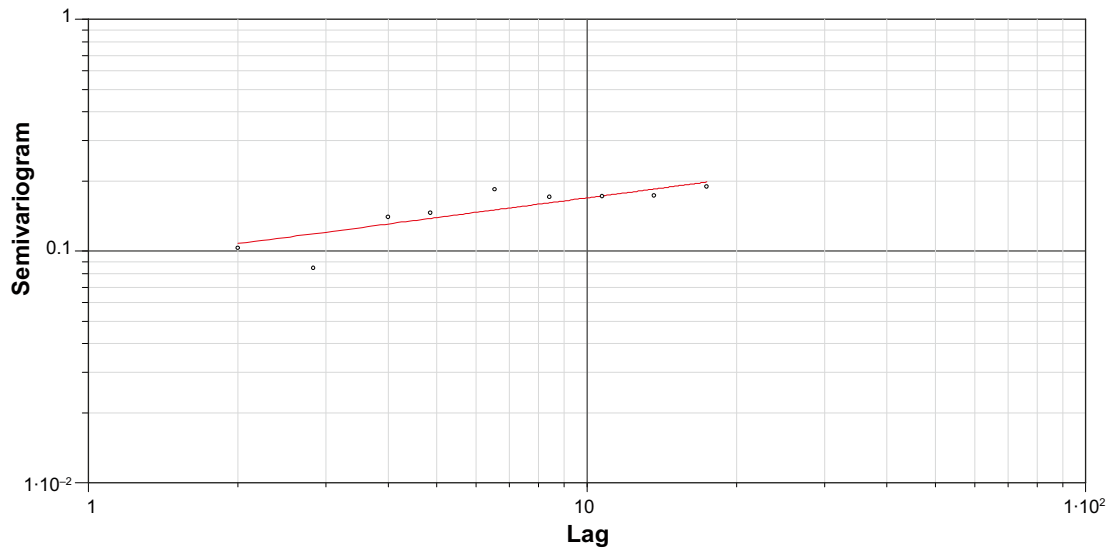
Figure 11-9. *Semivariogram for fracture intensity, AFM000054, NW Set, unlinked traces.*
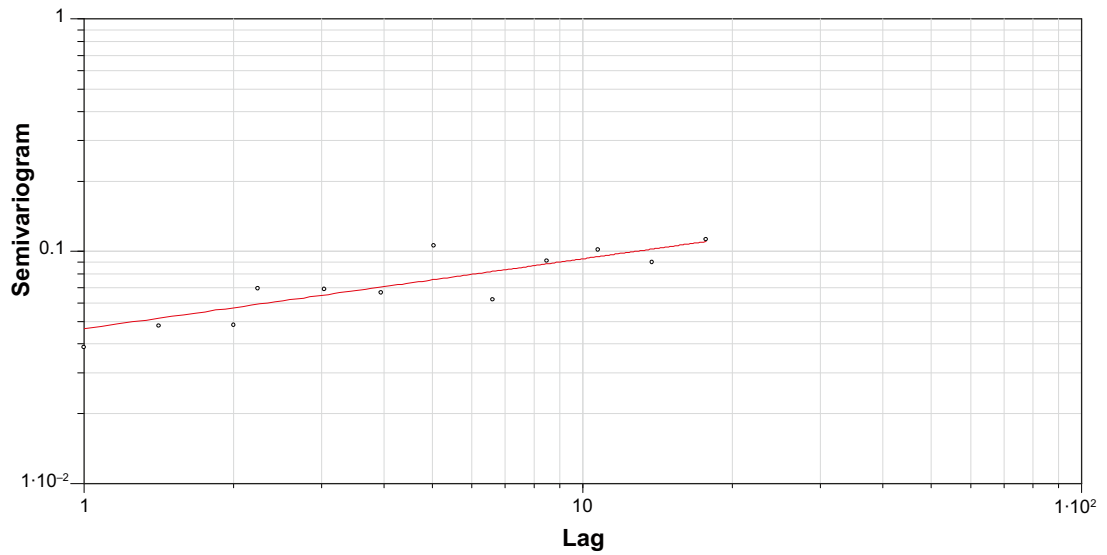
Figure 11-10. *Semivariogram for fracture intensity, AFM000054, SH Set, unlinked traces.*
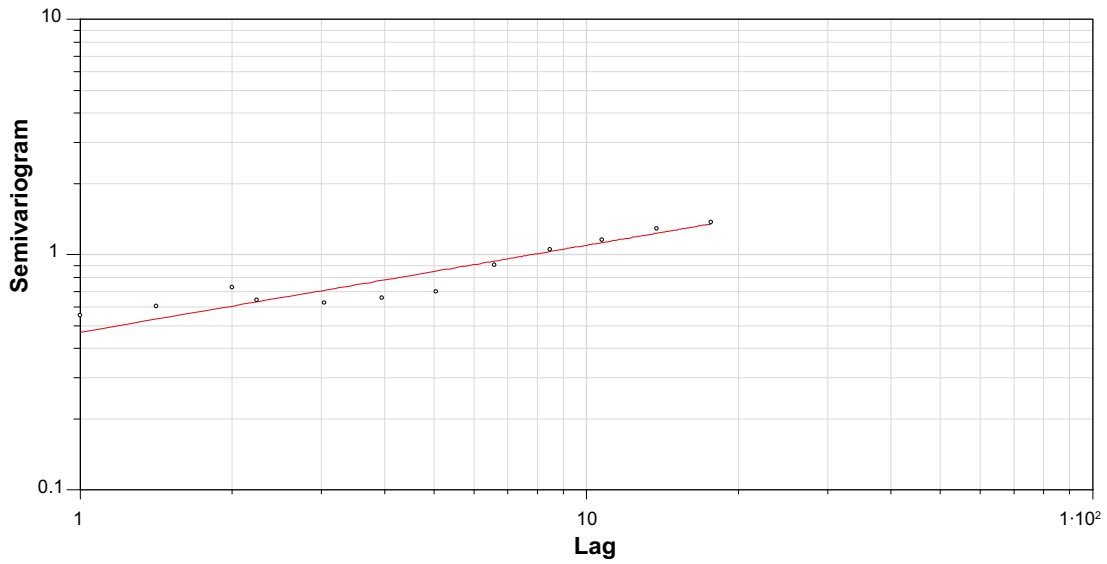
Figure 11-11. *Semivariogram for fracture intensity, AFM000053, WNW Set, unlinked traces.*
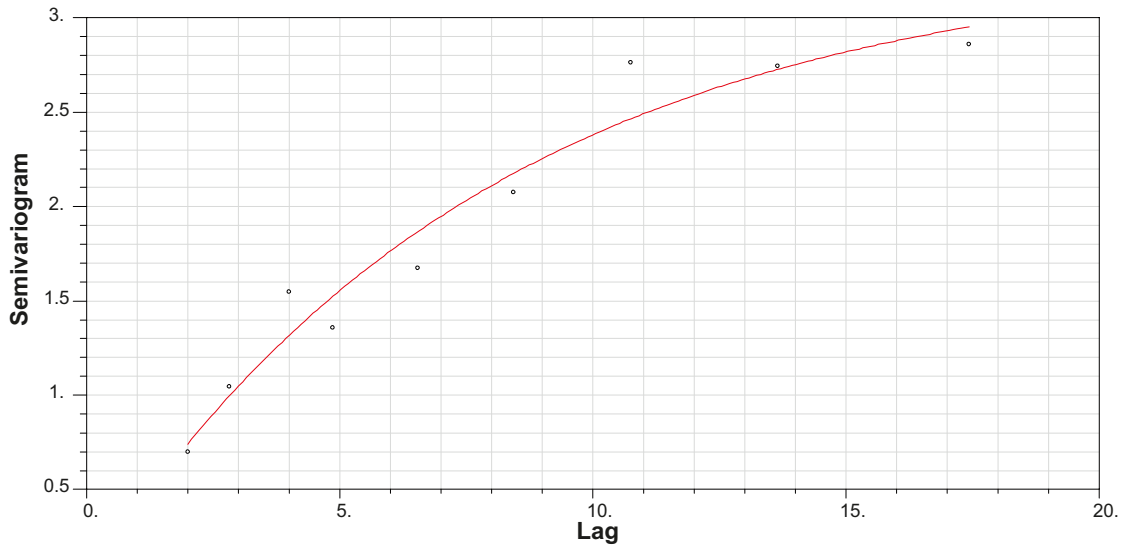
Figure 11-12. *Semivariogram for fracture intensity, AFM001097, NE Set, unlinked traces.*
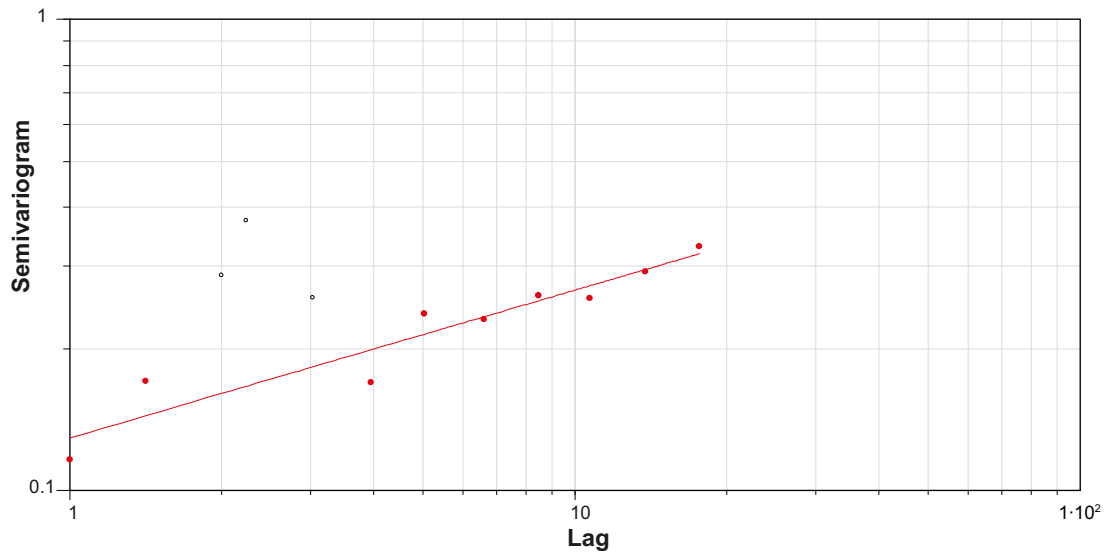
Figure 11-13. *Semivariogram for fracture intensity, AFM001097, NS Set, unlinked traces.*
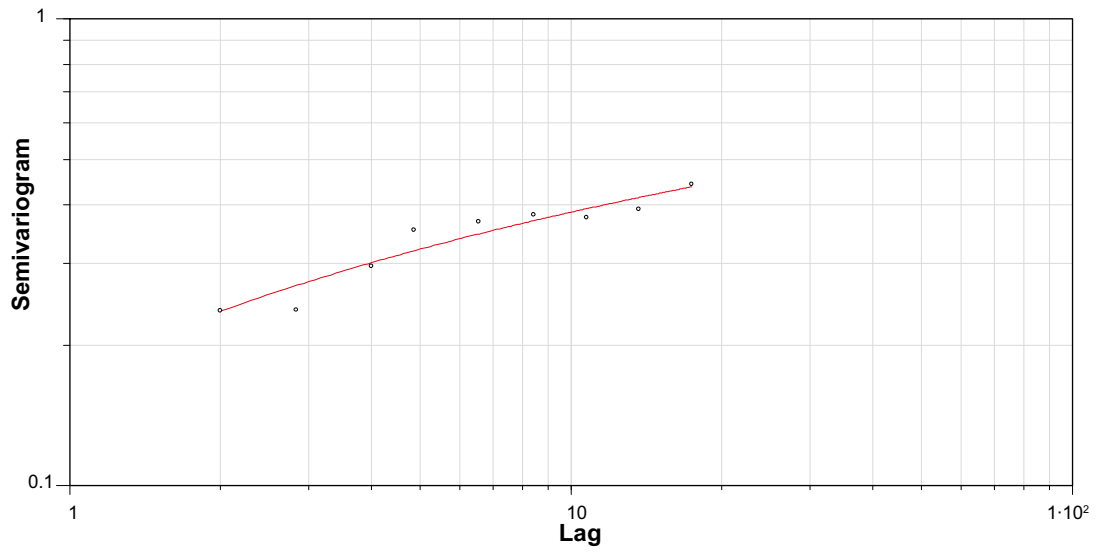
Figure 11-14. *Semivariogram for fracture intensity, AFM001097, NW Set, unlinked traces.*
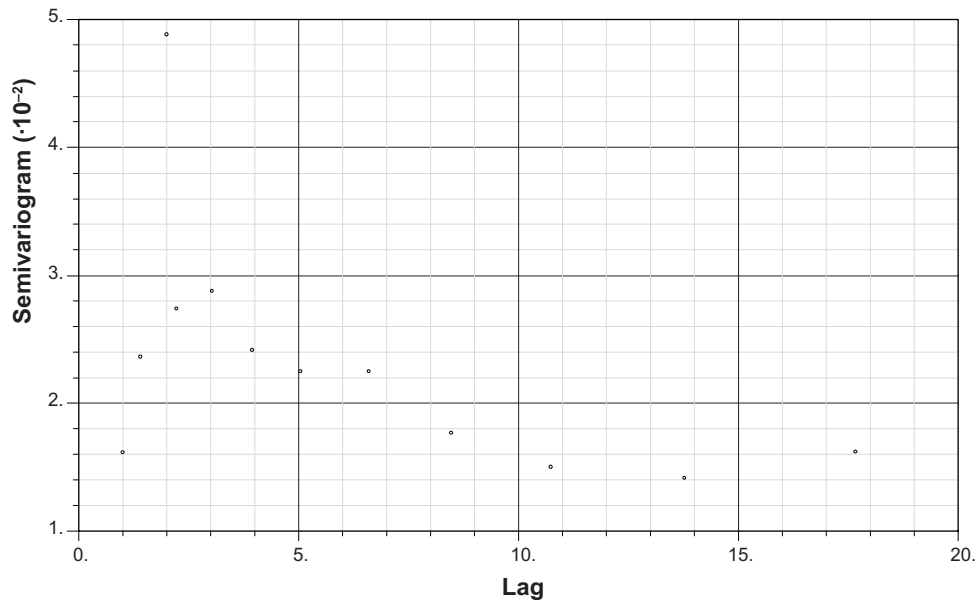
Figure 11-15. *Semivariogram for fracture intensity, AFM001097, SH Set, unlinked traces. Note that it was not possible to fit a model to this data.*
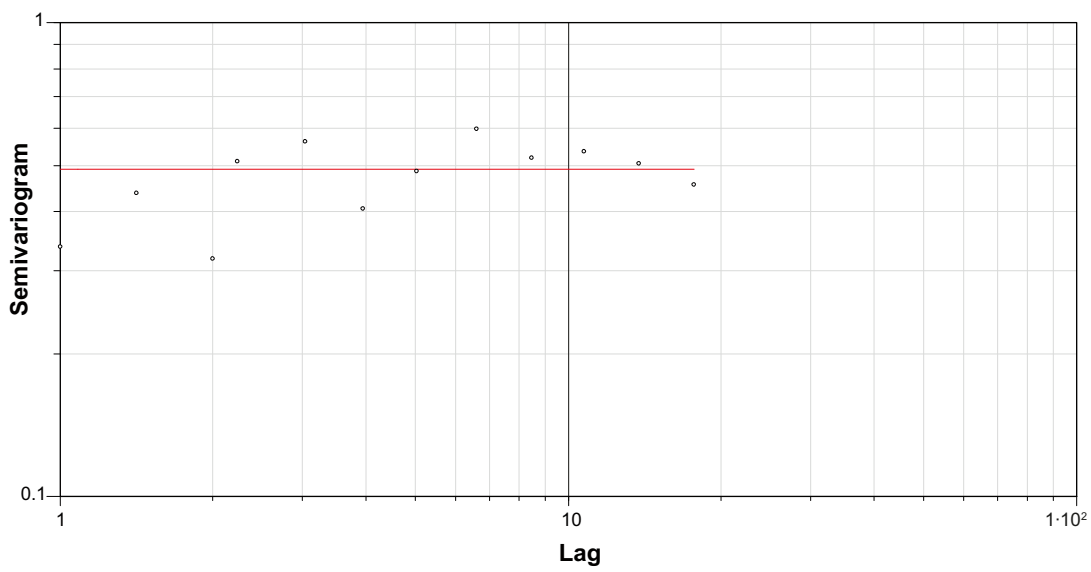
Figure 11-16. *Semivariogram for fracture intensity, AFM001097, EW Set, unlinked traces.*
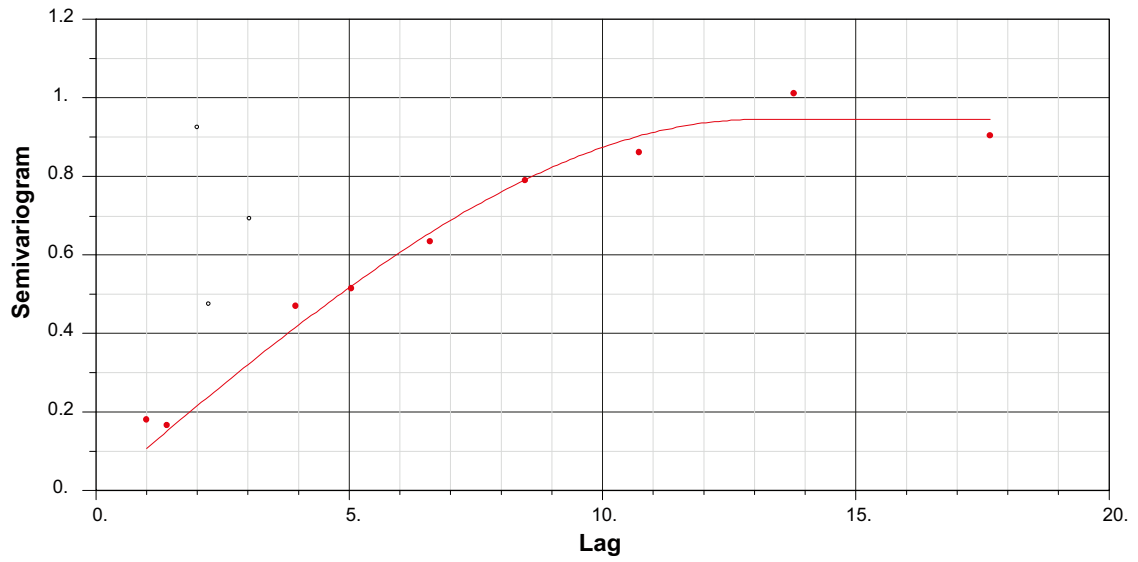
Figure 11-17. *Semivariogram for fracture intensity, AFM001098, EW Set, unlinked traces*
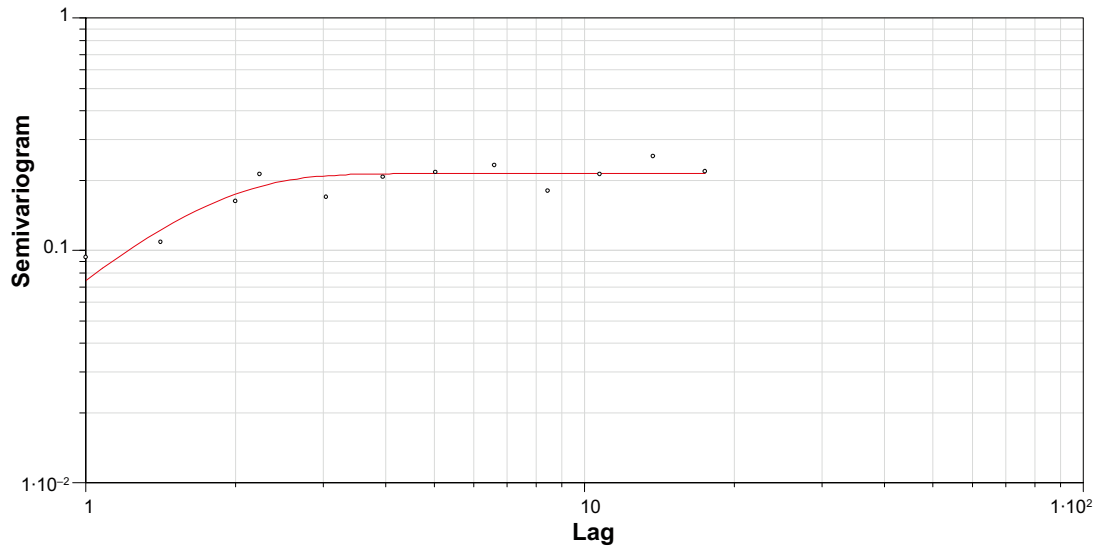
Figure 11-18. *Semivariogram for fracture intensity, AFM001098, NW Set, unlinked traces.*
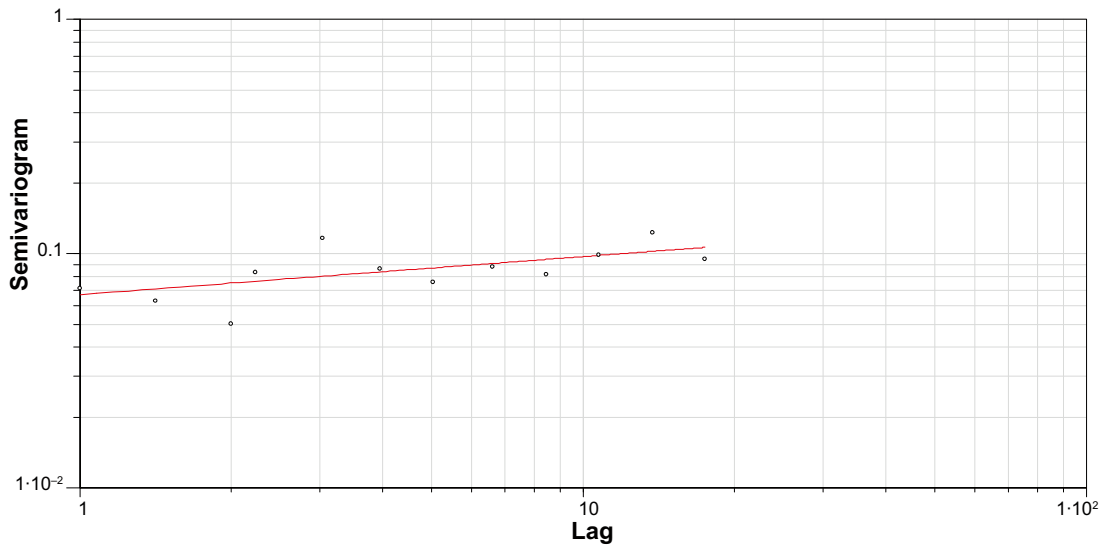
Figure 11-19. *Semivariogram for fracture intensity, AFM001098, SH Set, unlinked traces.*
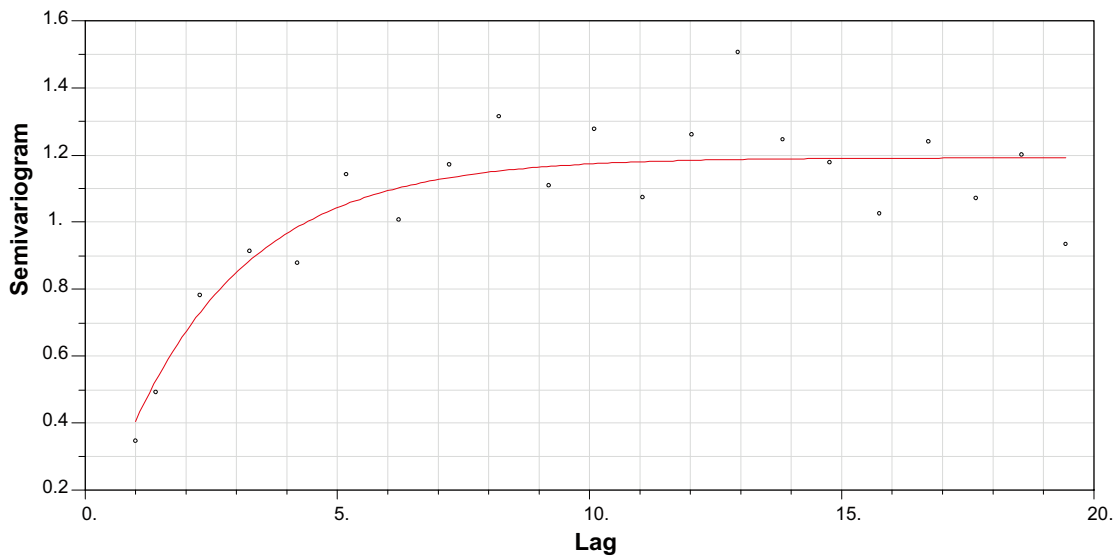
Figure 11-20. *Semivariogram for fracture intensity, AFM001098, NNE Set, unlinked traces.*
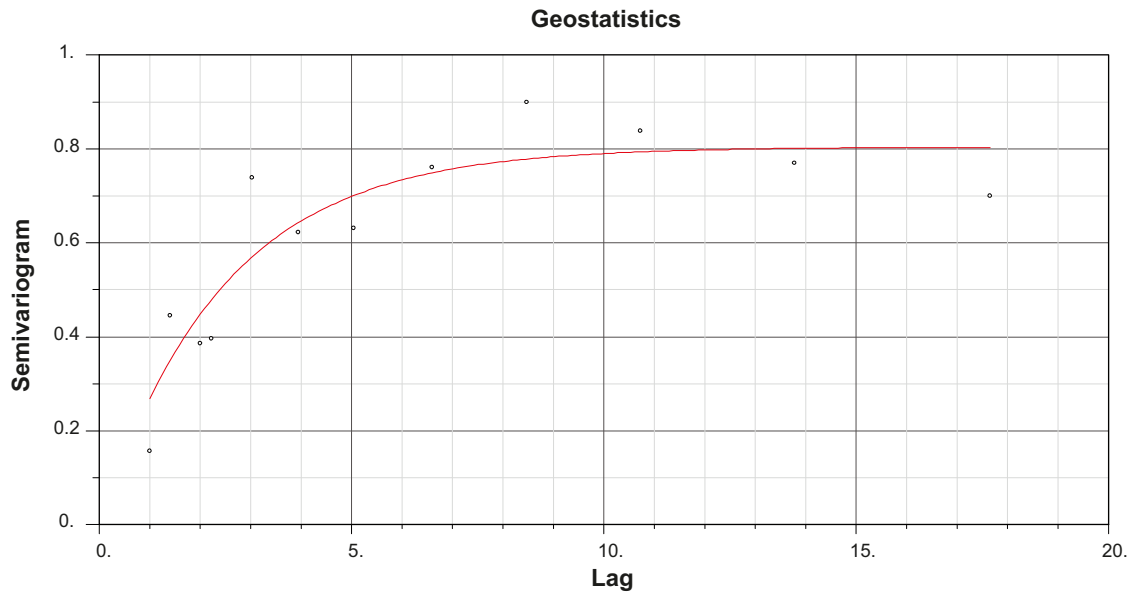
Figure 11-21. *Semivariogram for fracture intensity, AFM001098, WNW Set, unlinked traces.*
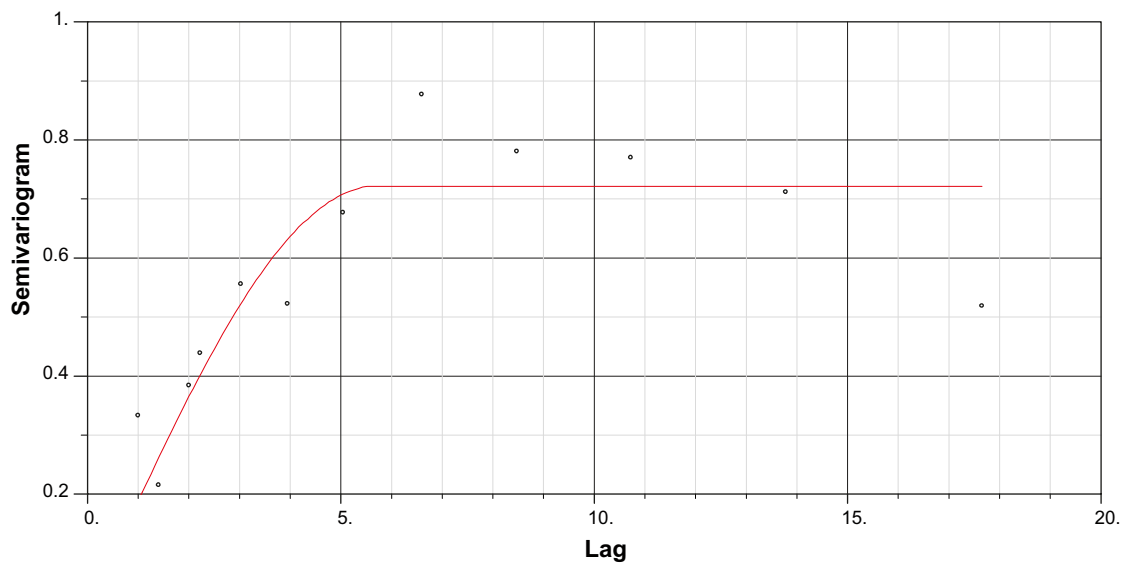
Figure 11-22. *Semivariogram for fracture intensity, AFM001243, NE Set, unlinked traces.*
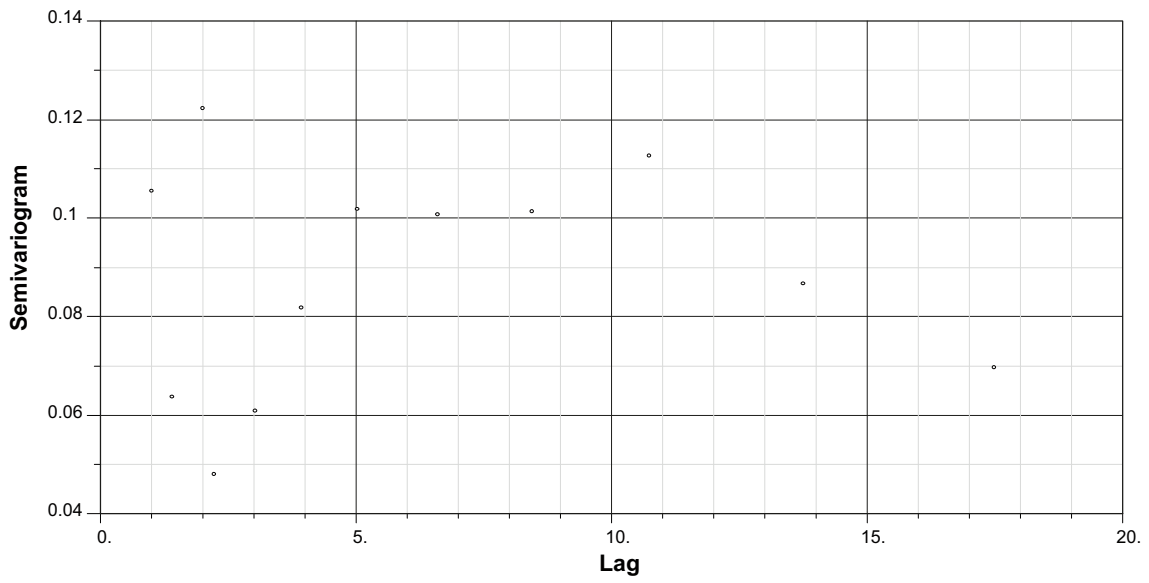
Figure 11-23. *Semivariogram for fracture intensity, AFM001243, NS Set, unlinked traces. Note that it was not possible to successfully fit a model to this data.*
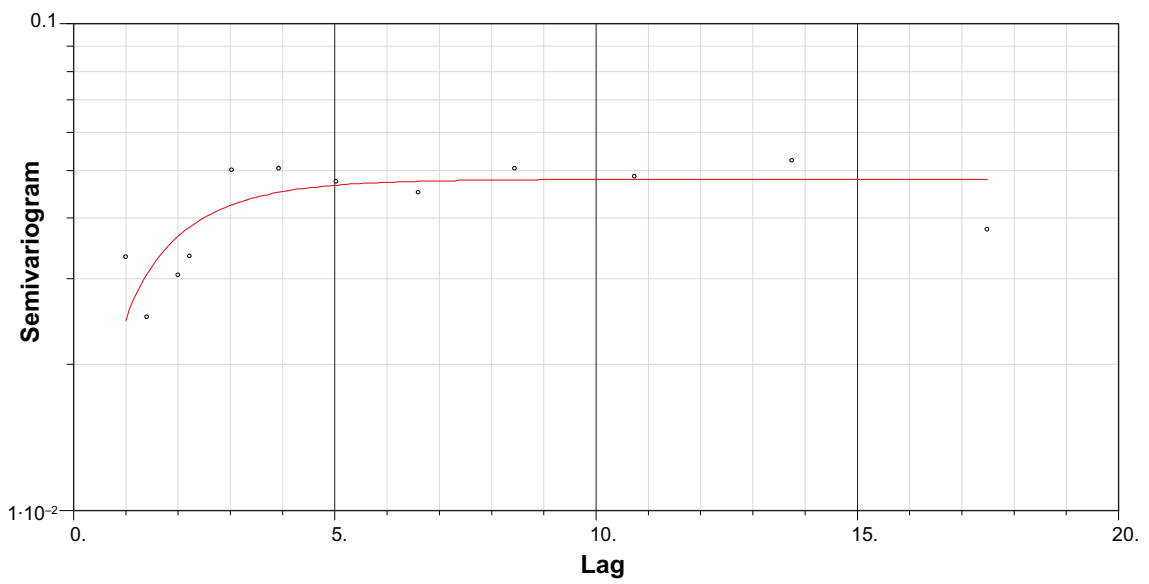
Figure 11-24. *Semivariogram for fracture intensity, AFM001243, SH Set, unlinked traces*
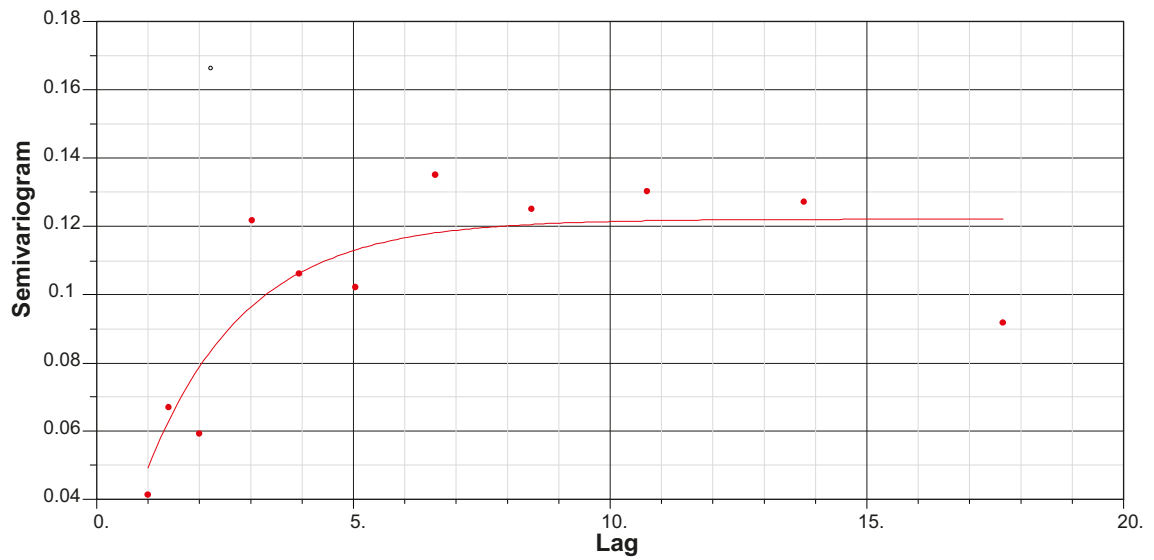
Figure 11-25. *Semivariogram for fracture intensity, AFM001243, WNW Set, unlinked traces.*
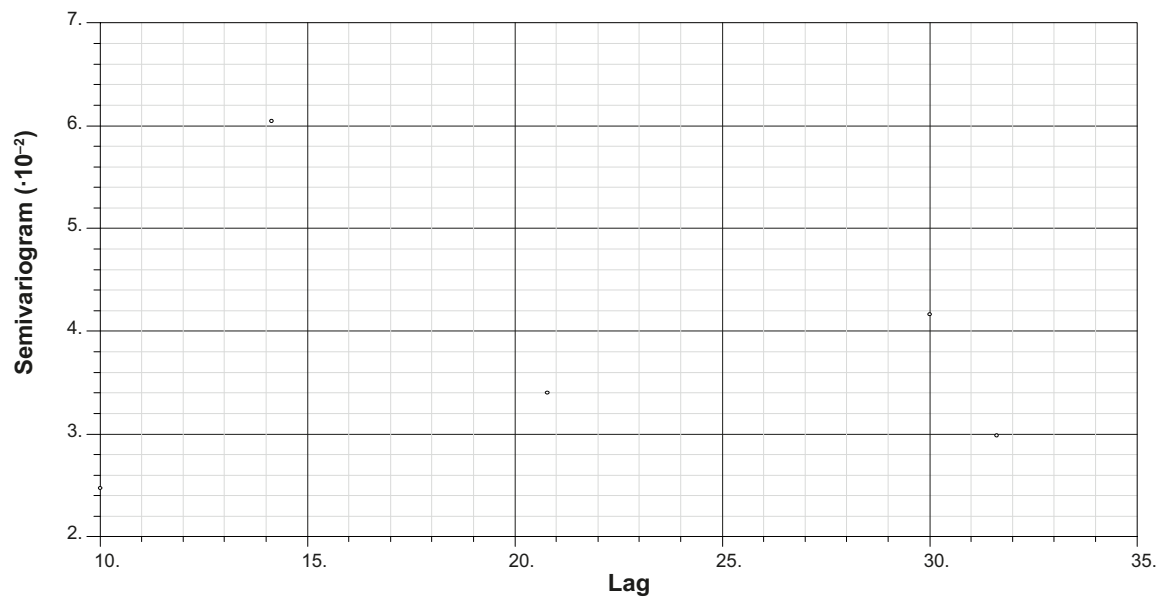
Figure 11-26. *Semivariogram for fracture intensity, AFM001244, NE Set, unlinked traces. Note that it was not possible to successfully fit a model to this data.*
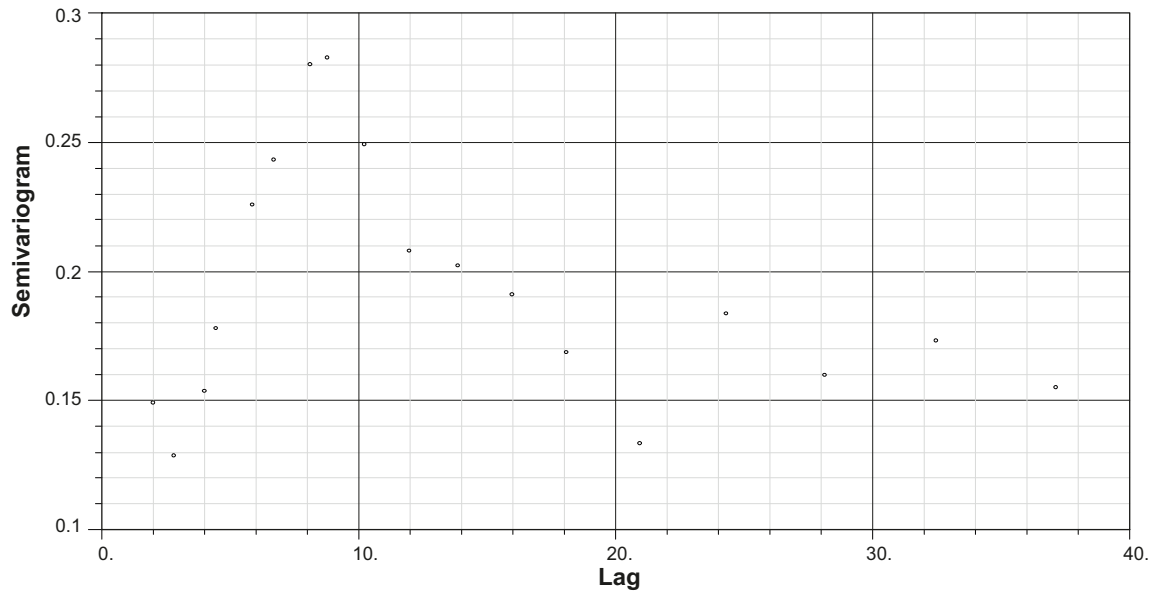
Figure 11-27. *Semivariogram for fracture intensity, AFM001244, NS Set, unlinked traces. Note that it was not possible to successfully fit a model to this data.*
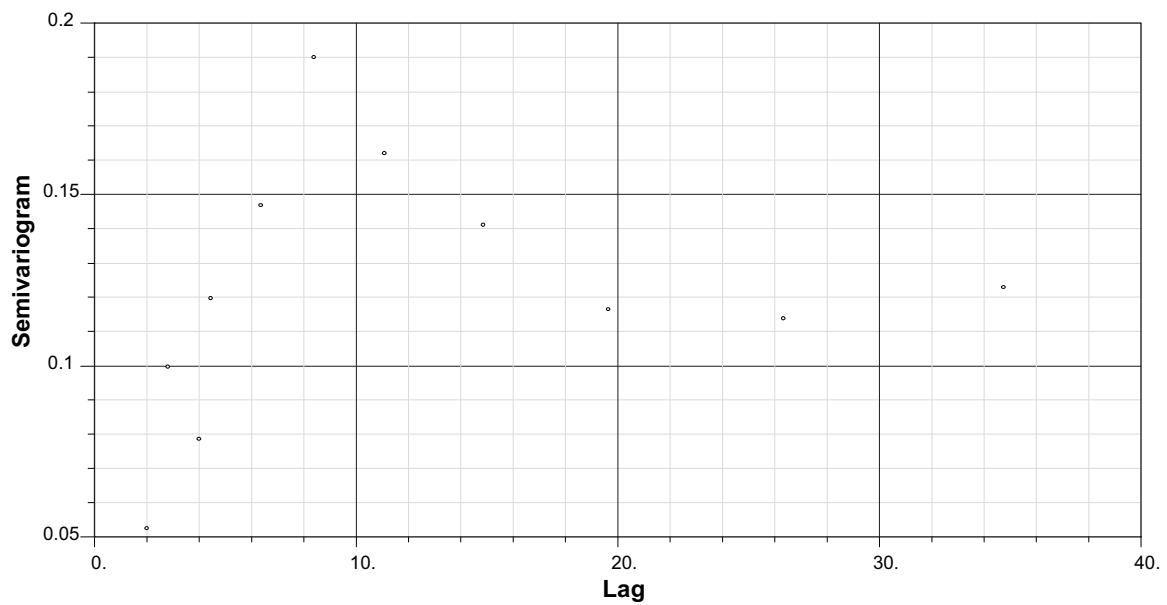
Figure 11-28. *Semivariogram for fracture intensity, AFM001244, NW Set, unlinked traces. Note that it was not possible to successfully fit a model to this data.*
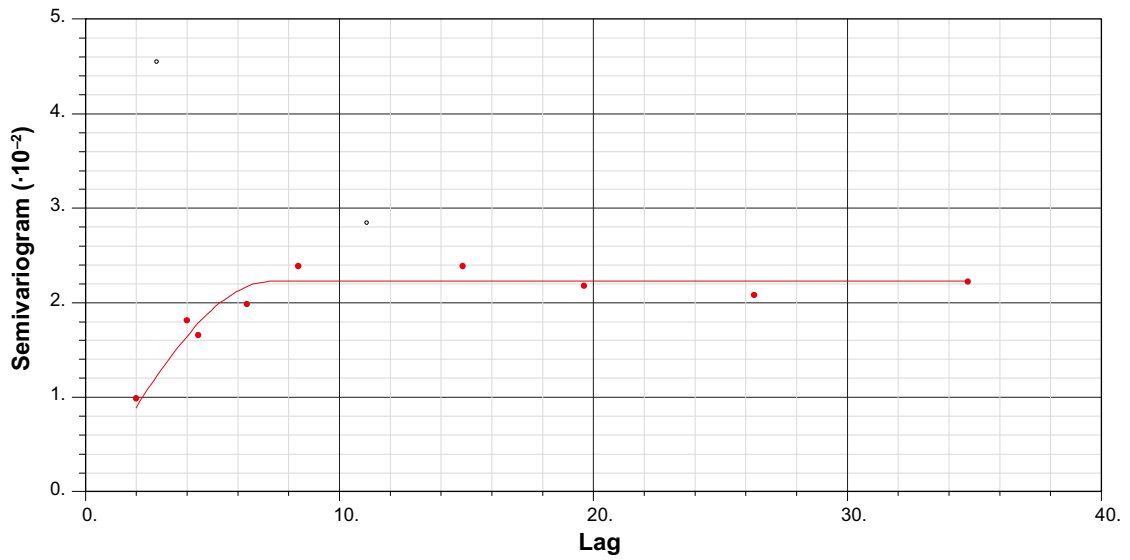
Figure 11-29. *Semivariogram for fracture intensity, AFM001244, SH Set, unlinked traces.*
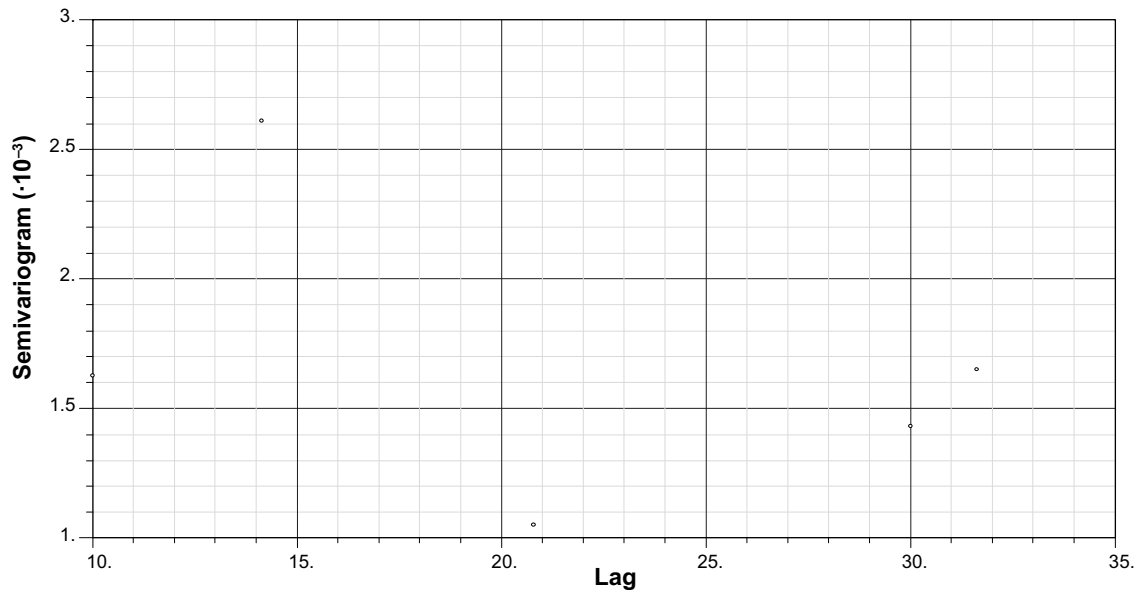
Figure 11-30. *Semivariogram for fracture intensity, AFM001244, EW Set, unlinked traces. Note that it was not possible to successfully fit a model to this data.*
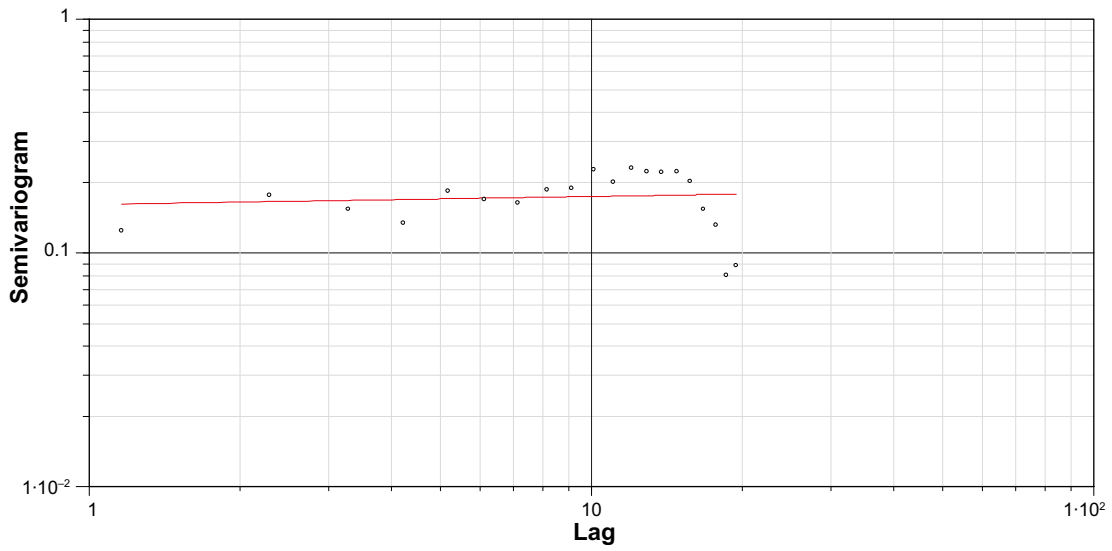
Figure 11-31. *Semivariogram for fracture intensity, AFM001264, NE Set, unlinked traces*
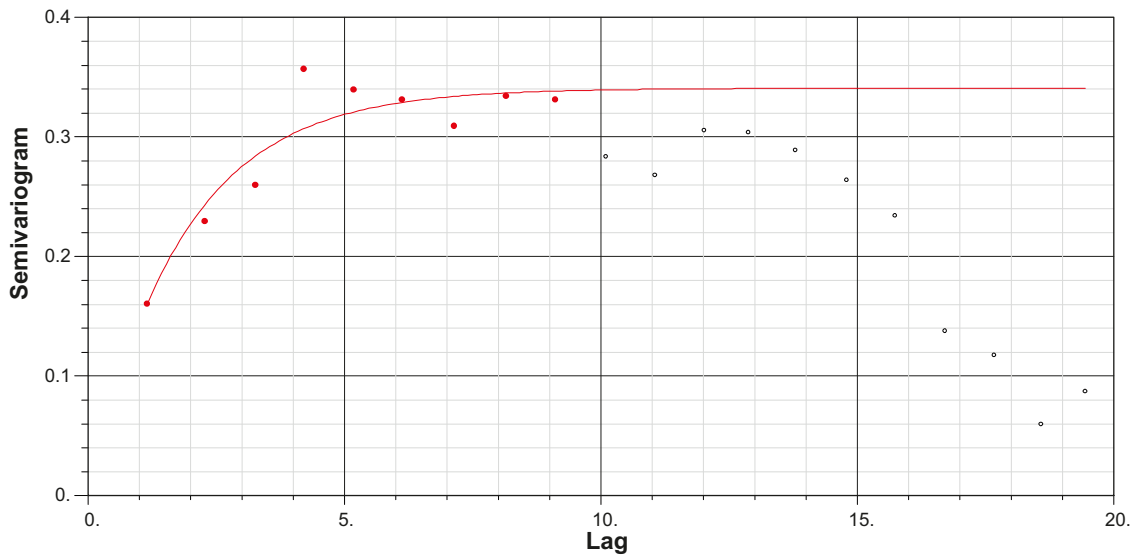
Figure 11-32. *Semivariogram for fracture intensity, AFM001264, NW Set, unlinked traces.*
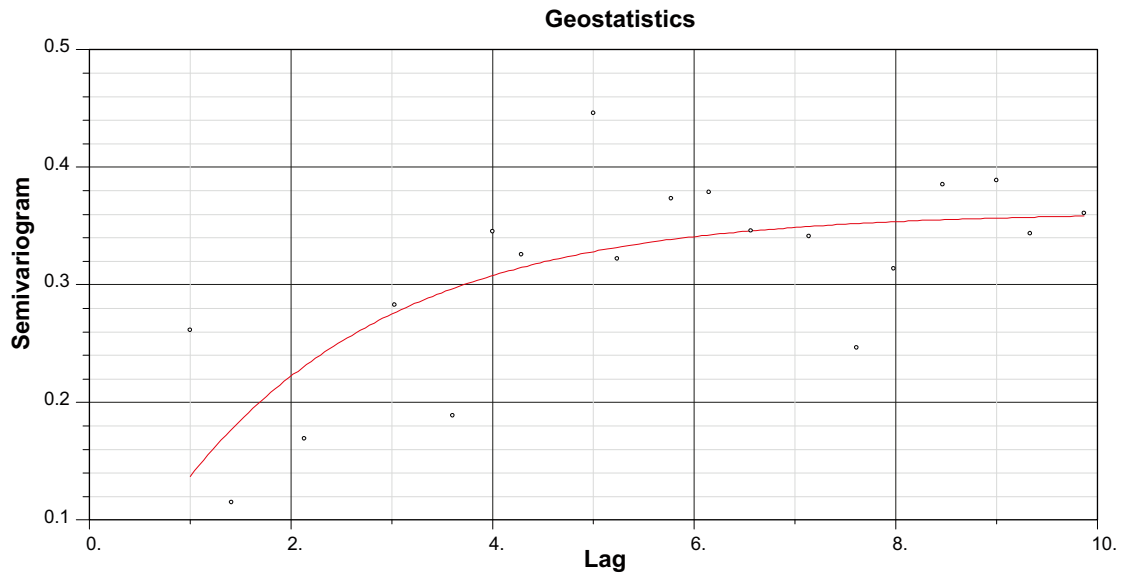
Figure 11-33. *Semivariogram for fracture intensity, AFM001264, SH Set, unlinked traces*
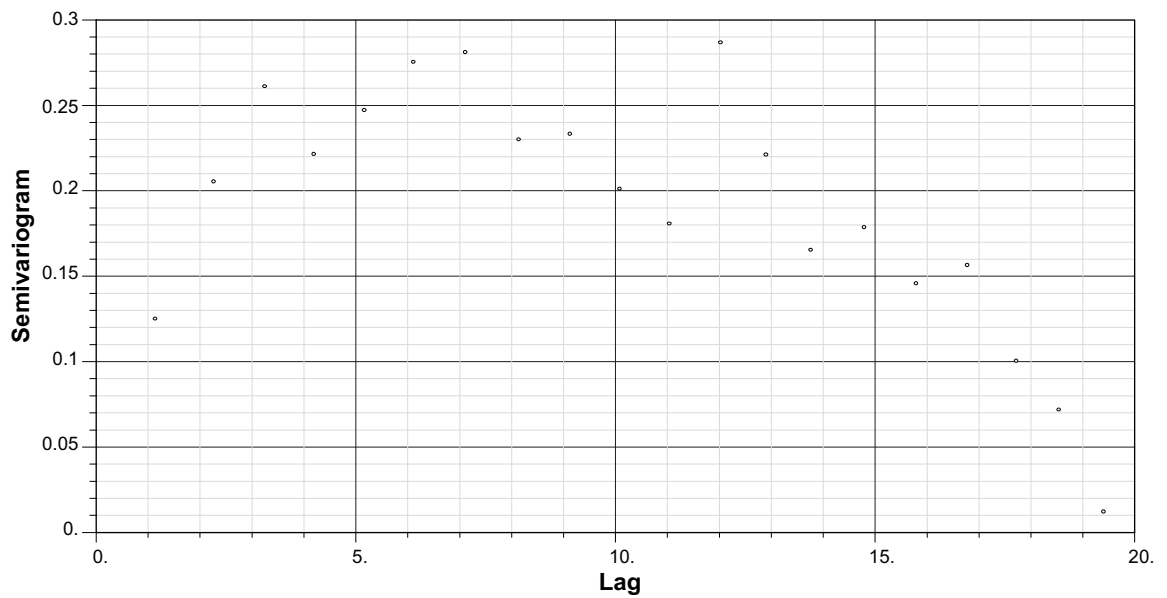
Figure 11-34. *Semivariogram for fracture intensity, AFM001264, ENE Set, unlinked traces. Note that it was not possible to successfully fit a model to this data.*
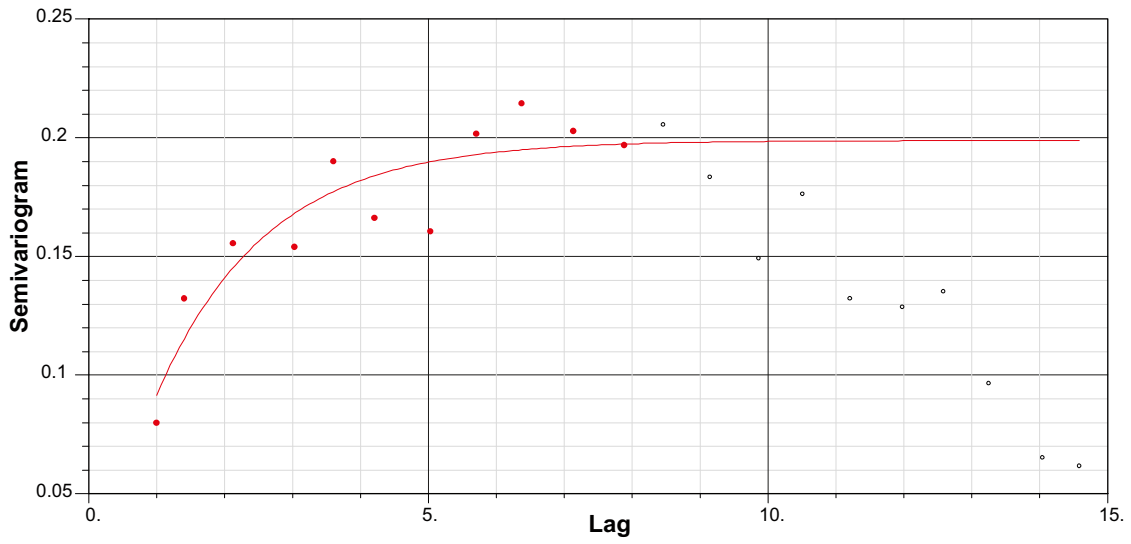
Figure 11-35. *Semivariogram for fracture intensity, AFM001264, WNW Set, unlinked traces.*
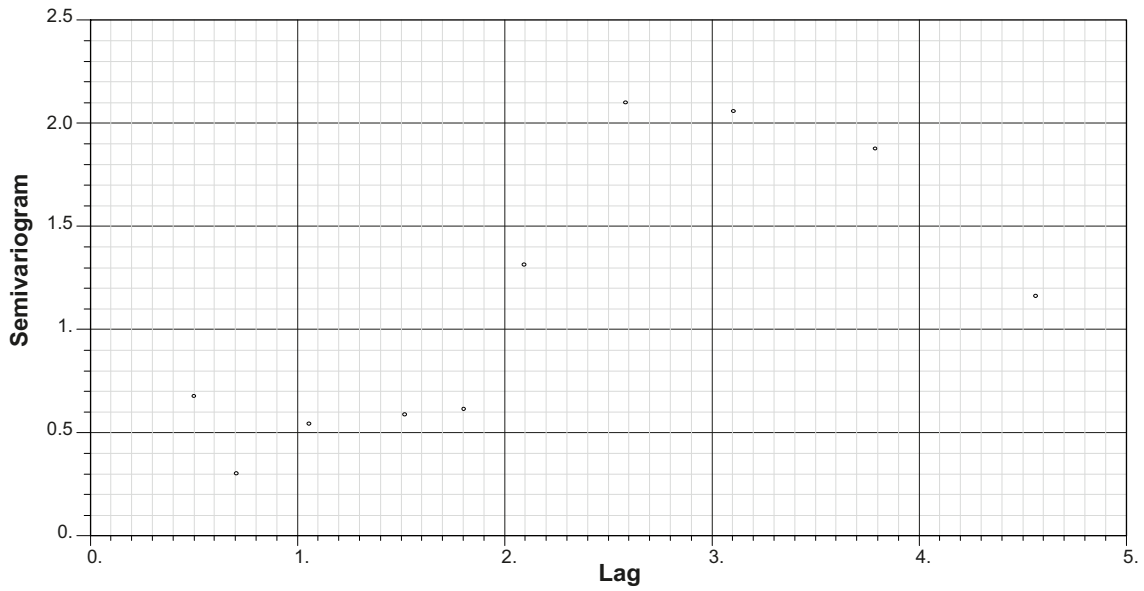
Figure 11-36. *Semivariogram for fracture intensity, AFM001265, NE Set, unlinked traces. Note that it was not possible to successfully fit a model to this data.*
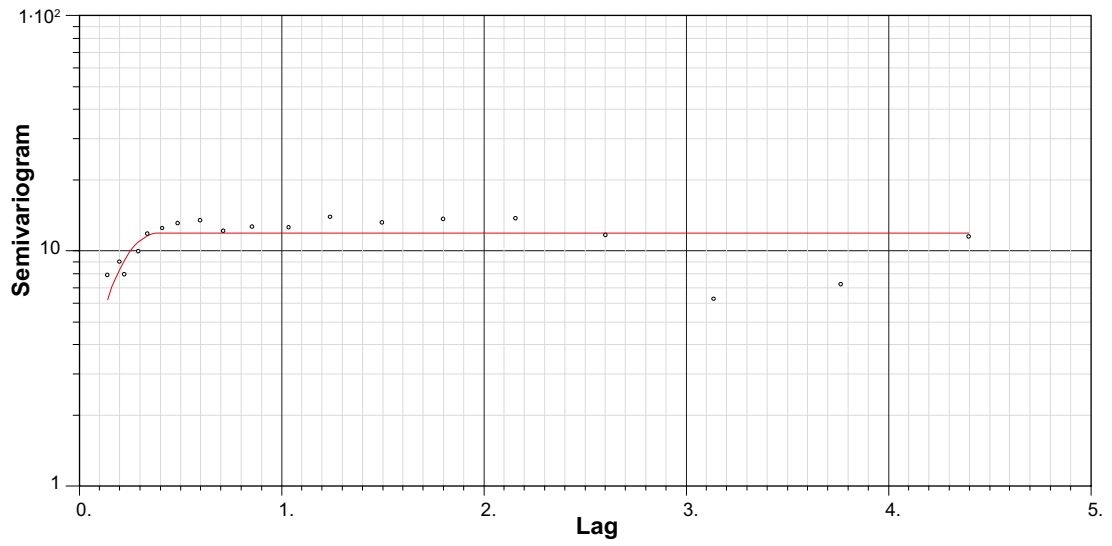
Figure 11-37. *Semivariogram for fracture intensity, AFM001265, EW Set, unlinked traces*
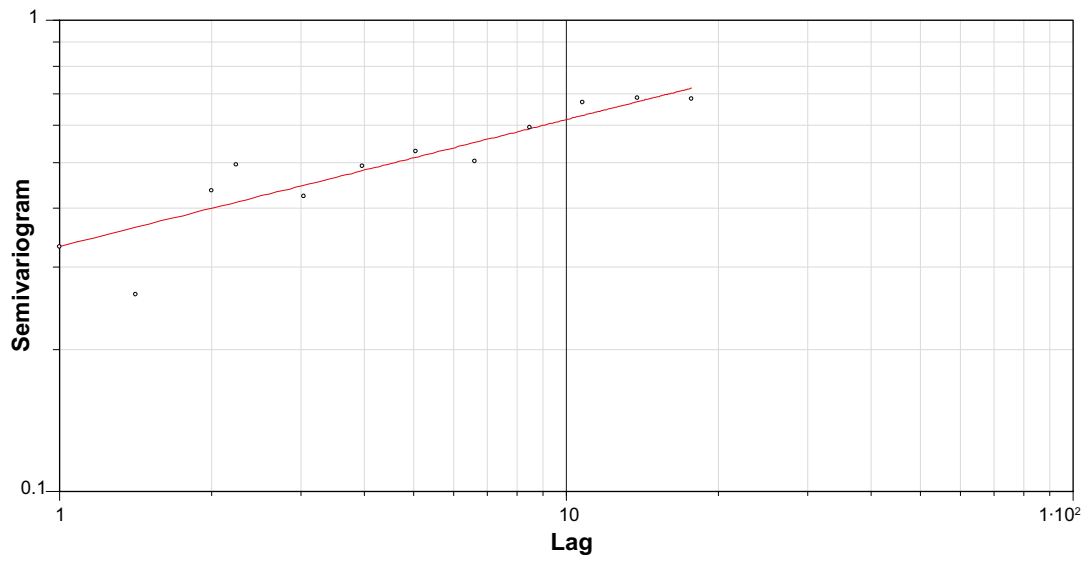
Figure 11-38. *Semivariogram for fracture intensity, AFM100201, NE Set, unlinked traces.*
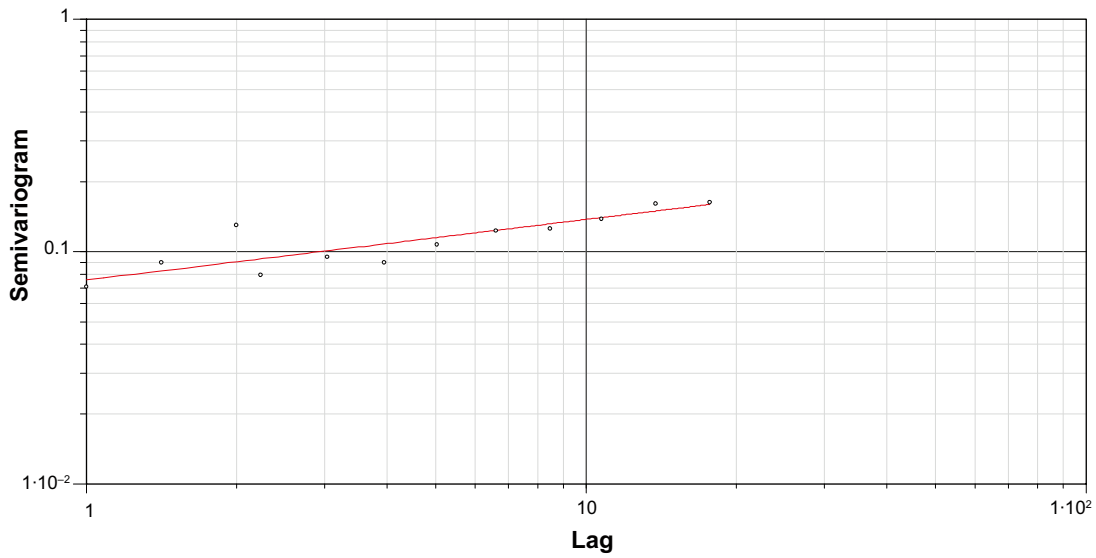
Figure 11-39. *Semivariogram for fracture intensity, AFM100201, NS Set, unlinked traces.*
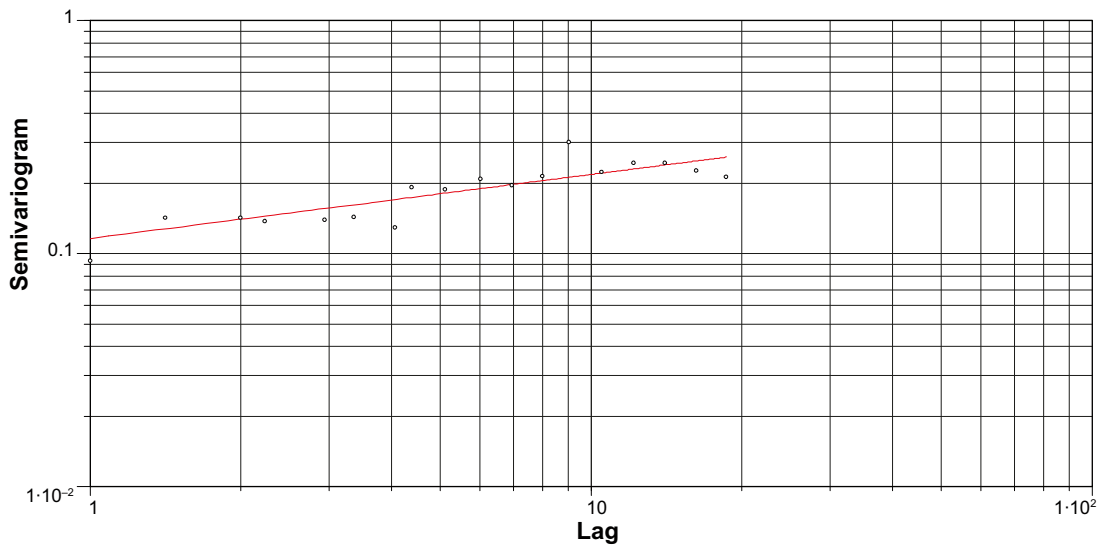
Figure 11-40. *Semivariogram for fracture intensity, AFM100201, NW Set, unlinked traces.*
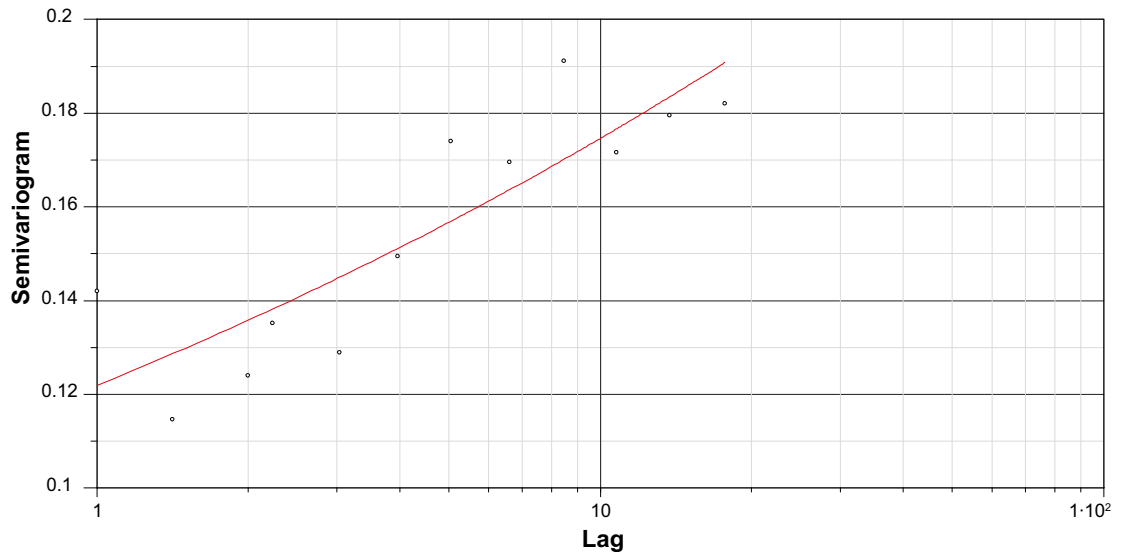
Figure 11-41. *Semivariogram for fracture intensity, AFM100201, SH Set, unlinked traces*
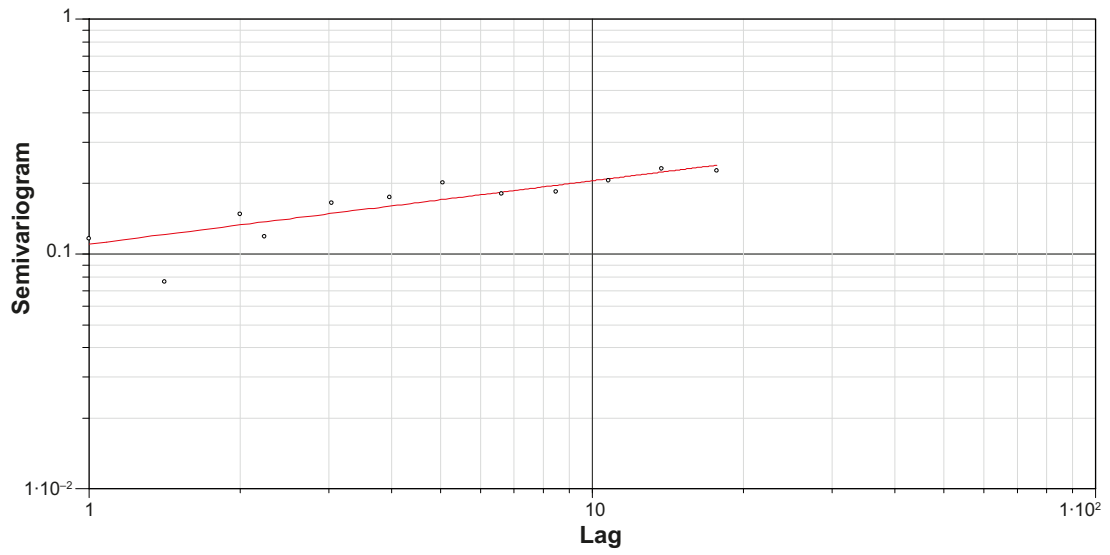
Figure 11-42. *Semivariogram for fracture intensity, AFM100201, EW Set, unlinked traces.*
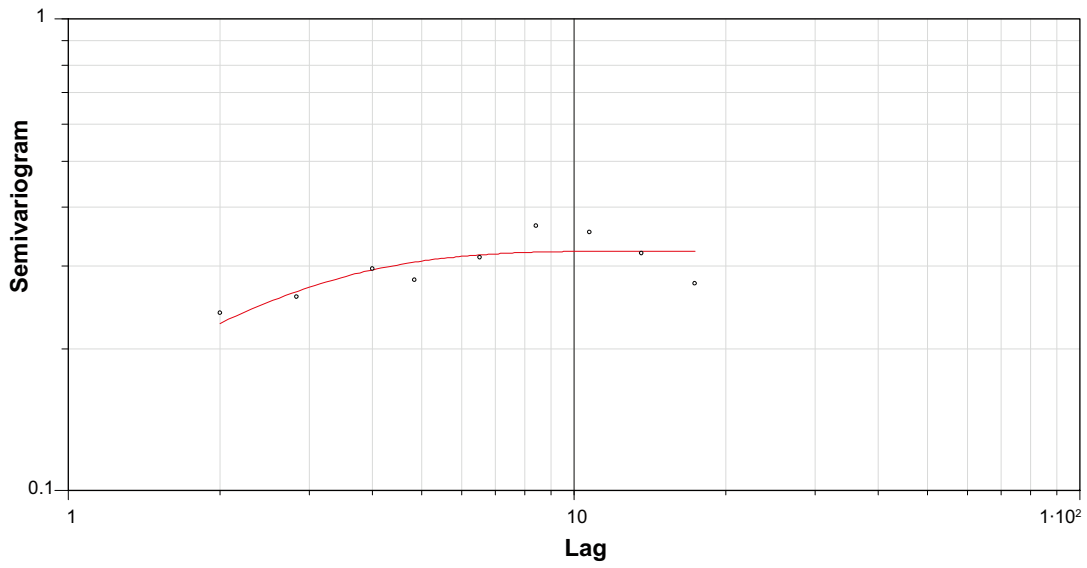
Figure 11-43. *Semivariogram for fracture intensity, AFM000053, NE Set, linked traces.*
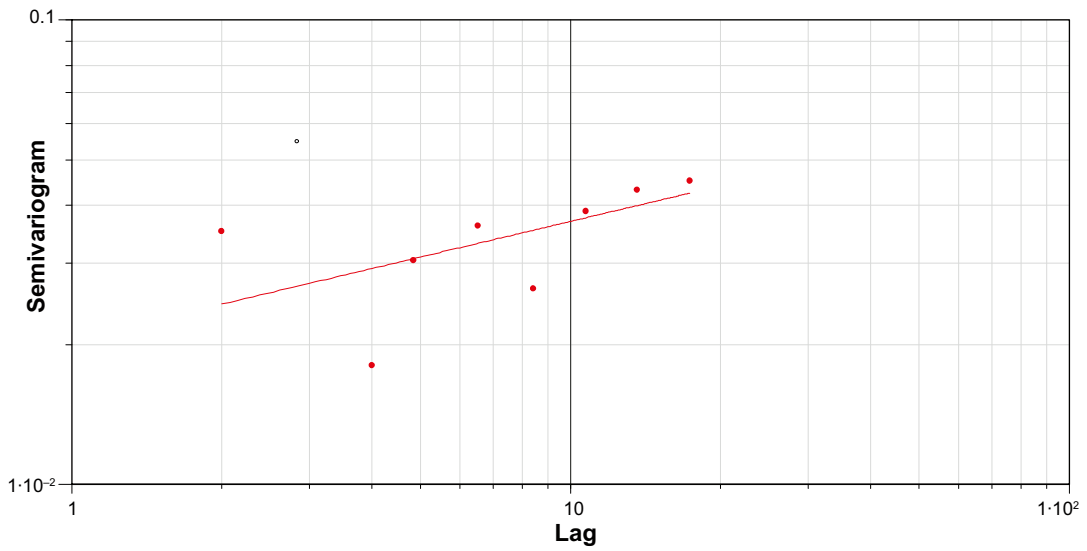
Figure 11-44. *Semivariogram for fracture intensity, AFM000053, NS Set, linked traces.*
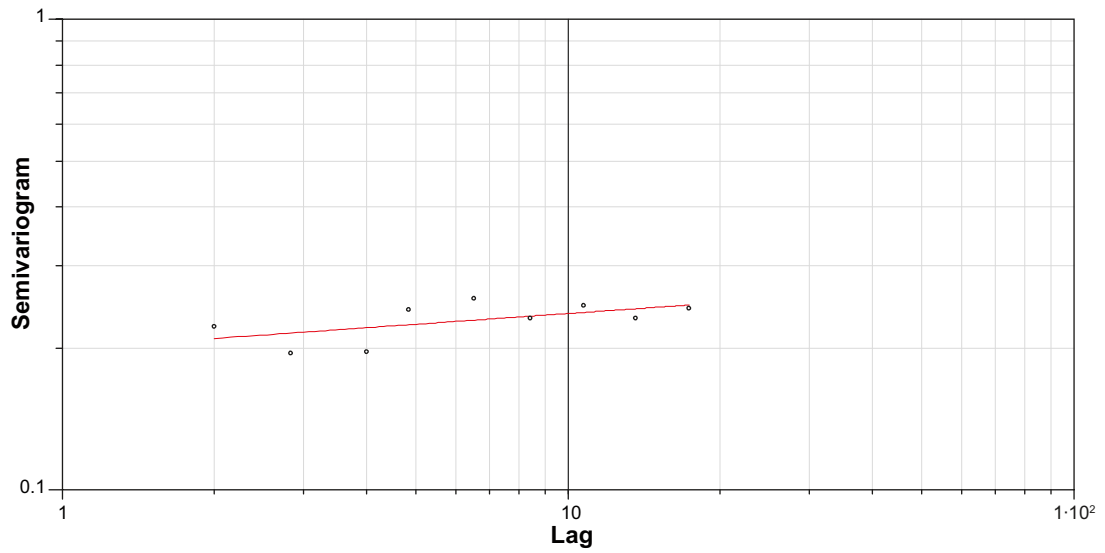
Figure 11-45. *Semivariogram for fracture intensity, AFM000053, NW Set, linked traces.*
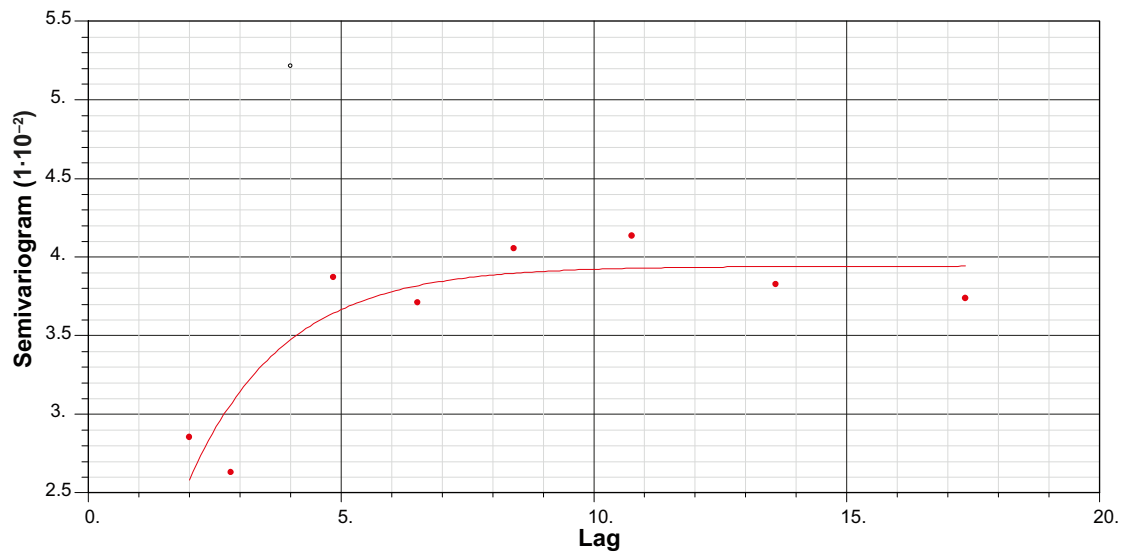
Figure 11-46. *Semivariogram for fracture intensity, AFM000053, SH Set, linked traces.*
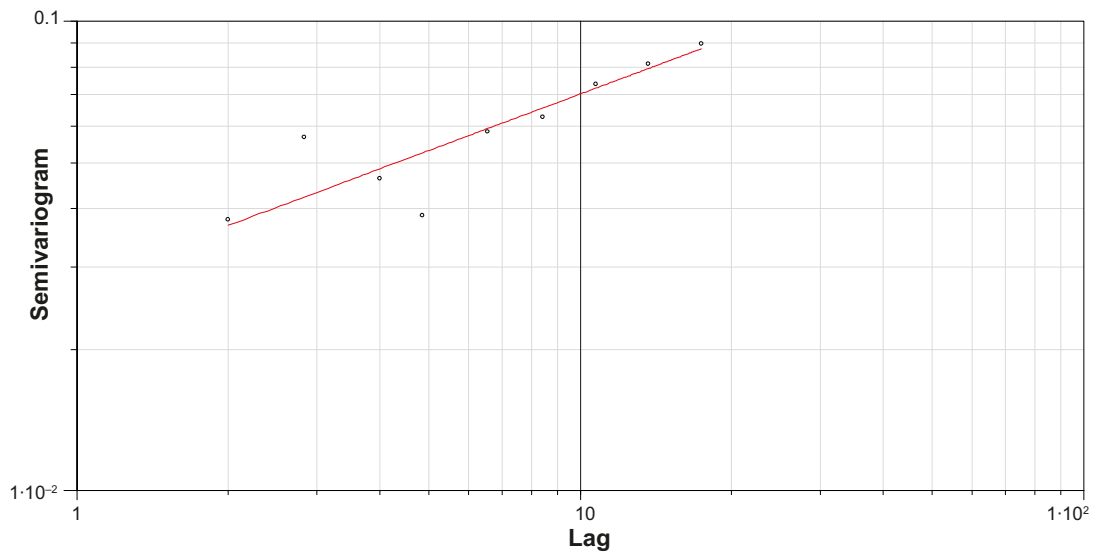
Figure 11-47. *Semivariogram for fracture intensity, AFM000053, ENE Set, linked traces.*
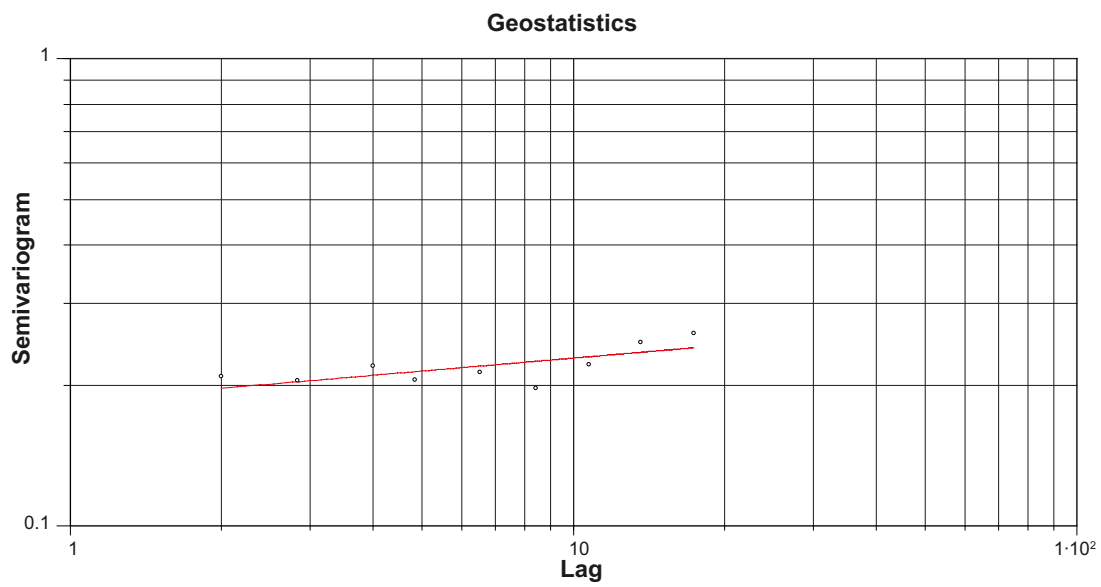
Figure 11-48. *Semivariogram for fracture intensity, AFM000053, WNW Set, linked traces.*

90
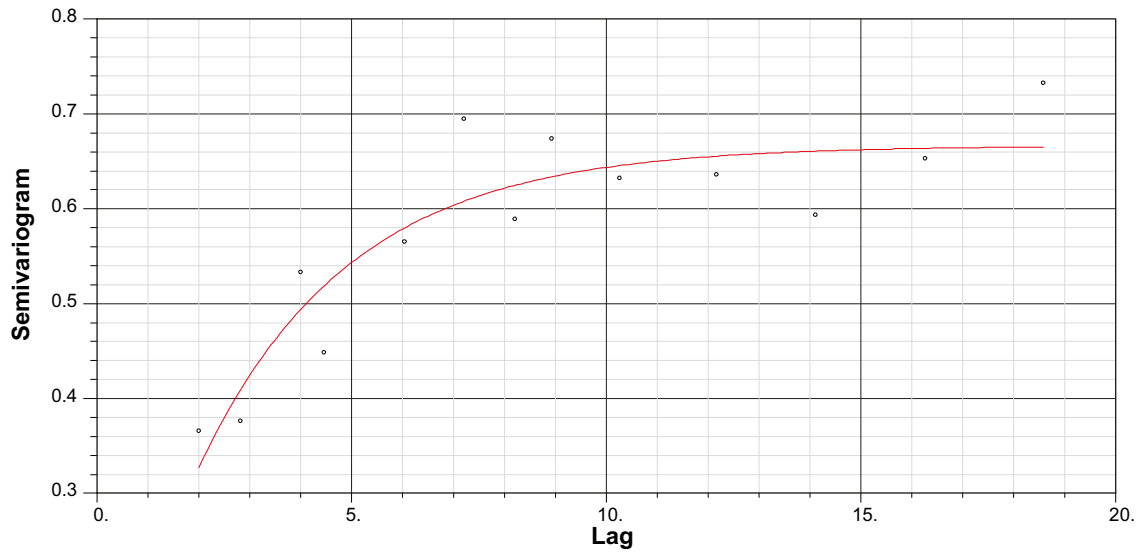
Figure 11-49. *Semivariogram for fracture intensity, AFM000054, NE Set, linked traces.*
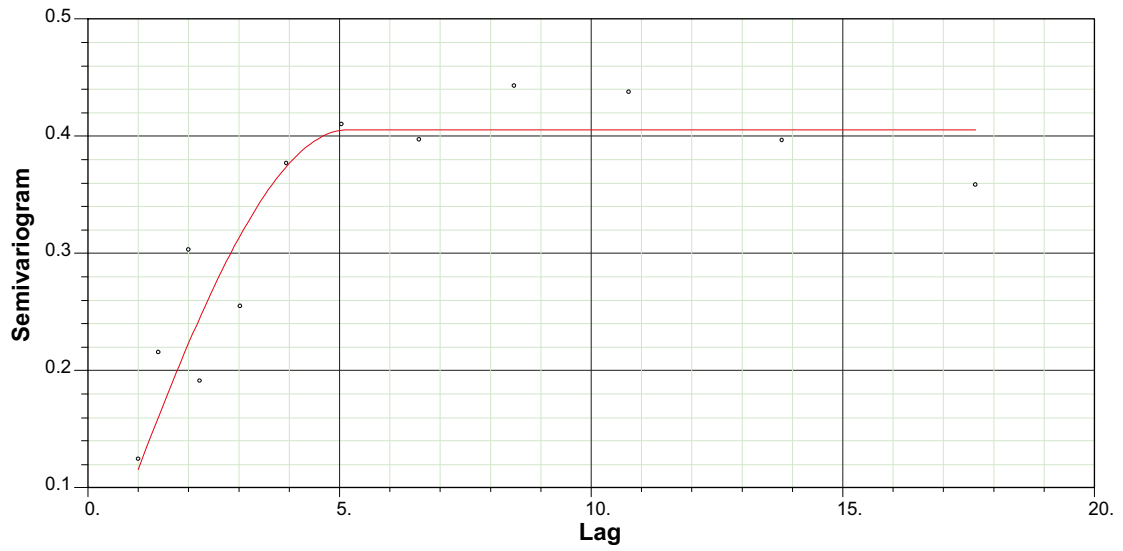
Figure 11-50. *Semivariogram for fracture intensity, AFM000054, NS Set, linked traces.*
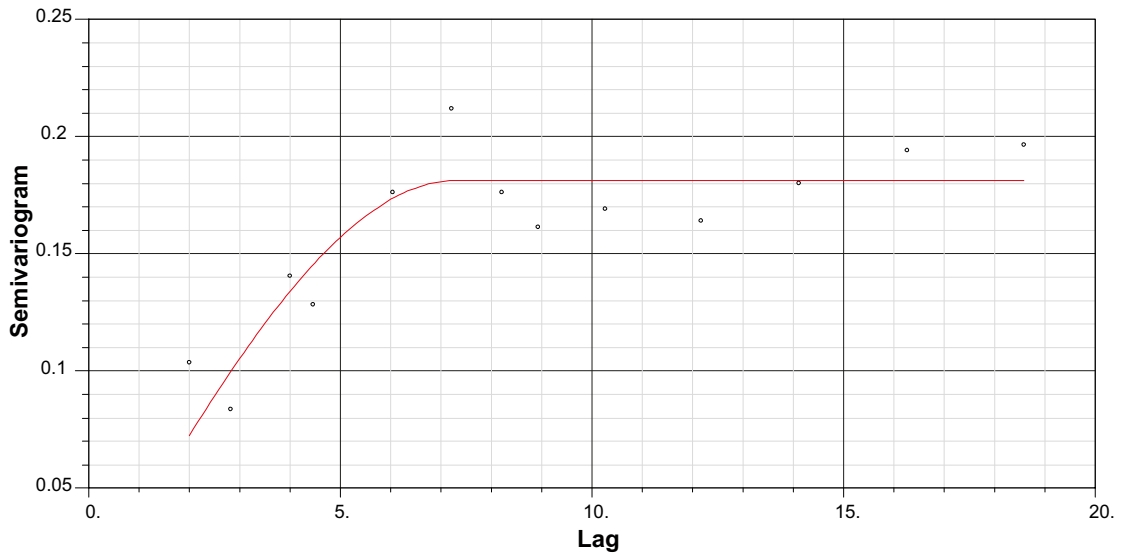
Figure 11-51. *Semivariogram for fracture intensity, AFM000054, NW Set, linked traces.*
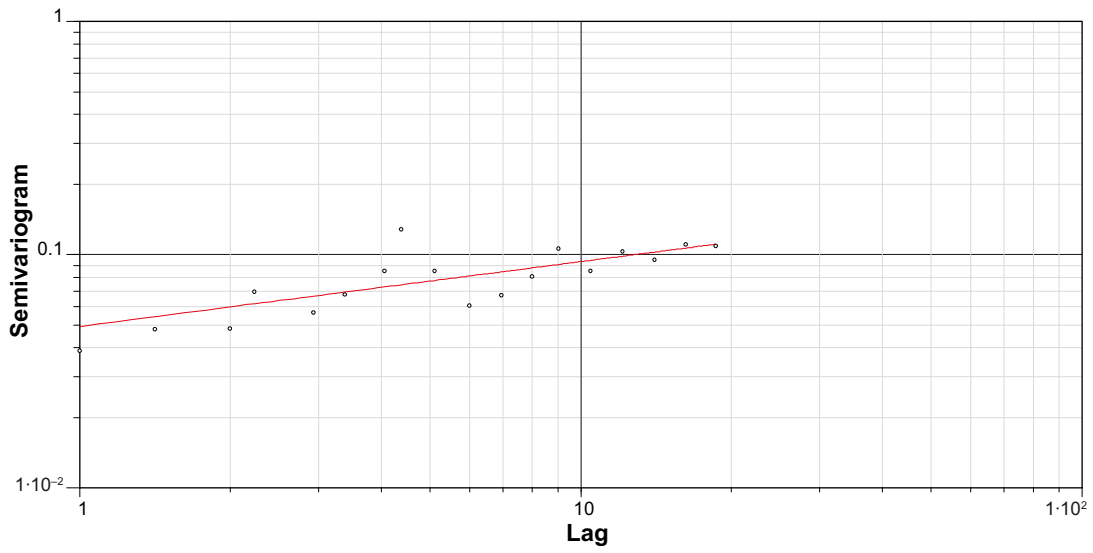
Figure 11-52. *Semivariogram for fracture intensity, AFM000054, SH Set, linked traces.*
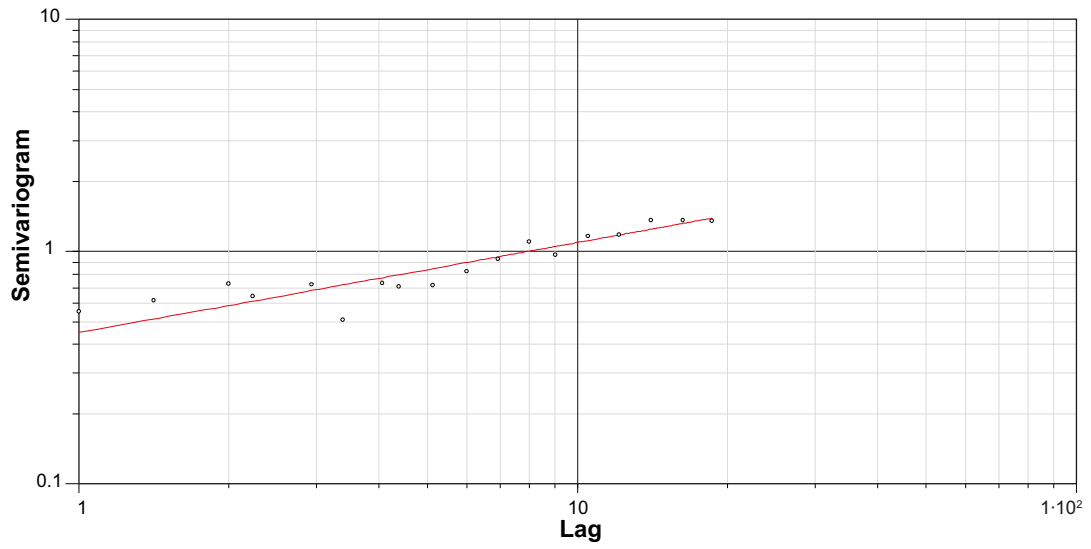
Figure 11-53. *Semivariogram for fracture intensity, AFM000054, WNW Set, linked traces.*
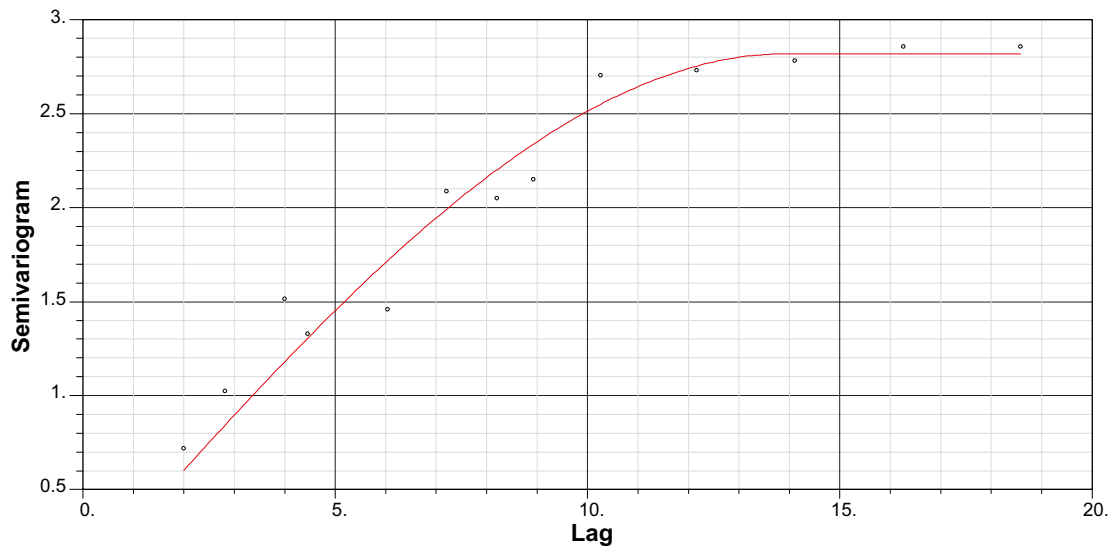
Figure 11-54. *Semivariogram for fracture intensity, AFM001097, NE Set, linked traces.*
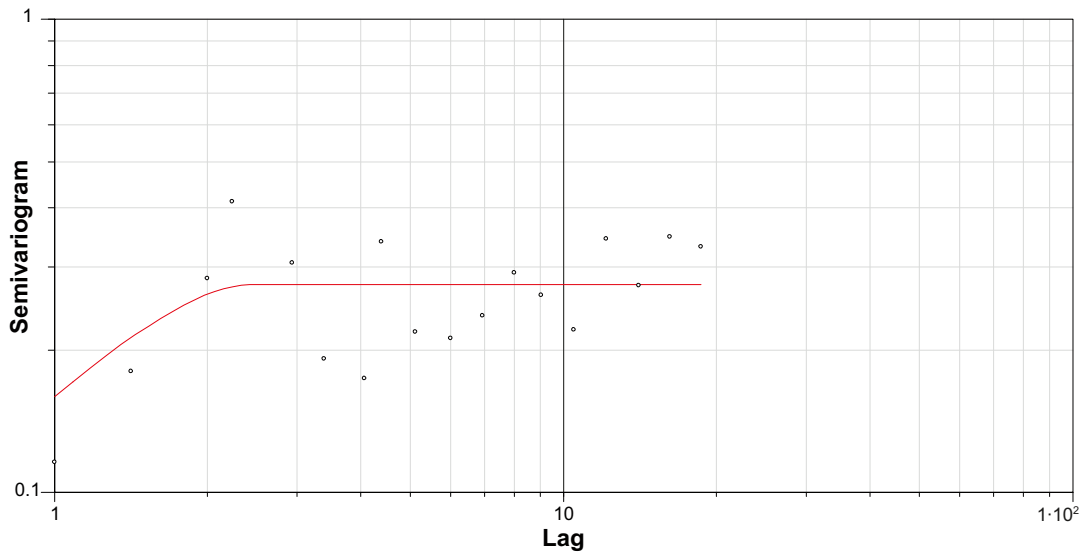
Figure 11-55. *Semivariogram for fracture intensity, AFM001097, NS Set, linked traces.*
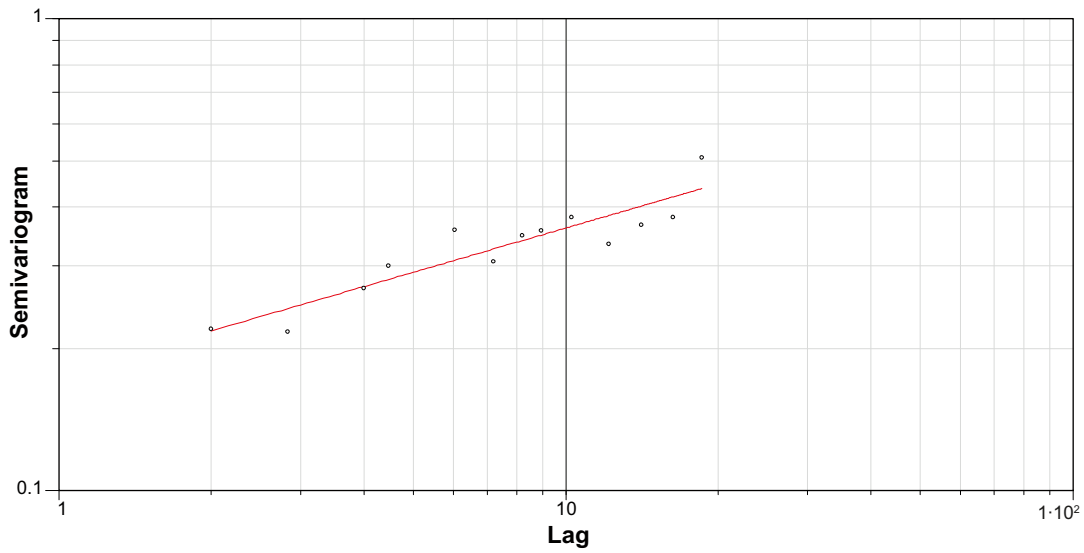
Figure 11-56. *Semivariogram for fracture intensity, AFM001097, NW Set, linked traces.*
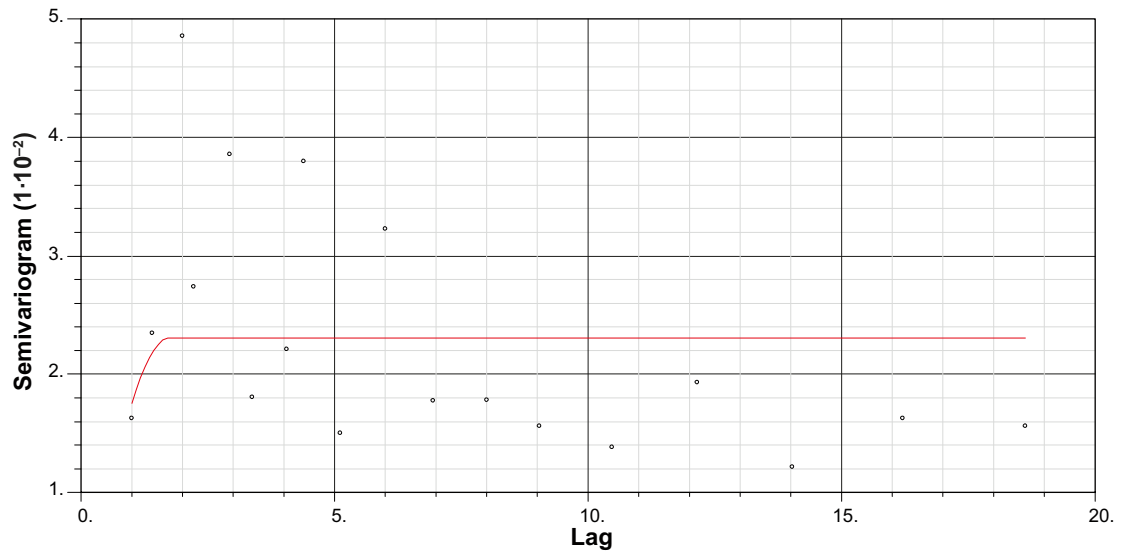
Figure 11-57. *Semivariogram for fracture intensity, AFM001097, SH Set, linked traces.*
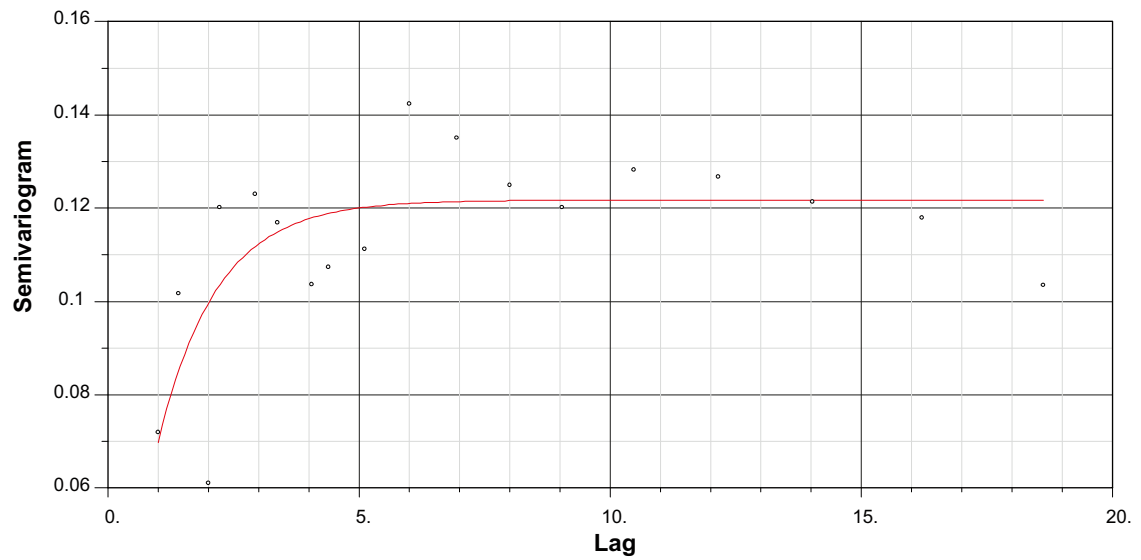
Figure 11-58. *Semivariogram for fracture intensity, AFM001097, EW Set, linked traces.*
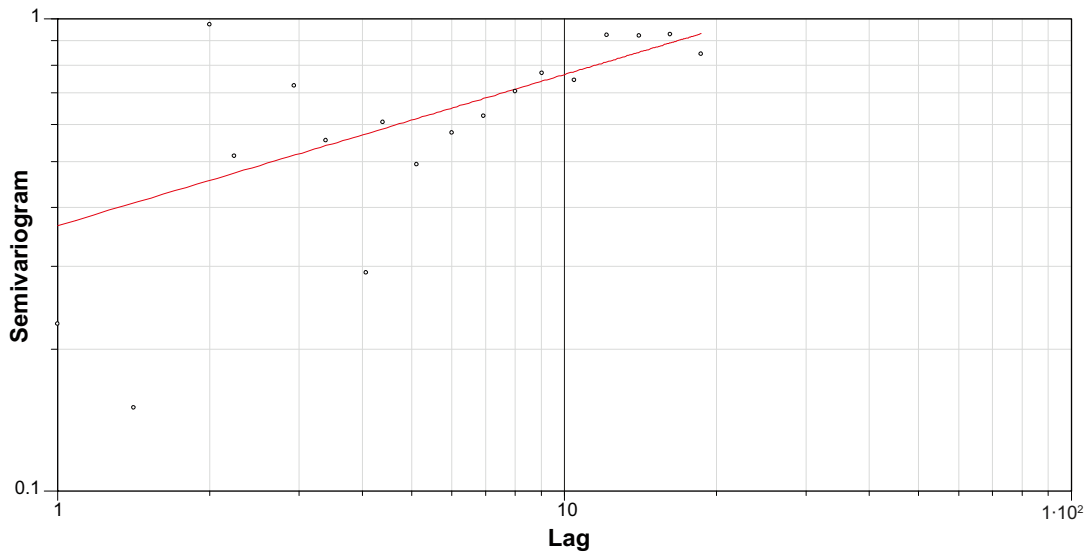
Figure 11-59. *Semivariogram for fracture intensity, AFM001098, NE Set, linked traces.*
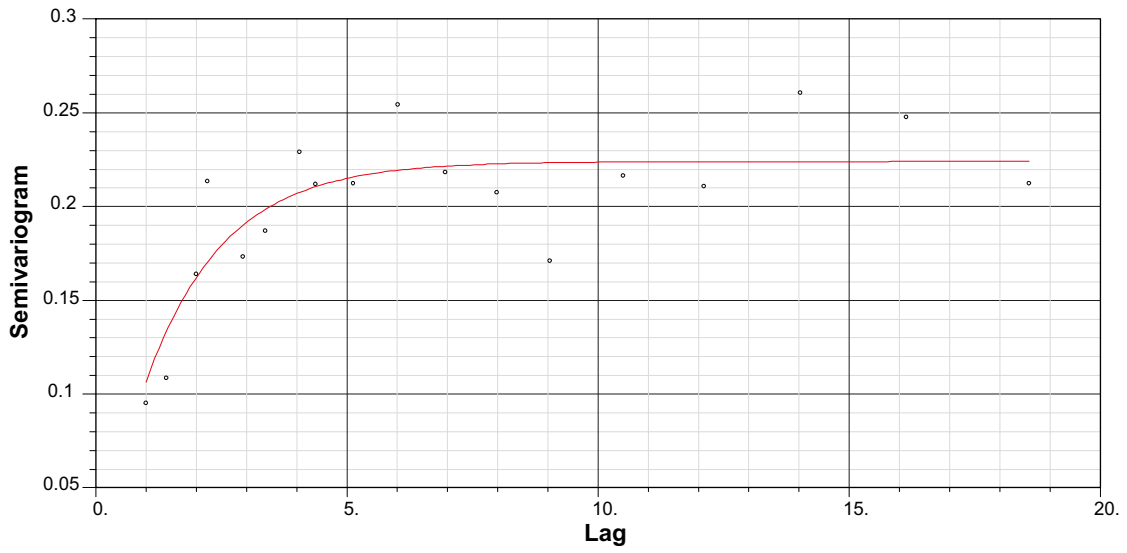
Figure 11-60. *Semivariogram for fracture intensity, AFM001098, NW Set, linked traces.*

96
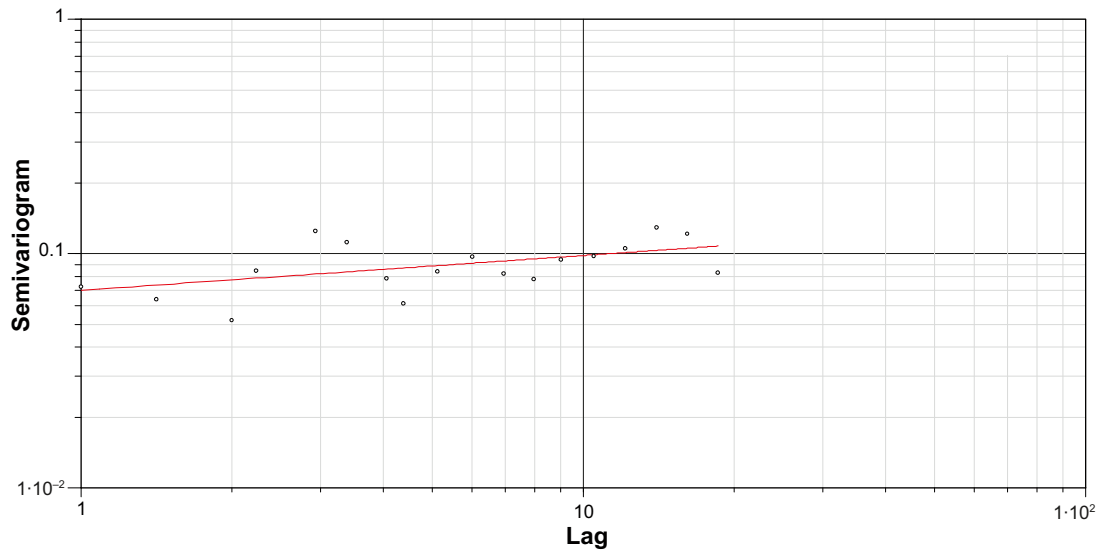
Figure 11-61. *Semivariogram for fracture intensity, AFM001098, SH Set, linked traces.*
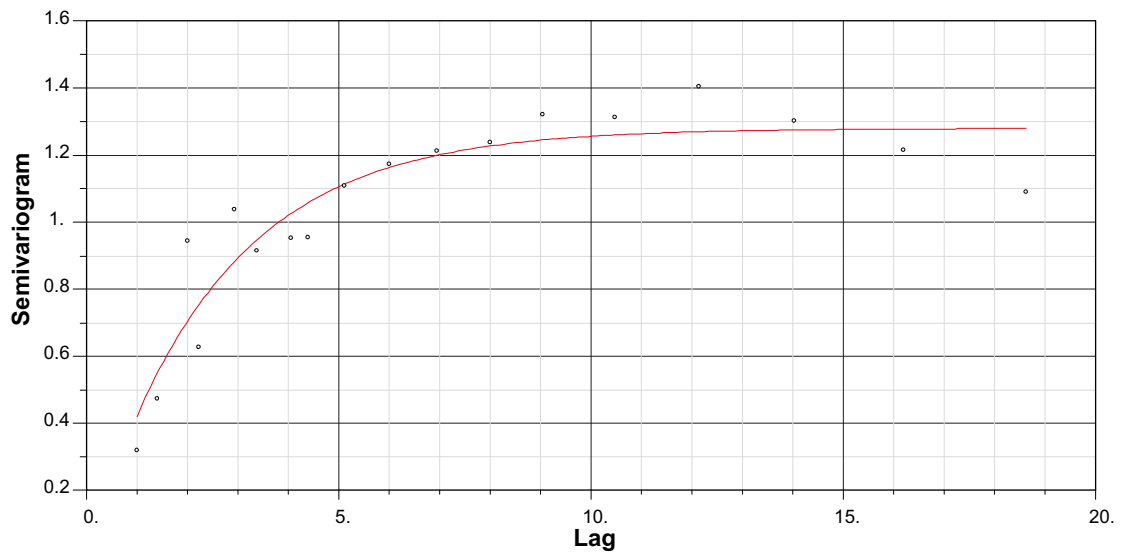
Figure 11-62. *Semivariogram for fracture intensity, AFM001098, NNE Set, linked traces.*
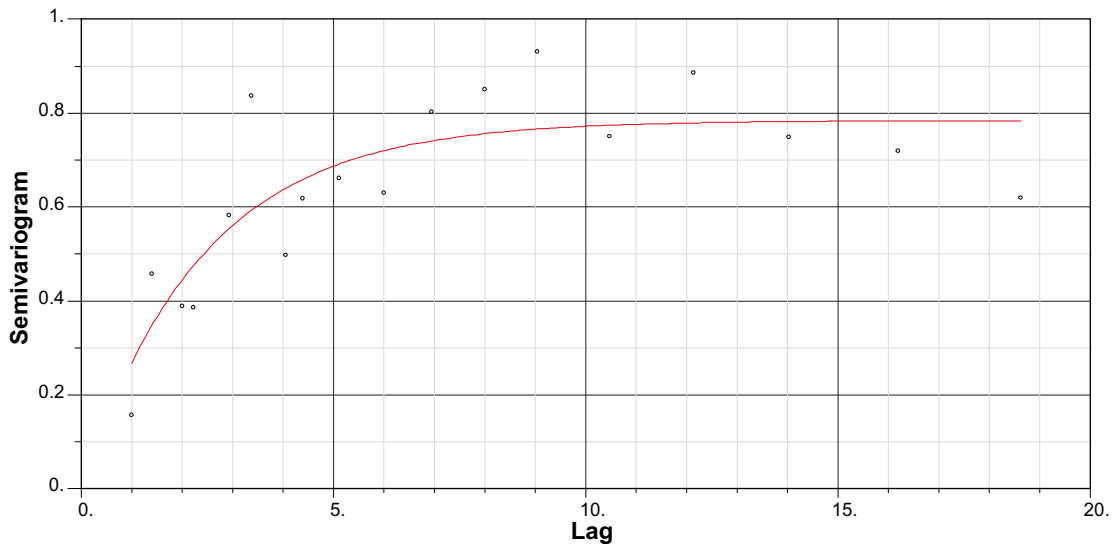
Figure 11-63. *Semivariogram for fracture intensity, AFM001098, WNW Set, linked traces.*
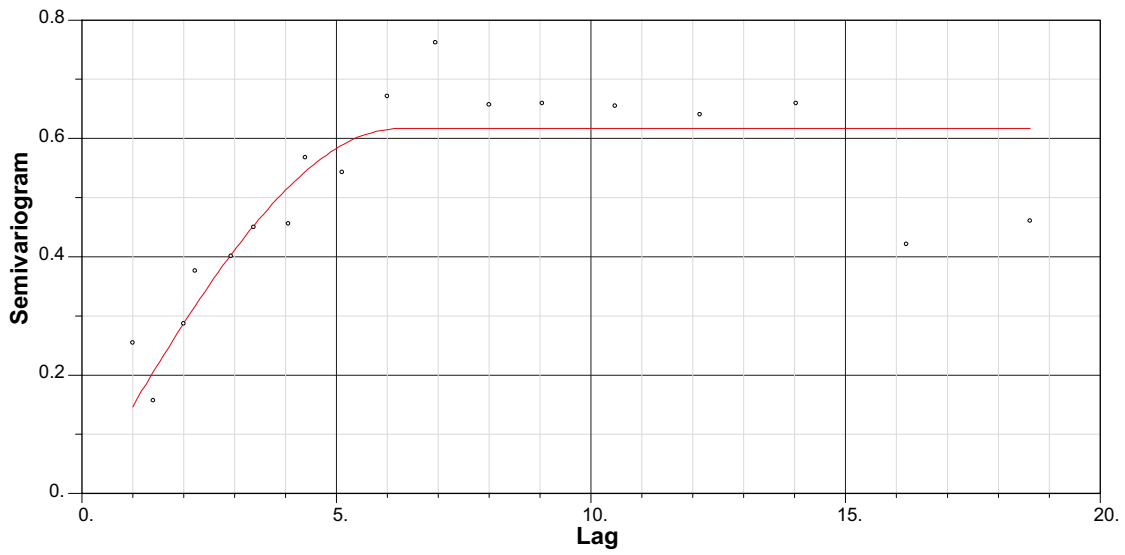
Figure 11-64. *Semivariogram for fracture intensity, AFM001243, NE Set, linked traces.*
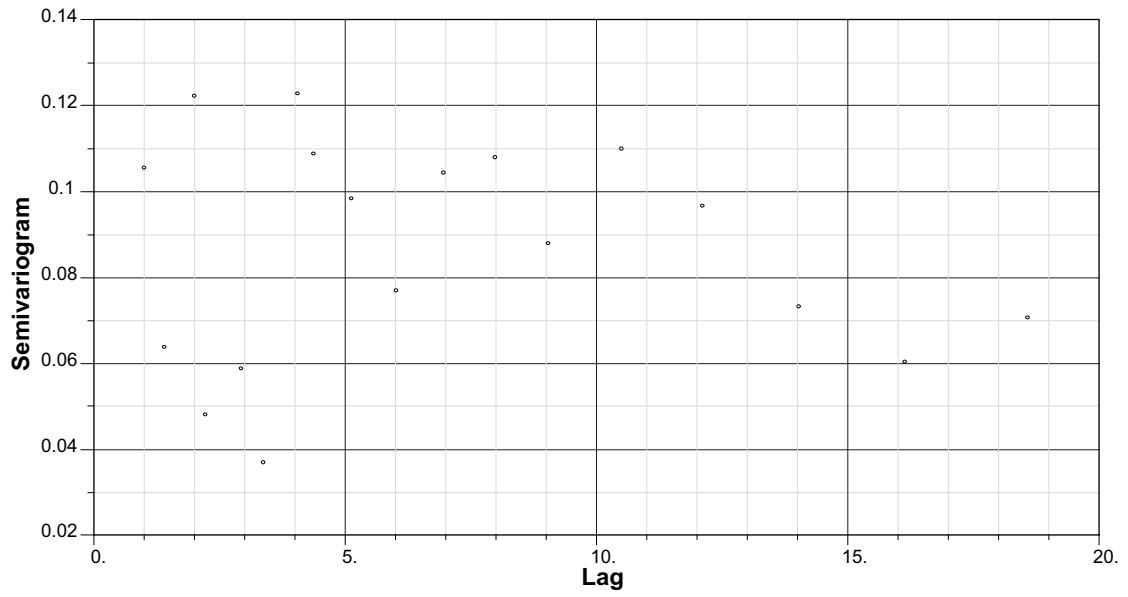
Figure 11-65. *Semivariogram for fracture intensity, AFM001243, NS Set, linked traces. Note that it was not possible to successfully fit a model to this data.*
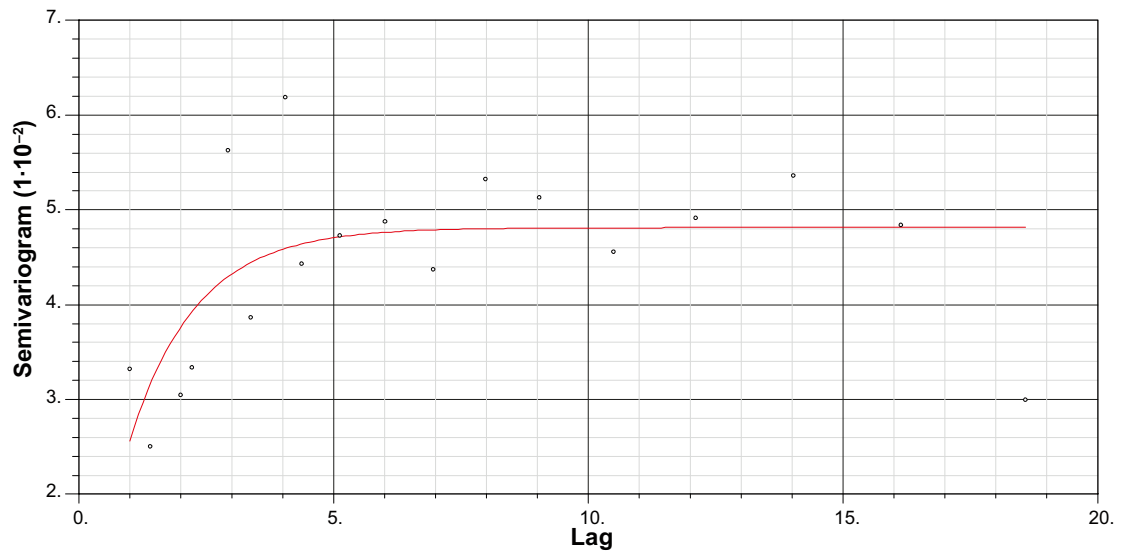
Figure 11-66. *Semivariogram for fracture intensity, AFM001243, SH Set, linked traces.*
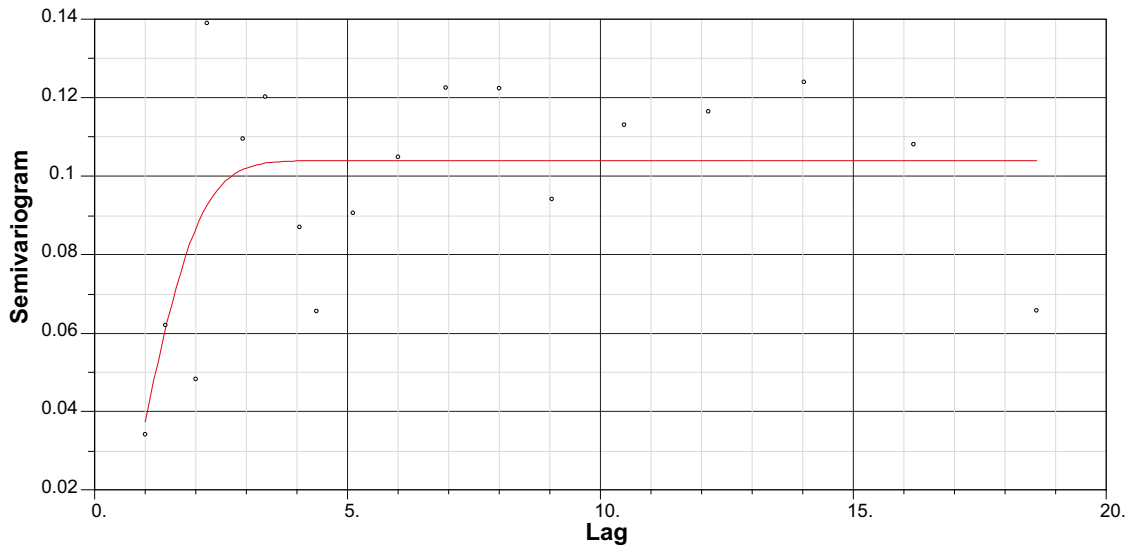
Figure 11-67. *Semivariogram for fracture intensity, AFM001243, WNW Set, linked traces*
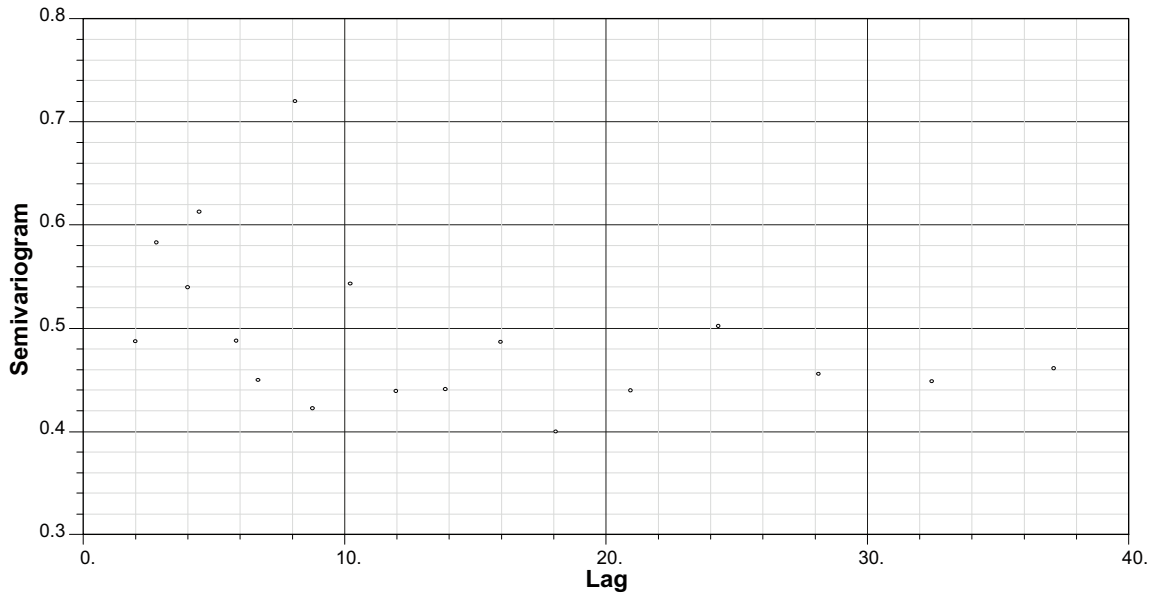
Figure 11-68. *Semivariogram for fracture intensity, AFM001244, NE Set, linked traces. Note that it was not possible to successfully fit a model to this data.*
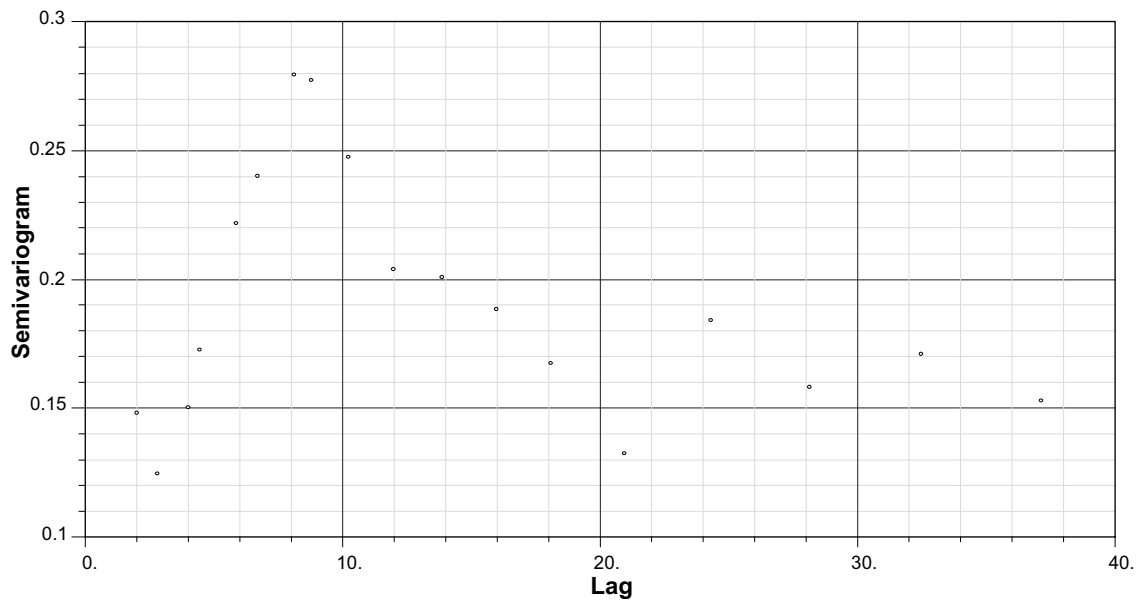
Figure 11-69. *Semivariogram for fracture intensity, AFM001244, NS Set, linked traces. Note that it was not possible to successfully fit a model to this data.*
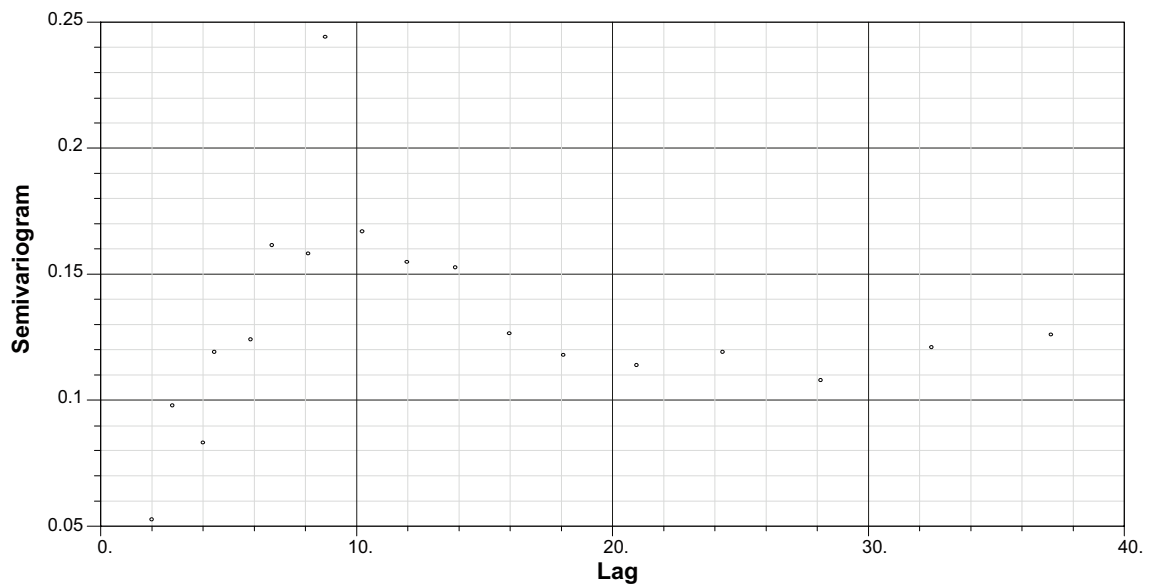
Figure 11-70. *Semivariogram for fracture intensity, AFM001244, NW Set, linked traces. Note that it was not possible to successfully fit a model to this data.*
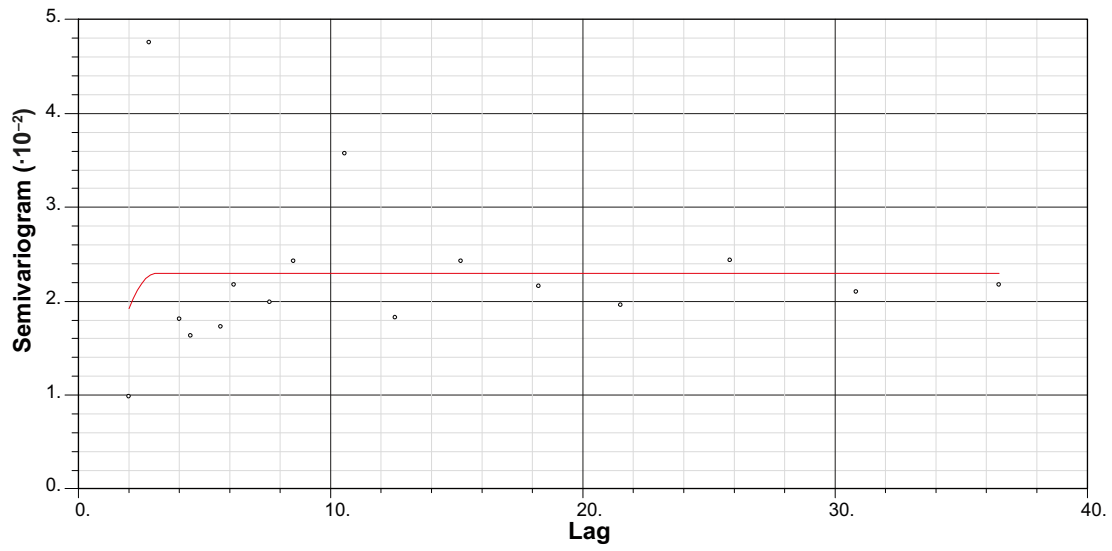
Figure 11-71. *Semivariogram for fracture intensity, AFM001244, SH Set, linked traces.*
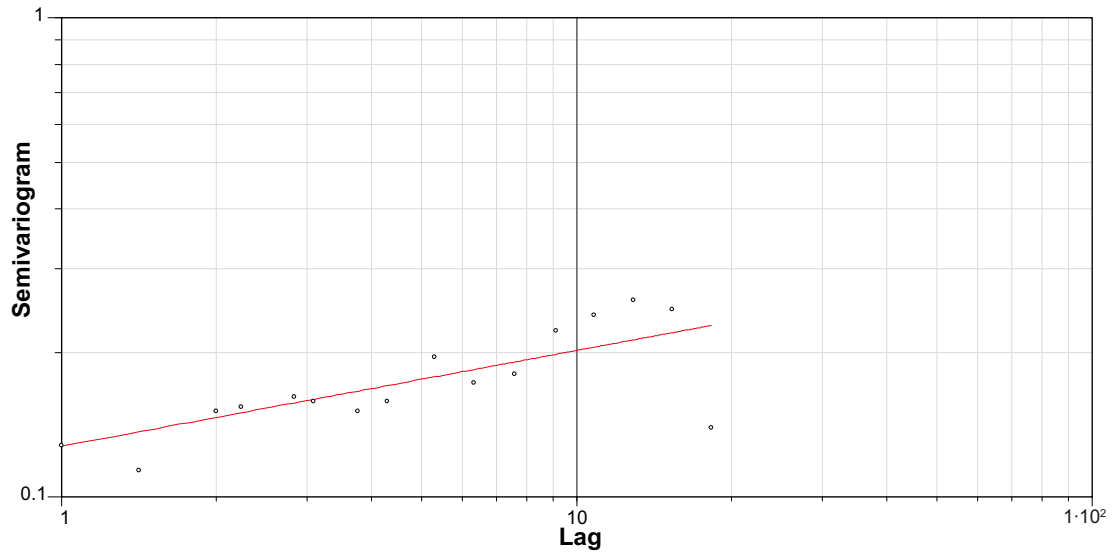
Figure 11-72. *Semivariogram for fracture intensity, AFM001264, NE Set, linked traces.*
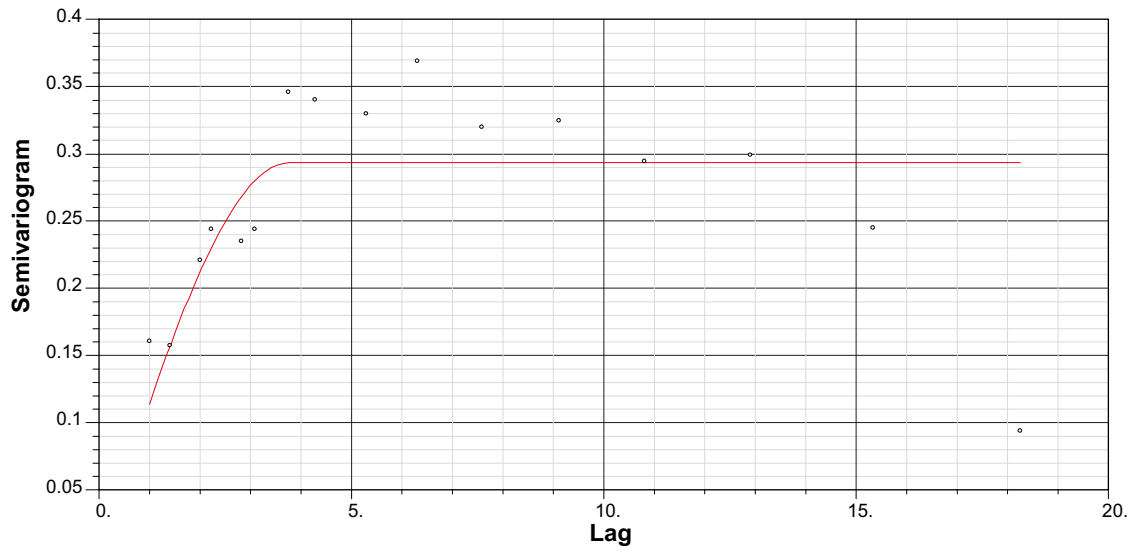
Figure 11-73. *Semivariogram for fracture intensity, AFM001264, NS Set, linked traces.*
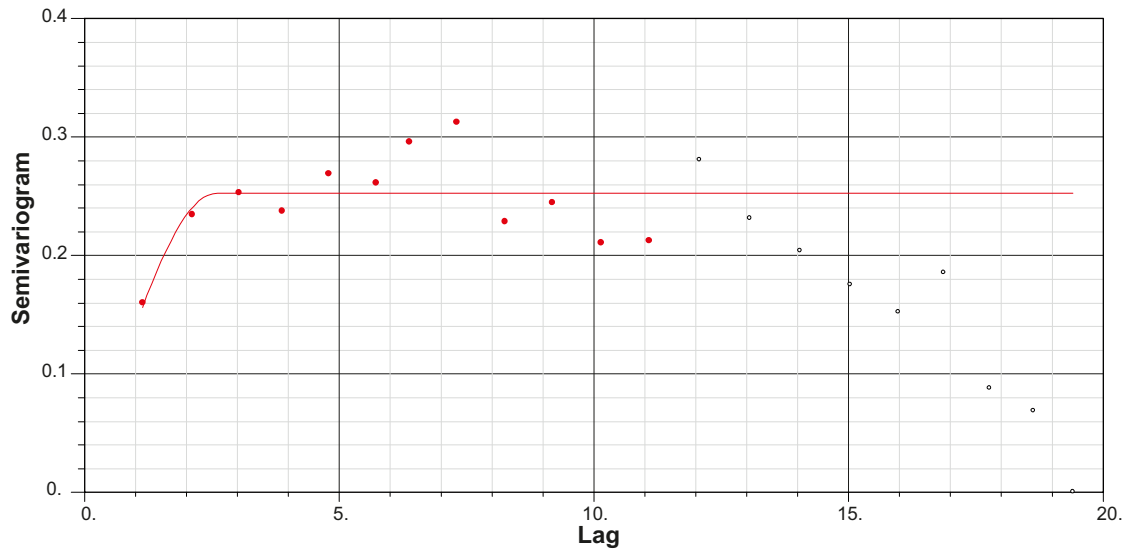
Figure 11-74. *Semivariogram for fracture intensity, AFM001264, NS Set, linked traces.*
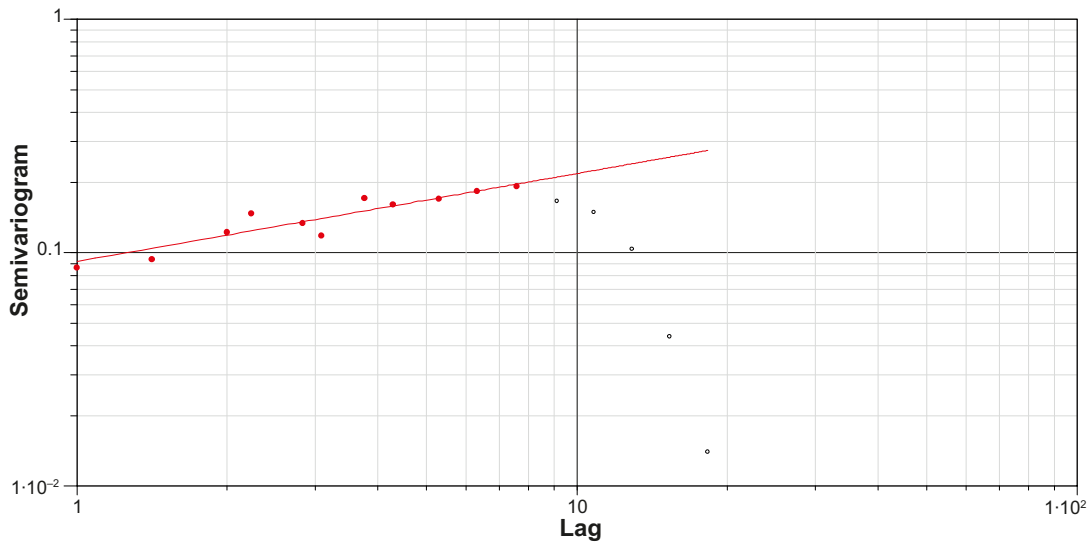
Figure 11-75. *Semivariogram for fracture intensity, AFM001264, SH Set, linked traces.*
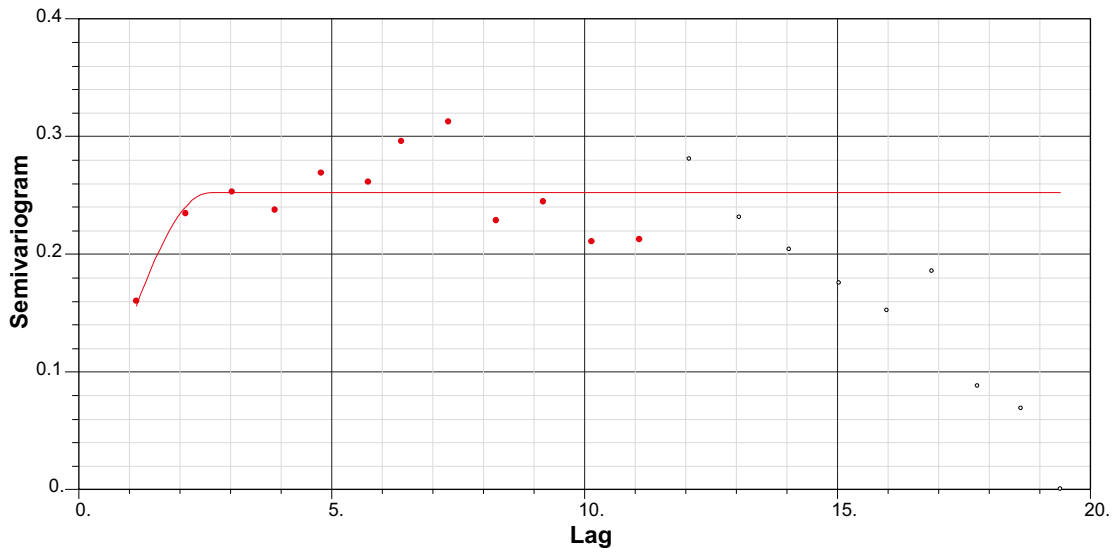
Figure 11-76. *Semivariogram for fracture intensity, AFM001264, ENE Set, linked traces.*
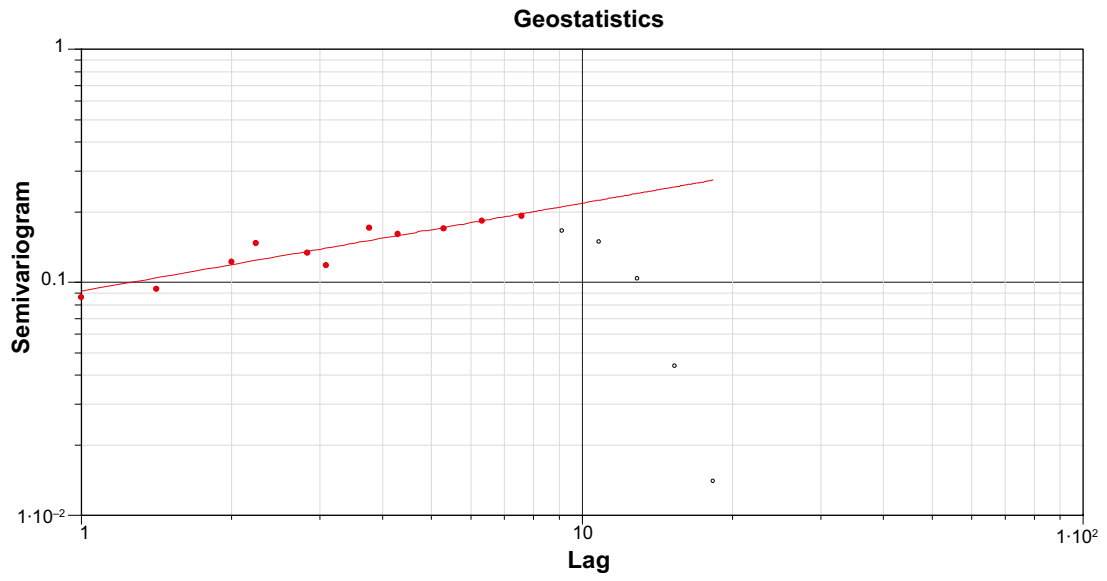
Figure 11-77. *Semivariogram for fracture intensity, AFM001264, WNW Set, linked traces.*
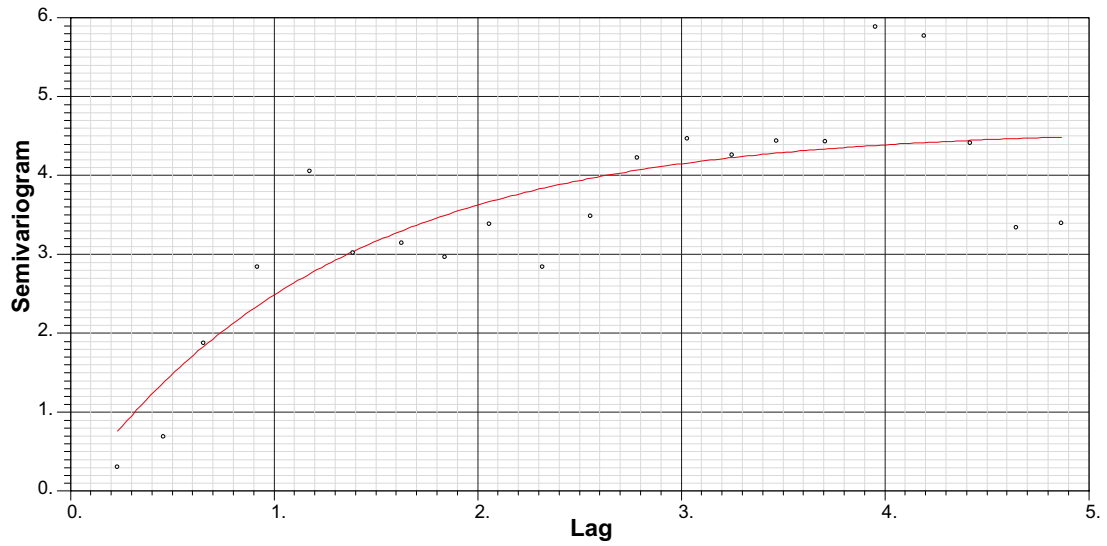
Figure 11-78. *Semivariogram for fracture intensity, AFM001265, NE Set, linked traces.*
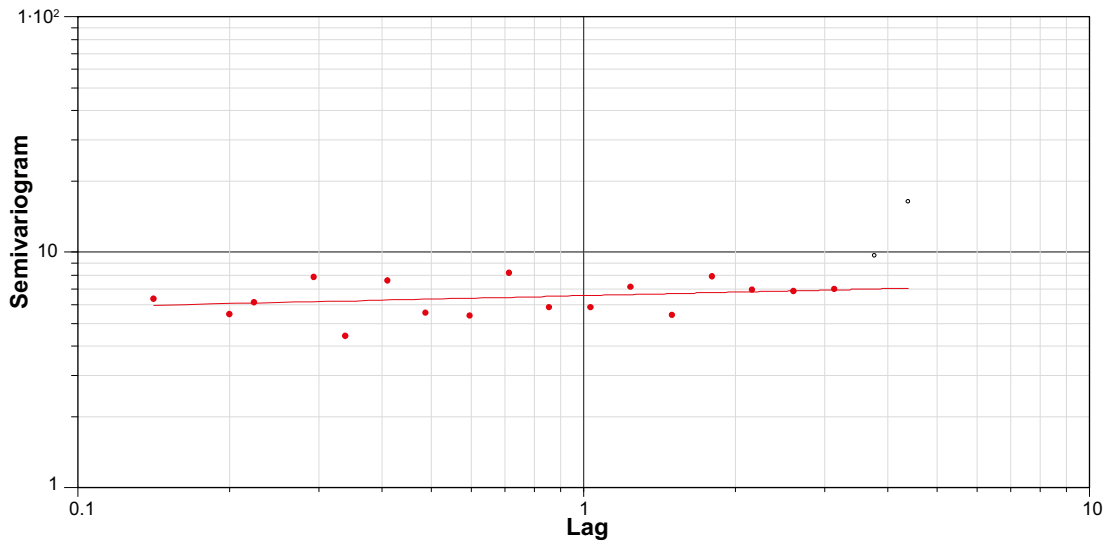
Figure 11-79. *Semivariogram for fracture intensity, AFM001265, EW Set, linked traces.*
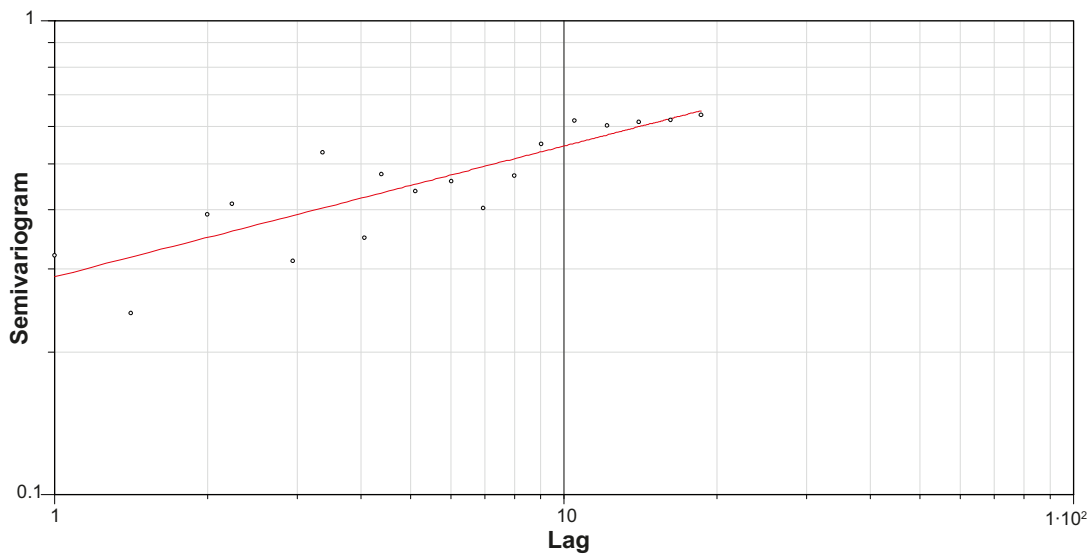
Figure 11-80. *Semivariogram for fracture intensity, AFM100201, NE Set, linked traces.*
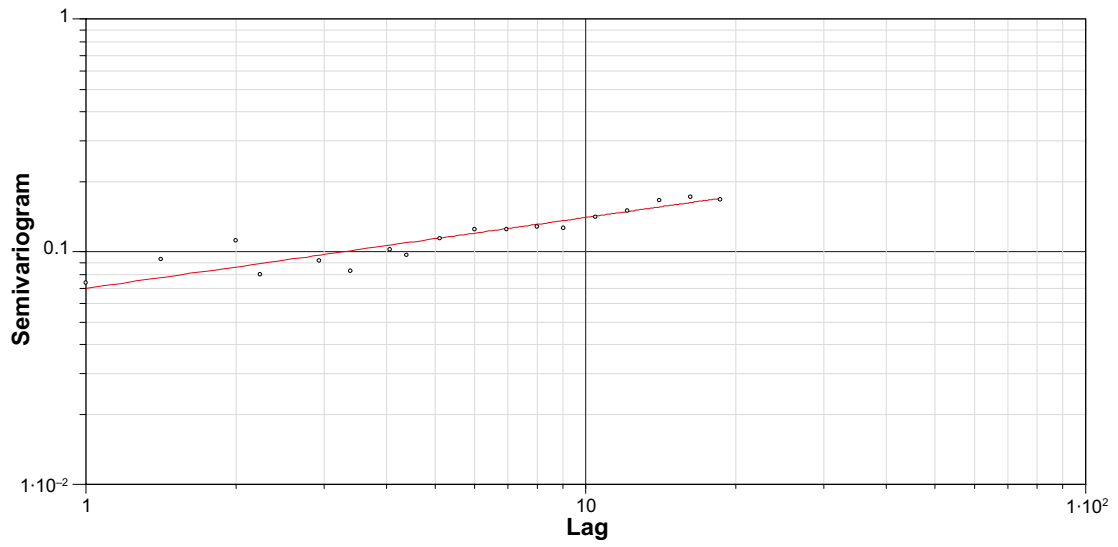
Figure 11-81. *Semivariogram for fracture intensity, AFM100201, NS Set, linked traces.*
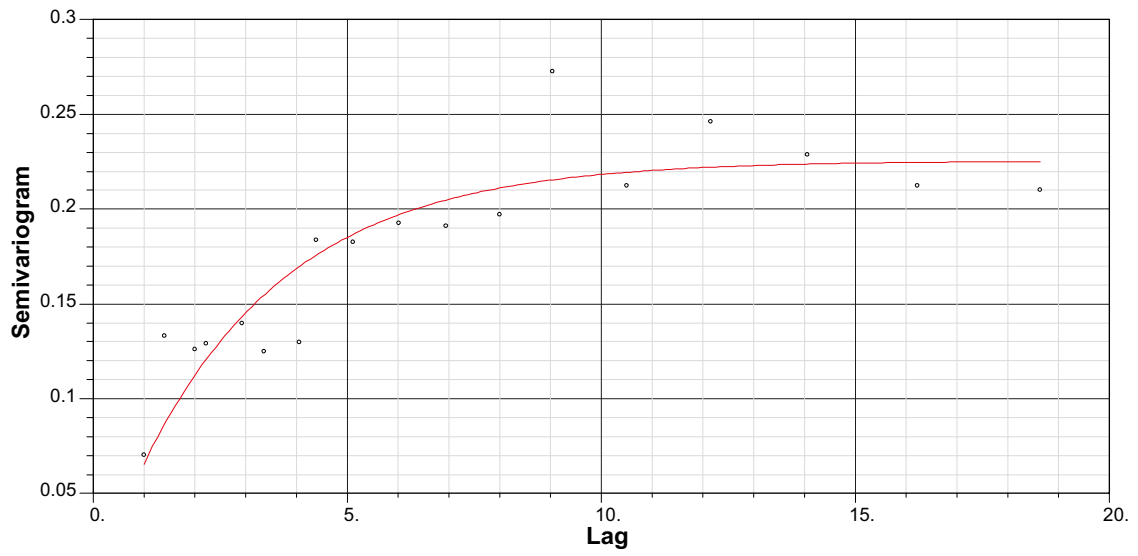
Figure 11-82. *Semivariogram for fracture intensity, AFM100201, NW Set, linked traces.*
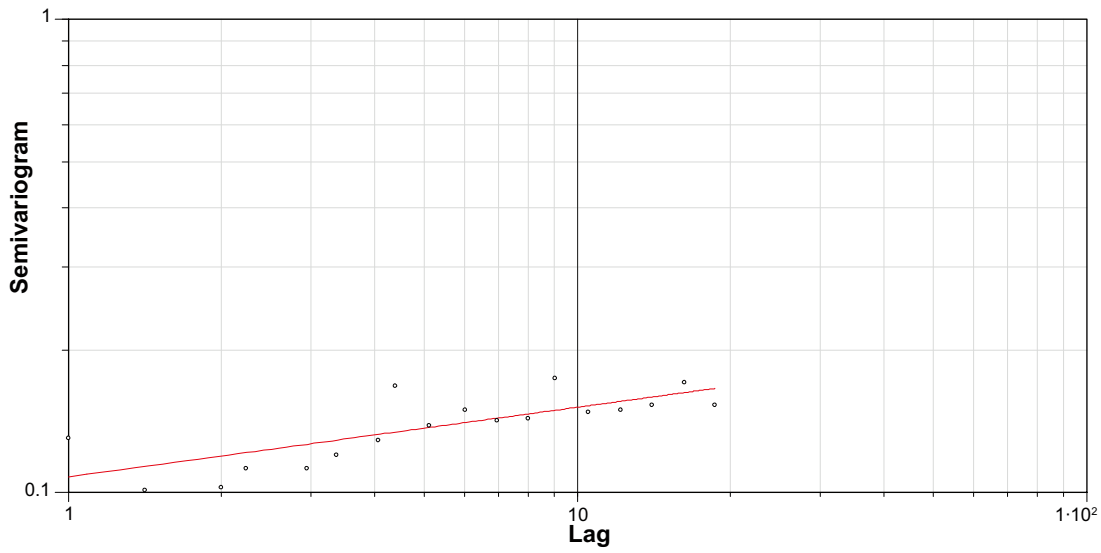
Figure 11-83. *Semivariogram for fracture intensity, AFM100201, SH Set, linked traces.*
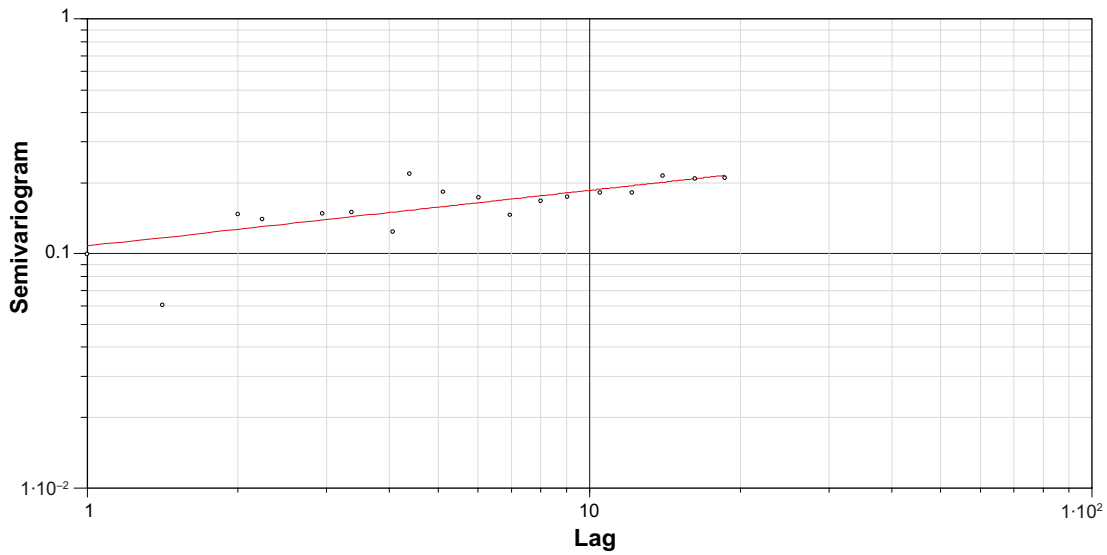
Figure 11-84. *Semivariogram for fracture intensity, AFM100201, EW Set, linked traces.*

Fracture Sets in Forsmark Cored Boreholes
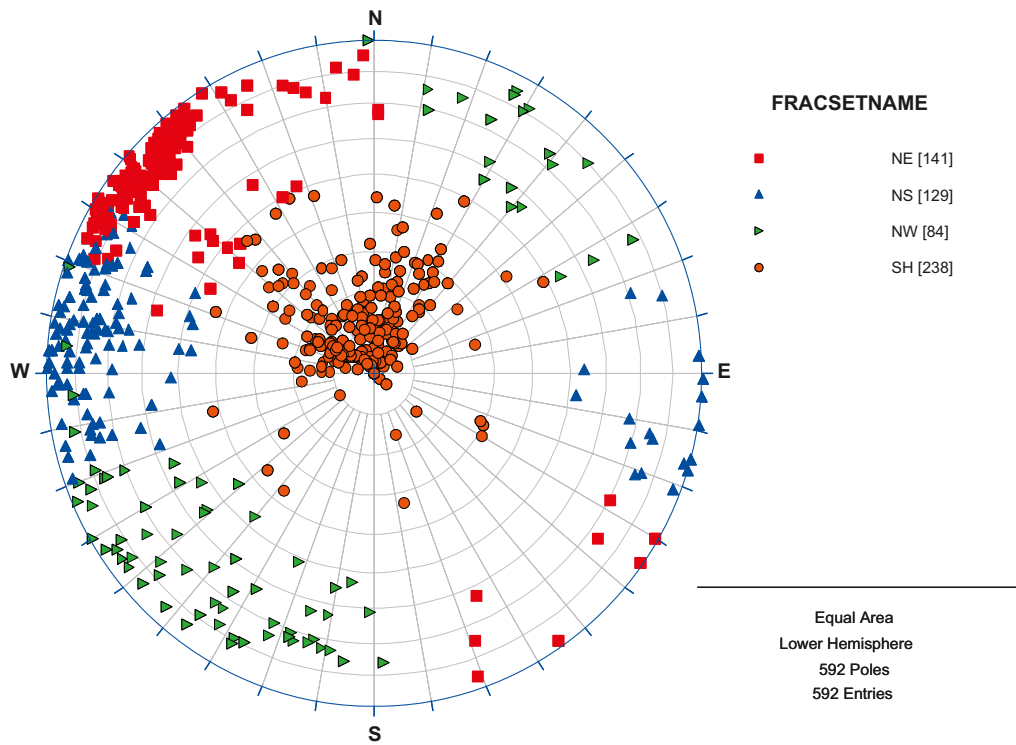
Figure 12-1. *Borehole KFM01A fracture sets, domain FFM01, fractures not affected by DZ*
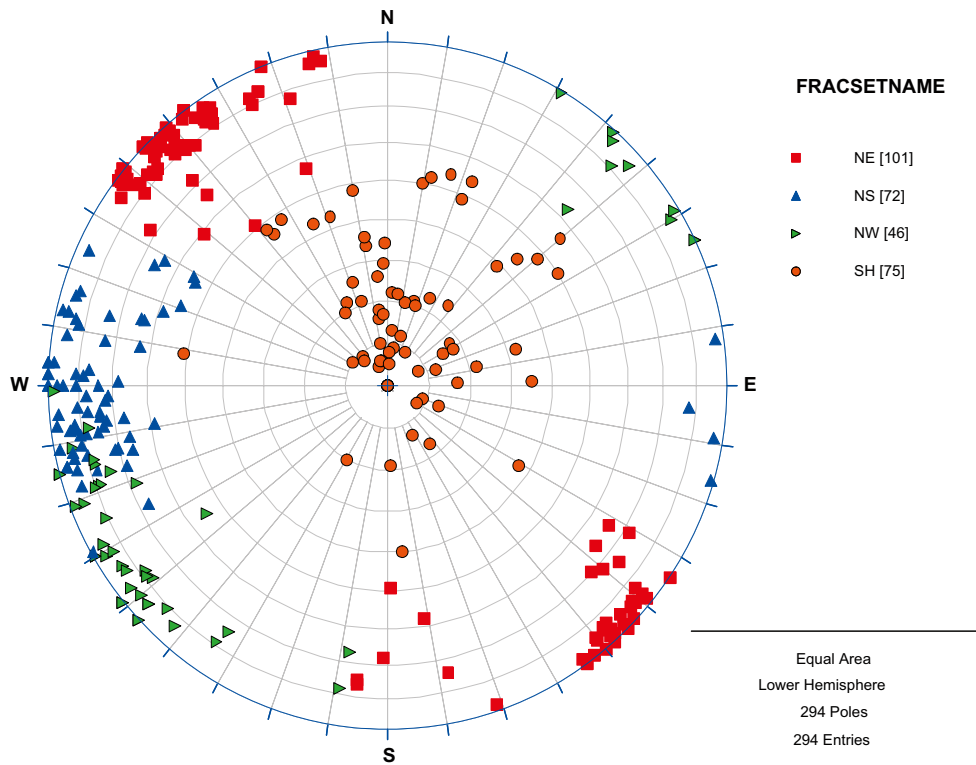
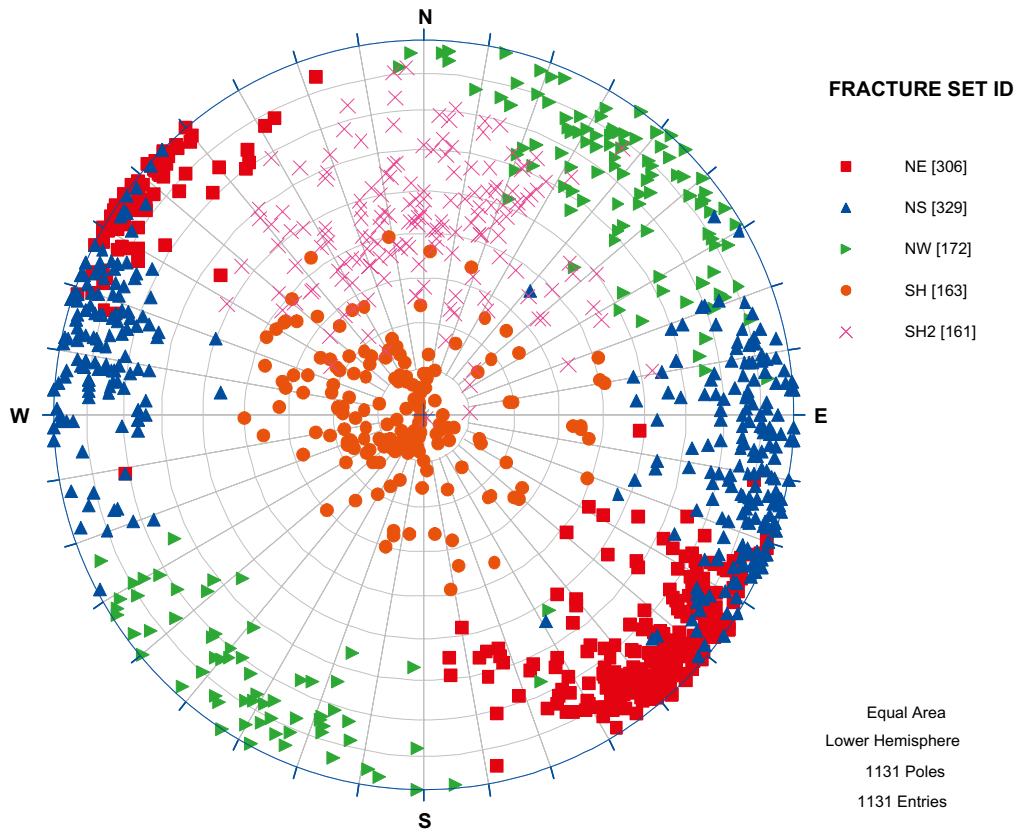***Figure 12-2.*** *Borehole KFM01B fracture sets, domain FFM01, fractures not affected by DZ*
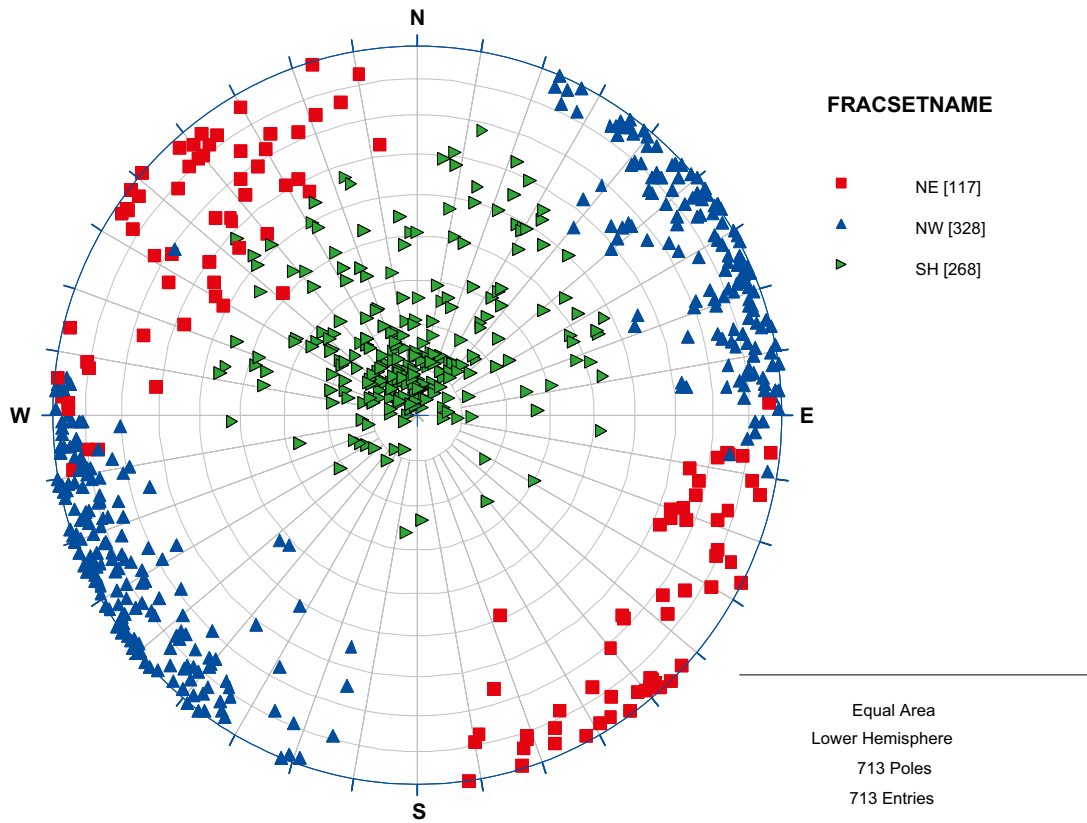
Figure 12-3. *Borehole KFM01D fracture sets, domain FFM01, fractures not affected by DZ*
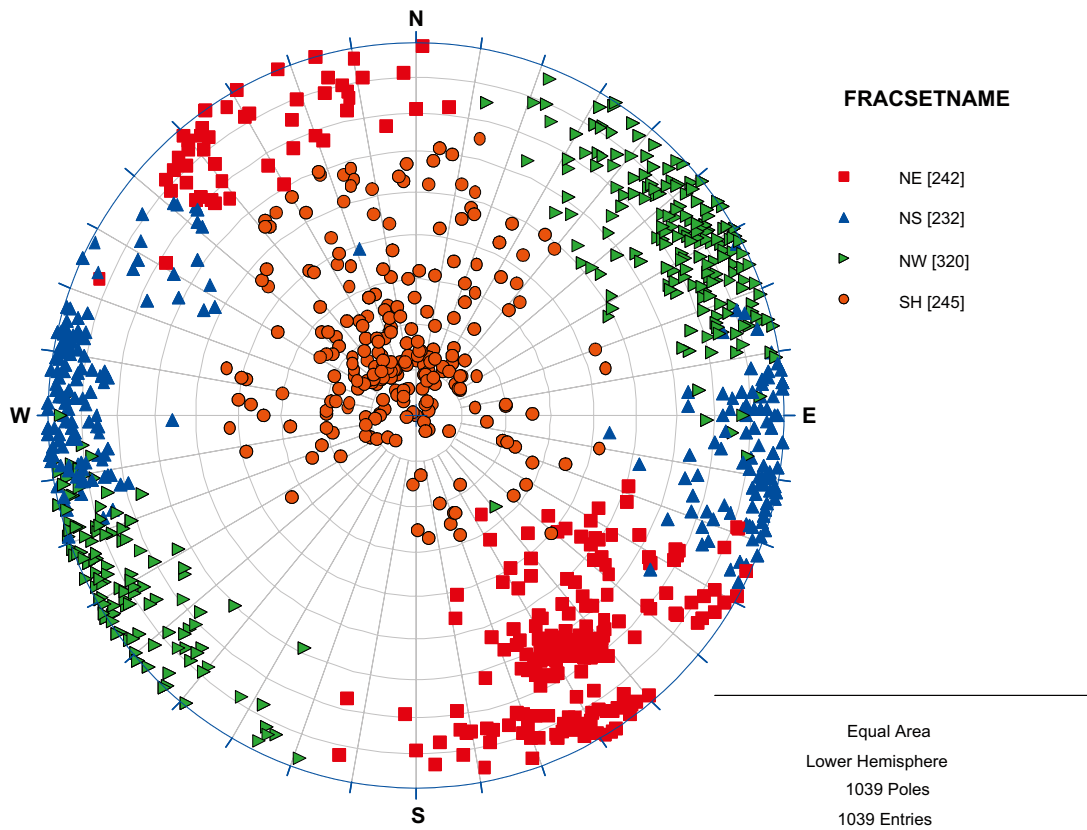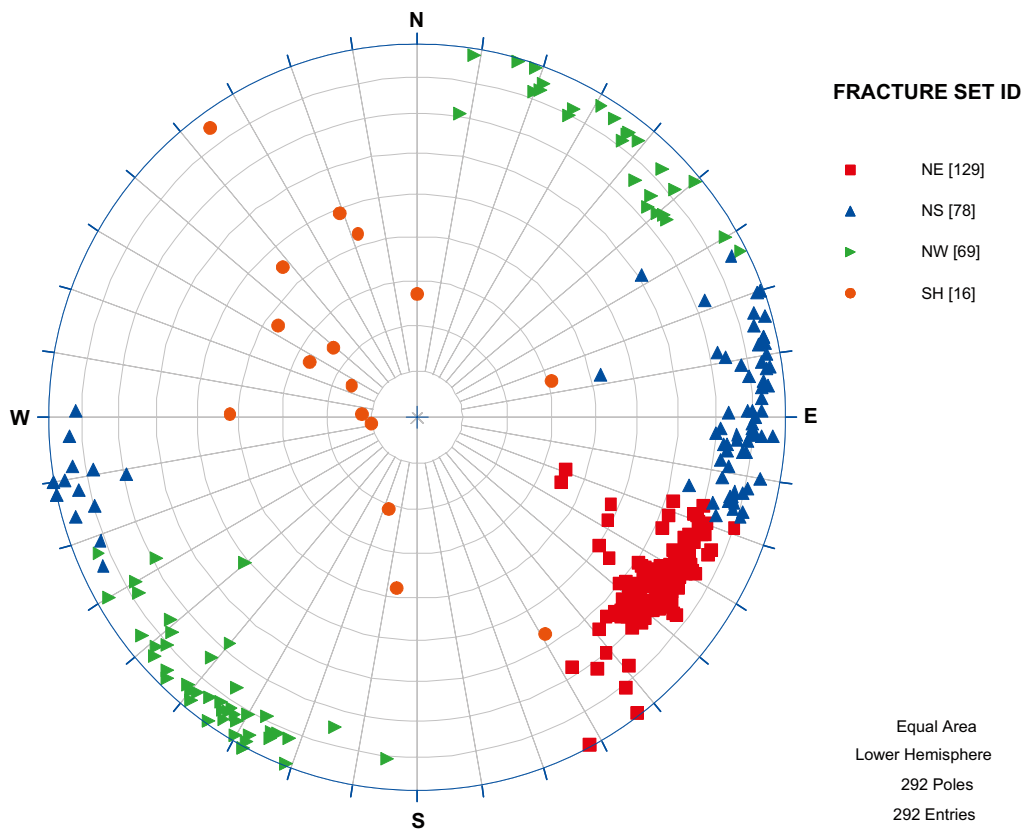

Figure 12-4. *Borehole KFM04A fracture sets, domain FFM01, fractures not affected by DZ.*
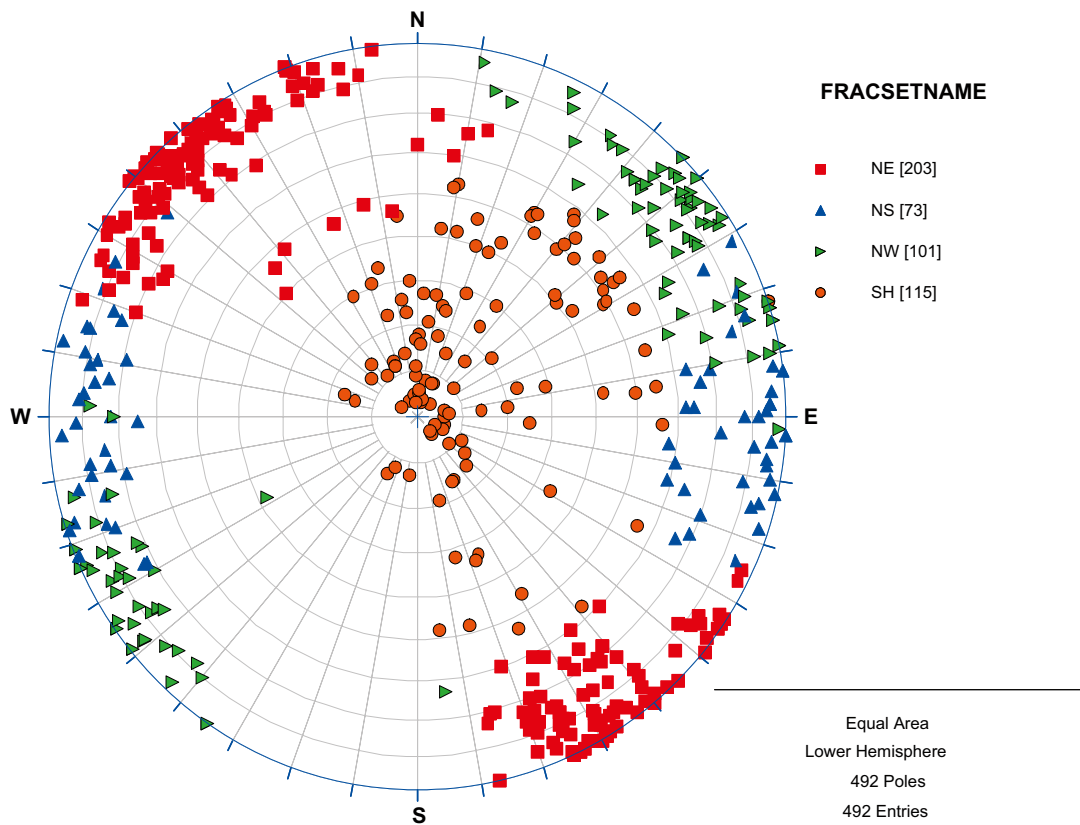
Figure 12-5. *Borehole KFM05A fracture sets, domain FFM01, fractures not affected by DZ.*
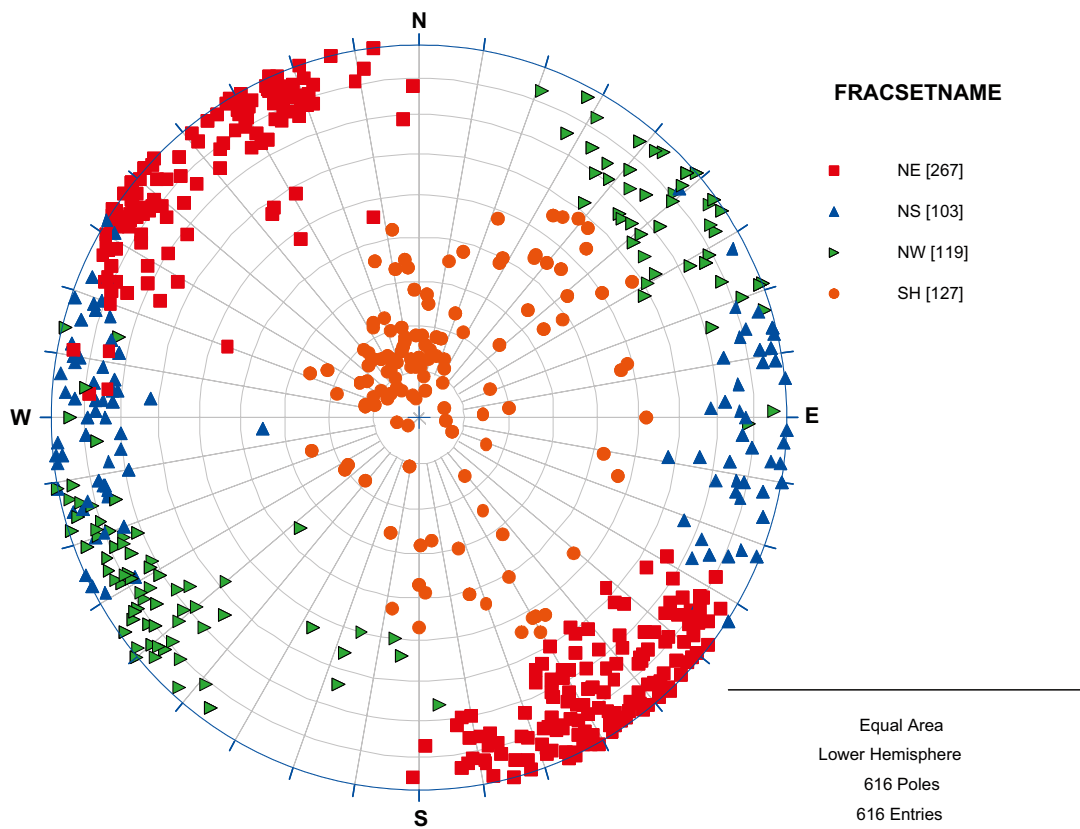
Figure 12-6. *Borehole KFM05A fracture sets, domain FFM01, fractures affected by DZ.*
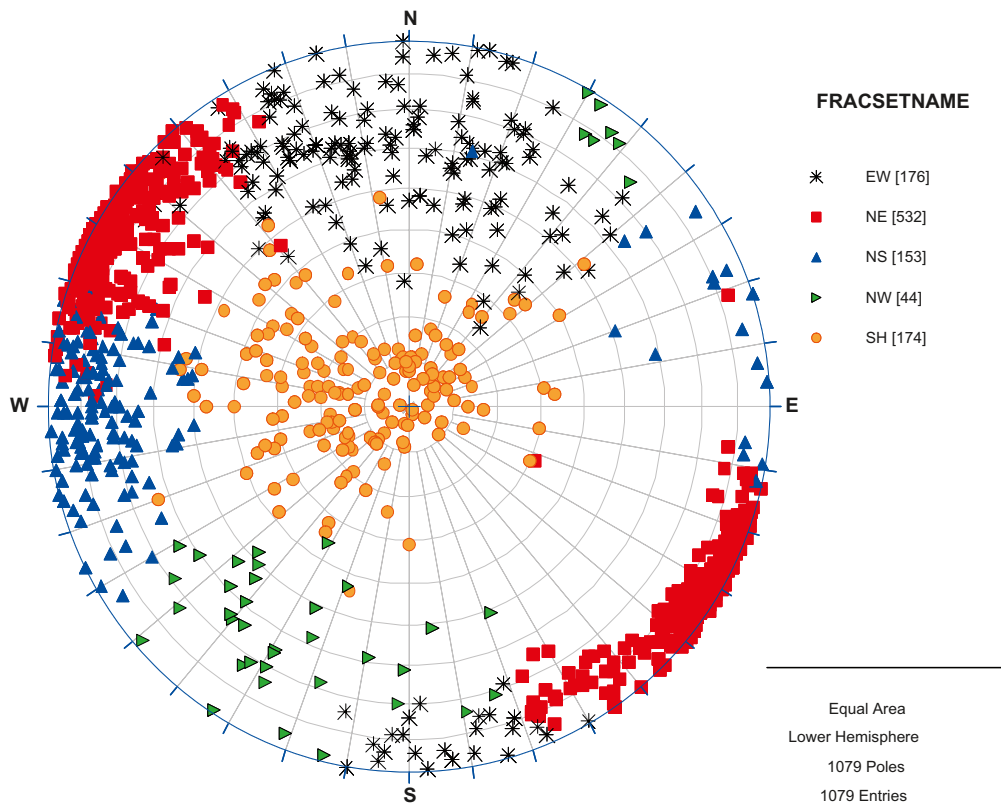
Figure 12-7. *Borehole KFM06A fracture sets, domain FFM01, fractures not affected by DZ.*
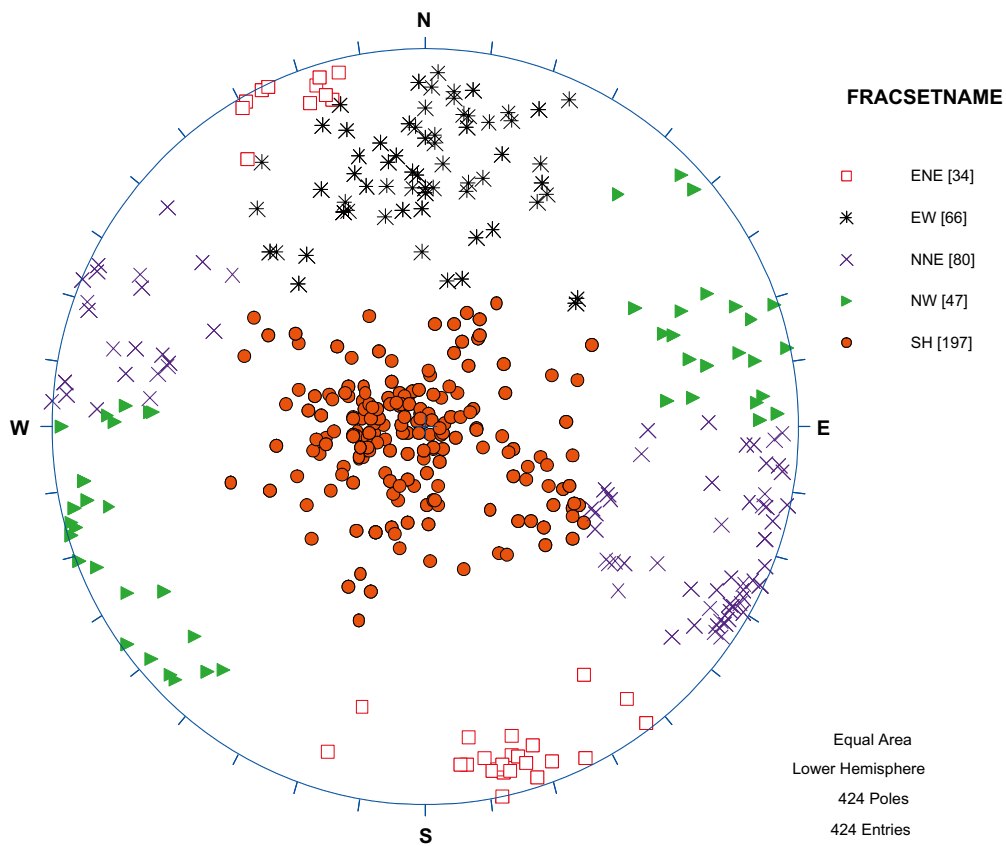
Figure 12-8. *Borehole KFM06C fracture sets, domain FFM01, fractures not affected by DZ.*
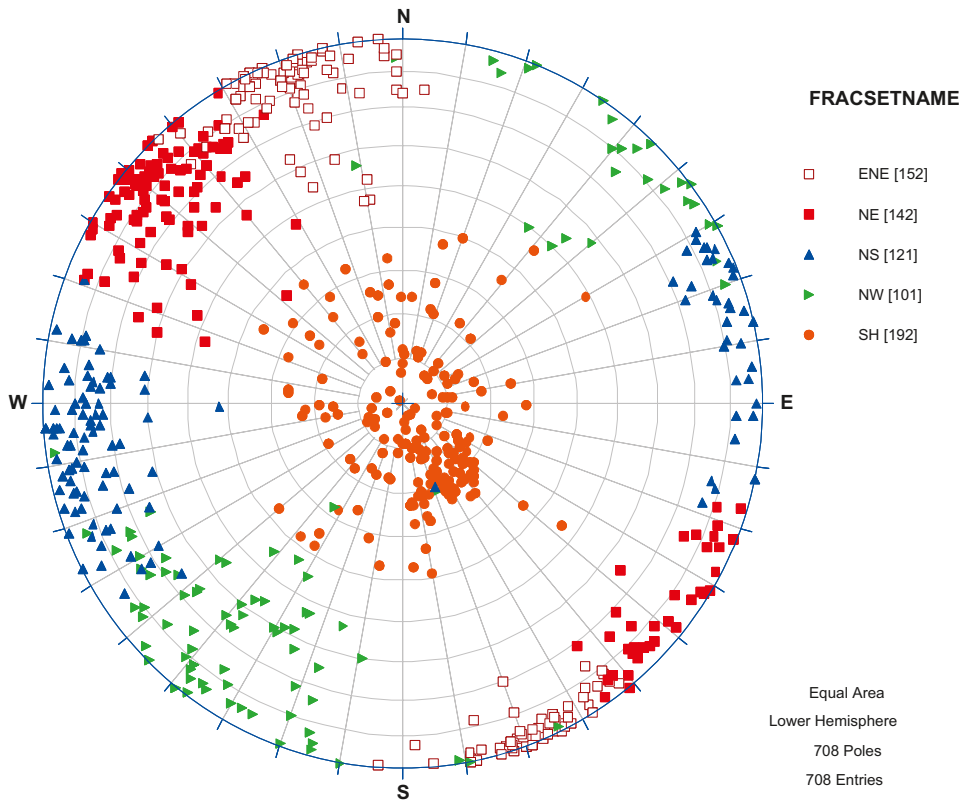
Figure 12-9. *Borehole KFM07A fracture sets, domain FFM01, fractures not affected by DZ.*
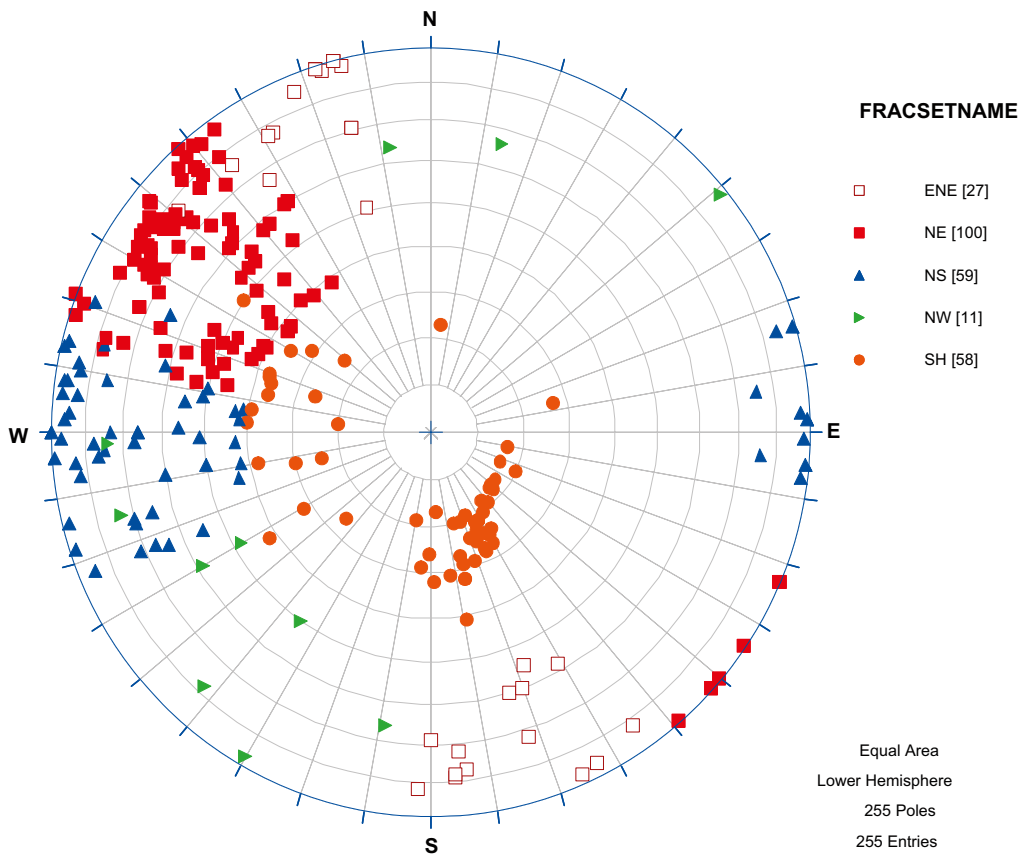
Figure 12-10. *Borehole KFM07A fracture sets, domain FFM01, fractures affected by DZ.*
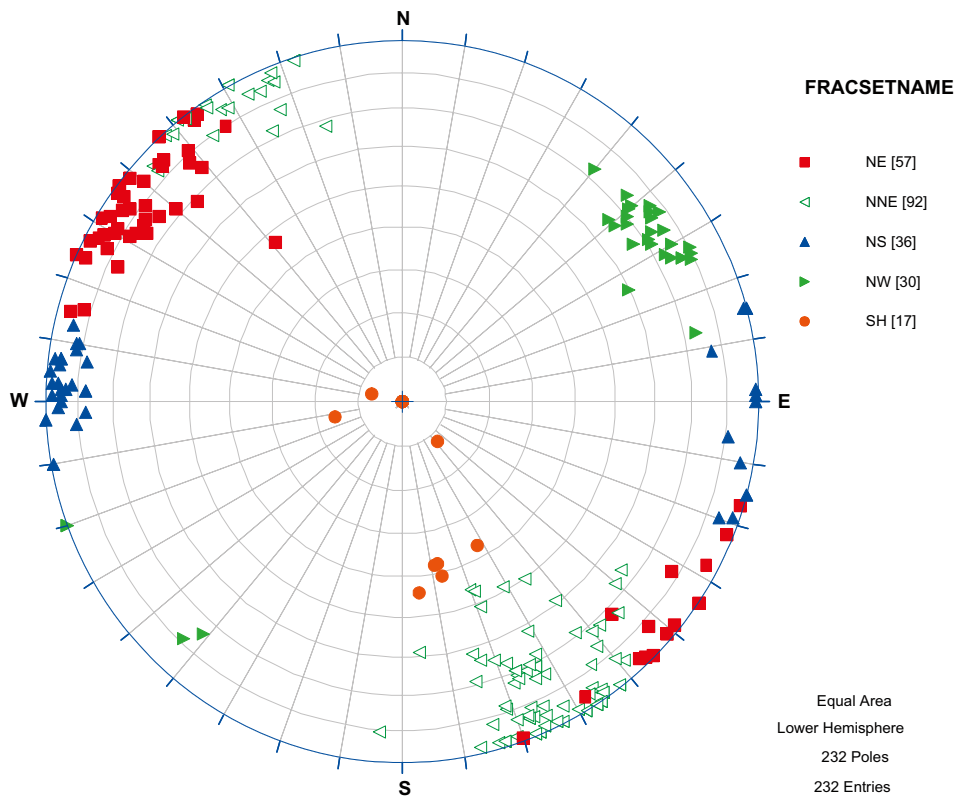
Figure 12-11. *Borehole KFM07B fracture sets, domain FFM01, fractures not affected by DZ.*
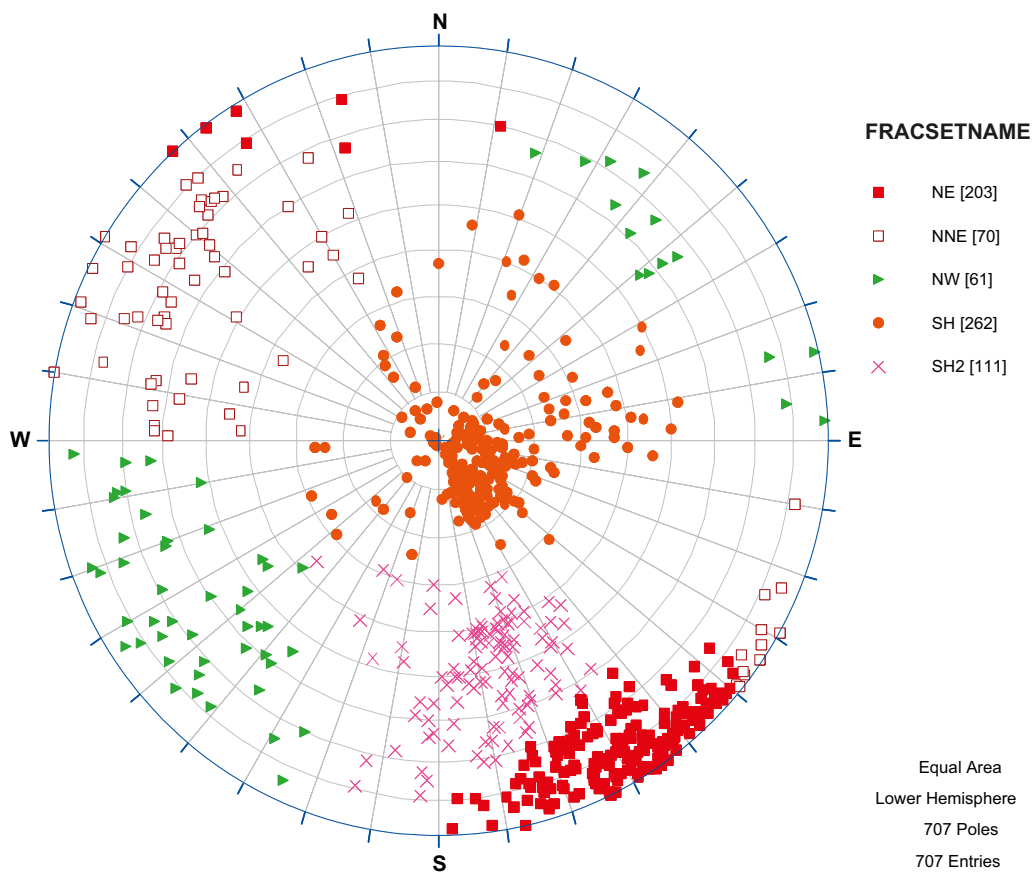
Figure 12-12. *Borehole KFM07C fracture sets, domain FFM01, fractures not affected by DZ.*
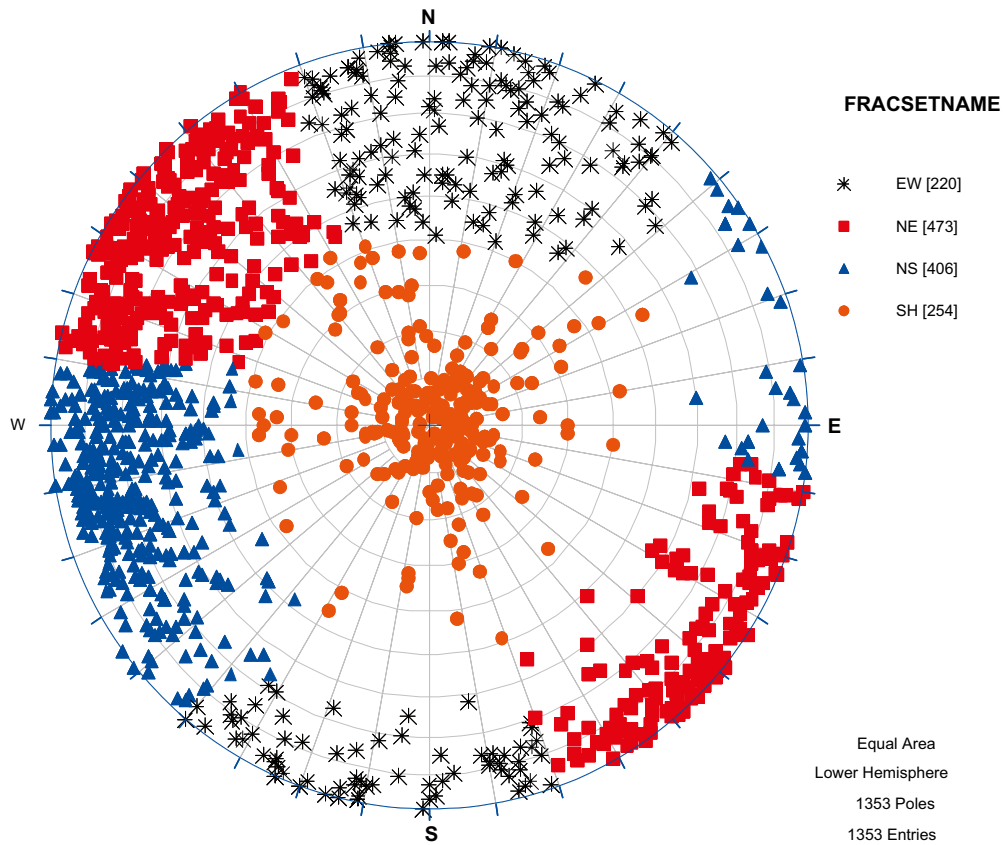
Figure 12-13. *Borehole KFM08A fracture sets, domain FFM01, fractures not affected by DZ.*
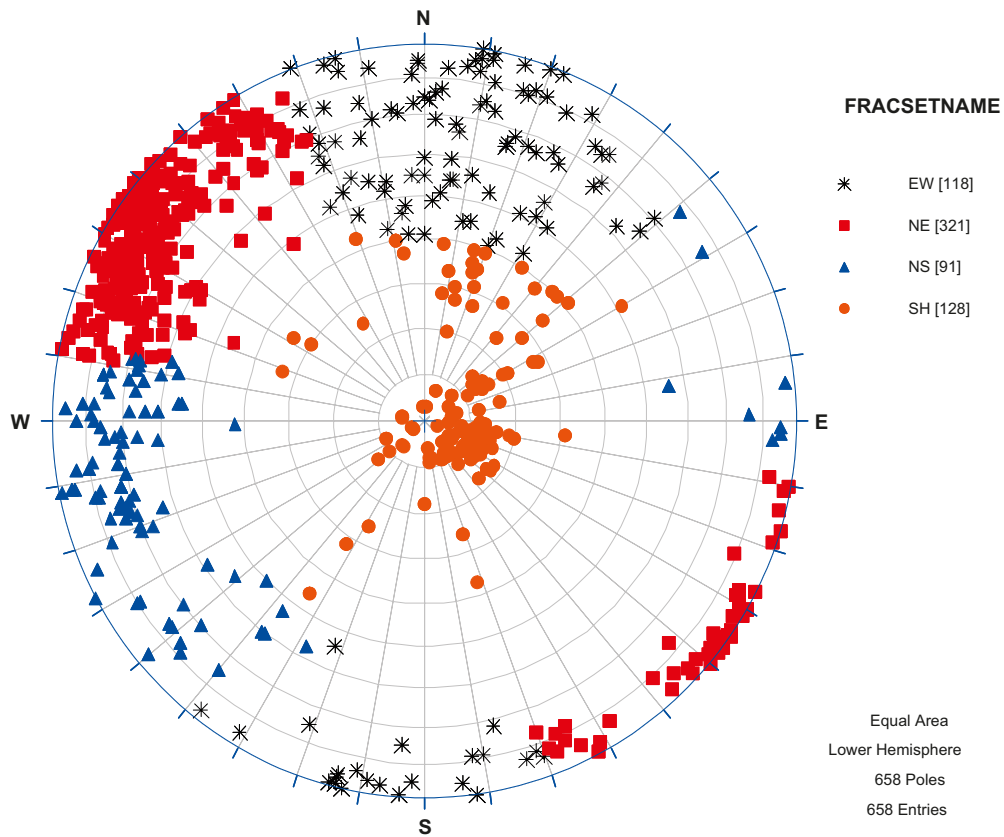
Figure 12-14. *Borehole KFM08A fracture sets, domain FFM01, fractures affected by DZ.*
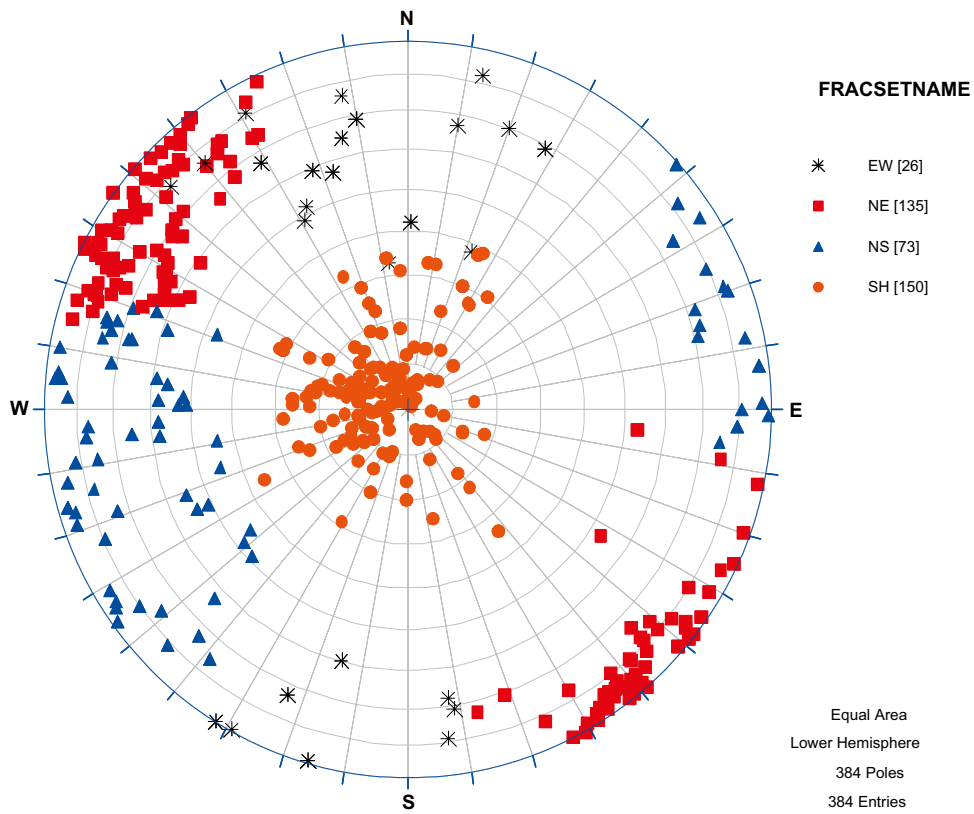
Figure 12-15. *Borehole KFM08B fracture sets, domain FFM01, fractures not affected by DZ.*
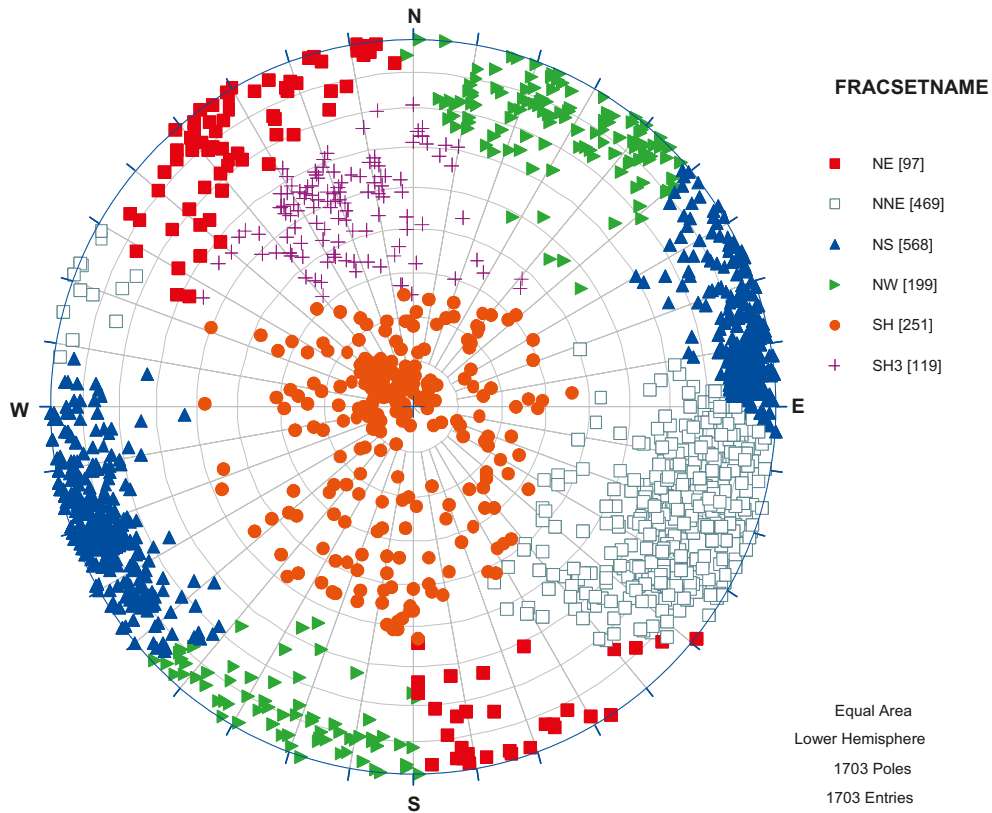
Figure 12-16. *Borehole KFM08C fracture sets, domain FFM01, fractures nor affected by DZ.*
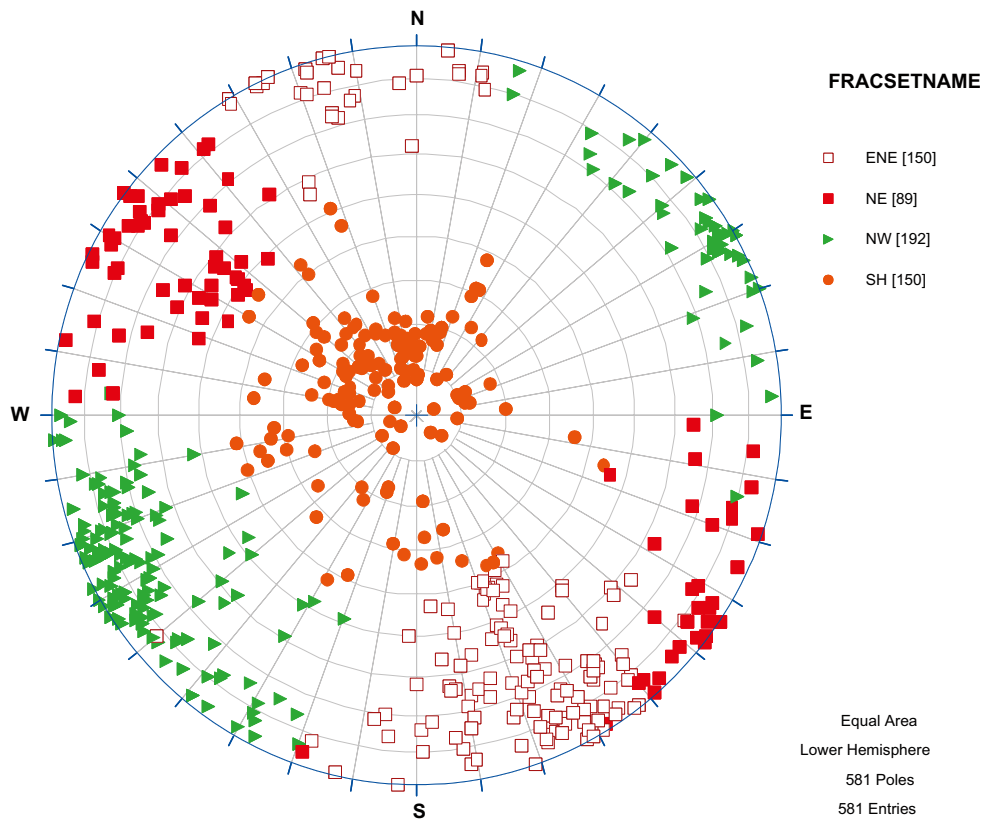
Figure 12-17. *Borehole KFM09A fracture sets, domain FFM01, fractures not affected by DZ.*
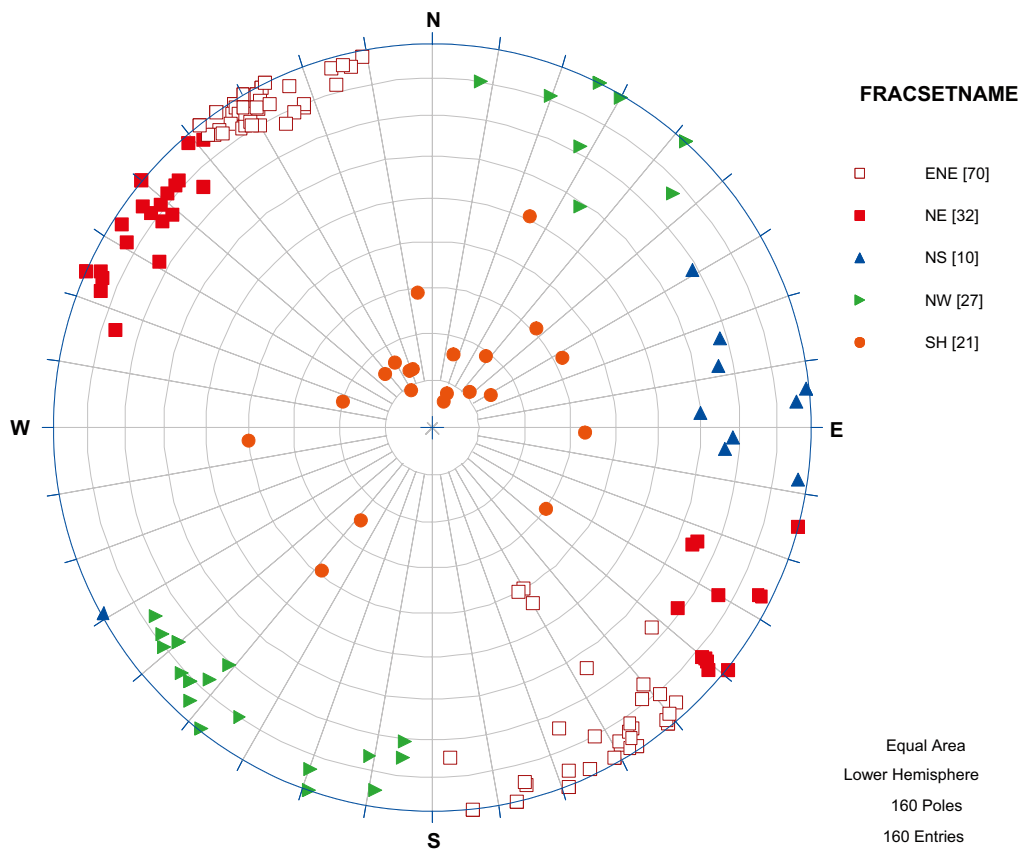
Figure 12-18. *Borehole KFM09B fracture sets, domain FFM01, fractures not affected by DZ.*
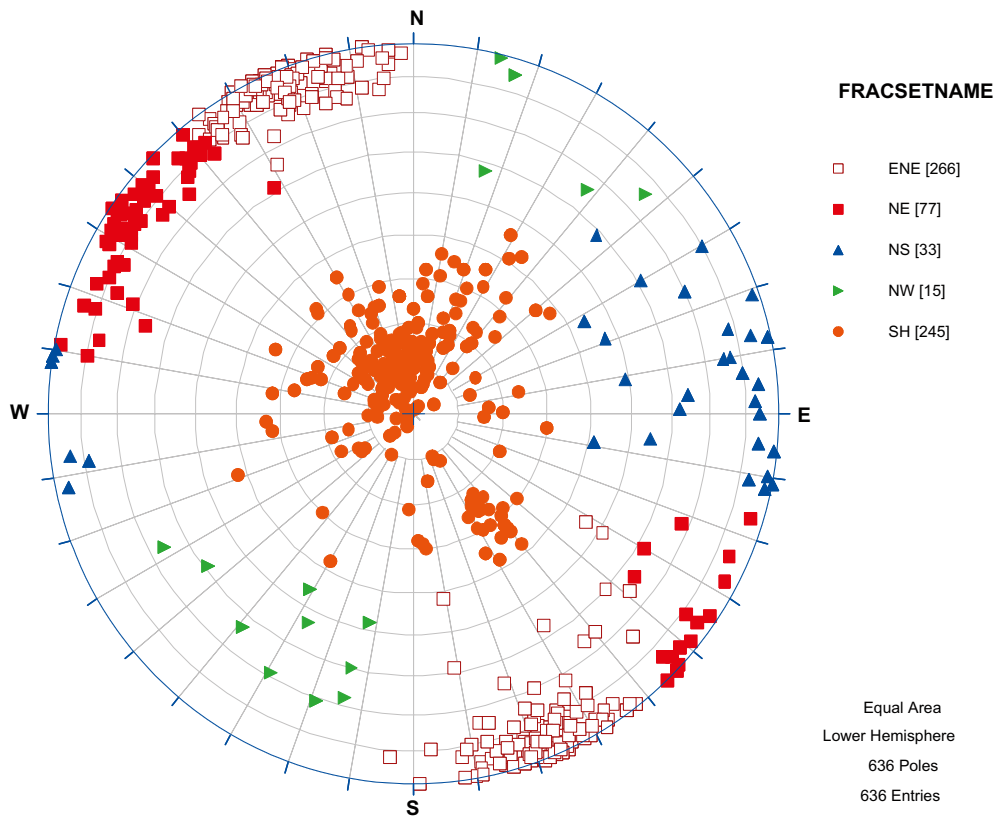
Figure 12-19. *Borehole KFM09B fracture sets, domain FFM01, fractures affected by DZ.*
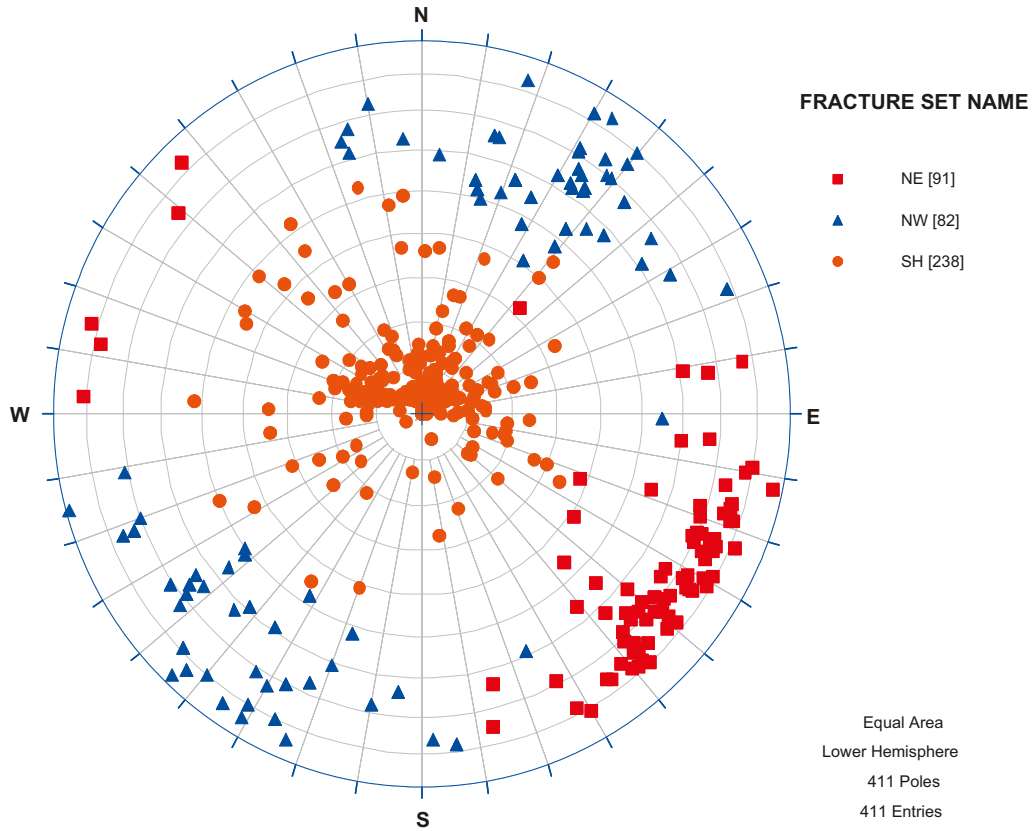
Figure 12-20. *Borehole KFM01A fracture sets, domain FFM02, fractures not affected by DZ.*
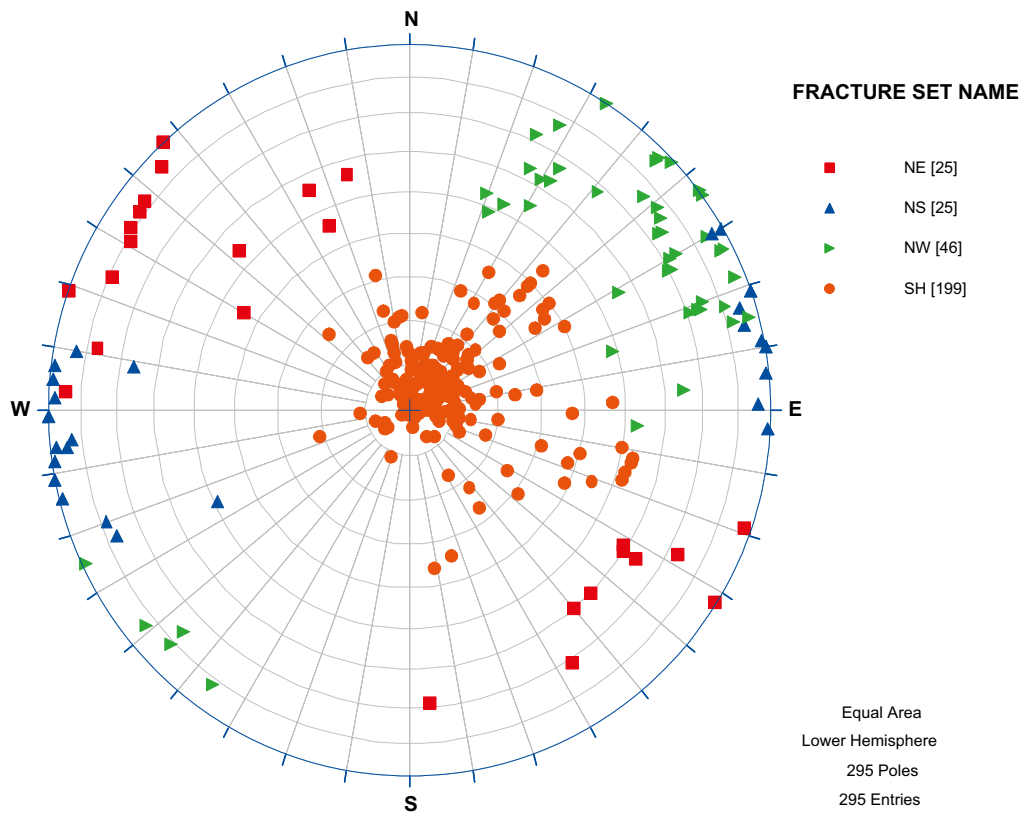
Figure 12-21. *Borehole KFM01B fracture sets, domain FFM02, fractures not affected by DZ.*
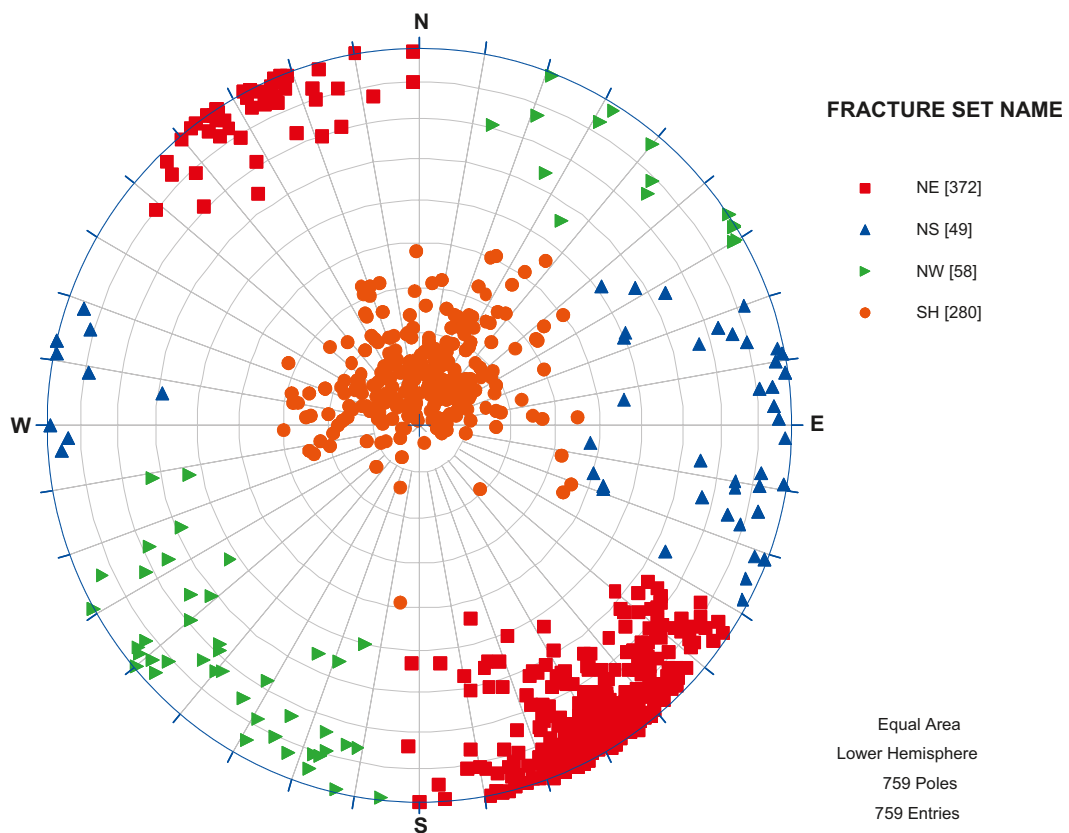
Figure 12-22. *Borehole KFM01C fracture sets, domain FFM02, fractures not affected by DZ.*
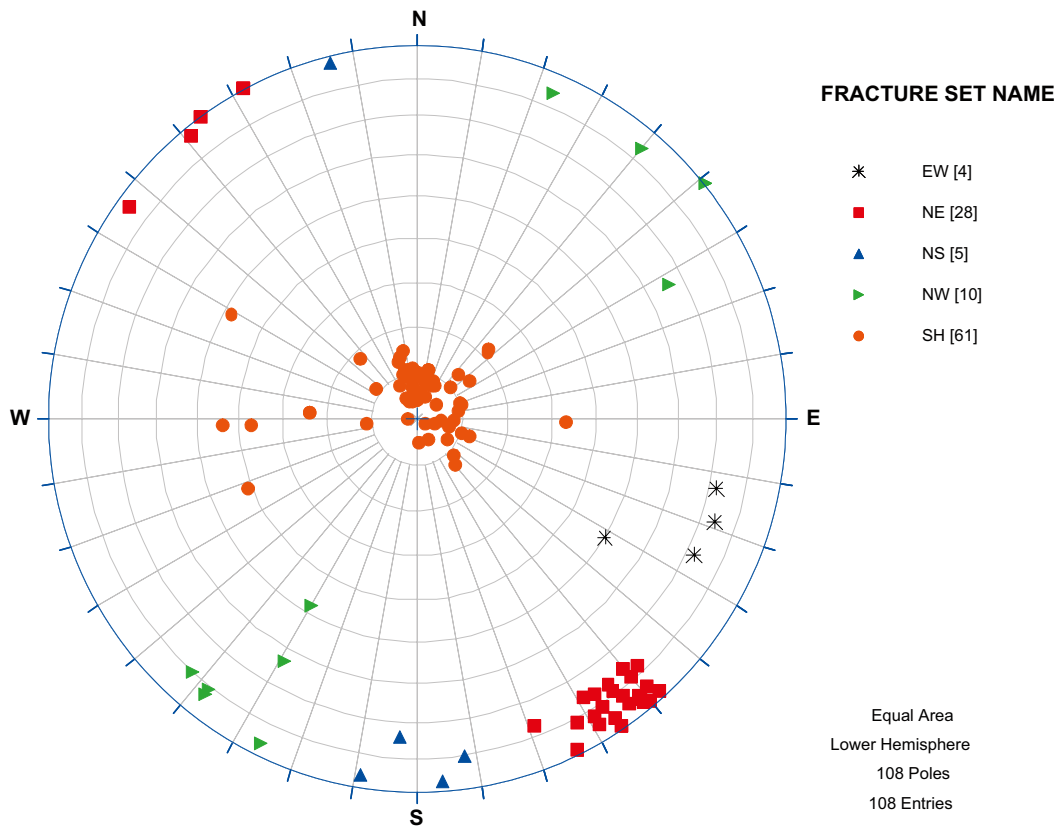
Figure 12-23. *Borehole KFM01C fracture sets, domain FFM02, fractures affected by DZ.*
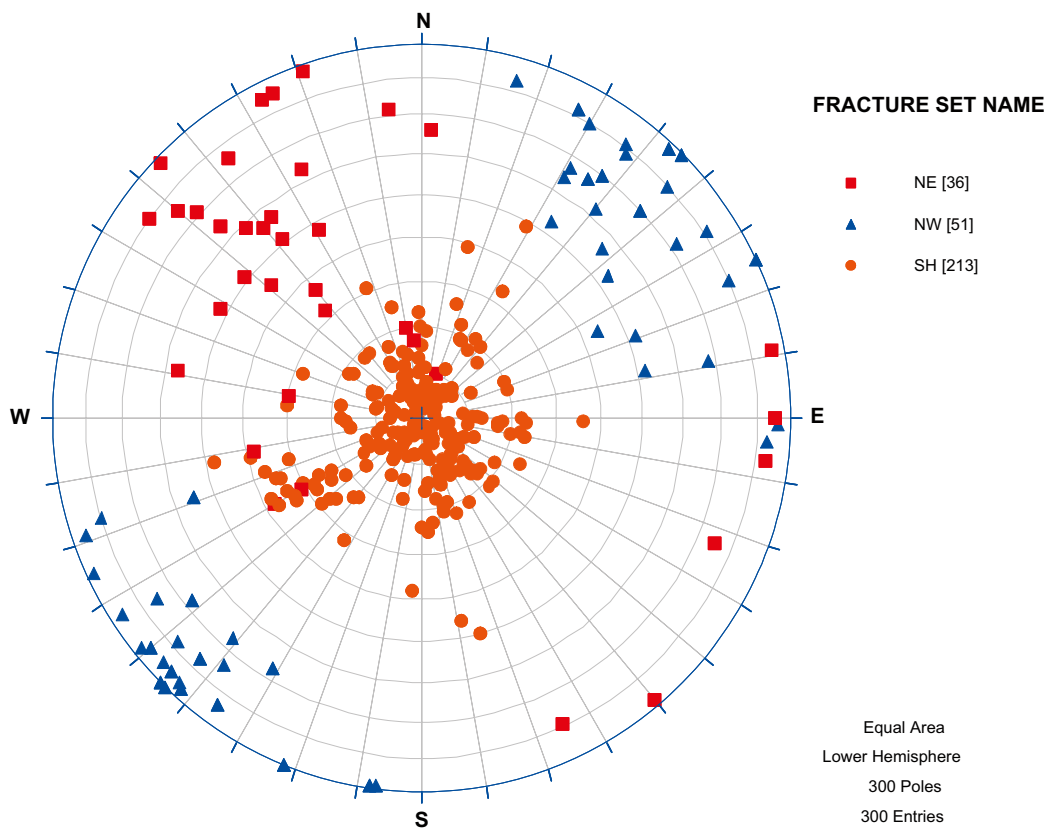
Figure 12-24. *Borehole KFM01D fracture sets, domain FFM02, fractures not affected by DZ.*

120
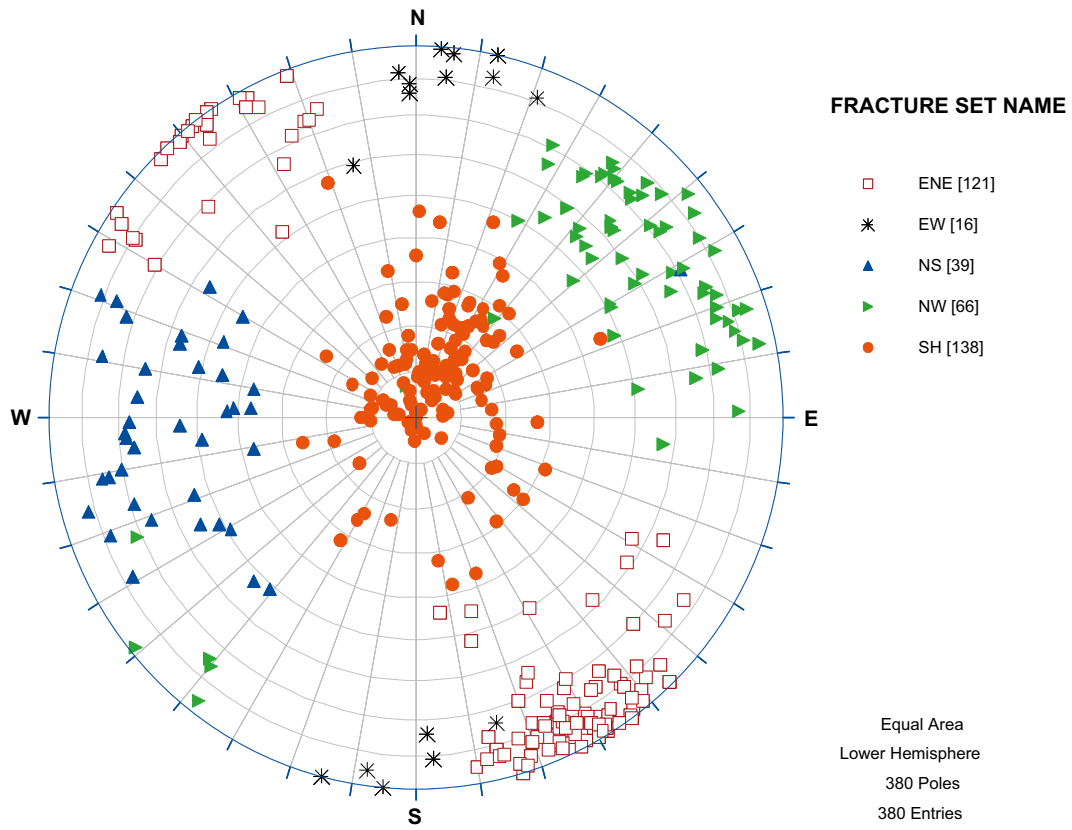
***Figure 12-25.** Borehole KFM05A fracture sets, domain FFM02, fractures not affected by DZ.*
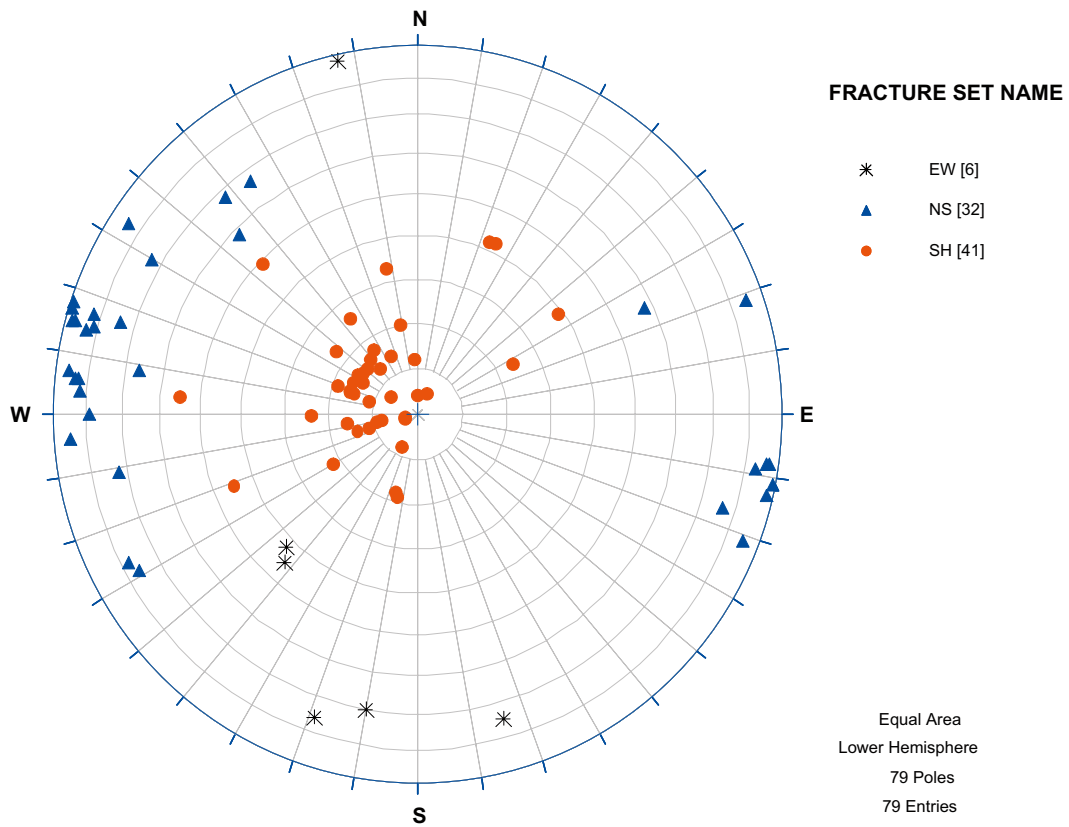
***Figure 12-26.** Borehole KFM06A fracture sets, domain FFM02, fractures not affected by DZ.*
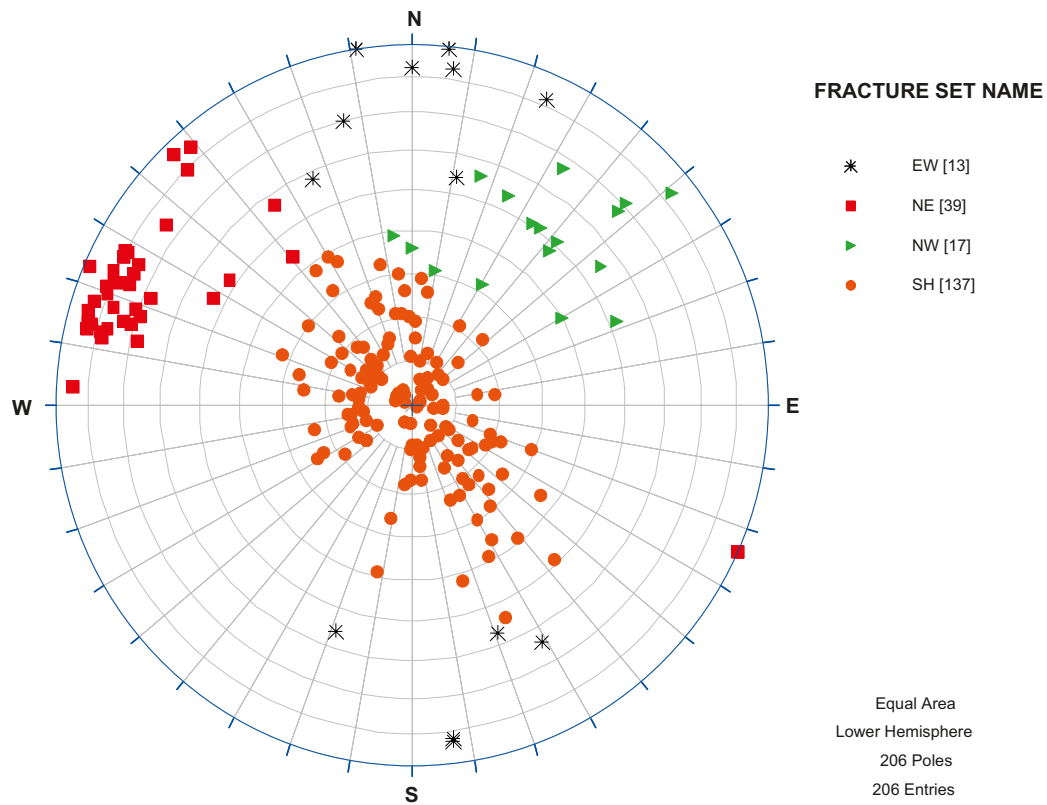
Figure 12-27. *Borehole KFM06B fracture sets, domain FFM02, fractures not affected by DZ.*
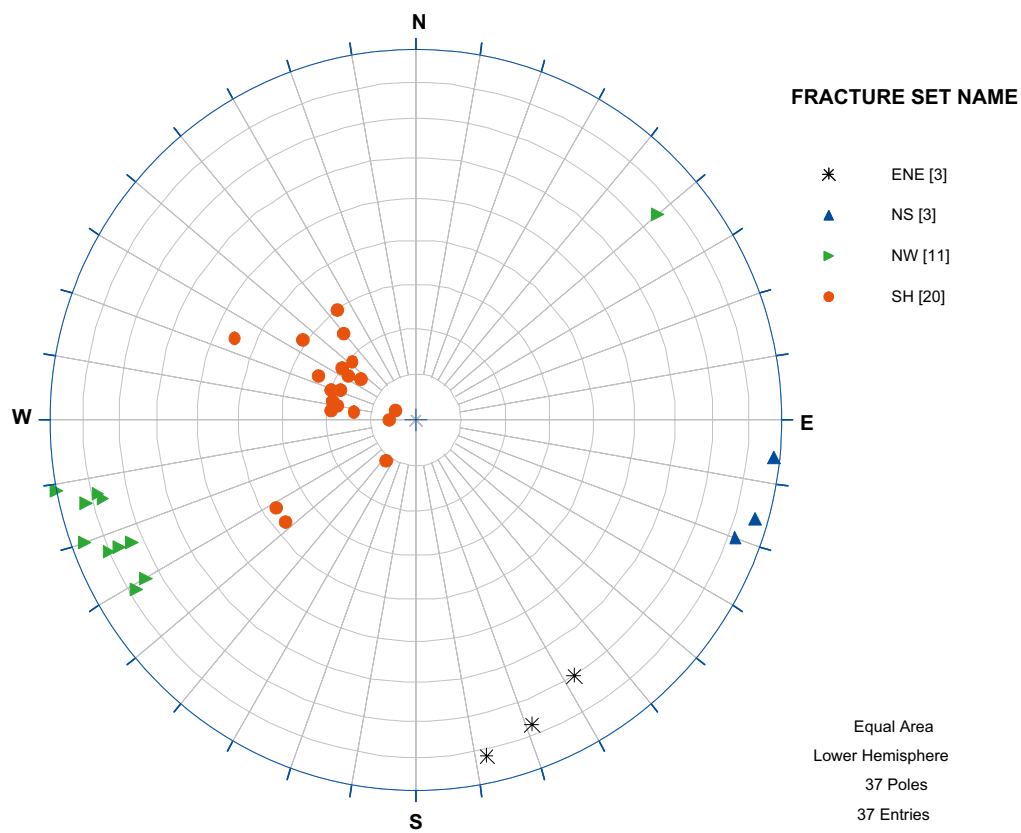
Figure 12-28. *Borehole KFM07A fracture sets, domain FFM02, fractures not affected by DZ.*
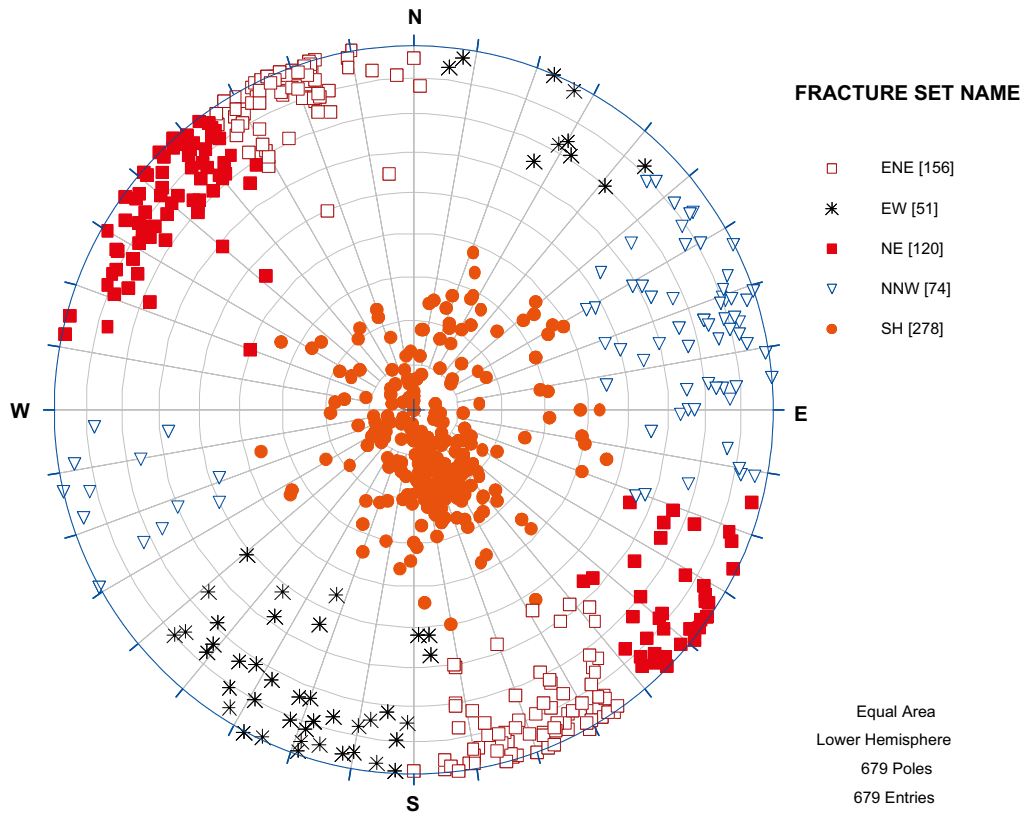
Figure 12-29. Borehole KFM07B fracture sets, domain FFM02, fractures not affected by DZ.
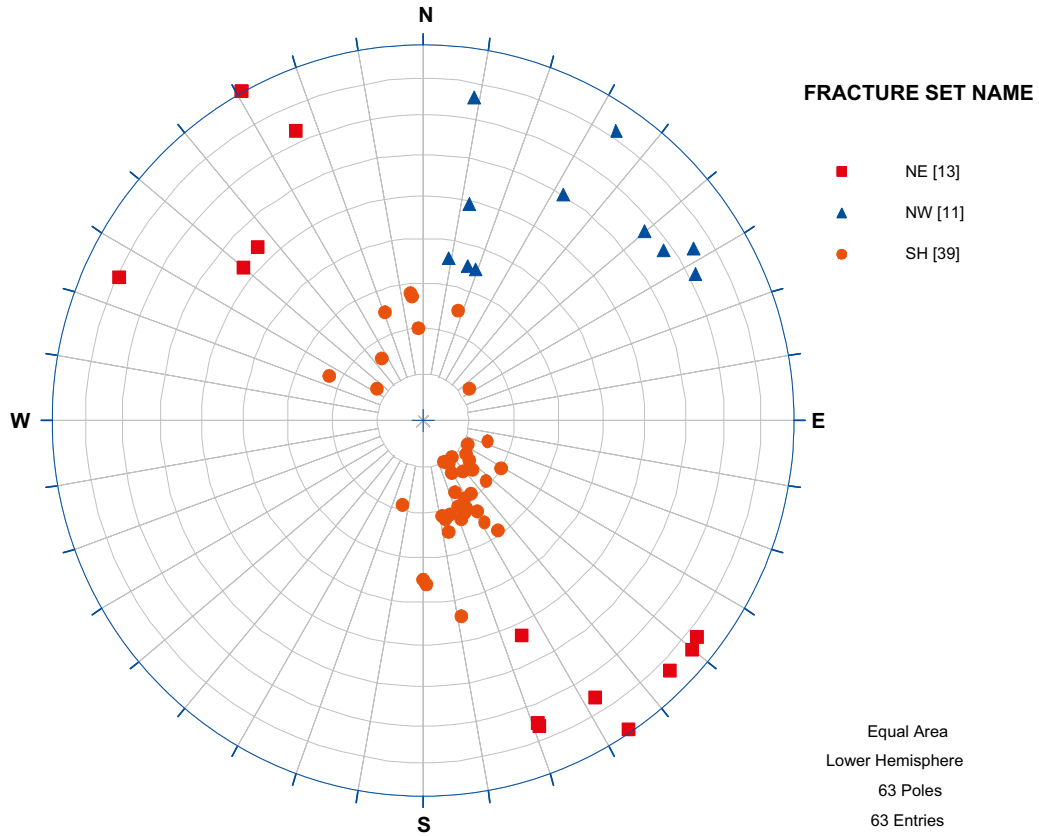
Figure 12-30. Borehole KFM07C fracture sets, domain FFM02, fractures not affected by DZ.

123
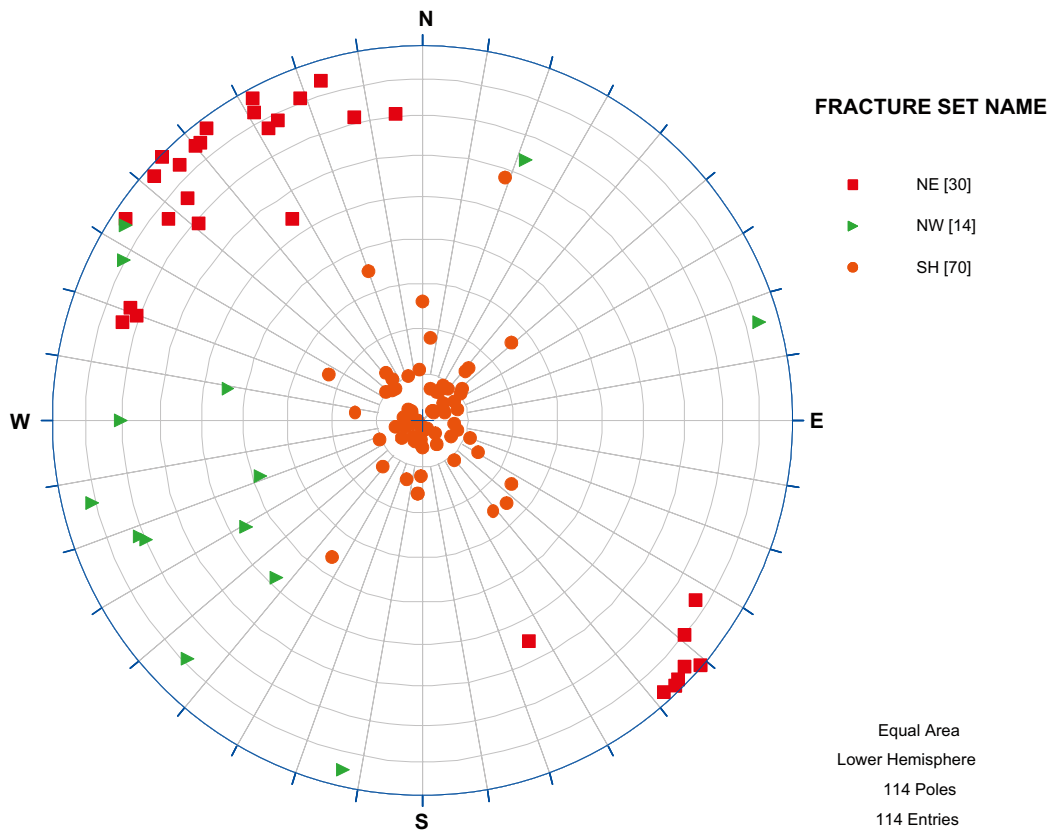
Figure 12-31. *Borehole KFM08B fracture sets, domain FFM02, fractures not affected by DZ.*
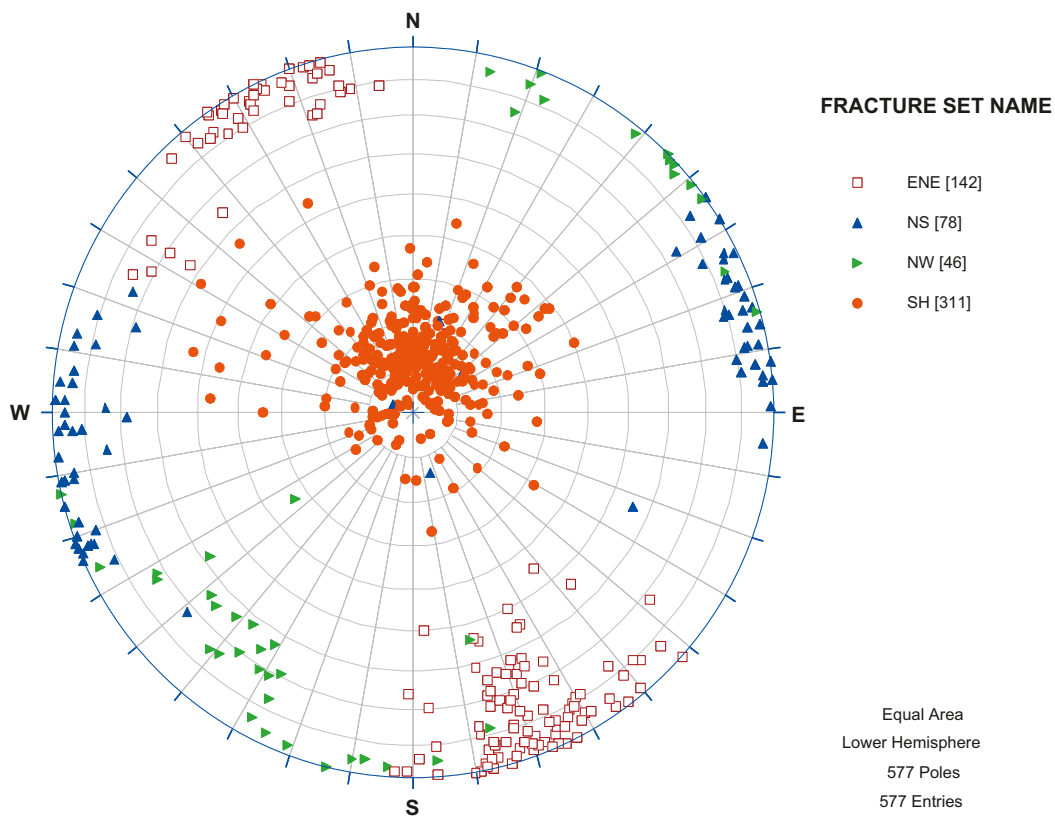
Figure 12-32. *Borehole KFM09A fracture sets, domain FFM02, fractures affected by DZ.*
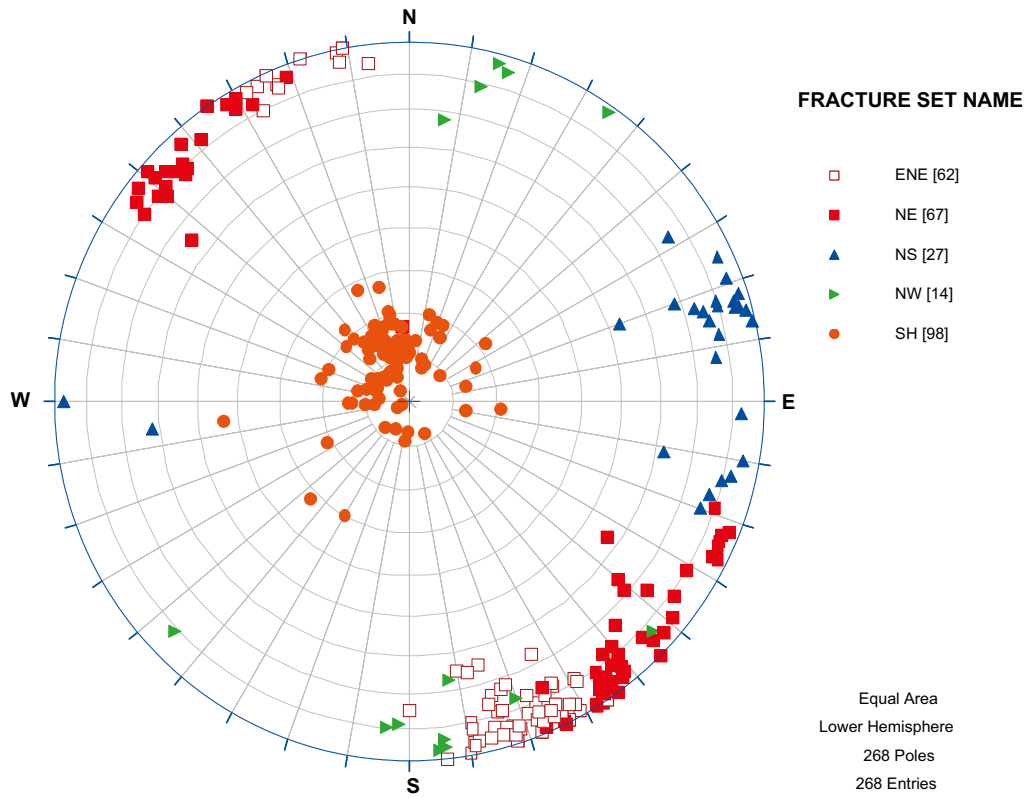
Figure 12-33. *Borehole KFM09B fracture sets, domain FFM02, fractures affected by DZ.*
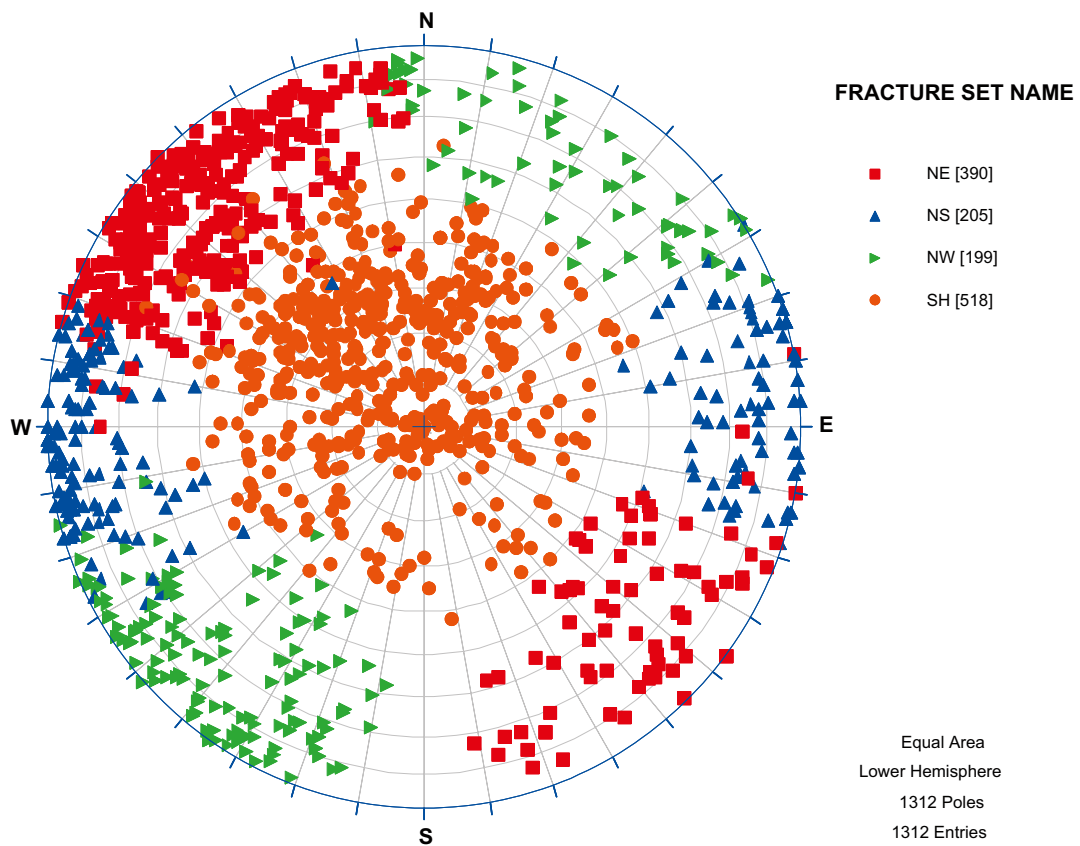
Figure 12-34. *Borehole KFM03A fracture sets, domain FFM03, fractures not affected by DZ.*
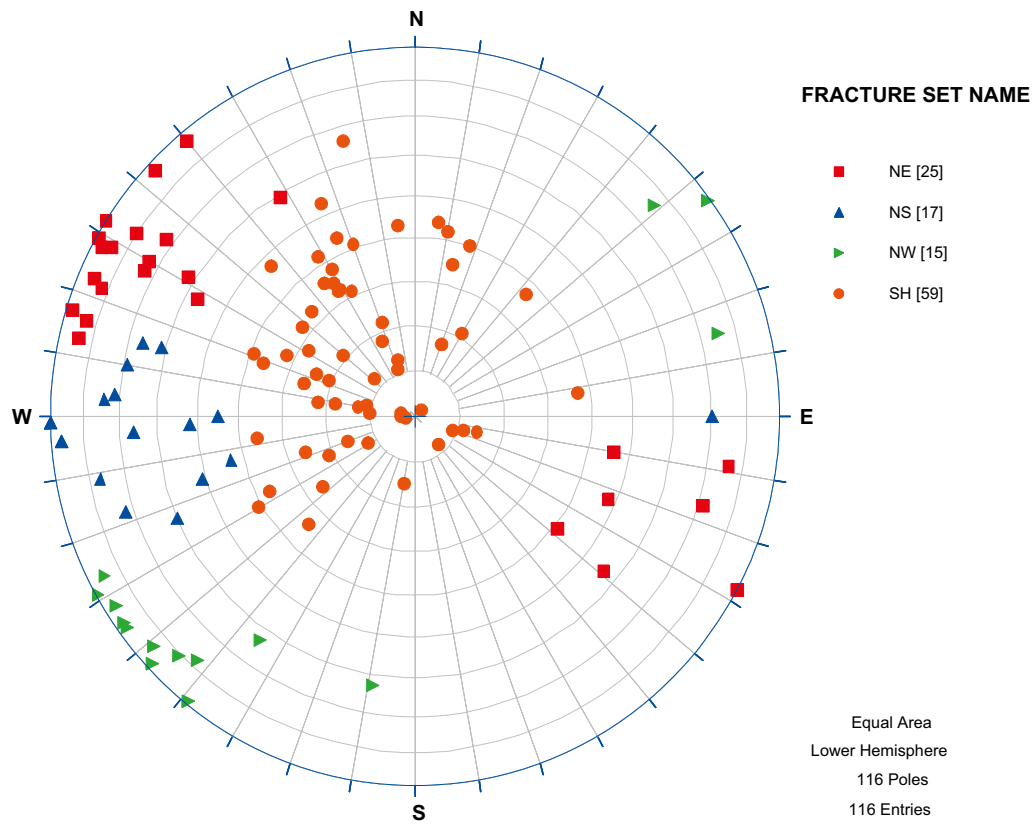
Figure 12-35. *Borehole KFM03B fracture sets, domain FFM03, fractures not affected by DZ.*
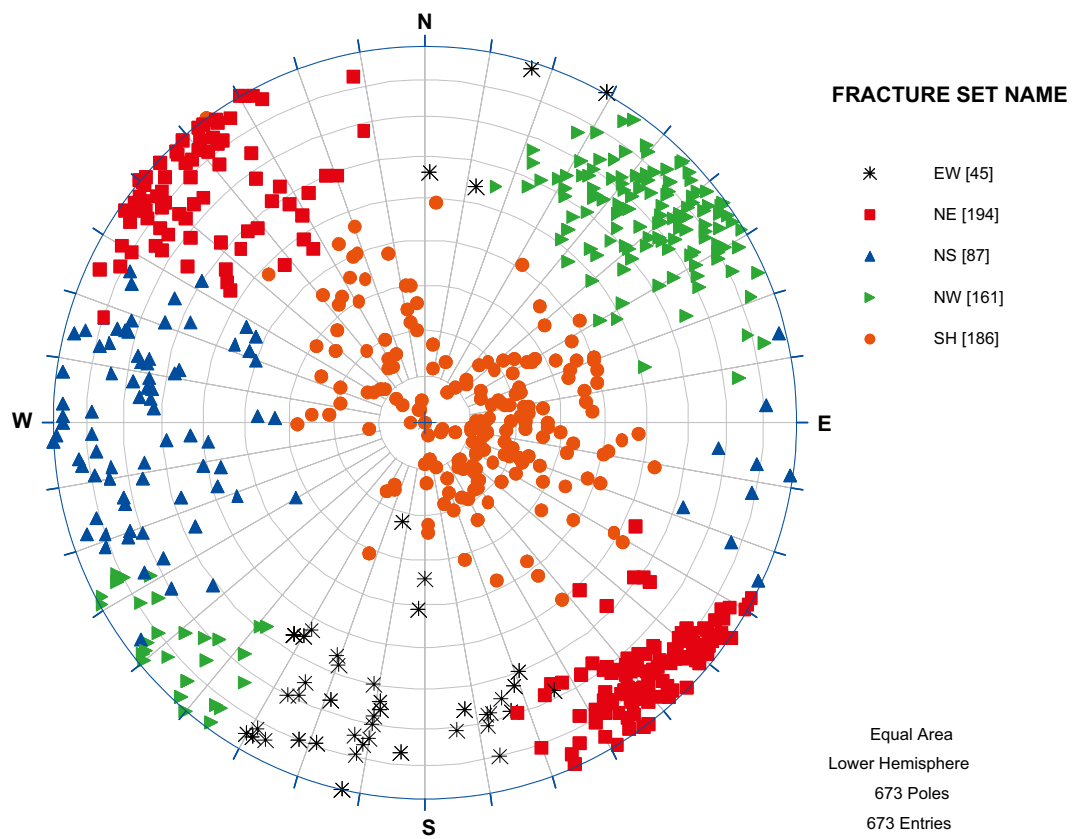
Figure 12-36. *Borehole KFM10A fracture sets, domain FFM03, fractures not affected by DZ.*
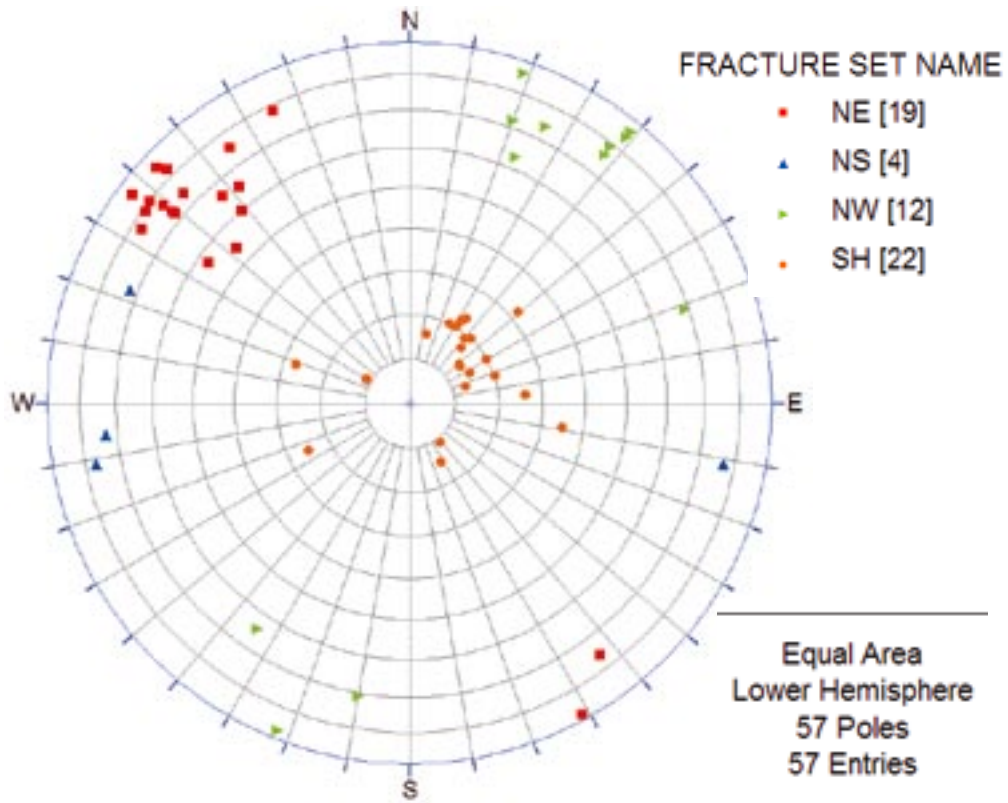
Figure 12-37. *Borehole KFM10A fracture sets, domain FFM03, fractures affected by DZ.*
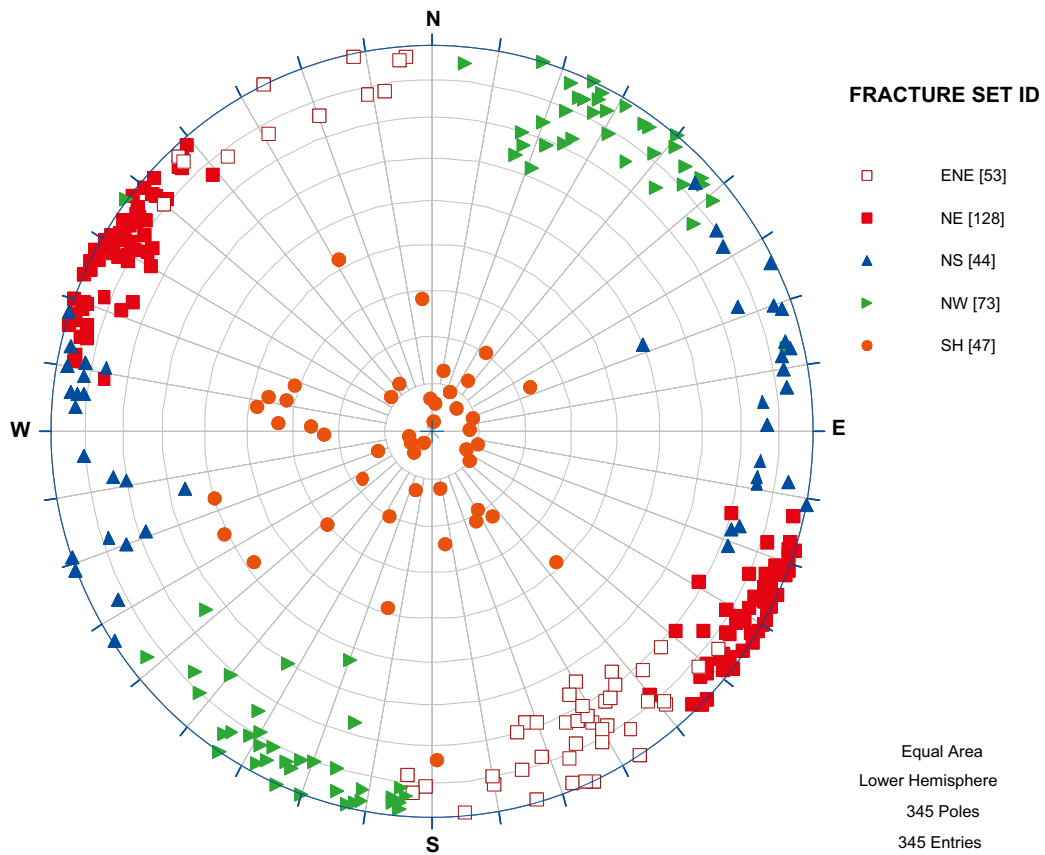
Figure 12-38. *Borehole KFM06A fracture sets, domain FFM06, fractures not affected by DZ.*

Figure 12-39. *Borehole KFM06C fracture sets, domain FFM06, fractures not affected by DZ.*

Figure 12-40. *Borehole KFM08C fracture sets, domain FFM06, fractures not affected by DZ.*

Fracture Intensity with Depth

**All figures are based on the 6m binned P$_{32}$ values for sections labeled 'Not Affected by DZ'.**
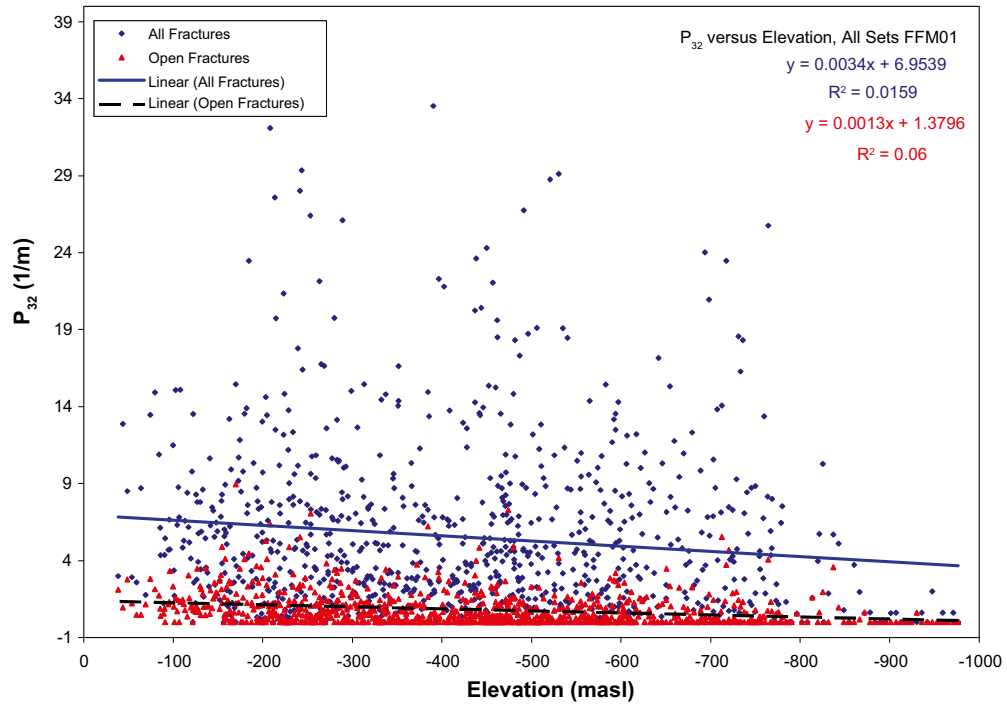
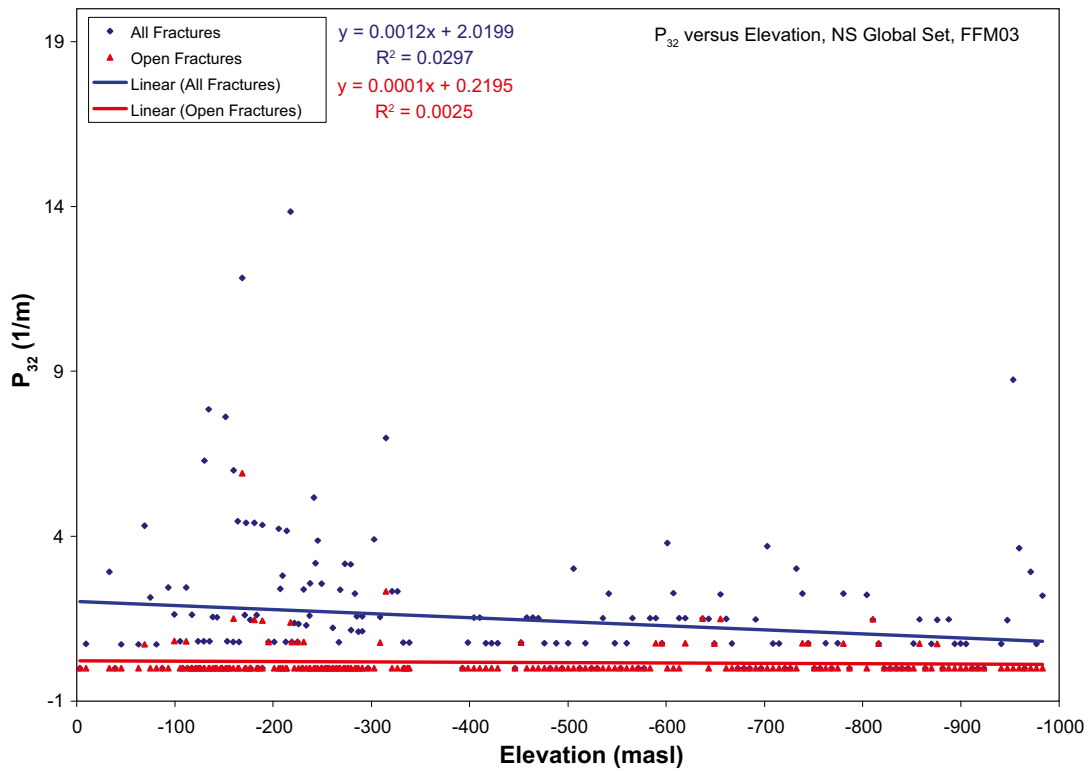*Figure 13-1.* *P$_{32}$ as a function of elevation, All Fractures, FFM01.*
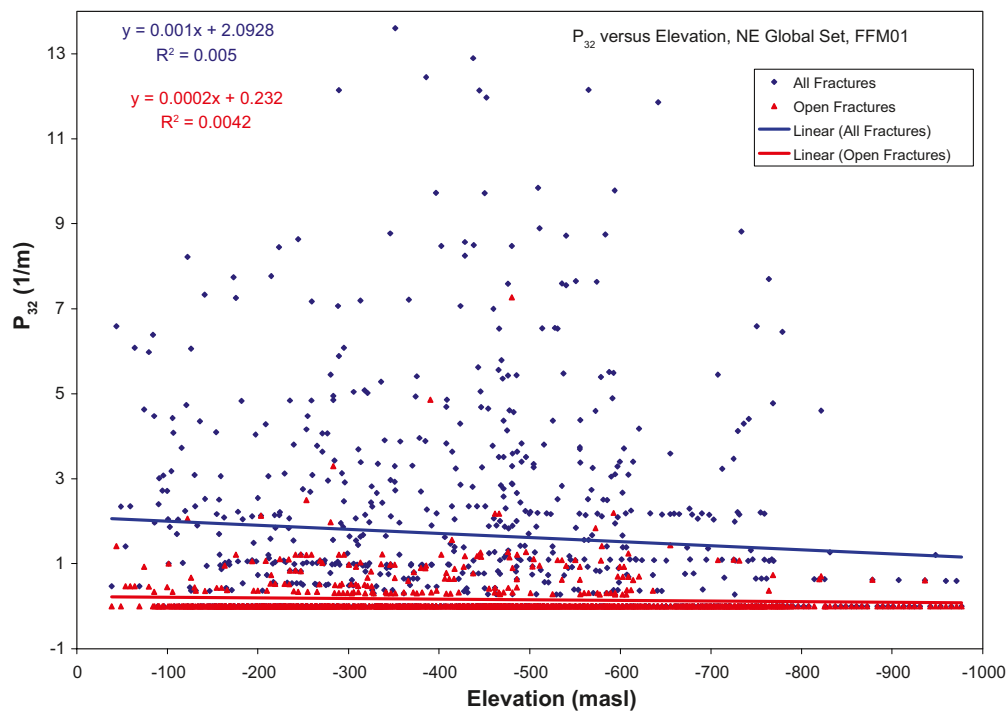
Figure 13-2. *P$_{32}$ as a function of elevation, NE Global Set, FFM01.*
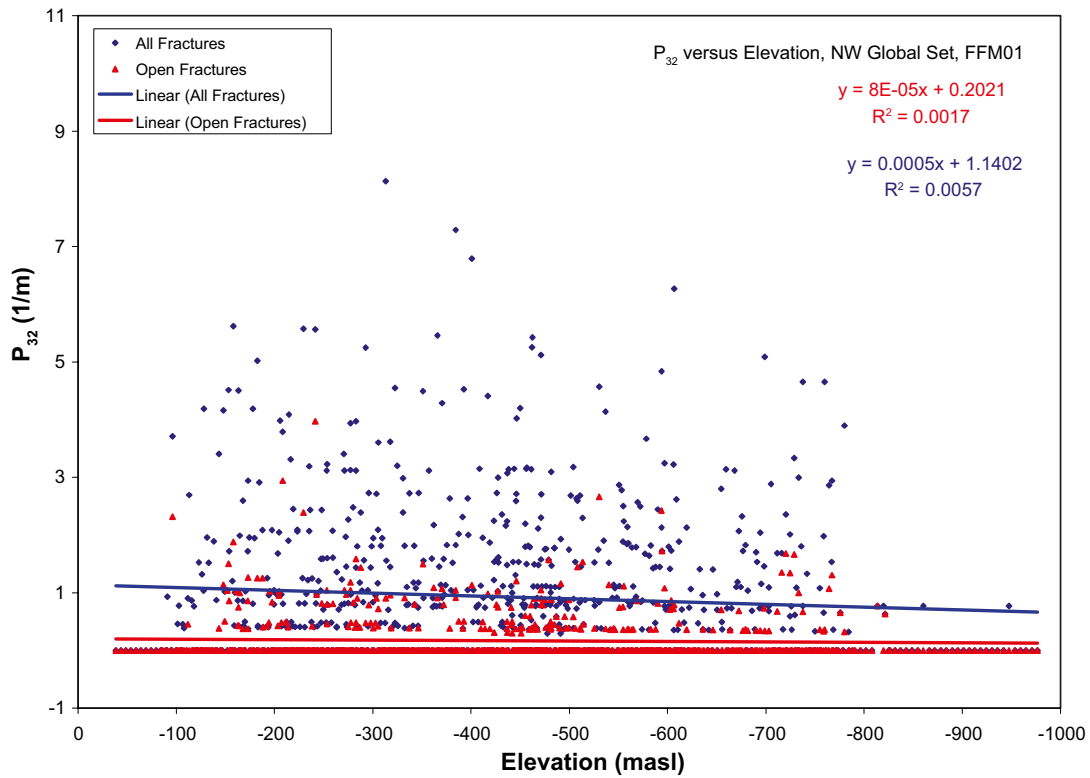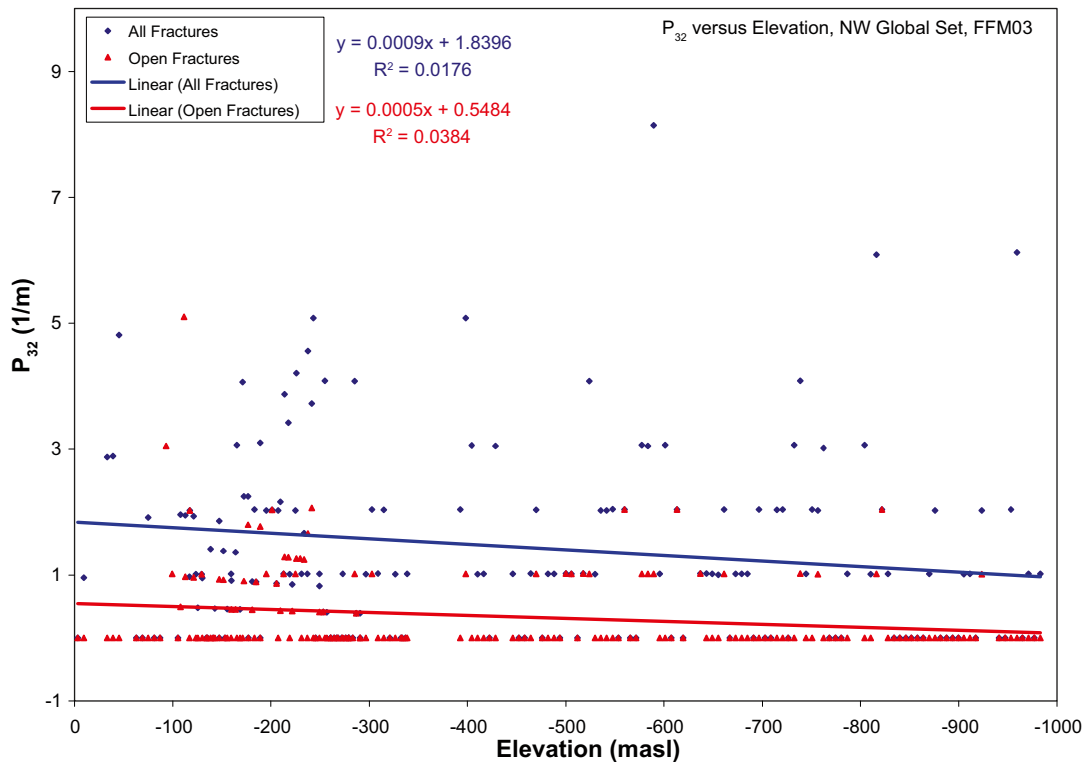
Figure 13-3. *P_{32} as a function of elevation, NW Global Set, FFM01.*
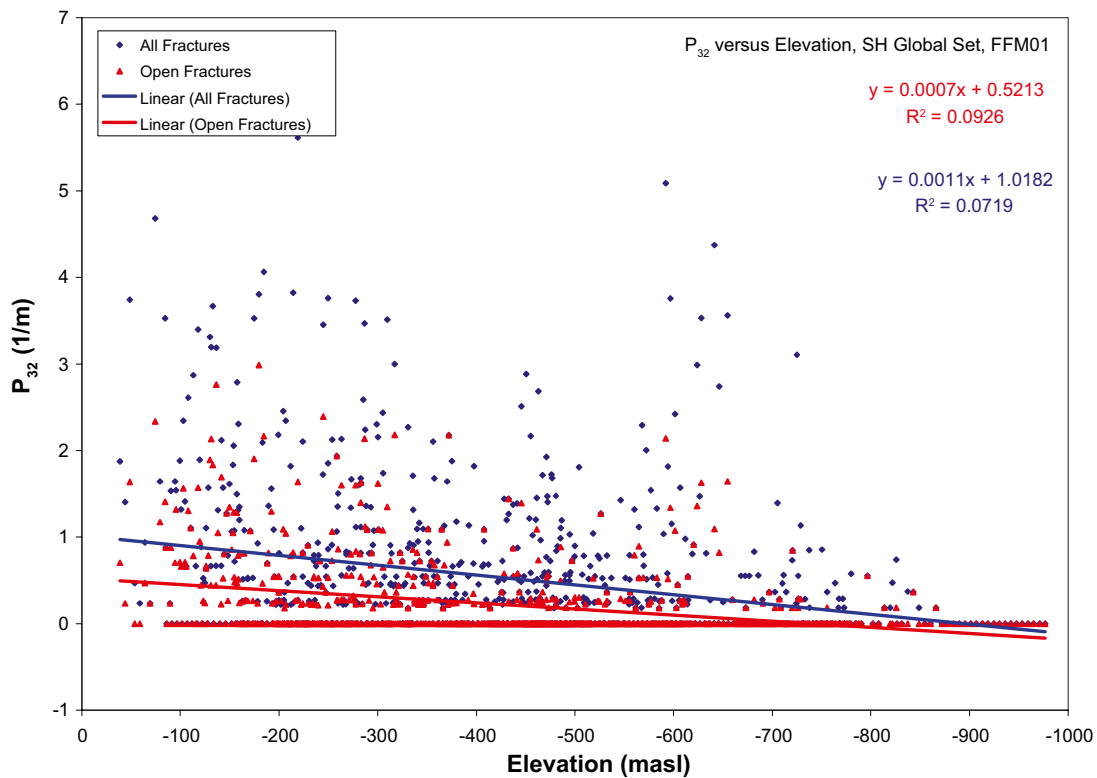
Figure 13-4. *P_{32} as a function of elevation, SH Global Set, FFM01.*
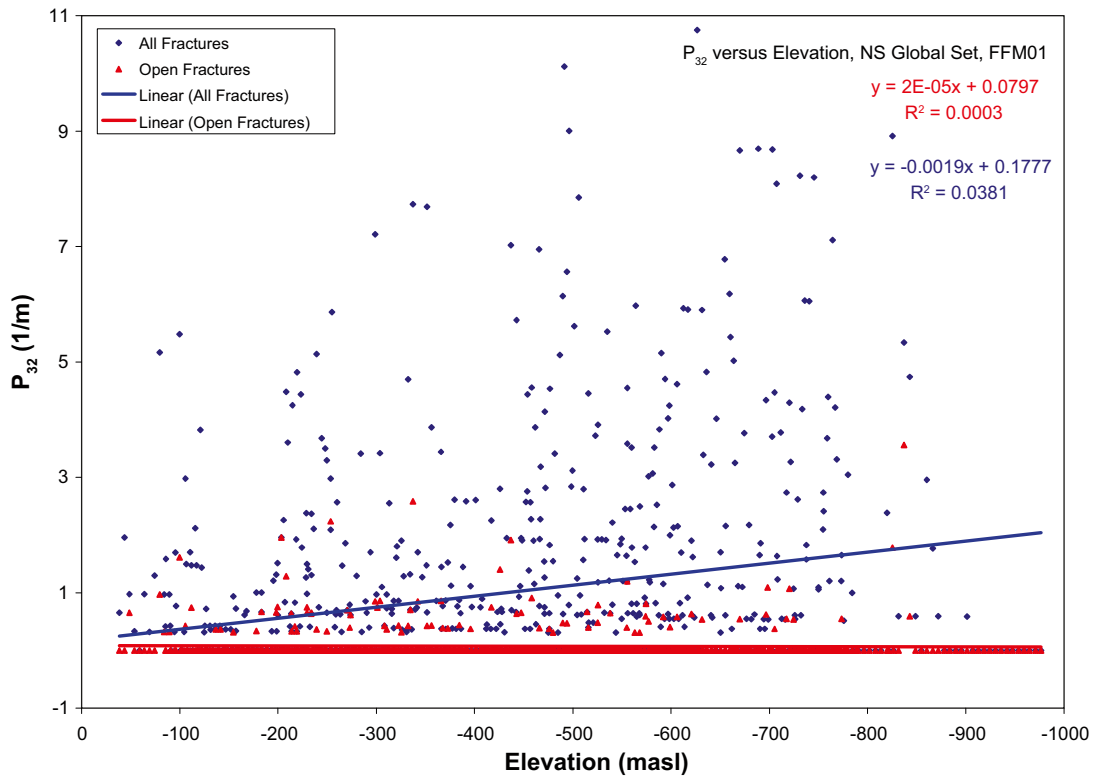
Figure 13-5. *P$_{32}$ as a function of elevation, NS Global Set, FFM01.*
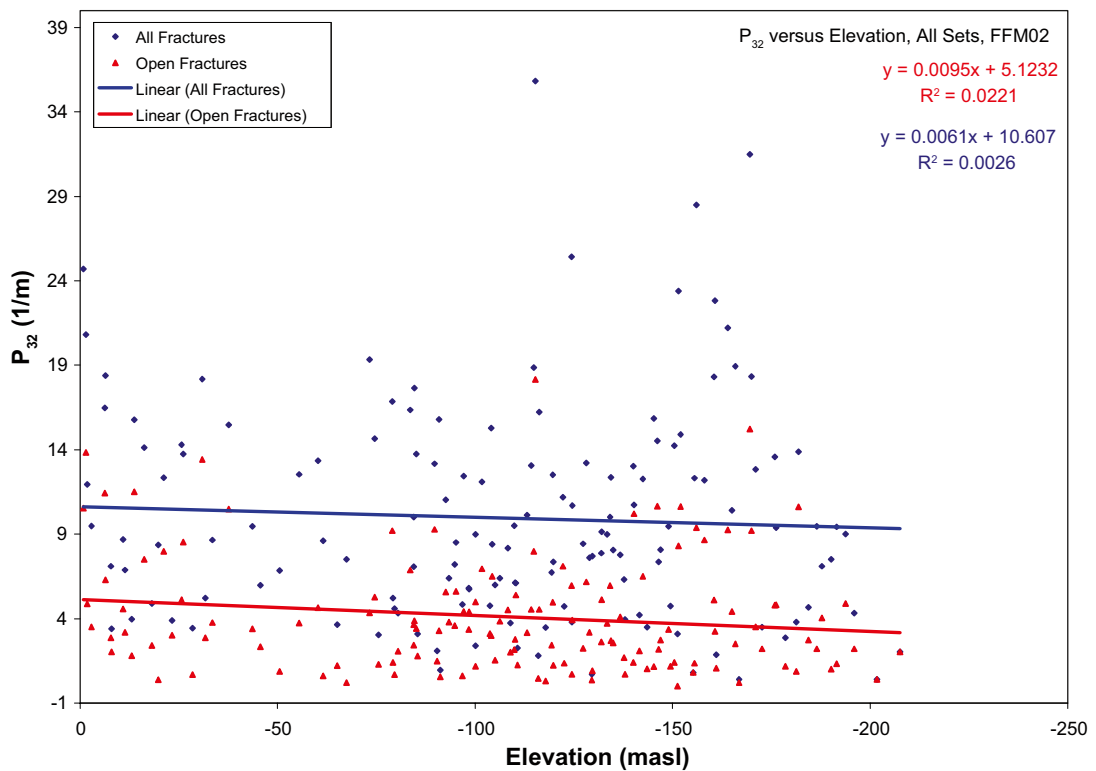
Figure 13-6. *P$_{32}$ as a function of elevation, All Fractures, FFM02.*
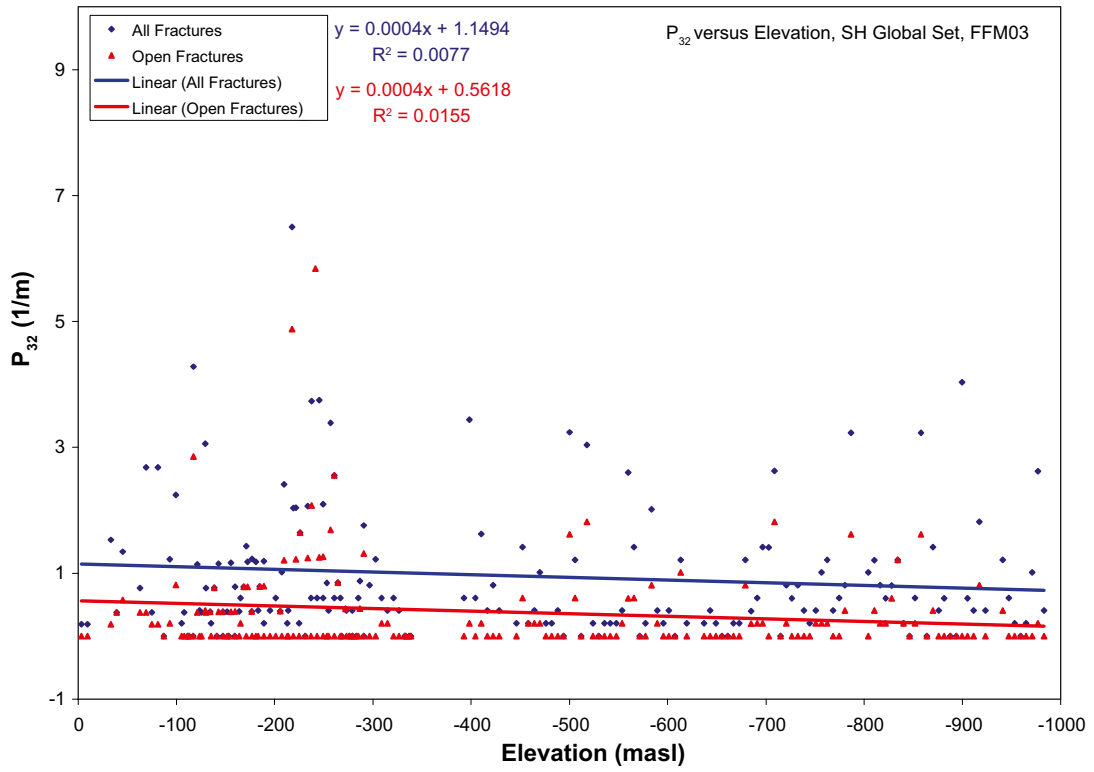
131
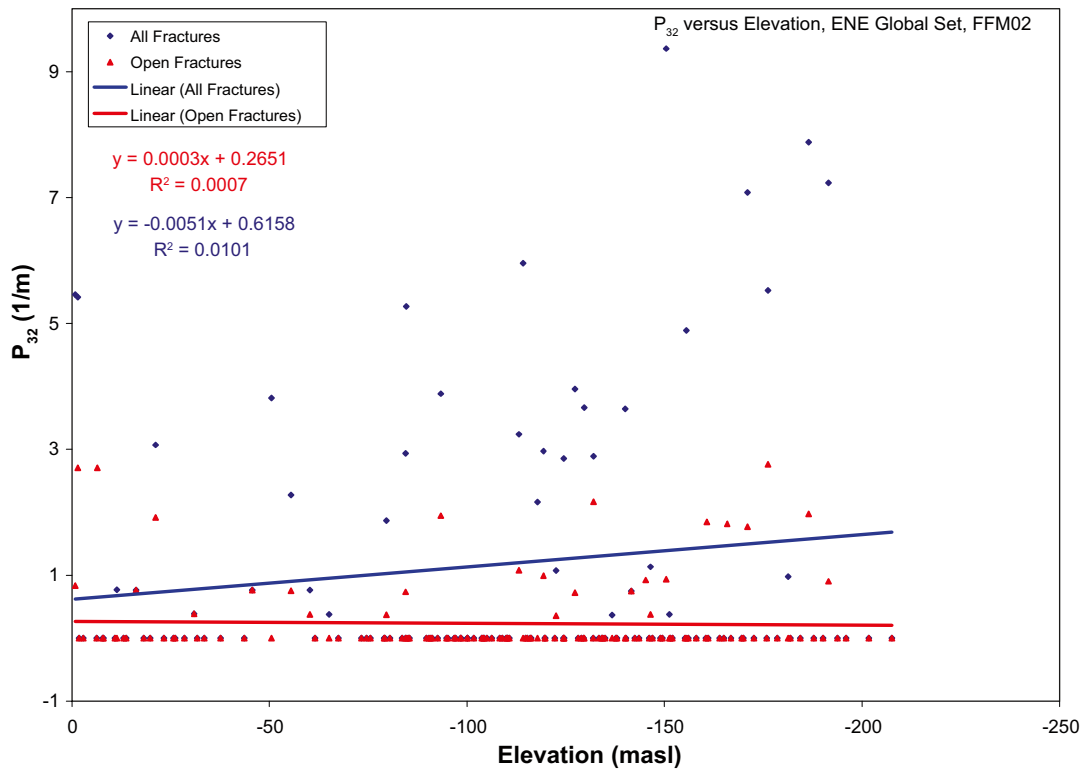
Figure 13-7. *P_{32} as a function of elevation, ENE Global Set, FFM02.*
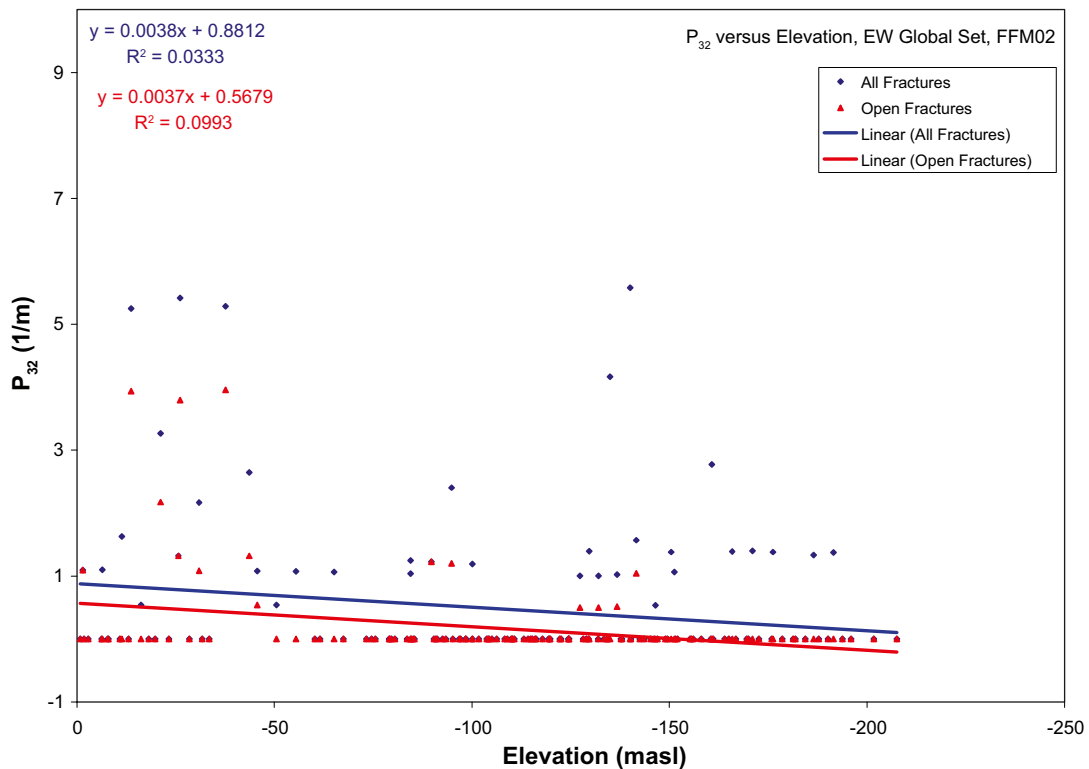
Figure 13-8. *P_{32} as a function of elevation, EW Global Set, FFM02.*
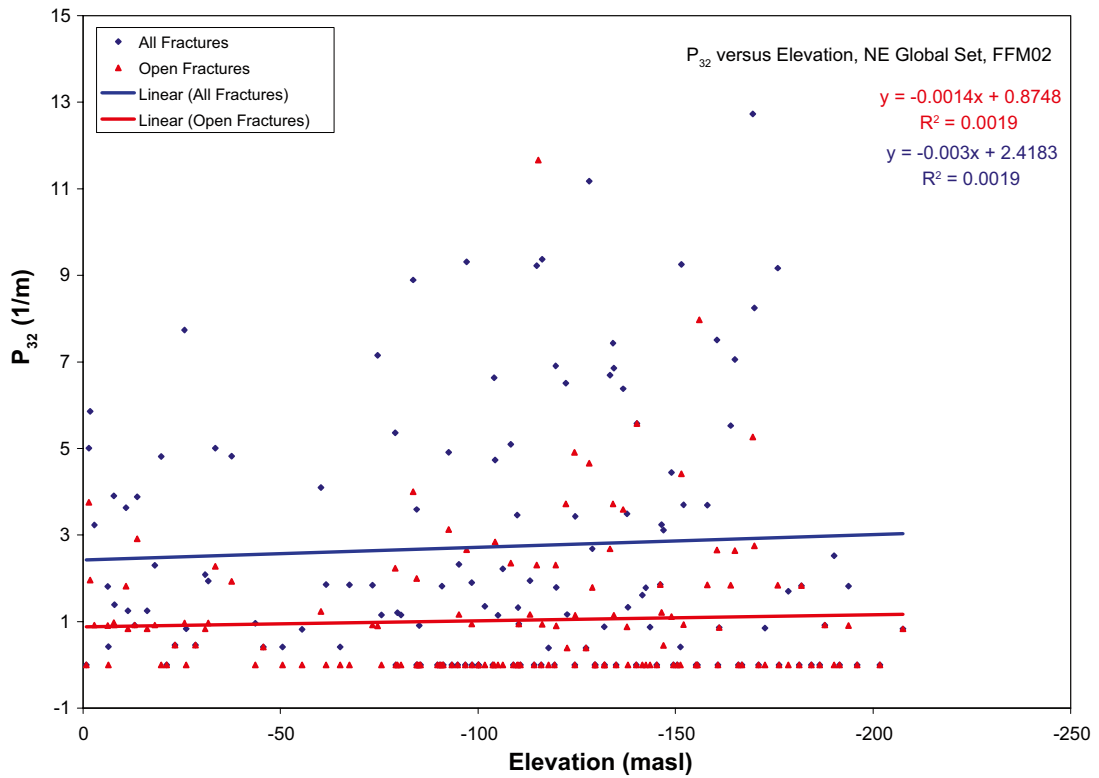
Figure 13-9. *P$_{32}$ as a function of elevation, NE Global Set, FFM02.*
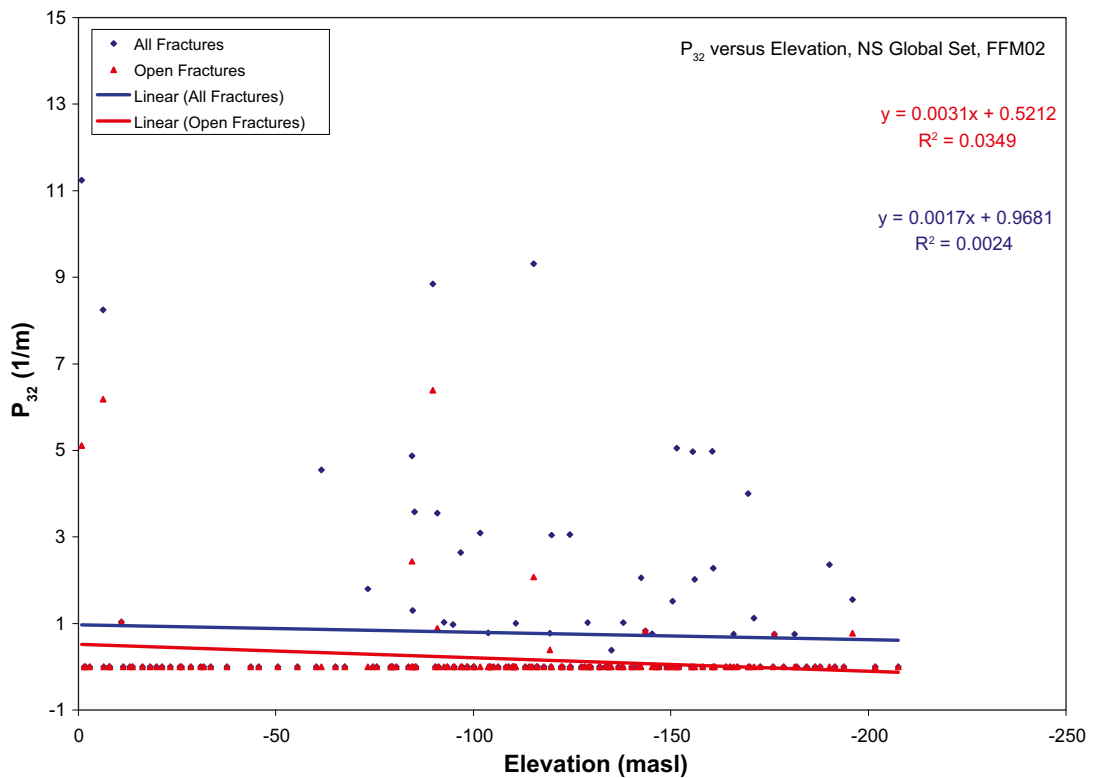
Figure 13-10. *P$_{32}$ as a function of elevation, NS Global Set, FFM02.*
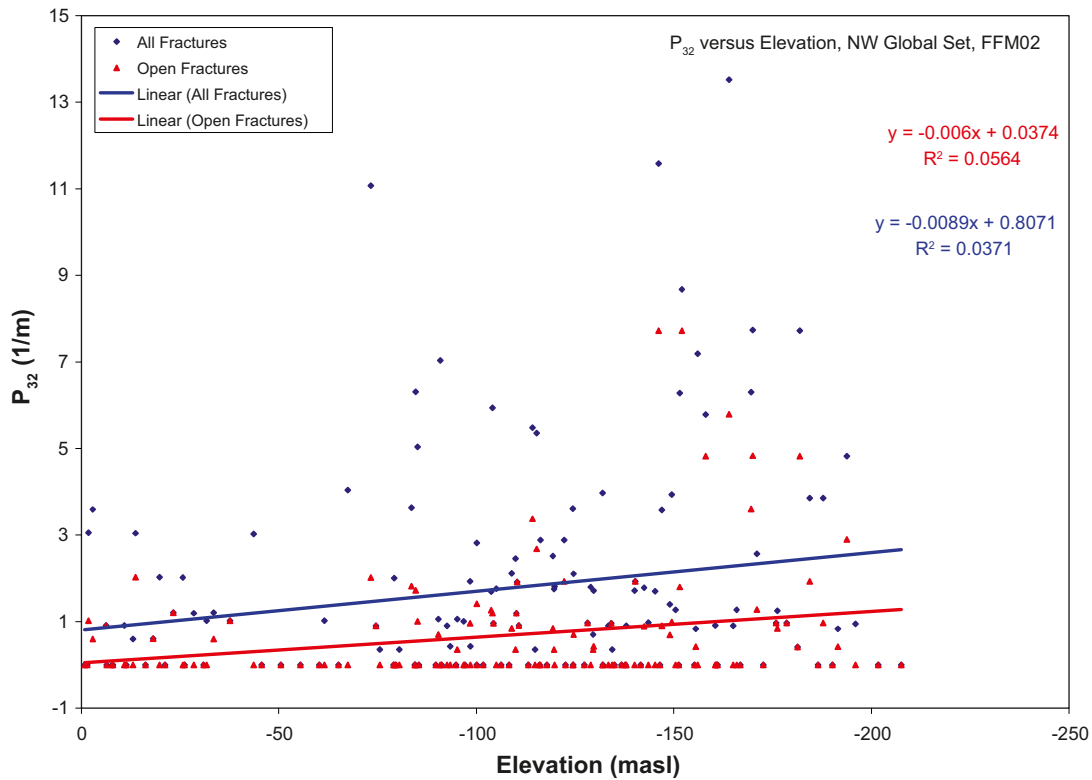
Figure 13-11. P_{32} as a function of elevation, NW Global Set, FFM02.
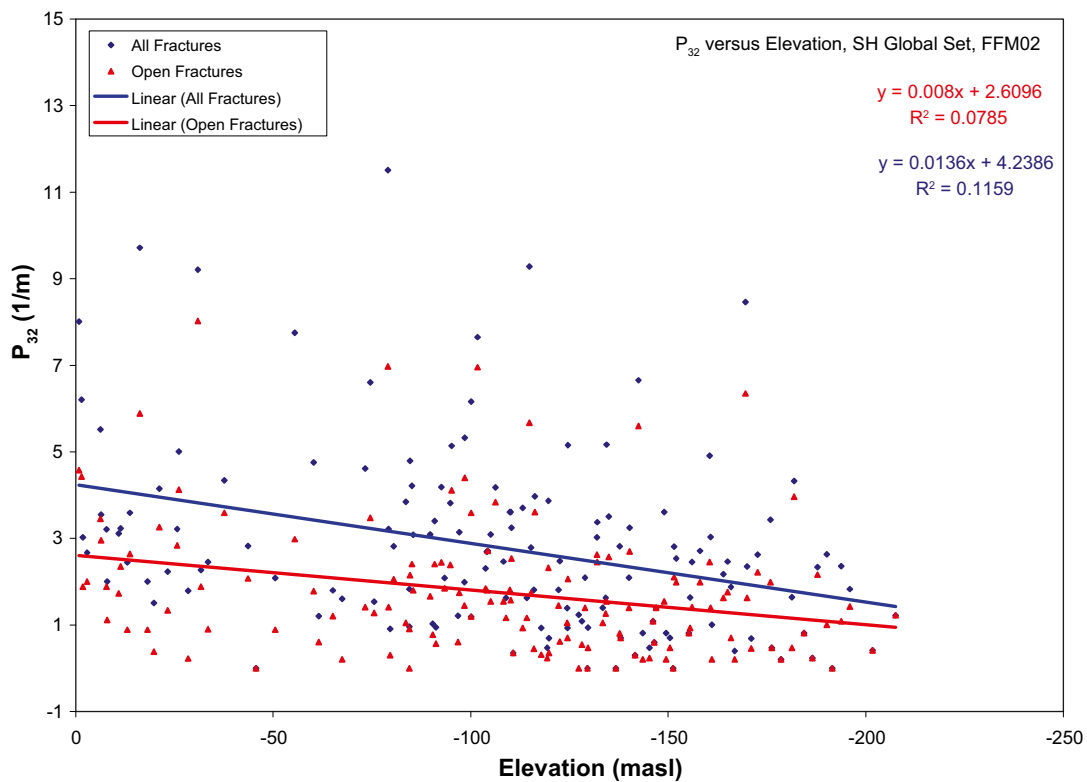
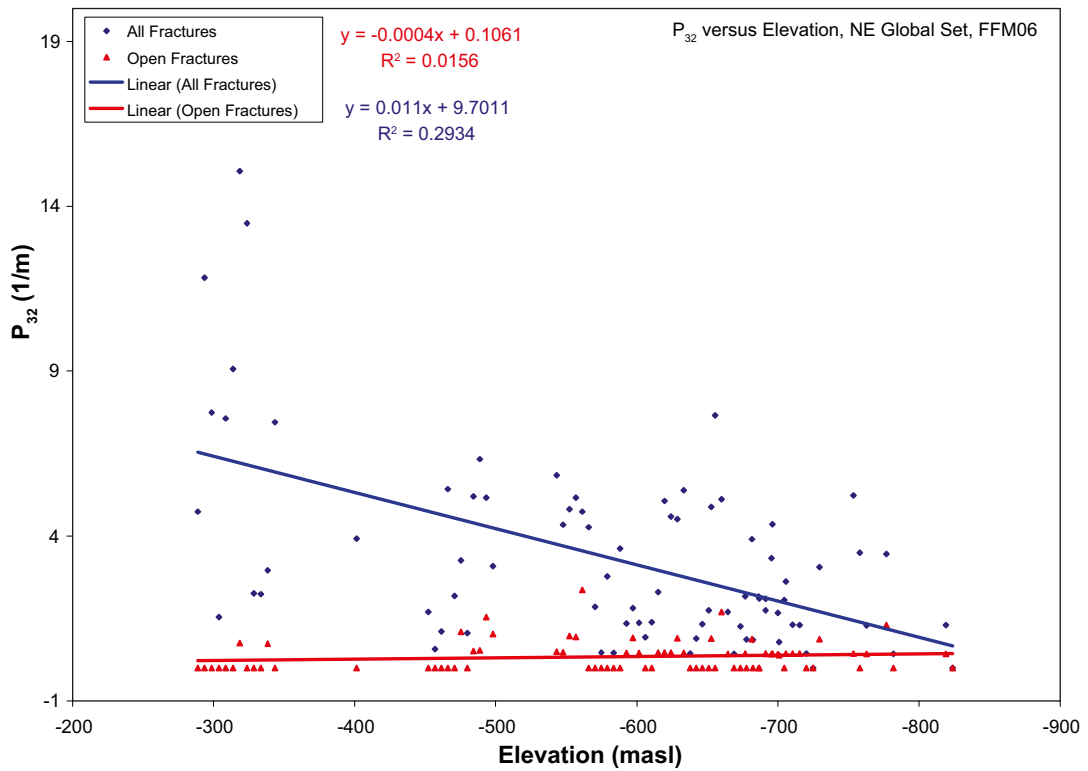**Figure 13-12.** P_{32} as a function of elevation, SH Global Set, FFM02.
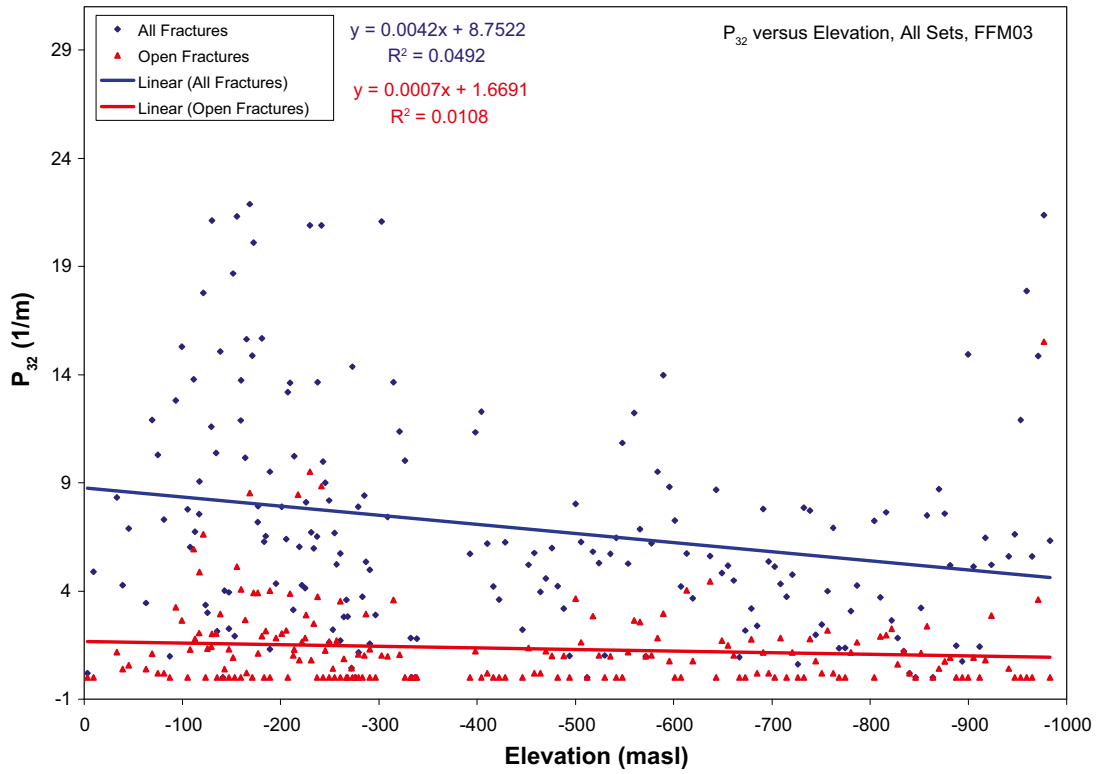
Figure 13-13. *P$_{32}$ as a function of elevation, All Sets, FFM03.*
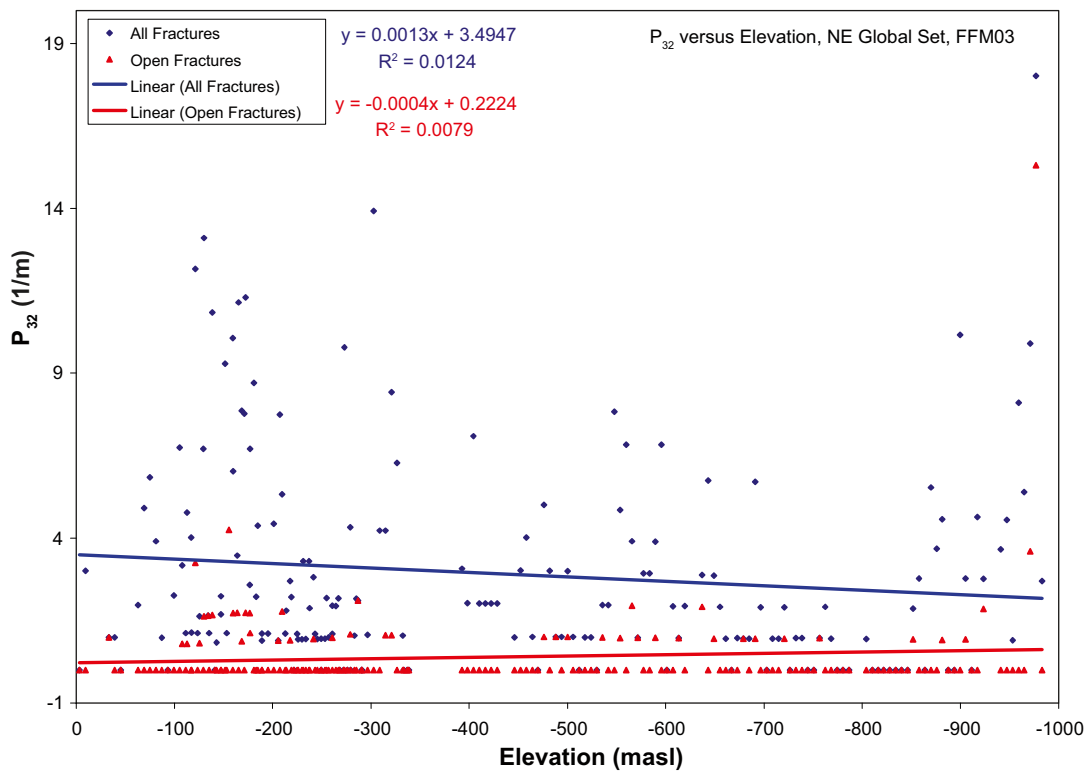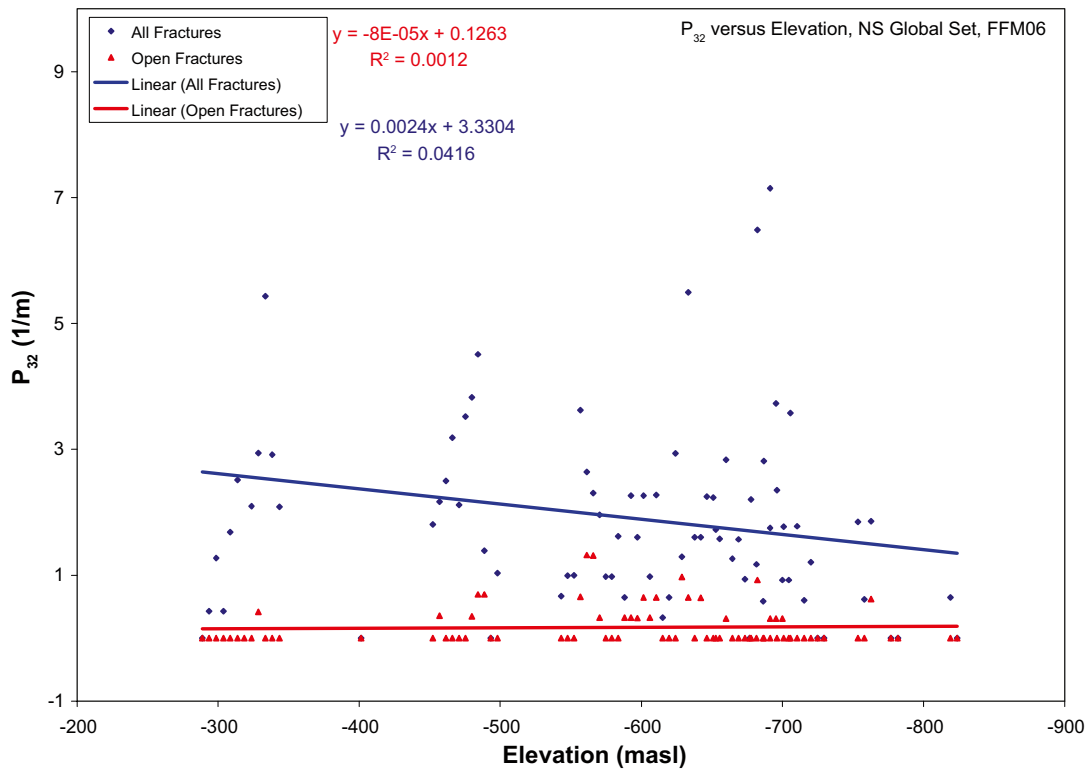

Figure 13-14. *P$_{32}$ as a function of elevation, NE Global Set, FFM03.*

Figure 13-15. *P_{32} as a function of elevation, NS Global Set, FFM03.*

Figure 13-16. *P_{32} as a function of elevation, NW Global Set, FFM03.*

Figure 13-17. *P_{32} as a function of elevation, SH Global Set, FFM03.*

Figure 13-18. *P_{32} as a function of elevation, NE Global Set, FFM06.*

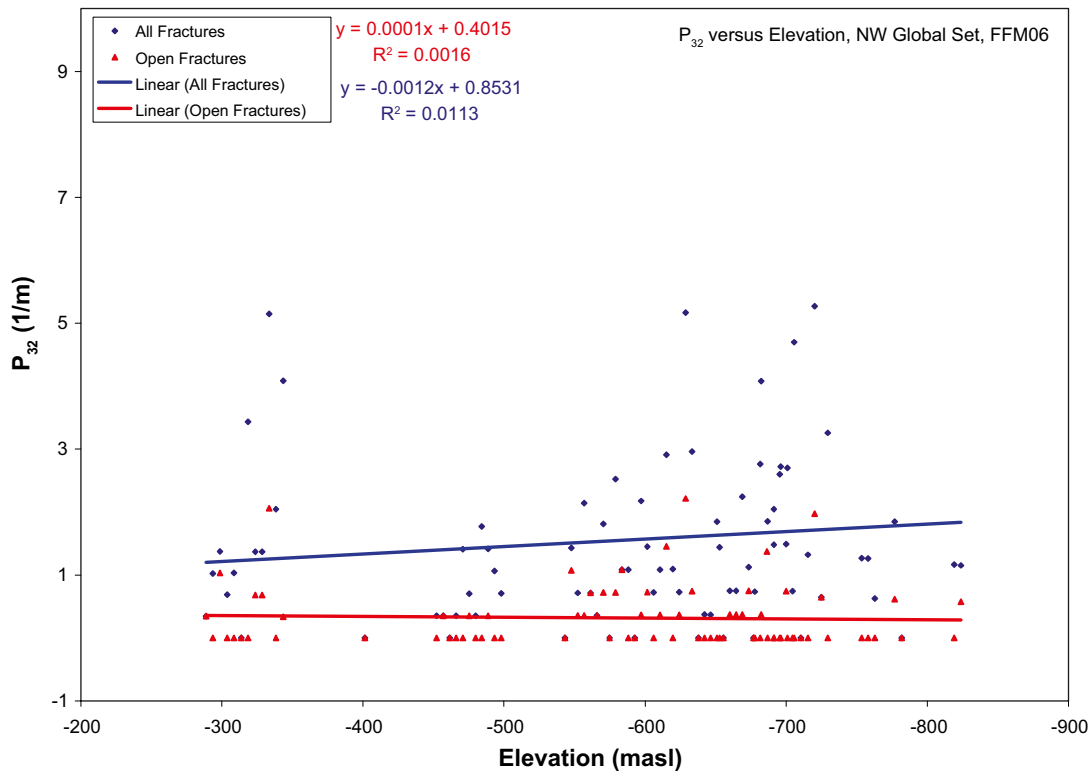**Figure 13-19.** *P$_{32}$ as a function of elevation, NS Global Set, FFM06.*
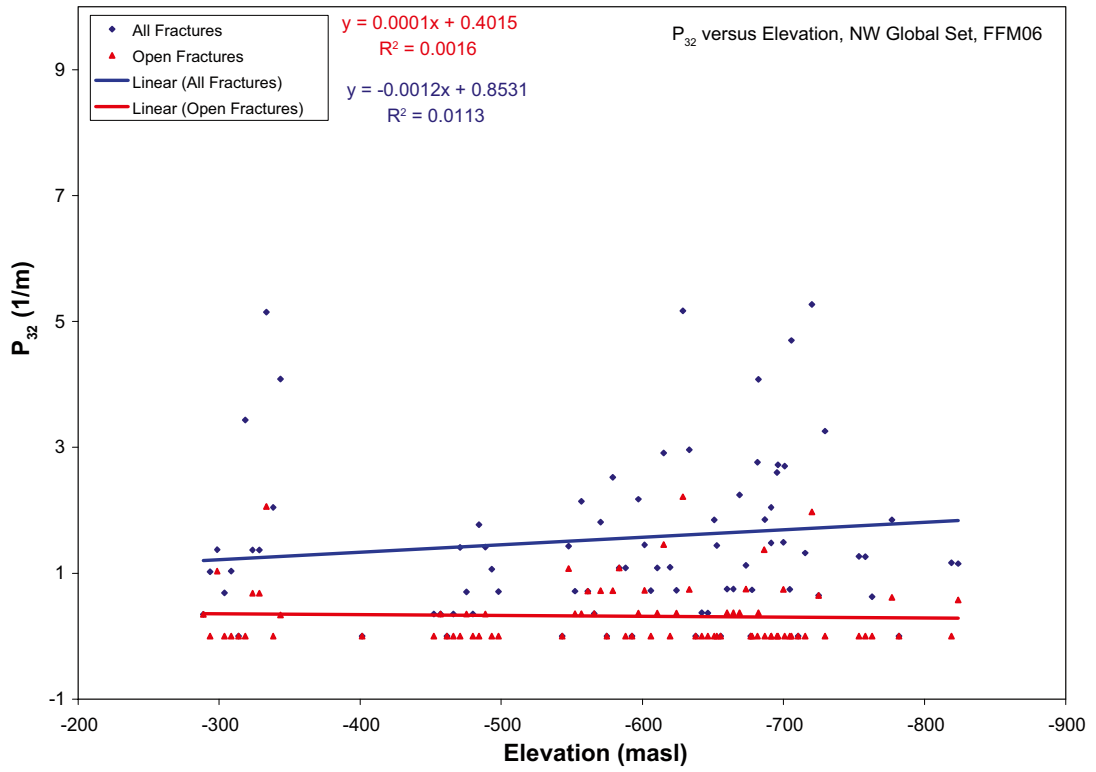

Figure 13-20. *P$_{32}$ as a function of elevation, NW Global Set, FFM06.*

Figure 13-21. *P₃₂ as a function of elevation, SH Global Set, FFM06.*